

REPORT DOCUMENTATION PAGE				Form Approved OMB No. 0704-0188		
Public reporting burden for this collection of information is estimated to average 1 hour per response, including the time for reviewing instructions, searching data sources, gathering and maintaining the data needed, and completing and reviewing the collection of information. Send comments regarding this burden estimate or any other aspect of this collection of information, including suggestions for reducing this burden to Washington Headquarters Service, Directorate for Information Operations and Reports, 1215 Jefferson Davis Highway, Suite 1204, Arlington, VA 22202-4302, and to the Office of Management and Budget, Paperwork Reduction Project (0704-0188), Washington, DC 20503.						
PLEASE DO NOT RETURN YOUR FORM TO THE ABOVE ADDRESS.						
1. REPORT DATE (DD-MM-YYYY) 5/28/99		2. REPORT DATE Final Report		3. DATES COVERED (From - To) 3/1/96 - 2/28/99		
4. TITLE AND SUBTITLE Hydrodynamic Interaction Between Olfactory Antennae and Odor Plumes				5a. CONTRACT NUMBER		
				5b. GRANT NUMBER N00014-96-1-0594		
				5c. PROGRAM ELEMENT NUMBER		
6. AUTHOR(S) M.A.R. Koehl				5d. PROJECT NUMBER		
				5e. TASK NUMBER		
				5f. WORK UNIT NUMBER		
7. PERFORMING ORGANIZATION NAME(S) AND ADDRESS(ES) The Regents of the University of California U.C. Berkeley, Dept. of Integrative Biology Berkeley, CA 94720-3140				8. PERFORMING ORGANIZATION REPORT NUMBER		
9. SPONSORING/MONITORING AGENCY NAME(S) AND ADDRESS(ES) Office of Naval Research 800 N. Quincy St. Arlington, VA 22217-5000				10. SPONSOR/MONITOR'S ACRONYM(S)		
				11. SPONSORING/MONITORING AGENCY REPORT NUMBER		
12. DISTRIBUTION AVAILABILITY STATEMENT Distribution Unlimited						
13. SUPPLEMENTARY NOTES						
14. ABSTRACT We studied the small-scale hydrodynamics of diverse olfactory antennae of marine animals to elucidate ways in which their physical structure and motion affect how they encounter the concentration distributions in odor plumes, and to gain insights for the design of man-made chemical sensors. The designs and motions of the lobster, crab, and mantis shrimp antennules we studied enhance their ability to take temporally and spatially discrete odor samples. We also measured turbulent water flow at several types of coastal field sites, simulated such turbulence in a flume (with Koseff at Stanford), and measured how the fine filaments of high concentration in a chemical plume are affected when antennules flick through them when an animal is different distances from an odor source.						
15. SUBJECT TERMS olfaction, antenna, plume, hydrodynamics						
16. SECURITY CLASSIFICATION OF:			17. LIMITATION OF ABSTRACT	18. NUMBER OF PAGES	19a. NAME OF RESPONSIBLE PERSON	
a. REPORT U	b. ABSTRACT U	c. THIS PAGE U	UL			
						19b. TELEPHONE NUMBER (Include area code)

19990614 019

~~DTIC QUALITY INSPECTED 4~~

DTIC QUALITY INSPECTED 4

FINAL REPORT

GRANT #: N000149610594

PRINCIPAL INVESTIGATOR: M. A. R. Koehl

INSTITUTION: University of California at Berkeley

GRANT TITLE: Hydrodynamic Interaction Between Olfactory Antennae and Odor Plumes

AWARD PERIOD: 3/1/96 - 2/28/99

OBJECTIVE: We study the hydrodynamic performance of olfactory antennae of marine animals, both to elucidate how they filter chemical cues from the environment and to gain insights for the design of man-made chemical sensors. The specific objective of this study was to elucidate ways in which the structure and the motions of olfactory antennae affect how they encounter the concentration distributions in odor plumes.

APPROACH: We have been comparing the flow through and molecule capture by arrays of chemosensory hairs on olfactory antennules from diverse marine crustaceans (lobsters, crabs, mantis shrimp). We use particle-image velocimetry to measure velocity profiles around dynamically-scaled physical models to study effects of antennule morphology and kinematics on flow near sensor surfaces. We determine how these flow fields affect the spatial and temporal patterns of molecule diffusion to the surfaces of the sensory hairs using a mathematical model. The parameters used to build our models are based on our morphometric (using SEM, TEM, light microscopy) and kinematic (using high-speed video) analyses of the antennules. We measure water velocity profiles and turbulence in the animals' habitats using acoustic doppler velocimetry; these field data are used by our collaborators at Stanford (J. Koseff) to design flow regimes in their flume that are relevant to real biosensors in coastal environments. Planar laser induced fluorescence is used to study the spatial and temporal distribution of concentration filaments in dye plumes in their flume. We place models of animals in these plumes to measure effects of flicking and distance from source on the spatio-temporal patterns of concentration encountered by antennules.

ACCOMPLISHMENTS: We have completed the kinematic and morphometric analyses of antennules of spiny lobsters (whose long antennules bear a complex, dense array of guard and sensory hairs), mantis shrimp (whose antennules bear a simple, sparse array of sensory hairs), and blue crabs (whose short antennules bear a dense brush of sensory hairs). We have used these data to construct dynamically-scaled physical models of the antennules of all these species and have completed the flow analyses for the lobsters and mantis shrimp (measurements for the crab antennules are underway). We have developed a reaction-diffusion model to calculate molecule arrival at the sensory hairs on antennules, and we have completed such calculations for mantis shrimp antennules. Water flow measurements have been made at a variety of shallow coastal habitats and our collaborators at Stanford have used these data to design flow regimes in their flume (see Koseff's progress reports for details of their accomplishments in producing and quantifying chemical plumes in their flume). We are in the midst of conducting the experiments in the Stanford flume using model organisms flicking antennules in plumes. We

have scheduled a collaboration for August, 1999, with Paul Moore (Bowling Green University) to repeat these experiments with an IVEC probe mounted among the sensory hairs on the antennule to simultaneously measure plume structure and the temporal pattern of molecule arrival at a hair within the array.

Educational Accomplishments: I have an AASERT in conjunction with the parent grant #N000149610594. The AASERT provided stipend for a number of graduate students who learned research approaches and techniques required for their dissertation research by working as assistants on the olfaction project. Funds from the parent grant also provided equipment and software for the olfaction project that was also available for student use in other projects. Undergraduate students (majoring in biology, engineering, or physics) were hired using funds from the parent grant and AASERT to participate in research in my laboratory. So far, three of these students have gone on to Ph.D. programs and one to become a lab technician in this field, and several are continuing in my lab.

CONCLUSIONS: The basic design of many antennules used by marine animals to capture odor molecules from the surrounding water is that of a moveable rod supporting an array of chemosensory hairs. These antennules are periodically moved through the water with a rapid flick and slower return stroke. The sensory hairs of some species splay apart during the flick, but not the return. The hairs on antennules from a variety of species operate at Reynolds numbers (Re) of order one. In this Re range, changes in hair speed and spacing have a pronounced effect on whether or not fluid penetrates into the spaces between hairs; increasing fluid penetration raises the rate of molecule arrival at the surfaces of the sensory hairs. The designs and motions of these antennules enhance their ability to take pulsatile odor samples that are temporally and spatially discrete from each other. Such sampling is desirable for olfactory probes used for determining position in an odor plume.

In the turbulent water flow typical of shallow coastal habitats, odor plumes are characterized by complex swirls of narrow filaments of high concentration near the odor source, but wider filaments of lower concentration farther from the source. Near the source, these filaments are so narrow that there can be differences along the length of an antennule in the odor concentrations arriving at sensory hairs, thus the spatial pattern of concentrations along an olfactory probe could be used to assess distance from an odor source. Antennule flicking does not disrupt these filaments upstream of the antennule, but does downstream, thus flicking frequency of an olfactory probe can be tuned to ambient current speed so that the probe can sample ambient filaments (for odor-tracing devices) or can sample well-stirred water (to measure chemical concentrations in the environment).

SIGNIFICANCE: By determining how the flow microenvironments and odorant encounter of olfactory antennules is affected by their structure and behavior in realistic odor plumes, we are discovering ways in which the physical design of an antenna affects how it filters chemical information from the environment. These basic rules provide insights for the design of man-made chemical sensors and also reveal how other filamentous biological devices work that capture molecules or particles from the surrounding fluid (e.g. gills, filter-feeding appendages).

AWARD INFORMATION: Mimi Koehl (P.I.):
Phi Beta Kappa Visiting Scholar, 1998-1999

Distinguished Alumni Award, Gettysburg College, 1998
 President-elect, Western Society of Naturalists, 1999
 Featured in: Sherrer, B. & B.S. Sherrer [eds.] (1996) *Notable Women Scientists in the Life Sciences*. Greenwood Pub, Westport, CN.
 Koehl research on hydrodynamics of hair-bearing appendages featured in BBC science documentary "Suspension Feeding" (filming done 12/98)
 Honoric Lectures: Keynote Thursday Night Speaker, Gordon Conference on Theoretical Biology and Biomathematics, 1996
 Cruickshank Lecturer, University of Rhode Island, 1997
 Keynote Speaker, Engineering Found'n International Symposium, 1998
 Plenary Lecturer, Oceanographic Society & IOC Meeting, Paris, 1998
 Weise Lecturer, Dauphin Island Marine Laboratory, 1999
 Keynote Lecturer, Symposium in Nonlinear Biology, 1999
 Illg Memorial Lecturer, Friday Harbor Laboratories, 1999

Marlene Martinez (graduate student):

Outstanding Graduate Student Instructor Award, U.C. Berkeley, 1999

Michael McCay (graduate student):

Dwight Davis Award, Soc. Integrative & Comparative Biology, 1999

Outstanding Graduate Student Instructor Award, U.C. Berkeley, 1999

Matthew McHenry (graduate student):

Outstanding Student Paper Award, Hon. Men., West.Soc.Naturalists, 1997

Best Student Paper Award, Soc. Integrative & Comparative Biology, 1998

Kimberly Quillin (graduate student):

Best Student Paper Award, Soc. Integrative & Comparative Biology, 1998

Winnie Lau and Jeff Goldman (undergraduates in Koehl lab):

Graduated with Honors, U.C. Berkeley

PUBLICATIONS AND ABSTRACTS:

(Due to page limit, only abstracts published in journals are listed.)

Koehl Papers and Abstracts (parent grant):

1. Goldman, J.A. and M. A. R. Koehl. Fluid dynamic design of lobster olfactory organs: High-speed kinematic analysis of antennule flicking by *Panulirus argus*. *Chem. Senses*. (in press).
2. Koehl, M. A. R. (1996) Small-Scale fluid dynamics of olfactory antennae. *Mar. Fresh. Behav. Physiol.* 27: 127-141.
3. Koehl, M. A. R. (1996) When does morphology matter? *Ann. Rev. Ecol. Syst.* 27: 501-542.
4. Koehl, M. A. R. (1998) Small-scale hydrodynamics of feeding appendages of marine animals. *Oceanography* 11 : 12 -14.
5. Koehl, M. A. R. Consequences of Size Change. In *Scaling in Biology*. J.Brown & G. West [eds.], Oxford Univ. Press. (in press)
6. Koehl, M. A. R. (1998) Small-scale hydrodynamics of particle and odorant capture by animals. (abstract) *Oceanography* 11: 20.
7. Mead, K. S., M. A. R. Koehl, and M. J. O'Donnell. Stomatopod sniffing: The scaling of chemosensory sensillae and flicking behavior with body size. *J. Exp. Mar. Biol. Ecol.* (in press).
8. Mead, K. S. and M. A. R. Koehl. Particle image velocimetry measurements of fluid flow through a model array of stomatopod chemosensory sensillae. (in prep.)
9. Moore, P., B. Best, R. Schneider, L. Gorski & M. Koehl (1996) Olfactory sampling in lobsters: Chemical dynamics during flicking and recovery in Maine and spiny lobsters (abst.). *Chem. Senses* 21: 645.

10. Shimeta, Jeff and M. A. R. Koehl (1997) Mechanisms of particle selection by tentaculate suspension feeders during encounter, retention, and handling. *J. Exp. Mar. Biol. Ecol.* 209: 47-73.
11. Stacey, M., K. Mead, and M. Koehl. Effect of flicking on the rates of diffusion of molecules in odor filaments to the chemosensory aesthetascs on stomatopod olfactory antennules. (in prep.)

Student Papers and Abstracts (AASERT and parent grant):

(Due to page limit, no "in prep." papers are listed.)

12. Jed, J. E. Ontogenetic changes in size and shape affect swimming performance in the scyphozoan medusa *Aurelia aurita*. *Mar. Biol.* (submitted).
13. Jed, J. E. (1996) Ontogenetic size and shape changes affect the mechanisms of jetting in the scyphozoan jellyfish *Aurelia aurelia*. (abstract). *Am. Zool.* 35: 7A.
14. Lau, W. and M. Martinez (1996) Hydrodynamics of the crab *Pachygrapsus crassipes* at two different microhabitats: Protected estuary and wave-swept rocky shore (abstract). *Am. Zool.* 35: 28A.
15. Martinez, M., R. Full & M. Koehl (1998) Underwater punting by an intertidal crab: A novel gait revealed by the kinematics of pedestrian locomotion in air vs. water. *J. Exp. Biol.* 201: 2609-2623.
16. Martinez, M. M. Running the surf: Hydrodynamics of the shore crab *Grapsus tenuicrustatus*. *J. Exp. Biol.* (submitted)
17. Martinez, M. M. (1996) Locomotor performance of subtidal, intertidal, and semi-terrestrial crabs in air vs. water. (abstract) *Am. Zool.* 36: 8A.
18. Martinez, M. M. (1999) Mechanics of pedestrian locomotion in water versus in air: An example from shore crabs. Pd.D. Dissertation, University of California, Berkeley.
19. McCay, M. G. (1996) Aerodynamic stability and maneuverability of gliding frogs. (abstract). *Am. Zool.* 36: 8A.
20. McCay, M. G. (1997) Aerodynamic stability and manoeuvrability of gliding frogs. (abstract). *J. Morph.* 232: 294.
21. McCay, M. G. (1998) A comparison of the aerodynamic stability of three species of neotropical tree frogs: How does stability change with gliding ability? (abstract). *Am. Zool.* 38: 150A.
22. McHenry, M. J. (1997) Twitching, twisting, and twirling in tunicate tadpole toddlers: The kinematics of swimming maneuvers by ascidian larvae. (abstract) *Am. Zool.* 38: 194A.
23. McHenry, M. & E. Azizi (1998) Like fish and flagellates: The 3D kinematics of swimming ascidian larvae. (abst.) *Am. Zool.* 37: 451A.
24. Mead, K.S. (1998) Size, speed, and stink: How the boundary layer surrounding stomatopod chemosensory setae during olfactory flicking changes as the animals grow. (abstract). *Am. Zool.* 38: 82A
25. Quillin, K. J. (1998) Ontogenetic scaling of hydrostatic skeletons: Geometric, static, and dynamic stress scaling of the earthworm *Lumbricus terrestris*. *J. Exp. Biol.* 201: 1871-1883.
26. Quillin, K. J. (1996) Kinematic scaling of hydrostatic skeletons: Peristaltic crawling in earthworms. (abstract). *Am. Zool.* 35: 9A.
27. Quillin, K. J. (1997) Ontogenetic scaling of force production in hydrostatic skeletons. (abstract). *Am. Zool.* 37: 176A.
28. Quillin, K. J. (1999) The mechanical scaling of hydrostatic skeletons: Ontogeny of earthworms *Lumbricus terrestris*. Pd.D. Dissertation, University of California, Berkeley.

SMALL-SCALE FLUID DYNAMICS OF OLFACTORY ANTENNAE

M. A. R. KOEHL

*Department of Integrative Biology, University of California, Berkeley, CA 94720-3140
e-mail: cnidaria@violet.berkeley.edu*

(Received April 1 1995; in final form May 31 1995)

A critical step in the process of olfaction is the arrival at the surface of a chemosensory structure of chemical signals from the environment. Many organisms use appendages bearing arrays of microscopic hairs to pick up chemical signals from the surrounding water or air. In this study a general model of fluid flow between neighboring hairs in an array is used to explore the effects of hair size, spacing, and speed on flow near olfactory hairs. If an array of hairs is moved more rapidly: 1) the volume flow rate through it rises, causing higher molecule encounter rates even though a smaller proportion of the odorants passing through the array have time to diffuse to hair surfaces, and 2) velocity gradients along hair surfaces become steeper, causing greater sensitivity to changes in odorant concentration. The more closely-spaced the hairs, the less sensitive they are to these effects of changing speed.

KEY WORDS: olfaction, chemosensation, antenna, low Reynolds number, boundary layer, diffusion

INTRODUCTION

The first step during olfaction is the arrival at the surface of a chemosensory structure of chemical signals from the environment. A diversity of organisms, including many zooplankton, use appendages bearing arrays of microscopic hairs to pick up chemical signals from the surrounding water or air (e.g., Atema, 1987; Laverack, 1988). The fluid flow field in the immediate vicinity of a sensory hair determines the rates at which molecules are captured. However, analyses of how these animals extract information from odor plumes, and efforts to characterize the kinetics of their olfactory neurons, will be compromised until we know more about how antennal morphology and motion determine small-scale fluid flow near (and hence the arrival of odorant molecules at) receptors. By elucidating basic rules about how morphology affects flow through arrays of olfactory hairs, we can also provide useful guidelines for the design of man-made chemical sensors, and for the analysis of other important biological structures bearing arrays of hairs, such as locomotory, filter-feeding, and gas-exchange appendages.

Importance of Fluid Motion to Olfaction

A critical step in the process of olfaction is the arrival of chemical signals from the environment to the surface of a chemosensory structure. This involves 1) the convection of odorant in the fluid from the source to the region of the sensor, and 2) diffusion from the bulk fluid to the surface of the sensor (DeSimone, 1981).

Odor plumes in the environment: Turbulent fluid motion on the scale of meters to centimeters determines the patchy structure of odor plumes in the environment (e.g. Csanady, 1973; Okubo, 1980), hence chemical signals in the fluid downstream from an odor source fluctuate (Aylor, *et al.*, 1976; Miksad and Kittredge, 1979; Murlis and Jones, 1981; Elkinton and Cardé, 1984; Atema, 1985; 1987; 1988; Murlis, 1986; Moore and Atema, 1988; 1991; Zimmer-Faust, *et al.*, 1988; Moore, *et al.*, 1989; 1991b; 1992; Murlis, *et al.*, 1992). The behavior of various aquatic and terrestrial animals in odor plumes has been studied, and the ways in which organisms might use the information in odor plumes has received much attention (e.g. Bossert and Wilson, 1963; Hamner and Hamner, 1977; Reeder and Ache, 1980; David, *et al.*, 1982; Devine and Atema, 1982; Bursell, 1984; Cardé, 1984; McPhie and Atema, 1984; Atema, 1985; 1988; Baker, 1989; Brady, *et al.*, 1989; Moore, *et al.*, 1991b; Murlis, *et al.*, 1992; Willis, *et al.*, 1991; 1994; Willis and Baker, 1994; Basil and Atema, 1994). However, the ability of a sensor to sample changes in odorant concentration as it moves relative to a plume depends on small-scale fluid flow near the sensory hairs, which is still poorly understood.

Small-scale fluid flow in the vicinity of sensory hairs: The number of molecules (N) captured per unit time (t) by an array of sensory hairs is given by:

$$N/t = (V/t)CP \quad (1)$$

where V is the volume of fluid moving through the array, C is the number of molecules per volume in the fluid, and P is the proportion of the molecules in the fluid that are captured. Both V/t and P depend on the small-scale fluid flow in the vicinity of the hairs.

Reynolds number (Re) represents the relative importance of inertial to viscous forces for a particular flow situation:

$$Re = LU/\nu \quad (2)$$

where L is a linear dimension such as hair diameter, U is fluid velocity relative to the hair, and ν is fluid kinematic viscosity. The Re 's of olfactory hairs on a variety of crustaceans and insects are low: 10^{-4} to 10 (Loudon, *et al.*, 1994). Although inertial effects cannot be ignored at the upper end of this Re range, the viscous flow near sensory hairs is laminar (i.e. fluid motion is smooth and orderly, with no turbulent mixing between adjacent streamlines or random fluctuations in velocity; Happel and Brenner, 1965; Vogel, 1994).

When fluid flows past a solid surface, the fluid in contact with the surface does not slip and a velocity gradient (boundary layer) develops in the fluid between the surface and the freestream flow (Figure 1, A). At low Re 's, such boundary layers are thick relative to the dimensions of the object. There is no turbulent mixing in a laminar boundary layer, hence molecular diffusion is the mechanism that moves odorants across streamlines towards or away from the sensor's surface. The distance travelled by a diffusing molecule is proportional to time $^{1/2}$ (Berg, 1993), so molecules in a streamline 10 times farther from the surface of a sensor than another streamline will take 100 times longer to arrive at the sensor's surface by diffusion.

Olfactory antennae often bear arrays of sensory hairs. Fluid can flow through or around a group of hairs. The leakiness (defined in Figure 1, B) of an array of hairs determines the volume flow rate (V/t) of fluid through the array (Figure 1, C). A row of hairs with low leakiness does not process much fluid per time, but the reduction of fluid velocity between neighbouring hairs allows a longer time for molecules to diffuse onto the hairs, thereby increasing the proportion (P) of the molecules in the fluid that are

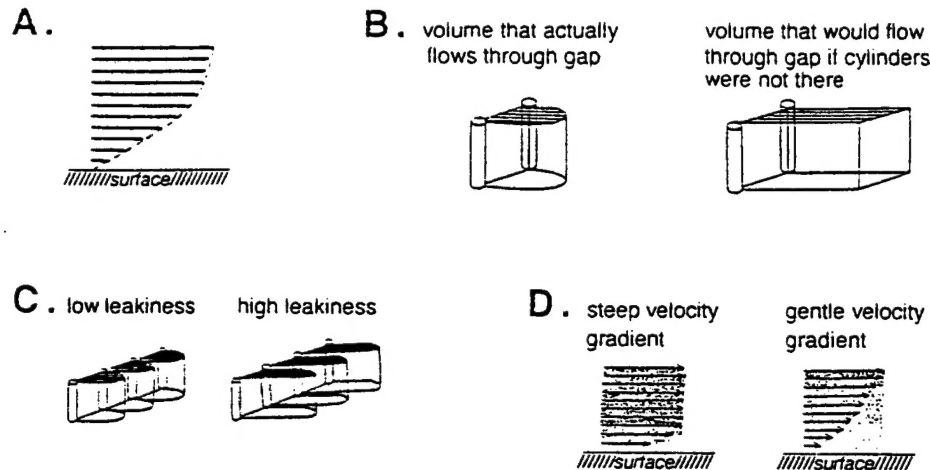


Figure 1 A. Diagram of a laminar boundary layer in the fluid moving with respect to a solid surface, such as the surface of a sensory hair. Arrows represent fluid velocity vectors at different heights above a point on the object. This represents the flow seen from the frame of reference of the object, and hence could represent flow past a stationary structure, or flow relative to an object moving through the fluid. B. "Leakiness" is defined as the ratio of the volume of fluid that actually moves between a pair of cylinders of unit length in a unit of time (shown on the left), to the volume of fluid that would move at freestream velocity (U_∞) through a gap of that width if the cylinders were not there to slow the flow (shown to the right). C. The flow rate (volume per time) of fluid moving through a leaky row of hairs (diagram on the right) is greater than through a less leaky row moving at the same velocity (diagram to the left). D. Diagram of a steep (left) and gentle (right) velocity gradient along a surface. The density of stippling in the fluid indicates the concentration of odorant molecules. In this example, a patch of light concentration odorant is being carried by in the ambient flow across the surface of a hair that had been in odorant-free fluid. The only way the molecules can reach the surface through these laminar velocity boundary layers is via molecular diffusion. Note that the surface with the gentle velocity boundary layer is "insulated" from this odor patch by a layer of slowly-moving "old" water.

caught (e.g. Fuchs, 1964; Davies, 1973; Pich, 1966; Rubenstein and Koehl, 1977; Murray, 1977; Shimeta and Jumars, 1991). However, although they are good at capturing a large percentage of the molecules in the fluid, hairs surrounded by thick boundary layers are insulated from rapid changes in the concentration of molecules in the ambient flow, as illustrated in Figure 1. D. These trade-offs illustrate the importance of understanding the factors that determine the small-scale flow around sensory hairs if we are to understand how antennae of different designs sample their fluid environments.

Importance of fluid transport of odorants to olfactory neurobiology: Although many efforts have been made to characterize the response characteristics (adaptation, flicker-fusion, dose-response, response threshold) of olfactory neurons of marine organisms such as crustaceans (e.g. Borroni and Atema, 1988; Voigt and Atema, 1990; Marscall and Ache, 1989; Moore, 1994), our lack of understanding of how small-scale flow affects arrival of odorant molecules makes these data difficult to interpret. Do the measurements reflect the properties of the nerves, or of the boundary layer around the sensor? Indeed, Moore, *et al.* (1991a) have lamented the lack of proper stimulus control in olfactory electrophysiological experiments.

While several authors have suggested that the time course of the initial phases of

neural responses to odorants might be determined by the transport of molecules to the receptor (Getchell and Getchell, 1977; DeSimone, 1981; Nachbar and Morton, 1981; Getchell, *et al.*, 1984; Moore, *et al.*, 1989; 1991b), others have argued that molecular diffusion may not be a limiting barrier to access to odor molecules (Boeckh, *et al.*, 1965; Futrelle, 1984; Mankin and Mayer, 1984). This issue has been addressed by a number of calculations of the diffusion of odor molecules to the surfaces of receptors (Adam and Delbrück, 1968; Berg and Purcell, 1977; Murray, 1977; DeSimone, 1981; Berg, 1983; Futrelle, 1984; Getchell, *et al.*, 1984; Kaissling, 1987). However, in spite of the importance of small-scale fluid flow to this process, information has been lacking about velocity profiles near hairs with neighbors. Therefore, various flow fields (such as flow around an isolated sphere or cylinder) have been assumed in these models that are not necessarily appropriate for antennae, hence applicability of model conclusions to various organisms is not yet clear.

Gleeson (1982) and Atema (1985) have pointed out that the morphology of the antennules of various decapod crustaceans with densely-packed hairs appears to inhibit flow and odor access, as corroborated by microelectrode measurements of reduced molecule fluxes within aesthetasc tufts on lobster lateral antennules, (Moore, *et al.*, 1989; 1991a), but not near smooth medial antennules. Antennal vibrating by insects (Schneider, 1964) and antennule flicking by crustaceans have been recognized as potential mechanisms of reducing boundary layer thickness, thereby increasing access of odors to receptor cells (e.g. Snow, 1973; Schmidt and Ache, 1979; Atema, 1985). Schmidt and Ache (1979) found that flicking enhanced the response of lobster olfactory receptors to changes in odor concentration, and Moore, *et al.* (1989; 1991a) found that pipette squirts to mimic flicking increased penetration of molecules into tufts of aesthetascs. Such periodic "sniffing" might provide a mechanism to get around the physical trade-off (mentioned above) between having a high P versus having a rapid response to a patch of odorant (i.e. "old" fluid can be "stripped off" olfactory hairs during a flick, yet fluid can be held between hairs when the antennule is not flicking, thereby allowing more of the molecules in that fluid the time to diffuse to receptors on the hairs' surfaces).

How Does the Morphology of an Array of Hairs Affect the Small-Scale Fluid Motion Through the Array?

We have used a combination of mathematical models (Cheer and Koehl, 1987a; 1987b) and dynamically-scaled physical models (Koehl, 1992; 1995; Loudon, *et al.*, 1994) to elucidate how the leakiness (Figure 1, B) of an array of hairs depends on factors such as hair diameter, spacing, length, speed relative to the fluid, and motion relative to nearby body surfaces. Such models enable us to vary one morphological or behavioral parameter at a time to ascertain the effects of each on performance. Since such controlled exploration of parameter space is not possible in comparative studies of different species, and since the small-scale flow around delicate, uncooperative, or very small organisms can be technically difficult to measure, models provide a useful complement to experiments with real organisms. Although the details of velocity profiles are difficult to measure around tiny hairs on living animals, the overall leakiness (which depends on those profiles) can sometimes be assessed to test the applicability of a model to the organism. The few measurements that have been made of the leakiness of arrays of hairs on arthropod appendages are consistent with the predictions of our mathematical and physical models (Koehl and Strickler 1981; Craig

and Chance, 1982; Vogel 1983; Cheer and Koehl 1987b; Koehl 1992, 1995). Our predictions match measured leakinesses very closely for hairs operating at Re 's of 10^{-1} and higher, and our physical models indicate that our under-estimation of the leakiness of copepod hairy appendages whose setae operate at lower Re 's (Koehl, 1992) is due to the interaction of those appendages with the body surface next to which they flap (Loudon, *et al.*, 1994).

The purpose of this study is to consider the general case of fluid flow between neighboring hairs to identify how hair size, speed, and spacing affect several aspects of fluid flow that are directly related to the performance of olfactory hairs: volume flow rate through an antenna, steepness of velocity gradient adjacent to a hair, and relative importance of fluid motion and molecular diffusion in getting odorant molecules to the surface of a sensory hair. Identifying such basic rules is a first step towards understanding the functional morphology of olfactory antennae, and may help us analyze the olfactory capabilities of planktonic animals whose sensors are technically difficult to study directly.

MATERIALS AND METHODS

I have employed velocity profiles calculated using the model of Cheer and Koehl (1987a) in order to estimate simple measures of various aspects of the performance of arrays of sensory hairs: leakiness and volume flow rate through the array, velocity profile steepness near the surface of an individual hair, and relative importance of fluid motion and of molecular diffusion in getting odorant molecules to the surface of a sensory hair. I have used these estimates of performance to explore the consequences of changing the behavior (velocity) or the morphology (inter-hair gap width) of rows of sensory hairs.

Model of Fluid Flow Between a Pair of Cylinders

Of the various methods that have been used to calculate the flow through arrays of hairs (reviewed in Koehl, 1995), the model of Cheer and Koehl (1987a) gives the best match to empirical data for biological antennae of finite width (Cheer and Koehl, 1987b). The details of this two-dimensional analytical model of fluid movement between a pair of circular cylinders at Re 's of 0.5 and lower are given in Cheer and Koehl (1987a). Fluid velocities far from the cylinders were calculated using Oseen's low- Re approximation of the Navier-Stokes equations (which includes inertial effects), velocities near the cylinders were calculated in bipolar coordinates using Stoke's low- Re approximation, and these two flow fields were put together using a matched asymptotic expansion technique. The fluid motion relative to the hairs (due either to motion of the antenna through the surrounding fluid, or to ambient wind or water currents past the antenna) was assumed to be normal to the plane of the row of hairs. The velocity vectors of the fluid moving between neighboring cylinders were used in all the calculations described below.

Leakiness

The "leakiness" of the gap between neighboring hairs was calculated as illustrated in Figure 1, B (Cheer and Koehl, 1987a).

Although such dimensionless indices as leakiness and Re are useful for seeing general patterns in the physical behavior of arrays of hairs, the performance consequences of changes in the morphology or motion of an array of hairs can be more easily illustrated by considering their effects on absolute flow rates and velocities for specific cases. Therefore, I have worked out the following examples for sensory hairs that are $1\text{ }\mu\text{m}$ in diameter.

Volume Flow Rate

An estimate of the volume (V) of fluid per time (t) moving through a unit area (A) normal to the flow direction of a filter or antenna composed of a row of hairs was calculated as:

$$V/(tA) = U_{\infty} Le g/(g + d), \quad (3)$$

where g is the width of the gap between neighboring hairs and d is the diameter of a hair. All calculations were done for a hair $1\text{ }\mu\text{m}$ in diameter.

Steepness of Velocity Gradient

The position closest to the surface of a hair for which velocity was calculated was $0.3\text{ }\mu\text{m}$ from the hair. The velocity of the fluid at that position ($U_{0.3\mu\text{m}}$) was used as an indicator of the steepness of the velocity gradient next to the hair. Calculations were done for hairs $1\text{ }\mu\text{m}$ and $0.1\text{ }\mu\text{m}$ in diameter.

Relative Importance of Fluid Flow and Diffusion in Molecule Encounter by a Hair

I used two simple indices to estimate the relative importance of fluid motion and of molecular diffusion in getting odorant molecules to the surface of a sensory hair in an array: Péclet number, and "diffusive spread" (both defined below).

Péclet number represents the importance of convection (i.e. fluid motion) relative to molecular diffusion for a particular mass transfer situation (Kaissling, 1987; Murray, 1977; Vogel, 1994). Péclet number ($Pé$) is given by

$$Pé = dU_{\infty}/D. \quad (4)$$

where d is hair diameter, U_{∞} is freestream fluid velocity relative to the hair, and D is the diffusion coefficient of the molecule of interest in the fluid. All calculations were done for a small molecule having a diffusion coefficient (D) of $10^{-9}\text{ m}^2/\text{s}$ in water at room temperature (Berg, 1993), and for hairs $1\text{ }\mu\text{m}$ in diameter. Péclet number plays a role in convective-diffusional mass transport processes somewhat comparable to the role of Re in inertial-viscous momentum transfer processes (Murray, 1977). Futrelle (1984) offered an intuitive description of $Pé$ saying it could be interpreted roughly as the ratio of the actual cross-sectional area of a hair to the effective cross-section of fluid from which a diffusing molecule has a "reasonable" chance of hitting the hair. The higher the Péclet number, the more important water flow is relative to molecular diffusion in getting molecules to the surface of the olfactory hair. However, because this rough measure does not take into account the effect of inter-hair gap width on velocity profiles along hair surfaces, I also utilized another rough estimate of the importance of diffusion relative to fluid flow in hair encounter by molecules, "diffusive spread".

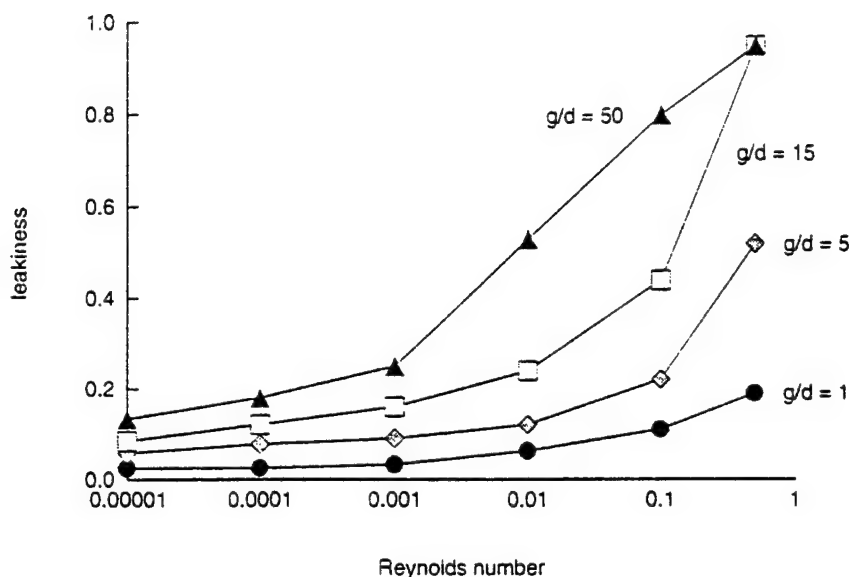


Figure 2 "Leakiness" (defined in Figure 1, B) plotted as a function of Reynolds number (log scale) for hairs at different distances apart. Each line represents a different gap (g = distance between neighboring hairs) to diameter (d = hair diameter) ratio.

As molecules in a patch diffuse via random thermal motion, their mean position does not change, but their spread about that mean increases with time. One measure of such diffusive spread of molecules along an axis is the root mean square displacement of those molecules at some time (r.m.s. displacement = $[2D t]^{1/2}$, where D is the diffusion coefficient and t is time); it represents the distance at which the chances are 32% that a molecule has wandered that far or farther (Berg, 1993). I calculated a rough estimate of how much diffusive spread there is away from a streamline during the time that a parcel of water in that streamline is "near" a hair. I focused on the streamline $0.3 \mu\text{m}$ from the hair's surface, and I estimated the time "near" a hair as the time (Δt) that it takes for a parcel of water in that streamline to travel the distance of the diameter (d) of the hair. I estimated "diffusive spread" (S) as the root mean square distance that molecules in that streamline could diffuse in Δt :

$$S = [2D d / U_{0.3\mu\text{m}}]^{1/2} \quad (5)$$

where $U_{0.3\mu\text{m}}$ is the velocity in the streamline at $0.3 \mu\text{m}$ from the surface of the hair. The greater this diffusive spread, the greater the likelihood that molecules arriving in a parcel of water in that streamline might diffuse to the surface of the hair. All calculations of S were done for hairs $1 \mu\text{m}$ in diameter and for small molecules having a diffusion coefficient (D) of $10^{-9} \text{ m}^2/\text{s}$ in water at room temperature.

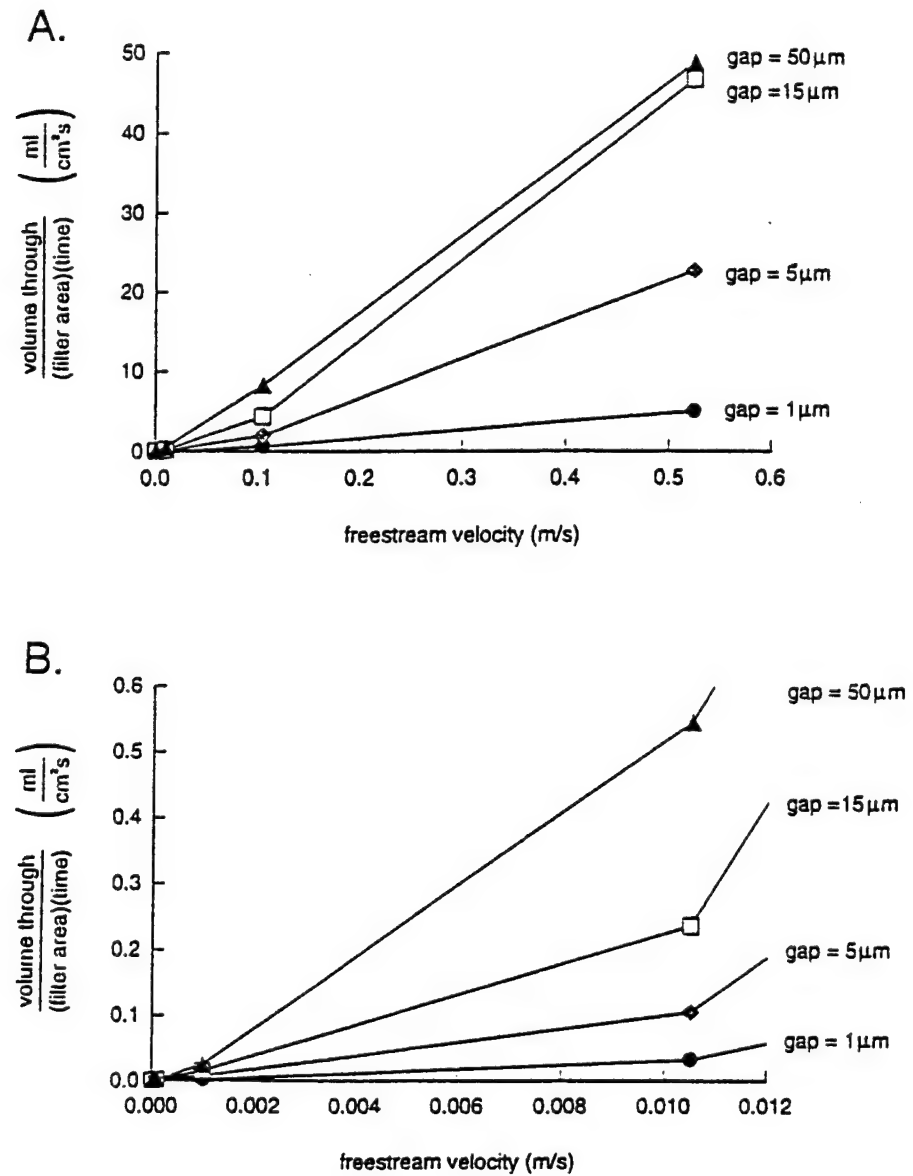


Figure 3 A. Volume (ml) of fluid per time (s) moving through a unit area (cm^2) of a filter or antenna composed of a row of hairs that are $1 \mu\text{m}$ in diameter, plotted as a function of freestream velocity (m/s: the velocity of the fluid in the environment relative to the antenna). Each line represents a different width of gap (μm) between neighboring hairs. B. Same as in A., but focusing on low freestream velocities.

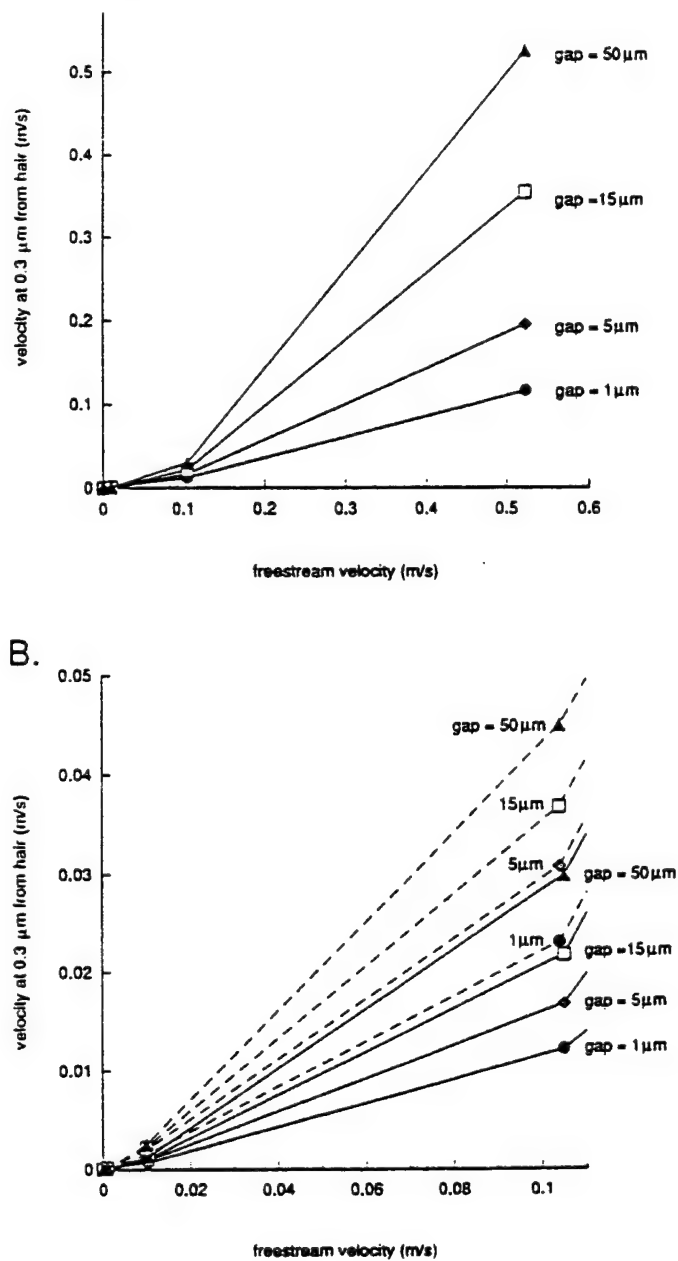


Figure 4 A. Velocity (m/s) in the fluid at a distance of 0.3 μm from the surface of a hair that is 1 μm in diameter, plotted as a function of freestream velocity (m/s). Each line represents a different width of gap (μm) between neighboring hairs. The higher the velocity at 0.3 μm from the hair, the steeper the velocity gradient along the surface of the hair. B. Same as in A, but focusing on low freestream velocities. Solid lines represent hairs that are 1 μm in diameter, and dashed lines represent hairs that are 0.1 μm in diameter.

RESULTS AND DISCUSSION

Effects of Morphology and Motion on Flow Between Hairs in an Array

The calculations described above reveal some general features about the design and deployment of appendages such as olfactory antennae composed of arrays of small hairs.

Leakiness: The leakiness of an array of hairs depends on Reynolds number (Re), as illustrated in Figure 2. At very low Re (10^{-3} and lower; i.e. for very small or slowly-moving sensory hairs) little fluid moves through the gap between neighboring hairs and the antenna behaves more like a paddle than like a sieve. In contrast, at higher Re 's (i.e. for larger or more rapidly-moving hairs), the array is leakier. At Re approaching 1, little fluid is dragged along with the hairs as they move and a hair-bearing antenna should be sieve-like. The Re of a sensory hair is modified if the hair changes in size (e.g. via growth of an individual, or through evolutionary change within a lineage) or if the fluid velocity relative to an antenna is altered (e.g. via swimming at a different speed, flicking the antenna, or moving to an area of different ambient current). Leakiness is changed little as Re is altered for hairs operating at very low Re 's, hence there is permission for variation in size or behavior without consequences to leakiness. In contrast, changing Re between 10^{-2} and 1 can lead to drastic changes in leakiness. Similarly, changes in the gap-to-diameter ratio (g/d) of a row of hairs has little effect on leakiness at very low Re , whereas moving hairs closer together can lead to drastic decreases in leakiness at higher Re 's. However, at Re 's approaching 1, hairs must be quite close together before gap width affects leakiness (for example, leakiness is the same for g/d 's of 15 and 50, but is much lower for a g/d of 5; Figure 2).

Volume flow rate: Obviously, the volume of fluid that can be processed per unit time by an antenna of a given area is increased if the velocity at which the sensory hairs are moved through the surrounding fluid is increased. The effect of velocity is more pronounced for arrays of hairs that have wide between-hair gaps (Figure 3). At high velocities, increasing the gap width increases the volume flow rate per area through the antenna if the hairs are very close together, but makes little difference if the hairs are farther apart (Figure 3, A). In contrast, at lower velocities, altering gap width alters volume flow rate per area through the antenna even for widely-spaced hairs (Figure 3, B).

Steepness of velocity gradient: As illustrated in Figure 1, D, the steeper the velocity gradient next to the surface of a sensory hair, the more quickly a change in ambient concentration of some odorant molecule will translate into a change in the rate of molecules arriving at the surface of the hair. Velocity gradients become disproportionately steeper as the velocity at which an antenna moves through the surrounding fluid is increased (Figure 4). The sensitivity of velocity gradient steepness to changes in antenna velocity is greater for arrays of hairs that are widely spaced than for those with narrow gap widths. Furthermore, for a given gap width and velocity, slim hairs have steeper velocity gradients along their surfaces than do wider hairs (Figure 4, B).

Relative importance of fluid flow and diffusion in molecule encounter by a hair: The slower the flow through an antenna, the greater the probability that an odorant molecule in the fluid moving through the antenna will have time to diffuse to the surface of an olfactory

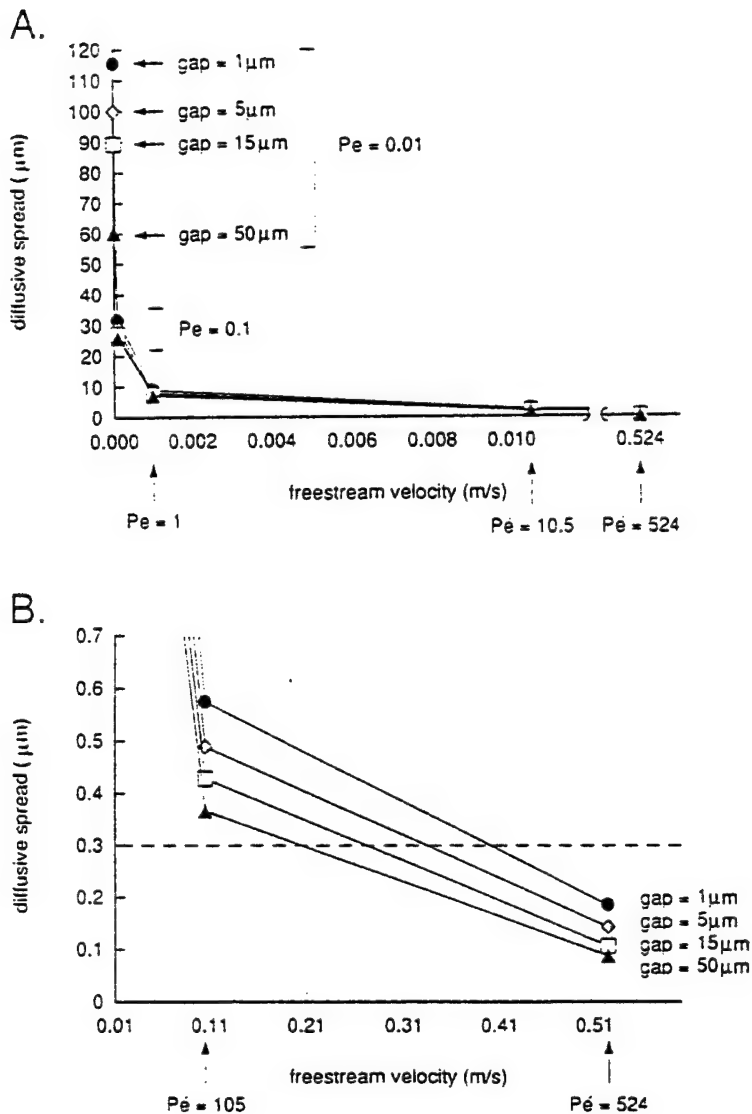


Figure 5 A. Diffusive spread (root-mean-square distance (μm)) that molecules in a streamline of water at a distance of $0.3\mu\text{m}$ from the surface of a hair could diffuse at right angles to that streamline in the time that it takes for a parcel of water in that streamline to travel the distance of the width of the hair ($1\mu\text{m}$)) plotted as a function of freestream velocity (m/s). The greater this r.m.s. distance, the greater the likelihood that molecules arriving in a parcel of water in that streamline might diffuse to the surface of the hair. Péclet numbers (Pe defined in the text) for the points plotted are indicated with arrows along the velocity axis or with brackets next to the points. All calculations were done for a small molecule having a diffusion coefficient (D) of $10^{-9}\text{ m}^2/\text{s}$ in water at room temperature. Each line represents a different width (μm) of gap between neighboring hairs. B. Same as in A, but focusing the higher freestream velocities. The dashed line indicates the distance of the streamline being considered from the surface of the hair.

hair. The Péclet numbers ($Pé$) shown along the velocity axis in Figure 5 represent the importance of fluid motion relative to molecular diffusion in getting molecules to the surfaces of hairs. Notice that the freestream velocity at which $Pé = 1$ for hairs $1\ \mu\text{m}$ in diameter is very low: $0.001\ \text{m/s}$. However, since flow through arrays of hairs can be slower than around isolated hairs at the same freestream velocity, the functional $Pé$'s of olfactory hairs may be lower than these estimates suggest, hence the freestream velocities at which $Pé = 1$ might be faster.

Diffusive spread (S , the root mean square distance that molecules might diffuse from a streamline during the time that a parcel of water in that streamline is "near" a hair) provides another index of the relative importance of diffusion in molecule capture by olfactory hairs. S is very low at freestream velocities above $0.001\ \text{m/s}$ (Figure 5, A), and at velocities of $0.01\ \text{m/s}$ only a small proportion of the molecules in the streamline $0.3\ \mu\text{m}$ from the hair should have time to diffuse to a hair (Figure 5, B). At very low freestream velocities (low $Pé$'s), narrower gaps between hairs lead to greater S , but at higher $Pé$'s, gap width has little effect on S .

These estimates of $Pé$ and S suggest that if hairy antennae are held still or moved very slowly, they will be good at harvesting via diffusion the molecules in the fluid trapped between the hairs, whereas if they are moved at velocities higher than about $1\ \text{mm/s}$, many of the molecules in the fluid processed by the antenna will "escape". Nonetheless, a greater number of molecules per time can be encountered by an array of hairs exposed to more rapid flow (e.g. Shimeta, 1993), and hence to a greater V/t (see equation 1). Therefore, if a zooplankter swims, produces a scanning current past its body (e.g. Koehl and Strickler, 1981), or flicks its antennae, it can increase its molecule encounter rate. Furthermore, the faster a zooplankter can move fluid relative to its olfactory hairs, the steeper the concentration gradient between "old" water along the hair's surfaces and "new" water containing a different concentration of odorant molecules, and hence the more sensitive to changes in odorant concentration such an antenna might be.

Thus, the first step in "filtering" olfactory signals from the environment can be due to the physical effects on molecule encounter rates caused by the fluid-moving behavior of the animal and by the morphology of its arrays of olfactory hairs, rather than by neural processing.

General Importance of Flow Through Arrays of Hairs

Many organisms from different phyla use appendages bearing arrays of hairs to perform a variety of important biological functions in addition to olfaction, including other mass exchange processes such as suspension-feeding and gas exchange, and momentum-exchange functions such as mechanoreception, swimming, or flying (e.g. Koehl 1992; 1995). Therefore, which morphological and behavioral factors determine the fluid motion through an array of cylinders is an issue of basic biological importance. One general conclusion of our modeling is that such hairy appendages are leaky sieve-like structures if their hairs operate at Re 's of 10^{-1} and higher, but are functionally more paddle-like (i.e. little of the fluid that they encounter flows through them) if their hairs operate at $Re \leq 10^{-2}$.

The conclusions of the general analysis presented here can be used to consider other molecule-capturing functions in addition to olfaction, such as gas exchange or capture of nutrient molecules. The rate of molecule encounter by a hair-bearing gill, feeding appendage, or antenna is enhanced if volume flow rate through such a structure is increased, even though the proportion of molecules encountered in each parcel of

water processed is reduced. Hairs that remove certain molecules from the fluid (such as those on gills or feeding appendages) can deplete the fluid near their surfaces of those molecules: the steeper the velocity gradient near the surface of a hair, the steeper the concentration gradient between the undepleted fluid and the hair, and hence the greater the rate of molecule encounter by the hair due to diffusion (e.g. Vogel, 1994; Shimeta and Jumars, 1991). Although olfactory antennae probably do not cause such local depletion of odorants, steeper velocity gradients can lead to increased sensitivity to changes in ambient odorant concentration, as discussed above. This study has shown that increases in freestream velocity increase both V/t and steepness of the velocity gradient near a hair, but that arrays of hairs with narrow gap widths are less sensitive to changes in freestream velocity than are those with more widely-spaced hairs. Furthermore, changes in gap width have bigger effects on diffusive spreading at low freestream velocities than they do in faster flow. In general, for all such hair-bearing appendages, the performance consequences of changes in behavior or morphology depend on the Reynolds number at which their hairs operate.

Acknowledgements

This research was supported by Office of Naval Research Grant #00014-90-J-1357 and by a John D. and Catherine T. MacArthur Foundation Fellowship Award. I am grateful to A. Cheer for calculating the velocity profiles from which the present analysis grew, to J. Jed for technical assistance, to C. Loudon for helpful comments on the manuscript, and to B. Ache, J. Atema, B. Best, C. Loudon, P. Moore, and J. Shimeta for useful discussions that helped shape my thinking about this problem.

References

- Adam, G. and Delbrück, M. (1968) Reduction in dimensionality in biological diffusion processes. In: *Structural Chemistry and Molecular Biology*: A. Rich and N. Davidson, eds., W. H. Freeman and Co., San Francisco, pp. 198–215.
- Atema, J. (1985) Chemoreception in the sea: Adaptations of chemoreceptors and behavior to aquatic stimulus conditions. *Soc. Exp. Biol. Symp.*, 39, 3887–3423.
- Atema, J. (1987) Aquatic and terrestrial chemoreceptor organs: Morphological and physiological designs for interfacing with chemical stimuli. In: *Terrestrial Versus Aquatic Life: Contrasts in Design and Function*, P. Dejours, ed., Liviana Press, pp. 303–316.
- Atema, J. (1988) Distribution of chemical stimuli. In: *Sensory Biology of Aquatic Animals*, J. Atema, R. R. Fay, A. N. Popper and W. N. Tavolga, eds., Springer-Verlag, New York, pp. 29–56.
- Aylor, D., Parlange, J.-Y. and Granett, J. (1976) Turbulent dispersion of dispersal in the forest and male gypsy moth response. *Env. Entomol.* 10, 211–218.
- Baker, T. C. (1989) Pheromones and flight behavior. In: *Insect Flight*, G. J. Goldsworthy and C. H. Wheeler, eds., CRC Press, Boca Raton, pp. 232–255.
- Basil, J. and Atema, J. (1994) Lobster orientation in turbulent odor plumes: simultaneous measurement of tracking behavior and temporal odor patterns. *Biol. Bull.*, 187, 272–273.
- Berg, H. C. (1993) *Random Walks in Biology*: Princeton University Press, Princeton, NJ.
- Berg, H. C. and Purcell, E. M. (1977) Physics of chemoreception. *Biophys. J.*, 20, 193–217.
- Boeckh, J., Kaissling, K. E. and Schneider, D. (1965) Insect olfactory receptors. *Cold Spring Harbor Symp. Quant. Biol.*, 30, 263–280.
- Borroni, P. F. and Atema, J. (1988) Adaptation in chemoreceptor cells I. Self-adapting backgrounds determine threshold and cause parallel shift of response function. *J. Comp. Physiol. A.*, 164, 67–74.
- Bossert, W. H. and Wilson, E. O. (1963) The analysis of olfactory communication among animals. *J. Theor. Biol.*, 5, 443–469.
- Brady, J., Gabriella, G. and Packer, M. J. (1989) Odour movement, wind direction, and the problem of host-finding by tsetse flies. *Physiol. Entomol.*, 14, 369–380.

- Bursell, E. (1984) Observations on the orientation of tsetse flies (*Glossina pallidipes*) to wind-borne odours. *Physiol Entomol.*, 9, 133-137.
- Cardé, R. T. (1984) Chemo-orientation in flying insects. In: *Chemical Ecology of Insects*. W. J. Bell and R. T. Cardé, eds., Elsevier Press, Amsterdam, pp. 109-134.
- Cheer, A. Y. L. and Koehl, M. A. R. (1987a) Paddles and rakes: Fluid flow through bristled appendages of small organisms. *J. Theor. Biol.*, 129, 185-199.
- Cheer, A. Y. L. and Koehl, M. A. R. (1987b) Fluid flow through filtering appendages of insects. *I.M.A. J. Math. Appl. Med. Biol.*, 4, 185-199.
- Craig, D. A. and Chance, M. M. (1982) Filter feeding in larvae of Simuliidae (Diptera: Culicomorpha): Aspects of functional morphology and hydrodynamics. *Can. J. Zool.*, 60, 712-724.
- Csanady, G. T. (1973) *Turbulent Diffusion in the Environment*. D. Reidel Publ. Co., Boston.
- David, C. T., Kennedy, J. S., Ludlow, A. R., Perry, J. N. and Wall, C. (1982) A reappraisal of insect flight towards a distant point source of wind-borne odor. *J. Chem. Ecol.*, 8, 1207-1215.
- Davies, C. N. (1973) *Air Filtration*. Academic Press, New York.
- DeSimone, J. A. (1981) Physicochemical principles in taste and olfaction. In: *Biochemistry of Taste and Olfaction*. R. H. Cagan and M. R. Kare, eds. Academic Press, New York, pp. 213-229.
- Devine, D. and Atema, J. (1982) Function of chemoreceptor organs in spatial orientation of the lobster, *Homarus americanus*: differences and overlap. *Biol. Bull.*, 163, 144-153.
- Elkinton, J. S. and Cardé, R. T. (1984) Odor dispersion. In: *Chemical Ecology of Insects*. W. J. Bell and R. T. Cardé, eds., Elsevier Press, Amsterdam, pp. 73-91.
- Fuchs, N. A. (1964) *The Mechanics of Aerosols*. Oxford University Press, Oxford.
- Futrelle, R. P. (1984) How molecules get to their detectors: The physics of diffusion of insect pheromones. *Trends Neurosci.* April: 116-120.
- Getchell, T. V. and Getchell, M. L. (1977) Early events in vertebrate olfaction. *Chem. Senses*, 2, 313-326.
- Getchell, T. V., Margolis, F. L. and Getchell, M. L. (1984) Perireceptor and receptor events in vertebrate olfaction. *Prog. Neurobiol.*, 23, 317-345.
- Gleeson, R. A. (1982) Morphological and behavioral identification of the sensory structures mediating pheromone reception in the blue crab, *Callinectes sapidus*. *Biol. Bull.*, 163, 162-171.
- Hamner, P. and Hamner, W. M. (1977) Chemosensory tracking of scent trails by the planktonic shrimp *Acetes sibogae australis*. *Science*, 195, 886-888.
- Happel, J. and Brenner, H. (1965) *Low Reynolds Number Hydrodynamics with Special Applications to Particulate Media*. Prentice-Hall, Englewood Cliffs, NJ.
- Kaissling, K. -E. (1987) *R. H. Wright lectures on insect olfaction*. K. Colbrow, ed., Simon Fraser Univ., Burnaby.
- Koehl, M. A. R. (1992) Hairy little legs: Feeding, smelling, and swimming at low Reynolds number. *Contemp. Math.*, 141, 33-64.
- Koehl, M. A. R. (1995) Fluid flow through hair-bearing appendages: Feeding, smelling, and swimming at low and intermediate Reynolds numbers. In: *Biological Fluid Dynamics*. T. Pedley and C. Ellington, eds., *Symp. Soc. Exp. Biol.* (in press).
- Koehl, M. A. R. and Strickler, J. R. (1981) Copepod feeding currents: food capture at low Reynolds number. *Limnol. Oceanogr.*, 26, 1062-1073.
- Laverack, M. S. (1988) The diversity of chemoreceptors. In: *Sensory Biology of Aquatic Animals*, J. Atema, ed., Springer-Verlag, New York, pp. 287-317.
- Loudon, C., Best, B. A. and Koehl, M. A. R. (1994) When does motion relative to neighboring surfaces alter flow through an array of hairs? *J. Exp. Biol.*, 193, 233-254.
- McPhie, D. and Atema, J. (1984) Chemical communication in lobsters: Information currents. *Biol. Bull.*, 167, 510-511.
- Mankin, R. W. and Mayer, M. S. (1984) The insect antenna is not a molecular sieve. *Experientia*, 40, 1251-1252.
- Marscall, H. -P. and Ache, B. W. (1989) Response dynamics of lobster olfactory neurons during simulated natural sampling. *Chem. Senses*, 14, 725.
- Miksad, R. W. and Kittredge, J. (1979) Pheromone aerial dispersion: A filament model. *14th Conf. Agric. For. Meteorol. Am. Meteorol. Soc.*, 1, 238-243.
- Moore, P. A. (1994) A model for adaptation and disadaptation in olfactory receptor neurons: Implications for the coding of temporal and intensity patterns in odor signals. *Chem. Senses*, 19, 71-78.
- Moore, P. A. and Atema, J. (1988) A model of a temporal filter in chemoreception to extract directional information from a turbulent odor plume. *Biol. Bull.*, 174, 355-363.
- Moore, P. A. and Atema, J. (1991) Spatial information in the three-dimensional fine structure of an aquatic odor plume. *Biol. Bull.*, 181, 408-418.
- Moore, P. A., Atema, J. and Gerhardt, G. A. (1991a) Fluid dynamics and microscale chemical movement in the chemosensory appendages of the lobster, *Homarus americanus*. *Chemical Senses*, 16, 663-674.

- Moore, P. A., Gerhardt, G. A. and Atema, J. (1989) High resolution spatio-temporal analysis of aquatic chemical signals using microchemical electrodes. *Chemical Senses*, 14, 829-840.
- Moore, P. A., Scholz, N. and Atema, J. (1991b) Chemical orientation of lobsters, *Homarus americanus*, in turbulent odor plumes. *J. Chem. Ecol.*, 17, 1293-1306.
- Moore, P. A., Zimmer-Faust, R. K., Weissburg, M. J., Parrish, J. M. and Gerhardt, A. (1992) Measurements of microscale patchiness in a turbulent aquatic odor plume using a semiconductor-based microprobe. *Biol. Bull.*, 183, 138-142.
- Murlis, J. (1986) The structure of odour plumes. In: *Mechanisms of Insect Olfaction*. T. L. Payne, ed., Clarendon Press, NJ, pp. 27-38.
- Murlis, J., Elkinton, J. S. and Cardé, R. T. (1992) Odor plumes and how insects use them. *Ann. Rev. Entomol.*, 37, 505-532.
- Murlis, J. and Jones, C. D. (1981) Fine-scale structure of odour plumes in relation to insect orientation to distant pheromone and other attractant sources. *Physiol. Entomol.*, 6, 71-86.
- Murray, J. D. (1977) Reduction of dimensionality in diffusion processes: Antenna receptors of moths. In: *Lectures on Nonlinear-Differential-Equation Models in Biology*. Oxford University Press, Oxford, pp. 83-127.
- Nachbar, R. B. and Morton, T. H. (1981) A gas chromatograph (GLC) model for the sense of smell: Variations of olfactory sensitivity with conditions of stimulation. *J. Theor. Biol.*, 84, 387-407.
- Okubo, A. (1980) *Diffusion and Ecological Problems: Mathematical Models*. Springer-Verlag, New York.
- Pich, J. (1966) Theory of aerosol filtration by fibrous and membrane filters. In: *Aerosol Science*. C. N. Davies, ed., Academic Press, New York, pp. 223-285.
- Reeder, P. B. and Ache, B. W. (1980) Chemotaxis in the Florida spiny lobster, *Panulirus argus*. *Anim. Behav.*, 28, 831-839.
- Rubenstein, D. I. and Koehl, M. A. R. (1977) The mechanisms of filter feeding: Some theoretical considerations. *Amer. Natur.*, 26, 981-994.
- Schmidt, B. C. and Ache, B. W. (1979) Olfaction: Responses of a decapod crustacean are enhanced by flicking. *Science*, 205, 204-206.
- Schneider, D. (1964) Insect antennae. *Ann. Rev. Entomol.*, 9, 103-122.
- Shimeta, J. (1993) Diffusional encounter of submicrometer particles and small cells by suspension feeders. *Limnol. Oceanogr.*, 38, 456-465.
- Shimeta, J. and P. A. Jumars. (1991) Physical mechanisms and rates of particle capture by suspension-feeders. *Oceanogr. Mar. Biol. Annu. Rev.*, 29, 191-257.
- Snow, P. J. (1973) The antennular activities of the hermit crab, *Pagurus alaskensis* (Benedict). *J. Exp. Biol.*, 58, 745-765.
- Vogel, S. (1983) How much air passes through a silkworm's antenna? *J. Insect Physiol.*, 29, 597-602.
- Vogel, S. (1994) *Life in Moving Fluids: The Physical Biology of Flow*, 2nd Edition. Princeton University Press, Princeton.
- Voigt, R. and Atema, J. (1990) Adaptation in chemoreceptor cells. III. Effects of cumulative adaptation. *J. Comp. Physiol. A.*, 166, 865-874.
- Willis, M. A. and Baker, T. C. (1994) Behaviour of flying oriental fruit moth males during approach to sex pheromone sources. *Physiol. Entomol.*, 19, 61-69.
- Willis, M. A., David, C. T., Murlis, J. and Cardé, R. T. (1994) Effects of pheromone plume structure and visual stimuli on the pheromone-modulated upwind flight of male gypsy moths (*Lymantria dispar*) in a forest (Lepidoptera: Lymantriidae). *J. Insect Behav.*, 7, 385-409.
- Willis, M. A., Murlis, J. and Cardé, R. T. (1991) Pheromone-mediated upwind flight of male gypsy moths, *Lymantria dispar*, in a forest. *Physiol. Entomol.*, 16, 507-521.
- Zimmer-Faust, R. K., Stanfill, J. M. and Collard, S. B. III (1988) A fast multi-channel fluorometer for investigating aquatic chemoreception and odor trails. *Limnol. Oceanogr.*, 33, 1586-1595.

FLUID DYNAMIC DESIGN OF LOBSTER OLFACTORY ORGANS:
HIGH-SPEED KINEMATIC ANALYSIS OF ANTENNULE FLICKING
BY *PANULIRUS ARGUS*

J. A. Goldman* and M. A. R. Koehl

Department of Integrative Biology

University of California

Berkeley, CA 94720-3140

* present address: Department of Zoology, Duke University, Durham, NC 27708-0325

KEY WORDS: aesthetasc, antennule, olfaction, lobster, Reynolds number

*Correspondence should be sent to: J. Goldman, Department of Zoology, Duke University,
Durham, NC 27708-0325, USA; FAX: (919) 684-6168; telephone: (919) 684-3592*

ABSTRACT

Many organisms use olfactory appendages bearing arrays of microscopic hairs to pick up chemical signals from the surrounding water or air. We report a morphometric and high-speed kinematic analysis of the olfactory organs (lateral flagella of the antennules, which bear chemosensory aesthetasc hairs) of the spiny lobster, *Panulirus argus*. *P. argus* sample specific locations by executing a rapid series of antennule flicks at one position, moving the antennule to a different spot, and then performing another series of flicks. Fluid motion around a hair depends on its Reynolds number (Re), which is proportional to both the diameter and speed of the hair. During a series of flicks, an antennule moves down rapidly (aesthetasc Re = 2) and up more slowly (Re = 0.5), pausing briefly (~0.16 s) before the next downstroke; antennule repositioning between series of flicks occurs on average at aesthetasc Re's = 0.8. Mathematical and physical modeling of fluid flow through arrays of closely-spaced cylinders reveals a transition between Re's $< 10^{-1}$, where arrays resist fluid penetration between hairs, and Re's > 1 , where they are quite leaky to fluid flow. Therefore, when antennules flick, "old" water is flushed out of the aesthetasc array during the leaky downstroke and is not picked up again during the less-leaky upstroke. For such a velocity asymmetry to result in a leakiness asymmetry, the hairs must operate in this critical Re range. That *P. argus* maintain this aesthetasc Re range as they grow provides further evidence of the importance of Re to antennule function. Our results suggest pulsatile sampling of parcels of water from a specific location when an antennule executes a series of flicks in one spot, and more-or-less continuous convective transport of odorants to the aesthetascs when an antennule sweeps to a new position between a series of flicks.

("sensing" on arthropods)

INTRODUCTION

A critical step in the process of olfaction is the arrival of chemical signals from the environment to the surface of a chemosensory structure. From a hydrodynamic standpoint, this process can be broken up into two regimes based on scale: (1) large-scale turbulent water flow transports the odorant plume from the source to the immediate vicinity of the sensor ; and (2) small-scale viscous flow and molecular diffusion govern the transport of the odorant to the surface of the sensor (e.g. DeSimone, 1981; Koehl, 1996). The first step in filtering the spatial and temporal information contained in odor plumes (e.g. Murlis, 1986; Weissburg and Zimmer-Faust, 1994; Willis, *et al.*, 1994; Atema, 1995) depends on the physical manner in which an olfactory structure affects fluid flow across its surfaces (e.g. Moore, *et al.*, 1989; Atema, 1995; Koehl, 1996).

Fluid Flow Around Arrays of Sensory Hairs at Low Reynolds Number

Many organisms use appendages bearing arrays of microscopic hairs to pick up chemical signals from the surrounding water or air. When a fluid moves past the surface of a structure, such as a sensory hair, the layer of fluid in contact with the surface does not slip relative to it, hence a velocity gradient develops in the fluid between the structure and the mainstream flow. The thickness of this velocity gradient depends on the Reynolds number (Re), which represents the relative importance of inertial to viscous forces for a particular flow:

$$Re = L \cdot U \cdot \rho / \mu,$$

where L is a linear dimension such as hair diameter, U is fluid velocity relative to the hair, and ρ and μ are fluid density and viscosity, respectively. The Re's of olfactory hairs on a variety of arthropods are low: 10^{-4} to 10 (Loudon, *et al.*, 1994). Although inertial effects cannot be ignored at the upper end of this Re range, the viscous flow near sensory hairs is laminar (i.e. fluid motion is smooth and orderly, with no random fluctuations in velocity; Happel and Brenner, 1965; Vogel, 1994). At these low Re's, laminar velocity gradients are thick relative to the dimensions of a hair (e.g. Cheer and Koehl, 1987). Since there is no turbulent mixing in a laminar

velocity gradient, molecular diffusion alone moves odorants across streamlines towards or away from the sensor's surface.

Theoretical analyses (Cheer and Koehl, 1987; 1988; Koehl, 1996) and model experiments (Koehl, 1992; 1996; Loudon, *et al.*, 1994) have elucidated how the steepness of velocity gradients adjacent to hairs and the leakiness of the array to fluid movement between neighboring hairs depends on hair speed, diameter, spacing, length, and motion relative to nearby body surfaces. Mathematical and physical modeling has shown a transition in the fluid dynamic performance of arrays of closely-spaced hairs at Re 's between 10^{-1} and 1: at low Re 's fluid flows around rather than through arrays of hairs, whereas at Re 's of 1 and higher, fluid readily moves between neighboring hairs, and hair-bearing appendages are quite leaky ("leakiness", defined in Cheer and Koehl, 1987, is a measure of the proportion of the fluid encountered by an array of hairs that flows through it rather than around it). Behaviors that can alter the leakiness of an array of hairs also changes across this Re range: moving more rapidly increases leakiness at Re 's of 10^{-1} to 1, whereas moving an appendage closer to a wall (such as the body surface) increases leakiness at lower Re 's. Therefore, determining how an olfactory appendage functions depends on knowing the Re at which its hairs operate.

A row of hairs with low leakiness does not process fluid rapidly, but low fluid velocity between neighboring hairs allows a long time for molecules to diffuse onto the hairs, and thus a large proportion of the molecules in the fluid may be caught (e.g. Murray, 1977; Rubenstein and Koehl, 1977; Shimeta and Jumars, 1991). However, a theoretical analysis by Koehl (1996) indicates that if an array of hairs is moved more rapidly: (1) the volume flow rate through it rises, increasing molecule encounter rates even though a smaller proportion of the odorants passing through the array have time to diffuse to hair surfaces, and (2) velocity gradients along hair surfaces become steeper, increasing sensitivity to changes in odorant concentration.

Although the few measurements that have been made of the leakiness of arrays of hairs on arthropod appendages are consistent with the predictions of our models (Koehl and Strickler, 1981; Vogel, 1983; Cheer and Koehl, 1988; Koehl, 1996), how the structure of and flow speed

past hair-bearing olfactory appendages affect molecule capture needs to be tested for diverse animal antennae. The first step in any such analysis is to quantify the morphology of the antenna and the water or air motion relative to it and, in particular, to determine the Re range in which the appendage operates. Therefore, the present study measures the morphology and kinematics of the olfactory antennules of the Florida spiny lobster, *Panulirus argus*, and determines the Re of its sensory hairs.

Antennule Flicking by Lobsters

The lateral branches (flagella) of the antennules of decapod crustaceans bear tufts of hairs in a great variety of arrangements (Laverack, 1988), and the aesthetasc hairs they bear serve an olfactory function (evidence reviewed by e.g. Atema, 1977; 1995; Gleeson, 1982; Grunert and Ache, 1988; Hallberg, *et al.*, 1992; Atema and Voigt, 1995). Decapod lateral antennules have been used as model systems for studying the electrophysiology of olfactory neurons (reviewed by e.g. Ache, 1982; 1988; Atema, 1985; Atema and Voigt, 1995); among the most extensively studied model species has been the lobster *P. argus* (e.g. Fuzessery, *et al.*, 1978; Schmidt and Ache, 1979; Bayer, *et al.*, 1980; Anderson and Ache, 1985; Marscall and Ache, 1989; Michel, *et al.*, 1991). The distal portion of the lateral branch of an antennule of *P. argus* bears rows of aesthetascs flanked by larger guard hairs (Grunert and Ache, 1988; Gleeson, *et al.*, 1993) (Figure 1). Ultrastructural studies (Grunert and Ache, 1988) showed that each *P. argus* aesthetasc contains several hundred chemoreceptor cells.

A variety of crustaceans flick their olfactory antennules. Schmidt and Ache (1979), Gleeson (1982), and Atema (1985) suggested that densely-packed hairs on the antennules of various crustaceans inhibit flow and odor access. This suggestion was corroborated by Moore, *et al.*'s (1989; 1991) microelectrode measurements of reduced molecule fluxes within aesthetasc tufts on the lateral flagella of the antennules of the clawed lobster, *Homarus americanus*, but not near their smooth medial flagella. Antennule flicking has been described as a mechanism of reducing velocity gradient thickness, thereby increasing access of odors to receptor cells (e.g. Schmidt and Ache, 1979; Atema, 1985), and synchronizing the arrival of signals along the

antennule (Gleeson, *et al.*, 1993). Several lines of evidence are consistent with this idea. Flow pulses onto the aesthetascs of antennule preparations (meant to mimic flicking) increased penetration of ^{tracer} molecules into aesthetasc tufts of *H. americanus* (Moore, *et al.*, 1989; 1991) and enhanced the response of *P. argus* olfactory receptor neurons to changes in odor concentration (Schmidt and Ache, 1979). ^{and of dye into aesthetasc cymys in *P. argus* (R. Gleeson '93)}

Although such experiments with antennule preparations reveal the importance of water motion to antennule reception of chemical signals, they cannot provide quantitative information about the effects of antennule flicking on the filtering of odorant signals unless they mimic the water flow relative to the aesthetascs during the course of a flick. Although video records of *P. argus* flicking have been made (Gleeson, *et al.*, 1993), the framing-rate of standard video is not fast enough to capture the details of this rapid motion. Therefore, the present study uses high-speed video analysis to quantify the kinematics of lateral antennule flicking by *P. argus*, providing the data necessary so future neurobiological experiments using antennule preparations can be designed to have biologically-relevant odorant delivery.

In addition, we provide values for the morphometric and kinematic parameters necessary to develop mathematical and physical models of *P. argus* antennules, and assess how these values vary across a range of body sizes. Such models permit measuring the details (which are unmeasurable on real flicking antennules) of the velocity gradients around and through arrays of aesthetascs. Such models also enable us to manipulate the design of the antennules (in ways not possible in experiments with living lobsters) to assess how morphological and kinematic parameters influence antennule performance. Although some morphological information for *P. argus* is available in the literature (Grunert and Ache, 1988; Gleeson, *et al.*, 1993), a number of fluid-dynamically-important parameters required for model development have not yet been measured

MATERIALS AND METHODS

Animals

Panulirus argus from Florida were kept in a 246 liter aquarium filled with artificial sea water ("Instant Ocean") at 25°C. Each lobster was fed one dead raw shrimp (approximately 50 to 150 g) every other day.

Kinematics

The kinematics of flicks by the lateral flagella of the antennules of *P. argus* were measured from high-speed video records made at 250 frames per second using a Kodak Ektapro TR High-Speed Video System with an intensified imager. Lobsters were placed in an aquarium (0.20 x 0.32 x 0.20 m) in artificial sea water at 25°C. We began videotaping when lobsters stood still with the lateral flagellum of one antennule flicking in a plane parallel to the camera lens. We analyzed the downstroke and upstroke of the first 15 flicks after taping began.

We analyzed the kinematics of antennule flicking using a Peak Performance Motion Analysis System (Peak Performance Technologies, version 5.0). We digitized the tip of the lateral flagellum of an antennule and the mid-point of the region of the flagellum bearing the tuft of aesthetascs at 0.04 s intervals to calculate their velocities. When the same video sequences were digitized on three separate days, the measurements of velocity were repeatable to the nearest 0.01 m/s. The lateral flagella of the antennules were flexible and bent as they were moved; thus, the angle of attack of a flagellum (the angle between the long axis of the antennule flagellum at some position along its length and the velocity vector of water motion relative to the flagellum) varied during a flick. Therefore, the angle of attack of the lateral flagellum of an antennule at the midpoint of its tuft of hairs was calculated as the angle between the instantaneous trajectory of that position on the flagellum and its instantaneous long axis.

Temporal and Spatial Pattern of Flicking

Video records of lobsters in the large aquarium were made using a Sony Hi-8 CCD-TR101 camcorder. No shrimp had been added to the aquarium for at least 24 hours prior to the videotaping, and about 30% of the water in the aquarium had been replaced by new artificial sea

parallel to the camera lens with the lateral hairs uppermost. The following parameters were digitized (as described above) using tracings on transparencies of video images of the three distal segments of the specimen: angles of the rows formed by the aesthetasc tips (o, p, q), width of the aesthetasc row at the tips (l), distances between the tips of the lateral-most aesthetascs in neighboring rows (n), distances between the tips of the ventral-most aesthetascs in neighboring rows (m), and angles of the aesthetascs to the stalk of the flagellum of the antennule (r, s, t, u) (Figure 1).

Repeated measurements of the same features were made on three separate days for both the SEM micrographs and the light microscope video images. We found that the measurements of angles were repeatable to the nearest 1° , and that the measurements of linear dimensions had two significant figures.

During a flick, the direction of water flow relative to the antennule is parallel to, but in the opposite direction from, the motion of the antennule. We measured the angle of the tuft of hairs on an antennule with respect to the water flow past the antennule during a flick (v) (Figure 2) from video records of the tips of antennules. We clamped antennules that had been removed from lobsters such that the long axis of the lateral flagellum was perpendicular to the lens of a video camera (Sony Hi-8 CCD-TR101). The joint at the base of the lateral flagellum only permits the branch to move in one plane relative to the base, hence we could manually push on the proximal end of the lateral flagellum to simulate the orientation of a flick. We digitized the angle between the trajectory of the flick and the tuft of hairs on the flagellum to the nearest 1° , as described above.

Statistics

Student's t tests were done as described by Zar (1974), and all other statistical analyses were conducted using Systat software (version 5.04).

Fig. 2
→

RESULTS

Morphology

The basic morphology of the hair-bearing region of the lateral flagellum of the antennule of a *P. argus* is illustrated in Figure 1. We measured a zig-zag arrangement of the tips of the aesthetascs (Table I), as was reported by Grunert and Ache (1988) and Gleeson, *et al.* (1993). Like Gleeson, *et al.* (1993), we also observed that the aesthetascs did not point directly into the flow during the flick downstroke, but rather were at an acute angle ($\alpha = 32^\circ \pm 4^\circ$, $n = 3$) with respect to the flow on the downstroke, and at an obtuse angle (148°) with respect to the flow during the upstroke (Figure 2).

Our morphometric data for the lateral flagella of the antennules of *P. argus* are reported in Table I. None of the morphological parameters listed in Table I changed significantly with carapace length (linear regression: slopes not significantly different from zero, $p > 0.05$ in all cases), suggesting that aesthetasc size, spacing, and orientation did not change as the lobsters grew, and that the numbers of aesthetascs and guard hairs per segment were maintained across the range of body sizes we studied. Gleeson, *et al.* (1993) also found no significant differences in aesthetasc morphology between the three lobsters they measured (carapace lengths from 0.058 to 0.076 m). Although the ^{diameter}width of the guard hairs did not change significantly across the size range we studied, the spacing between guard hairs along the length of the antennule did increase significantly ^{as a function of carapace length} (Figure 3, A and B), as did the width of the lateral flagellum of the antennule (Figure 3, C). Guard hair spacing and antennule width appeared to scale geometrically (e.g. Alexander, 1972) across the size range of *P. argus* we studied (the slopes of linear regressions of log-log plots of antennule width and of guard hair spacing versus carapace length were not significantly different from one, Student's *t*, $p > 0.05$ in all cases).

Kinematics of a Flick

The time course of the downward flick and the following upstroke are shown in Figure 4. Lobsters occasionally flicked downwards several times without intervening upstrokes; in these cases one long upstroke usually followed the series of downward flicks. During the more typical

single flicks, the downstroke generally lasted 0.15 to 0.20 s, while the upstroke was more variable in duration (0.20 to 0.90 s). The speed of the downstroke was much faster than that of the upstroke (Table II). While Gleeson, *et al.* (1993) estimated antennule velocity (by dividing excursion distance by flick duration) to be 0.077 m/s, our high-speed video analysis permitted us to resolve that downstroke velocities peaked at 0.09 m/s while upstroke velocities were only 0.02 m/s. Antennule bending and whiplashing during the flick caused the mid-point of the hair-bearing region of the lateral flagellum to slow before the flagellum tip at the end of the downstroke (Figure 4, A and C). The lateral flagella of the antennules bent as they moved through the water such that their instantaneous angles of attack varied with time (Figure 4, B - D). Nonetheless, the mean angle of attack during both the downstroke and the upstroke was 90°, and the angle of attack at the time of maximum velocity during the downstroke was 90° (Table II).

The speeds (Figure 5, A) and angles of attack (Figure 5, B) of flick downstrokes and upstrokes did not vary significantly with carapace length across the size range of animals we studied (linear regression, $p > 0.05$ in all cases).

Reynolds Numbers of Aesthetascs During Flicking

The Reynolds numbers ($Re = L U \rho / \mu$) of the aesthetascs during the flick downstrokes and upstrokes were calculated for each lobster (where L = aesthetasc diameter measured of each animal, U = mean speed of the midpoint of the hair tuft on the antennule measured for each animal, ρ = density of sea water at 25°C = 1023 kg/m³ (Zerbe & Taylor, 1953), and μ = viscosity of sea water at 25°C = 9.6 x 10⁻⁴ Pa·s (Sverdrup, *et al.* 1942)). We calculated the Re using three different speeds (U): the mean speed of the flick downstroke phase for the individual, the mean maximum speed attained during the downstroke for the individual, and the mean upstroke speed for the individual (Table II, Figure 5, C). The downstroke Re was significantly greater than the upstroke Re (Mann-Whitney U, $p = 0.008$). Furthermore, the Re 's of the downstrokes were always greater than or equal to one, while the Re 's of the upstrokes were always less than one.

Since aesthetasc dimensions and speeds did not vary with body size over the range we studied, the Re's of these sensory hairs did not vary significantly with carapace length (Figure 5, C) (linear regression: $p > 0.05$ in all cases).

Temporal and Spatial Pattern of Flicking

Fig 6
→ Examples of the antennule flicking patterns of *P. argus* are given in Figure 6. The lobsters typically flicked the lateral flagellum of an antennule several times in a row, and then paused for a few seconds before executing another series of flicks. Usually the tip of the antennule was moved a distance of several centimeters vertically and/or laterally to a new location during the pause, hence successive series of flicks sampled different positions in the water. Analysis of high-speed videos revealed that within a series of flicks at one position, the antennule was usually held stationary for a brief interval between successive flicks (e.g., for one animal that showed such stationary intervals 100% of the time, mean interval duration was 0.16 s, S.D. = 0.19, $n = 27$; for another individual that showed such intervals 68% of the time ($n = 28$), mean interval duration was 0.18 s, S.D. = 0.16, $n = 20$).

Antennule velocities during the repositioning that occurred between series of flicks were estimated from standard videos of undisturbed lobsters. Since lateral antennule motions did not always occur in the plane of the video, their analysis would have sometimes yielded underestimates of velocity. Therefore, we only measured the vertical velocities during repositioning of antennules for comparison with vertical velocities during flicking. Mean antennule vertical speed during repositioning was 0.012 m/s (S.D. = 0.007, $n = 13$) for one lobster, and 0.054 m/s (S.D. = 0.039, $n = 14$) for another, yielding a mean aesthetasc Re of 0.77 (S.D. = 0.70, $n = 2$ animals). Thus, the aesthetascs of these two lobsters operated at lower Re's during repositioning than they did during flick downstrokes, but at similar Re's to those during flick upstrokes.

Average flicking frequencies were quite variable, both within and between individuals. The frequencies we measured for undisturbed lobsters ($n = 4$) ranged between ~25 and ~90 flicks per minute (0.4 to 1.5 Hz). When shrimp were dropped into the aquarium, the lobsters began to

locomote so rapidly that it was impossible to digitize their antennule motions. However, in one such instance, we were able to count 59 flicks in 17 seconds (3.5 Hz) by a lobster that had been flicking at a rate of 87 flicks per minute (1.4 Hz) prior to the introduction of the shrimp. Flicking frequencies (0.6 Hz) of undisturbed lobsters calculated from data presented by Gleeson, *et al.* (1993) are consistent with our measurements. Gleeson, *et al.* (1993) also noted an increase in flicking frequency when food scent was introduced. In one case we were able digitize antennule flicking by an animal that had settled down to eat its shrimp (Figure 6, B); we found that the flicking behavior was similar to that prior to food introduction (Figure 6, A), although the range of vertical heights to which an antennule was repositioned between series of flicks was greater when the lobster was eating.

DISCUSSION

Flicking Behavior of *P. argus*

Our high-speed kinematic analysis of spiny lobsters, *Panulirus argus*, showed that when they flick their olfactory organs (the lateral flagella of their antennules), the sensory hairs (aesthetascs) on these structures operate at Reynolds numbers (Re) greater than one during the rapid downstroke, but at Re 's of around 0.5 during the slower upstroke. A spiny lobster samples different locations in the water by executing a series of such flicks in rapid succession at one position, and then moving the antennule to a different spot where it performs another series of rapid flicks. During the brief pauses between flicks within a series at one position, the antennules remain stationary, but during the repositioning that occurs between series of flicks, the aesthetascs encounter flow at Re 's around 0.8.

Maintainance of Local Flow Around Aesthetascs as Lobsters Grow

We found that the Reynolds number (Re), and thus the flow regime, of *P. argus* aesthetascs during flicking was maintained as body size changed. Although we only examined animals representing a 33% change in carapace length, our results are consistent with those of Best (1995), who found only a slight change in aesthetasc Re over a 20-fold range of carapace lengths for the clawed lobster, *Homarus americanus*. Such maintenance of aesthetasc Re during

lobster growth suggests that producing a specific water flow pattern near these olfactory hairs is important to their function in filtering odorant information from the environment.

Comparison of Antennule Flicking by *Panulirus* and by *Homarus*

Like *P. argus*, the clawed lobster, *Homarus americanus*, has served as a system for studying the neurobiology of olfactory organs (e.g. Derby and Atema, 1982; Borroni and Atema, 1988; Bayer, *et al.*, 1980; Voigt and Atema, 1990; Atema and Voigt, 1995). There are some intriguing contrasts and a number of similarities between the antennule designs and motions of these two species.

The antennules of clawed and spiny lobsters differ in both motion and the morphology. For example, the manner in which *H. americanus* and *P. argus* spatially sample the water around them is not the same. The excursion distance of a *H. americanus* flick (~14 to 15 mm; calculated from downstroke velocity and duration data reported in Moore, *et al.*, 1991) is roughly twice that of a *P. argus* flick (~6 mm, this study; ~9 mm, Gleeson, *et al.*, 1993), hence *H. americanus* sweep across larger parcels of water per flick than do *P. argus*. However, *P. argus* move the tips of their very long antennules to different positions between series of flicks, whereas *H. americanus* flick their relatively short antennules in a more spatially-restricted domain. Another striking difference between the two species is that the arrangement and orientation of the aesthetascs on their antennules differ, as will be discussed below.

Several parallels between the antennule flicking of clawed and spiny lobsters can be noted. Both *H. americanus* (Moore, *et al.*, 1991) and *P. argus* flick the lateral, but not the medial, flagellum of the antennule. Although actual velocities were not reported, *H. americanus* has been described as having a flick downstroke that is faster than the upstroke (Berg, *et al.*, 1992), as we have measured for *P. argus*. *H. americanus* can flick up to 4 Hz when "excited" (Berg, *et al.*, 1992), similar to our *P. argus* that flicked at 3.5 Hz when food was introduced into the aquarium.

Perhaps the most important similarity between the flicking of *P. argus* and *H. americanus* is that their aesthetascs operate in the same Reynolds number range. Re's we calculate for *H.*

americanus using published aesthetasc diameter (30 μm ; Moore, *et al.*, 1991) and antennule flicking velocities (0.12 to 0.15 m/s; Moore, *et al.*, 1991; Atema, 1995) are 3 to 4, comparable to those Best has measured for that species (personal communication, B. Best) and to those we have measured for the downstroke in *P. argus*. Furthermore, as mentioned above, both species maintain this aesthetasc Re across a range of body sizes. Is there anything special about the way that fluids move around hairs at these intermediate Re 's around one?

Lobster Aesthetascs Operate in a Critical Reynolds Number Range

Clawed and spiny lobsters appear to use different mechanisms to enhance water motion between aesthetascs during flicks and to resist it during between-flick intervals, but both the mechanisms they use to enhance this pulsatile sampling of odorants in their environments are especially effective at Re 's around one, which is the Re of their aesthetascs.

H. americanus aesthetascs splay apart during the downstroke and back together during the upstroke (Moore, *et al.*, 1991). They operate at a Re range in which changes in the gap width between closely-spaced hairs can produce very large changes in leakiness (Cheer and Koehl, 1987; Koehl, 1995; 1996), hence such aesthetasc splaying could lead to a substantial increase in flow between the hairs during the flick downstroke. In contrast, when the hairs move back closer together, water trapped between them should be less likely to be flushed away by ambient currents, and molecules in the trapped water can have time to diffuse to the aesthetasc surfaces. At higher or lower Re 's, this effect of hair-splaying on leakiness should not be as pronounced.

In contrast, the aesthetascs of *P. argus* do not splay apart during a flick (Gleeson, *et al.*, 1993), but water penetration between these aesthetascs may be enhanced by a different mechanism suggested by Gleeson, *et al.* (1993). While the aesthetascs of *H. americanus* are arranged in rows at right angles to the long axis of the antennule like bristles on a toothbrush (e.g. Fig. 3 in Atema, 1985) that face directly into the flow during a flick downstroke (e.g. Moore, *et al.*, 1991; personal communication, P. Moore), those of *P. argus* are bent into a zig-zag row along the antennule, and this row is oriented at 32° (this study) to 35° (Gleeson, *et al.*, 1993) to

the oncoming flow during a flick downstroke. Gleeson, *et al.* (1993) proposed that this configuration and orientation of aesthetascs serves to channel water flow between these sensory hairs during a flick. As with *H. americanus*, the Re range in which the aesthetascs of *P. argus* operate should enhance the differences in flow between the hairs during flick downstrokes and during inter-flick times. Because *P. argus* aesthetascs are flicked down at a Re greater than one and are moved between flicks at Re's of around 0.8, they operate in the Re range at which small changes in Re cause large changes in leakiness for closely-spaced hairs (Koehl, 1995). If they were flicked down at lower Re's (i.e. if they moved more slowly or had slimmer aesthetascs), not much new water would penetrate the aesthetasc array during the flick. If they operated at higher Re's between flicks (i.e. if they repositioned their antennules more rapidly or had bigger aesthetascs), most of the water encountered by the aesthetasc array during repositioning would flow through it rather than around it.

The mechanism described above should also lead to a difference in the leakiness of the aesthetasc array of a *P. argus* antennule during the flick downstroke (at $Re > 1$) and the slower upstroke (at $Re = 0.5$). We have estimated (using equation #3 in Koehl, 1996) that the volume of water flowing through the aesthetasc array during the rapid downstroke is about six times greater than that during the slow upstroke. Therefore, even though the antennule executes a reciprocal motion in which it ends up where it started before the flick, its aesthetascs do not end up surrounded by the same patch of water in which they started. The "old" water is flushed out during the leaky downstroke and is not picked up again during the less-leaky upstroke. For such a velocity asymmetry to result in a leakiness asymmetry, the hairs must operate in the critical Re range used by *P. argus* aesthetascs. We are presently testing these predictions using dynamically-scaled physical models.

Role of Convection and Diffusion in Transport of Molecules to Aesthetascs

Péclet number represents the importance of convection (i.e. fluid motion) relative to molecular diffusion for a particular mass transfer situation (e.g. Futrelle, 1984; Murray, 1977).

Péclet number (Pé) is given by

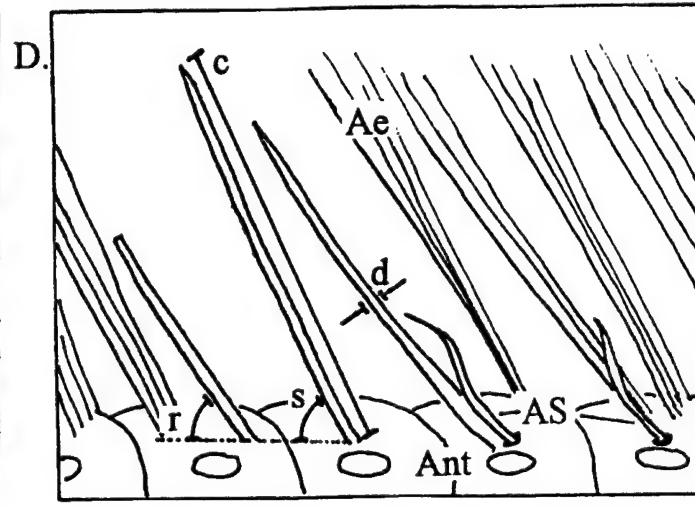
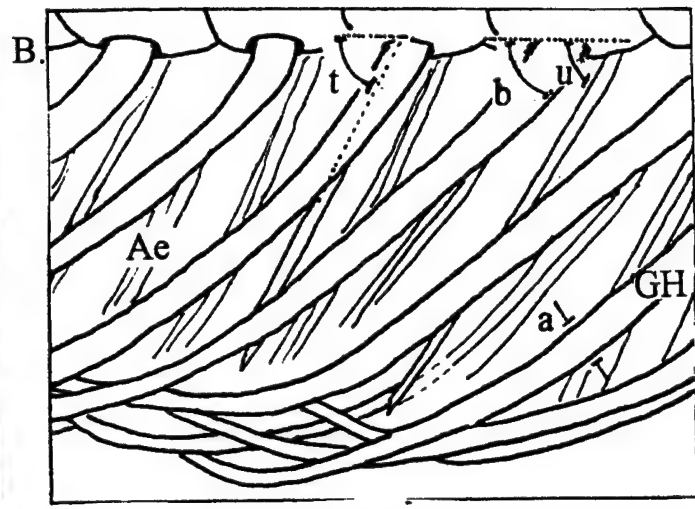
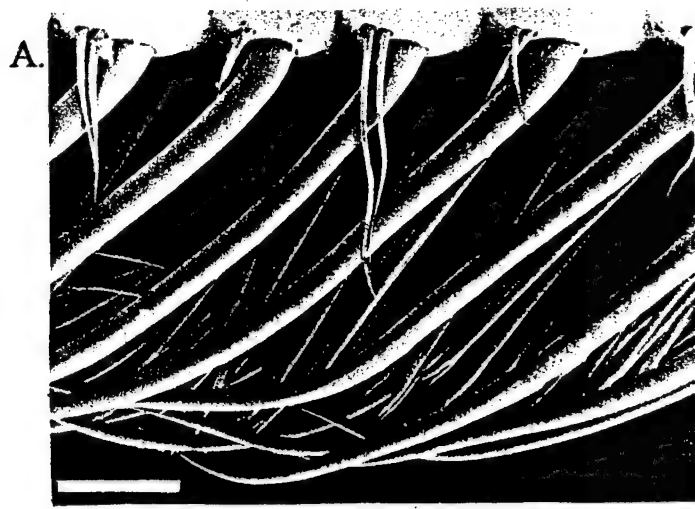
$$Pé = LU_{\infty} / D,$$

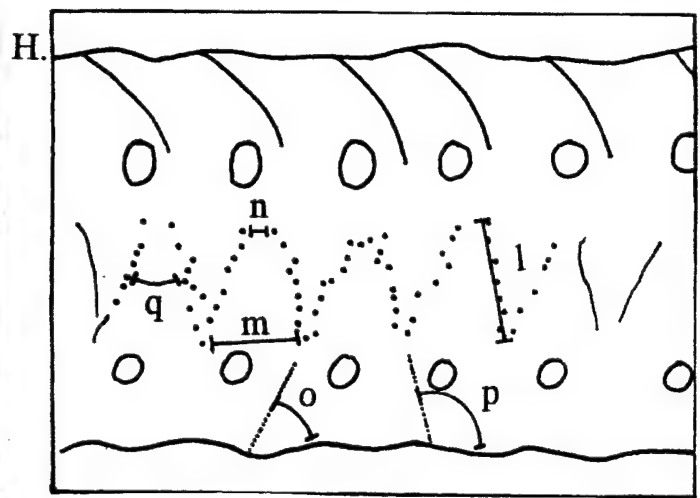
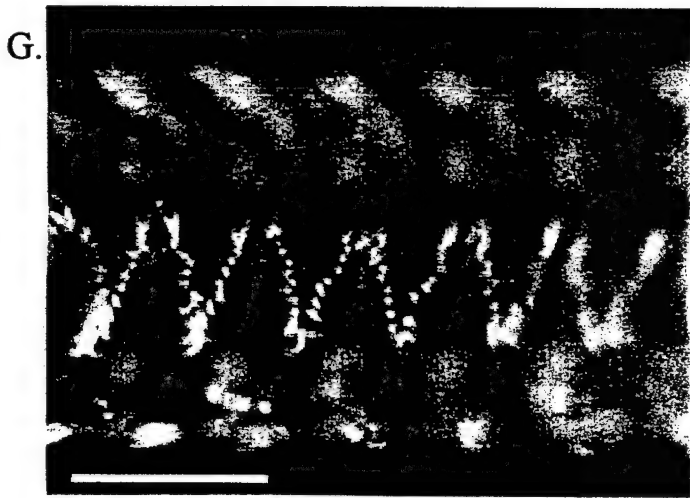
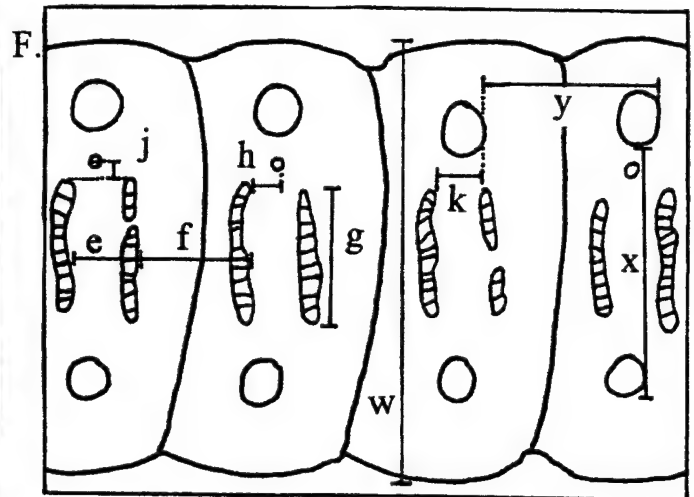
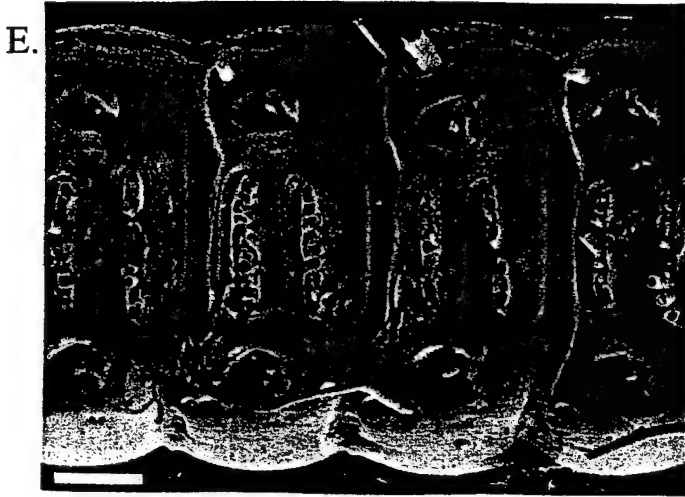
where L is a linear dimension such as hair diameter, U_{∞} is free stream fluid velocity relative to the hair, and D is the diffusion coefficient of the molecule of interest in the fluid. The higher the $Pé$, the more important is water flow relative to molecular diffusion in getting odorants to the surface of an olfactory hair.

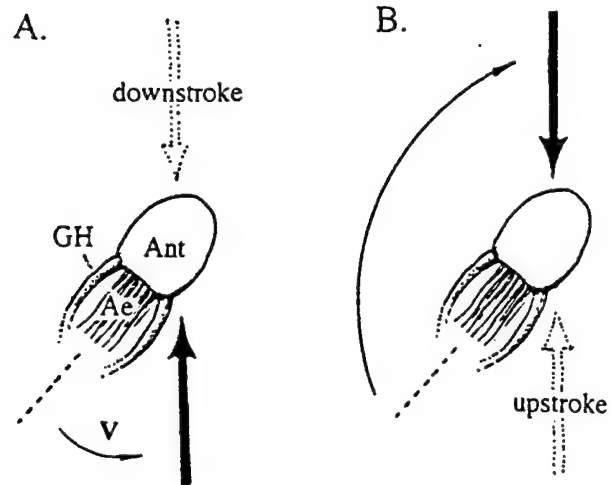
We calculated the $Pé$'s of *P. argus* aesthetascs, where L is mean aesthetasc diameter (2.2×10^{-5} m, Table I), D is the diffusion coefficient of a small molecule in water at 25°C (of order 10^{-9} m^2/s ; Berg, 1993), and U_{∞} is the water speed encountered by an aesthetasc in an array. We approximated U_{∞} as the maximum water velocity attained midway between adjacent aesthetascs; at a Re of 0.5 for arrays having a gap-to-diameter ratio of 1, this velocity is $\sim 20\%$ of the speed the array is moving (Cheer and Koehl, 1987), whereas at $Re \geq 1$ this velocity is about the same magnitude as the speed of the array (Abdullah and Cheer, unpublished calculations cited in Koehl, 1992). Using these model results and our measurements of antennule velocities to calculate rough approximations of U_{∞} 's, we estimated that the $Pé$ during a flick downstroke is about 1300, while during an upstroke and during repositioning the $Pé$ is about 100 to 200. $Pé$'s so far above one indicate that during both phases of the flick and during repositioning, convection rather than diffusion is the mechanism bringing odorants near aesthetascs. In contrast, during the brief intervals between the flicks in a series at one position, the antennule is held stationary, $Pé$ is essentially zero, and molecular diffusion is the mechanism bringing odorant molecules near the surfaces of the aesthetascs. Although these interflick intervals are only ~ 0.16 s, there is ample time for molecules to diffuse to the surfaces of the aesthetascs: the root mean square displacement of molecules by diffusion in such a time interval is $18 \mu\text{m}$ (r.m.s. displacement = $[2Dt]^{1/2}$, where D is diffusion coefficient and t is the time interval; Berg, 1993), greater than the half-gap width between adjacent aesthetascs (Figure 1). Of course, ambient water currents should also affect the velocities and $Pé$'s encountered by the aesthetascs (increasing or decreasing them, depending on the direction of ambient flow relative to antennule motions).

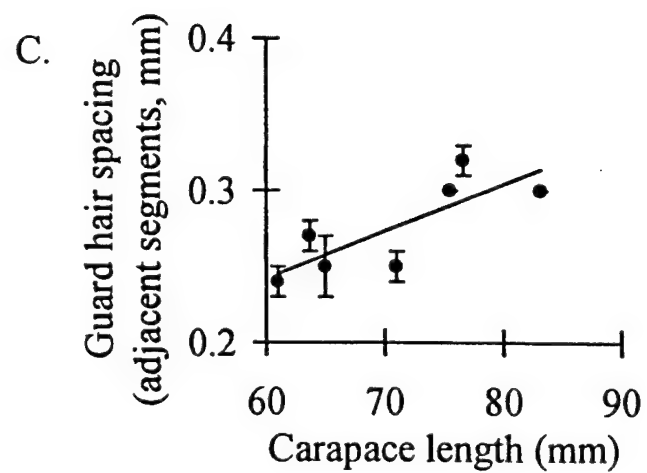
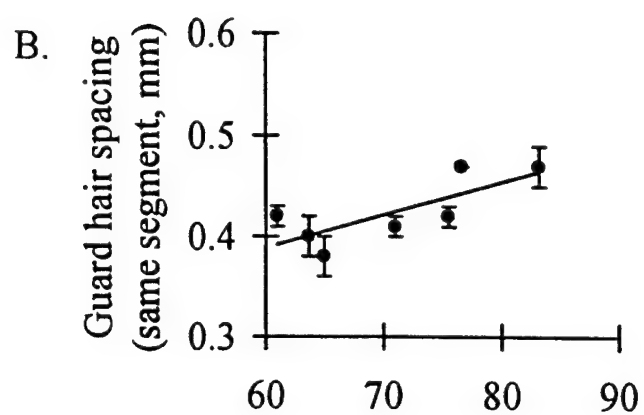
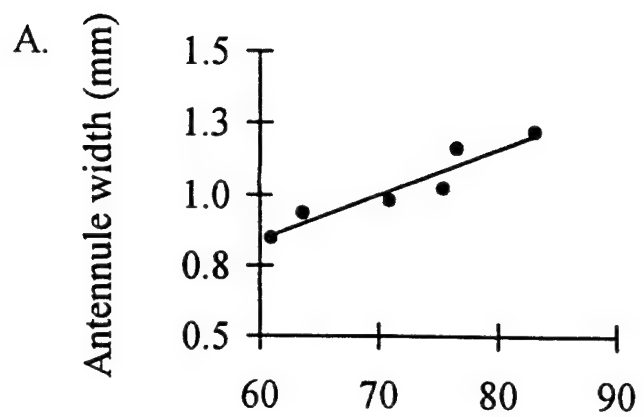
Table II. Kinematic parameters of the flick downstroke and upstroke of the lateral branch of the antennule of the lobster, *P. argus*. A mean velocity was calculated for each flick downstroke and upstroke, and the maximum speed attained during a downstroke was recorded. The mean values from 15 flicks per individual were calculated for these three speeds. These means were used to calculate the mean values reported below for 5 individuals.

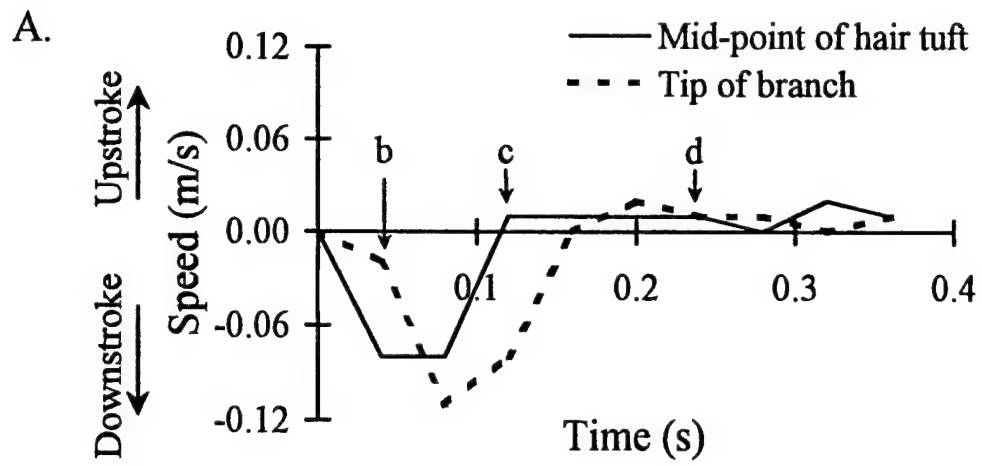
Kinematic parameter	Mean	S.D.
Angle of attack of antennule stalk (°)		
Mean at maximum downstroke speed	90	4
Mean during downstroke	90	10
Mean during upstroke	90	10
Speed (m/s)		
Maximum during downstroke	0.09	0.01
Mean during downstroke	0.06	0.01
Mean during upstroke	0.02	0.01
Aesthetasc Re (calculated from the following speeds)		
Mean maximum speed during downstroke	2	0.4
Mean speed during downstroke	1	0.5
Mean speed during upstroke	0.5	0.3











B.

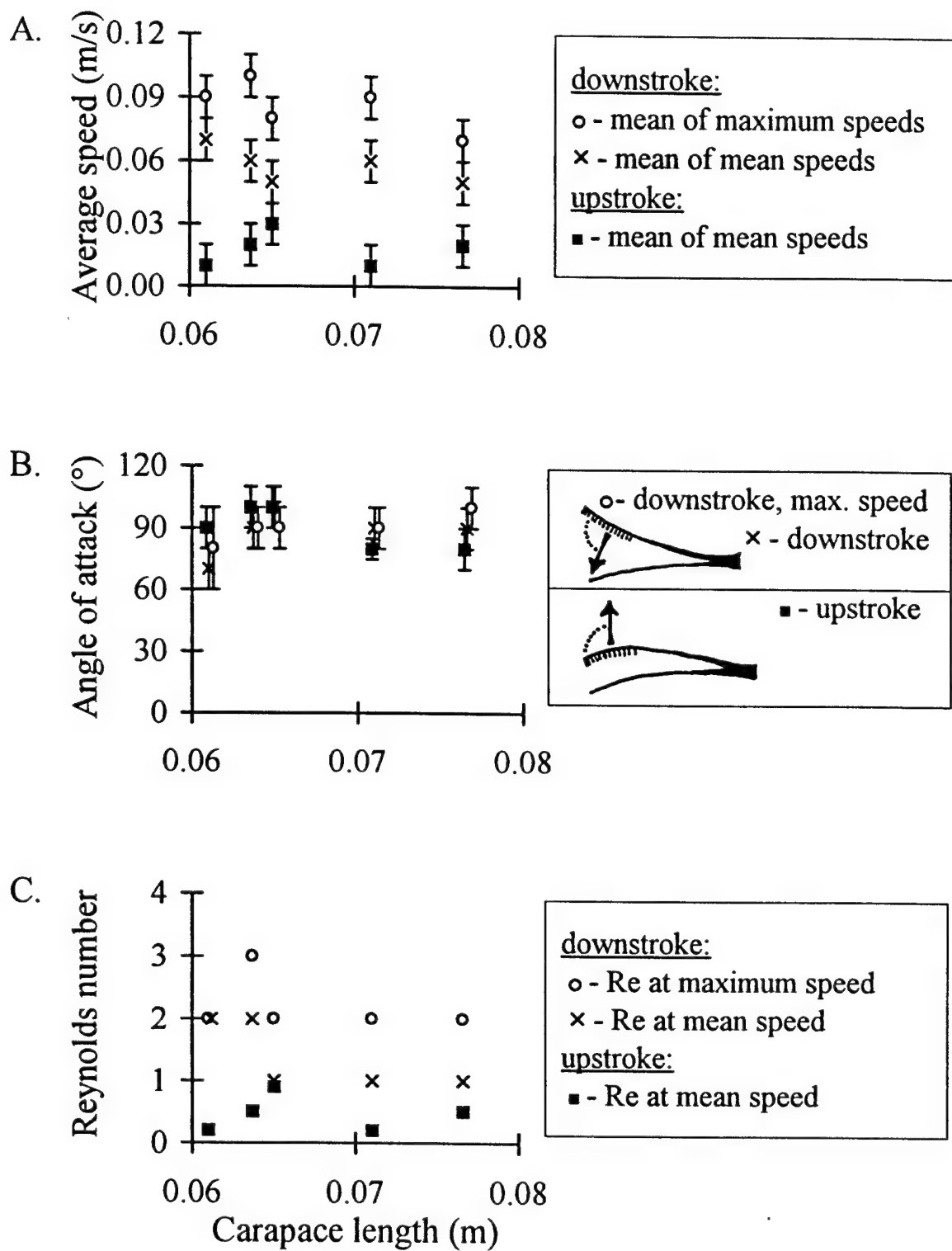


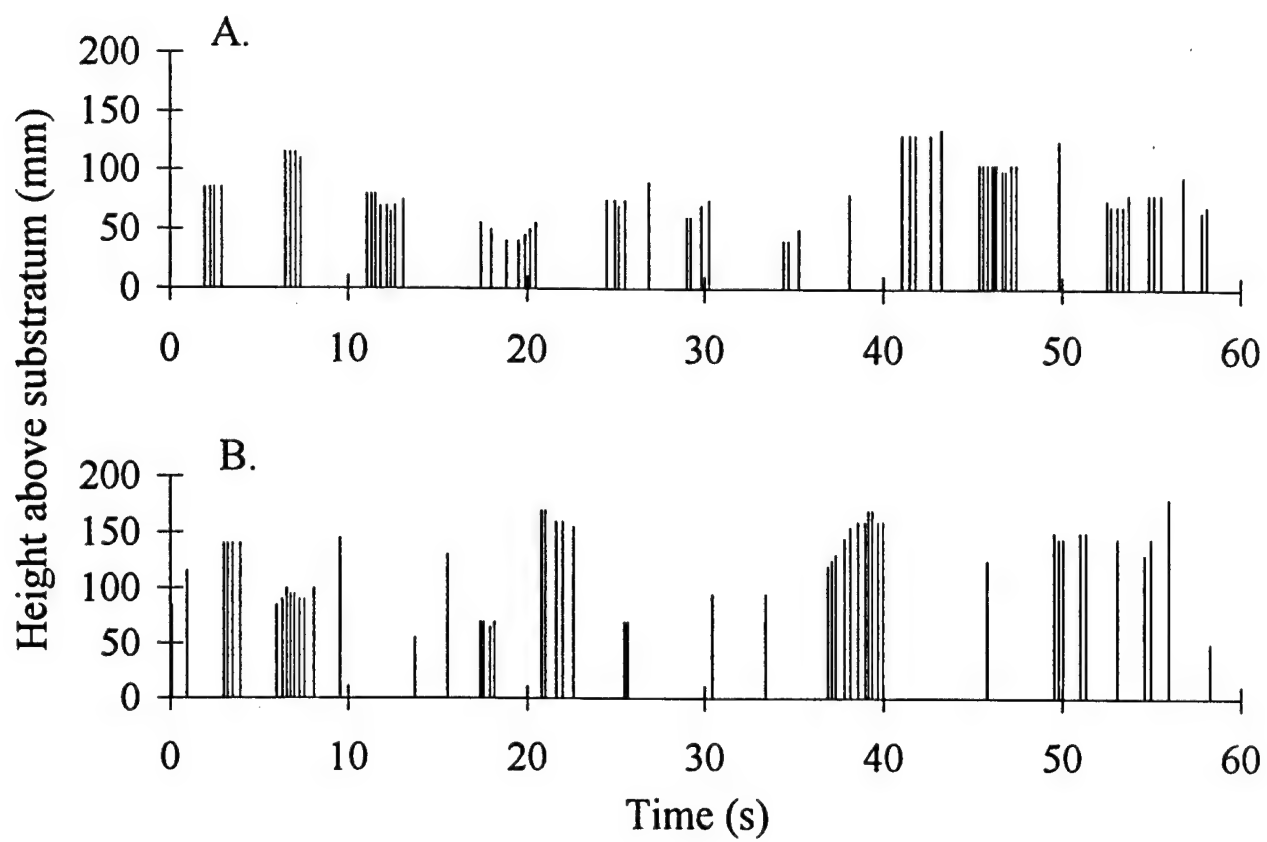
C.



D.







Crustacean antennule flicking has been hypothesized to be functionally like mammalian sniffing: during the flick "old" fluid trapped between the aesthetascs is replaced via convection by "new" fluid (e.g. Snow, 1973; Schmitt and Ache, 1979; Atema, 1985; Gleeson, *et al.*, 1993), resulting in a pulsatile (e.g. Atema, 1985) sampling of odors in the environment. However, our Pé calculations for *P. argus* suggest that, even though the aesthetasc rows are not very leaky during between-flick repositioning, there is significant augmentation of transport of water-borne molecules to the aesthetascs by convection as the antennules sweep to new locations (perhaps analogous to the smells that we experience while breathing). We therefore suggest that during a flick, the *P. argus* aesthetasc array is rapidly cleared of "old" water and filled with a specific parcel of "new" water from a particular location (perhaps analogous to us taking a sniff of air from a certain spot); molecules from that parcel of water diffuse to the aesthetascs during the brief interflick intervals when the antennule is stationary. Thus, we postulate for *P. argus*, that within a series of flicks, there is pulsatile sampling of parcels of water from a specific location, whereas between series of flicks, there is more-or-less continuous convective transport of odorants to the aesthetascs.

ACKNOWLEDGEMENTS

This research was supported by Office of Naval Research Grants #N00014-90-J-137 and #N00014-96-1-0594 to M.K. We are grateful to B. Ache and R. Gleeson for generously providing us with lobsters and antennules, as well as with the inspiration for this work. We thank R. Full for the use of his high-speed video system, R. Kram for assistance with high-speed videotaping, D. Davis for instruction in use of facilities in the Biological Sciences Electron Microscope Laboratory at U.C. Berkeley, the Duke University Morphometrics Laboratory for use of video and graphics equipment, M. O'Donnell for help with manuscript preparation, and S. Vogel for critical reading of a draft of this paper.

REFERENCES

- Alexander, R. McN. (1971) *Size and Shape*. Edward Arnold, London.
- Ache, B. W. (1982) Chemoreception and thermoreception. In H. L. Atwood and D. C. Standeman (eds.). *The Biology of the Crustacea*, Vol. 3. Academic Press, New York, pp. 369-393.
- Ache, B. W. (1988) Integration of chemosensory information in aquatic invertebrates. In Atema, et. al. (eds.). *Sensory Biology of Aquatic Animals*. Springer-Verlag. New York, pp. 387-401.
- Anderson, P. A. V. and Ache, B. W. (1985) Voltage and current clamp recordings of the receptor potential in olfactory cells in situ. *Brain Res.*, **338**, 273-280.
- Atema, J. (1977) Functional separation of smell and taste in fish and crustacea. In J. LeMagnen and L. MacLeod (eds.). *Olfaction and Taste IV*. Information Retrieval, London, pp. 165-174.
- Atema, J. (1985) Chemoreception in the sea: Adaptations of chemoreceptors and behavior to aquatic stimulus conditions. *Soc. Exp. Biol. Symp.*, **39**, 3887-3423.
- Atema, J. (1995) Chemical signals in the marine environment: Dispersal, detection, and temporal signal analysis. In Eisner, T. and Meinwals, J. (eds.), *Chemical Ecology: The Chemistry of Biotic Interactions*. National Academy Press, Washington, D.C., pp. 147-159.
- Atema, J. and Voigt, R. (1995) Behavior and sensory biology. In Factor, I. R. (ed.), *Biology of the Lobster Homarus americanus*. Academic Press, New York, pp. 313-348.
- Bayer, T. A., McClintock, T. S., Grunert, U., and Ache, B. W. (1980). Histamine-induced modulation of olfactory receptor neurones in two species of lobsters, *Panulirus argus* and *Homarus americanus*. *J. Exp. Biol.*, **145**, 133-146.
- Berg, H. C. (1983) *Random Walks in Biology*. Princeton University Press, Princeton, NJ.
- Berg, K., Voigt, R. and Atema, J. (1992) Flicking in the lobster *Homarus americanus*: Recordings from electrodes implanted in antennular segments. *Biol. Bull.*, **183**, 377-378.

- Best, B. A. (1995) Scaling and flow dynamics of crustacean antennules: What's flicking all about? *Am. Zool.*, **35**, 53A.
- Borroni, P. F. and Atema, J. (1988) Adaptation in chemoreceptor cells I. Self-adapting backgrounds determine threshold and cause parallel shift of response function. *J. Comp. Physiol. A.*, **164**, 67-74.
- Cheer, A. Y. L. and Koehl, M. A. R. (1987) Paddles and rakes: Fluid flow through bristled appendages of small organisms. *J. Theor. Biol.*, **129**, 185-199.
- Cheer, A. Y. L. and Koehl, M. A. R. (1988) Fluid flow through filtering appendages of insects. *I.M.A. J. Math. Appl. Med. Biol.*, **4**, 185-199.
- Derby, C. D. and Atema, J. (1988) Chemoreceptor cells in aquatic invertebrates: Peripheral mechanisms of chemical signal processing in decapod crustaceans. In Atema, J., *et al.* (eds.), *Sensory Biology of Aquatic Animals*. Springer-Verlag, New York, pp. 365-386.
- DeSimone, J. A. (1981) Physicochemical principles in taste and olfaction. In Cagan, R.H. and Kare, M. R. (eds.), *Biochemistry of Taste and Olfaction*. Academic Press, New York, pp. 213-229.
- Futrelle, R. P. (1984) How molecules get to their detectors: The physics of diffusion of insect pheromones. *Trends. Neurosci.*, **April**, 116-120.
- Fuzessery, Z. M., Carr, W. F. S., and Ache, B. W. (1978) Antennular chemosensitivity in the spiny lobster, *Panulirus argus*: Studies of taurine sensitivity receptors. *Biol. Bull.* **154**, 226-240.
- Gleeson, R. A. (1982) Morphological and behavioral identification of the sensory structures mediating pheromone reception in the blue crab, *Callinectes sapidus*. *Biol. Bull.*, **163**, 162-171.
- Gleeson, R. A., Carr, W. E. S., and Trapido-Rosenthal, H. G. (1993) Morphological characteristics facilitating stimulus access and removal in the olfactory organ of the spiny lobster, *Panulirus argus*: Insight from the design. *Chem. Senses*, **18**, 67-75.

- Grunert, U. and Ache, B. W. (1988) Ultrastructure of the aesthetasc (olfactory) sensilla of the spiny lobster *Panulirus argus*. *Cell Tissue Res.*, **251**, 95-103.
- Hallberg, E., Johansson, K.U.I., and Elofsson, R. (1992) The aesthetasc concept: Structural variations of putative olfactory receptor cell complexes in crustaceans. *Microsc. Res. Techn.*, **22**, 336-350.
- Happel, J. and Brenner, H. (1965) *Low Reynolds Number Hydrodynamics with Special Applications to Particulate Media*. Prentice-Hall, Englewood Cliffs, NJ.
- Koehl, M. A. R. (1992) Hairy little legs: Feeding, smelling, and swimming at low Reynolds number. *Fluid Dynamics in Biology. Contemp. Math.*, **141**, 33-64.
- Koehl, M. A. R. (1995) Fluid flow through hair-bearing appendages: Feeding, smelling, and swimming at low and intermediate Reynolds number. *Soc. Exp. Biol. Symp.*, **49**, 157-182.
- Koehl, M. A. R. (1996) Small-scale fluid dynamics of olfactory antennae. *Mar. Fresh. Behav. Physiol.*, **27**, 127-141.
- Koehl, M. A. R. and Strickler, J. R. (1981) Copepod feeding currents: food capture at low Reynolds number. *Limnol. Oceanogr.*, **26**, 1062-1073.
- Loudon, C., Best, B. A. and Koehl, M. A. R. (1994) When does motion relative to neighboring surfaces alter the flow through an array of hairs? *J. Exp. Biol.*, **193**, 233-254.
- Laverack, M. S. (1988) The diversity of chemoreceptors. In Atema, J. (ed.), *Sensory Biology of Aquatic Animals*. Springer-Verlag, New York, pp. 287-317.
- Marscall, H.-P. and Ache, B. W. (1989) Response dynamics of lobster olfactory neurons during simulated natural sampling. *Chem. Senses*, **14**, 725.
- Michel, W. C., McKlintock, T. S., and Ache, B. W. (1991) Inhibition of lobster olfactory receptor cells by an odor-activated potassium conductance. *J. Neurophysiol.*, **65**, 446-453.

- Moore, P. A., Gerhardt, G. A., and Atema, J. (1989) High resolution spatio-temporal analysis of aquatic chemical signals using microelectrochemical electrodes. *Chem. Senses*, **14**, 829-840.
- Moore, P. A., Atema, J., and Gerhardt, G. A. (1991) Fluid dynamics and microscale chemical movement in the chemosensory appendages of the lobster, *Homarus americanus*. *Chem. Senses*, **16**, 663-674.
- Murlis, J. (1986) The structure of odour plumes. In Payne, T. L., Birch, M. C., and Kennedy, C. E. J. (eds.), *Mechanisms of Insect Olfaction*, Clarendon Press, Oxford, pp. 27-38.
- Murray, J. D. (1977) Reduction of dimensionability in diffusion processes: Antenna receptors of moths. In Murray, J. D. (ed.), *Lectures on Nonlinear-Differential-Equation Models in Biology*. Oxford University Press, Oxford, pp. 83-127.
- Rubenstein, D. I. and Koehl, M. A. R. (1977) The mechanisms of filter feeding: Some theoretical considerations. *Am. Nat.*, **26**, 981-994.
- Schmidt, B. C. and Ache, B. W. (1979) Olfaction: Responses of a decapod crustacean are enhanced by flicking. *Science*, **205**, 204-206.
- Shimeta, J. and Jumars, P. A. (1991) Physical mechanisms and rates of particle capture by suspension-feeders. *Oceanogr. Mar. Biol. Annu. Rev.*, **29**, 191-257.
- Snow, P. J. (1973) The antennular activities of the hermit crab, *Pagurus alaskensis* (Benedict). *J. Exp. Biol.*, **58**, 745-765.
- Sverdrup, H. U., Johnson, M. W., and Fleming, R. H. (1942) *The Oceans: Their Physics, Chemistry, and General Biology*. Prentice-Hall, Inc., New York.
- Vogel, S. (1994) *Life in Moving Fluids: The Physical Biology of Flow*, 2nd Edition. Princeton University Press, Princeton.
- Vogel, S. (1983) How much air passes through a silkworm's antenna? *J. Insect Physiol.*, **29**, 597-602.
- Voigt, R. and Atema, J. (1990) Adaptation in chemoreceptor cells. III. Effects of cumulative adaptation. *J. Comp. Physiol. A*, **166**, 865-874.

- Weissburg, M. J. and Zimmer-Faust, R. K. (1994) Odor plumes and how blue crabs use them in finding prey. *J. Exp. Biol.*, **197**, 349-375.
- Willis, M. A., David, C. T., Murlis, J., and Carde, R. T. (1994) Effects of pheromone plume structure and visual stimuli on the pheromone-modulated upwind flight of male gypsy moths (*Lumantria dispar*) in a forest (Lepidoptera, Lymantriidae). *J. Insect Behav.*, **7**, 385-409.
- Zar, J. H. (1974) *Biostatistical Analysis*. Prentice-Hall, Inc., Englewood Cliffs, NJ.
- Zerbe, W.B. and Taylor, C.B. (1953) Sea water temperature and density reduction tables. In *Coast and Geodetic Survey Special Publication, no. 298*. U.S. Department of Commerce, Washington, D.C., pp. 18-19.

FIGURE LEGENDS

Fig. 1. Morphological parameters we measured of the hair-bearing region of the lateral branch of antennules of *P. argus* (w = width of lateral branch of antennule, x = distance between guard hairs along one segment, y = distance between guard hairs on adjacent segments, Ant = antennule, GH = guard hair, Ae = aesthetasc, AS = asymmetric sensilla; all other code letters defined in Table I). The distal end of the antennule is to the left in all pictures. A. SEM of a medio-lateral view of the ventral portion of a left antennule, showing the guard hairs and aesthetascs. (Scale bar = 200 μm) B. Tracing of the SEM in A, showing morphological parameters measured. C. SEM of a dorso-lateral view of the right side of a right antennule from which the guard hairs have been removed to show the aesthetascs and assymetric sensilla. (Scale bar = 150 μm) D. Tracing of the SEM in C, showing morphological parameters measured. E. SEM of a ventro-lateral view of a left antennule from which the guard hairs, aesthetascs, and assymetric sensilla have been removed. (Scale bar = 150 μm) F. Tracing of the SEM in E, showing morphological parameters measured. G. Light micrograph of a ventro-lateral view of a left antennule from which the guard hairs have been removed. Only the tips of the aesthetascs are in the plane of focus. (Scale bar = 500 μm) H. Tracing of the micrograph in G, showing morphological parameters measured.

Fig. 2. Diagram of a cross-section of the lateral branch of the right antennule (as viewed from its distal end) of a *P. argus* showing the orientation of the aesthetascs with respect to the direction of antennule flicking. The direction of antennule motion is indicated by the dotted arrow, and the direction of water motion relative to the antennule is indicated by the solid arrow. (Ant = lateral flagellum of antennule, Ae = aesthetascs, GH = guard hair). A. During the downstroke (angle v is defined Table I). B. During the upstroke.

Fig. 3. Morphological parameters that varied significantly with body size, plotted as a function of carapace length. A. Antennule width (linear regression: $y = 0.016x - 0.13$, $r^2 = 0.90$, $p =$

0.004). B. Distance between guard hairs on the same segment of the antennule ($y = 0.003x + 0.19$, $r^2 = 0.60$, $p = 0.04$). C. Distance between guard hairs on adjacent segments ($y = 0.003x + 0.06$, $r^2 = 0.65$, $p = 0.03$). Each symbol in B and C represents the mean value of all the measurements (error bars = one standard deviation, $n = 3$) of that parameter made for an individual lobster, while in A only one measurement per animal is reported.

Fig. 4. Example of the kinematics of a flick by the lateral flagellum of the antennule of a *P. argus*. A. Graph of the speed of the tip (dashed line) and the midpoint of the tuft of hairs (solid line) of a flicking antennule as a function of time. The downstroke speeds are indicated by negative values and the upstroke speeds by positive values. B. Frame of a high-speed video of an antennule at the stage during its flick that corresponds to stage "b" indicated on the graph in A. Arrows indicate the velocity of motion of the lateral flagellum of the antennule at its tip and at the midpoint of the tuft of hairs. (size scale bar = 10 mm; velocity scale shown in C) C. Frame of a high-speed video of an antennule at the stage in its flick that corresponds to "c" indicated on the graph in A. (velocity scale bar = 0.05 m/s; size scale shown in B). D. Frame of a high-speed video of the antennule at the stage during its flick that corresponds to "d" indicated on the graph in A. (size scale shown in B; velocity scale shown in C)

Fig. 5. Kinematic parameters plotted as a function of carapace length. Each symbol represents the mean value of fifteen digitized flicks per individual, and the value for each of those flicks represents the mean of the measurements made for the frames digitized for that flick (the number of frames digitized varied depending on the duration of the flick). Error bars in A and B represent \pm one S.D. A. Speed of antennule measured at the midpoint of the tuft of hairs: \circ = maximum speed attained during a downstroke, \times = mean speed during an entire downstroke, \blacksquare = mean speed during an entire upstroke. B. Angle of attack of antennule (angle between the long axis of the antennule at the midpoint of the tuft of hairs and the velocity vector of water motion relative to the antennule, as indicated by the dotted angles on the diagram): \circ = angle at the time

of maximum downstroke speed, \times = mean angle during an entire downstroke, \blacksquare = mean angle during an entire upstroke. C. Reynolds number (Re) of aesthetascs: \circ = Re calculated using the mean of the maximum speed attained during a downstroke, \times = Re calculated using the mean of the mean speeds during entire downstrokes, \blacksquare = Re calculated using the mean of the mean speeds during entire upstrokes.

Fig. 6. Examples of the temporal and spatial patterns of antennule flicking by *P. argus*. Each flick is represented by a line that intersects the time axis at the instant (to the nearest 0.033 s) that the flick began. The height of each line represents the height above the substratum of the tip of the lateral flagellum of the antennule at the onset of each flick. A. Antennule flicking by an undisturbed lobster standing still in a 65 gallon aquarium to which no food (shrimp) had been added during the previous 24 hours. B. Antennule flicking by the same lobster eating a shrimp. A dead shrimp was dropped into the aquarium 1 min after the flicking sequence in A was recorded, and the lobster locomoted quickly and seized the prey. The sequence in B was recorded about 6 min later, after the lobster settled down in one spot and was eating the shrimp.

Table I. Morphological parameters of the lateral antennule of the lobster, *P. argus*. Values are means of the mean values from *s* measures of *n* individuals. Codes refer to Figures 1 and 2.

Code	Morphological feature (units)	Mean	S.D.	n	s
a	Guard hair diameter (μm)	60	9	7	3
b	Guard hair angle ($^{\circ}$)	39	4	7	3
c	Aesthetasc length ^a (μm)	720	50	7	6
d	Aesthetasc diameter ^a (μm)	22	3	7	6
e	Distance between aesthetasc rows on same segment (μm)	110	10	7	3
f	Distance between aesthetasc rows on adjacent segments (μm)	170	20	7	3
g	Width of aesthetasc row at base ^a (μm)	230	20	7	6
h	Distance between aesthetasc row and guard hair (μm)	60	10	7	3
i	Number of aesthetascs per row ^a	10	1	7	6
j	Distance laterally of asymmetric sensillum from aesthetascs (μm)	31	6	7	3
k	Distance proximally of asymmetric sensillum from aesthetascs (μm)	40	10	7	3
l	Width of aesthetasc row at tips ^a (μm)	220	27	6	6
m	Distance between tips of the ventral-most aesthetascs in the rows on a segment (μm)	196	44	6	3
n	Distance between tips of the lateral-most aesthetascs in the rows on a segment (μm)	53	10	6	3
o	Acute angle formed by tip of distal aesthetasc row and longitudinal axis of antennule ($^{\circ}$)	70	5	6	3
p	Obtuse angle formed by tips of proximal aesthetasc row and longitudinal axis of antennule ($^{\circ}$)	107	8	6	3
q	Acute angle formed by tips of distal and tips of proximal aesthetasc rows ^b ($^{\circ}$)	39	8	6	6
r	Angle between lateral-most aesthetasc in the distal row and antennule ($^{\circ}$)	48	5	6	3
s	Angle between lateral-most aesthetasc in the proximal row and antennule ($^{\circ}$)	55	9	6	3
t	Angle between ventral-most aesthetasc in the distal row and antennule ($^{\circ}$)	54	6	6	3
u	Angle between ventral-most aesthetasc in the proximal row and antennule ($^{\circ}$)	50	6	6	3
v	Angle ventrolaterally of tuft with respect to the flow during downstroke ($^{\circ}$)	32	4	3	1

^a No significant difference was found between proximal and distal rows of aesthetascs (Wilcoxon signed ranks test, $p > 0.05$) and the results reported are pooled.

^b No significant difference was found between angles formed by rows on same segment and those formed by rows on adjacent segments (Wilcoxon signed ranks test, $p > 0.05$). The results reported are pooled.

WHEN DOES MORPHOLOGY MATTER?

M. A. R. Koehl

Department of Integrative Biology, University of California, Berkeley, California
94720-3140

KEY WORDS: performance, ecomorphology, novelty, constraint, Reynolds number

ABSTRACT

The performance of an organism is the crucial link between its phenotype and its ecological success. When does an organism's morphology affect its performance? Quantitative mechanistic analyses of how function depends on biological form have shown that the relationship between morphology and performance can be nonlinear, context-dependent, and sometimes surprising. In some cases, small changes in morphology or simple changes in size can lead to novel functions, while in other cases changes in form can occur without performance consequences. Furthermore, the effect of a specific change in morphology can depend on the size, shape, stiffness, or habitat of an organism. Likewise, a particular change in posture or behavior can produce opposite effects when performed by bodies with different morphologies. These mechanistic studies not only reveal potential misconceptions that can arise from the descriptive statistical analyses often used in ecological and evolutionary research, but they also show how new functions, and novel consequences of changes in morphology, can arise simply as the result of changes in size or habitat. Such organismal-level mechanistic research can be used in concert with other tools to gain insights about issues in ecology (e.g., foraging, competition, disturbance, keystone species, functional groups) and evolution (e.g., adaptation, interpretation of fossils, and origin of novelty).

INTRODUCTION

The biological literature abounds with qualitative arguments about the selective advantages of particular morphological traits; more recently such qualitative arguments have been replaced by quantitative correlations between structural or performance characteristics of organisms and their fitness or ecological role.

Such qualitative or statistical statements are often made without a mechanistic understanding of how the morphological traits affect performance. Nonetheless, the performance of an organism is recognized as the crucial link between its phenotype and its ecological success (e.g. 7, 8, 20, 45, 91, 104, 198, 228, 229).

The purpose of this article is to draw together for ecologists and evolutionary biologists examples of the nonlinear, context-dependent, and sometimes surprising relationships between the morphology and performance of organisms. These nonintuitive effects, which have been revealed by mechanistic organismal-level investigations, are often missed in descriptive statistical or phylogenetic studies that use morphological or performance data. I have two goals in reviewing this information: One is to warn about the misconceptions that can arise from descriptive statistical studies that are blind to mechanism, and the other is to point out ways in which such organismal-level mechanistic information can be used to gain insights about issues in ecology (e.g. foraging, competition, disturbance, keystone species, functional groups) and evolution (e.g. adaptation, interpretation of fossils, and origin of novelty).

Some Definitions

I define the *morphology* of an organism as its structure on any level of organization from molecular to organismal, and I define *performance* as a measure of ability to carry out a specific function. Although some authors (8, 45) consider behavioral and physiological traits as morphology, I view them here as functions (although this distinction can sometimes be blurred—75). Furthermore, while some authors (8, 45) define performance as a measure of whole-organism capacity, I also consider performance of parts of organisms (e.g. appendages, enzymes). A *function* of a structure is simply a function the structure is capable of doing [i.e. *fundamental niche* sensu, (198); *performance* sensu, (63)], whereas a *role* of a structure is a use to which the structure is put by an organism in a given environment [i.e. *realized niche* sensu, (98); *behavior* sensu, (63)] (20, 60, 134). How well a structure performs a role (such as food-gathering) is often assumed to affect the fitness of the organism (e.g. 60, 134), although fitness may depend most on the performance of rare life-or-death roles (such as escape maneuvers) (198). *Fitness* is the number of zygotes or surviving offspring, corrected for rate of population growth, produced by an individual during its lifetime (45).

The Biomechanical Approach to Studying Effects of Morphology on Performance

There is a long history of research on the relationship between biological structure and function (reviewed by 137, 158, 229, 232, 234). One approach to

functional morphology is biomechanics, the application of quantitative engineering techniques to study how organisms perform mechanical functions and interact with their physical environments. Biomechanists are concerned with elucidating the basic physical rules governing how biological structures operate, identifying physical constraints on what organisms can do, evaluating which structural characteristics affect performance, and analyzing the mechanisms responsible for the effects of morphological differences on performance (e.g. 3, 4, 35, 40, 44, 45, 54, 60, 104, 131, 134, 153, 166, 185, 198, 224, 226, 228, 230, 234). Although some biomechanists have been accused of assuming that natural selection has led to the morphologies being studied (e.g. 232), many of us simply focus on the mechanisms by which form affects function without making inferences about evolutionary origin. In addition to being a legitimate field on its own, biomechanics has also served as the handmaiden of other disciplines (232), providing useful tools for studying questions in ecology as well as in evolutionary biology and paleontology.

EXAMPLES OF SURPRISES THAT ORGANISMAL-LEVEL MECHANISTIC STUDIES REVEAL ABOUT HOW MORPHOLOGY AFFECTS PERFORMANCE

Many quantitative studies of the effects of morphology on performance are reviewed in biomechanics books (e.g. 3, 35, 40, 153, 166, 185, 224, 226, 230). My purpose here is not to summarize the field, but rather to focus on examples of the nonlinear and context-dependent ways in which performance depends on structure. After introducing basic types of nonlinear relationships between structure and function, I describe two examples of how the relationship between morphology and performance can be surprising (fluid dynamics of little hairs, and effects of body shape and texture on drag). I then discuss in more general terms the categories of nonintuitive effects of morphology on performance that we should keep in mind when using morphological data to address ecological or evolutionary questions.

Overview of Nonlinear Effects of Morphology on Performance

If the quantitative relationship between a measure of performance and a measure of morphology is nonlinear, then there are ranges of the morphological parameter where modifications of structure make little difference, and other ranges where small morphological changes can have large consequences. For example, an asymptotic curve is shown in Figure 1a: increasing the number of receptor sites on a cell increases the rate at which it adsorbs molecules when receptor numbers are low, but offers little improvement when receptor numbers are high (17).

An example of an exponential curve is shown in Figure 1b: Differences in the size of small prey have little effect on predator handling time and hence on the prey's likelihood of being eaten, whereas differences in body size between larger prey can have a big effect on the danger of becoming a meal (46). [Of course, once prey become large enough that they escape in size from predation (179), differences in size once again become unimportant to the risk of being eaten.] Many aspects of mechanical performance also have exponential relationships to morphological features [e.g. deflection of a bending beam bearing a given load $\propto \text{length}^3$; weight borne by a skeleton $\propto \text{body volume} \propto \text{length}^3$; volume flow rate through a pipe $\propto \text{diameter}^4$; and many others described in e.g. (2, 3, 154, 166, 226, 230)]. Thus, performance of functions like skeletal support should be insensitive to structural variation at small size but very sensitive to morphological changes at large size.

If the relationship between performance and a morphological variable goes through a maximum or a minimum (Figure 1c), then the effect of increasing the morphological variable reverses once it passes a critical value. We are used to trying to relate such maxima and minima to the peaks and troughs in adaptive landscapes (e.g. 58, 104). In addition, we might also consider that passing through such an inflection point represents the acquisition of a novel consequence for a particular type of morphological change. For example, if a heated body is surrounded by a non-heat-producing layer (e.g. extracellular cuticle, mucus, or fur), thickening that layer enhances the rate of heat loss from the body until a critical outer radius is reached, above which further thickening of the layer reduces heat loss (Figure 1c) (192). This critical radius concept from heat transfer physics was used to argue that naked baby mammals and birds would lose heat faster if they had feathers or fur (12), but calculations by Porter et al (192) showed the critical radius to be too small to be relevant (Figure 1c). Furthermore, when the non-heat-producing layer surrounding the body was assumed to be porous (like feathers or fur containing air spaces), the calculated resistance to heat loss was much greater than when the insulating layer was assumed to be solid (Figure 1d) (192). This example illustrates the importance of doing quantitative assessments of how morphology affects performance and of using biologically relevant assumptions in calculations.

Now, armed with the idea that the effect of morphology on performance is sometimes nonlinear, I provide some examples of various types of surprising relationships between morphology and performance.

Performance of Hairy Little Legs

Many animals from different phyla use appendages bearing arrays of hairs to perform important biological functions such as suspension-feeding, gas exchange, olfaction, mechanoreception, and swimming or flying (Figure 2a-e).

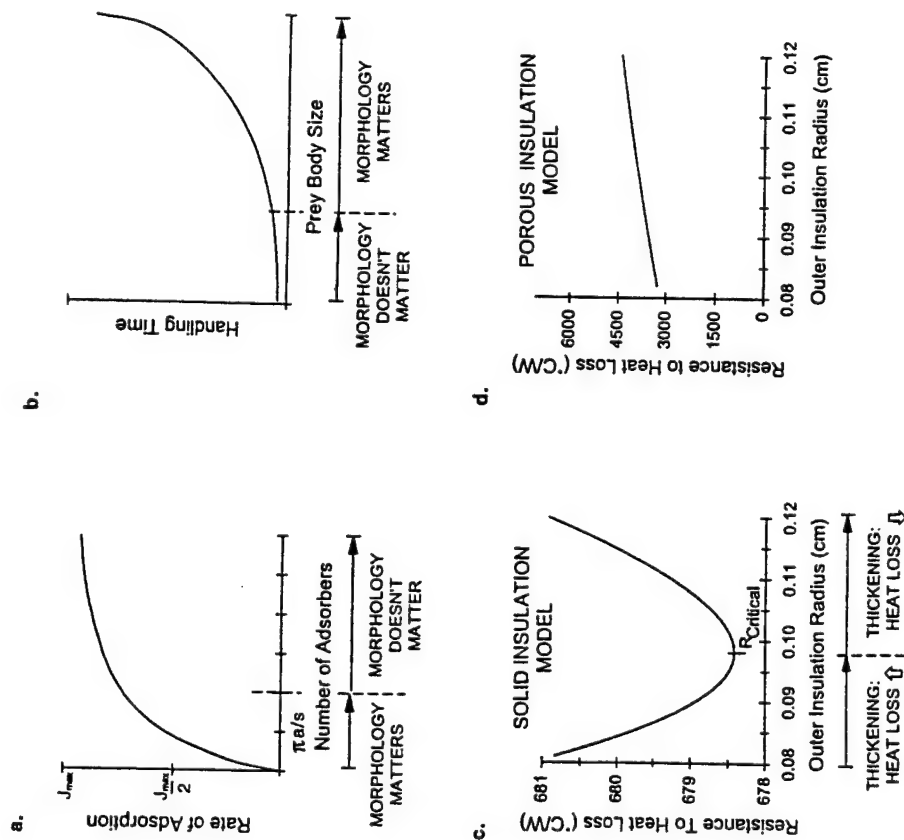


Figure 1 Examples of the relationship between performance (y axis) and morphology (x axis). (a) Rate of molecule adsorption (molecules per time, where J_{max} = number of molecules per time captured by a sphere whose entire surface is adsorbing receptor sites) of a spherical cell, plotted as a function of the number of adsorbing receptor sites on the cell (where a = radius of cell, s = radius of a single receptor site). [Curve calculated using equation 8 in (17)]. (b) Handling time for a predator to eat a prey organism (the higher the value, the better the performance of the prey), plotted as a function of prey body size. [Redrawn by digitizing one of the curves in Figure 6.3 of (46)]. (c) Resistance to heat loss by a heated cylindrical body (diameter = 0.16 cm) surrounded by a layer of solid insulation, plotted as a function of the outer radius of the body plus insulation. Resistance was calculated for heat loss by conduction through the insulation, and by free convection and radiation from the outer surface of the insulation. [Redrawn by digitizing the total resistance curve in Figure 2 of (192)]. (d) Resistance to heat loss by the same heated cylindrical body, but with porous insulation. [Redrawn by digitizing the free-convection curve in Figure 6 of (192)].

To carry out any of these functions, an array of hairs must interact with the water or air around it; thus, to understand how appendage morphology affects performance we must analyze the fluid dynamics of arrays of hairs.

Reynolds number (Re) represents the relative importance of inertial to viscous forces for a particular flow situation ($Re = LU/\nu$) where L is a linear dimension such as hair diameter, U is fluid velocity relative to the hair, and ν is kinematic viscosity of the fluid (226). At high Re 's (e.g. large, rapidly moving structures), inertial forces predominate, so flow is messy and turbulent, whereas at low Re 's (e.g. small, slowly moving structures), viscosity damps out disturbances in the fluid, hence flow is smooth and orderly. When fluid flows past a solid surface, the fluid in contact with the surface does not slip relative to the surface, and a velocity gradient (boundary layer) develops between the surface and the freestream flow. At low Re 's, boundary layers are thick relative to the dimensions of the structure.

Most of the types of hairs listed above operate at Re 's of order 10^{-3} to 10 (119). If the layers of fluid stuck to and moving with the hairs in an array are thick relative to the gaps between hairs, little fluid leaks through the array. Since performance of the functions listed above depends on the leakiness of hair-bearing appendages (reviewed in 119, 120), the effects of hair spacing and Re (size or speed) on leakiness have been explored using mathematical and physical models (Figure 2f) (29, 30, 78, 118–120). Although hairy appendages look like sieves, they are not always leaky: at $Re < 10^{-3}$, so little fluid leaks through the gaps between neighboring hairs that arrays of hairs function like paddles; in contrast, at $Re > 10^{-2}$, fluid flows readily between the hairs and arrays behave like leaky filters. Another surprising discovery is that at $Re < 10^{-3}$, changes in morphology (hair diameter or spacing) or behavior (speed) have little effect on leakiness (i.e. there is permission for morphological and behavioral diversity without performance consequences), whereas at Re 's of 10^{-2} to 10^{-1} , changes in size or speed can have a big effect on leakiness. Moreover, at Re 's of 10^{-2} to 10^{-1} , decreasing gap width reduces leakiness, whereas at $Re = 1$, changes in hair spacing affect leakiness only when hairs are quite close together. The effect of a morphological change can also reverse at a critical Re : adding more hairs to an array reduces leakiness if $Re < 1$, but has the opposite effect if $Re > 1$ (D Abdullah, personal communication; 119). The leakiness of an array is increased when it moves near a wall (such as the body surface) if $Re < 10^{-2}$ (146)—thus the behavior that can alter leakiness changes as an animal grows (i.e. altering appendage distance from the body when $Re < 10^{-2}$, versus changing appendage speed when $Re > 10^{-2}$).

The hairy feeding appendages (second maxillae, M2's) of calanoid copepods (Figure 3) provide a biological example of the consequences of these physical

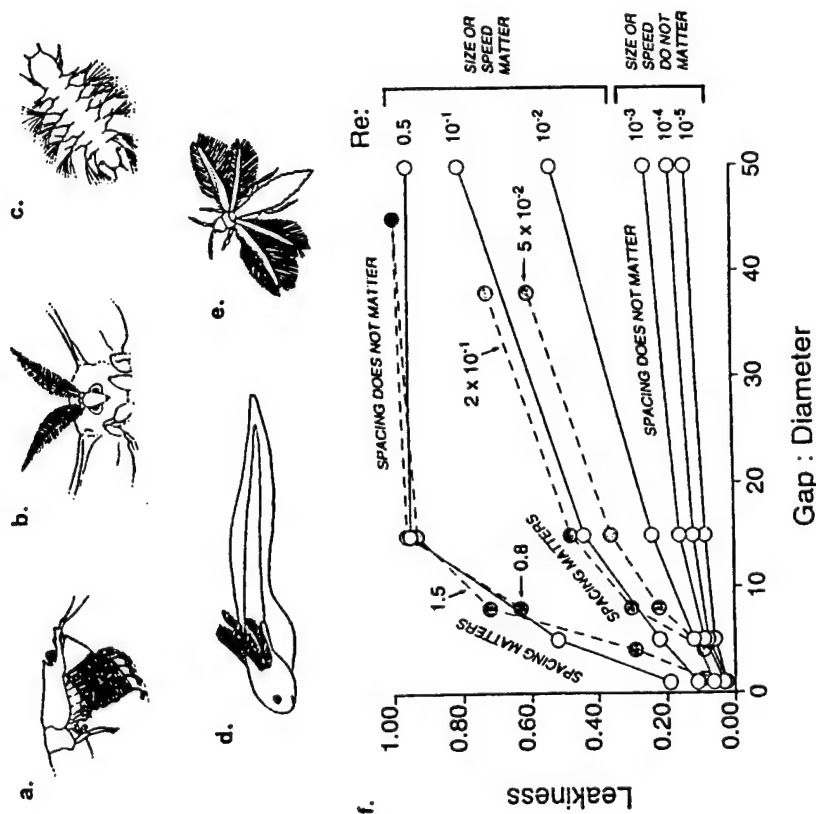


Figure 2 Examples of hair-bearing appendages that serve different functions: (a) suspension-feeding legs of a euphausiid, Phylum Arthropoda; (b) olfactory antenna of a male moth, Phylum Arthropoda; (c) swimming parapodia of a nereid larva, Phylum Annelida; (d) external gills of a larval African lungfish, Phylum Chordata; wings of a thrips, Phylum Arthropoda. (e) Plot of leakiness (volume of fluid flowing through the gap between adjacent hairs divided by the volume of fluid that would flow through a space of that width if the hairs were not there) as a function of gap:diameter ratio of neighboring hairs. Open circles and solid lines represent leakiness calculated using the model of Cheer & Koehl (30). Grey circles and dashed lines represent leakiness measured during towing experiments with comb-like physical models of Hansen & Tiselius (78). Each line represents a different Re , as indicated by the numbers near the lines. [Redrawn from Figures 1 and 3 in (119)].

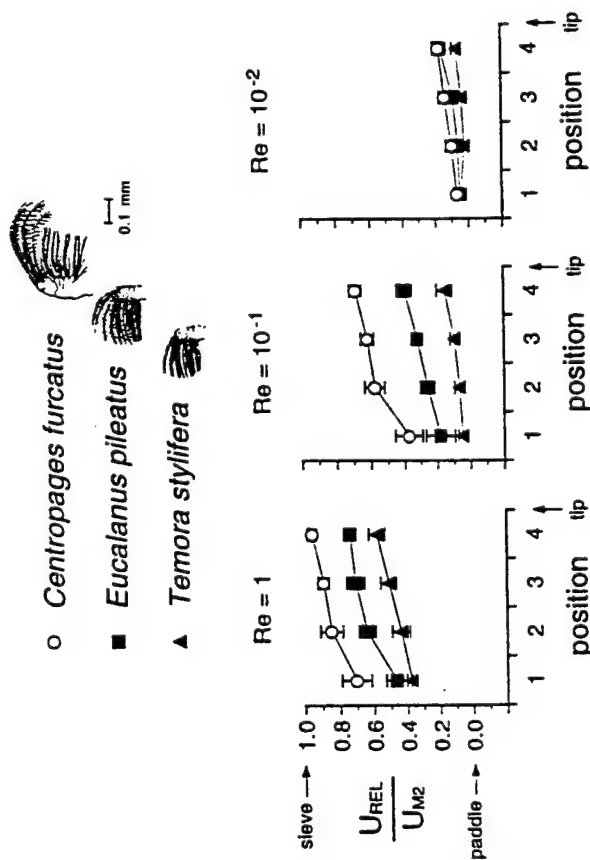


Figure 3 Fluid movement through dynamically scaled physical models of the M2's (pictured at the top) of *C. furcatus* (open circles), *E. pileatus* (grey squares), and *T. stylifera* (black triangles). The mean values of U_{REL}/U_{M2} (where U_{REL} is the absolute value of the fluid velocity relative to the M2, and U_{M2} is the velocity of the M2) for each section along the length of the model (section 1 near base, 4 near tip) are plotted for models run at a Re of 1 (left graph), 10^{-1} (middle graph), and 10^{-2} (right graph). Error bars indicate one standard deviation ($N = 3$ to 12). The lower the value of U_{REL}/U_{M2} , the less leaky (i.e. the more paddle-like) the M2. Note that the coarseness of the mesh of the M2's affects leakiness at Re 's of 1 and 10^{-1} , but not at 10^{-2} . *C. furcatus* operate their M2's at $Re \approx 1$ (at which the M2's are sieve-like), *T. stylifera* at $Re \approx 10^{-2}$ (at which the M2's are paddle-like), and *E. pileatus* at $Re \approx 10^{-2}$ to 10^{-1} (a range in which the M2 leakiness varies). (Redrawn from Figure 14 in 119).

rules (118, 119). Copepods capture single-celled algae by flinging apart their pair of M2's and then squeezing them back together (114). Some species (e.g. *Centropage typicus*) that have coarsely meshed M2's, whose setae (hairs) operate at $Re \approx 1$, have leaky M2's and filter their food from the water during the squeeze; in contrast, other species (e.g. *Temora stylifera*) that have finely meshed, slowly moving M2's, whose setae operate at $Re \approx 10^{-2}$, have paddle-like M2's that capture food by drawing a parcel of water containing an algal cell toward the mouth during the fling. Thus, even though their M2 feeding motions look qualitatively similar, the physical mechanisms by which these two copepods capture food are different because they operate at Re 's above

and below the transition from paddle to sieve. Some copepods (e.g. *Eucalanus pileatus*) are plastic in their behavior and can switch their M2 speed, and thus leakiness, for different functions; note that only organisms operating in this transitional Re range can alter their leakiness by this means.

Thus, quantitative study of mechanism has revealed the conditions under which permission exists for morphological diversity of hairy appendages with little consequence to performance, versus conditions under which simple changes in hair speed, size, or spacing can lead to novel physical mechanisms of operation.

Effects of Body Shape and Texture on Fluid Dynamic Drag

Drag is the hydrodynamic force tending to push a body in the direction of fluid movement relative to the body (explained in e.g. 25, 40, 113, 226), hence drag tends to dislodge sessile organisms and to resist the motion of swimming, flying, and sinking creatures. At low Re 's, drag is due to skin friction (the viscous resistance of the fluid in the boundary layer around the body to being sheared as the fluid moves past the body), so greater wetted area leads to higher friction. At high Re 's drag is due to skin friction plus form drag (the pressure difference across the body due to the formation of a wake on the downstream side of the body). The bigger the wake, the higher the form drag; hence any morphological feature that moves the flow separation point (i.e. the place the wake starts to form) rearward along a body reduces drag at high Re . The drag coefficient (C_D) is a dimensionless measure of the drag-inducing effect of body shape.

Streamlining (putting a long, tapered end on the downstream side of a body) is one familiar way to reduce form drag, although the increased area raises skin friction. For large, fast organisms operating at high Re , streamlining reduces the net drag, but for small, slow organisms at low Re , streamlining increases the drag. For example, C_D 's of globose ammonoid shells are lower than C_D 's of flat, streamlined shells at $Re < 100$, but the reverse is true for larger shells at higher Re (95). Similarly, drag on small ($Re = 1$ to 10) benthic stream invertebrates is lowered if their shape becomes more hemispherical, but is lowered on larger animals ($Re = 1000$) if they become more flattened (216). Nonetheless, most lotic invertebrates do not change shape as they grow, having streamlined profiles even when small (215). However, even though streamlining doesn't work when small stream insects are exposed to slow currents, flat body shapes do reduce hydrodynamic-resistance to their higher- Re escape maneuvers (34). For animals like these insects that can cross a Re transition by changing their speed, the Re of the activity that has the greatest impact on fitness (e.g. escape) appears to be the Re for which the body shape is drag-reducing.

Another morphological feature that has different effects on drag at different Re 's is surface roughness (25, 109, 223, 226) (Figure 4). As the Re of a

bluff body increases (i.e. as a nonstreamlined organism grows or moves more rapidly), C_D drops when flow in the boundary layer along the body's surface suddenly becomes turbulent and carries the separation point rearward, producing a smaller wake and lower form drag. At Re 's below point A in Figure 4, surface texture is buried in the boundary layer and has no effect on drag, whereas at very high Re 's surface bumps can protrude through the boundary layer and increase skin friction drag. However, surface roughness can trip the boundary layer to go turbulent at a lower Re than for a smooth body. Thus, there is a range of Re 's (between A and B, Figure 4) in which a bumpy surface reduces drag on a bluff body. The shape of an organism's body affects whether or not this drag-reducing effect of bumpy skin occurs: Net drag on streamlined bodies is simply increased by surface texture once the critical Re is reached (A, Figure 4). The verrucae on sea anemones do not affect drag because the animals' Re 's are below the transition Re (109). In contrast, tubercles increase

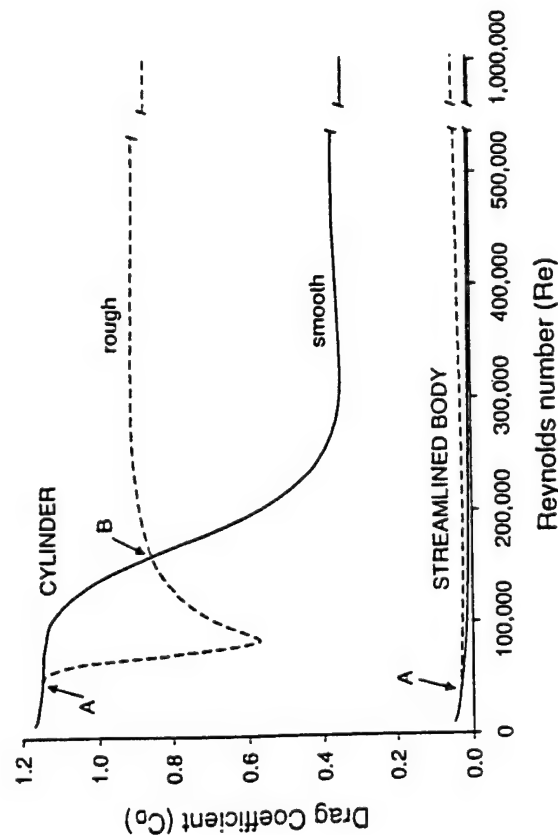


Figure 4 Plot of drag coefficient ($C_D = 2D/(\rho S U^2)$, where D = drag, ρ = fluid density, S = plan area of body, U = fluid velocity relative to body) as a function of Reynolds number ($Re = \rho U L / \mu$, where L = linear dimension of body, μ = dynamic viscosity of fluid) for a cylinder at right angles to the flow, and for a streamlined body (note that both axes of graph are log scales). The solid lines indicate bodies with smooth surfaces, and the dashed lines indicate bodies with rough surfaces. A indicates the onset of turbulence in the boundary layer, and B indicates the point beyond which roughness increases drag on the cylinder. (Redrawn using data digitized from Figure 5.8 in 226).

the drag on a swordfish's high- Re sword, but induce a turbulent boundary layer over the fish's body such that net drag on the whole fish is reduced (25, 223).

Both the examples described above (leakiness of hair-bearing appendages and drag on bodies) involve structures moving relative to the surrounding air or water, and both illustrate that the performance consequences of particular morphological characters depend on Re . I now discuss in more general terms the categories of nonintuitive effects of morphology on performance that we should keep in mind when using morphological data to address ecological or evolutionary questions.

Morphology Does Not Affect Performance

When the morphology of a structure does not affect the performance of some function, there is permission for diversity of form and for assumption of other functions.

MORPHOLOGICAL FEATURES THAT HAVE LITTLE EFFECT ON PERFORMANCE Denny (42) found that lift is more important than drag in removing limpets from the substratum; thus features affecting only drag do not influence limpet performance at resisting ambient flow. Limpets show high diversity in the shell characters that affect drag.

Organisms that swim by flapping appendages at high Re can generate thrust to propel the body by using either drag or lift on the appendages. Vogel (226) noted that appendage shape has a big influence on lift-based swimming performance but makes little difference to drag-based propulsion, and he thus predicted that multifunctional appendages should use drag to generate thrust. Indeed, the walking appendages of polychaetes, ducks, muskrats, and freshwater turtles all use drag-based propulsion during swimming, whereas the lift-based flippers of sea turtles serve poorly as walking legs.

In some cases only part of a structure is critical to performance, so there is permission for diversity of form of the noncritical regions of the structure. For example, the morphology of the petiole and basal lobes of a tree leaf determine how easily it rolls up in the wind, but the diversity of form of the rest of the leaf does not affect performance of this drag-reducing rolling (225, 226). Butterflies bask in the sun to warm up, using their wings as solar panels. Dark wings absorb more heat, but since most of the heat transferred to the body comes from the basal region of a wing, there is permission for the rest of the wing to sport defensive or cryptic color patterns without interfering with thermoregulatory ability (235). At Re 's where surface roughness affects drag, bumps on the anterior and widest regions of a body are very important to drag, whereas texture on the posterior region of a body makes little difference (25).

PERMISSION FOR DIVERSITY OF MORPHOLOGY AND KINEMATICS AT SMALL SIZE As mentioned above, skeletal structures should be insensitive to structural variation at small size. Indeed, there is variability in the ossification of bones (i.e. in their material stiffness—35; in very small salamanders—77). Similarly, the tiny stalks of the fruiting bodies of cellular slime molds show simple geometric scaling, in contrast to large biological columns (e.g. tree trunks, leg bones) that as they grow must become disproportionately wide relative to their length to support body weight (22, 154).

There are also biofluiddynamic functions whose performance is insensitive to morphology or kinematics at small size, such as the hair-spacing and surface roughness examples described above. Many small free-swimming organisms create feeding currents past themselves by flapping appendages. Calculation of the scanning currents produced by different types of appendage motions shows that for each technique, the energy cost per volume of water scanned changes very little if animals depart from optimal appendage kinematics (although which scanning technique is most efficient depends on the size of an animal's target zone—the distance at which it can perceive and capture prey) (31).

Another example of permission for kinematic diversity at small size is provided by basilisk lizards, which run on the surface of water (66, 67). The force to support the lizard's body during this sort of locomotion is provided by an upward impulse as the foot slaps onto the water surface, followed by an upward impulse as the foot strokes down into the water. Comparison of water-surface running by basilisks of different sizes revealed that small animals, which have the capacity to generate a large force surplus relative to their body weight, varied their kinematics considerably without performance consequences, whereas larger animals, which can generate barely enough force to support their weight, were constrained to a narrow range of leg and foot motions to run successfully on water. Indeed, in the field juveniles often run on water simply to move to another sunning spot, whereas adults venture onto the water only under duress.

Small Changes in Morphology or Simple Changes in Size Lead to Novel Functions

We should expect transitions in hydrodynamic or aerodynamic function as organisms grow or clades evolve through different Re ranges. Examples of such transitions were described above for the leakiness of hairy appendages and the drag on streamlined or rough bodies. Other examples can be found in ontogenetic studies of swimming. For instance, as brine shrimp larvae get bigger, even though the flapping motion of their appendages does not change, their propulsive mechanism switches from drag-based rowing at low Re to inertial swimming at higher Re (241, 242). Similarly, larval fish switch from drag-

based swimming at low Re to inertial propulsion when they grow to higher Re (14, 176), and intermittent swimming becomes more energetically advantageous as the importance of viscous force declines at higher Re (237). Another example is provided by scallops, which swim by jet propulsion by squirting water out of the mantle cavity while clapping their shells together. Very small juvenile scallops cannot use this inertial mode of locomotion effectively and are sedentary; larger scallops can jet, and once at $Re > 3000$, they can also use lift to get up off the substratum; however, when very large they become poor swimmers again, as their shells grow too heavy relative to the thrust they can generate (36, 147).

Functional transitions accompanying size changes can also be found for organisms moving through air. For example, wing shapes that optimize gliding performance of plant seeds or animals depend on Re: short, wide wings are better at small size, whereas long, narrow wings enhance gliding at large size (51). An example of how isometric size changes in the absence of shape changes have the potential to generate novel functions is provided by the experiments of Kingsolver & Koehl (105, 107) that tested the aerodynamic and thermoregulatory consequences of changes in the length of protowings on models of fossil insects. At small body size, short thoracic protowings can improve thermoregulatory performance, although they have negligible effect on aerodynamic gliding, parachuting, or turning performance; in contrast, protowings of the same relative length on a larger insect can improve aerodynamic performance. This illustrates that it is physically possible for a simple increase in body size to cause a novel function (i.e. a solar panel can become a wing) without requiring the invention of a novel structure. (However, whether protowings served these aerodynamic or thermoregulatory roles in early insects is just as speculative as other feasible hypotheses, like sexual signaling, gas exchange, or skimming along the surface of a body of water.)

Another example of a functional switch accompanying a simple continuous change in morphology is provided by the chitinous exoskeleton (perisarc) of hydroid colonies (92) (Figure 5a). If bent too far, perisarc kinks like a beer can, damaging the tissue inside (Figure 5b). Perisarc, which has annulated regions and internodes, is thickened with time. Tissue damage from kinking is worse in annulated regions than internodes when perisarc is thin near the growing tips of colonies, but as the perisarc is thickened, these roles reverse and the annulated regions provide protection from damage when the colony is subjected to large bends (Figure 5c,d).

Dimensionless numbers, such as Re, that express the relative importance of various physical factors affecting a process, can provide us with hints of other places to look for functional shifts. For example, Froude number (gravity

relative to inertia) is a good predictor of gait changes in pedestrian locomotion (e.g. 5), while reduced frequency (accelerational relative to steady-state flow) indicates the importance of nonsteady-state mechanisms of generating lift and thrust in swimming or flying (e.g. 37), and Péclet number (fluid convection relative to molecular diffusion) indicates the importance of bulk air or water movement in getting molecules to the surface of a collecting device such as a gill or olfactory antenna (120).

Effects of a Morphological Trait Depend on Other Characteristics of an Organism's Body

Single traits should not be studied in isolation (68), not only because multiple traits can affect a particular aspect of performance (e.g. 4), but also because both the magnitude and direction of the performance consequences of a particular morphological change can depend on other aspects of an organism's structure.

An example of the interactive effect of several traits on performance is provided by flying frogs, tree frogs that glide through the forest canopy and that have a unique suite of derived morphological characters, including enlarged hands and feet. An aerodynamic study using physical models of flying and nonflying frogs on which such characters could be modified one at a time revealed that the effects of the flyer traits on aerodynamic performance were nonadditive (48). For example, all the flyer traits occurring together improved turning performance significantly more than expected from the sum of their individual effects. However, for certain aspects of aerodynamic performance, the effect of the co-occurrence of flyer traits depended on body size: Gliding performance was improved more than expected only for small frogs, whereas parachuting performance was improved less than expected only for large frogs.

Performance of a structure at one level of organization can depend on morphology at another level of organization. In the following examples, the deformability of a structure (which depends on tissue microarchitecture and molecular composition—e.g. 224, 230) can affect the consequences of variation in gross morphology. While Lauder (132) has proposed a phylogenetic method to examine the independence of different levels of organization during evolution, mechanistic studies like those cited below reveal the physical reasons that performance depends on the interaction of different levels of structure.

Flexible sessile organisms experience lower drag forces than do rigid ones of the same shape because the deformable organisms are passively blown into more streamlined shapes (e.g. 109, 115, 225, 226). Flexibility also determines whether or not body shape even affects flow forces. Because of passive streamlining, the drag coefficients of various species of floppy intertidal algae are similar when water velocities are high enough to cause damage, even though

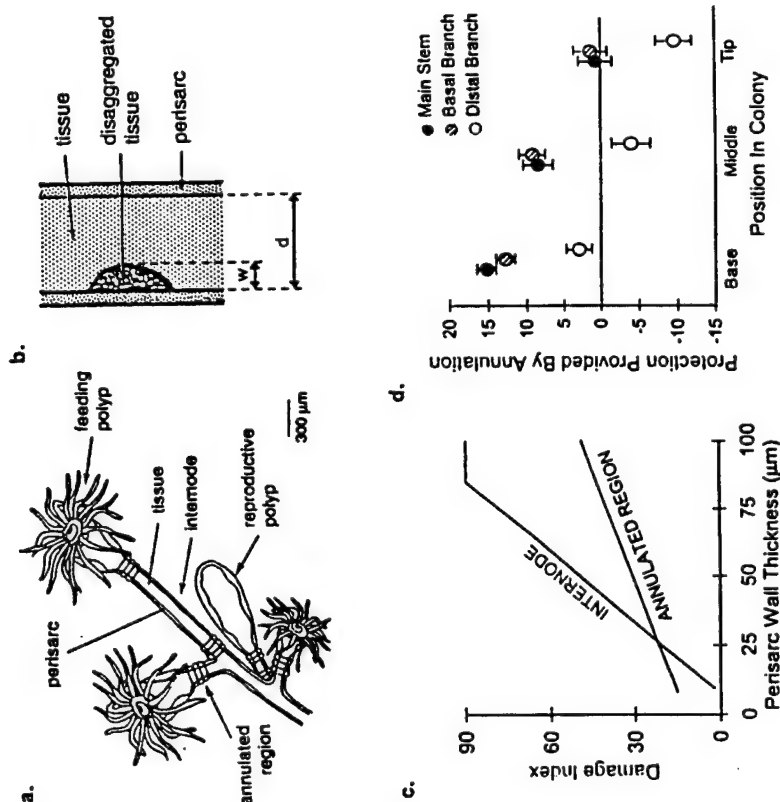


Figure 5 Perisarc of the hydroid *Obelia longissima*: (a) Diagram of the tip of a branch of a colony, showing the annulated and internode regions of the perisarc. (b) Diagram of the tissue damage (disaggregated tissue) caused by perisarc kinking when bent (w = width of damaged tissue, d = diameter of tissue inside the perisarc). (c) Damage index ($\arcsin w/d$), plotted as a function of perisarc wall thickness for internode and annulated regions. The internode line levels off at a damage index of 90, indicating complete tissue damage. [Redrawn by digitizing the regression lines in Figure 7, Chapter 1, of (92).] (d) Index of protection from damage (a measure of the protection of soft tissue afforded by the presence of annulations in the perisarc, given by the difference between tissue damage in the internode region and tissue damage in the annulated region) for different regions of hydroid colonies. Error bars = 95% confidence intervals (n = 93 per group). Positive values indicate that annulations protect from damage, whereas negative values indicate that annulations make damage worse. [Redrawn using data digitized from Figure 8, Chapter 1, of (92).]

they have very different shapes (28). In contrast, blade shape does affect drag for the less flexible blades of bull kelp (121). Denny (42) has suggested that once a lineage has become sufficiently flexible, shape may be removed from further selection by drag.

Flexibility can also determine the consequences of growth for organisms of a given shape, as illustrated by model studies of planar sessile organisms (122). If a planar rigid organism (e.g. a platy hydrocoral) lengthens in a wave-swept habitat, the hydrodynamic force it bears rises, whereas if a very flexible organism lengthens (e.g. a floppy alga that can move back and forth with the flow), the force on its holdfast remains low (Figure 6). However, a flexible organism in waves must grow to a critical size before it can benefit from "going with the flow": A floppy creature can move with the flow only until it reaches the end of its tether, at which point the water moves past it and it must bear the hydrodynamic force (115). Thus, algae that are short relative to the distance the water travels in a wave before it reverses direction do experience an increase in force as they grow (64). Furthermore, an organism of intermediate flexural stiffness can deflect enough to move with the flow only after the organism has become sufficiently long (deflection of a cantilever $\propto \text{length}^3$), so as it grows, the force rises, then plateaus, and then decreases (Figure 6). Flexibility also determines which sort of flow habitat is most mechanically stressful: For rigid organisms, waves produce larger forces than do unidirectional currents of the

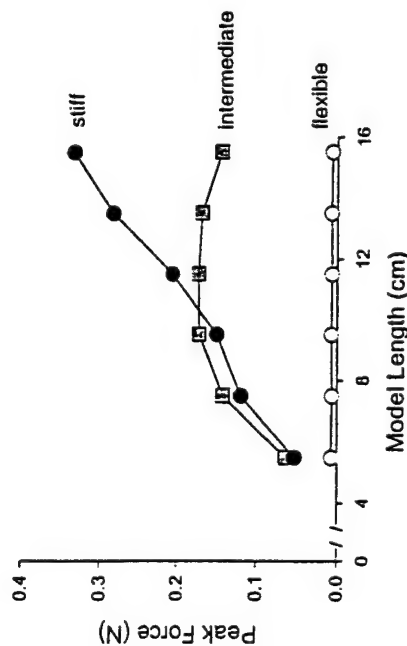


Figure 6 Peak hydrodynamic force measured on models of planar benthic organisms of different stiffnesses exposed to oscillatory flow in a wave tank, plotted as a function of model length. Error bars, which represent 95% confidence intervals ($n = 5$ per point), are smaller than the symbols used on the graph. The models maintained constant width and thickness as they "grew" (M Koehl, T Hunter, and J Jett, unpublished data).

same peak velocity, whereas the opposite is true for flexible organisms (122). Another example of the consequences of flexibility is provided by protozoans that locomote by undulating flagella that bear hairs (mastigonemes). Both fluid dynamical analysis (52) and observations of swimming protozoans (86) show that when mastigonemes are stiff, protozoans swim in the same direction as the direction of wave propagation along the flagellum, whereas when mastigonemes are flexible, the organisms swim in the opposite direction (as do protozoans without mastigonemes).

Effects of a Morphological Trait Depend on Habitat

The performance of an organism is meaningful only in the context of the environment in which the organism lives (e.g. 63, 74, 109). The following examples illustrate not only that changes in habitat can have profound effects on performance, but also that the consequences of a morphological modification can depend on the environment.

One environmental variable whose effect on performance has received much attention from biologists is temperature. Temperature is perhaps the most commonly used abscissa on graphs in physiology books, and the effects of temperature on important biological and ecological processes such as locomotor performance, predator-prey interactions and foraging strategies, development rate and life history patterns, and habitat use are well documented (e.g. 32, 63, 81, 82, 87, 90, 189–191). Other more subtle effects of temperature on mechanical performance include changes in the mechanical properties (such as stiffness, resilience, strength, and toughness) of biological tissues (e.g. 110, 112, 224, 230), and a shift in the Reynolds number of aquatic organisms [due to changes in kinematic viscosity, which nearly doubles between 0° and 20°C, as well as to changes in the rate of movement of some species (e.g. 187, 188, 215, 226, 245)]. Therefore, the body speeds and sizes at which Reynolds number-dependent functional shifts occur depend on habitat temperature. Obviously the temperature changes that accompany diurnal and seasonal cycles, climate shifts, microhabitat changes, and species range extensions can have profound effects on the performance of organisms with given morphologies.

Another obvious feature of the physical environment that can have enormous mechanical and physiological consequences is whether an organism is surrounded by air or water. The transition between aquatic and terrestrial habitats has been made in the evolution of many lineages. This transition between water and air is also made during the ontogeny of some species (e.g. with aquatic larvae and terrestrial adults) and is made daily by intertidal organisms and by animals that locomote between the two habitats (e.g. littoral crabs, diving birds). The consequences to performance of moving between these two media are reviewed by Denny (41) and Vogel (226).

Benthic marine organisms are exposed to unidirectional currents at some sites, but to waves (oscillatory flow with high accelerations) at others. The morphology of a spawning animal in waves does not affect gamete dispersal (123), although it does in gentler unidirectional flow (221). Similarly, streamlining works only if flow direction can be predicted, and hence it is ineffective at wavy sites (42, 109). Furthermore, the consequences of growth to a stiff organism's risk of dislodgment by hydrodynamic forces are different in the two types of habitats. The attachment strength of a sessile organism depends on holdfast or foot area ($\propto L^2$), and the drag and lift it must withstand in unidirectional flow depends on plan area ($\propto L^2$), whereas the acceleration reaction force in waves depends on body volume ($\propto L^3$) (e.g. 40, 109). Therefore, wave-swept organisms have a physical constraint on body size not experienced by creatures in steady currents (43).

Flow conditions in the environment affect the feeding performance of many aquatic animals that make their living by filtering small organisms and particles from the surrounding water. For example, ambient flow velocity affects not only the volume of water per time that a passive benthic suspension feeder can process for food and the amount of particulate material stirred up in the water (e.g. 171), but the velocity also determines the efficiency (proportion of encountered particles that are captured) and the size-selectivity of a filter of a given morphology (e.g. 204, 209). In addition, the turbulence (random fluctuations in velocity) of the flow can alter feeding performance of both planktonic (e.g. 151, 203, 210) and benthic (e.g. 183) suspension feeders. However, whether turbulence enhances or inhibits feeding rate depends on the morphology, swimming mode, and physical capture mechanism(s) used by an organism (209, 210).

An organism's performance can depend on the morphology of its neighbors. For example, the structure of canopies of terrestrial plants, or of aquatic sessile animals or macrophytes, affects the microclimate that they and the other organisms living among them encounter, often buffering them from fluctuations and extremes in environmental conditions (e.g. 56, 109, 115, 121, 157, 244). Similarly, the arrangement of individuals in aggregations of sessile benthic invertebrates, such as tubicolous phoronids and polychaetes, can affect the feeding and spawning performance of individuals within the aggregation (100, 101, 220, 221). Whether neighbors improve or harm the performance of a benthic animal depends on morphology. For example, the feeding performance of encrusting bryozoans is enhanced by upstream neighbors (but only if ambient flow is fast), whereas that of arborescent forms is reduced (172–174). Furthermore, physical constraints on organisms in aggregations can sometimes be different from those on solitary individuals: e.g. sea palm kelp in dense stands

can support their crowns of blades on slimmer, taller stipes without buckling because they lean on their neighbors (85).

Another example of how habitat can alter the effect of a morphological feature on performance is provided by arboreal lizards. The effect of leg length on sprint speed depends on the diameter of the branch on which an animal runs (145).

Consequences of Behavior Depend on Morphology

I define behavior as an action taken by an organism, ranging from simple kinematics or assumption of a posture to complex interactions with other organisms. The consequences of a particular behavior can depend on the morphology of the organism. For example, the flying frogs described above take on a characteristic posture when airborne, with knees pulled forward and feet spread out laterally. Emerson & Koehl (47) discovered via model experiments that when frogs assume the flying posture, parachuting performance of the flyer morph improves whereas that of the nonflyer morph worsens; gliding performance worsens much more for the nonflyer than the flyer, and only turning performance improves for both morphs. Another example is provided by copepods (119): Although *E. pileatus* can alter the leakiness of their M2's by changing speed (from $Re \simeq 10^{-2}$ to $Re \simeq 10^{-1}$), if *T. stylifera* changed the speed of their more finely meshed M2's over the same Re range, leakiness would not change (Figure 2).

Functional Equivalency: "There's More Than One Way to Skin A Cat"

Evolutionary biologists (e.g. 58, 152) and ecologists (e.g. 219) have recognized that organisms can play the same role in a variety of ways. Studies of natural history and behavior reveal how different organisms perform the same task. For example, several taxa of lizards have the ability to dive into sand but utilize different techniques that involve distinct exaptations in each case (6); three species of snakes eat whiptail lizards, but use different methods to capture them (73); and a variety of mechanisms can play the same role in predator defense (50).

Biomechanical studies elucidate the physical principles underlying how different structures can serve the same mechanical function. For example, many animals in different phyla reinforce their soft tissues with mineral inclusions (e.g. spicules, sclerites, ossicles) whose bizarre shapes are so specific that they are used as taxonomic characters. Analysis of the mechanics of spicule-reinforced tissues as filled-polymer composite materials revealed that the stiffening effect of spicules depends on the surface area of the spicule-tissue interaction, but that the particular combination of spicule sizes, shapes, and numbers

used to produce that surface area in a volume of tissue matters little to performance (112). Many other examples of functional equivalency can be found by considering the flexural stiffness (resistance to bending, EI) or torsional stiffness (resistance to twisting, τJ) of organisms. Both depend on the product of the elastic modulus (resistance to deformation, E in tension or τ in shear) of the tissues from which a structure is made, and to I or J, shape properties of the structure (proportional to radius⁴) (e.g. 230). Thus, organisms can produce a flexible structure via the microarchitecture of their tissues or via the gross morphology of cross-sectional shape. Simple examples of both can be found among cnidarians: Flexible joints in some sea fans occur at regions of lower E (due to sclerite microarchitecture of the tissue) (162), whereas the bending joints in sea anemones (e.g. 111) and the torsional joints in sea pens (18) are due solely to local reductions in I or J.

Another example of functional equivalency is provided by the phenotypic plasticity of giant bull kelp in different water-flow habitats. As they grow, the kelp maintain the same ratio of stress (force per cross-sectional area) required to break the stipe (stem) to stress imposed on the stipe by hydrodynamic forces; they can do so by altering a variety of morphological traits: blade shape (affecting drag), stipe diameter (affecting stress), or stipe material properties (affecting strength) (102).

Summary: Nonlinear Context-Dependent Effects of Morphology on Performance

When does the morphology of an organism affect its performance? For structures that perform mechanical functions (e.g. skeletal support, locomotion, food capture), the relationships between morphological dimensions and measures of performance can be quantified using physical principles. Although many biomechanical studies have shown how particular aspects of performance are affected by defined changes in morphology, others have revealed cases in which changes in form can occur without performance consequences. Quantitative mechanistic studies of how function depends on form have also produced some intriguing surprises. For example, in some cases small changes in morphology or simple changes in size can lead to novel functions. Furthermore, the effect of a specific change in morphology can depend on the size, shape, stiffness, or habitat of an organism. Likewise, a particular change in posture or behavior can produce opposite effects when performed by bodies with different morphologies.

What implications do these findings have for ecologists and evolutionary biologists? I devote the rest of this review to pointing out ways in which quantitative mechanistic organismal-level research can be a useful tool in the arsenal of approaches for attacking ecological and evolutionary questions. I

mention misconceptions that can arise by ignoring mechanism, but I also point out limitations of the mechanistic approach.

WHY SHOULD ECOLOGISTS CARE ABOUT THE MECHANISMS BY WHICH MORPHOLOGY AFFECTS PERFORMANCE?

Mechanistic Versus Phenomenological Approaches

Why should ecologists worry about how individual organisms work when they are studying populations, communities, or ecosystems? Both quantitative empirical studies and mathematical models of ecological processes can use either a phenomenological or a mechanistic approach (see historical review in 180). If we focus on phenomenological analysis of a population, community, or ecosystem, we are concerned *that* organisms perform certain processes (e.g. consume certain prey, overgrow neighbors, migrate, produce offspring) at defined rates, rather than worrying about the details of *how* they perform these activities. In contrast, mechanistic studies assume that particular processes at the organismal level are important in governing the behavior of a system at a larger level of organization, such as a population, community, or ecosystem. The pros and cons of phenomenological versus mechanistic approaches are reviewed in (116, 138, 194, 200, 206). Phenomenological models can be powerful tools for making short-term predictions about systems for which descriptive data are available. Although mechanistic models generally do not fit the data as well as phenomenological models and may be complicated and slow to provide answers, the development of mechanistic models can lead to an understanding of how a system works. A number of examples of how mechanistic studies have provided ecological insights are reviewed in (194, 206).

Organismal-level mechanistic information about how performance depends on morphology not only can reveal limitations to the interpretation of phenomenological data, they can also provide insights about the mechanisms underlying ecological processes.

Morphology as a Tool to Infer Function or Ecological Role: Usefulness and Problems of this Phenomenological Approach

BACKGROUND One common type of ecomorphological study is the statistical description of patterns of distribution of morphologies with aspects of the environment, community structure, or ecological roles organisms play (reviewed by 198, 199, 207). Such studies do not directly assess the functional meaning of morphological variables, but rather they assume that the ecological characteristics of a species can be inferred from its morphology (198). These

descriptive studies are an effective way to reveal patterns that can guide further mechanistic research and that can aid in interpretation of fossil communities or poorly studied recent communities, but they are limited in their ability to establish cause and effect (88). The dangers of making spurious conclusions about causes using statistical tests based on descriptive models have been reviewed in 96.

IMPORTANCE OF MECHANISTIC INFORMATION The examples described above of the many ways in which the relationship between morphology and function can be surprising and complex should caution us against expecting simple correlations between structure and function to yield reliable predictions of performance. However, mechanistic studies can yield quantitative expressions of the basic physical rules governing how a type of biological structure operates. Such mechanistic equations can be powerful tools for predicting the effects of specific morphological parameters on defined aspects of function, even in cases where the effects are nonlinear and context-dependent.

Although there are certainly instances when the function of an organism has been inferred successfully from its structure alone (reviewed in 133, 228), many other cases exemplify the problems of trying to read function from morphology without the aid of mechanistic information (discussed by 59, 68). Anyone trying to infer function from morphology should be aware of the following potential problems when descriptive statistical studies are done without mechanistic analysis:

1. Statistical analyses may not reveal a connection between structure and function in cases for which the effects of morphology on performance are nonlinear, or for which different mechanisms can play similar roles, as illustrated by the examples described above.
2. Statistical studies can also fail to reveal a mechanistic relationship between a structural feature and performance if the feature studied is only one of several that affects the performance (4). For example, the adhesive force holding a tree frog to a surface is proportional to toepad area, but measures of angles of surfaces at which frogs slipped off (sticking performance) did not correlate with toepad area because sticking performance is also inversely related to a frog's weight (44). Similarly, frog leg length did not correlate with jumping distance (45), and fish streamlining did not correlate with swimming speed, because both aspects of performance also depend on muscle mass, arrangement, and power output (4).
3. Statistical studies can find correlations between morphological features and performance or fitness that are not causally related when other correlated

but unmeasured morphological variables are responsible for the performance differences assessed (7, 88, 96, 133, 134).

4. Greene (72), who found that morphology was a poor predictor of lizard diets, stressed the importance of the ecological context in which an organism operates. For example, function is difficult to infer from morphology when information is lacking about the trade-offs to which a structure is subjected if it serves more than one role (133). Furthermore, we may waste time correlating unimportant aspects of performance to morphological characters if we do not base our studies on natural history observations of what organisms actually do in the field (e.g. 73) and on quantification of physical conditions actually encountered by organisms in nature (e.g. 40, 42, 102, 109, 113, 190).

Organismal Mechanistic Studies Shed Light on Ecological Questions

BACKGROUND Processes acting at the level of individual organisms can determine the properties of populations, communities, and ecosystems (reviewed by 116, 198), hence the effects of morphology on performance can have important ecological consequences (e.g. 7, 16, 44, 53, 88, 206, 232). For example, biomechanical analyses reveal the mechanisms responsible for differences in susceptibility of intertidal organisms of various morphologies to removal by waves (e.g. 40, 42, 43, 109, 110, 113, 115, 124); such wave-induced disturbance is important in determining the structure of intertidal communities (e.g. 180, 181, 213). Biophysical analyses of heat and water exchange between animals and the environment reveal where and when particular species can be active, and hence such analyses point out morphological constraints on habitat use, on ecological interactions such as competition or predation (e.g. 71, 81, 82, 189–191), and on reproductive strategies (e.g. 103). Similarly, flight aerodynamics provides a mechanistic explanation for the patterns of foraging and competition by hummingbirds living at different altitudes (55), and of foraging and habitat use by bats of different morphologies (170), while swimming hydrodynamics and head biomechanics do so for fish (e.g. reviewed by 228, 236). Likewise, biophysical studies reveal physical constraints on the distribution and ecological interactions of plants of different morphologies (e.g. 166, 169). Mechanistic studies such as these also enhance theoretical ecology by elucidating factors that can be ignored versus those that must be included in mechanistic ecological models, by testing the assumptions of such models, and by providing realistic values for parameters used in model calculations (88, 116).

INSIGHTS PROVIDED BY RECOGNITION OF NONLINEAR, CONTEXT-DEPENDENT EFFECTS OF MORPHOLOGY ON PERFORMANCE Although the literature abounds with examples of how ecological studies are enriched by information about how organisms function, the nonlinear context-dependent effects of morphology on performance reviewed here may be especially useful in providing insights in the developing area of "context-dependent ecology." Evidence is accumulating (193, 219) that the ecological role played by a particular species, as well as its impact on community structure and ecosystem dynamics, depends on the ecological context (e.g. physical conditions, time since disturbance, ecosystem productivity).

Keystone species (e.g. 155, 156, 178), now defined as those species whose impact on a community or ecosystem is disproportionately large relative to their abundance or biomass (193), may not be dominant controlling agents in all parts of their range or at all times in the succession of a community (examples tabulated in 193). By weaving together organismal-level studies of how habitat affects performance with data about the ecological patterns characterizing situations in which a sometimes-keystone species does play a significant role, we may reveal the mechanisms responsible for the context-dependency of its importance. Although such studies have not, to my knowledge, been conducted yet, an example can be pieced together using information in the literature. Biomechanical analyses reveal that kelp with weak, deformable tissues can resist breakage by stretching like extensible shock absorbers when hit by waves. A context-dependent performance consequence of this mechanism (which depends on the microarchitecture of the tissue) is that such kelp are generally quite tough but can break easily if the long-duration waves that accompany storms stretch them beyond their limit (113, 114). A storm can clear an area of kelp when broken plants become entangled with their neighbors, which then also break (114, 124). An ecological study of the role of sea urchins in benthic communities showed that these animals are keystone grazers that control community composition in areas where kelp are absent, but not where kelp are present and they have plenty of drift algae to eat; storms can cause a community to convert from a kelp bed to a "barrens" controlled by urchin grazing (79). Thus, information about the organismal-level mechanical performance of kelp can shed light on the issue of when sea urchins are keystone species.

Functional groups (e.g. 218, 219) are suites of species that play equivalent roles in an ecosystem. Understanding the mechanisms responsible for functional equivalency at the organismal level may help us identify the circumstances under which one species can play the same ecological role as another. Again, an example can be pieced together from published studies about the convergence

of ecological roles played by mussels (*Mytilus californianus*) on wave-swept rocky shores in Washington state and tunicates (*Pyura praeputialis*) in similar habitats in Chile (182). Both species are competitive dominants that can form mat-like monocultures of individuals attached to each other; interstices in these mats provide protected habitats for an assemblage of small organisms. The formation of holes ("patches") in these mats of competitive dominants is an important process affecting the diversity of the rocky shore community by providing space on the substratum to sessile species that would otherwise be out-competed (180, 181). A biomechanical analysis of the physical mechanisms by which patches are produced in mussel beds revealed that the same morphological features that lead to the ecological convergence of these mussels and tunicates also are responsible for patch initiation. The pressure difference between the slowly moving water in the interstices below the mats and the rapidly moving water in a breaking wave above the mats cause lift forces high enough to rip chunks of the mat away (39). Analysis of forces on individual mussels indicated that waves do not exert forces large enough to wash them away (39). Thus, evidence that the performance consequences of a given morphology are very different when in an aggregation than when isolated leads to this insight about why competitively dominant mat-forming intertidal species are also subject to patch formation.

Conclusions

Ecologists should care about the mechanisms by which morphology affects performance for two reasons. Knowledge of these mechanisms can reveal the limitations of interpretation of descriptive phenomenological information. Mechanistic information also can provide insights about processes affecting the structure of populations, communities, and ecosystems.

WHY SHOULD EVOLUTIONARY BIOLOGISTS CARE ABOUT THE MECHANISMS BY WHICH MORPHOLOGY AFFECTS PERFORMANCE?

Observations about the nonlinear context-dependent relationship between morphology and performance can provide insights about the evolution of biological structure to researchers using a variety of approaches: the externalists, who emphasize natural selection and the performance or fitness of different phenotypes in the environment (reviewed by 10, 229, 233); the paleontologists, who interpret fossil evidence about the history of evolution; and the internalists, who focus on the generation of form and on the ontogenetic mechanisms that might constrain phenotypic variation or produce novelty (reviewed by 10, 23, 65, 83, 161, 233).

Externalists: The Study of Adaptations

BACKGROUND Traditionally, when biologists noted correlations between particular morphological features and certain habitats or lifestyles of organisms, they referred to such features as adaptations (discussed by 20, 63). However, since Gould & Lewontin (68) harpooned this plausible-argument approach to identifying which traits are adaptations, the topic of adaptation has been contentious (144, 152). Today a morphological feature can strictly be called an adaptation only if it promotes the fitness of the organism and if it arose via natural selection for its present role (69). Although these requirements are difficult to satisfy, various research methodologies for identifying adaptations have been proposed (6–8, 16, 60, 62, 63, 73, 130, 131, 134, 136, 197, 198, 239). Many of these schemes incorporate the “morphology → performance → fitness” paradigm.

Arnold (7) formalized an emerging conceptual framework for studying the selective advantage of morphological features: The morphology of an organism can determine its performance, which in turn can affect fitness. This approach, which has become the “central paradigm in ecomorphology” (198), uses natural variation in populations to seek correlations between morphology and performance, and between performance and fitness (e.g. 7, 8, 63, 228). When this paradigm is followed, the primary goal of studying performance is to identify how morphological features interact with each other and the environment to affect fitness (45). This popular quantitative approach is a powerful tool for demonstrating natural selection in the field and for revealing patterns that suggest which morphological features might be adaptive in which ecological contexts.

IMPORTANCE OF MECHANISTIC INFORMATION The examples described above of the nonlinear ways in which morphology can affect performance illustrate that the “morphology → performance” connection can be complex and surprising. Nonetheless, many studies using the “morphology → performance → fitness” methodology have relied on statistical correlations between morphological features and performance or fitness but have not included mechanistic analyses of how the features cause the correlated effects (e.g. 11, 16, 44, 49, 61, 63, 70, 97, 98, 127, 142, 143, 198, 199, 228). Even the classic studies correlating garter snake performance with morphology (11, 97), morphology with fitness (9), and performance with fitness (98) have not been complemented by experimental studies investigating the mechanisms by which vertebral number or tail length produce differences in burst speed, or by which burst speed improves survivorship.

Because the morphology → performance → fitness methodology is descriptive rather than mechanistic, a major limitation of this approach, discussed by

Arnold (7) and others (e.g. 88, 96, 133, 134), is that unmeasured morphological variables (that correlate with those that are measured) may be responsible for the performance differences assessed, and that unmeasured aspects of performance (that correlate with those assessed) may be the actual focus of selection. In addition, we must remember the other warnings (listed in the Morphology as a Tool to Infer Function or Ecological Role section above) about misconceptions that can arise when mechanism-blind correlations are made between morphology and performance. Hence, one means by which organismal-level mechanistic studies can enhance research in evolutionary biology is by providing the information necessary to prevent such misinterpretations of correlational data.

ADAPTATION CANNOT BE INFERRED FROM EFFECTS OF MORPHOLOGY ON PERFORMANCE Both mechanistic and correlational studies that focus only on the relationship between structure and performance can be misleading when used to infer adaptation. An untested assumption underlying many such studies is that a performance advantage translates into increased fitness (discussed by 7, 15, 45). There are a number of limitations of performance testing that call this assumption into question:

1. The aspect of performance measured may not be important to the biology of the organism in nature (74, 135, 228), or may play a different role in the life of the organism than we assumed. For example, tall, slim benthic organisms made of stiff, brittle tissues are susceptible to breakage in waves (seemingly “poor” performance), but breakage can be an important mechanism of asexual reproduction and dispersal by corals with such morphologies, which can therefore thrive on wave-swept reef crests (reviewed in 113). Similarly, rapidly growing seaweeds with weak stipes and holdfasts (“poor” performance) may be as successful in habitats where they can reproduce before seasonal storms hit as are stronger kelp (“good” performance) that grow more slowly, but that survive the storms (115).
2. Most performance studies are done on adults, even though organisms change properties as they grow and environments vary with time (diurnally, seasonally, and from year to year). The examples of the size-dependent and context-dependent effects of morphology on performance cited above should make us realize the importance of assessing performance at different stages in an organism’s ontogeny. One way to deal with this problem is to devise performance measures, such as the environmental stress factor described in (102), that relate the performance of an organism at each stage of its ontogeny to the environmental conditions it encounters at that stage.

3. Lack of information on the genetic basis of the morphological or performance differences studied limits the evolutionary conclusions that can be drawn from such experiments (108).
4. Morphological features that improve performance do not necessarily arise via natural selection (discussed by e.g. 69, 83, 131). Some features may be epiphenomena of how a structure is produced (e.g. 68, 83), such as the ridges on clam shells that may improve burrowing (208), or the shapes of sea urchin skeletons that correlate with their water-flow habitats (13). Sometimes wear and tear in the environment can improve the performance of a structure. For example, pruning of kelp by limpet foraging can reduce their chances of being ripped away by storm waves (19), chipping of barnacle shells by wave-borne debris can produce more breakage-resistant shapes (186), wear of radular teeth in snails can sharpen their cutting edges (83), and passive orientation of gorgonian sea fans by hydrodynamic forces (231) can increase their suspension-feeding rates (139). Of course, the growth rules and breakage patterns described above could themselves be the result of natural selection.

Paleontologists: The Interpretation of Fossils

BACKGROUND The ways in which morphological data are used to infer the function of fossil organisms are reviewed by Hickman (83, 84), Lauder (133), and Van Valkenburgh (222). Perhaps the most commonly used approach is analogy with living species of similar morphology. Analogy arguments are most convincing if the living organisms that possess a particular structure all use it in the same way, and if the structure does not appear in the fossil record before its hypothesized function was possible (e.g. features for arboreality should not precede the origin of vascular plants—222). Homology among living species can also be used to infer the functions of extinct organisms: Ancestral character states of functions are determined by mapping functions of living organisms onto a phylogeny; then the functions of extinct taxa are inferred by their position within particular clades (75). Another approach to inferring the function of extinct organisms is the paradigm method in which morphological features are compared with theoretical optimal designs for particular functions. If a fossil structure is close to the ideal design for accomplishing some function, it is inferred that the fossil structure probably served that function (84, 133, 222, 229). This approach has limited usefulness since there are many reasons that a structure might not be optimal for a function that it serves (e.g. 42, 57, 58, 68, 72, 152, 177, 217, 232). Both the analogy and paradigm methods suffer from the problems (discussed above) of assuming that morphology is a reliable predictor of function, while the homology method is only as reliable as the phylogenetic hypothesis on which it is based.

USEFULNESS AND LIMITATIONS OF MECHANISTIC STUDIES One way to avoid these problems is to conduct performance tests using physical or mathematical models of fossil organisms (e.g. 105, 107, 133, 196). Obviously this approach is limited to testing hypotheses about physical functions. Furthermore, even if such biomechanical studies show that a fossil structure could have carried out some task or improved the performance of some function, that does not reveal the role that morphological feature served in the life of the organism; the best we can hope to accomplish with such quantitative studies is to reject functional hypotheses that are physically impossible (105–107, 133).

Several potential pitfalls of mechanistic analyses of fossil function are illustrated by the study of Marden & Kramer (149, 150), who presented an intriguing argument by analogy with living stoneflies that the protowings of early insects served in skimming or sailing locomotion on the surface of water. They showed by wing-trimming experiments that skimming and sailing performance are improved by increasing wing length. However, in interpreting these results they fell prey to a flaw in logic and they ignored available evidence on the phylogenetic relationships of the organisms involved. The flaw in logic was the assertion (148) that evidence supporting one functional hypothesis (surface skimming) implies rejection of alternate hypotheses (e.g. parachuting, gliding, thermoregulation), even though these alternative functions may not be mutually exclusive (107). The phylogenetic faux pas was the proposition that surface skimming represents an intermediate stage in the evolution of insect wings in Pterygotes, and this ancestral function has been retained by primitive stoneflies. This interpretation ignores the fact that stoneflies are members of the Neoptera, whose wing characteristics are considered to represent a derived condition (240). Without phylogenetic support, all the feasible scenarios proposed for the evolution of insect wings remain speculative (240).

Internalists: Study of the Origin of Evolutionary Novelty

The mechanisms by which novel phenotypes arise during evolution and the mechanisms responsible for the rapid morphological transformations that are recorded in the fossil record are challenging and contentious issues in evolutionary biology (history reviewed by 58, 65). Evidence emerging from mechanistic studies about the nonlinear size- and context-dependent effects of morphology on performance suggest another simple mechanism by which evolutionary novelty might arise.

BACKGROUND Evolutionary novelty or innovation has been defined in various ways (233): Some investigators require that it be a qualitative deviation in morphology (10, 160, 161), whereas others refer to a morphological, physiological, or behavioral change that permits the assumption of a new function (15, 94, 168). A key innovation is a novel feature that characterizes a clade and allows

a subsequent diversification of the lineage (20, 134, 136, 140, 175, 202). The concept of key innovation has been criticized (e.g. 33, 94, 136) for a variety of reasons, including the difficulty of choosing which feature is the novelty and of demonstrating the causal link between that feature and a subsequent increased speciation rate. Nonetheless, various methodologies have been proposed to identify key innovations (e.g. 136, 212), and a number of examples of key innovations have been proposed (e.g. 134). A key adaptation is a novelty that reduces the costs of tradeoffs between various functions a species performs, thereby permitting that species to invade a niche when the incumbent species in that niche becomes extinct (201). A preadaptation is a feature that acquires a new biological role when organisms interact with their environment in a different way (e.g. 20, 57, 227). A preadaptation becomes an exaptation, a trait whose origins in a clade were due to selective pressures different from those that currently maintain it (69).

The idea of uncoupling (or decoupling) has provided a conceptual framework for much of the discussion of the origin of novelty (e.g. 10, 57, 128, 134, 202, 233). The basic argument is that coupling (e.g. one structure serving several functions, some function depending on several interrelated structures, or a change in one structure necessitating changes in others via pleiotropic effects or via their interconnection during morphogenesis) leads to evolutionary stasis because of the difficulty of changing one trait without negative effects on other features coupled to it (132). Examples of decoupling permitting evolutionary change (reviewed in 128, 202) include duplication of structural elements (if one set takes on a new function, the original function is not compromised), and loss of an old function (the structures that once performed it are free to be involved in new functions). However, some authors have argued that phenotypic plasticity permits suites of coupled characters to change in a coordinated way such that a complex organism's phenotype can shift rapidly with little genetic change (160, 238).

SOURCES OF NOVELTY: NEW BEHAVIORS AND CHANGES IN DEVELOPMENTAL PROGRAM

There are different views about the origin of novelty. While some investigators argue that behavioral shifts precede structural changes, others focus on the origins of new morphologies during development.

Behavioral shifts may precede morphological or physiological changes because behavior is more labile than morphology, and because natural selection should favor individuals showing compensatory behavior if the environment changes (e.g. 89, 161, 168, 227, 238; and others reviewed by 47, 72, 234).

Range expansion into a novel habitat can also provide a new set of selective forces on a population (examples discussed in 134). Furthermore, changes in the motor pattern controlling the kinematics of existing structures can produce novel functions (133). Once new behaviors or functions are acquired, selection should favor morphological variations that facilitate the new activity (161).

Small modifications in developmental program can lead to large changes in morphology (i.e. novelties) (e.g. 1, 23, 65, 94, 160, 161, 195). While the basic conceptual framework for this view has been formalized in terms of heterochrony (changes in the relative rates of different developmental processes) (e.g. 1), the nuts-and-bolts evidence for how changes in development can occur is coming from mechanistic studies, such as those of homeobox genes (reviewed by 65) and of the biomechanics of morphogenesis (reviewed by 38, 117).

MECHANISTIC STUDIES REVEAL ANOTHER POTENTIAL SOURCE OF NOVELTY
New functions and novel consequences of changes in morphology can arise simply as the result of physics. As the examples described above illustrate, a simple change in environmental physical conditions or in body size can sometimes suffice to alter function. Although I think that both behavioral changes and alterations in developmental programs are important sources of novelty, it is possible for innovation to occur without either.

Mechanistic studies also illustrate that a common form of decoupling can be simply the lack of dependence of performance on morphology. Such permission for diversity of form without performance consequences may free structures to vary randomly or to respond to selection on other functions.

Although many ecomorphologists view size as a confounding factor in their analyses and propose various statistical techniques to eliminate size effects (e.g. 63, 228), I think it is important to consider size effects if one is addressing evolutionary questions. Most studies of size in biology have focused on the allometric changes required to maintain function as organisms grow or lineages evolve (e.g. 2, 27, 46, 102, 125, 126, 154, 167, 184, 205). If size changes over evolutionary time, such allometric growth of different parts of organisms might lead to new arrangements of these components and hence to innovations (e.g. 1, 136, 165). Of course, another way to think about allometry is to consider that if organisms do not change their form as they enlarge, their function does change, and such functional changes might be a source of evolutionary novelty.

There is ample evidence for selection on body size (reviewed by e.g. 24), and there are many examples in the fossil record of size changes within lineages over evolutionary time (reviewed by e.g. 93, 125, 126). The evolutionary trend in many, but certainly not all (93), lineages is that size increased with time (Cope's rule). This may be an artifact of better preservation and bias in observation of large organisms in the fossil record (125), or it may be that the

founders of lineages tended to be small, and as size diversified, descendants on average got larger (93, 214). Fossil evidence indicates that many higher taxa arose from small ancestors (214). Stanley (214) suggested that small organisms were more likely to be founders of lineages than were large ones because little organisms are less subject to allometric constraints and therefore are more likely to give rise to novel types, while LaBarbera (126) pointed out that, even if the probability of breakthrough is the same at all body sizes, there are more small species.

The species diversity of small organisms is greater than that of large ones (e.g. 125, 163, 211), but the causes remain the subject of speculation (e.g. 33). One view is that there are fewer physical constraints on body form at small size (e.g. 21, 214). Another view is that ecosystems have more niches at small size (125) due to the fractal nature of habitats (159, 243).

The observations compiled above lead me to speculate about another potential mechanism to add to the list of ways of generating evolutionary innovation. Morphological and kinematic diversity may accumulate at small size without functional consequence, but such novelties may not assume new functional roles until there is a size increase and morphology matters. The structural diversity that did not affect performance at small size might gain functional significance at larger size; not only might features that were selectively neutral at small size become subject to selection at larger size, but novel functions might also become physically possible. Müller (160) has also suggested that evolutionary innovation should be associated with changes in size, basing his argument on evidence that size changes in developing embryos can affect pattern formation, thereby producing novelties in adult morphology.

If size changes tend to lead to evolutionary innovation, then I might speculate that the rate of evolutionary change would correlate with the rate of size change in a lineage. If we turn to the fossil record for evidence, and if we assume that short taxon longevity is a rough indication of rapid evolutionary change (i.e. high rates of modification or extinction), then the data from Hallam (76) for Jurassic ammonites and bivalves (replotted in Figure 7) is consistent with my speculation, but this obviously bears further investigation.

The Phylogenetic Approach and the Usefulness of Mechanistic Morphological Research

Modern studies of adaptation stress the importance of integrating analyses of structure, function, and fitness with phylogenetic history (16, 26, 45, 63, 68, 73, 80, 88, 89, 99, 129, 131, 136, 141, 144, 198, 222, 239). Unfortunately, enthusiasm for this approach has produced a climate in which mechanistic research can be dismissed when done without a phylogeny in hand. This dismissal ignores

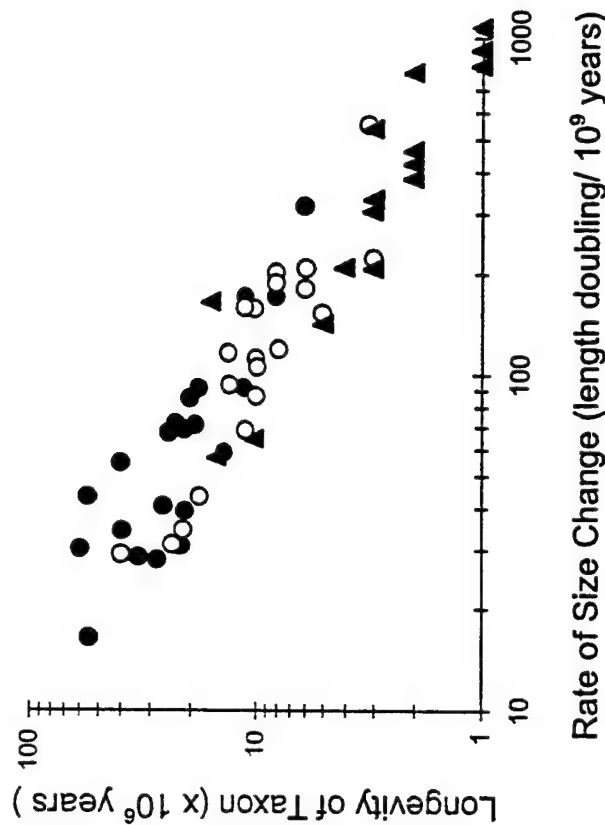


Figure 7 Longevity of each taxon in the fossil record, plotted as a function of the rate of change of body size, for Jurassic bivalved mollusks (circles) and ammonites (triangles). Solid symbols represent genera, and open symbols represent species. [Replotted using data digitized from Figure 1 of (76).]

the fact many mechanistic studies do not have the identification of adaptations as their goal, but rather simply seek to unravel how (i.e. mechanism of operation), not why (i.e. evolutionary history) performance depends on morphology. I hope that the examples cited in this review will serve as a reminder that such mechanistic "how" information can also provide insights about evolutionary questions.

CONCLUSIONS

Quantitative mechanistic analyses of how function depends on biological form, and on the ecological context in which an organism operates, should complement descriptive statistical and phylogenetic studies to provide insights about ecological and evolutionary questions. Such quantitative studies have shown that the relationship between morphology and performance is often nonlinear and sometimes surprising. These mechanistic studies not only reveal potential misconceptions that can arise from the descriptive statistical analyses often used

in ecological and evolutionary research, but they also show how new functions, and novel consequences of changes in morphology, can arise simply as the result of changes in size or habitat.

"... You ask me whom the Macrocystis alga hugs in its arms?
Study, study it, at a certain hour, in a certain sea I know.
... Or the crystal architecture of the sea anemone?
... I will tell you the ocean knows this, that life in its jewel boxes
is endless as the sand, ...
... I walked around as you do, investigating..."

Pablo Neruda, *Enigmas* (164)

ACKNOWLEDGMENTS

I am grateful to the following people for leads into the literature and/or discussions that helped shape my thinking about the issues addressed above: S Arnold, S Emerson, R Full, H Greene, R Huey, T Hunter, D Jablonsky, J Kingsolver, A Kohn, G Lauder, G Oster, R Paine, M Power, M Slatkin, S Stearns, J Valentine, S Vogel, D Wake, M Wake, S Wainwright, and the participants in Integrative Biology 231 and 290 at University of California, Berkeley. I thank H Greene, K Quillin, and P Wainwright for helpful comments on the manuscript. My data presented here were gathered with support from National Science Foundation Grant #OCE-9217338 and Office of Naval Research Grant #N00014-90-J-1357. M O'Donnell helped prepare the manuscript; T Cooper, J Jed, and K Quillin made the figures.

Any Annual Review chapter, as well as any article cited in an Annual Review chapter, may be purchased from the Annual Reviews Preprints and Reprints service.
1-800-347-8007; 415-259-5017; email: arpr@class.org
Visit the Annual Reviews home page at
<http://www.annualreviews.org>

Literature Cited

- Alberch P, Gould SJ, Oster GF, Wake DB. 1979. Size and shape in ontogeny and phylogeny. *Palaeobiology* 5:296-317.
- Alexander RM. 1971. *Size and Shape*. London: Edward Arnold.
- Alexander RM. 1983. *Animal Mechanics*. Oxford: Blackwell Sci. 2nd ed.
- Alexander RM. 1990. Apparent adaptation and actual performance. *Evol. Biol.* 25:357-73.
- Alexander RM, Jayes AS. 1983. A dynamic similarity hypothesis for the gaits of quadrupedal mammals. *J. Zool.* 201:135-52.
- Arnold EN. 1995. Identifying the effects of history on adaptation: origins of different sand-diving techniques in lizards. *J. Zool.* 235:351-88.
- Arnold SJ. 1983. Morphology, performance and fitness. *Am. Zool.* 23:347-61.
- Arnold SJ. 1986. Laboratory and field approaches to the study of adaptation. See Ref. 54, pp. 157-79.
- Arnold SJ. 1988. Quantitative genetics and selection in natural populations: microevolution of vertebral numbers in the garter snake *Thamnophis elegans*. In *Proc. 2nd Int. Conf. on Quant. Genet.*
- BS Weir, J Eisen, MJ Goodman, G Namkoong. pp. 619-36. Sunderland, MA: Sinauer.
- Arnold SJ, Alberch P, Csányi V, Dawkins RC, Emerson SB, et al. 1989. Group Report: How do complex organisms evolve? See Ref. 232a, pp. 403-33.
- Arnold SJ, Bennett AF. 1988. Behavioral variation in natural populations. V. Morphological correlations of locomotion in the garter snake, *Thamnophis radix*. *J. Linn. Soc.* 34:175-90.
- Balmer RT, Strobosch AD. 1977. Critical size of newborn homeotherms. *J. Appl. Physiol.* 42:571-77.
- Baron CJ. 1991. What functional morphology cannot explain: a morphogenetic model of sea urchins and a discussion of the role of morphogenetic explanations in evolutionary morphology. In *The Unity of Evolutionary Biology*, ed. EC Dudley, pp. 471-88. Portland, OR: Dioscorides.
- Batty RS. 1984. Development of swimming movements and musculature of larval herring (*Clupea harengus*). *J. Exp. Biol.* 37:129-53.
- Benkman CW, Lindholm AK. 1991. The advantages and evolution of a morphological novelty. *Nature* 349:519-20.
- Bennett AF, Huey RB. 1990. Studying the evolution of physiological performance. *Oxford Surv. Evol. Biol.* 7:251-84.
- Berg HC, Purcell EM. 1977. Physics of chemoreception. *Biophys. J.* 20:193-219.
- Best BA. 1983. Mechanics of orientation in sea pens: a rotational one line joint. *J. Biomech.* 16:297.
- Black R. 1976. The effects of grazing by the limpet, *Acaezia intessa* on the kelp, *Egregia laevigata*, in the intertidal zone. *Ecology* 57:265-77.
- Bock WJ, von Wahlert G. 1965. Adaptation and the form-function complex. *Evolution* 19:269-99.
- Bonner JT. 1968. Size change in development and evolution. *The Paleontol. Soc. Mem.* 2:1-15.
- Bonner JT. 1981. Evolutionary strategies and developmental constraints in cellular slime molds. *Am. Nat.* 119:530-52.
- Bonner JT, ed. 1982. *Evolution and Development*. Berlin: Springer-Verlag.
- Bonner JT, Horn HS. 1982. Selection for size, shape, and developmental timing. See Ref. 23, pp. 259-76.
- Bushnell DM, Moore KJ. 1991. Drag reduction in nature. *Annu. Rev. Fluid Mech.* 23:65-79.
- Cadle JE, Greene HW. 1993. Phylogenetic patterns, biogeography, and the ecological structure of neotropical snake assemblages. In *Species Diversity in Ecological Communities: Historical and Geographical Perspectives*, ed. RE Ricklefs, D Schlüter, pp. 281-93. Chicago: Univ. Chicago Press.
- Calder WA III. 1984. *Size, Function and Life History*. Cambridge, MA: Harvard Univ. Press.
- Carrington E. 1990. Drag and dislodgement of an intertidal macroalga: consequences of morphological variation in *Mastocarpus papillatus* Kutzing. *J. Exp. Mar. Biol. Ecol.* 139:185-200.
- Cheer AYL, Koehl MAR. 1988. Fluid flow through insect filters. *JMA J. Math. Appl. Med. Biol.* 4:185-99.
- Cheer AYL, Koehl MAR. 1988. Paddles and rakes: fluid flow through bristled appendages of small organisms. *J. Theor. Biol.* 129:17-39.
- Childress S, Koehl MAR, Miksis M. 1987. Scanning currents in Stokes flow and the efficient feeding of small organisms. *J. Fluid Mech.* 177:407-36.
- Cossins AR, Bowler K. 1987. *Temperature Biology of Animals*. London: Chapman & Hall.
- Cracraft J. 1990. The origin of evolutionary novelties: pattern and process at different hierarchical levels. See Ref. 167a, pp. 21-46.
- Craig DA. 1990. Behavioral hydrodynamics of *Cloeon dipterum* larvae (Ephemeroptera: Baetidae). *J. North Am. Benthol. Soc.* 9:346-57.
- Currey J. 1984. *The Mechanical Adaptations of Bones*. Princeton, NJ: Princeton Univ. Press.
- Dadswell MJ, Weihs D. 1990. Size-related hydrodynamic characteristics of the giant scallop, *Placopodium magellanicus* (Bivalvia: Pectinidae). *Can. J. Zool.* 68:778-85.
- Daniel TL, Webb PW. 1987. Physical determinants of locomotion. In *Comparative Physiology: Life in Water and on Land*, ed. P. Dejours, L. Bolis, CR Taylor, ER Weibel, Padova: Liviana.
- Davidson LA, Koehl MAR, Keller R, Oster GF. 1995. How do sea urchins gas-triulate? Distinguishing between mechanisms of primary invagination using biomechanics. *Development* 121:2005-18.
- Denny MW. 1987. Lift as a mechanism

- of patch initiation in mussel beds. *J. Exp. Mar. Biol. Ecol.* 113:231-45.
40. Denny MW. 1988. *Biology and the Mechanics of the Wave-Swept Environment*. Princeton, NJ: Princeton Univ. Press.
 41. Denny MW. 1993. *Air and Water*. Princeton, NJ: Princeton Univ. Press.
 42. Denny MW. 1994. Roles of hydrodynamics in the study of life on wave-swept shores. See Ref. 228a, pp. 169-204.
 43. Denny MW, Daniel T, Koehl MAR. 1985. Mechanical limits to the size of wave-swept organisms. *Ecol. Monogr.* 55:69-102.
 44. Emerson SB. 1991. The ecomorphology of Bornean tree frogs (family Rhacophoridae). *Zool. J. Linn. Soc.* 101:337-57.
 45. Emerson SB, Arnold SJ. 1989. Intra- and interspecific relationships between morphology, performance and fitness. See Ref. 232a, pp. 295-314.
 46. Emerson SB, Greene HW, Charnov EL. 1994. Allometric aspects of predator-prey interactions. See Ref. 228a, pp. 123-39.
 47. Emerson SB, Koehl MAR. 1990. The interaction of behavioral and morphological change in the evolution of a novel locomotor type: "Flying" frogs. *Evaluation* 44:1931-46.
 48. Emerson SB, Travis J, Koehl MAR. 1990. Functional complexes and additivity in performance: a test case with "flying" frogs. *Evolution* 44:2153-57.
 49. Endler J. 1986. *Natural Selection in the Wild*. Princeton, NJ: Princeton Univ. Press.
 50. Endler JA. 1986. Defense against predators. See Ref. 54, pp. 109-34.
 51. Ennos AR. 1989. The effect of size on the optimal shapes of gliding insects and seeds. *J. Zool.* 219:61-69.
 52. Fauci L. 1996. Computational modeling of the fluid dynamics of locomotion. *Am. Zool.* In press.
 53. Feder ME, Lauder GV. 1986. Commentary and conclusion. See Ref. 54, pp. 180-89.
 54. Feder ME, Lauder GV, eds. 1986. *Predator-Prey Relationships: Perspectives and Approaches from the Study of Lower Vertebrates*. Chicago: Univ. Chicago Press.
 55. Feinsinger P, Colwell RK, Terborgh J, Chaplin SB. 1979. Elevation and the morphology, flight energetics, and foraging ecology of tropical hummingbirds. *Am. Nat.* 113:481-97.
 56. Fonseca MS, Fisher JS, Ziemann JC, Thayer GW. 1982. Influence of the sea-grass *Zostera marina* L., on current flow. *Estuar. Coast. Shelf Sci.* 15:351-54.
 57. Frazetta TH. 1975. *Complex Adaptations in Evolving Populations*. Sunderland, MA: Sinauer. 267 pp.
 58. Futuyama DJ. 1986. *Evolutionary Biology*. Sunderland, MA: Sinauer. 2nd ed.
 59. Gans C. 1966. Some limitations and approaches to problems in functional anatomy. *Folia Biotheor.* 6:41-50.
 60. Gans C. 1986. Functional morphology of predator-prey relationships. See Ref. 54, pp. 6-23.
 61. Garland T Jr. 1983. The relation between maximum running speed and body mass in terrestrial mammals. *J. Zool.* 99:157-70.
 62. Garland T Jr. 1994. Why not to do two-species comparative studies: limitations on inferring adaptation. *Physiol. Zool.* 67:797-828.
 63. Garland T Jr, Losos JB. 1994. Ecological morphology of locomotor performance in squamate reptiles. See Ref. 228a, pp. 240-302.
 64. Gaylord B, Blanchette CA, Denny MW. 1994. Mechanical consequences of size in wave-swept algae. *Ecol. Monogr.* 64:287-313.
 65. Gilbert SF, Opitz JM, Raff RA. 1996. Resynthesizing evolutionary and developmental biology. *Dev. Biol.* 173:357-72.
 66. Glasheen JW. 1995. *Strange locomotion: from humans running on their hands to lizards running on water*. PhD diss. Dept. Org. Evol. Biol., Harvard.
 67. Glasheen JW, McMahon TA. 1996. Weight support on the water surface in Basilisk lizards. *Nature*. 380:340-42.
 68. Gould SJ, Lewontin RC. 1979. The spandrels of San Marco and the panglossian paradigm: a critique of the adaptationist programme. *Proc. R. Soc. London Ser. B* 205:581-98.
 69. Gould SJ, Vrba ES. 1982. Exaptation: a missing term in the science of form. *Paleobiology* 8:4-15.
 70. Grant BR, Grant PR. 1989. Natural selection in a population of Darwin's finches. *Am. Nat.* 133:377-93.
 71. Grant BW, Porter WP. 1992. Modeling global macroclimatic constraints on ectotherm energy budgets. *Am. Zool.* 32:154-78.
 72. Greene HW. 1982. Dietary and phenotypic diversity in lizards: Why are some organisms specialized? In *Environmental Adaptation and Evolution*, ed. D
 73. Mossakowski, G Roth, pp. 107-28. New York: Gustav Fisher.
 74. Greene HW. 1986. Diet and arboreality in the emerald monitor, *Varanus praxinus*, with comments on the study of adaptation. *Feldiana Zool.* 31:1-12.
 75. Greene HW. 1986. Natural history and evolutionary biology. See Ref. 54, pp. 99-108.
 76. Greene HW. 1994. Homology and behavioral repertoires. In *The Hierarchical Basis of Comparative Biology*, ed. BK Hall, pp. 369-90. San Diego, CA: Academic.
 77. Hallam A. 1975. Evolutionary size increase and longevity in Jurassic bivalves and ammonites. *Nature* 258:493-96.
 78. Hanken J. 1985. Morphological novelty in the limb skeleton accompanies miniaturization in salamanders. *Science* 229:871-74.
 79. Hansen B, Tiesius P. 1992. Flow through the feeding structures of suspension feeding zooplankton: a physical model approach. *J. Plankton Res.* 14:821-34.
 80. Harrold C, Reed DC. 1985. Food availability, sea urchin grazing, and kelp forest community structure. *Ecology* 66:1160-69.
 81. Harvey PH, Pagel MD. 1991. *The Comparative Method in Evolutionary Biology*. Oxford: Oxford Univ. Press.
 82. Heinrich B. 1979. *Bumblebee Economics*. Cambridge, MA: Harvard Univ. Press.
 83. Heinrich B. 1993. *The Hot-blooded Insects: Strategies and Mechanisms of Thermoregulation*. Berlin: Springer-Verlag.
 84. Hickman CS. 1980. Gastropod radulae and the assessment of form in evolutionary paleontology. *Paleobiology* 6:276-94.
 85. Hickman CS. 1988. Analysis of form and function in fossils. *Am. Zool.* 28:775-93.
 86. Holbrook NM, Denny M, Koehl MAR. 1991. Interstitial "trees": consequences of aggregation on the mechanical and photosynthetic characteristics of sea palms. *J. Exp. Mar. Biol. Ecol.* 146:39-67.
 87. Holwill MEJ, Sleigh MA. 1967. Propulsion by hispid flagella. *J. Exp. Biol.* 47:267-76.
 88. Huey RB. 1982. Temperature, physiology, and the ecology of reptiles. In *Biology of Reptilia*, ed. C Gans, pp. 25-91. New York: Academic.
 89. Huey RB, Bennett AF. 1986. A comparative approach to field and laboratory studies in evolutionary biology. See Ref. 54, pp. 82-98.
 90. Huey RB, Bennett AF. 1987. Phylogenetic studies of coadaptation: preferred temperatures versus optimal performance temperatures of lizards. *Evolution* 41:1098-115.
 91. Huey RB, Kingsolver JG. 1993. Evolutionary responses to extreme temperatures in ectotherms. *Am. Nat.* 143:S21-S46.
 92. Hunter T. 1988. *Mechanical design of hydroids: flexibility, flow forces and feeding in Obelia longissima*. PhD dissertation Zool., Univ. Calif., Berkeley.
 93. Jablonski D. 1996. Body size and macroevolution. In *Evolutionary Paleobiology: Essays in Honor of James W. Valentine*, ed. D Jablonski, DH Erwin, JH Lipps, pp. 256-89. Chicago: Univ. Chicago Press. In press.
 94. Jablonski D, Bottjer DJ. 1990. The ecology of evolutionary innovation: the fossil record. See Ref. 167a, pp. 253-88.
 95. Jacobs DK. 1992. Shape, drag, and power in ammonoid swimming. *Paleobiology* 18:203-20.
 96. James FC, McCulloch CE. 1990. Multivariate analysis in ecology and systematics: Panacea or Pandora's Box? *Ann. Rev. Ecol. Syst.* 21:129-66.
 97. Jayne BC, Bennett AF. 1989. The effect of tail morphology on locomotor performance of snakes: a comparison of experimental and correlative methods. *J. Exp. Zool.* 252:126-33.
 98. Jayne BC, Bennett AF. 1990. Scaling of speed and endurance in garter snakes: a comparison of cross-sectional and longitudinal allometries. *J. Zool.* 220:257-77.
 99. Jensen JS. 1990. Plausibility and testability: assessing the consequences of evolutionary innovation. See Ref. 167a, pp. 171-90.
 100. Johnson AS. 1986. *Consequences of individual and group morphology: a hydrodynamic study of the benthic suspension-feeder *Phoronopsis viridis**. PhD dissertation Univ. Calif., Berkeley.
 101. Johnson AS. 1990. Flow around Phoronids: consequences of a neighbor to suspension feeders. *Limnol. Oceanogr.* 35:1395-401.
 102. Johnson AS, Koehl MAR. 1994. Main-

- tenance of dynamic strain similarity and environmental stress factor in different flow habitats: Thallus allometry and material properties of a giant kelp. *J. Exp. Biol.* 195:381-410
103. Kingsolver JG. 1983. Ecological significance of flight activity in *Colias* butterflies: implications for reproductive strategy and population structure. *Ecology* 64:546-51
 104. Kingsolver JG. 1988. Thermoregulation, flight, and the evolution of wing pattern in Pierid butterflies: the topography of adaptive landscapes. *Am. Zool.* 28:899-912
 105. Kingsolver JG, Koehl MAR. 1985. Aerodynamics, thermoregulation, and the evolution of insect wings: differential scaling and evolutionary change. *Evolution* 39:488-504
 106. Kingsolver JG, Koehl MAR. 1989. Selective factors in the evolution of insect wings: response to Kukulova-Peck. *Can. J. Zool.* 67:785-87
 107. Kingsolver JG, Koehl MAR. 1994. Selective factors in the evolution of insect wings. *Annu. Rev. Entomol.* 39:425-51
 108. Kingsolver JG, Woods HA, Gilchrist G. 1995. Traits related to fitness. *Science* 267:396
 109. Koehl MAR. 1977. Effects of sea anemones on the flow forces they encounter. *J. Exp. Biol.* 69:87-105
 110. Koehl MAR. 1977. Mechanical diversity of the connective tissue of the body wall of sea anemones. *J. Exp. Biol.* 69:107-25
 111. Koehl MAR. 1977. Mechanical organization of cantilever-like sessile organisms: sea anemones. *J. Exp. Biol.* 69:127-42
 112. Koehl MAR. 1982. Mechanical design of spicule-reinforced connective tissues: stiffness. *J. Exp. Biol.* 98:239-68
 113. Koehl MAR. 1984. How do benthic organisms withstand moving water? *Am. Zool.* 24:57-70
 114. Koehl MAR. 1984. Mechanisms of particle capture by copepods at low Reynolds number. In *Trophic Interactions in Aquatic Ecosystems*, ed. DL Meyers, JR Strickler, pp. 135-160. Boulder, CO: Westview
 115. Koehl MAR. 1986. Seaweeds in moving water: form and mechanical function. In *On the Economy of Plant Form and Function*, ed. TJ Givnish, pp. 603-34. Cambridge: Cambridge Univ. Press
 116. Koehl MAR. 1989. From individuals to populations. In *Perspectives in Ecology*
 117. May SA, Levin, pp. 39-53. Princeton, NJ: Princeton Univ. Press
 118. Koehl MAR. 1992. Hairy little legs: feeding, smelling, and swimming at low Reynolds number. *Contemp. Math.* 141:33-64
 119. Koehl MAR. 1995. Fluid flow through hair-bearing appendages: feeding, smelling, and swimming at low and intermediate Reynolds number. In *Biological Fluid Dynamics*, ed. CP Ellington, TJ Pedley. Soc. Exp. Biol. Symp. 49:157-82
 120. Koehl MAR. 1996. Small-scale fluid dynamics of olfactory antennae. *Mar. Freshwater Behav. Physiol.* 27:127-41
 121. Koehl MAR, Alberte RS. 1988. Flow, flapping, and photosynthesis of thacral-gae: functional consequences of undulate blade morphology. *Mar. Biol.* 99:435-44
 122. Koehl MAR, Hunter T, Jed J. 1991. How do body flexibility and length affect hydrodynamic forces on sessile organisms? *Am. Zool.* 31:A60
 123. Koehl MAR, Powell TM. 1996. Effects of benthic organisms on mass transport at wave-swept rocky shores. *Eos, Trans. Am. Geophys. Union* 76:OS69
 124. Koehl MAR, Wainwright SA. 1977. Mechanical adaptations of a giant kelp. *Limnol. Ocean.* 22:1067-71
 125. LaBarbera M. 1986. The evolution and ecology of body size. In *Patterns and Processes in the History of Life*, ed. DM Raup, D Jablonski, pp. 69-98. Berlin: Springer-Verlag
 126. LaBarbera M. 1989. Analyzing body size as a factor in ecology and evolution. *Annu. Rev. Ecol. Syst.* 20:97-117
 127. Lande R, Arnold SJ. 1983. The measurement of selection on correlated characters. *Evolution* 37:1210-26
 128. Lauder GV. 1981. Form and function: structural analysis in evolutionary morphology. *Paleobiology* 7:430-42
 129. Lauder GV. 1982. Introduction. In *Form and Function: A Contribution to the History of Animal Morphology*, ed. ES Russell, pp. xi-xiv. Chicago: Univ. Chicago Press
 130. Lauder GV. 1990. Functional morphology and systematics: studying functional patterns in an historical context. *Annu. Rev. Ecol. Syst.* 21:317-40
 131. Lauder GV. 1991. Biomechanics and evolution: integrating physical and historical biology in the study of complex systems. See Ref. 196, pp. 1-19
 132. Lauder GV. 1991. An evolutionary perspective on the concept of efficiency: How does function evolve? In *Efficiency and Economy in Animal Physiology*, ed. RW Blake, pp. 169-84. Cambridge: Cambridge Univ. Press
 133. Lauder GV. 1995. On the inference of function from structure. In *Functional Morphology in Vertebrate Paleontology*, ed. JJ Thomason, pp. 1-18. Cambridge: Cambridge Univ. Press
 134. Lauder GV, Crompton AW, Gans C, Hanken J, Liem KF, et al. 1989. Group Report: How are feeding systems integrated and how have evolutionary innovations been introduced? See Ref. 232a, pp. 97-115
 135. Lauder GV, Leroi AM, Rose MR. 1993. Adaptations and history. *TREE* 8:294-97
 136. Lauder GV, Liem KF. 1989. The role of historical factors in the evolution of complex organismal functions. See Ref. 232a, pp. 63-78
 137. Lauder GV, Wainwright PC. 1992. Function and history: the pharyngeal jaw apparatus in primitive ray-finned fishes. In *Systematics, Historical Ecology, and North American Freshwater Fishes*, ed. RL Mayden, pp. 455-71. Stanford: Stanford Univ. Press
 138. Lehman JT. 1986. Grazing, nutrient release, and their importance on the structure of phytoplankton communities. In *Trophic Interactions within Aquatic Communities*, ed. DG Meyers, JR Strickler, pp. 49-72. AAAS Sel. Symp. 85
 139. Levesee GJ. 1976. Flow and feeding in fan-shaped colonies of the gorgonian coral, *Leptogorgia*. *Biol. Bull.* 151:344-56
 140. Liem KF. 1973. Evolutionary strategies and morphological innovations: Cichlid pharyngeal jaws. *Syst. Zool.* 22:425-41
 141. Liem KF. 1990. Key evolutionary innovations, differential diversity, and synecomorphy. See Ref. 167a, pp. 147-70
 142. Losos JB. 1990. Ecomorphology, performance capability, and scaling of West Indian *Anolis* lizards: an evolutionary analysis. *Ecol. Monogr.* 60:369-88
 143. Losos JB. 1990. The evolution of form and function: morphology and locomotor performance in West Indian *Anolis* lizards. *Evolution* 44:1189-203
 144. Losos JB, Miles DB. 1994. Adaptation, constraint, and the comparative method: phylogenetic issues and methods. See Ref. 228a, pp. 60-98
 145. Losos JB, Sinervo B. 1989. The effects of morphology and perch diameter on sprint performance in West Indian *Anolis* lizards. *J. Exp. Biol.* 145:23-30
 146. Loudon C, Best BA, Koehl MAR. 1994. When does motion relative to neighboring surfaces alter the flow through an array of hairs? *J. Exp. Biol.* 193:233-54
 147. Manel JL, Dadswell MJ. 1993. Swimming of juvenile sea scallops, *Placopecten magellanicus* (Gmelin): a minimum size for effective swimming? *J. Exp. Mar. Biol. Ecol.* 174:137-75
 148. Marden JH. 1995. How insects learned to fly. *The Sciences* 35:26-30
 149. Marden JH, Kramer MG. 1994. Surface-skimming stoneflies: a possible intermediate stage in insect flight evolution. *Science* 266:427-30
 150. Marden JH, Kramer MG. 1995. Locomotor performance of insects with rudimentary wings. *Nature* 377:332-34
 151. Marrasé C, Costello JH, Granata T, Strickler JR. 1991. Grazing in a turbulent environment: energy dissipation, encounter rates, and efficacy of feeding currents in *Centropages hamatus*. *Proc. Natl. Acad. Sci. USA* 87:1653-57
 152. Mayr E. 1983. How to carry out the adaptationist program? *Am. Nat.* 121:324-34
 153. McMahon TA. 1984. *Muscles, Reflexes, and Locomotion*. Princeton, NJ: Princeton Univ. Press
 154. McMahon TA, Bonner JT. 1983. *On Size and Life*. New York: Freeman
 155. Menge BA, Berlow EL, Blanchette CA, Navarrete SA, Yamada SB. 1994. The keystone species concept: variation in interaction strength in a rocky intertidal habitat. *Ecol. Monogr.* 64:249-87
 156. Mills LS, Soule MB, Doak DF. 1993. The keystone-species concept in ecology and conservation. *BioScience* 43:219-24
 157. Monteith JL, Unsworth MH. 1990. *Principles of Environmental Physics*. London: Edward Arnold. 2nd ed.
 158. Moore JA. 1987. *Science as a Way of Knowing V—Form and Function*. Chicago: Am. Soc. Zool. 220 pp.
 159. Morse DR, Lawton JH, Dodson MM, Williamson MH. 1985. Fractal dimension of vegetation and the distribution of arthropod body lengths. *Nature* 314:731-33
 160. Müller GB. 1990. Developmental mech-

161. Müller GB, Wagner GP. 1991. Novelty in evolution: restructuring the concept. *Ann. Rev. Ecol. Syst.* 22:229-56.
162. Muzik K, Wainwright SA. 1977. Morphology and habitat of five Fijian sea fans. *Bull. Mar. Sci.* 27:308-37.
163. Nee S, Lawton JH. 1996. Body size and biodiversity. *Nature* 380:672-73.
164. Neruda P. 1971. Enigmas. In *Neruda and Vachello: Selected Poems*, ed. R Bly, pp. 131-32. Boston: Beacon.
165. Newell ND. 1949. Phylogenetic increase, an important trend illustrated by fossil invertebrates. *Evolution* 3:103-24.
166. Niklas KJ. 1992. *Plant Biomechanics: An Engineering Approach to Plant Form and Function*. Chicago: Univ. Chicago Press.
167. Niklas KJ. 1994. *Plant Allometry: The Scaling of Form and Process*. Chicago: Univ. Chicago Press.
- 167a. Nitecki MW, ed. 1990. *Evolutionary Innovations*. Chicago: Univ. Chicago Press.
168. Nitecki MW. 1990. The plurality of evolutionary innovations. See Ref. 167a, pp. 3-18.
169. Nobel PS. 1983. *Biophysical Plant Physiology and Ecology*. San Francisco: Freeman.
170. Norberg UM. 1994. Wing design, flight performance, and habitat use in bats. See Ref. 228a, pp. 205-29.
171. Nowell ARM, Jumas PA. 1984. Flow environments of aquatic benthos. *Ann. Rev. Ecol. Syst.* 15:303-28.
172. Okamura B. 1984. The effects of ambient flow velocity, colony size, and upstream colonies on the feeding success of bryozoa. I. *Bugula stolonifera* (Ryland), an arborescent species. *J. Exp. Mar. Biol. Ecol.* 83:179-93.
173. Okamura B. 1985. The effects of ambient flow velocity, colony size, and upstream colonies on the feeding success of bryozoa. II. *Conopeum reticulatum* (Linnaeus), an encrusting species. *J. Exp. Mar. Biol. Ecol.* 89:69-80.
174. Okamura B. 1988. The influence of neighbors on the feeding of an epifaunal bryozoan. *J. Exp. Mar. Biol. Ecol.* 120:105-23.
175. Olson EC. 1965. Summary and comment. *Syst. Zool.* 14:337-42.
176. Osse JWM, Drost MR. 1983. Hydrodynamics and mechanics of fish larvae. *Pol. Arch. Hydrobiol.* 36:455-66.
177. Oster GF, Wilson EO. 1978. *Caste and Ecology in the Social Insects*. Princeton, NJ: Princeton Univ. Press.
178. Paine RT. 1966. Food web complexity and species diversity. *Am. Nat.* 100:65-75.
179. Paine RT. 1976. Size-limited predation: an observational and experimental approach with the *Mytilus-Pisaster* interaction. *Ecology* 57:858-73.
180. Paine RT. 1994. *Marine Rocky Shores and Community Ecology: An Experimentalist's Perspective*. Oldendorf/Luhe, Germany: Ecology Inst. 152 pp.
181. Paine RT, Levin SA. 1981. Intertidal landscapes: disturbance and the dynamics of pattern. *Ecol. Monogr.* 51:145-78.
182. Paine RT, Suchanek TH. 1983. Convergence of ecological processes between independently evolved competitive dominants: a tunicate-mussel comparison. *Evolution* 37:821-31.
183. Patterson MR. 1991. The effects of flow on polyp-level prey capture in an octocoral, *Alcyonium Siderium*. *Biol. Bull.* 180:92-102.
184. Pedley TJ, ed. 1977. *Scale Effects in Animal Locomotion*. London: Academic.
185. Pennycuik CJ. 1992. *Newton Rules Biology*. New York: Oxford Univ. Press.
186. Pentecheff ND. 1991. Resistance to crushing from wave-borne debris in the barnacle *Balanus glandula*. *Mar. Biol.* 110:399-408.
187. Podolsky RD. 1993. Separating the effects of temperature and viscosity on swimming and water movement by sand dollar larvae (*Dendraster excentricus*). *J. Exp. Biol.* 176:207-21.
188. Podolsky RD. 1994. Temperature and water viscosity: physiological versus mechanical effects on suspension feeding. *Science* 265:100-4.
189. Porter WP, Grant BW. 1992. Modeling global macroclimatic constraints on ectotherm energy budgets. *Am. Zool.* 32:154-78.
190. Porter WP, Mitchell JW, Beckman WA, DeWitt CB. 1973. Behavioral implications of mechanistic ecology: thermal and behavioral modelling of desert ectotherms and their microenvironment. *Oecologia* 13:1-54.
191. Porter WP, Mitchell JW, Beckman WA, Tracy CR. 1975. Environmental constraints on some predator-prey interactions. In *Perspectives of Biophysical Ecology*, ed. DM Gates, RB Schmerl, pp. 347-64. New York: Springer-Verlag.
192. Porter WP, Parkhurst DF, McClure PA. 1986. Critical radius of endotherms. *Am. J. Physiol.* 250:699-707.
193. Power ME, Tilman D, Estes JA, Meyer BA, Bond WJ, et al. 1996. Challenges in the quest for keystones. *BioScience*. In press.
194. Price MVE. 1986. Symposium: mechanistic approaches to the study of natural communities. *Am. Zool.* 26:3-106.
195. Raff RA, Parr BA, Parks AL, Wray GA. 1990. Heterochrony and other mechanisms of radical evolutionary change in early development. See Ref. 167a, pp. 71-98.
196. Rayner JMV, Wootton RJ, eds. 1991. *Biomechanics in Evolution*. Cambridge: Cambridge Univ. Press.
197. Reilly SM, Lauder GV. 1992. Morphology, behavior, and evolution: comparative kinematics of aquatic feeding in salamanders. *Brain Behav. Evol.* 40:182-96.
198. Reilly SM, Wainwright PC. 1994. Conclusion: ecological morphology and the power of integration. See Ref. 228a, pp. 339-54.
199. Ricklefs RE, Miles DB. 1994. Ecological and evolutionary inferences from morphology: an ecological perspective. See Ref. 228a, pp. 13-41.
200. Rigler FH. 1982. Recognition of the possible: an advantage of empiricism in ecology. *Can. J. Fish. Res. Aquat. Sci.* 39:1323-31.
201. Rosenzweig ML, McCord RD. 1991. Incumbent replacement: evidence for long-term evolutionary progress. *Phyleology* 17:202-13.
202. Roth G, Wake DB. 1989. Conservation and innovation in the evolution of feeding in vertebrates. See Ref. 232a, pp. 7-21.
203. Rothschild BJ, Osborn TR. 1988. Small-scale turbulence and plankton contact rates. *J. Plankton Res.* 10:465-74.
204. Rubenstein DI, Koehl MAR. 1977. The mechanisms of filter feeding: some theoretical considerations. *Am. Nat.* 111:981-94.
205. Schmidt-Nielsen K. 1984. *Scaling: Why is Animal Size So Important?* Cambridge: Cambridge Univ. Press.
206. Schoener TW. 1986. Mechanistic approaches to community ecology: a new reductionism? *Am. Zool.* 26:81-106.
207. Sebens KP, Done TJ. 1992. Water flow, growth form and distribution of scleractinian corals: Davies Reef (GBR), Australia. *Proc. 7th Int. Coral Reef Symp.*
208. Seilacher A. 1973. Fabricational noise in adaptive morphology. *Syst. Zool.* 22:451-65.
209. Shimeta J, Jumas PA. 1991. Physical mechanisms and rates of particle capture by suspension-feeders. *Oceanogr. Mar. Biol. Annu. Rev.* 29:191-257.
210. Shimeta J, Jumas PA, Lessard EJ. 1995. Influences of turbulence on suspension feeding by planktonic protozoa: experiments in laminar shear fields. *Limnol. Ocean.* 40:845-59.
211. Siemann E, Tilman D, Haarstad J. 1996. Insect species diversity, abundance and body size relationships. *Nature* 380:704-6.
212. Slowinski JB, Goyer C. 1993. Testing whether certain traits have caused amplified diversification: an improved method based on a model of random speciation and extinction. *Am. Nat.* 142:1019-24.
213. Sousa WP. 1984. The role of disturbance in natural communities. *Ann. Rev. Ecol. Syst.* 15:1353-91.
214. Stanley SM. 1973. An explanation for Cope's rule. *Evolution* 27:1-26.
215. Statzner B. 1988. Growth and Reynolds number of lotic macroinvertebrates: a problem for adaptation of shape to drag. *Oikos* 51:84-87.
216. Statzner B, Holm TF. 1989. Morphological adaptation of shape to flow: macroinvertebrates around lotic macroinvertebrates with known Reynolds numbers at quasi-natural flow conditions. *Oecologia* 78:145-57.
217. Stearns SC. 1982. On fitness. In *Environmental Adaptation and Evolution*, ed. D Mossakowski, G Roth, pp. 3-17. New York: Gustav Fischer.
218. Steneck RS, Dehler MN. 1994. A functional group approach to the structure of algal-dominated communities. *Oikos* 69:476-98.
219. Stone R. 1996. Taking a new look at life through a functional lens. *Science* 269:316-17.
220. Thomas FIM. 1994. Morphology and orientation of tube extensions on aggregations of the polychaete annelid *Phragmatopoma californica*. *Mar. Biol.* 119:525-34.
221. Thomas FIM. 1994. Transport and mixing of gametes in three free-spawning polychaete annelids *Phragmatopoma californica* (Fewkes), *Sabellaria cemen-tarium* (Moore), and *Schizobranchia insignis* (Rush). *J. Exp. Mar. Biol. Ecol.*

- 179:11-27
222. Van Valkenburgh B. 1994. Ecomorphological analysis of fossil vertebrates and their paleocommunities. See Ref. 228a, pp. 140-68
223. Videler JJ. 1995. Body surface adaptations to boundary-layer dynamics. In *Biological Fluid Dynamics*. Soc. Exp. Biol. Symp., ed. CP Ellington, TJ Pedley, 49:1-20. London: Co. Biol.
224. Vincent JV. 1990. *Structural Biomaterials*. Princeton, NJ: Princeton Univ. Press
225. Vogel S. 1993. When leaves save the tree. *Nat. Hist.* 102:58-62
226. Vogel S. 1994. *Life in Moving Fluids*. Princeton, NJ: Princeton Univ. Press, 2nd ed.
227. von Wahlert G. 1965. The role of ecological factors in the origin of higher levels of organization. *Syst. Zool.* 14:288-300
228. Wainwright PC. 1994. Functional morphology as a tool in ecological research. See Ref. 228a, pp. 42-59
- 228a. Wainwright PC, Reilly SM, eds. 1994. *Ecological Morphology: Integrative Organismal Biology*. Chicago: Univ. Chicago Press
229. Wainwright PC, Reilly SM. 1994. Introduction. See Ref. 228a, pp. 1-12
230. Wainwright SA, Biggs WD, Currey JD, Gosline JW. 1976. *Mechanical Design in Organisms*. Princeton, NJ: Princeton Univ. Press
231. Wainwright SA, Dillon JR. 1969. On the orientation of sea fans (genus *Gorgonia*). *Biol. Bull.* 136:130-39
232. Wake DB. 1982. Functional and evolutionary morphology. *Perspect. Biol. Med.* 25:603-20
- 232a. Wake DB, Roth G, eds. 1989. *Complex Organismal Functions: Integration and Evolution in Vertebrates*. New York: Wiley & Sons
233. Wake DB, Roth G. 1989. The linkage between ontogeny and phylogeny in the evolution of complex systems. See Ref. 232a, pp. 361-77
234. Wake MH. 1992. Morphology, the study of form and function, in modern evolutionary biology. In *Oxford Surveys in Evolutionary Biology*, ed. D Futuyma, J Antonovics, pp. 289-346. New York: Oxford Univ. Press
235. Wasserthal LT. 1975. The role of butterfly wings in regulation of body temperature. *J. Insect Physiol.* 21:1921-30
236. Webb PW. 1986. Locomotion and predator-prey relationships. See Ref. 54, pp. 24-41
237. Weihs D. 1980. Energetic significance of changes in swimming modes during growth of larval anchovy *Engraulis mordax*. *Fish. Bull. Fish Wildl. Serv. US* 77:597-604
238. West-Eberhard MJ. 1989. Phenotypic plasticity and the origins of diversity. *Annu. Rev. Ecol. Syst.* 20:249-78
239. Westneat MW. 1995. Systematics and biomechanics in ecomorphology. *Environ. Biol. Fish.* 44:263-83
240. Will KL. 1995. Piecemeal surface-skimming and insect flight evolution. *Science* 270:1684-85
241. Williams TA. 1994. Locomotion in developing *Artemia* larvae: mechanical analysis of antennal propulsors based on large-scale physical models. *Biol. Bull.* 187:156-63
242. Williams TA. 1994. A model of rowing propulsion and the ontogeny of locomotion in *Artemia* larvae. *Biol. Bull.* 187:164-73
243. Williamson MH, Lawton JH. 1988. Fractal geometry of ecological habitats. In *Habitat Structure: The Physical Arrangement of Objects in Space*, ed. SS Bell, ED McCoy, HR Mushinsky, pp. 69-86. New York: Routledge, Chapman & Hall
244. Worcester SE. 1994. Adult rafting versus larval swimming: dispersal and recruitment of a botryllid ascidian on eelgrass. *Mar. Biol.* 121:309-17
245. Young CM. 1995. Behavior and locomotion during the dispersal phase of larval life. In *Ecology of Marine Invertebrate Larvae*, ed. LR McEdward, pp. 249-78. Boca Raton, FL: CRC

Small-Scale Hydrodynamics of Feeding Appendages of Marine Animals

M.A.R. Koehl

Dept. of integrative Biology • University of California • Berkeley, California 94720 USA

Many animals in the ocean use appendages bearing arrays of hairs to capture molecules from the surrounding fluid (e.g. feathery gills take up oxygen; olfactory antennae capture odorants), to capture food particles (e.g. hairy suspension-feeding appendages catch single-celled algae), or to move the fluid around them (e.g. setulose appendages are used to swim or create ventilatory currents). Since hairy little appendages serve such important biological functions in animals from so many phyla, we have been trying to elucidate the basic rules governing how they all work.

Hydrodynamics of "Hairy Little Legs"

The performance of all the functions mentioned above (e.g. capturing molecules or particles; moving water) depends on how the arrays of hairs interact with the water around them (e.g. Koehl, 1981; 1995; Childress, et al., 1987). Therefore, the first step in analyzing how hairy appendages work is to figure out how fluid moves around and through them. The Reynolds number (Re) of a structure moving through a fluid represents the relative importance of inertial to viscous forces determining how the fluid moves; $Re = \rho LU / \mu$, where L is a linear dimension of the structure, U is fluid velocity relative to it, and ρ and μ are the density and viscosity (resistance to being sheared) of the fluid (e.g. Vogel, 1994). At high Re (e.g. large, rapidly-moving structures), inertial forces predominate and flow is messy and turbulent, whereas at low Re (e.g. small, slowly-moving structures), viscosity damps out disturbances in the fluid and flow is smooth and orderly. When fluid flows past a solid surface, the fluid in contact with the surface does not slip relative to the surface and a velocity gradient develops between the surface and the freestream flow. At low Re , this layer of sheared fluid between the surface of a moving structure and the still surrounding fluid is thick relative to the dimensions of the structure (e.g. Koehl, 1981; 1995). If we calculate the Re at which the hairs on the types of appendages listed above operate (using hair diameter for L), we find that they range between 10^{-5} and 10 (Rubenstein & Koehl, 1977; Koehl and Strickler, 1981;

... the first step in analyzing how hairy appendages work is to figure out how fluid moves around and through them.

Cheer and Koehl, 1987; 1988; Loudon, et al., 1994; Koehl, 1995). In this Re range viscosity is very important in determining flow patterns (although we cannot ignore the effects of inertia at the upper end of this Re range, Cheer and Koehl, 1987; 1988; Koehl, 1992; 1995). Since humans operate at high Re (approximately 10^6 when swimming), we cannot trust our intuitions when considering the viscous flow around arrays of little hairs.

In order to understand how arrays of hairs capture molecules or particles, or push fluids around, the first thing that we need to figure out is whether fluid flows through the gaps between the hairs in an array, or flows around the sides of the array rather than through it. We have defined the "leakiness" of an array of hairs as the proportion of the water encountering the gap between adjacent hairs that actually flows through the gap (Cheer and Koehl, 1987). The leakiness of a hair-bearing structure determines whether or not the structure can function as a filter, and it also affects the flux of molecules to hair surfaces and the ability of the appendage to generate thrust or lift (e.g. Koehl, 1995; 1996a). Since there is diversity in the size, structure, and behavior of hair-bearing appendages, another important piece of the puzzle that we have to address

is how the morphology and motion of a hairy leg affect its leakiness (Koehl, 1983; 1995; 1996b; Loudon, et al., 1994).

A general model of flow between neighboring hairs permits us to examine how the size, spacing, and speed of an array of hairs affect its leakiness (Cheer and Koehl, 1987; 1988). At small hair sizes ($Re = 10^{-5}$ to 10^{-3}), arrays of hairs have very low leakiness (i.e. only a small proportion of the water or air encountered actually goes through the gaps between hairs, while most flows around the array) and function like non-porous paddles. In contrast, from Re of 10^{-2} to 1, a transition in leakiness occurs: a structure that functioned like a paddle at low speed and small size becomes a leaky sieve at faster speed or larger size. We can apply these general principles to study how "hairy little legs" (such as the feeding appendages of copepods) work, and how their structure and behavior affect their performance.

Oceanography: Before we close, what about some general comments on Year of the Ocean?

Gaffney: The year is not over yet. The President, Vice President, Secretary of Commerce, Secretary of the Navy all showed up at the National Oceans Conference, in addition to a whole lot of good looking and important people. I don't recall, since I started hanging around this political-oceanography business in 1975, a better dialogue or critical mass of folks together. I am very happy that the Secretary of the Navy John Dalton, a former submariner, has become so personally interested in oceanography. He has played a personal role in the Navy's investment in the exposition in Lisbon. He was there for the opening. He was a co-sponsor for the Ocean Conference and participated personally and vigorously and went to tens of briefings on exactly how that conference would be set up and run perfectly. He offered the site for the conference at the Naval Postgraduate School, and he has become a vigorous, comfortable co-chairman of the National Ocean Research Leadership Council of the National Oceanographic Partnership Program. I think that is three times a miracle-and we've had many Secretaries of the Navy that have been interested in oceanography. I can name several of them, but Secretary Dalton has been more interested than any one else. That is just really great news for ONR who has a very large segment of its money invested in oceanography, and the Chief of Naval Research by law reports to the Secretary of the Navy. To have your boss intimately interested in the largest chunk of your investment is great. So, to me, the Year of the Ocean was a magnificent success.

We are a maritime nation and I think it is insane for the United States not to understand why the ocean is a part of why we are a great nation—it acts as both an insulator, and a conductor of this country. It keeps the bad things away, but it also brings us to the rest of the world. To not understand that medium is insane.

The Navy needs to understand maritime weather on the oceans, and that's what makes the Navy and the Marine Corps different from the other services. The Year of the Oceans put a spotlight on that. When the


*We are a maritime nation
and I think it is insane
for the United States
not to understand
why the ocean is a part of
why we are a great nation—
it acts as both an insulator,
and a conductor of this country.*

Secretary of the Navy gets involved in the Year of the Oceans, 45 admirals get involved as well, whether they like it or not, and now they all know about it.

Oceanography: Finally, consider the TOS international audience and a young graduate in ocean scientist coming into the research community right now. What is your advice?

Gaffney: What is your goal in life? Do you want to make a difference, live in a nice place, have adventure, or make a lot of money? Some of those things apply to research oceanographers, some don't. You're probably not going to be real rich. You'll probably be away from home a lot. On the other hand, you'll definitely have more adventures than your buddy down the street will.

And you've got to want to do something that is very important—I think the world is figuring out that the ocean is very important. We see threats to the environment. There's an awful lot of speculation whether there is global change going on and we have the chance to determine whether or not that is happening, and do something about it. The next generation is going to do something about that—the old guys are not going to do anything about that. The people in school, the post-docs now are going to have to wrestle with that problem and it could be a major issue. Just think of this. About 50%-maybe 75% of the world's population lives within 200km of the ocean, attracted by good recreation, better weather, and transportation options. Before the people you're talking about die, the population of the earth—at the rate we're going now—will double. I predict the same ratio will live along the shores—the stresses that will put on the edge of the ocean are incredible.

So I believe there is an incredible amount of work out there. Will you get rich? No. Will you do important, maybe the most important things for the planet? Yes, I think so. Will it be adventurous? Yes, absolutely. I would encourage you to go into the field, but if you go in thinking you're going to make a lot of money, be a millionaire being an ocean researcher, don't. 

Copepod Feeding Appendages

Calanoid copepods are abundant planktonic crustaceans that play a critical link in many marine food webs between single-celled algae and higher trophic levels such as fish. Since copepod feeding is so ecologically important, many studies measuring copepod feeding rates and selectivity have been conducted (reviewed in Koehl, 1984). To complement these studies, we have been working to figure out the physical mechanisms copepods use to catch particles like single-celled algae.

High-speed microcinematography of seawater labeled with dye and released from micropipettes near the animals while they were catching food particles revealed the appendage and water motions involved in copepod feeding (Koehl and Strickler, 1981; Koehl and Paffenhöfer, unpubl. data). The last stage in particle capture is performed by a pair of setulose appendages, the second maxillae (M2's; Fig. 1), that fling apart from each other and then squeeze back together again. Some species perform this capture motion with their setae (hairs) operating at Re of order 1, whereas others do it at hair Re as low as 10^{-2} (Koehl, 1981; Koehl and Strickler, 1981; Koehl, 1992; 1995). Remember, this represents the critical Re range in which the transition occurs between non-leaky paddle-like behavior and leaky sieve-like function.

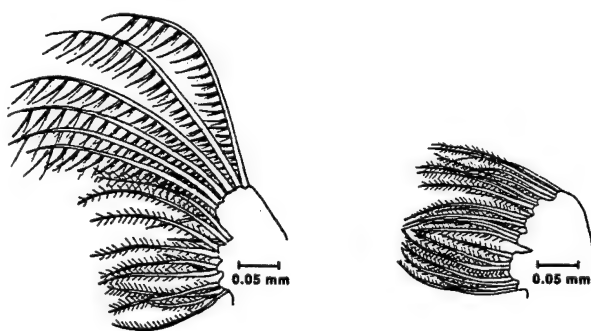
Analysis of the motions of M2's, particles, and dye in the movies of feeding copepods revealed that species such as *Centropages velificatus* that have coarsely-meshed M2's (Fig. 1) whose setae (hairs) operate at $Re = 1$, have leaky M2's and filter their food from the water during

... even though their feeding motions look qualitatively similar, the physical mechanisms by which these two copepods capture food are different ...

during the fling (Koehl 1981; Koehl and Strickler, 1981; Koehl, 1995). Thus, even though their M2 feeding motions look qualitatively similar, the physical mechanisms by which these two copepods capture food are different because they operate at Re above and below the transition from paddle to sieve. These copepod M2's provide examples of hairy appendages that look similar to each other and that move qualitatively in the same way, but that capture algal cells by different mechanisms during that motion simply because they operate at Reynolds

numbers on either side of the transition in leakiness.

We have been using physical models of copepod M2's to tease out whether leakiness is affected by the coarseness of the mesh of hairs on the M2's as well as by their speed. Like mathematical models, physical models permit us to vary only one parameter at a time to quantify its effects while holding all the other vari-



Centropages velificatus *Temora stylifera*

Figure 1. Diagrams of second maxillae from the calanoid copepods *Centropages velificatus* (whose setae operate at Reynolds numbers of order 1) and of *Temora stylifera* (whose setae operate at Reynolds numbers of order 10^{-2}).

the squeeze (Koehl, 1995). In contrast, other species such as *Temora stylifera* that have finely-meshed (Fig. 1), slowly-moving M2's whose setae operate at $Re = 10^{-2}$, have paddle-like M2's that capture food by drawing a parcel of water containing an alga towards the mouth

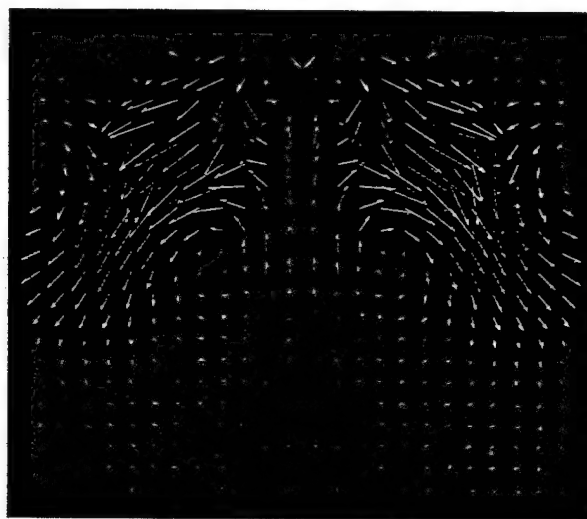


Figure 2. Diagram of the net displacement of water produced by the "fling-and-squeeze" motion of a pair of food-particle-capturing appendages (second maxillae, M2's) of the calanoid copepod *Centropages velificatus* (arrows indicate water direction and their color represents distance moved: blue ~ 460 μ m, green ~ 230 μ m, red < 1 mm). The gray bars indicate the positions of the M2's (390 μ m long) after the fling-and-squeeze is completed, and the gray circles represent the hinges between the M2's and the body surface of the animal. We are looking down on the anterior end of a copepod that is vertical in the water; the body of the animal is at the top of the picture, the M2's are on the ventral surface, and the mouth is midway between the M2's. During the fling, the M2's rotate away from each other, and during the squeeze, they rotate back towards each other. Some copepods operate their M2's so slowly that little water flows through the array of setae (hairs) on an M2, which therefore functions like a paddle moving water containing food particles towards the mouth. In contrast, *C. velificatus* moves its M2's more rapidly and water flows through rather than around the array of hairs on each M2. These leaky M2's can filter particles from the water moving through them, whereas paddle-like M2's cannot. As this diagram indicates, water is drawn towards the mouth and is passed laterally through the M2's when a *C. velificatus* does a fling-and-squeeze. This flow visualization was made using a dynamically-scaled physical model of a pair of *C. velificatus* M2's attached to a body surface, and this image was produced by T. Cooper using the particle image velocimetry program described by Cowan and Monismith (1997).

ables constant (Koehl, 1992; 1995); such manipulations are not possible in comparative studies with real animals. If a physical model and the prototype M2's are geometrically similar and operate at the same Re, then the ratios of the velocities and the forces at comparable positions in the flow field around the model are the same as those around the M2 (Vogel, 1994). Therefore, we can slowly flap large models of copepod M2's in high viscosity mineral oil at the Re used by the copepods, and we can also change the speeds of the models to make them operate at different Re used by other

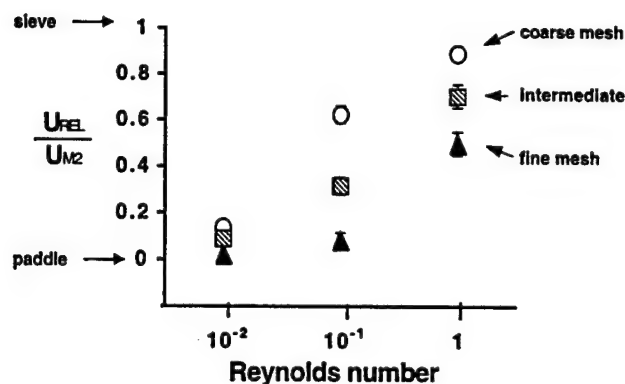


Figure 3. Flow through the middle of the array of hairs on models of the second maxillae of calanoid copepods: *Centropages velificatus* (coarse mesh of hairs on the second maxillae; indicated by circles), *Eucalanus pileatus* (intermediate mesh; shown by squares), and *Temora stylifera* (fine mesh; indicated by triangles). U_{REL} is the velocity of fluid between the hairs relative to the hairs, and U_M is the speed of the second maxilla; the ratio U_{REL}/U_M is an indication of leakiness (values near one are leaky and sieve-like, while values near zero are un-leaky and paddle-like). Even though *C. velificatus* operate their second maxillae at seta Reynolds numbers of order 1, while the other two species operate at Re of order 10^{-2} , we could run the models at any Re we chose. These experiments showed that at a Reynolds number of 10^{-2} , the coarseness of the mesh of hairs on a second maxilla makes no difference to its leakiness, whereas at Reynolds numbers of 10^{-1} and 1, coarsely-meshed appendages are leakier than finely-meshed ones (error bars indicate one standard deviation, $n = 3$ to 12).

species. By videotaping the paths of neutrally-buoyant marker particles in the fluid, we have measured the flow produced during the fling and squeeze (Fig. 2) and we have used these data to calculate the M2 leakiness. From such experiments we learned that the coarser the mesh, the leakier the M2's at $Re \geq 10^{-1}$, but that at $Re = 10^{-2}$, mesh coarseness has no effect on leakiness (Fig. 3). Although this result—that the morphology of an appendage only affects its performance at some Re, but not at others—seems non-intuitive, it was predicted from the basic physics of how fluids flow around cylinders (Cheer and Koehl, 1987; 1988; Koehl, 1992; 1995). We are now applying the same principles to investigate molecule capture by “hairy little noses” (e.g. we are studying the hydrodynamic design of olfactory antennules of a variety of crustaceans) (Koehl, 1996b).

REFERENCES

- Cheer, A. Y. L. and M. A. R. Koehl, 1987: Paddles and rakes: Fluid flow through bristle appendages of small organisms. *J. Theor. Biol.*, 129, 17-39.
- Cheer, A. Y. L. and M. A. R. Koehl, 1988: Fluid flow through filtering appendages of insects. *I.M.A. J. Math. Appl. Med. Biol.*, 4, 185-199.
- Childress, S., M. A. R. Koehl, and M. Miksis, 1987: Scanning currents in Stokes flow and the efficient feeding of small organisms. *J. Fluid Mech.*, 177, 407-436.
- Cowen, E.A., and S.G. Monismith, 1997: A hybrid digital particle tracking velocimetry technique. *Experiments in Fluids*, 22, 199-211.
- Koehl, M. A. R., 1981: Feeding at low Reynolds number by copepods. *Lectures in Mathematics in the Life Sciences*, 14, 89-117.
- Koehl, M. A. R., 1983: The morphology and performance of suspension-feeding appendages. *J. Theor. Biol.*, 105, 1-11.
- Koehl, M. A. R., 1984: Mechanisms of particle capture by copepods at low Reynolds number: Possible modes of selective feeding. In: *Trophic Interactions Within Aquatic Ecosystems*. D. L. Meyers and J. R. Strickler, eds., Westview Press, 135-160.
- Koehl, M. A. R., 1992: Hairy little legs: Feeding, smelling, and swimming at low Reynolds number. *Fluid Dynamics in Biology. Contemporary Mathematics*, 141, 33-64.
- Koehl, M. A. R., 1995: Fluid flow through hair-bearing appendages: Feeding, smelling, and swimming at low and intermediate Reynolds number. *Soc. Exp. Biol. Symp.*, 49, 157-182.
- Koehl, M. A. R., 1996a: When does morphology matter? *Ann. Rev. Ecol. Syst.*, 27, 501-542.
- Koehl, M. A. R., 1996b: Small-Scale fluid dynamics of olfactory antennae. *Mar. Fresh. Behav. Physiol.*, 27, 127-141.
- Koehl, M. A. R. and J. R. Strickler, 1981: Copepod feeding currents: Food capture at low Reynolds number. *Limnol. Oceanogr.*, 26, 1061-1073.
- Loudon, C., B. A. Best, and M. A. R. Koehl, 1994: When does motion relative to neighboring surfaces alter the flow through an array of hairs? *J. Exp. Biol.*, 193, 233-254.
- Rubenstein, D. I. and M. A. R. Koehl, 1977: The mechanisms of filter feeding: Some theoretical considerations. *Amer. Natur.*, 111, 981-994.
- Vogel, S., 1994: *Life in Moving Fluids: The Physical Biology of Flow*, 2nd Edition. Princeton University Press, Princeton.

Consequences of Size Change During Ontogeny and Evolution

M. A. R. Koehl

Changes in body size can occur during the lifetime of an individual organism as it grows, or can occur over many generations during the evolution of a lineage. Most studies of body size either explore how function is maintained at different sizes, or seek mechanistic explanations for the patterns we see in how features such as shape, metabolic rate, or life history vary with body size [7, 41, 53] (e.g., Brown this volume; Biewener this volume). My purpose here is to complement this literature about the consequences of *being* one size or another with an exploration of some of the functional consequences of *changing* size.

Function can shift as size changes, but the particular consequences of a size change can depend on factors such as the environment and morphology of the organism. This chapter focuses first on functional consequences of changing size, and then considers how the effects of morphological features on performance can be altered as size changes. This chapter concludes by considering how the consequences of a size change might be affected by: (1) the size range in which the change occurs, (2) the habitat, and (3) the structural design of the organism. I introduce each of these topics with a few examples, mostly biomechanical, and then discuss in more general terms their ecological or evolutionary consequences.

1 TRANSITIONS IN FUNCTION AS SIZE CHANGES

1.1 EXAMPLES OF FUNCTIONAL SHIFTS ACCOMPANYING SIZE CHANGE

1.1.1 Shifts in Hydrodynamic Function. Many important biological processes (such as respiration, and locomotion) depend on how organisms interact with the fluid medium, water or air, around them. The Reynolds number (\mathcal{R}) of a structure moving through a fluid represents the relative importance of inertial to viscous forces determining how the fluid moves ($\mathcal{R} = LU/\nu$, where L is a linear dimension of the structure, U is fluid velocity relative to it, and ν is kinematic viscosity of the fluid) [58]. At high \mathcal{R} 's (e.g., large, rapidly moving structures), inertial forces predominate and flow is messy and turbulent, whereas at low \mathcal{R} 's (e.g., small, slowly moving structures), viscosity damps out disturbances in the fluid and flow is smooth and orderly. Thus, we should expect changes in biological processes that involve fluids as body size (and hence \mathcal{R}) changes.

1.1.2 Hairy Little Legs. Many animals from different phyla use appendages bearing arrays of hairs (Figure 1(a)–(e)) to capture molecules from the surrounding fluid (e.g., feathery gills or olfactory antennae), to capture particles (e.g., hairy suspension-feeding appendages), or to move the fluid around them (e.g., setulose appendages used to fly, swim, or create ventilatory currents). When a particular type of structure is so ubiquitous among organisms and serves such critical biological functions, it is important to figure out how it works, and how its function is affected by its size.

The performance of all the functions mentioned above (e.g., capturing molecules or particles, moving water or air) depend on how the arrays of hairs interact with the fluid around them. Therefore, the first step in analyzing how these structures work is to figure out how fluid moves around and through them. The \mathcal{R} 's at which the hairs on the types of structures listed above operate [8, 9, 30, 35, 39, 52] (using hair diameter for L) range between 10^{-5} and 10. In this \mathcal{R} range viscosity is very important in determining flow patterns (although we cannot ignore the effects of inertia at the upper end of this \mathcal{R} range). When fluid flows past a solid surface, the fluid in contact with the surface does not slip relative to the surface and a velocity gradient develops between the surface and the free-stream flow. The layer of fluid along a solid surface in which this velocity gradient exists is called the boundary layer. Similarly, when a structure moves through water or air, the fluid contacting its surface is carried along with it and a boundary layer of sheared fluid develops along the structure's surface. The lower the \mathcal{R} , the thicker this layer of sheared fluid can be relative to the dimensions of the structure. Thus, in the case of viscous flow around a hair, the layer of fluid moving along with the hair can be quite thick relative to the hair's diameter, and little fluid may move through the gaps between adjacent hairs in an array [8, 9, 30]. Furthermore,

← antennae
(plural)

*we're working on
the quality of this
figure. good! It looks pretty bad now.*

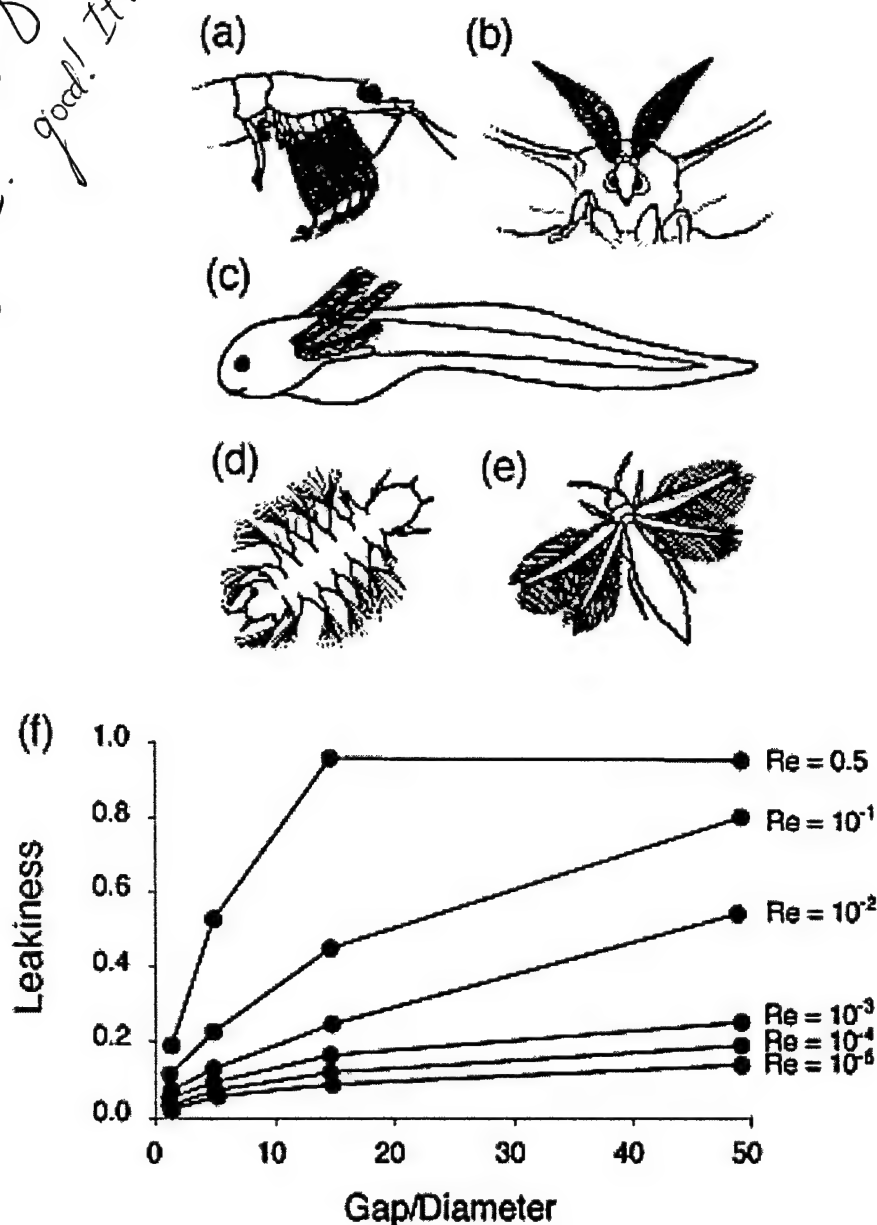


FIGURE 1 (a) Suspension-feeding appendages of a euphausiid ("krill"), Phylum Arthropoda. (b) Olfactory antennae of a male moth, Phylum Arthropoda. (c) External gills of a larval African lungfish, Phylum Chordata. (d) Swimming parapodia of a nereid larva, Phylum Annelida. (e) Wings of a thrips, Phylum Arthropoda. (f) Leakiness to fluid flow of the gap between neighboring hairs, plotted as a function of the ratio of the width of that gap to the diameter of a hair (redrawn from Koehl [32]). Each line represents a different Reynolds number.

flow is laminar (i.e., there is no turbulent mixing) in the \mathcal{R} range in which these hairs operate; hence, the only way that molecules can be spread across streamlines is via molecular diffusion. Since humans operate at high \mathcal{R} , we cannot trust our intuitions when considering the viscous flow around arrays of little hairs.

In order to understand how arrays of hairs capture molecules and particles, or push fluids around, the first thing that we need to figure out is whether fluid flows through the gaps between the hairs in an array, or flows around the array rather than through it. The leakiness (the proportion of the fluid encountering a gap between two hairs that flows through the gap rather than around the perimeter of the array of hairs [8]) of a hair-bearing structure determines, for example, whether or not the structure can function as a filter, the flux of molecules to hair surfaces, and the ability of the appendage to generate thrust or lift [30, 31]. Therefore, size (\mathcal{R}) should affect all of these leakiness-dependent functions.

A general model of flow between neighboring hairs permits us to examine how the size, spacing, and speed of an array of hairs affects its leakiness (Figure 1(f)). Each line in Figure 1 represents a different \mathcal{R} (i.e., a different size). At small hair sizes ($\mathcal{R} = 10^{-5}$ to 10^{-3}), arrays of hairs have very low leakiness (i.e., only a small proportion of the water or air encountered actually goes through the gaps between hairs, while most flows around the array) and function like nonporous paddles. In contrast, from \mathcal{R} 's of 10^{-2} to 1, a transition in leakiness occurs: a structure that functioned like a paddle at small size becomes a leaky sieve at larger size and filtering becomes possible. Thus, as hair-bearing appendages change size across this critical \mathcal{R} range, their function switches.

A biological example of this transition in leakiness is provided by calanoid copepods, abundant planktonic crustaceans that play a critical link in many marine food webs between single-celled algae and higher trophic levels such as fish. Copepods capture single-celled algae using a pair of hairy feeding appendages, the second maxillae (M2's), which they fling apart from each other and then sweep back together [35]. Some species perform this capture motion with their setae (hairs) operating at \mathcal{R} 's of order 10^{-2} ; their nonleaky, paddlelike M2's capture food by drawing a parcel of water containing an alga toward the mouth during the fling. In contrast, other species operate their M2's at setal \mathcal{R} 's of one and filter their food from the water as they sweep toward each other. Thus, even though their M2 feeding motions look qualitatively similar, the physical mechanisms by which these two species of copepods capture food are different because they operate at \mathcal{R} 's above and below the transition from paddle to sieve [30]. These results suggest that we might expect similar functional transitions during the ontogeny of the many aquatic larvae with setulose appendages that grow across this hair \mathcal{R} range where the transition in leakiness occurs.

1.1.3 Swimming. Other examples of transition in hydrodynamic function as size (R) changes are provided by studies of the ontogeny of swimming. As brine shrimp larvae get bigger, their propulsive mechanism switches from drag-based rowing at low R to inertial swimming at higher R , even though the flapping motion of their appendages does not change [61, 62]. Similarly, larval fish switch from drag-based swimming at low R to inertial propulsion when they grow to higher R [4, 47]. Furthermore, as larval fish increase in size and the importance of viscous force declines at higher R , intermittent swimming becomes more energetically advantageous [60]. Scallops provide another example of transitions in swimming performance with changes in body size [11, 40]. Scallops swim by jet propulsion by squirting water out of the mantle cavity while clapping their shells together. Very small juvenile scallops cannot use this inertial mode of locomotion effectively and are sedentary, whereas larger scallops can jet; once $R > 3000$, scallops are big enough to use lift to get up off the substratum. However, when scallops grow even larger, they become poor swimmers again as their shells grow too heavy relative to the thrust they can generate.

1.1.4 Walking on Water. Whether or not animals can walk on water depends on their size. Some animals, such as water striders, are held up by the surface tension acting along the perimeters of their feet. Since the force holding the animal up is proportional to length, while the weight of the animal is proportional to volume, there is a body size above which animals cannot use the surface-tension mechanism to walk on water [1].

Some larger animals, such as basilisk lizards, can run on water using a different physical mechanism: the force to support the lizard's body is provided by an upward impulse as the foot slaps onto the water surface, followed by an upward impulse as the foot strokes down into the water [17, 18]. There is also an upper limit to the body size for which this mechanism of locomotion on a water surface can work, since the weight that must be supported increases at a greater rate with body size than does the upward force that can be generated by the feet. These lizards also provide an example of another functional shift that can sometimes accompany increases in body size: at small size there can be permission for diversity in the ways in which the animals move their appendages without serious performance consequences, whereas at larger size limb movements can have a critical effect on performance [31]. Small basilisks, which have the capacity to generate a large force surplus relative to their body weight, can vary their limb movements considerably and still remain atop the water, whereas larger animals, which can generate barely enough force to support their weight, are constrained to a narrow range of leg and foot motions to run successfully on water [17, 18]. In the field, juveniles often run on water simply to move to another sunning spot, whereas adults venture onto the water only under duress.

just checking that there should be two upward impulses here

yes - there are two impulses

1.1.5 Solar Panels and Wings. An example of how an isometric change in body size has the potential to generate novel function is provided by wind-tunnel experiments using models of fossil insects of a range of sizes [26, 27]. The physical models were used to test various hypotheses about the aerodynamic and thermoregulatory consequences of changes in the length of protowings on early insects. At small body size, short thoracic protowings improved thermoregulatory performance, but had negligible effect on aerodynamic gliding, parachuting, or turning performance; in contrast, protowings of the same relative length on larger models improved aerodynamic performance. This illustrates that it is physically possible for a simple increase in body size to cause a novel function (i.e., a solar panel can become a wing) without requiring the invention of a novel structure. (Of course, whether or not protowings served thermoregulatory or aerodynamic roles in early insects remains speculative, as do other feasible hypothesized functions, such as sexual signaling, gas exchange, or skimming along the surface of a body of water.)

1.1.6 Trophic Role. Examples of functional shifts that accompany size change can be found in ecological studies of the trophic roles played by certain species of animals as they grow. For instance, some benthic marine worms that feed on sediment particles as adults have juvenile stages that are herbivorous or carnivorous. This size-dependent switch in feeding mode is thought to occur because the guts of little juveniles are too small to permit adequate digestion of nutrient-poor sediment particles [22, 24, 51]. Similarly, the type of prey that can be caught and ingested by certain species of predators can shift as body size increases (e.g., snakes [19], fish [46]).

Some species of prey grow large enough to become invulnerable to particular species of predators. The classic example of this type of switch in function that occurs as organisms grow is the size refuge attained by large mussels, *Mytilus californianus*, from predation by starfish (*Pisaster ocraceus*) [49]. Since *M. californianus* are important competitors for space on rocky shores along the Pacific coast of North America, their ability to undergo a transition from being the preferred prey of *P. ocraceus* to being not eaten by this keystone predator can have profound effects on the structure of the communities of organisms in these habitats [49, 50].

1.2 WHERE TO EXPECT FUNCTIONAL SHIFTS TO OCCUR AS SIZE CHANGES

There are bound to be many yet to be studied examples of functional shifts that occur as size changes. Some hints of where to expect such changes in function can be gleaned from the dimensionless numbers, worked out by engineers, to describe the relative importance of different physical factors involved in a process. In some of the examples cited above, the relative importance of inertia to viscosity (\mathcal{R}) depends on size (L). For biological functions involving momentum exchange between organisms and the water or air around them (e.g.,

Make this parenthetical a footnote?

No - please leave it as it is.

swimming, flying, ventilation, circulation), we can expect to find functional shifts as \mathcal{R} changes. Similarly, for biological functions involving transport of molecules, such as gas exchange, nutrient uptake, or smelling, the importance of fluid motion relative to molecular diffusion is given by the Péclet number ($Pé = LU/D$, where L is a linear dimension, U is velocity of the fluid relative to the structure, and D is the diffusion coefficient of the molecule of interest in the fluid) [58]. Like \mathcal{R} , $Pé$ depends on size (L). Pedestrian locomotion (walking, running) and swimming at the air-water interface depend on the importance of gravity relative to inertia (Froude number $= U^2/[gL]$, where g is the acceleration due to gravity), which also depends on size (L). ~~\times~~

no exponent

1.3 ECOLOGICAL AND EVOLUTIONARY SIGNIFICANCE OF FUNCTIONAL SHIFTS THAT OCCUR AS SIZE CHANGES

The examples cited above are but a few of the transitions in function that must accompany the size changes that occur during the ontogeny of an individual or the evolution of lineage. An important ecological consequence of such transitions is that a single species can play several different roles in a community if, for example, their feeding mode or their vulnerability to predation or physical disturbance changes as they grow [46, 49, 50]. An important evolutionary consequence of functional transitions that accompany size change is that new selective pressures on morphology can occur if a novel function is acquired as a lineage changes size over evolutionary time [26, 30].

2 TRANSITIONS IN THE EFFECTS OF MORPHOLOGY AND BEHAVIOR AS SIZE CHANGES

2.1 EXAMPLES OF SIZE-DEPENDENT CONSEQUENCES OF MORPHOLOGY AND BEHAVIOR

2.1.1 Hairy Little Legs. The hairy legs mentioned above provide examples of how the effects of a particular morphological characteristic or type of behavior can be altered as size changes. We have been using mathematical [8, 9, 30] and physical models [30, 38] to quantify how various structural or kinematic features of a row of hairs might affect its leakiness. For example, hair spacing has virtually no effect on leakiness at hair \mathcal{R} 's of order 10^{-3} and lower, but as size increases to \mathcal{R} 's of 10^{-2} to 1, spacing has an enormous effect on flow through the array of hairs. At even larger sizes ($\mathcal{R} > 1$), hair spacing once again has no effect on leakiness (unless hairs are very close together) (Figure 1). Adding more hairs to a row of hairs reduces the leakiness of the array if $\mathcal{R} < 1$, but has the opposite effect at larger size ($\mathcal{R} > 1$). Similarly, as size changes, there are transitions in which behaviors can affect the leakiness of hairy appendages. For example, moving the appendage near a wall (such as the body surface) increases leakiness at \mathcal{R} 's of 10^{-2} and lower, but not at

larger size. In contrast, speeding up appendage movement only affects leakiness at \mathcal{R} 's between 10^{-2} and one, but not at smaller or larger sizes. Thus, for hair-bearing appendages, a continuous change in size can lead to a discontinuous change in how particular morphological or behavioral traits affect performance.

2.1.2 Streamlining. The effect of body shape on drag depends on the size of the organism. Drag, a force which tends to push an organism in the direction that water or air flows past it, is due to skin friction (the resistance of the fluid in the boundary layer around the body to being sheared) at low \mathcal{R} 's, but is due to skin friction plus form drag (the net pressure on a body behind which a wake has formed) at high \mathcal{R} 's [58]. Streamlined body shapes (those with a long, tapered downstream end) reduce form drag compared with bluff body shapes of the same width because smaller wakes form behind the streamlined bodies, although the larger area of the long, tapered tail raises skin friction. Drag coefficient (C_D) is a dimensionless index of how drag-inducing a body shape is. For large organisms operating at high \mathcal{R} 's, at which form drag is much greater than skin friction, streamlining reduces C_D , but for small organisms at low \mathcal{R} that only experience skin friction, streamlining increases C_D . For example, C_D 's of globose ammonoid shells are higher than C_D 's of flat, streamlined shells at $\mathcal{R} > 100$, but the reverse is true for smaller shells at lower \mathcal{R} [23]. Similarly, the C_D of small ($\mathcal{R} = 1$ to 10) benthic stream invertebrates is lower if their shape is more hemispherical, whereas the C_D of larger animals is lower ($\mathcal{R} = 1000$) if they are more flattened [56].

2.1.3 Bumpy Skin. Body size determines whether or not bumps on the skin of an organism affect drag [6, 28, 57, 58]. When organisms are small, surface texture is buried in the boundary layer and has no effect on drag, whereas at very high \mathcal{R} 's surface bumps can protrude through the boundary layer and increase skin friction drag. The net drag on streamlined bodies is simply increased by skin bumps once the critical \mathcal{R} (i.e., size) is reached. Changes in body size have more complex consequences for organisms that are not streamlined: at small sizes (\mathcal{R} 's) surface texture has no effect on drag, whereas at large sizes surface bumps increase the drag; however, at intermediate sizes surface bumps have the opposite effect and *decrease* the drag (mechanisms explained in Vogel [58] and Koehl [31]).

2.1.4 Gliding. The wing shape that improves the distance traveled by gliding animals or plant seeds depends on body size. Short, wide wings enhance gliding at small size, whereas long, narrow wings improve performance at large size [14].

2.2 ECOLOGICAL AND EVOLUTIONARY CONSEQUENCES OF SIZE-DEPENDENT CONSEQUENCES OF MORPHOLOGY AND BEHAVIOR

The effects of structure or kinematics on performance can shift as size changes. Therefore, if size changes during the evolution of a lineage, then selection for different morphologies or behaviors can occur for the large species than for the small ones, even if their function does not change. Ecomorphologists and paleontologists use morphological characters of organisms to infer their ecological roles, their function, or their performance of particular tasks relative to other organisms (reviewed in Koehl [31]). In doing so, they should be aware that a particular morphological trait may have very different effects on the performance of small organisms than it does on the functioning of larger ones. Which morphologies correlate with particular ecological roles can depend on size.

...for the large species rather than for the small ones...

3 THE CONSEQUENCES OF SIZE CHANGES DEPEND ON SIZE

3.1 EXAMPLES OF SIZE-DEPENDENT EFFECTS OF SIZE CHANGE

In the introductory chapter of this book, Brown discusses examples of plotting power functions on both linear and logarithmic axes. If we look at linear plots of the performance of some process as a function of body size, it is easy to see that various aspects of performance vary with body size in nonlinear ways. The size ranges for which such nonlinear plots have steep slopes are the ranges in which a change in size can have important consequences. In contrast, within the size ranges for which the slope is very shallow, modifications of size make little difference to performance. If the sign of the slope of such a plot changes, then an increase in size can have the opposite effect for small organisms than for large ones.

3.1.1 Exponential Relationships Between Size and Performance. An example of an exponential curve is shown in Figure 2, a plot of predator handling time as a function of prey size [13]. Differences in the size of small prey have little effect on predator handling time and hence on the prey's likelihood of being eaten, whereas differences in body size between larger prey can have a big effect on the danger of becoming a meal.

Many aspects of mechanical performance also have exponential relationships to size. For example, the deflection of a bending beam bearing a distributed load is proportional to its length⁴, so the effect of a 10-cm increase in the height of a sessile, cantileverlike organism of a given width being bent by ambient water flow is small if the organism is short, but is large if an organism of the same width is tall [31]. There are many other examples of exponential relationships between function and size [1, 2, 41, 42, 58, 59], including the

length⁴

This should be length followed by the exponent 4

an alternative would be to write: "length raised to the fourth power"

or, to be consistent with p.B, this could be the capital letter "L" with the exponent 4

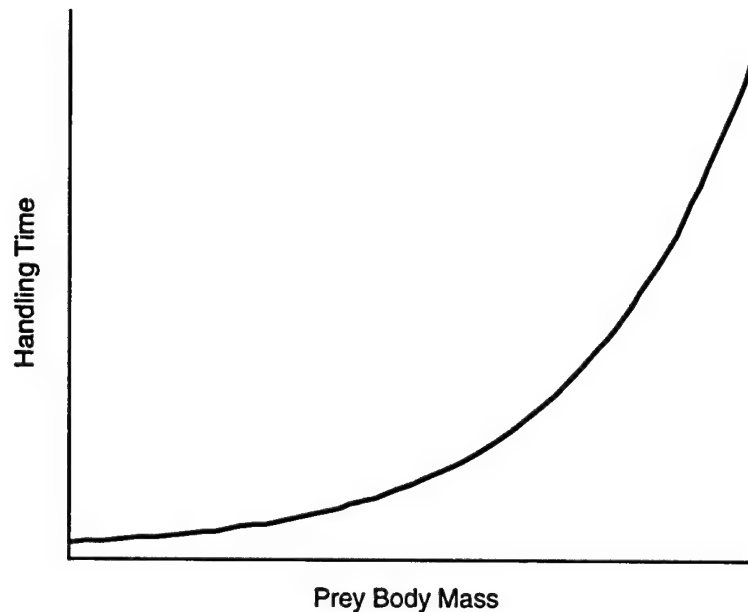


FIGURE 2 Handling time for a predator, plotted as a function of the body size of the prey (redrawn from a curve calculated by Emerson et al. [13]).

volume of fluid per time that can be pushed through a pipe (such as a blood vessel) by a given pressure difference, which is proportional to pipe diameter d , or the weight that must be borne by a skeleton, which is proportional to body volume ($\propto \text{length}^3$).

3.1.2 Optimal Sizes. If the plot of some aspect of an organism's performance as a function of body size goes through a maximum or a minimum, then the effect of increasing size reverses once it passes a critical value. One of many examples of how the consequence of a change in size can reverse as size increases is provided by Sebens [54], who analyzed the energetics of suspension-feeding animals. The energy available for growth and reproduction increases as such animals get larger up to a point, beyond which further increments in size have the opposite effect and reduce the excess energy for growth and gonad (Figure 3). We usually consider such curves in the context of optimization analyses [3, 48], and we try to relate such maxima and minima to the peaks and troughs in adaptive landscapes [16, 25]. In addition, we might also consider that passing through such an inflection point represents the acquisition of a novel consequence for a size change.

use the symbol " \propto "
or write \propto
"proportional to"

This should say:
(proportional to
 length^3)

(or "proportional
to L^3 " to
be consistent with
page 13)

this should be
by diameter followed
by the exponent d

An alternative
would be to say
"diameter raised
to the fourth
power."

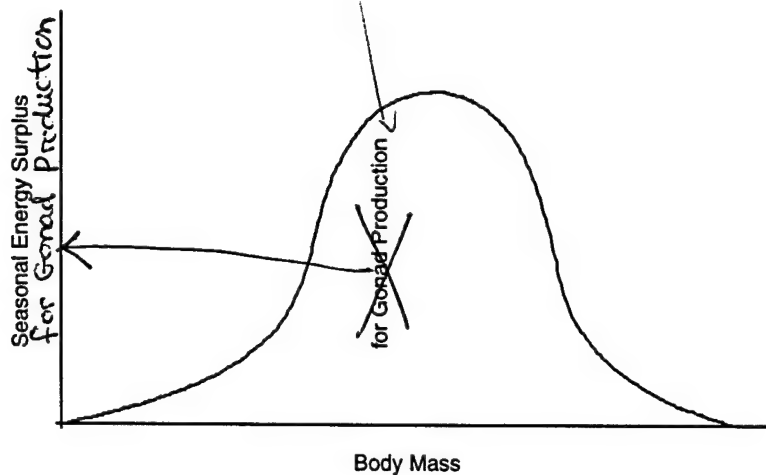


FIGURE 3 Energy surplus available for gonad production for an entire season, plotted as a function of the body mass of a passive suspension feeder, when prey sizes are normally distributed (redrawn from a curve calculated by Sebens [54]).

4 THE CONSEQUENCES OF SIZE CHANGE DEPEND ON MORPHOLOGY

4.1 EXAMPLES OF MORPHOLOGY-DEPENDENT EFFECTS OF SIZE CHANGE

4.1.1 Hairy Legs. Our recent work using dynamically scaled physical models to study the water flow through the setulose feeding appendages of copepods has shown that morphology affects the size at which the transition occurs between functioning like a nonleaky paddle and working like a leaky sieve. Coarsely meshed appendages become filters at smaller size than do appendages bearing closely spaced hairs [34].

4.1.2 Hydrodynamic Forces on Sessile Marine Organisms in Waves. The structure of the skeletal support tissues of sessile marine organisms can affect the hydrodynamic consequences of increasing size [31]. The microarchitecture of the support tissues determines their resistance to deformation, which in turn affects the flexural stiffness of the organism. Many marine organisms attached to the substratum, such as stony corals, are supported by stiff skeletal materials. In contrast, others like flexible gorgonians and seaweeds are made of tissues that are less stiff and can bend when subjected to hydrodynamic forces. All these attached organisms risk being dislodged or broken by ocean waves. We have been studying how the stiffness of their tissues affects the magnitude of the hydrodynamic forces they experience in the back-and-forth

*oops - just "coral"
should go in index -
I goofed with my
highlighter*

The label for the y-axis is missing!

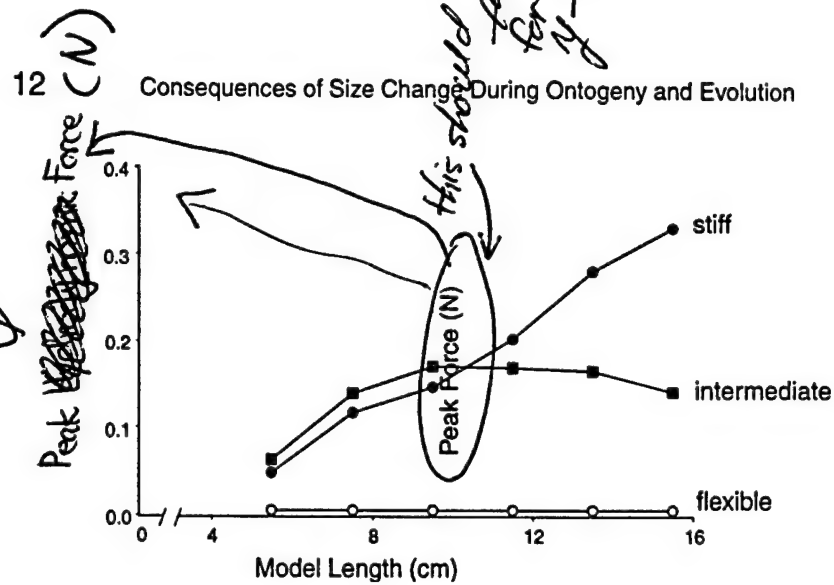


FIGURE 4 Peak hydrodynamic force in oscillatory flow measured on models of upright, planar benthic organisms, plotted as a function of model length. Each line represents a different flexural stiffness. (Redrawn from Koehl [31]).

accelerational flow they experience in waves. One approach that we have used is to build models of generic organisms, holding shape constant but using different materials to provide a range of flexural stiffness. We measured the hydrodynamic forces on such models of different lengths in a wave tank (Figure 4). As the stiff models "grew," the force increased. In contrast, the very flexible models flopped over into more streamlined shapes and went with the flow such that the force they bore did not measurably increase with length. A third type of size-dependent behavior was shown by the models of intermediate stiffness: lengthening increased hydrodynamic forces on short models, had no effect on models of intermediate length, and decreased forces on long models. Since deflection of a cantilever depends on length⁴, the longer the models of intermediate stiffness become, the more they bend over and go with the flow.

4.2 ECOLOGICAL AND EVOLUTIONARY CONSEQUENCES OF MORPHOLOGY-DEPENDENT CONSEQUENCES OF SIZE CHANGE

If the effects of changing size depend on structure, then the consequences of growth or of evolutionary shifts in size can be different for organisms of various morphologies. Ecological modelers should be mindful that a single size-dependent expression may not describe the function of diverse members of a community. Furthermore, when organisms alter their morphology during ontogeny, the quantitative relationship between certain aspects of performance and body size can change. For example, when copepods shift from the body form of the nauplius larva to the morphology of the copepodid stages, the slope

← length⁴
 ↑
 length followed by the exponent 4 —
 or else say "length raised to the fourth power"

↑
 or "L⁴"
 to be consistent with page 13

of the log-log plot of mass-specific metabolic rate as a function of body mass switches from ~ 1 (indicating little change as size increases) to $\ll 1$ (indicating a decline as size increases) [15]. Thus, a single size-dependent expression may not even describe a single species in a community.

5 THE CONSEQUENCES OF SIZE CHANGE DEPEND ON HABITAT

5.1 EXAMPLES OF HABITAT-DEPENDENT EFFECTS OF SIZE CHANGE

5.1.1 Hydrodynamic Forces on Sessile Organisms. The effect of size on the hydrodynamic forces on stiff sessile organisms depends on whether they live in habitats exposed to waves or to unidirectional water currents [12]. When exposed to waves, organisms experience acceleration reaction force as well as drag. The acceleration reaction force is proportional to the volume of the organism, and hence increases with L^3 , while the attachment area of the organism ~~goes as~~ L^2 . Therefore, in wave-swept habitats an increase in body size leads to an increase in the probability of being swept off the shore by waves. In contrast, sessile organisms in habitats subjected to unidirectional water currents only experience drag force, which depends on their projected area. Since both drag and attachment strength are proportional to L^2 , growth does not impose an increased risk of being ripped off the substratum like it does in wave-swept habitats.

Water-flow habitat also affects the consequences of growth for flexible organisms, but differently from stiff organisms [31]. In unidirectional currents, both the drag and attachment strength of flexible creatures are proportional to L^2 , as for stiff organisms. However, flexible organisms in the back-and-forth flow of waves can experience a reduction in hydrodynamic forces as they increase in length beyond the distance the water travels before it stops and flows back the other way, as measured on real kelp in the field as well as on models in a wave tank [33].

5.1.2 Spawning by Sessile Organisms. Many attached marine organisms spawn gametes into the surrounding water. An increase in body height improves gamete transport and mixing in gentle currents, but has no effect in turbulent waves [31].

5.1.3 Suspension Feeding by Colonial Animals. The effect of an increase in the size of a colony of suspension-feeding bryozoans can depend on the hydrodynamic environment in which the colony lives [44, 45]. An increase in colony size can lead to a decrease in particle-capture rate per zooid in habitats characterized by slow currents, as upstream zooids deplete the water of food. However, in habitats exposed to rapidly flowing water, colony growth has the opposite effect on feeding rates per zooid: larger colonies are more effective than small

is proportional
to

uncertain what you mean by
"goes as L^2 "

ones at slowing the water flowing through them enough that zooids can catch and hold on to food particles.

5.2 ECOLOGICAL AND EVOLUTIONARY CONSEQUENCES OF HABITAT-DEPENDENT CONSEQUENCES OF SIZE CHANGE

Since the performance consequences of changing size can depend on habitat, analyses of size and scaling should be done in the context of the environment in which the organisms live. Furthermore, the habitat dependence of the effects of size suggests that, when organisms disperse to new habitats or when the environment changes, selection on body size can change. Striking examples of this are provided by the evolutionary size changes exhibited by isolated populations of mammals on islands where resource availability and predation pressure are different from those on the mainland (e.g., Lomolino [37]).

6 EVOLUTIONARY CONSEQUENCES OF SIZE CHANGES

6.1 ANOTHER POSSIBLE MECHANISM FOR THE ORIGIN OF NOVELTY

A variety of mechanisms have been proposed for the origin of novelty during the process of evolution (reviewed by Koehl [31]). Size change should be added to the list. There is ample evidence for selection on body size, and there are many examples in the fossil record of size changes within lineages over evolutionary time (reviewed by Koehl [31]). Many studies of organism size have explored how body allometry permits function to be maintained at different sizes. However, another way to think about allometry is to consider that if organisms do *not* change their form as they change in size, their function *is* altered, and such functional shifts might be a source of evolutionary innovation.

One obvious mechanism by which a change in body size might lead to evolutionary novelty is that a structure acquires a new function once size crosses some threshold. That structure then becomes subject to a different suite of selective pressures than it was when it performed the old function at the former size. A similar mechanism by which size change might contribute to evolutionary novelty is that morphological and kinematic diversity might accumulate at small size without consequences to the performance or fitness of the organisms, but might gain functional significance and thus become subject to natural selection at larger size (reviewed by Koehl [31]).

A third mechanism by which size change might lead to evolutionary innovation is that size differences in developing embryos can affect pattern formation, thereby producing novelties in adult morphology (reviewed by Koehl [31]).

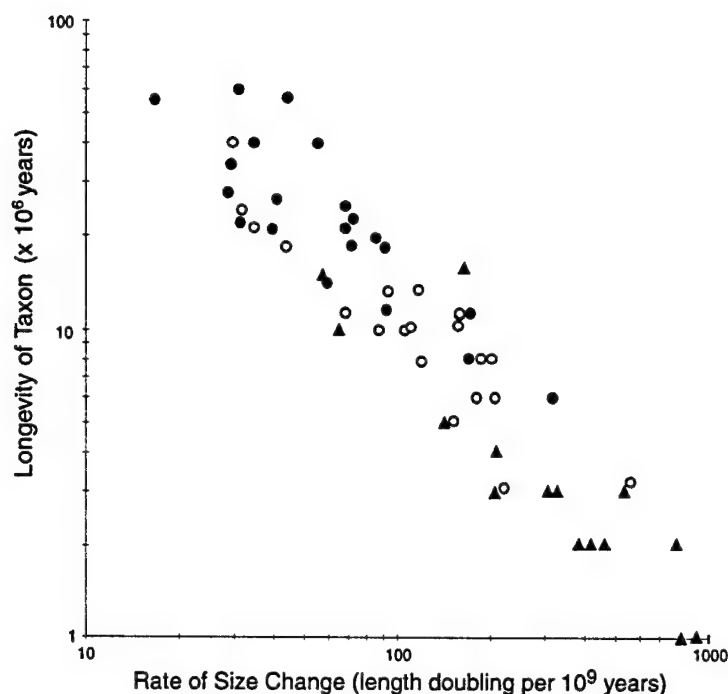


FIGURE 5 Longevity of each taxon in the fossil record, plotted as a function of the rate of change of body size, for Jurassic ammonites (each triangle represents a genus) and bivalved mollusks (each black circle represents a genus; each open circle represents a species). (Redrawn from Koehl [31]; data from Hallam [20].)

6.2 POSSIBLE EFFECTS OF SIZE CHANGE ON RATES OF EVOLUTION

Since shifts in size can be accompanied by alterations in function and changes in the consequences of particular morphological features, a reasonable speculation might be that rapid evolutionary change should tend to occur when size changes within a lineage. If we assume that short taxon longevity is a rough indication of rapid evolutionary change (i.e., high rates of modification or extinction), then Jurassic ammonites and bivalves (Figure 5) provide fossil evidence consistent with this speculation, but obviously this issue requires further study. For example, extinction might be due to acquisition of "poor" function accompanying a size change in the face of a shifting abiotic or biotic environment, or it might be the consequence of random events. Nonetheless, the pattern revealed by Hallam's data is intriguing.

7 CONCLUSIONS

Changes in body size can occur during the ontogeny of an individual or during the evolution of a lineage. The examples of the consequences of such size changes cited in this chapter illustrate that the effects of becoming larger or smaller are complicated, can involve dramatic transitions in function, and can depend on the morphology and habitat of the organisms. My point in raising these examples is *not* that the consequences of changing size are too complex to be understood using simple rules. Quite to the contrary, my point is that basic physical principles permit us to understand and to predict such transitions in the functional consequences of size changes.

ACKNOWLEDGMENTS

I am grateful to the following people for leads into the literature and/or discussions that helped shape my thinking about the issues addressed above: J. Brown, H. Greene, D. Jablonsky, J. Kingsolver, R. Paine, J. Valentine, S. Vogel, S. Wainwright, and the participants in the biomechanics discussion group at the University of California, Berkeley. I thank K. Bishop for preparing the figures. My data presented here were gathered with support from National Science Foundation Grant #OCE-9217338, Office of Naval Research Grant #N00014-96-1-0594, and a MacArthur Fellowship.

REFERENCES

- [1] Alexander, R. M. *Size and Shape*. London: Edward Arnold, 1971.
- [2] Alexander, R. M. *Locomotion of Animals*. New York & Glasgow: Blackie, 1982.
- [3] Alexander, R. M. *Optima for Animals*. London: Edward Arnold, 1982.
- [4] Batty, R. S. "Development of Swimming Movements and Musculature of Larval Herring (*Clupea harengus*).*" J. Exp. Biol.* **37** (1984): 129-153.
- [5] Berg, H. C., and E. M. Purcell. "Physics of Chemoreception." *Biophys. J.* **20** (1977): 193-219.
- [6] Bushnell, D. M., and K. J. Moore. "Drag Reduction in Nature." *Ann. Rev. Fluid Mech.* **23** (1991): 65-79.
- [7] Calder, W. A., III. *Size, Function, and Life History*. Cambridge, MA: Harvard University Press, 1984.
- [8] Cheer, A. Y. L., and M. A. R. Koehl. "Fluid Flow through Filtering Appendages of Insects." *I.M.A.J. Math. Appl. Med. Biol.* **4** (1987): 185-199.
- [9] Cheer, A. Y. L., and M. A. R. Koehl. "Paddles and Rakes: Fluid Flow through Bristled Appendages of Small Organisms." *J. Theor. Biol.* **129** (1987): 17-39.

- [10] Craig, D. A. "Behavioral Hydrodynamics of *Cloeon dipterum* Larvae (Ephemeropter: Baetidea)." *J. N. Am. Benthol. Soc.* **9** (1990): 346-357.
- [11] Dadswell, M. J., and D. Weihs. "Size-Related Hydrodynamic Characteristics of the Giant Scallop, *Placopecten magellanicus* (Bivalvia: Pectinidae)." *Can. J. Zool.* **68** (1990): 778-785.
- [12] Denny, M. W., T. Daniel, and M. A. R. Koehl. "Mechanical Limits to the Size of Wave-Swept Organisms." *Ecol. Monogr.* **55** (1985): 69-102.
- [13] Emerson, S. B., H. W. Greene, and E. L. Charnov. "Allometric Aspects of Predator-Prey Interactions." In *Ecological Morphology: Integrative Organismal Biology*, edited by P. C. Wainwright and S. M. Reilly, 123-139. Chicago: University of Chicago Press, 1994.
- [14] Ennos, A. R. "The Effect of Size on the Optimal Shapes of Gliding Insects and Seeds." *J. Zool., Lond.* **219** (1989): 61-69.
- [15] Epp, R. W., and W. M. Lewis, Jr. "The Nature and Ecological Significance of Metabolic Changes During the Life History of Copepods." *Ecology* **611** (1980): 259-264.
- [16] Futuyma, D. J. *Evolutionary Biology*. Sunderland, MA: Sinaur Associates, 1986.
- [17] Glasheen, J. W. "A Hydrodynamic Model of Locomotion in the Basilisk Lizard." *Nature* **380** (1996): 340-342.
- [18] Glasheen, J. W., and T. A. McMahon. "Weight Support on the Water Surface in Basilisk Lizards." *Nature* **380** (1996): 340-342.
- [19] Godley, J. S. "Foraging Ecology of the Striped Swamp Snake, *Regina alleni* in Southern Florida." *Ecol. Monogr.* **50** (1980): 411-436.
- [20] Hallam, A. "Evolutionary Size Increase and Longevity in Jurassic Bivalves and Ammonites." *Nature* **258** (1975): 493-496.
- [21] Hansen, B., and P. Tiselius. "Flow through the Feeding Structures of Suspension Feeding Zooplankton: A Physical Model Approach." *J. Plankton Res.* **14** (1992): 821-834.
- [22] Hentschel, B. T. "Spectrofluorometric Quantification of Neutral and Polar Lipids Suggests a Food-Related Recruitment Bottleneck for Juveniles of a Deposit-Feeding Polychaete Population." *Limnol. Oceanogr.* **43** (1998): 543-549.
- [23] Jacobs, D. K. "Shape, Drag, and Power in Ammonoid Swimming." *Paleobiology* **18**(1992): 203-220.
- [24] Jumars, P. A., L. M. Deming, J. A. Baross, and R. A. Wheatcroft. "Deep-Sea Deposit-Feeding Strategies Suggested by Environmental and Feeding Constraints." *Phil. Trans. Roy. Soc. Lond. Sec. A* **331** (1990): 85-101.
- [25] Kingsolver, J. G. "Thermoregulation, Flight, and the Evolution of Wing Pattern in Pierid Butterflies: The Topography of Adaptive Landscapes." *Am. Zool.* **28** (1988): 899-912.
- [26] Kingsolver, J. G., and M. A. R. Koehl. "Aerodynamics, Thermoregulation, and the Evolution of Insect Wings: Differential Scaling and Evolutionary Change." *Evolution* **39** (1985): 488-504.

note: This is the same book as is cited for ref. #57, so their format should be done the same way

company of Biologists publisher?

J. Jed
need initials for Jed, maybe more info not yet

need reference pops! it's the same paper

- [27] Kingsolver, J. G., and M. A. R. Koehl. "Selective Factors in the Evolution of Insect Wings." *Ann. Rev. Entomol.* **39**(1994): 425-451.
- [28] Koehl, M. A. R. "Effects of Sea Anemones on the Flow Forces They Encounter." *J. Exp. Biol.* **69** (1977): 87-105.
- [29] Koehl, M. A. R. "Mechanisms of Particle Capture by Copepods at Low Reynolds Number: Possible Modes of Selective Feeding." In *A.A.A.S. Selected Symposium #85: Trophic Interactions within Aquatic Ecosystems*, edited by D. L. Meyers and J. R. Strickler, 135-160. Boulder, CO: Westview Press, 1984.
- [30] Koehl, M. A. R. "Fluid Flow through Hair-Bearing Appendages: Feeding, Smelling, and Swimming at Low and Intermediate Reynolds Number." In *Biological Fluid Dynamics. Soc. Exp. Biol. Symp.*, Vol. 49, edited by C. P. Ellington and T. J. Pedley, 157-182, 1995.
- [31] Koehl, M. A. R. "When Does Morphology Matter." *Ann. Rev. Ecol. System.* **27** (1996): 501-542.
- [32] Koehl, M. A. R. "Small-Scale Fluid Dynamics of Olfactory Antennae." *Mar. Fresh. Behav. Physiol.* **27** (1996): 127-141.
- [33] Koehl, M. A. R. Unpublished data.
- [34] Koehl, M. A. R., and J. Jed. Unpublished data.
- [35] Koehl, M. A. R., and J. R. Strickler. "Copepod Feeding Cuments: Food Capture at Low Reynolds Number." *Limnol. Oceanogr.* **26** (1981): 1062-1073.
- [36] Koehl, M. A. R., and S. A. Wainwright. "Mechanical Adaptations of a Giant Kelp." *Limnol. Oceanogr.* **22** (1977): 1067-1071.
- [37] Lomolino, M. V. "Body Size of Mammals on Islands: The Island Rule Reexamined." *Amer. Natur.* **125** (1985): 310-316.
- [38] Loudon, C., and M. A. R. Koehl. 1994.
- [39] Loudon, C., B. A. Best, and M. A. R. Koehl. "When Does Motion Relative to Neighboring Surfaces Alter the Flow through an Array of Hairs?" *J. Exp. Biol.* **193** (1994): 233-254.
- [40] Manuel, J. L., and M. J. Dadswell. "Swimming of Juvenile Sea Scallops, *Placopecten magellanicus* (Gmelin): A Minimum Size for Effective Swimming." *J. Exp. Mar. Biol. Ecol.* **174** (1993): 137-175.
- [41] McMahon, T. A., and J. T. Bonner. *On Size and Life*. New York: W. H. Freeman, 1983.
- [42] Niklas, K. J. *Plant Biomechanics: An Engineering Approach to Plant Form and Function*. Chicago: University of Chicago Press, 1992.
- [43] Niklas, K. J. *Plant Allometry: The Scaling of Form and Process*. Chicago: University of Chicago Press, 1994.
- [44] Okamura, B. "The Effects of Ambient Flow Velocity, Colony Size, and Upstream Colonies on the Feeding Success of Bryozoa. I. *Bugula stolonifera* (Ryland), an Arborescent Species." *J. Exp. Mar. Biol. Ecol.* **83** (1984): 179-193.
- [45] Okamura, B. "The Effects of Ambient Flow Velocity, Colony Size, and Upstream Colonies on the Feeding Success of Bryozoa-II. *Conopeum ret-*

- icalum* (Linnaeus), an Encrusting Species." *J. Exp. Mar. Biol. Ecol.* **89** (1985): 69-80.
- [46] Osenberg, C. W., E. E. Werner, G. C. Mittelbach, and D. J. Hall. "Growth Patterns in Bluegill (*Lepomis macrochirus*) and Pumpkinseed (*L. gibbosus*) Sunfish: Environmental Variation and the Importance of Ontogenetic Niche Shifts." *Can. J. Fish. Res. Aquatic Sci.* **45** (1988): 17-26.
- [47] Osse, J. W. M., and M. R. Drost. "Hydrodynamics and Mechanics of Fish Larvae." *Pol. Arch. Hydrobiol.* **36** (1983): 455-466.
- [48] Oster, G. F., and E. O. Wilson. *Caste and Ecology in the Social Insects*. Princeton, NJ: Princeton University Press, 1978.
- [49] Paine, R. T. "Size-Limited Predation: An Observational and Experimental Approach with the *Mytilus*-*Pisaster* Interaction." *Ecology* **57** (1976): 858-873.
- [50] Paine, R. T. ~~*Marine Rocky Shores and Community Ecology: An Experimentalist's Perspective*~~, edited by O. Kinne. Oldendorf/Luhe: Ecology Institute, 1994.
- [51] Penry, D. L., and P. A. Jumars. "Gut Architecture, Digestive Constraints and Feeding Ecology of Deposit-Feeding and Carnivorous Polychaetes." *Oecologia* **82** (1990): 1-11.
- [52] Rubenstein, D. I., and M. A. R. Koehl. "The Mechanisms of Filter Feeding: Some Theoretical Considerations." *Amer. Natur.* **111** (1977): 981-994.
- [53] Schmidt-Nielsen, K. *Scaling: Why Is Animal Size So Important?* Cambridge: Cambridge University Press, 1984.
- [54] Sebens, K. P. "The Limits to Indeterminate Growth: An Optimal Size Model Applied to Passive Suspension Feeders." *Ecology* **63** (1982): 209-222.
- [55] Statzner, B. "Growth and Reynolds Number of Lotic Macroinvertebrates: A Problem for Adaptation of Shape to Drag." *Oikos* **51** (1988): 84-87.
- [56] Statzner, B., and T. F. Holm. "Morphological Adaptation of Shape to Flow: Microcurrents Around Lotic Macroinvertebrates with Known Reynolds Numbers at Quasi-Natural Flow Conditions." *Oecologia* **78** (1989): 145-157.
- [57] Videler, J. J. "Body Surface Adaptations to Boundary-Layer Dynamics." In *Biological Fluid Dynamics, Soc. Exp. Biol. Symp.* **49**, edited by C. P. Ellington and T. J. Pedley, 1-20. London: Company of Biologists, 1995.
- [58] Vogel, S. *Life in Moving Fluids*. Princeton, NJ: Princeton University Press, 1994.
- [59] Wainwright, S. A., W. D. Biggs, J. D. Currey, and J. W. Gosline. ~~*Mechanical Design in Organisms*~~, edited by E. Arnold. Princeton: Princeton University Press, 1976.

no - It is a whole
need title of chapter and page
range
book -
Kinne is
the editor
of the
series of
books.

need title of chapter and page
range
no - it's the
whole book.

omit.

- [60] Weihs, D. "Energetic Significance of Changes in Swimming Modes During Growth of Larval Anchovy *Engraulis mordax*." *Fishery Bull. Fish Wildl. Serv. US* 77 (1980): 597-604.
- [61] Williams, T. A. "Locomotion in Developing Artemia Larvae: Mechanical Analysis of Antennal Propulsors Based on Large-Scale Physical Models." *Biol. Bull.* 187 (1994): 156-163.
- [62] Williams, T. A. "A Model of Rowing Propulsion and the Ontogeny of Locomotion in Artemia Larvae." *Biol. Bull.* 187 (1994): 164-173.

SSP-06: Small Scale Hydrodynamics of Particle and
Odorant Capture by Animals

M. A. R. Koehl (cnidaria@socrates.berkeley.edu),
Department of Integrative Biology, University of
California at Berkeley 94720-3140, USA

Many marine animals use appendages bearing arrays of hairs to capture food or molecules from the surrounding fluid, or to locomote or create currents past themselves. The performance of these functions by hair-bearing appendages depends on how much of the fluid that they encounter flows through the gaps between the hairs rather than around the perimeter of the whole array. We have conducted high-speed kinematic analyses of various hair-bearing structures (e.g. particle-capturing appendages of copepods; olfactory antennae of various crustaceans) and have used these data to design dynamically-scaled physical models. We have used flow visualizations around the physical models as well as mathematical models to elucidate the factors that determine the leakiness of an array of hairs. Our work has revealed that different aspects of morphology and behavior are important in determining the performance of hairy appendages at different Reynolds numbers.

(1998) *Oceanography* 11: 26.

**STOMATOPOD SNIFFING: THE SCALING OF CHEMOSENSORY
SENSILLAE AND FLICKING BEHAVIOR WITH BODY SIZE**

January 30, 1999

K.S. Mead¹, M.A.R. Koehl¹, and M. J. O'Donnell²

1. Department of Integrative Biology

VLSB 3060, University of California, Berkeley 94720-3140.

(correspondence address)

Telephone: (510) 643-9048

Fax: (510) 643-6264

email: kmead@socrates.berkeley.edu

2. Department of Biological Sciences

Stanford, California 94305

submitted to JEMBE 1/30/99
in press: accepted 5/28/99

Abstract:

Many crustaceans detect odors from distant sources (such as conspecifics or prey items) by using chemosensory sensillae (aesthetascs) on their antennules. The morphology and arrangement of the aesthetascs on the antennule and the movement of the antennule through the surrounding fluid during olfactory sampling affect the flow of odorants around the sensillae and thus odorant access to receptors inside the aesthetascs. We examined fluid flow around the olfactory appendages of the stomatopod Gonodactylus mutatus, a crustacean with excellent olfactory capabilities, a simple arrangement of aesthetascs on their antennules, and a ten-fold range in post-metamorphic body sizes. Using morphometric and kinematic measurements, we calculated several hydrodynamic parameters including the aesthetasc Reynolds number (Re), the leakiness of the setal array, and flow rate through aesthetascs and determined how these descriptors of fluid flow changed as the animals increased in size. We found that G. mutatus aesthetascs operate over a range of Re where the leakiness of the aesthetasc array is very sensitive to changes in antennule speed and setal dimension. As a result, the rate of fluid flow through the array of aesthetascs varies by a factor of two during different odor-sampling motions of the antennule, and changes over two hundred-fold as the animals increase in size. The increases in Re , leakiness, and flow rate as the stomatopods grow suggest that stomatopods alter their odor sampling paradigm as they mature, corresponding to changes in diet, preferred habitat, and behavior.

Keywords: Aesthetasc; Antennule flicking; Boundary layer; Chemosensory; Hydrodynamic; Reynolds number; Stomatopod

1. Introduction

1.1 Chemoreception and aesthetascs

Marine crustaceans use their sense of smell to detect prey items, gain information about conspecifics, and avoid predators (Ache, 1982; Atema and Voigt 1995; Zimmer-Faust, 1989). Most crustaceans, including lobsters, crabs, crayfish, prawns, leptostracans, anaspidans, mysids, amphipods, tanaids, isopods, ostracods, phyllopods, cumaceans, and stomatopods detect odors from distant sources by using chemosensory sensillae called aesthetascs (Heimann, 1984; Hallberg, et al., 1993). The aesthetascs are stiff, cuticular hair-like structures organized in arrays on the antennules (Figure 1; Hallberg, et al., 1993). Odors from food and other sources exist as patches or plumes of odorant molecules in the surrounding fluid. In order for chemoreception to work, the odor molecules must first be transported to the surface of the aesthetasc. The morphology of the aesthetascs, their arrangement on the antennule, and the movement of the antennule relative to ambient water motion affect the flow of water bearing odorants around the sensillae. This in turn affects the transport of odorants to the aesthetasc surface and hence to the chemoreceptors within the sensillae. Thus, the structure and deployment of the antennules affect the ability of the animal to identify the contents of the plume and locate its source.

1.2 Water flow affects odor molecule capture by aesthetascs

Many crustaceans sample their chemical environment by rapidly flicking their antennules through the surrounding fluid (Schmidt and Ache, 1979). Because the fluid at

the interface with a solid surface, such as the surface of the antennule, does not move with respect to it (the “no-slip condition”), a velocity gradient forms in the fluid between the antennule and the mainstream flow. Typically, the distance from the surface to the point where the velocity is 99% of the mainstream velocity is called the boundary layer (e. g. Vogel, 1994). The faster the motion of the body through the fluid (or the faster the free-stream fluid motion relative to the body), the thinner the boundary layer. The thickness of the boundary layer is very important for olfaction because it can act as a barrier to odorant access to the aesthetascs. While odorants can be very rapidly transported through the environment in currents (at speeds on the order of centimeters to meters per second), the time required to cross the boundary layer depends on the much slower process of molecular diffusion. Dimensional analysis indicates that the average time t required for a molecule to cross a boundary layer of thickness x is proportional to the square of the thickness of the boundary layer:

$$t \propto \frac{x^2}{D}, \quad \text{Equation 1}$$

where D is the coefficient of diffusion (m^2/s). Amino acids, to which many crustaceans are responsive, typically have molecular diffusion coefficients on the order of $10^{-9} \text{ m}^2/\text{s}$ in water. Therefore, while it might take 1 s for an amino acid to travel a meter in an ambient water current moving from a dead fish to the edge of a $100 \text{ }\mu\text{m}$ boundary layer of water around a crustacean’s aesthetasc, it might take 10 seconds on average to cross the remaining $100 \text{ }\mu\text{m}$. Furthermore, if the animal is able to reduce the boundary layer coating its aesthetasc to just $50 \text{ }\mu\text{m}$ (by flicking more rapidly, for example), the time to

diffuse across the boundary layer surrounding the aesthetasc decreases to 2.5 s on average. Thus the structure of the boundary layer regulates the rate of odorant access to the receptors in the aesthetascs.

To analyze the water flow past aesthetascs, we must consider the boundary layers around a number of cylindrical setae (the aesthetascs) attached to another cylinder (the antennule) when the animal is moving this appendage through the surrounding seawater during a flick. There is no simple formula for the boundary layer in this situation, but we know that the structure of the boundary layer depends on many variables, including the length and diameter of the aesthetascs, the gap between aesthetascs, their orientation on the antennule, antennule diameter, the mainstream velocity, the density of the fluid and the dynamic viscosity of the fluid (Schlichting, 1979; Koehl, 1995).

One simple way to start understanding this complicated flow situation is to calculate the Reynolds number (Re) that describes the fluid flow around the aesthetascs during flicking. Re is a dimensionless parameter that represents the ratio of inertial to viscous forces involved in a particular flow situation:

$$\text{Re} = \frac{\rho LU}{\mu} \quad \text{Equation 2}$$

where ρ is the density of the fluid (here the density of sea water at 25 °C, 1023 kg/m³), U is a velocity (here the antennule velocity relative to the ambient flow), L is a length unit (here the diameter of the aesthetasc), and μ is the dynamic viscosity of the fluid (here the viscosity of sea water at 25 °C, 0.97 x 10⁻³ Pa s) (Vogel, 1994). In general, $\text{Re} < 1$ indicates that viscous forces are dominant and $\text{Re} > 1$ suggests that inertial forces are

important. For a given aesthetasc diameter, a large Re indicates that the boundary layer is thin relative to the dimensions of the object, and a small Re suggests that the boundary layer is thick relative to the body. If Re is low and boundary layers are thick relative to the diameters of the setae in an array, then little fluid may penetrate into the array.

Leakiness is a measure of fluid penetration through the gaps in an array of setae. Leakiness is defined as the ratio of the volume of fluid that flows through a gap between two cylinders in a unit of time to the volume of fluid that would have flowed through the same area in that unit of time if the cylinders had not been present (Figure 2; Cheer and Koehl, 1987; Koehl, 1995). Leakiness can then be used to calculate the amount of fluid that flows between adjacent rows of aesthetascs per unit of time (flow rate) during different parts of the flick.

Since Reynolds number is proportional to setal (e.g. aesthetasc) diameter, and since leakiness and flow rate depend on aesthetasc diameter and spacing (Koehl, 1995), the growth of an animal might affect the performance of olfactory antennules. Furthermore, since Re , leakiness, and flow rate also depend on velocity, the kinematics of antennule movements can also affect their performance. In order to examine the effects of aesthetasc size and antennule velocity on olfactory performance, we have investigated the morphological and kinematic changes in the antennules of a crustacean, the stomatopod *Gonodactylus mutatus*, as it grows from its post-settlement size to its largest adult size. We have used Re , leakiness, and flow rate as performance indicators.

1.3 Stomatopod antennules and aesthetascs

We are using stomatopod antennules as a model system for examining the effect of aesthetasc morphology, aesthetasc arrangement on the antennule, and antennule movement on odorant access in marine crustaceans. Stomatopods (also known as mantis shrimp) are aggressive shrimp-like crustaceans that live in burrows in mudflats or in coral reef rubble in tropical and semi-tropical habitats. In addition to using chemical information to find food and mates, and to avoid predators (Caldwell, 1979; 1985), stomatopods depend highly on their sense of smell to identify burrows (which are critical to their feeding, reproduction, and survival during molts) whose inhabitants they can eject through aggressive interactions (Caldwell, 1979; 1985). Stomatopods appear to recognize by odor the individuals they have beaten and the ones by which they have been defeated in previous contests, and appear to lose this ability when their aesthetascs are removed (Caldwell, 1985).

The stomatopod antennules are preoral segmented appendages that end in two long flagellae and a robust filament that emerges from the base of the lateral flagellum and lies between the two flagellae (Figure 1A, B). The aesthetascs are arranged in rows of three (one row per segment) on the outer portion of the dorsal side of the filament (Figure 1C, D). In addition to the aesthetascs, there is one unobtrusive recumbent seta (of unknown function) per filament segment (Figure 1D).

Stomatopods are excellent subjects for chemosensory studies for several reasons. 1) The simple arrangement of aesthetascs on their antennules facilitates mathematical and physical modeling of fluid flow around these sensillae. In comparison, chemosensory sensillae in crabs and lobsters are highly complex (Gleeson, 1982; Grünert and Ache, 1988). For example, the spiny lobster's olfactory organ consists of hundreds of tightly

packed aesthetascs arranged in a zig-zag fashion in surrounded by large curved guard hairs, asymmetric hairs, and companion hairs (Gleeson, et al., 1993). 2) The fact that stomatopods rely on their aesthetascs to recognize odors from specific individuals (Caldwell, 1979; 1985; 1987) indicates that aesthetasc function is important to the animal. The ease of obtaining juveniles and adults spanning an almost 10-fold range of body lengths within a species and the ease of maintaining stomatopods in the laboratory add to their experimental tractability.

In this study, we concentrate on the small, shallow subtidal tropical species of stomatopod, Gonodactylus mutatus. While little has been published on the life history of G. mutatus, work on G. bredini, a closely-related species, showed that post-larvae (7-12 mm rostrum-telson length) live in interstices on the surface of coral rubble and subsist on planktonic material and organic films (Caldwell, et al., 1989). Larger G. bredini (12-15 mm body length) move into well-defined burrows in coral rubble and begin hunting small crabs, molluscs, and worms during foraging forays from their burrows (Caldwell, et al., 1989). During our field collections of G. mutatus, we noted the same size-dependent patterns in habitation and foraging. G. mutatus males begin breeding when they are 25-30 mm, and females when they are 35-40 mm (Caldwell, pers. comm.). The largest G. mutatus (mostly females) reach a maximum body length of about 55 mm (Caldwell, pers. comm.).

The purpose of this study was to determine the Reynolds number of G. mutatus aesthetascs, and hence the leakiness and flow rate through arrays of aesthetascs on the antennules of these stomatopods. Since water flow through an aesthetasc array (and hence odorant access) depends on the velocity of antennule motion, we studied temporal

variation in velocity within a flick. Reynolds number and flow through aesthetasc arrays depend on aesthetasc size and spacing as well as on velocity, so we also investigated how the morphology and behavior of G. mutatus antennules scale as the animals grow. We did so for juveniles and for sexually mature males and females to determine if stomatopods of different life stages sample their chemical environment differently.

2. Materials and Methods

2.1 Collection and maintenance of animals.

Gonodactylus mutatus were collected from coral rubble on sand flats (water depth 0.7-1.5 meters) in Kaneohe Bay, Oahu, HI. Animals were maintained separately in small containers of artificial seawater ("Instant ocean") at 25 °C, and were fed life adult Artemia (brine shrimp) twice per week.

2.2 Measuring and sexing animals.

Prior to each observation or antennule sampling, each animal's total body length (rostrum to telson), carapace length, rostrum length, and antennule length were measured using Mitutoyo digital calipers. Males were identified by the presence of a pair of claspers behind the third pair of walking legs. Live animals less than 13 mm long could not be reliably sexed using external characters and thus were recorded as "juvenile".

2.3 Scanning electron microscopy.

Excised antennules were fixed in 2% glutaraldehyde in 0.1 M sodium cacodylate

buffer, pH 7.2, for 3 hours to several days. The specimens were post-fixed in osmium tetroxide, washed in cacodylate buffer, and dehydrated in an alcohol series. The specimens were dried in a critical point dryer (Samdri PVT-3B, Tousimis Research Corp.), mounted on SEM stubs, and then coated with a 20 nm layer of gold (Polaron E-5400 sputter coater). Specimens were examined using a ISI-DS-130 scanning electron microscope, with a 10 kV beam. Micrographs were taken of the aesthetasc-bearing filament of each antennule from the side and from the top. Measured quantities are indicated in Figure 2. Each parameter was measured on the micrograph using Mitutoyo digital calipers. Each measurement was repeated at the same position three times to assess measurement precision (within 0.5%). Each parameter was then measured at five replicate sites that were chosen using a grid and a random number generator. Values compared between animals of different sizes were taken from the middle of the aesthetasc tuft.

2.4 Staining.

Aesthetasc permeability to small molecules in an aqueous solution was examined by exposing live stomatopods to a 0.01% solution of methylene blue in artificial seawater (32 ppt) for 1-60 minutes (after Slifer, 1960). The animals were rinsed in clean seawater for 5 minutes and examined under a dissecting microscope (Leica M28, 6.3-50x). This protocol indicated which portions of the aesthetasc are permeable to small molecules, a necessary requirement for olfaction. Permeable areas remained blue after rinsing. Occasionally nerve fibers inside the aesthetasc also stained blue.

2.5 Videomicrography.

Gonodactylus mutatus (50 live animals and 10 dead specimens) ranging in size from 7.6 mm to 55 mm were videotaped at 60 frames per second through a dissecting scope (Leica M28, 6.3-50x) using an Optronics Engineering LE 470 camera and a Sony SVO-5800 VCR. In early investigations, the animals were free to move around in a small dish of sea water; in later sessions, stomatopods were immobilized by placing them side, ventral, or dorsal surface up and covering their carapace and telson with dental wax. Flagella length, width, and thickness, filament length, width, and thickness, distance between aesthetasc rows, angle of aesthetasc insertion, and aesthetasc length were measured from single frames on a VCR monitor using Mitutoyo digital calipers and a protractor.

2.6 High speed video and digitization.

To investigate antennule kinematics, thirteen animals ranging in length from 8.4 mm to 53 mm were placed one at a time into a glass or plexiglass aquarium with an artificial burrow. The glass aquarium used for larger animals measured 17.5 cm (height, H) x 12 cm (width, W) x 23 cm (length, L). The artificial burrow used for large animals consisted of a plastic vial with a hole (13 mm diameter) in its lid, which was screwed into a partition at a distance of 4 cm from the front wall of the aquarium. Mirrors placed at an angle of 45° from the burrow made three-dimensional video analysis possible, although subsequent calculations showed that two-dimensional video analysis was sufficient when flicks were chosen whose movement was within the focal plane (see Results). Smaller animals were filmed in a plexiglass aquarium 6 cm (W) x 6 cm (H) x 8 cm (L). A divider

with one of three interchangeable burrows (pipette tips of various sizes) was placed 2 cm from the front wall. Burrow sizes in the small aquarium were 2.3 mm, 5.0 mm, or 6.25 mm in diameter. All animals were given 1-2 days before they were videotaped to acclimate to the tank and to find the burrow. After being deprived of food for a day, the stomatopod was videotaped at 250 frames per second using a high-speed video system (NAC color high speed video, hsv-1000 fps). Fiber optics lamps (Cole Parmer 9741-50) were used as a light source to minimize heating the aquarium. The water in the aquarium was kept at 25 °C. The temperature of the water in the aquarium was monitored frequently since any increase in temperature would affect flicking both by increasing the animal's metabolic rate and by decreasing the viscosity of the sea water. Brine shrimp odorant was prepared by placing a high concentration of living adult Artemia in artificial seawater for 1-2 days, and then pouring off the liquid. When we injected 2-5 ml brine shrimp odor into the top portion of the tank out of a stomatopod's field of view, the stomatopod began moving its antennules rapidly in a stereotypic flicking behavior called "antennulation" (Caldwell, 1979). These movements were captured on video, and analyzed using image digitization software from Peak Motus Performance Technologies (version 2.0). The positions of the base of the antennule, the distal end of the propus, the tips of the flagellae, and the tip of the aesthetasc-bearing filament were recorded 250 times per second. 10 flicks were digitized per animal. Digitized data files were scaled (from pixels to mm) within Peak Motus and exported to Microsoft Excel 5.0 spreadsheets. We calculated linear and angular filament tip displacement, and maximum and mean antennule velocities tangential to the arc inscribed by the filament tip of the antennule for both strokes of the flick. We also calculated the maximum and mean

angular velocities for the two strokes of the flick, and the position of the aesthetasc-bearing antennule filament relative to the base of the antennule at the beginning and end of each flick.

2.7 Leakiness and flow rate calculations.

Leakiness is the ratio of the volume of fluid that flows between adjacent rows of aesthetascs in a unit of time to the volume of fluid that would have flowed through the same area in the unit of time if the aesthetascs were not there (Figure 2). We made estimates of the leakiness of the gaps between rows of aesthetascs by assuming that a row of three closely-spaced aesthetascs oriented with the long axis of the row perpendicular to the flow functioned as a single cylinder. We used aesthetasc diameter and the mean tangential velocity of the aesthetasc-bearing filament tip to calculate Reynolds number (Equation 2). We used the distance between aesthetascs as the gap width and aesthetasc diameter as the cylinder diameter to calculate the gap:diameter ratio (G/D). These values of Re and G/D were used to read estimates of leakiness on the graphs in Figures 3 and 10 in Koehl (1995). The leakiness values that we used for $Re < 0.5$ were calculated from the mathematical model generated by Cheer and Koehl (1987), while leakiness values for higher Re s were determined from tow-tank experiments with comb-like physical models by Hansen and Tiselius (1992). When necessary, we interpolated values between the points plotted in Figures 3 and 10 in Koehl (1995) by making the simplifying assumption that leakiness increases linearly with G/D and with Re in the narrow range between points. We calculated the rate of fluid flow (volume/time) between two adjacent rows of aesthetascs to be:

$$\text{flow rate} = L_a L_g V * \text{leakiness} * \sin \alpha \quad \text{Equation 3}$$

where L_a is the aesthetasc length, L_g is the distance between adjacent rows of aesthetascs, V is tangential velocity of the filament tip during the portion of the flick under study, and α is the angle at which the aesthetascs are inserted into the antennule filament (Figure 1). This calculation makes the assumption that leakiness and flow rate are independent of position along the aesthetasc. Leakiness should be lower near the bases of the aesthetascs due to the boundary layer along the filament surface and should be higher near the filament tips (Best, Loudon, and Koehl, unpublished data), so our calculation of flow rate based on mid-aesthetasc leakiness is just a rough estimate. We also calculated the volume/time of fluid processed by an entire array of aesthetascs by calculating the flow rate between each pair of adjacent aesthetasc rows. Since the antennule filament in G. mutatus is rigid, we assumed that the velocity with which an aesthetasc moves through the fluid is a linear function of the aesthetasc's position on the antennule, and adjusted the velocity and leakiness for each pair of adjacent aesthetasc rows accordingly.

2.8 Analysis and statistics.

We plotted various antennule and aesthetasc morphological and kinematic parameters as a function of stomatopod rostrum-telson length. We then calculated Standard Model I linear regressions examining the scaling of these elements with body size using the statistics package in Microsoft Excel 5.0. Because standard least-squares linear regressions of allometric relationships with a low r^2 can lead to an underestimate of

the slope (LaBarbera, 1989), we estimated the effect of the error of the independent variable on the slope. We used the reliability ratio κ (where $\kappa = r$, and r is the correlation between repeated measurements of stomatopod rostrum-telson length; Fuller, 1987) to estimate the measurement error in our independent variable (Johnson and Koehl, 1994). We then corrected the slope by multiplying the slope by $1/\kappa$. Minimum significant differences (used to determine if regression slopes differed significantly from each other) were calculated using the Tukey-Kramer method (Sokal and Rohlf, 1995).

2.9 Flicking frequency.

Segments of high-speed video showing rapid flicking movements were digitized and analyzed as above. Stomatopods intersperse bouts of intensive flicking with periods of quiescence of varying lengths. Flicking frequencies within bouts of at least four flicks were calculated. Five flicking frequencies were calculated per specimen.

3. Results

3.1 Stomatopod rostrum-telson length. Our measurements of stomatopod rostrum-telson lengths generated a reliability ratio κ of 0.99.

3.2 External aesthetasc morphology.

Gonodactylus mutatus aesthetascs are thin cuticularized structures that are enlarged at the base, and have an annulus about 60% of the distance along the aesthetasc from the base (Figure 1D). As animals grow from 8 to 55 mm rostrum-telson length, the number of

rows of aesthetascs increases from 3 to 18, and aesthetasc length increases from 150 to 550 μm (Figure 3A, 3D; Table I). The length and diameter of the filament on which the aesthetascs are borne also increases with body size (Figure 3B and 3C; Table I). In contrast, the angle at which the aesthetascs are inserted into the filament and the distance between the rows of aesthetascs do not vary with body size (Figures 3E, 3F, Table I).

Associated with each row of aesthetascs is a small seta (4-5 μm diameter) of unknown function, possibly analogous to the asymmetric mechanosensory sensillae of the spiny lobster Panulirus argus (Gleeson *et al.*, 1993). The medial and lateral flagellae of a stomatopod antennule also bear setae (that are not aesthetascs); these are 60-100 μm long and 4-5 μm in diameter.

Measurements from scanning electron micrographs indicate that aesthetasc diameter and the diameter of the presumptive asymmetric sensillae increase with body size (Figure 4A, 4B; Table I), whereas the diameters of the setae on the medial and lateral flagellae do not increase with body size (Figure 4C; Table I).

While aesthetascs show sexual dimorphism in some decapods, cladocerans, mysids, copepods, anaspids, amphipods, tanaids, and cumaceans (Hallberg *et al.*, 1992), there is no significant morphological difference between the antennules or aesthetascs of male and female Gonodactylus mutatus. The slopes of linear regressions of all structural parameters tested (number of aesthetasc rows, filament length, filament diameter, aesthetasc length, aesthetasc angle, and distance between rows of aesthetascs) as a function of total body length show no significant differences between males and females (Table I).

3.3 Internal aesthetasc and filament morphology.

Dye studies showed that the aesthetasc cuticle is readily permeable to methylene blue after only a few seconds of exposure to the dye. This suggests that the cuticle is permeable to other small molecules, such as amino acids. Cuticle permeability is a minimum requirement for identifying the sensillae as aesthetascs, since the odorants need to be able to penetrate the cuticle in order to gain access to chemoreceptors on the surface of sensory nerves inside the aesthetasc. The cuticle appeared to be permeable to dye along the entire length of the aesthetasc. After rinsing, the dye was darkest in small (20-30 μm diameter) cord-like structures inside the filament, tentatively identified as nerve bundles.

3.4 Kinematics.

Stomatopod investigatory antennulation consists of a series of small flicks of one or both antennules. Antennulation usually consists of several rapid flicks along a single axis, followed by a pause as the stomatopod repositions its antennules, and then begins to flick again (Figure 5A). The right and left antennules can flick in synchrony or independently (Figure 5B). Each flick starts with a rapid, outward lateral movement followed by a slower return medial movement (Figure 5C). The outward movement lasts for 33 ± 2 ms and the return motion lasts for 43 ± 3 ms regardless of body size. Figure 6 shows that seen from the front, flicks can start at almost any angle.

As long as we chose flicks whose entire motion was within the focal plane of the camera, 2-D and 3-D analysis gave trajectories and velocities that agreed to within 5%. Three-dimensional analysis confirmed that the flicks that we chose were representative of

the entire population of flicks in terms of duration, tangential velocity, angular velocity, and flicking frequency.

In all flicks the mean tangential velocity of the aesthetasc-bearing filament is 1.90 (SE = 0.03, n = 130) times as large during the lateral part of the flick as it is during the medial motion of the flick. The maximum tangential filament velocity is 1.88 (SE = 0.02, n = 130) times larger than the mean lateral tangential velocity (Figure 7A). Similarly, maximum angular velocities are on average 2.29 (SE = 0.04, n = 130) times greater than lateral angular velocities, which are 2.08 (SE = 0.02, n = 130) times greater than medial angular velocities (Figure 7B). Tangential filament velocities (maximum, lateral and medial) do not appear to change with body size when animals are small (rostrum-telson length 8-25 mm). Once the animals have a rostrum-telson length greater than 25 mm, tangential filament velocities increase 3-4 fold with body size (Figure 7A). Lateral velocities increase faster with body size in males than in females (Table II). Angular filament velocities do not change significantly with body size (Figure 7B, Table II).

3.5 Reynolds number.

Figure 8 shows how the Reynolds number (Re) varies with body size. Re is 1.91 (SE = 0.03, n = 130) times greater during the lateral (outward) motion of the flick than during the medial (return) motion. The combined increase in aesthetasc size and in antennule tangential velocity causes the Re of the lateral movement of the antennule (Re_{lateral}) to increase from 0.2 to 1.8 and Re_{medial} to increase from 0.1 to 0.9 as the animals increase in size from 8 mm to 52 mm rostrum-telson length (Figure 8). There is no statistically significant difference between the Reynolds numbers of male and female Gonodactylus

mutatus (Table II).

3.6 Leakiness.

Figure 9 shows the mean leakiness during the lateral and medial parts of the flick. Note that there is a general increase in leakiness with body size, and that an average of 1.23 (SE = .01, n = 130) times more fluid leaks through the aesthetascs during the outward part of the flick than during the return part of the flick. There is no statistically significant difference in leakiness between male and female stomatopods (Table II).

3.7 Flow rate.

The volume of fluid that flows between adjacent rows of aesthetascs per unit time is 2.36 (SE = .05, n = 130) times greater during the lateral motion of the flick than during the medial motion of the flick (Figure 10). Flow rate between one pair of adjacent aesthetasc rows increases more than 20-fold as the animals increase in size from 8 to 55 mm rostrum-telson length. Flow rate between all aesthetasc rows on an antennule filament increases more than 200-fold as the animals grow over the same range of body sizes (Figure 11). In both cases, the difference in flow rate between males and females is not statistically significant. (Table II).

3.8 Flicking frequency.

Maximum flicking frequency increased from 2 to 7 flicks per second as the total body length increased from 8 to 52 mm (Figure 11).

4. Discussion

Odorant access to the aesthetascs on stomatopod olfactory antennules is affected by flow near the aesthetascs when the animals flick their antennules. We have used kinematic and morphological data to calculate estimates of the water flow between rows of aesthetascs of stomatopods as they grow from newly-settled juveniles to mature males and females. Such water flow should affect how these animals sample their chemical environments.

4.1 Flow through the aesthetasc array during a flick.

The Reynolds number (Re) of the flow around the aesthetascs during the outward part of the flick is always greater than the Re of the flow around the aesthetascs during the return inward part of the flick. The mean ratio of outward Re to inward Re is 1.91 (SD = 0.03 , n = 130). Both mathematical models (Cheer and Koehl, 1987; Koehl, 1995; 1996) and physical models (Hansen and Tiselius, 1992; Louden *et al.*, 1994; Koehl, 1995) of flow between neighboring cylinders in an array suggest that the leakiness of an array of closely-spaced hairs (gap-to-diameter ratios of 10 or lower, as found in the spacing of rows of aesthetascs along stomatopod antennules) operating in the Re range of stomatopod aesthetascs (Re = 0.1- 1.8) is very sensitive to changes in Re. This suggests that stomatopod antennules operate in a Re range that enhances the difference in leakiness between the fast outward part of the flick and the slower return. Thus, new water and any odorants it may bear should penetrate the aesthetasc array more during the leaky lateral motion than during the slower medial motion of a flick. One consequence of this

difference in leakiness is that the water surrounding the aesthetascs at the end of a flick is different from the water surrounding them before the flick, even when the aesthetascs return to their original position. This mechanism has been suggested for the antennules of spiny lobsters, which also show an asymmetry in aesthetasc Re during the downward versus upward portions of a flick (Goldman and Koehl, in review).

Another consequence of the difference in aesthetasc Re between the outward and return parts of the flick is that the boundary layer around the aesthetascs is thinner during the outward motion than during the return motion. Hence the time needed for odorants to diffuse from newly-sampled water to the aesthetasc is less during the lateral movement than during the medial stroke. When flow rates through an array of setae are high and boundary layers are thin, the number of molecules captured per time by the setae is greater than when flow rates are low and boundary layers are thick (e.g. Shimeta and Jumars, 1991; Koehl, 1996). The shorter response time and higher capture rate when flow rate is high and boundary layers are thin suggests that changes in odor molecule concentration may be important cues under these conditions (Koehl, 1996). In contrast, when flow rates through an array of hairs are low, there is more time for molecules in the water being sampled to diffuse to hair surfaces. Under these conditions, a greater proportion of the molecules in the sample water are caught (e.g. Rubenstein and Koehl, 1977; Koehl, 1996), although response time may be long and capture rates low.

The difference in Re of the outward and inward parts of a stomatopod antennule flick suggest that the rapid outward motion removes "old" already-sampled water from the aesthetasc array and allows penetration of new odorant-bearing water close to aesthetasc surfaces, similar to the downstroke of a lobster antennule flick (e.g. Schmidt and Ache ,

1979; Moore, et al., 1991; Goldman and Koehl, in review). Goldman and Koehl (in review) suggested that this difference in odorant access during different portions of the flick contributes to the ability of a flicking antennule to take discrete temporal and spatial samples of their chemical environment.

4.2 Scaling of antennules as stomatopods grow.

Because stomatopod aesthetascs operate in a Re range in which flow rate through the aesthetasc array is very sensitive to changes in Re , the size (L in equation 1) and speed (U in equation 1) changes that occur as animals grow might affect antennule performance. The smallest stomatopods operate their antennules at aesthetasc Res of 0.1-0.2, while large stomatopods operate at aesthetasc Res between 1 and 2 (Figure 8). Therefore, the aesthetascs of small stomatopods have relatively thick boundary layers, low leakiness, and little water flowing between adjacent rows, whereas those of large animals develop thin boundary layers, show high leakiness, and have proportionally more fluid flowing between the rows of aesthetascs (Figures 9-11).

The differences in aesthetasc Re , leakiness, and flow rate of small and large stomatopods could have several functional consequences. The higher flow rate through the aesthetasc arrays of large stomatopods should enable them to shed “old” water from their antennules more quickly and completely than small animals can. Furthermore, the thinner boundary layers that form around the aesthetascs of large stomatopods should permit more rapid odorant diffusion to aesthetasc surfaces than for smaller animals. Thus, large animals should be more sensitive than small ones to changes in odorant concentration and should be able to take more temporally and spatially discrete samples

of their chemical environment when they flick. However, while the thick boundary layers surrounding the aesthetascs of small animals mean that odorant diffusion is slow, the reduced fluid flow may allow a greater proportion of odorant molecules to diffuse to the sensillum before they are swept away than for large animals.

4.3 Changes in stomatopod behavior and ecology with size and age.

Several aspects of stomatopod life history suggest that the ecological requirements for smelling may change as stomatopods grow and mature. Since newly-settled Gonodactylus are not yet territorial, do not have social interactions that require recognition of individual conspecifics, and do not hunt motile prey (Caldwell, et al., 1989), they may not rely heavily on smell at this stage. After animals grow to body lengths of 12-15 mm, they start to engage in contests over burrows in coral rubble (Caldwell, et al., 1989). Furthermore, as the animals grow, the size and speed of their preferred prey (crabs, molluscs, worms) increases (Caldwell et al., 1989). G. mutatus begin breeding when they reach rostrum-telson lengths of 35-40 mm (R. Caldwell, pers. comm.). Assessing burrow inhabitants (for mate choice or habitat competition), burrow defense, and finding prey are likely to require rapid chemosensory sampling. The fact that social interactions and aggression, hunting of prey, and mating become increasingly important as stomatopods grow suggests that gathering olfactory information becomes more critical to stomatopods at the sizes at which their aesthetasc arrays become leakier (permitting greater odorant penetration) and the frequency of olfactory flicking increases.

4.4 Comparison with antennules of other crustaceans.

The kinematics and the morphometrics of the antennules of the spiny lobster, Panulirus argus (Gleeson, et al., 1993; Goldman and Koehl, in review), and the American lobster, Homarus americanus (Moore and Atema, 1991; Best, 1995) have been analyzed and can be compared with those of the stomatopod, G. mutatus. These two species of lobsters bear their aesthetascs on the terminal portion of the lateral branch of each antennule. P. argus aesthetascs operate at a Re of 2 on the downstroke and at a Re of 0.5 during the upstroke (Goldman and Koehl, in review), while the aesthetascs of H. americanus operate at Res of 3-4 (Moore and Atema, 1991; Best, pers. comm.). In contrast to stomatopods, lobsters maintain the same aesthetasc Re as they grow (Best, 1995; Goldman and Koehl, in review). Best (1995), who observed that aesthetasc Re was conserved over a twenty-fold increase in body length, suggested that the nature of the flow around the sensory hairs and antennules may be very important to the processing of information during chemoreception. Goldman and Koehl (in review) suggested that lobsters maintain the Re of their aesthetascs as they grow in a range where the difference in leakiness is enhanced between the rapid downstroke and the slower upstroke. Because aesthetasc kinematics have only been quantified for a few species, it is not clear whether maintaining Re (as lobsters do) or increasing Re (as stomatopods do) as animals grow is more prevalent.

Conclusion

Our study of the flicking kinematics and the morphology of the olfactory antennules of the stomatopods Gonodactylus mutatus revealed that their olfactory setae, the

aesthetascs, operate at a range of Reynolds numbers where the leakiness of an array is very sensitive to changes in speed and setal dimensions. As a consequence the flow rate of water through the array of aesthetascs is greater during the rapid lateral motion of an antennule flick than during the following slower motion. This leakiness asymmetry suggests that “old” water that has already been sampled is shed from the aesthetascs during the rapid lateral motion while “new” water and the odorants it carries penetrate the array, and then are retained during the slower medial motion. As stomatopods grow and mature, the Re of their aesthetascs increases nine-fold, aesthetasc leakiness doubles, and flow rate through the aesthetasc arrays increases by a factor of 200. These changes in antennule hydrodynamics, which should improve the sensitivity of the antennules to changes in odorant concentration from one flick to the next, accompany behavioral and ecological changes that the stomatopods undergo as they grow. As these animals grow in size and mature, their increasing ability to acquire rapid, accurate olfactory information is undoubtedly important as they step up their efforts to hunt animal prey, to compete for burrows, and to seek mates.

Acknowledgements

We are grateful to R. Caldwell for his invaluable advice and support. We thank C. Fiedler and the staff at Hawaii Institute for Marine Biology where the animals were collected, P. Sicurello for instruction in SEM, K. Vetter for assistance in the field, the biomechanics group at U. C. Berkeley, F. Grasso, and H. Trapido-Rosenthal for instructive feedback. These experiments were funded by ONR grant N00014-96-1-0594 to M. Koehl.

References

- Ache, B. W., 1982. Chemoreception and thermoreception. In: H. L. Atwood and D. C. Standeman (eds) *The Biology of Crustacea*, Vol. 3. New York Academic Press: pp. 369-393.
- Atema, J. and R. Voigt, 1995. Behavior and sensory biology. In: J. R. Factor (ed) *Biology of the Lobster Homarus americanus*. San Diego, CA. Academic Press: pp. 313-348.
- Best, B., 1995. Scaling and flow dynamics of crustacean antennules: What's flicking all about? *Am. Zool.* 35, 53A
- Caldwell, R.L., 1979. Cavity occupation and defensive behaviour in the stomatopod Gonodactylus festae: evidence for chemically mediated individual recognition. *Anim. Behav.* 27:194-201.
- Caldwell, R.L., 1985. A test of individual recognition in the stomatopod Gonodactylus festae. *Anim. Behav.* 33:101-106.
- Caldwell, R. L., 1987. Assessment strategies in stomatopods. *Bull. Mar. Sci.* 41: 135-150.
- Caldwell, R. L., G. K. Roderick, and S. M. Shuster, 1989. Studies of predation by Gonodactylus bredini. In: E. A. Ferrero (ed.), *Biology of Stomatopods*. Collana UZI, Selected Symposia and Monographs, Mucchi Editore, Modena. pp. 117-131.
- Cheer, A. Y. L. and M. A. R. Koehl, 1987. Paddles and rakes: fluid flow through bristled appendages of small organisms. *J. theor. Biol.* 129: 17-39.

- Derby, C. D., 1982. Structure and function of cuticular sensilla of the lobster Homarus americanus. J. Crust. Biol. 2: 1-21.
- Gleeson, R. A., 1982. Morphological and behavioral identification of the sensory structures mediating pheromone reception in the blue crab, Callinectes sapidus. Biol. Bull. 163: 162-171.
- Gleeson, R. A., W. E. S. Carr, and H. G. Trapido-Rosenthal, 1993. Morphological characteristics facilitating stimulus access and removal in the olfactory organ of the spiny lobster, Panulirus argus: insight from the design. Chem. Senses. 18: 67-75.
- Goldman, J. and M. A. R. Koehl. Fluid dynamic design of lobster olfactory organs: high-speed kinematic analysis of antennule flicking by Panulirus argus. Chem. Senses (in review).
- Grünert, U. and B. W. Ache, 1988. Ultrastructure of the aesthetasc (olfactory) sensilla of the spiny lobster, Panulirus argus. Cell Tissue Res. 251: 95-103.
- Hallberg, E., K.U.I. Johansson, and R. Elofsson, 1992. The aesthetasc concept: structural variations of putative olfactory receptor cell complexes in Crustacea. Micros. Res. and Tech. 22: 325-335.
- Hansen, B. and P. Tiselius, 1992. Flow through feeding structures of suspension feeding zooplankton: A physical model approach. J. Plankton Res. 14: 821-834.
- Heimann, P., 1984. Fine structure and molting of the aesthetasc sense organs on the antennules of the isopod, Asellus aquaticus (Crustacea). Cell Tissue Res. 235: 117-128.
- Johnson, A. S. and M. A. R. Koehl, 1994. Maintenance of dynamic strain similarity and environmental stress factor in different flow habitats: thallus allometry and material properties of a giant kelp. J. exp. Biol. 195: 381-410.

- Koehl, M. A. R., 1993. Hairy little legs: feeding, smelling, and swimming at low Reynolds numbers. *Contemp. Math.* 141: 33-64.
- Koehl, M. A. R., 1995. Fluid flow through hair-bearing appendages: feeding, smelling and swimming at low and intermediate Reynolds numbers. In *Biological Fluid Dynamics*, ed. C. P. Ellington, T. J. Pedley. *Soc. exp. Biol. Symp.* 49:157-182.
- Koehl, M. A. R., 1996. Small-scale fluid dynamics of olfactory antennae. *Mar. Fresh. Behav. Physiol.* 27: 127-141.
- Koehl, M. A. R., 1996. When does morphology matter? *Annu. Rev. Ecol. Syst.* 27: 501-542.
- LaBarbara, M., 1989. Analyzing body size as a factor in ecology and evolution. *Ann. Rev. Ecol. Syst.* 20: 97-117.
- Louden, C., B. Best, and M. A. R. Koehl, 1994. When does motion relative to neighboring surfaces alter the flow through arrays of hairs? *J. exp. Biol.* 193: 233-254.
- Moore, P. A., J. Atema, and G. A. Gerhardt, 1991. Fluid dynamics and microscale chemical movement in the chemosensory appendages of the lobster, Homarus americanus. *Chem. Senses.* 16: 663-674.
- Morin, M., M. Spoto, and E. A. Ferrero, 1989. Spatio-temporal analysis of grooming behavior of *Squilla mantis* (Crustacea, Stomatopoda). In: E. A. Ferrero (ed.), *Biology of Stomatopods. Collana UZI, Selected Symposia and Monographs*, Mucchi Editore, Modena. pp. 105-116.
- Rubenstein, D. I., and M. A. R. Koehl, 1977. The mechanisms of filter feeding: some theoretical considerations. *Am. Nat.* 111: 981-994.

Saus, A., M. Riba, R. Eizaguirre, and C. Lopez, 1997. Electroantennogram, wind tunnel, and field responses of the male Mediterranean corn borer, Sesamia nonagrioides, to several blends of its sex pheromone components. Entomol. Exp. et Appl. 52: 121-127.

Schlichting, H, 1979. Boundary-layer theory, seventh edition. McGraw-Hill, Inc. London. 817 pp.

Schmidt, B. C. and B. W. Ache, 1979. Olfaction: responses of a decapod crustacean are enhanced by flicking. Science 205: 204-206.

Shimeta, J. and P. Jumars, 1991. Physical mechanisms and rates of particle capture by suspension feeders. Oceanogr. Mar. Biol. Ann. Rev. 29: 191-257.

Slifer, E. H., 1960. A rapid and sensitive method for identifying permeable areas in the body wall of insects. Ent. News 71: 179-182.

Sokal, R. R. and F. J. Rohlf, 1995. Biometry, third edition. W. H. Freeman and Company. 887 pp.

Vogel, S., 1994. Life in Moving Fluids, second edition. Princeton University Press, Princeton, N.J. 467 pp.

Zimmer-Faust, R. K. 1989. The relationship between chemoreception and foraging behavior in crustaceans. Limnol. Oceanogr. 34: 1364-1374.

Table Legends:

Table I. Scaling of structural features of the antennule filament bearing the aesthetascs in the stomatopod *Gonodactylus mutatus*. Model I linear regressions with slopes corrected for error in measurement of the total body length ($\kappa=0.99$). For categories 1-6, $n = 60$ (18 males, 29 females, 13 juveniles). $n = 9$ for categories 7-9 (2 males, 3 females, 4 juveniles). MSD = minimum significant difference.

Table II. Scaling of the filament tangential velocity, Reynolds number describing flow around the aesthetascs, leakiness, flow rate, and flicking frequency with body size. Model I linear regressions with slopes corrected for error in measurement of the total body length ($\kappa=0.99$). $n = 13$ (4 males, 5 females, 2 juveniles), except for category 9 ($n = 11$; 3 males, 4 females, 2 juveniles). MSD = minimum significant difference.

Table I. Scaling of structural features of the antennule filament bearing the aesthetascs in the stomatopod *Gonodactylus mutatus*: Model I Linear regressions

Category	Sex	R ²	Slope	Y-Intercept	p slope =0	95% confidence	MSD
number of aesthetasc rows per mm rostrum-telson length)	male	.93	.31±.02	.36±.76	<.000001	.26-36	.07
	female	.86	.28±.02	1.0±.89	<.000001	.23-32	.06
aesthetasc filament length (μm) per mm rostrum-telson length	male	.84	76±8	56±291	<.000001	58-94	24
	female	.67	56±8	497±308	<.000001	41-72	23
filament diameter (μm) per mm rostrum-telson length	male	.49	1.54±.39	106±14	.001	.71-2.4	1.16
	female	.43	2.28±.51	66±21	.0001	1.25-3.32	1.47
aesthetasc length (μm) per mm rostrum-telson length	male	.003	.28±1.4	328±47	.84	-2.6-3.2	4.04
	female	.26	3.8±1.2	195±50	.005	1.25-6.3	3.55
aesthetasc angle (degrees) per mm rostrum-telson length	male	.03	-.06	52±3	.52	-.26-.14	.28
	female	.006	.028±.069	51±3	.68	-.11-.17	.20
distance between aesthetasc rows (μm) per mm rostrum-telson length	male	.08	-.63±.55	163±19	.27	-1.8-.5	1.63
	female	.04	.52±.50	116±21	.31	-.5-1.6	1.47
aesthetasc diameter (μm) per mm rostrum-telson length	both	0.7	.197±.049	7.8±2	.005	.08-.314	
asymmetric sensillum diameter (μm) per mm rostrum-telson length	both	0.9	.07±.01	1.5±0.4	.001	.044-.099	
seta diameter on lateral, medial flagellae (μm) per mm rostrum- telson length	both	0.04	.017±.032	4.0±1.3	.65	.92-7.02	

Table II. Scaling of the filament tangential velocity, Reynolds number describing flow around the aesthetascs, leakiness, flow rate, and flicking frequency with body size: Model I Linear regressions

Category	Sex	R ²	Slope	Y- Intercept	p slope =0	95% confidence intervals	MSD
Filament maximum tangential velocity (mm/s per mm rostrum-telson length)	male	.87	5.1±1.4	-73±54	.070	-1-11.1	6.3
	female	.52	2.1±1.2	37±47	.17	-1.6-5.8	4.6
Filament mean tangential velocity during the lateral flick stroke (mm/s per mm rostrum-telson length)	male	.94	3.4±.6	-64±.23	.029	.85-6.1	2.7
	female	.47	.72±.44	38±18	.20	-.7-2.1	1.7
Filament mean tangential velocity during the medial flick stroke (mm/s per mm rostrum-telson length)	male	.70	1.5±.7	-21±26	.16	-1.5-4.4	3.2
	female	.41	.19±.13	25±5.4	.249	-.2-.61	0.51
Filament maximum angular velocity (degrees/s per mm rostrum-telson length)	male	.78	.55±.20	23±8	.11	-10-56	.9
	female	.09	.20±.36	37±15	.62	-10-83	1.41
Filament mean angular velocity during the lateral part of the stroke (degrees/s per mm rostrum-telson length)	male	.98	.64±.07	-4±3	.01	-15-7	.3
	female	.11	-.15±.26	27±10	.58	-5-60	1.02
Filament mean angular velocity during the lateral part of the stroke (degrees/s per mm rostrum-telson length)	male	.11	.16±.32	4±12	.67	-49-56	1.44
	female	.001	-.01±.22	11±9	.97	-17-39	.86
Reynolds number describing the lateral flick stroke (Re per mm rostrum-telson length)	male	.94	.067±.012	-1.4±.47	.03	.016-.117	.054
	female	.81	.027±.007	.029±.3	.036	.003-.05	.027
Reynolds number describing the medial flick stroke (Re per mm rostrum-telson length)	male	.77	.03±.01	-.53±.43	.12	-.019-.79	.045
	female	.88	.01±.002	.14±.085	.019	.003-.0	.0079
Mean leakiness during the lateral flick stroke (leakiness per mm rostrum-telson length)	male	.65	.013±.007	.25±.26	.19	-.016-.043	.032
	female	.01	- .001±.004	.79±.15	.85	-.013-.011	.016
Mean leakiness during the medial flick stroke (leakiness per mm rostrum-telson length)	male	.62	.016±.009	.02±.009	.21	-.020-.056	.041
	female	.08	.003±.005	.51±.2	.64	-.013-.018	.020
Mean flow rate during outward part of flick (mm ³ /s per mm rostrum-telson length)	male	.93	.17±.03	-4.03±1.26	.036	.028-.31	.14
	female	.14	.031±.044	.69±1.77	.53	-.11-.17	.17
Mean flow rate during return part of flick (mm ³ /s per mm rostrum-telson length)	male	.44	.085±.067	-1.96±2.55	.33	-.2-.37	.30
	female	.11	.01±.02	.36±.66	.57	-.04-.06	.08
Maximum flicking frequency (flicks/s per mm rostrum-telson length)	male	.87	-.04±.02	8.6±.63	.23	-.24-.16	.09
	female	.87	.06±.03	4.0±1.1	.16	-.06-.18	.12

Figure Legends

Figure 1. Antennule and aesthetasc structure. A. Overview of the terminal portion of a Gonodactylus mutatus antennule. The middle and lateral flagellae, and the aesthetasc-bearing filament of the lateral flagellum are shown. B. SEM of an antennule from a small G. mutatus (rostrum-telson length 11 mm), showing the two flagellae, the filament, and aesthetascs. C. Line drawing of the distal part of the filament that branches off of the lateral flagellum. The aesthetascs are arranged in rows of three on the dorsal side of the filament, with one bundle per segment. D. SEM of part of the aesthetasc-bearing filament of a large G. mutatus (rostrum-telson length 55 mm). Note the enlarged base of the aesthetascs, the “annulus” part way along the aesthetasc, and the narrow asymmetric hair that emerges from the back of each row of three aesthetascs. Abbreviations are as follows: ad = aesthetasc diameter, aes = aesthetasc, ah = asymmetric hair, ai = angle of insertion, al = aesthetasc length, ann = annulus, fil = antennule filament, ft = filament thickness, fw = filament width, lf = lateral flagellum, mf = medial flagellum, set = seta (non-aesthetasc).

Figure 2. Orientation of aesthetascs relative to flow and leakiness during flicking. A. The axis of each row of aesthetascs is perpendicular to the axis of the filament and parallel to the direction of flow. B. Leakiness is the ratio of the volume of fluid that flows between adjacent rows of aesthetascs in a unit of time (dotted volume) to the volume of fluid that would have flowed through the same area in the unit of time if the aesthetascs were not there (unfilled volume).

Figure 3. Scaling of structural elements with body size. Data are means and standard errors from 61 specimens studied through dissecting scope. Solid squares are males, open triangles are females, and grey circles are juveniles. Linear regressions shown are based on all 61 specimens. A. Aesthetasc bundles. B. Filament length. C. Filament diameter. D. Aesthetasc length. E. Aesthetasc angle. F. Distance between rows of aesthetascs.

Figure 4. Scaling of structural elements with body size. Data are means and standard errors for 9 animals examined in SEM. A. Aesthetasc diameter. B. Diameter of asymmetric sensillae. C. Diameter of setae on medial and lateral flagellae.

Figure 5. Flick parameters for a 52 mm (rostrum-telson length) stomatopod. A. Stomatopods antennulate in bursts of flicks. B. Right and left antennules flick in synchrony or independently. C. Profile of a typical flick.

Figure 6. Orientation of olfactory flicks. A. Front view of stomatopod showing position and direction of flicks relative to rostrum. During a flick, the antennule can move in and out of the plane of the figure (open triangle), in a dorso-ventral direction (solid triangle), or in a combination of the two axes. The outward or dorsal movement is termed the lateral portion of the flick, and the inward or ventral motion is called the medial part of the flick. B. Flick orientation relative to rostrum. Starting position of 108 digitized flicks relative to rostrum. From the observer's point of view facing the stomatopod, all flicks starting on the left moved in a clockwise direction and then returned to their initial

position. Conversely, all flicks starting on the right moved in a counter-clockwise direction before returning to their initial position.

Figure 7. Scaling of velocity of aesthetasc tip with body size. Data are means and standard errors from high speed video measurements of 13 specimens. 10 flicks were digitized per individual. A. Maximum tangential velocity (grey symbols), mean tangential velocity during the lateral motion of the flick (filled symbols), mean tangential velocity during the medial motion of the flick (open symbols). B. Maximum angular velocity (grey symbols), mean angular velocity during the outward motion of flick (filled symbols), mean angular velocity during the return motion of flick (open symbols). In both A. and B, triangles represent females, squares indicate males, and circles show juveniles. Solid lines show linear regressions for males, dashed lines show linear regressions for females.

Figure 8. Scaling of Reynolds number with body size. Length element = aesthetasc diameter. Data are means and standard errors from calculated Reynolds numbers for 13 specimens. Lateral motion of flick (filled symbols), medial motion of flick (open symbols). Triangles indicate females and squares show males. Solid lines show linear regressions for males, dashed lines show linear regressions for females.

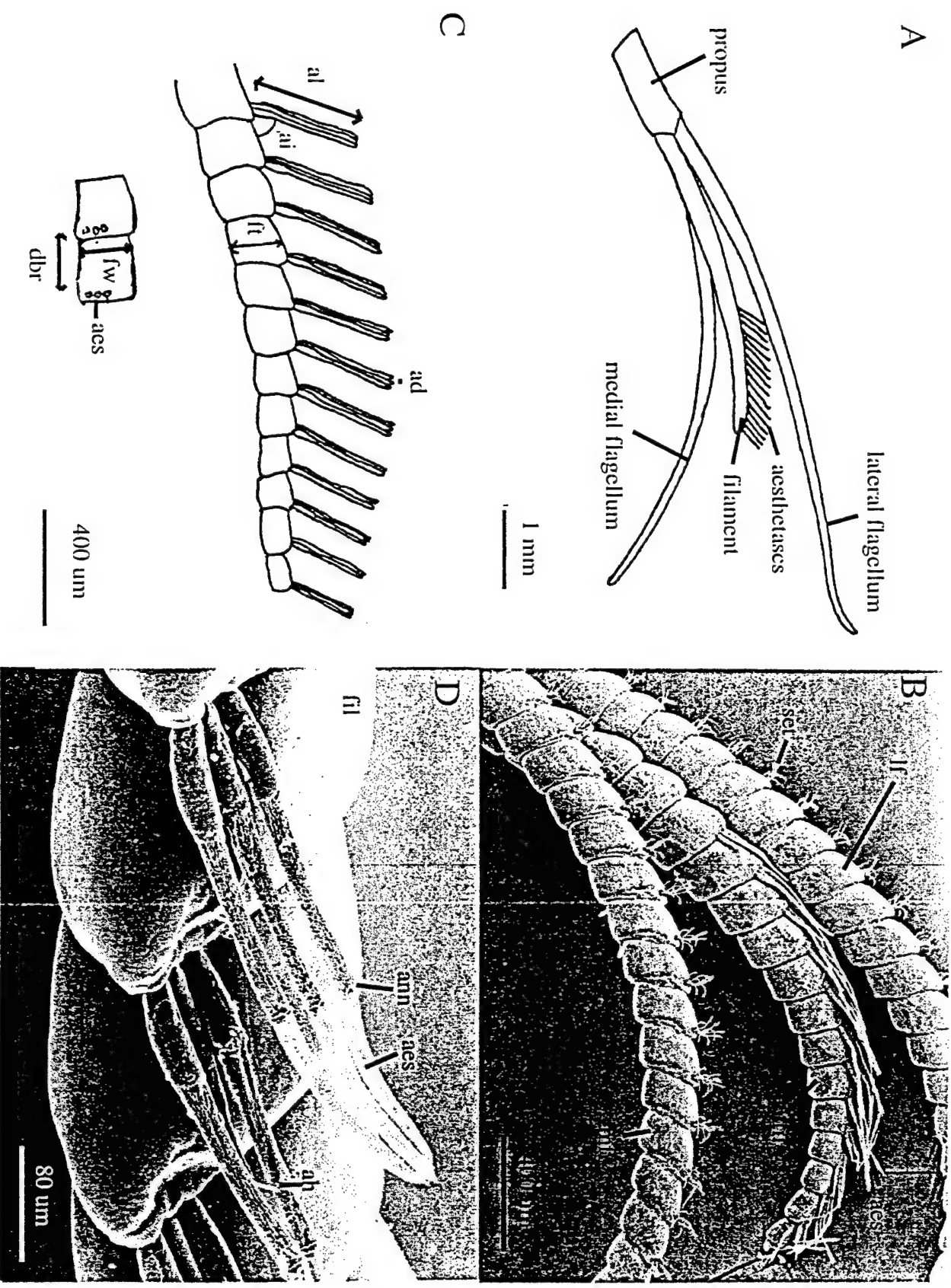
Figure 9. Calculated leakiness during flicking. Data are means and standard errors of the leakiness between adjacent aesthetasc rows of 13 specimens. Lateral motion of flick (filled symbols), medial motion of flick (open symbols). Triangles indicate females and

squares show males. Solid lines show linear regressions for males, dashed lines show linear regressions for females.

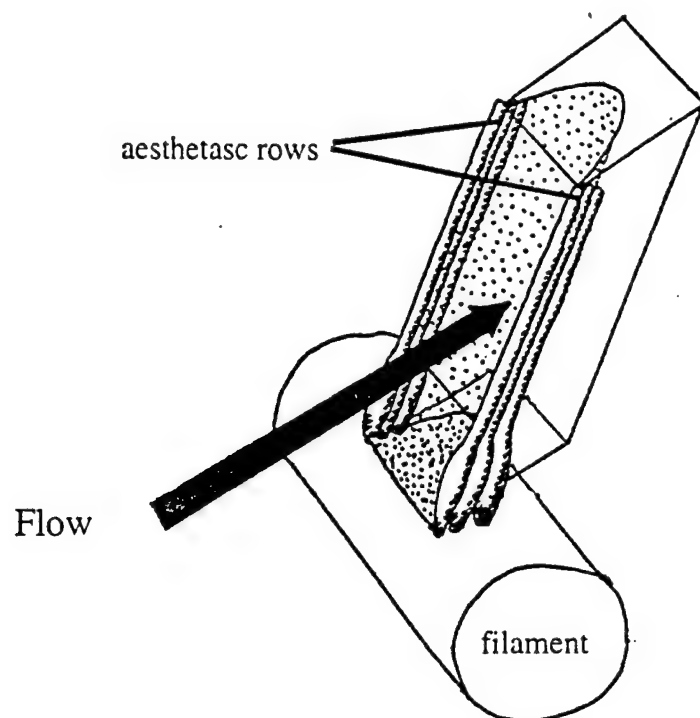
Figure 10. Flow rate between adjacent rows of aesthetascs. Data are means and standard errors of the flow rate between two adjacent aesthetasc rows near the tip of the aesthetasc-bearing filament. N=13. Lateral motion of flick (filled symbols), medial motion of flick (open symbols). Triangles indicate females and squares show males. Solid lines show linear regressions for males, dashed lines show linear regressions for females.

Figure 11. Flow rate between all aesthetasc rows on an antennule. Data are means and standard errors of the flow rate between all the aesthetasc rows on the aesthetasc-bearing filament. N=13. Lateral motion of flick (filled symbols), medial motion of flick (open symbols). Triangles indicate females and squares show males. Solid lines show linear regressions for males, dashed lines show linear regressions for females.

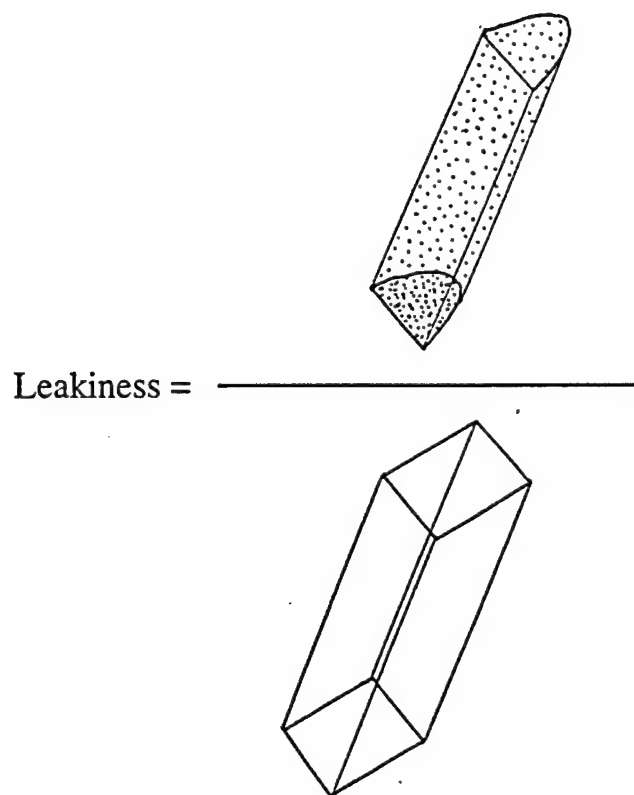
Figure 12. Maximum flicking frequency. Data are maximum flicking frequencies of bouts lasting for at least five flicks. N = 13. Triangles indicate females, squares show males, and circles are juveniles.

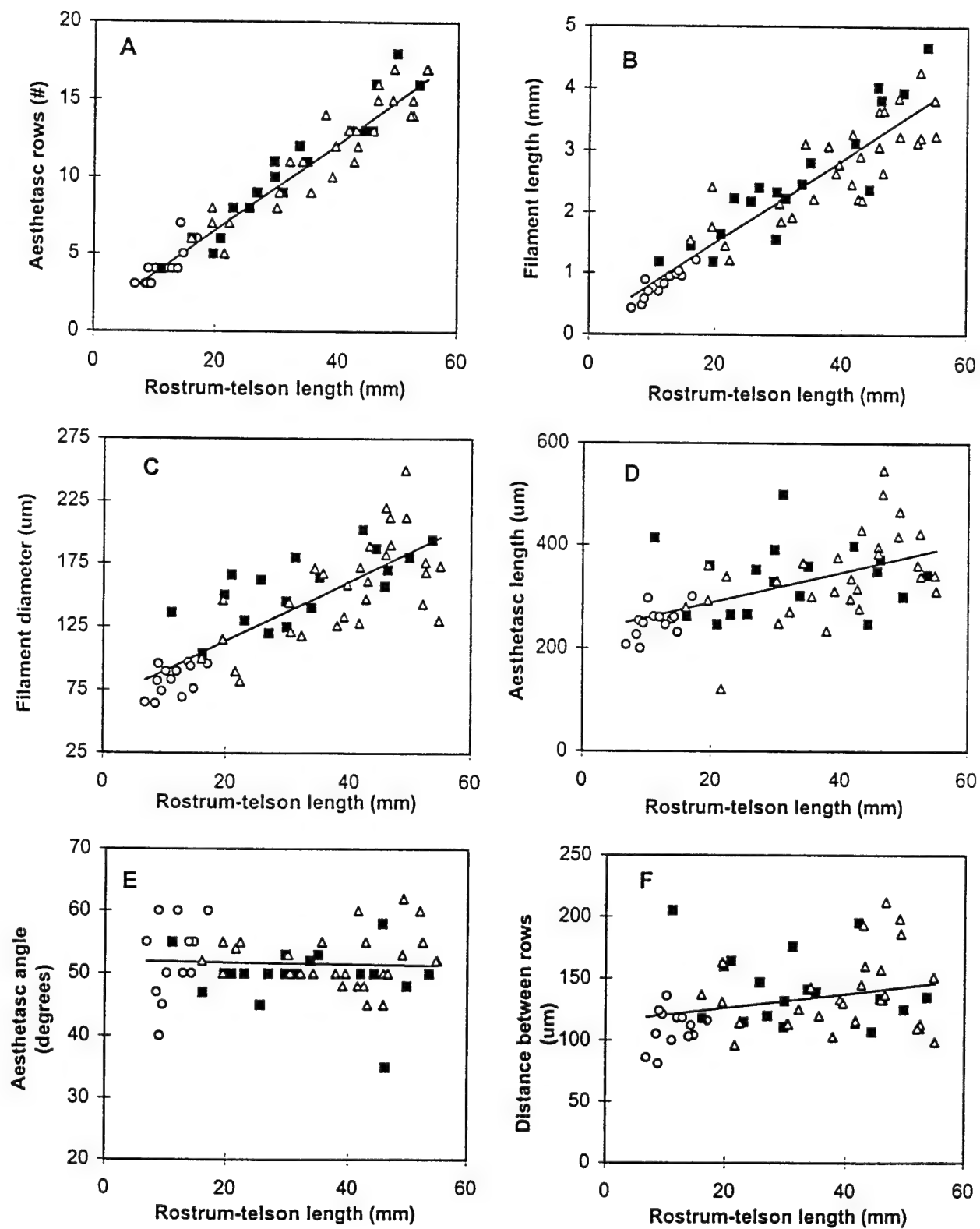


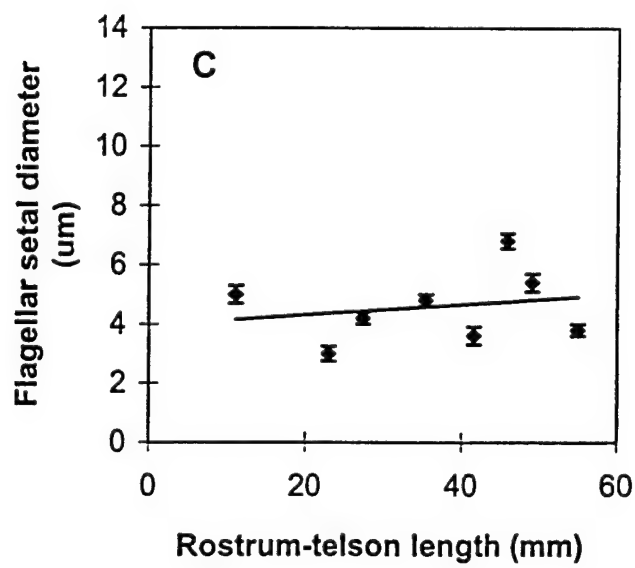
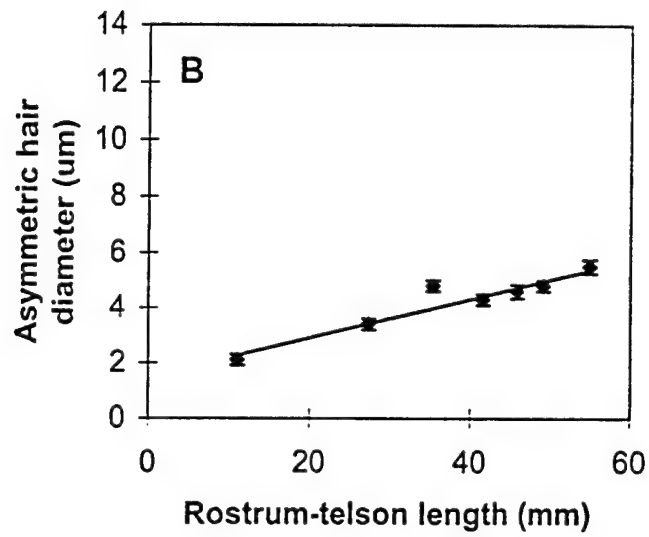
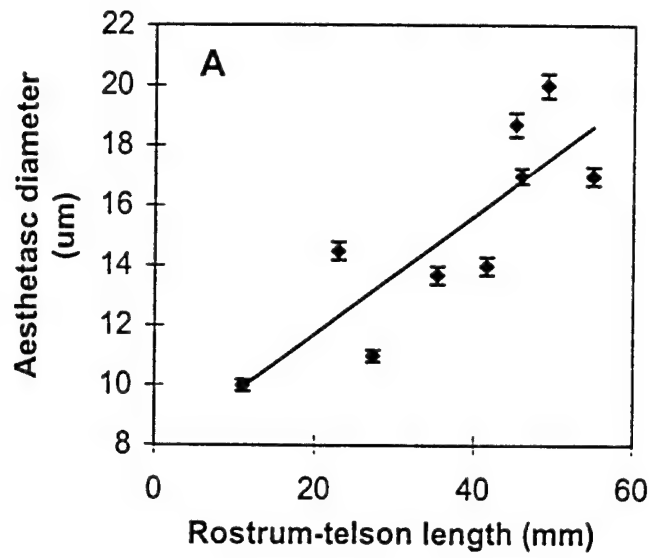
A

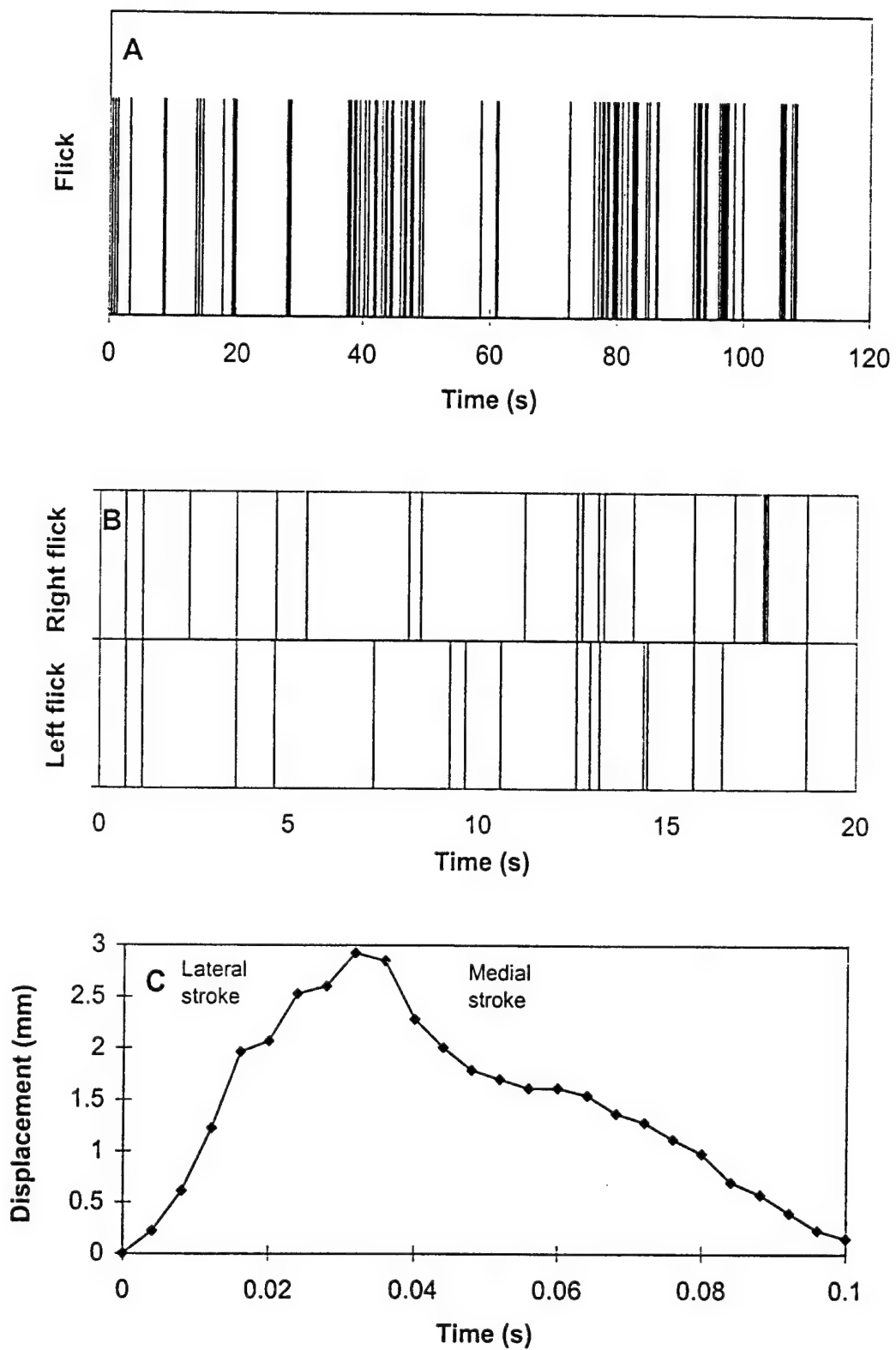


B

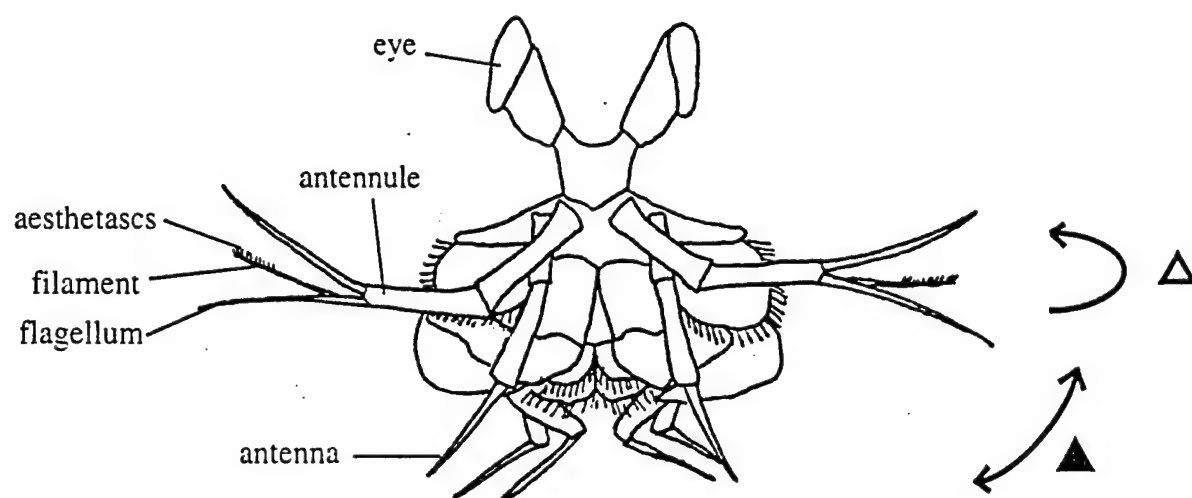




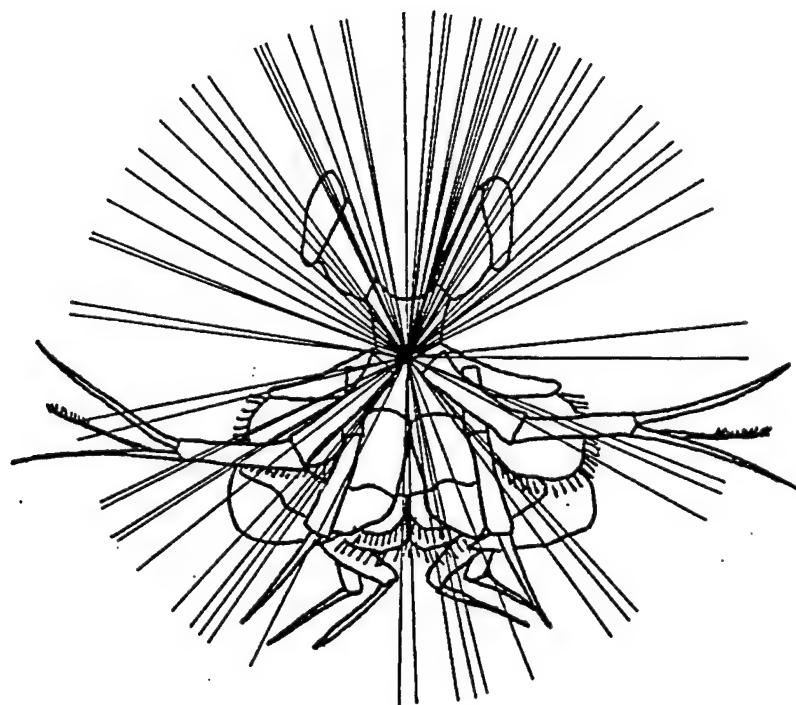


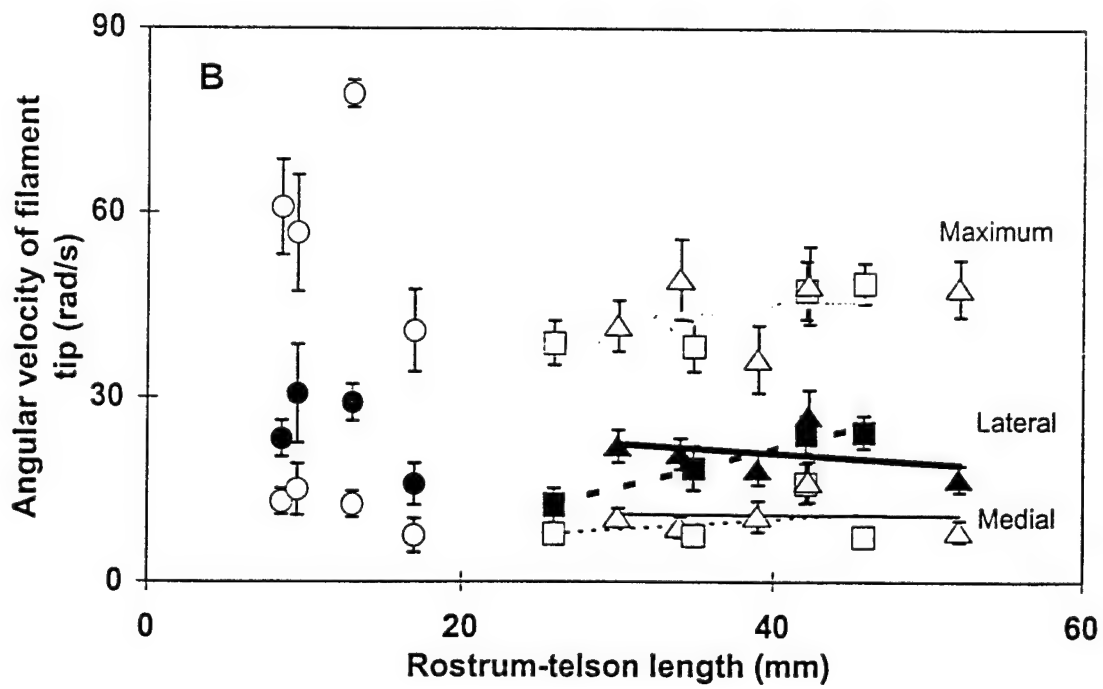
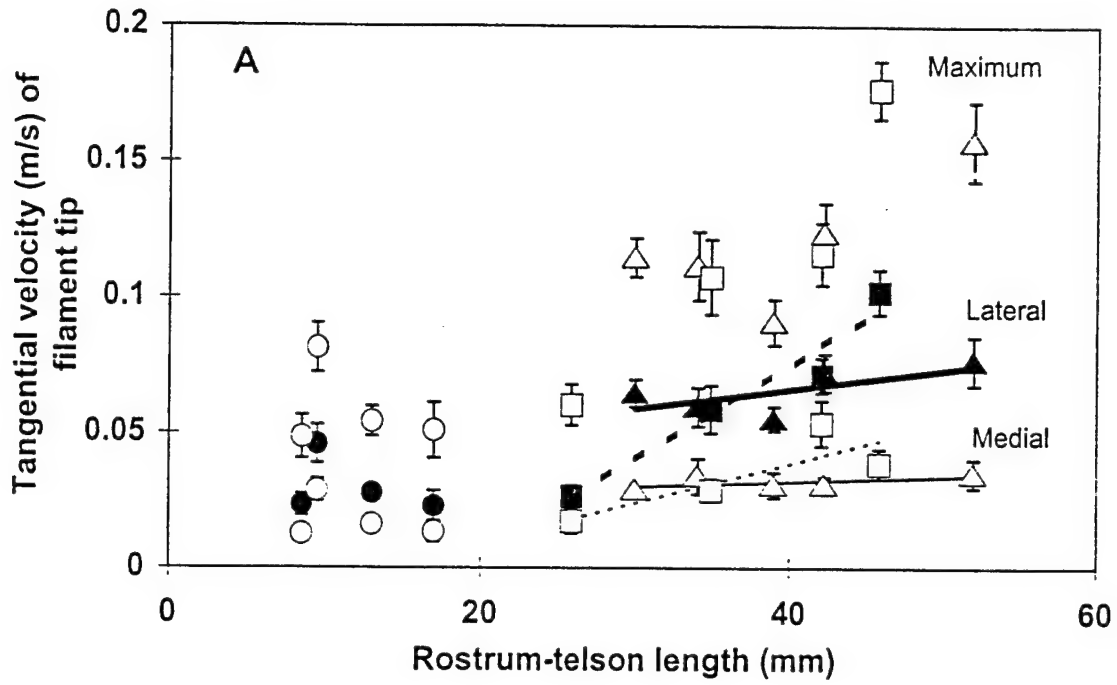


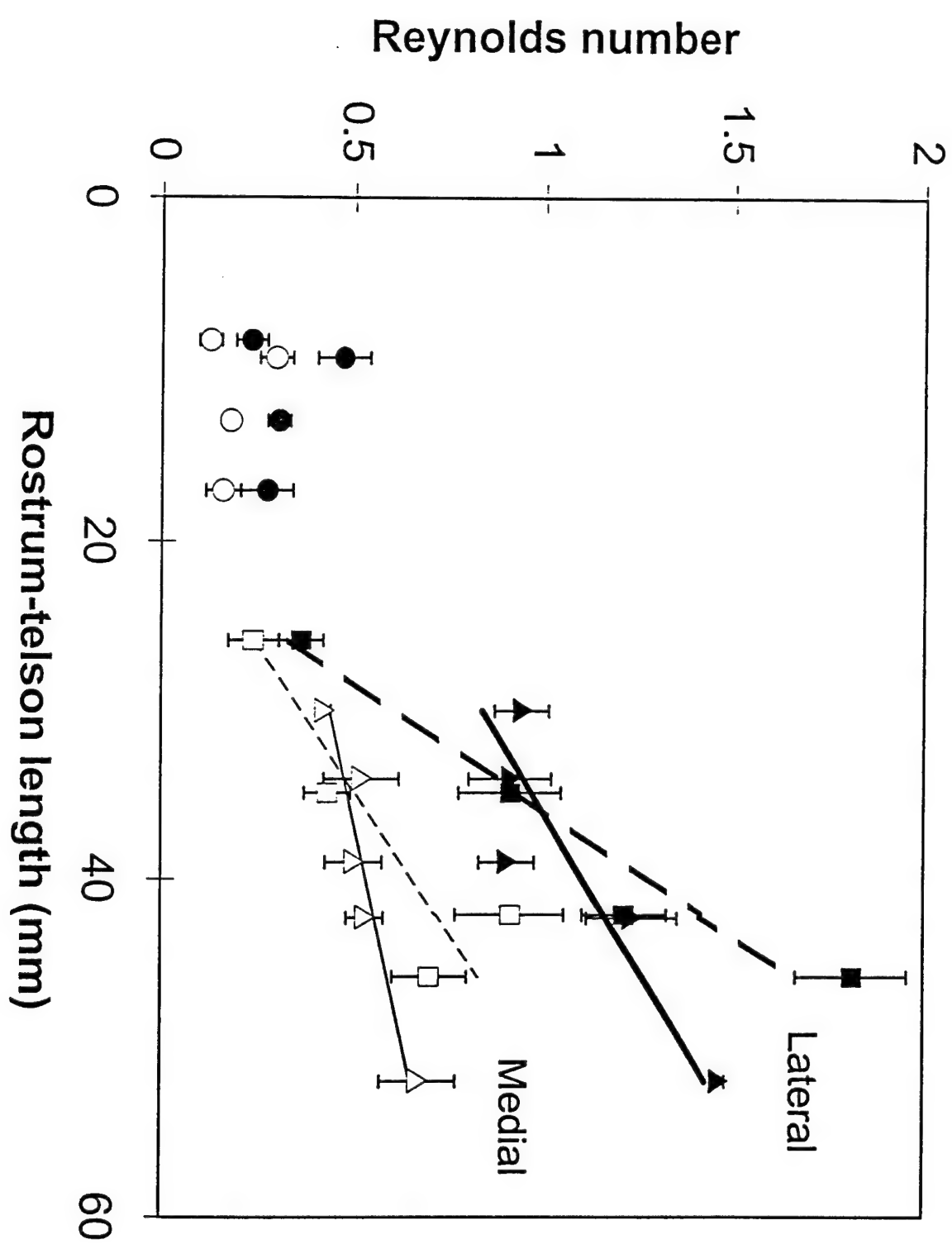
A.

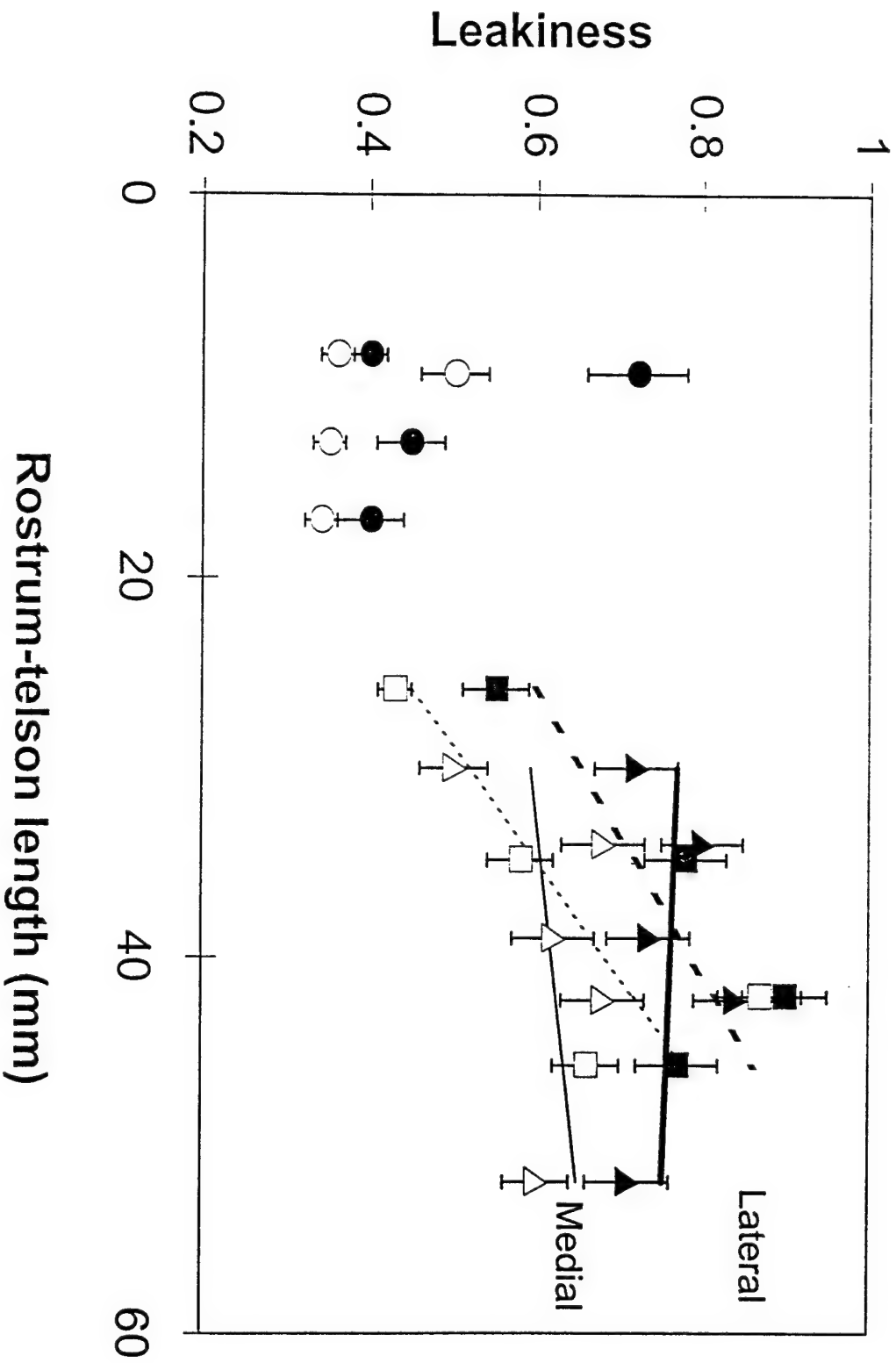


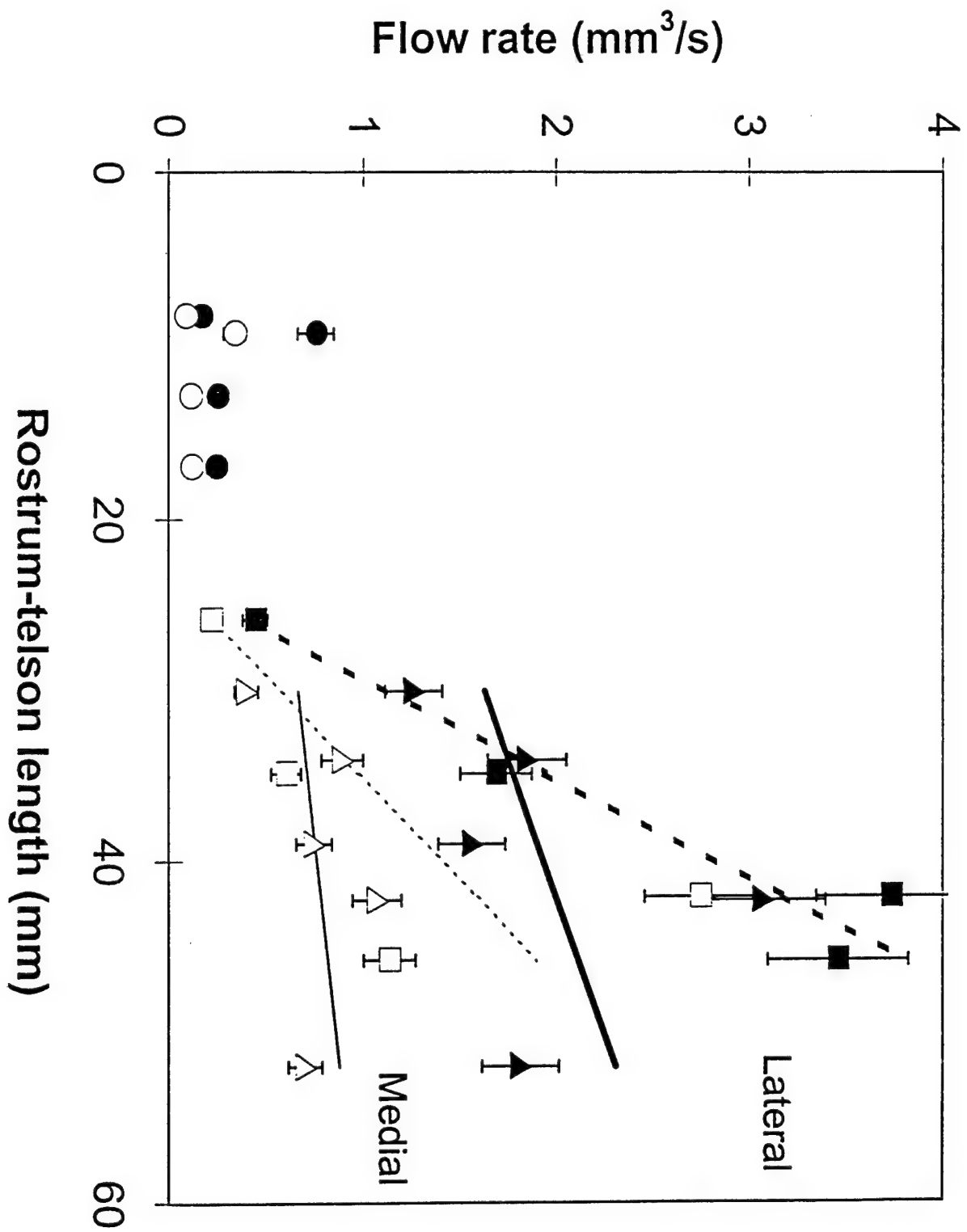
B.

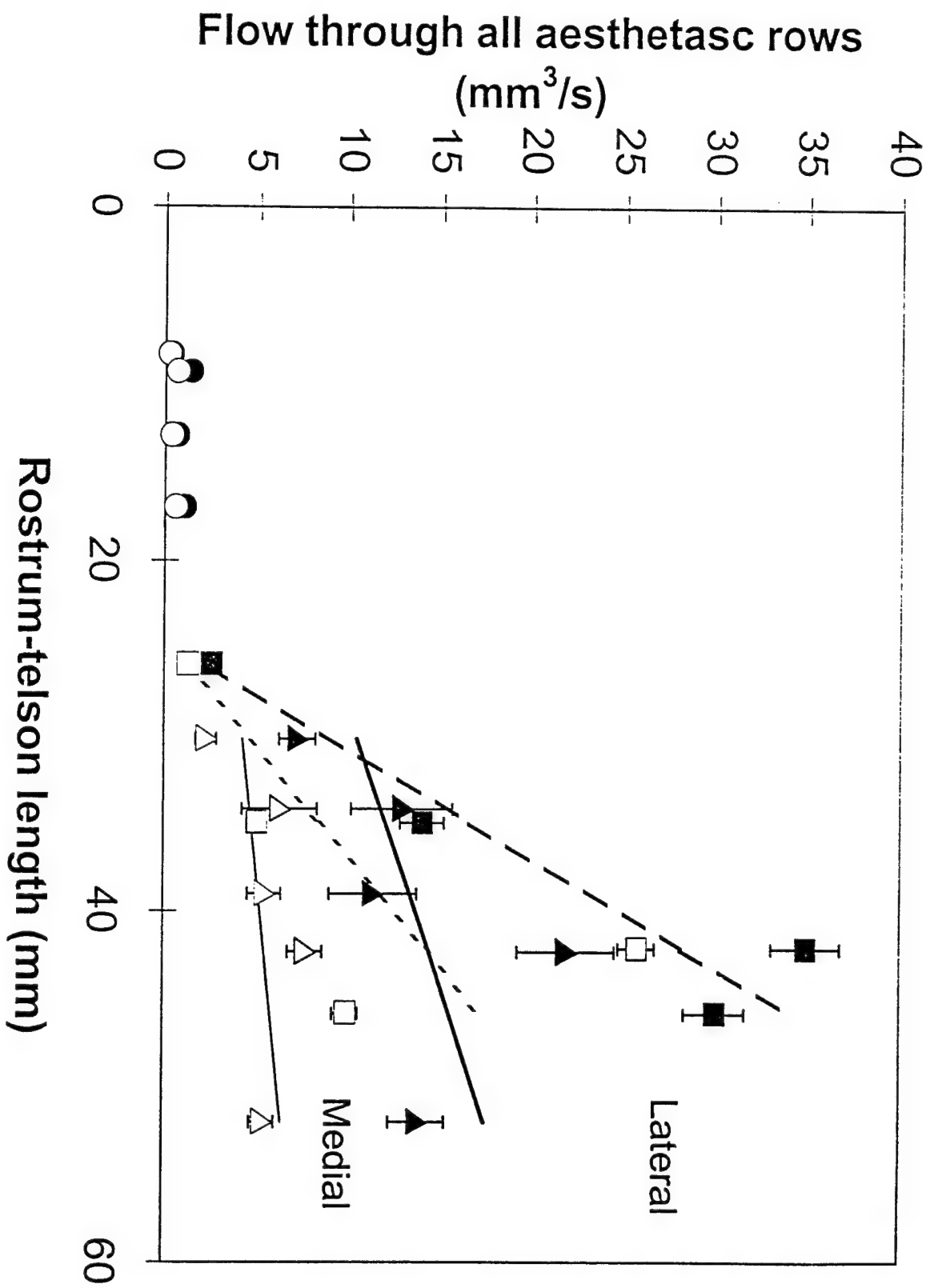


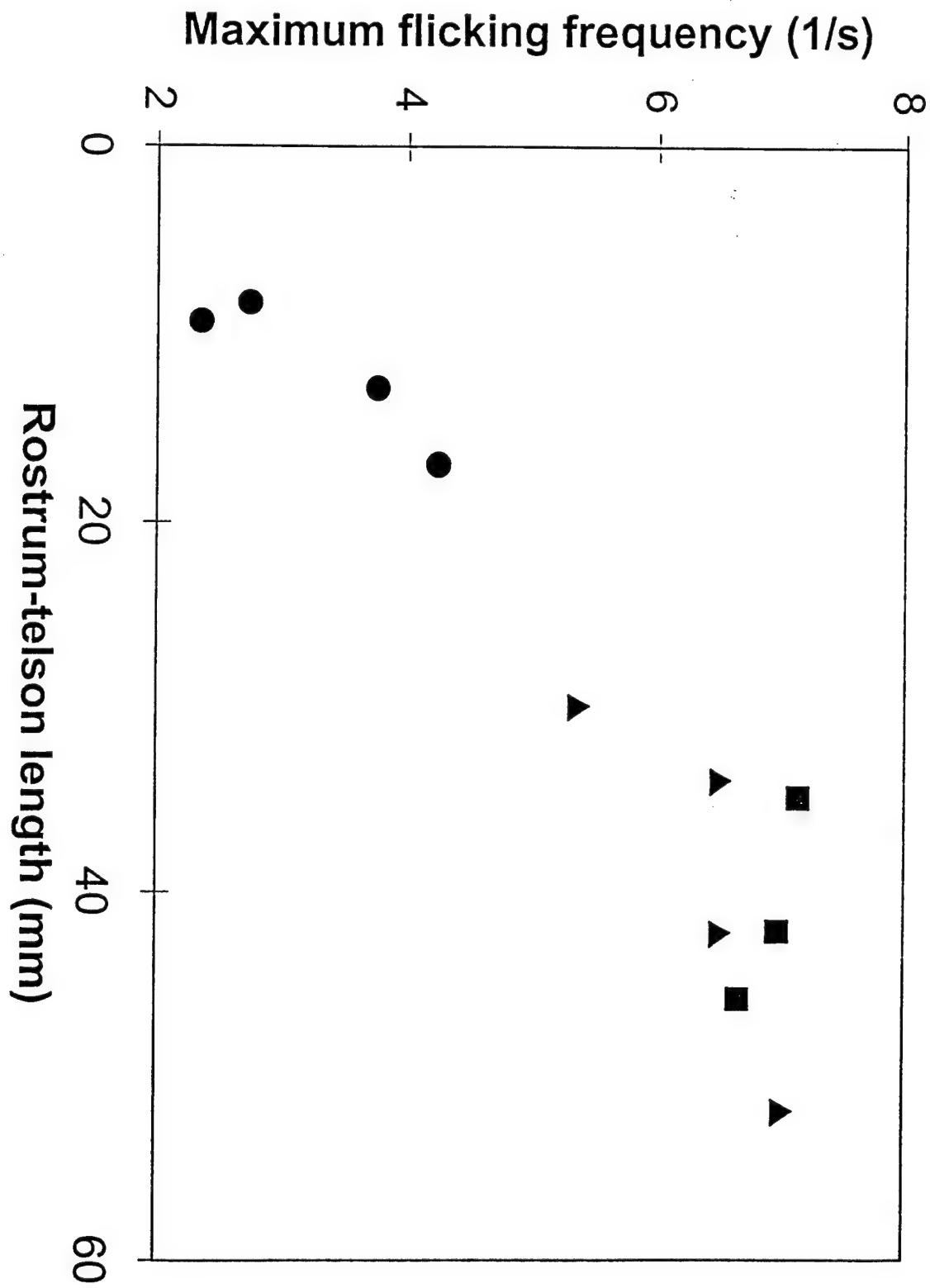












204. Olfactory sampling in lobsters: chemical dynamics during flicking and recovery in the Maine and spiny lobster

Paul A. Moore, Barb Best¹, Robb Schneider, Lydell Gorski² and Mimi A.R. Koehl²

¹Department of Biological Sciences, Bowling Green State University, Bowling Green, OH 43403, ²Department of Biology, Colby College, Waterville, ME 04901 and ²Department of Integrative Biology, University of California at Berkeley, Berkeley, CA 94720-3140, USA

For many organisms, the generation of fluid flow is necessary to bring chemical signals from the environment to microscale environment of the receptor cells. Crustaceans have various mechanisms that enhance the movement of water, and thus, chemical signals, near chemosensory appendages. For example, the flicking by the lateral antennule of lobsters is thought to enhance the delivery of odorant molecules to the sensory aesthetascs on the antennules. By coupling detailed video analysis of antennule movement with microscale electrochemical measurements, it is possible to examine how flicking and recovery influences fluid flow and chemical dynamics in the local environment around aesthetascs. We have mounted a IVEC probe on the lateral antennules of both the Maine, *Homarus americanus*, and spiny, *Paralichthys interruptus*, lobsters and used dopamine as a model for an odorant molecule. Lateral antennules with electrodes were then mounted onto complete carapaces with a mechanical device was constructed that allowed us to 'flick' antennules to simulate the flick of a live lobster. Models were placed in a flow tank and an odor plume of dopamine and fluorescein was released upstream. Video records of flicks were synched with 50 Hz IVEC chemical recordings. Results show that flicking increases the probability that the antennule will encounter odor patches. Flicking increases the concentration detected by the electrode and odorant arrives at the IVEC probed located amongst the aesthetascs after the flick is completed. The results from these studies are critical to the understanding of the chemical dynamics that occur during olfactory sampling and may lead to new insights into the physical design of olfactory appendages.

(1996) Chemical Senses 21:645.

Aims and Scope

The journal provides a forum for work in the biochemistry, physiology, behaviour, and genetics of marine plants and animals in relation to their ecology; all levels of biological organization will be considered, including studies of ecosystems and ecological modelling. The main emphasis of the journal lies in experimental work, both from the laboratory and the field. Descriptive studies will, however, be acceptable if they elucidate general ecological principles. Papers describing important new techniques, methods, and apparatus will also be considered. All papers will be refereed by experts before acceptance for publication. In all cases proofs will be sent to authors. The editors, referees, and publisher will make every effort to expedite publication and the cooperation of authors in this task is welcomed.

Managing Editors

Brian L. Bayne, Plymouth Marine Laboratory, Prospect Place, West Hoe, Plymouth PL1 3DH, UK
F. John Vernberg, Belle W. Baruch Institute for Marine Biology and Coastal Research, University of South Carolina, Columbia, SC 29208, USA

Associate Editors

Ron S. Burton, Marine Biology Research Division 0202, Scripps Institution of Oceanography, University of California, San Diego, 9500 Gilman Drive, La Jolla, CA 92093-0202, USA
Robin N. Gibson, Dunstaffnage Marine Laboratory, P.O. Box 3, Oban, Argyll PA34 4AD, UK
Stephen F. Stancyk, Belle W. Baruch Institute for Marine Biology and Coastal Research, University of South Carolina, Columbia, SC 29208, USA
Richard Warwick, Plymouth Marine Laboratory, Prospect Place, West Hoe, Plymouth PL1 3DH, UK

Consulting and Book Review Editor

Margaret Barnes, Dunstaffnage Marine Laboratory, P.O. Box 3, Oban, Argyll PA34 4AD, UK

Editorial Board

S.S. Bell, Tampa, FL, USA
R. Black, Netherlands, Australia
B.E. Brown, Newcastle upon Tyne, UK
C.A. Butman, Woods Hole, MA, USA
J.H. Christy, Balboa, Panama
A. Clarke, Cambridge, UK
C.M. Duarte, Blanes, Spain
T. Ebert, San Diego, CA, USA
K.J. Eckelbarger, Walpole, ME, USA
J. Field, Cape Town, South Africa
D.R. Fielder, St. Lucia, QLD, Australia
J. Grant, Halifax, NS, Canada
K. Hirayama, Nagasaki, Japan
R.E. Hodson, Athens, Georgia, USA
I.R. Joint, Plymouth, UK
J.M. Jones, Port Erin, UK
T. Kikuchi, Kumamoto, Japan
P. Mladenov, Dunedin, New Zealand
G.S. Moreira, Sao Paulo, Brazil
N.J.P. Owens, Newcastle upon Tyne, UK
J.A. Pechenik, Medford, MA, USA
N. Polunin, Newcastle upon Tyne, UK
D. Raffaelli, Aberdeenshire, UK
D. Randall, Vancouver, BC, Canada
B. Santelices, Santiago, Chile
J.R. Sargent, Stirling, UK
D.O. Skibinski, Swansea, UK
V. Smetacek, Bremerhaven, Germany
C.D. Todd, St. Andrews, UK
A.J. Underwood, Sydney, Australia
R.E. Weber, Aarhus, Denmark
D.J. Wildish, St Andrews, Canada

Publication information: *Journal of Experimental Marine Biology and Ecology* (ISSN 0022-0981). For 1997 volumes 205-215 are scheduled for publication. Subscription prices are available upon request from the Publisher. Subscriptions are accepted on a prepaid basis only and are entered on a calendar year basis. Issues are sent by surface mail except to the following countries where air delivery via SAL mail is ensured: Argentina, Australia, Brazil, Canada, Hong Kong, India, Israel, Japan, Malaysia, Mexico, New Zealand, Pakistan, PR China, Singapore, South Africa, South Korea, Taiwan, Thailand, USA. For all other countries airmail rates are available upon request. Claims for missing issues should be made within six months of our publication (mailing) date.

Orders, claims, and product enquiries: please contact the Customer Support Department at the Regional Sales Office nearest you:

New York: Elsevier Science, P.O. Box 945, New York, NY 10159-0945, USA; Tel. (+1)212-633-3730; [Toll free number for North American customers: 1-888-4ES-INFO (437-4636)]; Fax (+1)212-633-3680; E-mail usinfo@elsevier.com
Amsterdam: Elsevier Science, P.O. Box 211, 1000 AE Amsterdam, The Netherlands; Tel. (+31)20-4853757, Fax (+31)20-4853432, E-mail nlinfo@elsevier.nl
Tokyo: Elsevier Science, 9-15 Higashi-Azabu 1-chome, Minato-ku, Tokyo 106, Japan; Tel. (+81)3-5561-5033, Fax (+81)3-5561-5047, E-mail ky04013@niftyserve.or.jp
Singapore: Elsevier Science, No. 1 Temasek Avenue, #17-01 Millenia Tower, Singapore 039192; Tel. (+65)434-3727, Fax (+65)337-2230, E-mail asiainfo@elsevier.com.sg

Back volumes: Please contact the Publisher.



Journal of Experimental Marine Biology and Ecology,
209 (1997) 47-73

JOURNAL OF
EXPERIMENTAL
MARINE BIOLOGY
AND ECOLOGY

Mechanisms of particle selection by tentaculate suspension feeders during encounter, retention, and handling

Jeff Shimeta*, M.A.R. Koehl

Department of Integrative Biology, University of California, Berkeley, CA 94720-3140, USA

Received 1 September 1995; revised 28 May 1996; accepted 19 June 1996

Abstract

Selection among food particles can occur during any of the successive steps in suspension feeding: particle encounter, retention, and handling. We made predictions for mechanical particle-size selection in encounter and retention by tentaculate suspension feeders (e.g., polychaetes, ctenidarians, and echinoderms), and we measured concurrent selection during each step in feeding for two species of spionid polychaetes (*Pseudopolydora paucibranchiata* Okuda and *Pseudopolydora kempii japonica* Imajima and Hartman). In flume experiments we measured selection between two sizes of plastic beads was measured in flume experiments using video analyses of encounter and retention, and we determined handling selection by subsequent examination of gut contents. Encounter was strongly biased toward large particles, as predicted for the physical mechanism of direct interception. In contrast, retention was often biased toward small particles, as predicted by a model of the balance of forces on an encountered particle (i.e., an adhesive force which promotes retention vs. drag and lift forces which may cause particle loss). Handling was also biased toward small particles, apparently by active rejection of large particles. Flow speed and palp width affected selection only during particle retention. As predicted by the retention model, the retention bias toward smaller particles was stronger at higher flow speed and for worms with narrower palps. Retention mechanics alone thereby resulted in small worms ingesting relatively fewer large particles (and more small particles) in fast flow than they did in slow flow. Furthermore, in fast flow small worms ingested relatively fewer large particles than did larger worms. Given the wide range of particle sizes and types available in the field, retention mechanics can directly influence feeding ecology by placing constraints of flow speed and appendage size on the diet obtainable by tentaculate suspension feeders. Copyright © 1997 Elsevier Science B.V. All rights reserved.

Keywords: Particle selection; *Pseudopolydora kempii japonica*; *Pseudopolydora paucibranchiata*; Spionid polychaete; Suspension feeding; Tentacle

*Corresponding author. Address for correspondence: MS#11, Woods Hole Oceanographic Institution, Woods Hole, MA 02543-1053, USA. Tel.: (508) 289-3448; fax: (508) 457-2194; e-mail shimeta@tides.whoi.edu

0022-0981/97/\$17.00 Copyright © 1997 Elsevier Science B.V. All rights reserved
P/I S0022-0981(96)02684-6

1. Introduction

Suspension feeding is a multi-step process, with the possibility of passive mechanical selection or active behavioral selection among food particles occurring at several stages prior to ingestion. A wide variety of potential food items is available in suspension, and selection among them has numerous implications for animal nutrition and food-web dynamics (e.g., Jørgensen, 1966; Sebens and Koehl, 1984; Kiefer and Berwald, 1992). Potential selection criteria include particle size, shape, specific gravity, stickiness, and taste. In order to understand and to predict how selection depends on factors such as particle characteristics, animal morphologies, and flow environments, passive-mechanical and behavioral mechanisms operating during the separate steps in particle capture and handling must be elucidated.

The first step in suspension feeding is particle encounter (Fig. 1). A suspended particle contacts the capture device (e.g., tentacle) by one of several mechanisms: direct interception, inertial impaction, diffusional encounter, or gravitational deposition (Rubenstein and Koehl, 1977). These mechanisms depend on the small-scale fluid and particle dynamics near the particle-capturing structure (reviewed by Shimeta and Jumars, 1991). The second step in suspension feeding is particle retention, which is required for successful capture of an encountered particle. Although some retention mechanisms, such as trapping particles against a sieve structure or securing particles with nematocysts, have been studied extensively, other retention mechanisms, such as mucous adhesion or surface electrostatics, have received less attention (Shimeta and Jumars,

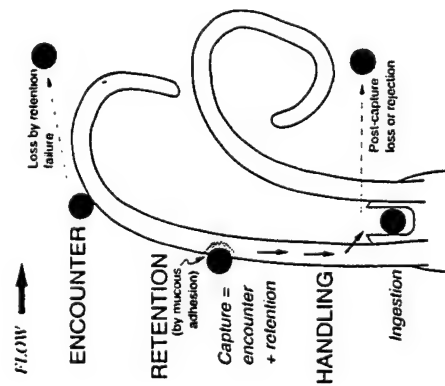


Fig. 1. Component steps in suspension feeding, illustrated for a bidentaculate spionid polychaete. A particle is encountered, then either lost or retained (i.e. captured, depending on a retention mechanism such as mucous adhesion), and finally handled until it is either ingested, rejected, or lost. Shading around the captured particle represents the mucous bond.

1991). The third step in suspension feeding is particle handling, i.e., transport to the mouth by mechanisms such as ciliary beating or motion of the particle-capturing appendage. During post-capture handling, both physical and behavioral mechanisms can determine whether a captured particle is ingested or lost. These mechanisms can include passive mechanical loss due to strong flow forces or sorting limitations, and active behavioral rejection of unwanted particles.

The ingested spectrum of food particles can differ from that available in suspension because of selection during encounter, retention, and/or handling, but no previous study has quantified all of these stages in feeding. Most predictions of mechanical selection by suspension feeders derive from the particle-size dependency in encounter models. However, few tests of models have involved measurement of true particle encounter. More often, particle capture or ingestion has been measured, and the steps of retention and handling have been assumed to involve no losses of particles (reviewed by Shimeta and Jumars, 1991). Several investigators have suggested that reduced capture or ingestion rates in high velocities are caused by strong drag forces that limit particle retention (e.g., Rubenstein and Koehl, 1977; Patterson, 1984; Okamura, 1984, 1985; McFadden, 1986), but this hypothesis has not been verified with quantitative measures of retention efficiencies. Examples of studies that have considered some of the component steps in suspension feeding include that of Appelmanns (1994), who investigated particle selection in both capture and handling by an echinoderm larva, and that of Leonard et al. (1988), who separated encounter from retention in their analysis of particle capture by a crinoid. An analogous dissection of the component mechanisms of selection in tentaculate deposit feeding was introduced by Jumars et al. (1982). Taghon (1982) suggested that drag forces in strong flow might shift the deposit-feeding selectivity of spionid polychaetes to smaller particles, which is a hypothesis similar to the one we present below for particle retention by suspension feeders.

We modeled passive mechanical selection based on particle size by tentaculate suspension feeders, emphasizing influences of ambient flow speed and tentacle size on selectivity. By 'tentaculate suspension feeder' we mean an animal that captures suspended particles on one or more cylindrical structures that do not allow trapping against a sieve, and that depends primarily on ambient flow to produce a particle flux to these structures. Tentaculate suspension feeders thereby include, e.g., various polychaetes, cnidarians, and echinoderms. Our use of the term 'tentacle' includes structures otherwise referred to as, e.g., tentacles, palps, tube feet, and even mucous threads. We focused on particle size because it often relates to food value; e.g. caloric content generally scales with volume among organic particles, and with surface area among organically coated mineral grains. We tested our predictions by measuring selectivity in each step of feeding using two species of spionid polychaetes. Spionids are widely distributed and abundant worms that suspension and deposit feed with a pair of mucus-coated palps (e.g., Taghon et al., 1980; Dauer et al., 1981). Shimeta (1996) found that particle size-selective ingestion by the spionid *Pseudopolydora paucibranchiata* varied with ambient flow speed and animal size in both feeding modes, and he suggested that mechanisms of particle capture on the palps were responsible for the observed patterns of selectivity. Our model predictions and experiments provide a general framework for interpreting such selective suspension feeding.

2. Theory and predictions

2.1. Particle encounter

We predicted that encounter is biased toward larger particles. As explained below, however, we were unable to predict whether the strength of this bias varies with velocity and tentacle size; our null hypothesis was that selective encounter is independent of these variables. We treated only encounter by direct interception, which is considered the predominant mechanism for most non-motile food particles (Shimeta and Jumars, 1991). Our predictions might not apply to those animals and/or situations in which ciliary currents around tentacles (e.g., Mayer, 1994), or responses of cilia to approaching particles (e.g., Strathmann, 1987), influence interception.

Encounter by direct interception occurs when a particle follows a streamline that brings its center within one particle radius of a tentacle (Rubenstein and Koehl, 1977). The particle radius (r_p) itself defines the limiting streamline for contact. Therefore, the volume of water from which particles are encountered (and hence, the encounter rate, E) is directly related to particle size, i.e., $E \propto r_p^n$, where $n > 0$. Encounter is thus biased toward larger particles, and the strength of the bias depends on the exponent, n . Rubenstein and Koehl (1977), Shimeta and Jumars (1991) and Shimeta (1993) gave analytical models for the rate and efficiency of direct interception of spherical particles when both the tentacle Reynolds number (Re_t) and the ratio of particle radius to tentacle radius (r_p/r_t) are less than 0.1 ($Re_t = 2 r_t U/\nu$, where U is free-stream velocity and $\nu = \text{kinematic viscosity} = 0.01 \text{ cm}^2 \text{ s}^{-1}$). However, many tentaculate suspension feeders (e.g., polychaetes, ophiuroids, crinoids, holothuroids, sea anemones, corals, sea pens) experience $Re_t \geq 1$ because they feed at relatively high velocities with relatively large tentacles, or they experience $r_p/r_t \geq 1$ because they encounter relatively large particles (Shimeta and Jumars, 1991). Increasing Re_t above 0.1 can strengthen the r_p -dependence of encounter rate by enhancing streamline compression around the tentacle (Shimeta and Jumars, 1991). However, increasing r_p/r_t above 0.1 can reduce the r_p -dependence by creating interference to contact that is stronger for larger particles due to interaction between flow fields around the tentacle and the particle (cf. Davies, 1973). Therefore, we determined experimentally the strength of the encounter bias for large particles, as well as its dependence on velocity and tentacle diameter.

2.2. Particle retention

We made the following predictions, each derived below from a model of retention mechanics for an isolated tentacle, where trapping against a sieve cannot occur. First, smaller particles are preferentially retained over larger particles, except when all particles being compared are much smaller than the tentacle diameter. Second, the retention bias toward smaller particles is stronger for narrower tentacles than it is for wider tentacles, except when all tentacles being compared are much larger than the particles. Third, the efficiency of retention (i.e., proportion of encountered particles that are captured) is inversely related to velocity. Fourth, the retention bias toward smaller particles is stronger in faster flow than it is in slower flow. We refer to mucous adhesion

throughout this analysis because it is important in retention for a variety of polychaetes, echinoderms, and some cnidarians (e.g., Jørgensen, 1966; Pentreath, 1970; Lewis and Price, 1975; Jumars et al., 1982; Sebens and Koehl, 1984; Lahaye and Jangoux, 1985). Nematocysts (e.g., Mariscal, 1974; Conklin and Mariscal, 1976) and possibly surface electrostatics (e.g., LaBarbera, 1978) are important retention mechanisms for some tentaculate suspension feeders, and our qualitative predictions should apply to these cases as well.

Retention of a particle encountered on an isolated tentacle requires the force promoting adhesion to equal or exceed the sum of the forces resisting adhesion:

$$F_A \geq F_D + F_L + F_G, \quad (1)$$

where F_A , F_D , F_L , and F_G are the adhesive, drag, lift and gravitational forces on the particle, respectively. This force balance assumes (1) that prey are not live, or at least not able to exert a significant struggling force against retention, (2) that gravity resists retention, requiring either that the tentacle is oriented vertically or that the particle is not encountered exactly on the top of the tentacle, and (3) that the drag force (oriented downstream) acts in a direction away from the tentacle, requiring that the particle is encountered at any position other than at the center of the upstream side of the tentacle. Indeed, most particles are not encountered along the center, stagnation streamline (Shimeta and Jumars, 1991). The forces can be parameterized for spherical particles and substituted into Eq. (1) as follows:

$$\sigma_B A_C \geq 0.5 \rho C_D \langle u^2 \rangle A_p + 0.5 \rho C_L \langle u^2 \rangle A_p + (\rho_p - \rho) g V_p, \quad (2)$$

where σ_B is the breaking stress of the particle-tentacle bond, A_C is the area of contact made between the particle and tentacle, C_D and C_L are the drag and lift coefficients, $\langle u^2 \rangle$ is the average of the squared local velocity over the particle, A_p is the exposed cross-sectional area of the particle, ρ_p and ρ are the particle and fluid densities, g is the gravitational acceleration, and V_p is the particle volume. Particle retention can be quantified as the retention efficiency, $R = \text{proportion of encountered particles that are captured}$.

The gravitational force is generally insignificant relative to the drag and lift forces for most particles under typical feeding conditions. Of the examples in Fig. 2a, only very large organic particles (e.g., larvae) and mineral grains of coarse-silt or larger size can reach $F_G > 0.1 [F_D + F_L]$, and only in very slow flows ($\leq \text{order } 1 \text{ cm s}^{-1}$). Organic particles (e.g., algal cells) often experience a greater applied force than do denser but smaller mineral grains (Fig. 2b), because of the greater contribution of the drag and lift forces relative to the gravitational force, thus favoring retention of the denser particles. F_G can be important for selective retention among similarly sized particles that differ greatly in specific gravity (e.g., a mineral grain and an algal cell), but again only in very slow flows (Fig. 2b). For the sake of clarity in our presentation we assume $F_G = 0$ (although we consider the implications of specific gravity where they might be important). Therefore, retention requires

$$\sigma_B A_C \geq 0.5 \rho \langle u^2 \rangle A_p (C_D + C_L). \quad (3)$$

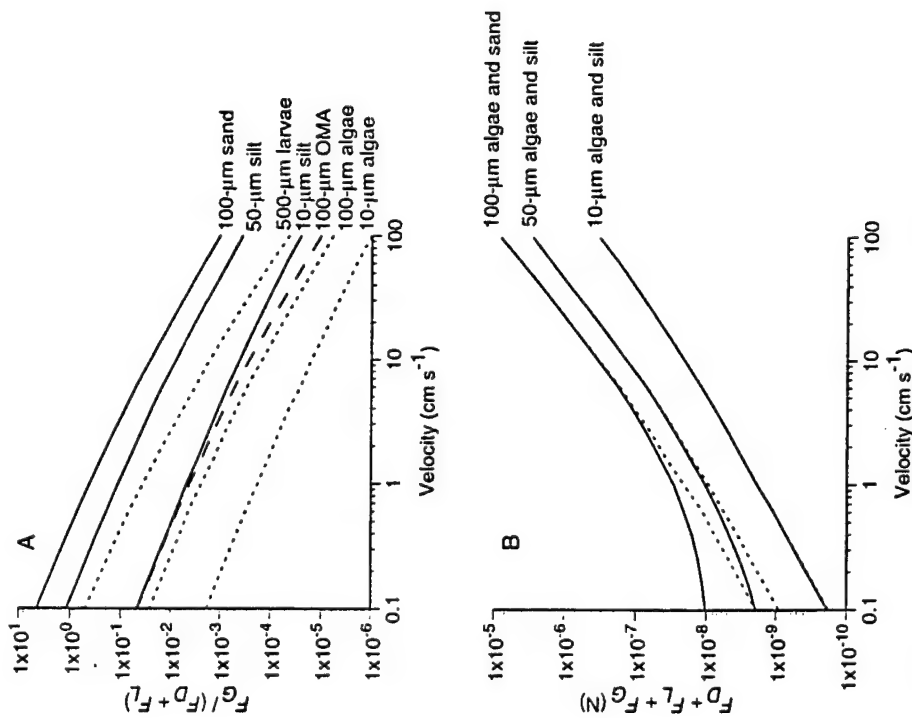


Fig. 2. Calculated (Eq. (2)) drag (F_D), lift (F_L), and gravitational (F_G) forces resisting retention of encountered, spherical particles. Dotted lines represent organic particles, dashed line indicates organic-mineral aggregates (OMA), and solid lines are mineral grains. Values of $(r_p - r_t)$ are taken from Gibbs (1985) for OMA, Jackson (1989) for larva, and Butman (1986) for larva, and $\rho_p - \rho = 1.63$ for mineral grains. (A) illustrates the contribution of F_G relative to F_D and F_L . (B) illustrates the influence of particle specific gravity on the sum of forces experienced by particles of similar size (algae and mineral grains).

Our first two predictions concerning selective retention were derived from a qualitative argument considering the dependence of contact area, A_c , on relative sizes of the particle (r_p) and tentacle (r_t). Particles that are much smaller than the tentacle can be well-embedded in mucus upon contact (Fig. 3a). (Tentacle compliance that allows the surface to wrap at least partially around the particle can create a similar effect.) In the

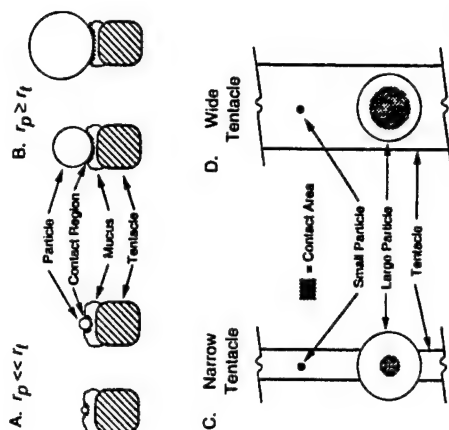


Fig. 3. Contact-area relations between a particle and a tentacle, drawn for mucous retention as an example. Shading represents mucous bond. (A), (B) cross-sectional views through tentacle, coated with mucus on upper surface; r_p and r_t are the radius of the particle and tentacle, respectively. Smaller particles should be retained preferentially over larger particles in case (B). (C), (D) frontal views of tentacle, with mucous bonds visible through particles. The retention bias toward smaller particles should be stronger in case (C) than in case (D).

limit of $r_p \leq r_t$, particles of different sizes should have a contact area that varies approximately in direct proportion with their surface area ($\propto r_p^2$). In contrast, when the particle size is similar to or larger than that of the tentacle, contact area cannot remain proportional to particle area (Fig. 3b).

The first prediction was therefore that smaller particles are preferentially retained over larger particles, except among particles that are all much smaller than the tentacle diameter. In the latter case ($r_p \leq r_t$, Fig. 3a), A_c and thus the adhesive force rise at least as rapidly with particle size (approximately $\propto r_p^2$) as do the drag and lift forces. We say 'at least' because, although F_D and F_L depend directly on particle cross-sectional area (A_p), they in fact have functions that are weaker than r_p^2 , due to the inverse dependence of the drag and lift coefficients (C_D and C_L) on r_p . For the relevant range of particle Reynolds number, C_D varies from $\propto r_p^{-1.0}$ to ca. $\propto r_p^{-0.4}$ as velocity and/or particle size increase (Vogel, 1994; 1994); C_L for hemispheres against a boundary has the same functionality as C_D (Chepil, 1958). In contrast, among particles that are roughly similar to or larger than the size of the tentacle, contact area does not maintain proportionality with particle area (Fig. 3b), and at some point A_c becomes a weaker function of r_p than are the drag and lift forces. The result is that retention is increasingly likely to fail as particle size increases, and thus smaller particles are preferentially retained. (Note that if the gravitational force (F_G) is important, as for very large or dense particles in slow flow (cf. Fig. 2), the retention bias toward small particles can be even stronger, because the sum of forces resisting retention (Eq. (2)) then scales with r_p^3 .)

Our second prediction, a corollary to the first, was that variation in tentacle diameter

should have virtually no effect on retention if r_t is consistently $> r_p$; otherwise, the narrower the tentacle, the stronger the bias toward retaining small particles. Tentacles of two different widths can create the same contact area with a small particle that in each case satisfies the condition $r_p < r_t$ (Fig. 3c, d), and thus they have similar retention efficiency. In contacting a much larger particle, however, the smaller tentacle can have poorer retention than the larger tentacle because of a reduced contact area (Fig. 3c). The retention bias toward smaller particles is therefore stronger among narrower tentacles than it is among wider tentacles.

The third and fourth predictions resulted from the velocity dependence of the drag and lift forces (Eq. (3)). Because these forces increase with velocity, while the adhesive force is independent of velocity, we predicted that retention efficiency falls as velocity rises. Furthermore, we predicted that the bias toward retaining smaller particles increases at higher velocities due to the nonlinearities in the drag and lift forces with respect to velocity and particle size. Larger particles experience a greater increase in $(F_D + F_L)$ in response to rising velocity than do smaller particles. Using our experimental conditions as an example, an increase in velocity from 1.3 to 9.1 cm s⁻¹ caused $(F_D + F_L)$ on 80 μ m spheres to rise by 1.9×10^{-7} N (or by a factor of 9.8x), while $(F_D + F_L)$ on 33 μ m spheres rose by only 6.2×10^{-8} N (or by a factor of 8.5x). Because adhesive failure depends on the applied force exceeding a threshold corresponding to the adhesive force, the absolute rise in $(F_D + F_L)$ is of more importance than the proportional rise.

2.3. Particle handling

Tentaculate suspension feeders from many phyla display selectivity during post-capture handling, which might be passive and/or active (e.g., Pentreath, 1970; Winston, 1978; Dauer, 1984, 1985; Holland et al., 1986), and little information is available on the role of particle size per se (except, e.g., Nicol, 1930; Bonar, 1972). We therefore made no predictions regarding handling selection based on particle size.

3. Materials and methods

3.1. Animal collection and maintenance

We collected the spionid polychaetes *Pseudopolydora paucibranchiata* Okuda from an intertidal fine-sand flat in Bodega Bay, CA, and *Pseudopolydora kempi japonica* Inajima and Hartman from an intertidal silty-sand flat at the Richmond Field Station (University of California) in San Francisco Bay, CA. Animals were sieved onto a 500 μ m mesh screen in the field and brought to U.C. Berkeley, where they were kept in aerated sea water at 13°C. Worms were separated from their tubes and preliminary measures of palp width were made for each worm with an eyepiece micrometer under a dissecting microscope while they were anesthetized in 4% MgCl₂ in sea water. Plastic pipettor tips (0.75 cm widest i.d.), with the narrow end sealed, were filled with 250 μ m sieved sediment from the collection sites and stored vertically. Each worm was placed on the sediment surface in a pipettor tip and was allowed to burrow and build a new

tube. Worms in pipettor tips were kept submerged in trays of sea water from the Bodega Bay Marine Lab and fed a ground paste of Gerber® mixed cereal for one to four days before experiments were conducted.

3.2. Flume experiments

Experiments were run at 13°C in a recirculating flume as described by Shimeta (1996). The flume floor was clean, except for a 2 cm wide strip of 2 mm sand cemented near the channel entrance that ensured development of a turbulent boundary layer when the flume was run at low velocities. The flume was filled 4.3 cm deep with sea water passed through a 5 μ m mesh filter bag. The working section of the flume included a removable Plexiglas plate with holes into which the pipettor tips containing individual worms fit snugly and were held flush with the flume floor. Worms were aligned in a single row parallel to the flow, separated from each other by 3.75 cm. This separation distance (ca. 37 worm-tube diameters) was sufficient to prevent the wake of a worm's tube from influencing the flow around a downstream neighbor (Nowell and Jumars, 1984).

We ran experiments with spherical polystyrene beads that were neutrally buoyant (specific gravity 1.02), which ensured that they were not available to the worms by deposit feeding. We purchased beads in two size classes, nominally 25–38 μ m and 75–90 μ m (Solotill Labs, Inc.). These diameters fall within the range for particles in suspension in the field (e.g., algal cells, microzooplankters, detritus, mineral grains, and organic-mineral aggregates). Beads were rinsed with distilled water and wet-sieved between 15 and 45 μ m Nitex screens (small bead-size class) or between 75 and 100 μ m Nitex screens (large bead-size class) to eliminate any overlap in size ranges. The mean diameters in the two size classes, as measured under a dissecting microscope, were 33.2 μ m (± 6.0 μ m s.e., $n = 54$) and 80.0 μ m (± 7.7 μ m s.e., $n = 46$). When examining beads on videotapes or in experimental samples, all beads < 60 μ m were scored as 'small' and all beads ≥ 60 μ m were scored as 'large'.

The two size classes of beads were added to the flume with 20 ml of filtrate from Gerber® mixed cereal (ground in sea water and passed through a 10 μ m filter) to stimulate feeding. For determination of concentrations by microscope counts, the particle suspension was sampled repeatedly throughout experiments by withdrawing 40 ml isokinetically through a Pasteur pipette at 3 mm height in the working section of the flume using a peristaltic pump. The mean concentrations of small and large beads were 853 ml⁻¹ (± 81 ml⁻¹ s.e., $n = 8$) and 722 ml⁻¹ (± 48 ml⁻¹ s.e., $n = 8$), respectively. The mean proportion of the suspension composed of large beads was 0.46 (± 0.02 s.e., $n = 8$). A size-frequency distribution from other experiments performed with this bead mixture is shown in Shimeta (1996).

Six worms of one species were placed in the flume at a time. Worms of both species held their palps in the water column to suspension feed almost exclusively throughout all experiments. Each worm was videotaped while feeding at constant flow velocity for at least 15 min. Videotapes were recorded on a Panasonic AG7350 SVHS VCR using a Watec WAT-902 CCD camera, a Nikon PB-6 extension bellows, and a Nikon Micro-Nikkor 105 mm macro lens. Lighting was provided overhead by a fiber-optic lamp

Table 1
Flow parameters calculated from suspended-bead trajectories

<i>P. paucibranchiata</i>		
U_{mean} (cm s ⁻¹)	1.3 ± 0.2 (n = 25)	9.1 ± 2.1 (n = 50)
u , (cm s ⁻¹)	0.39	1.6
<i>P. kempii japonica</i>		
U_{mean} (cm s ⁻¹)	1.8 ± 0.1 (n = 20)	7.4 ± 1.9 (n = 40)
u , (cm s ⁻¹)	0.66	1.3

U_{mean} = mean velocity 3 mm above the bed, u , = shear velocity. Columns indicate treatments applied to each species.

covered by red acetate to prevent light avoidance by worms. Each *P. paucibranchiata* individual was videotaped at one of two velocity settings (Table 1), after which it was removed from the flume. The sealed end of the pipettor tip was cut off and the contents were rinsed with 20% formalin in sea water into a vial to preserve the worm for later analysis of beads that were ingested during videotaping. Too few individuals of *P. kempii japonica* were available to allow independent samples between velocity settings, so a single group of worms was videotaped at two different velocities (Table 1). After the high-velocity treatment the worms were removed and preserved for later analysis of beads ingested during that treatment.

3.3. Data analysis

We viewed videotapes on a Sony PVM-1341 Trinitron monitor. Flow parameters were measured from videotaped segments of the flowing particle suspension in the absence of worms, assuming that the neutral buoyancy of the beads made them adequate flow markers. Mean velocities were determined from measurements to the nearest mm of bead displacements over a 10-frame segment of videotape. Mean velocities are reported (Table 1) for 3 mm above the flume floor (U_{mean}), which is the approximate height of the worms' palps (cf. Shimeta, 1996). Vertical profiles of mean velocity were used to calculate the shear velocity (u), a measure of bottom shear stress) from the slope of the best linear fit to the natural log of height vs. mean velocity (Nowell and Jumars, 1987).

Particle encounter and capture were quantified by frame-by-frame viewing of the videotapes of feeding. The magnification was such that the smallest beads (15 μ m) appeared 2 mm in size on the monitor. Palp width for each worm was measured to the nearest mm on the monitor in the middle of the portion that was viewed, and this width measure was used in all data analyses. For each species, an encounter between a bead and a palp in the high-velocity treatment was defined to occur when a bead stopped, in contact with the palp, for at least two video frames (0.0333 s). In the low-velocity treatment for each species, the frame-number criterion for encounter was extended in proportion with the ratio of U_{mean} in the two treatments (Table 1). Thus, for *P. paucibranchiata*, the frame-number criterion at the low velocity was $(9.1/1.3) \times 2 = 14$

frames (0.233 s). For *P. kempii japonica*, the frame-number criterion at low velocity was $(7.4/1.8) \times 2 = 8$ frames (0.133 s). For each worm, the first 50 encounters were scored for bead size. A capture of a bead was defined to occur when an encountered bead began to move proximally along the surface of a palp, indicating that manipulative control of the bead had been achieved by the worm. For each worm, the first 50 captures were scored for bead size. The retention efficiency of each bead-size class was determined from the number of captures scored among the first 50 encounters.

To determine the numbers of beads of each size class that were ingested during videotaping, each fixed worm was retrieved from its tube, cleaned of any adhering beads under a dissecting microscope, and placed into a plastic microfuge tube containing chlorine bleach. After the body tissue was dissolved, the remaining bead sample from the gut was transferred to a Sedgwick–Rafter counting chamber and counted under a dissecting microscope. We assumed that all ingested beads were obtained by suspension feeding because the specific gravity reported for the beads matched that measured for the flume water (1.02), and beads did not accumulate on the flume floor during experiments. Only worms that had ingested at least 50 beads were included in statistical analyses of encounter, capture, retention, and ingestion. This arbitrary criterion was adopted to ensure that the particle suspension was acceptable to those individuals (cf. Hentschel, 1996; Shimeta, 1996), and for the ingestion data to at least match the sample sizes of 50 beads scored for encounter, capture, and retention.

We expressed the relative numbers of small and large beads in a sample (i.e., ambient suspension, or beads encountered, beads captured, or beads ingested by a worm) as the proportion of the sample composed of large beads (P_L , calculated as the number of large beads divided by the sum of the number of small and large beads). When compared between the successive steps in feeding, differences in this proportion reveal whether any selectivity between the bead sizes occurred during encounter, retention, or handling. Spearman's rank correlation coefficients were calculated with Systat 5.1 software. Significance values for the Spearman coefficients, as well as Wilcoxon rank sums (2-sample) and signed ranks (paired-sample) tests, were calculated following Conover (1980). Nonparametric linear regressions were calculated following Tate and Clelland (1957).

4. Results

4.1. General observations of feeding behavior

Measurements of ciliary-current velocities around the palps suggested that a passive mechanical process of direct interception was a valid first approximation for the particle-encounter mechanism. Following an extended period of suspension feeding by *P. paucibranchiata*, flow in the flume was stopped and palps remained vertical in the water column for several minutes, during which time we observed suspended beads to be occasionally entrained into a ciliary current. From videotaped sequences of these events, we measured the maximal particle velocity (among 5 measured particle trajectories) in the ciliary current to have a mean value of 0.13 cm s^{-1} ($\pm 0.01 \text{ s.e.}$, $n = 6$ worms), and

there was no relation to palp size. To determine roughly whether this ciliary current was strong enough to influence particle trajectories in the presence of ambient flow, we compared it with calculations of velocity in the boundary layer around a cylinder normal to a flow. Using numerical solutions for flow at cylinder $Re=1, 2, 5$, and 10 (Keller and Takami, 1966; Takami and Keller, 1969; Dennis and Chang, 1970), we calculated that the minimal velocity along the limiting trajectory for direct interception (i.e., one particle radius from the cylinder) ranged from 0.25 to 8.0 cm s^{-1} for parameter values corresponding to our particle diameters, palp diameters, and upstream flow velocities. Although we could not measure the ciliary current in the presence of ambient flow, nor did we look for ciliary-reversal responses to particles nearing the palps (cf. Strathmann, 1987), we concluded that the ciliary current had a minor influence on the trajectories of particles approaching the palps because its maximal velocity was at most only 0.02 to 0.5 times the calculated particle velocities in flow.

Mucous adhesion appeared to be the primary mechanism of particle retention for both species when feeding in flow. Dauer (1984, 1985) alternatively suggested, based on observing the spionids *Sirethaspio benedicti* and *Parapionospio pinnata* in still water and examining excised palps, that particles were retained by being flicked onto the frontal groove of a palp by the latero-frontal cirri; mucus-bound particles were then transported in the frontal groove to the mouth. In contrast, we observed beads in flowing water to be contacted and retained either directly on the frontal groove or on the lateral surfaces of palps. Because beads caught on the sides of palps often remained there for several seconds or longer before being transferred to the frontal groove, we inferred that ciliary flicking was not required for initial particle retention. Rather, mucus was apparently responsible for their retention, as evidenced by the fact that, when retention failed, laterally encountered beads sometimes hung on briefly by a thread of mucus before fully breaking away.

Particle handling and rejection behavior were also similar in both species. Once a particle was captured, its subsequent loss during transport into the tube was extremely rare. Rejected particles were transported, singly or in small aggregates, out of the tube along the frontal groove of the palp; particles were then moved laterally out of the groove and were lost. We did not quantify particle rejection because it was sometimes difficult to distinguish between aggregates of rejected beads and small, loosely compacted fecal pellets, which were also released by a similar mechanism. Nonetheless, we inferred that differences between the captured and ingested proportions of beads of different sizes were the result of particle rejection.

4.2. *Pseudopolydora paucibranchiata*

When feeding in slowly flowing water ($U_{3mm}=1.3 \text{ cm s}^{-1}$), *P. paucibranchiata* showed no significant correlations between palp width and P_e (proportion of the sample composed of large beads) for either encounter, capture, or ingestion (Fig. 4a). P_e for encounter was always above the ambient P_e in suspension; thus, encounter was biased for large beads. The values of P_e for capture essentially overlap those for encounter, suggesting that there was no selective retention based on bead size. The net result is that capture was biased for large beads relative to their availability in suspension, and this

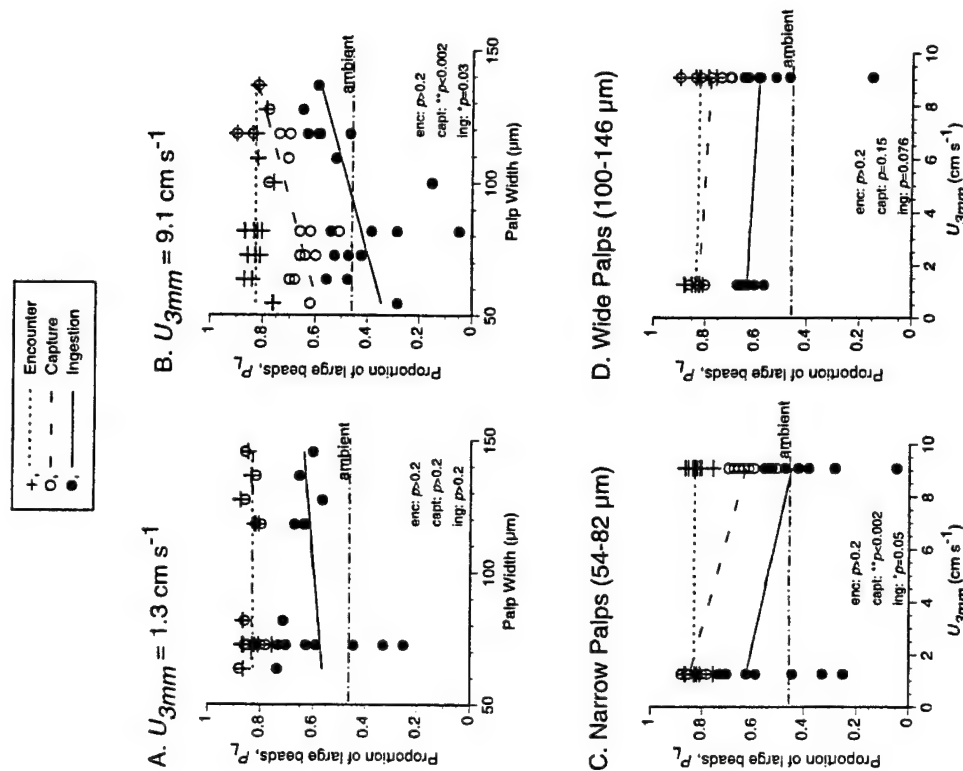


Fig. 4. Concurrent encounter, capture, and ingestion by *Pseudopolydora paucibranchiata*. Ordinates show the proportion of the sample composed of large beads (P_e). The dotted-dashed line indicates the proportion of the ambient suspension composed of large beads. Data aligned at a single palp width in A and B correspond to a single worm (although there is overlap where more than one worm of a single palp width was included). (A) lines through the data are nonparametric linear regressions meant only to aid the eye in seeing trends. Spearman rank correlation coefficients (r_s) are as follows ($n=15$; 2-tailed p values are shown on figure). Encounter $r_s=0.14$; capture $r_s=0.037$; ingestion $r_s=-0.068$. (B) lines are as in panel A; correlation coefficients are as follows ($n=18$). Encounter $r_s=-0.074$; capture $r_s=0.70$; ingestion $r_s=0.52$. (C) data for worms with narrow palps from panels A and B. Lines through the data connect medians between the two velocities. Two-tailed p values from Wilcoxon rank sums tests comparing medians are shown ($n=9, 10$). (D) data for worms with wide palps from panels A and B; lines are as in Panel C. Two-tailed p values from comparisons of medians are shown ($n=6, 8$).

bias was due to selection only at the step of encounter. Finally, the P_L values for ingestion were lower than those for capture, suggesting that large beads were preferentially rejected during post-capture handling. Nonetheless, the median P_L for ingestion was still higher than the ambient P_L ($p < 0.005$), meaning that the net result of capture and ingestion was a bias for large beads eaten relative to their availability in suspension (although there were three worms with narrow palps that ingested a lower P_L than ambient; Fig. 4a).

Although the encountered P_L values still did not correlate with palp width in more rapidly flowing water ($U_{3mm} = 9.1 \text{ cm s}^{-1}$), both the captured P_L and the ingested P_L values showed significant positive correlation with palp width (Fig. 4b); i.e., worms with wider palps captured and ingested relatively more large beads (and fewer small beads) than did worms with narrower palps. As at the lower velocity, the encountered P_L values were above the ambient P_L for the suspension, indicating that encounter was biased for large beads. Furthermore, for nearly every worm the P_L values for capture were below those for encounter, suggesting that the retention step was biased for small beads; this bias was stronger for worms with narrower palps. Although the apparent retention bias for small beads partially offset the encounter bias for large beads, all of the P_L values for capture were above the ambient P_L in the suspension, meaning that there was a net bias for capture of large beads relative to their availability. As at the lower velocity, the P_L values for ingestion were lower than those for capture, suggesting that large beads were preferentially rejected during post-capture handling. The direct relationship between palp width and the P_L for ingestion paralleled the corresponding relationship with the captured P_L (tested below; Fig. 6), suggesting that the dependence of ingested P_L on palp width is produced entirely by the palp-width-dependent bias during particle retention.

We divided the experimental worms into two size classes according to palp width ('narrow palp' = 54–82 μm , and 'wide palp' = 100–146 μm) to test for an influence of velocity in each size class. The narrow-palp worms showed no difference between the P_L values for encounter at the two velocities, but the P_L values for capture and ingestion each dropped at the higher velocity (Fig. 4c). Therefore, the narrow-palp worms captured and ingested relatively fewer large beads (and more small beads) as the velocity rose. The median P_L for ingestion by narrow-palp worms was higher than the ambient P_L at 1.3 cm s^{-1} ($p = 0.05$) but not at 9.1 cm s^{-1} ($p = 0.23$); therefore, the combined process of capture and ingestion had a net bias for large beads relative to their availability at the low velocity, but it was nonselective at the high velocity. In contrast, the P_L values of wide-palp worms for encounter, capture, and ingestion each showed no significant difference between the two velocities (Fig. 4d). The median P_L for ingestion in this size class was greater than the ambient P_L ($p = 0.007$), indicating that the combined process of capture and ingestion had a net bias for large beads relative to their availability.

Because there were no significant differences among the encountered P_L for different palp widths or at different velocities, we pooled the data for determining the functional dependence of encounter rate (E) on particle size (r_p). The exponent in the model, $E \propto r_p^n$, was calculated by using our data to solve the expression, $E_L/E_S = (C_L r_L / C_S r_S)^n$, where C = particle concentration and the subscripts 'L' and 'S' indicate the large and small beads, respectively. The mean value of the exponent was 2.00 (± 0.27 s.e., $n = 33$).

Retention efficiencies (R = proportion of encountered beads that were captured) for small and large beads (R_S and R_L , respectively) were measured directly by viewing individual encounter events. At the slow velocity ($U_{3mm} = 1.3 \text{ cm s}^{-1}$) neither R_S nor R_L correlated with palp width (Fig. 5a). Furthermore, at 1.3 cm s^{-1} there was no significant difference between R_S and R_L for either the narrow-palp or the wide-palp worms (Fig. 5c, d), i.e., there was no retention bias at the low velocity. In contrast, in faster flow (9.1 cm s^{-1}), R_L was significantly lower than R_S for both size classes of worms (Fig. 5c, d), meaning that a retention bias for small beads appeared at this velocity. Note, however, that the retention bias among the wide-palp worms was apparently not strong enough to have caused a significant difference in the captured proportion of large beads between the two velocities (Fig. 4d). Indeed, the retention bias was stronger among the narrow-palp worms, as evidenced most clearly by the fact that at 9.1 cm s^{-1} R_L was positively correlated with palp width while R_S was independent of palp width (Fig. 5b). Finally, both the narrow-palp and the wide-palp worms showed significant reductions in both R_S and R_L at the higher velocity compared to the lower velocity (Fig. 5c, d).

Particle selection during post-capture handling is illustrated by plotting the ratio of the ingested P_L to the captured P_L (Fig. 6), thus indicating the extent to which handling alters the captured proportion of large beads. A value of 1.0 indicates that rejection of captured beads before ingestion was nonselective; values below 1.0 indicate that large beads were preferentially rejected. All worms at both velocities preferentially lost large beads (Fig. 6), as is evident on Fig. 4 by the fact that all P_L values for ingestion were lower than those for capture. The nonsignificant correlation coefficients in Fig. 6 reveal that the degree of this handling bias did not relate to palp width. Neither the narrow-palp nor the wide-palp worms showed a significant difference in handling bias between the two velocities ($p > 0.1$ for each). The mean value of ingested/captured P_L for the pooled data was 0.68 (± 0.20 s.e., $n = 33$).

4.3. *Pseudopolydora kempji japonica*

Like *P. paucibranchiata*, *P. kempji japonica* feeding in slow flow ($U_{3mm} = 1.8 \text{ cm s}^{-1}$) showed no significant correlations between palp width and P_L for either encounter or capture (Fig. 7a). All P_L values were above the ambient P_L in suspension; thus, encounter and net capture were both biased for large beads relative to their availability. However, the values of P_L for capture generally were slightly below the corresponding values for encounter ($p < 0.005$), suggesting a slight retention bias for small beads. For both species feeding in slow flow, the large-particle bias in capture was due to encounter.

In faster flow (7.4 cm s^{-1}) *P. kempji japonica* again showed patterns very similar to those of *P. paucibranchiata* in faster flow. There was no correlation between palp width and the P_L values for encounter, and the encountered P_L was again above the ambient P_L for the suspension (Fig. 7b), indicating an encounter bias for large beads. In contrast, there were significant positive correlations between palp width and both the captured P_L and the ingested P_L . Worms with wider palps therefore captured and ingested relatively more large beads (and fewer small beads) than did worms with narrower palps. For most worms the P_L values for capture were below those for encounter, suggesting that

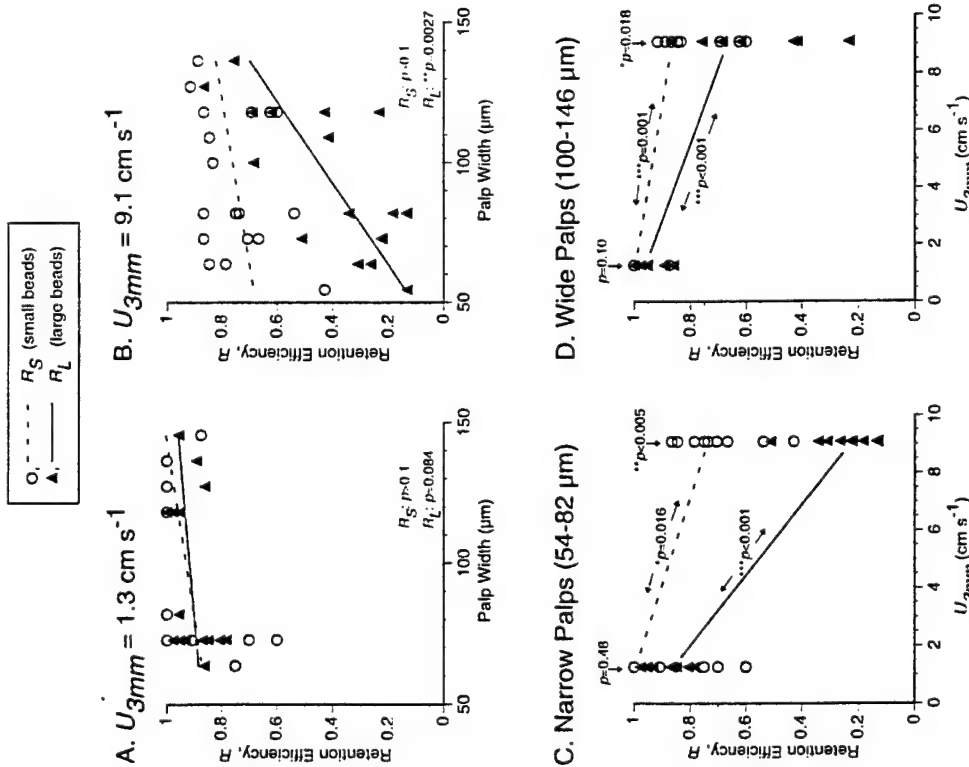


Fig. 5. Retention efficiencies of small and large beads (R_S and R_L) for *Pseudopolydora paucibranchiata*. R = number of captured beads divided by number of encountered beads. (A) Lines through the data are nonparametric linear regressions meant only to aid the eye in seeing trends. Spearman rank correlation coefficients (r_s) are as follows ($n = 15$; one-tailed p values are shown on figure): R_S $r_s = 0.35$; R_L $r_s = 0.38$. (B) Lines are as in panel A; correlation coefficients are as follows ($n = 18$): R_S $r_s = 0.31$; R_L $r_s = 0.65$. (C) Retention efficiencies for worms with narrow palps from panels A and B. Lines through the data connect medians between the two velocities. One-tailed p values from Wilcoxon rank sums tests comparing medians are shown on the lines connecting medians ($n = 9$, 10). One-tailed p values from Wilcoxon signed ranks tests comparing R_S vs. R_L at a single velocity are shown above the data at each velocity ($n = 9$, 10). (D) Retention efficiencies for worms with wide palps from panels A and B; lines are as in panel C. One-tailed p values from comparisons of medians are shown on the lines connecting medians ($n = 6$, 8). One-tailed p values from comparisons of R_S vs. R_L at a single velocity are shown above the data at each velocity ($n = 6$, 8).

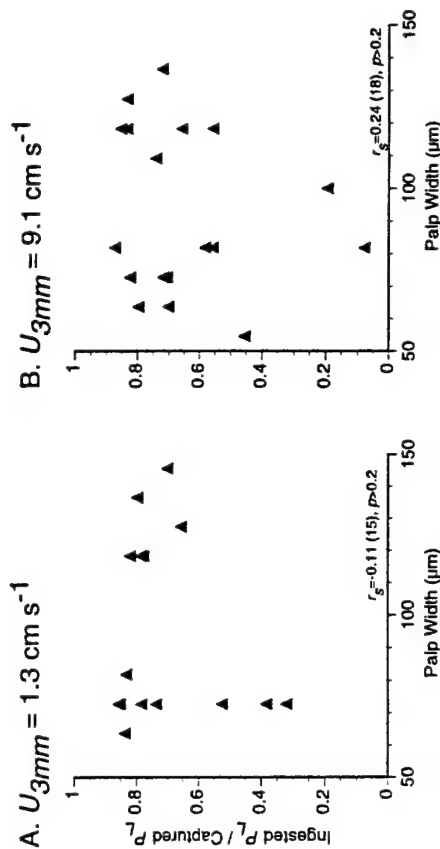


Fig. 6. Post-capture handling selection by *Pseudopolydora paucibranchiata*. Ordinates show the P_L for ingestion divided by the P_L for capture from data in Fig. 4. Values below 1.0 indicate preferential rejection of large beads. Spearman rank correlation coefficients (r_s) are shown with sample sizes and two-tailed p values.

retention was biased toward small beads; this bias was stronger for worms with narrower palps. Although the apparent retention bias toward small beads partially offset the encounter bias toward large beads, the P_L values for capture were above the ambient P_L of the suspension in all but one case (the worm with narrowest palps). Therefore, there was a net bias for capture of large beads relative to their availability. The P_L for ingestion was only measured after worms fed at 7.4 cm s^{-1} (Fig. 7b), and these values were consistently lower than the P_L for capture, suggesting that large beads were preferentially lost during post-capture handling as well. The capture and ingestion data are parallel (tested below; Fig. 9), indicating that the dependence of ingested P_L on palp width was produced entirely by the palp-width dependent bias during particle retention, as we observed for *P. paucibranchiata*.

We divided the experimental worms into two palp-width classes ('narrow palp' = 87–127 μm , and 'wide palp' = 136–200 μm) to test for an influence of velocity within each size class. In each palp-width class, there were two or three worms that were only videotaped in one of the two velocity treatments; these worms have been omitted from statistical tests that compare size classes between the two treatments, i.e. only the paired data were analyzed. The narrow-palp worms showed no difference between the P_L values for encounter at the two velocities, but the P_L values for capture dropped at the higher velocity (Fig. 7c). Therefore, as for *P. paucibranchiata*, the narrow-palp worms captured relatively fewer large beads (and more small beads) as the velocity rose. The median P_L for ingestion at 7.4 cm s^{-1} among narrow-palp *P. kempii japonica* was not different from the ambient P_L ($p = 0.40$), indicating that overall ingestion was nonselective relative to bead availability. In contrast, the wide-palp worms showed no difference between the two velocities in either the P_L values for encounter or the P_L

values for capture (Fig. 7d). As for *P. paucibranchiata*, the median P_L for ingestion among wide-palp *P. kempi japonica* in faster flow was significantly greater than the ambient P_L ($p < 0.005$), showing that the combined process of capture and ingestion had a net bias for large beads relative to their availability in suspension.

Because the same worms were used in experiments at each velocity, we separately determined in each treatment the functional dependence of encounter rate on particle size. Calculating the exponent in the model, $E \propto r^n$, as we did above for *P. paucibranchiata*, we obtained at 1.8 cm s^{-1} a mean value of $1.95 (\pm 0.34 \text{ s.e., } n = 15)$, and at 7.4 cm s^{-1} a mean of $1.90 (\pm 0.34 \text{ s.e., } n = 18)$. There was no significant difference between either of these estimated exponents and that from the *P. paucibranchiata* data ($p = 0.61$ using $U_{3mm} = 1.8 \text{ cm s}^{-1}$ and $p = 0.28$ using $U_{3mm} = 7.4 \text{ cm s}^{-1}$ in *t*-tests).

Retention efficiencies (R_s and R_L) for *P. kempi japonica* feeding in slow flow (1.8 cm s^{-1}) showed no statistically significant correlations with palp width (Fig. 8a), as was observed for *P. paucibranchiata*. However, unlike *P. paucibranchiata* in slow flow, both palp-width classes of *P. kempi japonica* individuals feeding at 1.8 cm s^{-1} had significantly lower retention efficiencies for large beads than for small beads (Fig. 8c, d), i.e., the worms showed a bias for retention of small beads at the lower velocity. The strength of this bias, expressed as R_L/R_s , showed no correlation with palp width ($p > 0.1$). Worms also showed a retention bias for small beads when feeding in faster flow (7.4 cm s^{-1}), with R_L significantly lower than R_s for both narrow-palp and wide-palp worms (Fig. 8c, d). R_s and R_L were each positively correlated with palp width at the higher velocity (Fig. 8b), but the relationship was clearly steeper for the large beads. The retention bias for small beads was therefore stronger for the narrow-palp worms; R_L/R_s was directly correlated with palp width (Spearman rank correlation coefficient $r_s = 0.63$, $p = 0.0036$). Finally, R_s and R_L both fell at the higher velocity for small-palp worms (Fig. 8c), but only R_L dropped for large-palp worms (Fig. 8d). Within both palp-width classes of worms, the retention bias for small beads strengthened at the higher velocity ($p < 0.005$ for small-palp worms and $p = 0.01$ for large-palp worms, testing R_L/R_s between the two velocities).

Particle selection during post-capture handling at 7.4 cm s^{-1} (Fig. 9) showed preferential rejection of large beads by all *P. kempi japonica* individuals tested, and, as for *P. paucibranchiata*, the strength of this handling bias did not relate to palp width. The mean value of ingested/captured P_L was $0.66 (\pm 0.18 \text{ s.e., } n = 18)$, which was not significantly different from that for *P. paucibranchiata* ($p = 0.20$).

5. Discussion

Particle-size selection occurred during each step in the suspension-feeding process of two species of spionid polychaetes. Large particles were selected during encounter; small particles were often selected during retention; and small particles were selected during handling. Particle retention was the only step in the feeding process that was affected by ambient flow speed or by the width of an animal's palps. Therefore, retention mechanics were ultimately responsible for the influences of flow speed and palp width on selective ingestion.

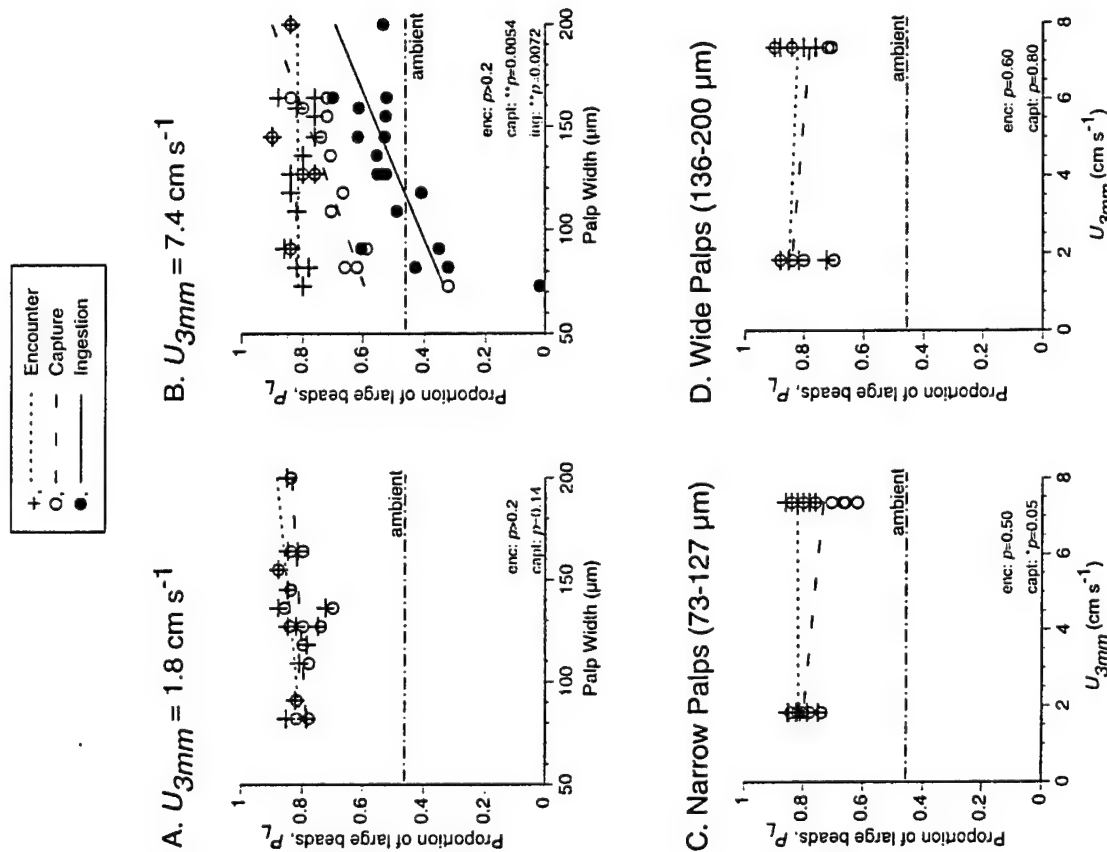


Fig. 7. Concurrent encounter, capture, and ingestion by *Pseudopolydora kempi japonica*. The format is as in Fig. 4. (A) correlation coefficients (r_s) are as follows ($n = 15$). Encounter $r_s = 0.31$; capture $r_s = 0.41$. (B) correlation coefficients are as follows ($n = 18$). Encounter $r_s = -0.0058$; capture $r_s = 0.65$; ingestion $r_s = 0.63$. (C) two-tailed p values from Wilcoxon signed ranks tests comparing medians are shown ($n = 8$). (D) two-tailed p values from comparisons of medians are shown ($n = 6$).

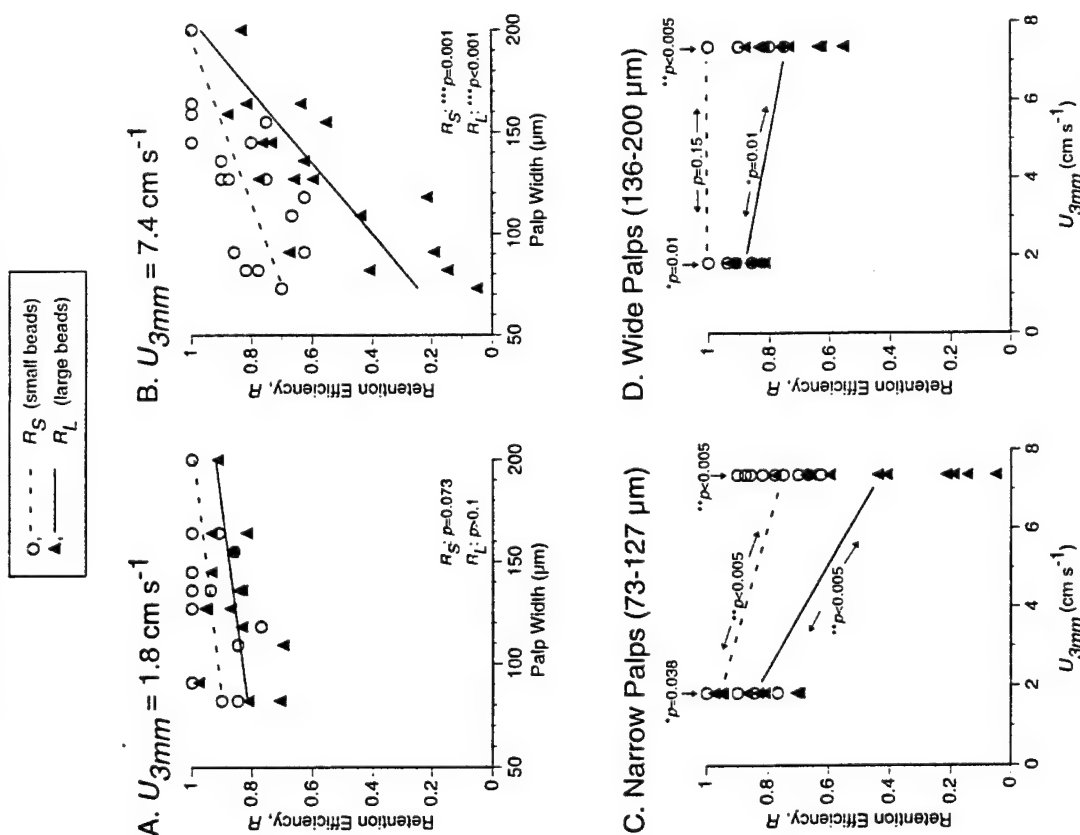


Fig. 8. Retention efficiencies of small and large beads (R_S and R_L) for *Pseudopolydora kempii japonica*. The format is as in Fig. 5. (A) correlation coefficients (r_s) are as follows ($n=15$), R_S $r_s=0.40$; R_L $r_s=0.28$. (B) correlation coefficients are as follows ($n=18$), R_S $r_s=0.69$; R_L $r_s=0.77$. (C) one-tailed p values from Wilcoxon signed ranks tests comparing medians are shown on the lines connecting medians ($n=8$). One-tailed p values from Wilcoxon signed ranks tests comparing R_S vs. R_L at a single velocity are shown above the data at each velocity ($n=8, 10$). (D) one-tailed p values from comparisons of medians are shown on the lines connecting medians ($n=6$). One-tailed p values from comparisons of R_S vs. R_L at a single velocity are shown above the data at each velocity ($n=7, 8$).

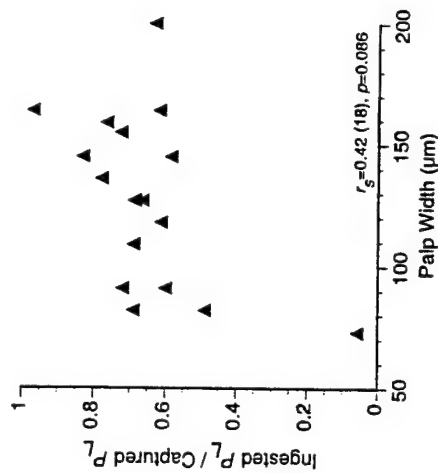


Fig. 9. Post-capture handling selection by *Pseudopolydora kempii japonica* at $U_{3mm}=7.4 \text{ cm s}^{-1}$. Ordinate shows the P_L for ingestion divided by the P_L for capture from data in Fig. 7B. The Spearman rank correlation coefficient (r_s) is shown with sample size and two-tailed p value.

5.1. Particle encounter

We found that the first step in the suspension-feeding process, particle encounter, showed a consistent bias for large particles. Such an encounter bias is predicted for the mechanism of direct interception by models of the physical processes by which particles contact filters (e.g., Rubenstein and Koehl, 1977; Shimeta and Jumars, 1991; Shimeta, 1993). However, these models of direct interception cannot be applied quantitatively to our experiments because our tentacle Reynolds numbers ($Re_t=0.7$ to 1.5) and ratios of particle-to-tentacle radius ($r_p/r_t=0.2$ to 1.5) were higher than those assumed by the models ($Re_t<0.1$, $r_p/r_t<0.1$). We therefore determined empirically that encounter was proportional to $r_p^{1.9-2.0}$. Thus, for the range of Re_t and r_p/r_t we used, which are typical of many tentaculate suspension feeders (Shimeta and Jumars, 1991), a small increase in particle size leads to a large increase in encounter rate.

The size-selectivity of encounter was not affected by flow speed or palp width for the range of tentacle Reynolds numbers and particle sizes used in our experiments. Therefore, all worms in a population experiencing a similar range of velocities in the field should encounter particles from suspension with the same bias.

5.2. Particle retention

An encountered particle is retained by a tentacle if the adhesive force holding it to the tentacle is greater than the sum of the drag and lift forces tending to remove it. As predicted, we found that increases in ambient flow speed caused decreases in particle retention efficiency by spionid palps. Our data corroborate suggestions by other authors

that retention efficiency is inversely related to velocity (e.g., Rubenstein and Koehl, 1977; Patterson, 1984; Okamura, 1984, 1985) and are similar to the results reported by McFadden (1986) for particle retention by a suspension-feeding soft coral. However, if lift and drag are very small relative to the adhesive force (e.g., if particles are much smaller than the tentacle, or if the ambient velocity is slow), then particle retention efficiency can be independent of flow speed. We found this to be the case only for the largest *P. kempii japonica* individuals when capturing the small particles. Similarly, Leonard et al. (1988) found retention to be independent of velocity for a suspension-feeding crinoid in slow flow ($0.9\text{--}6.4\text{ cm s}^{-1}$).

We also found that small particles were retained preferentially relative to large particles if the ambient flow was sufficiently fast, as predicted by considering the mechanics of retention. When the retention bias was present, the degree of selectivity was directly related to flow speed. Thus, flow speed in the habitat of such worms can determine whether and how strongly their particle retention is size-selective. Loudon (1990) also reported a retention efficiency bias towards small particles by caddisfly nets.

Also as predicted, we found that the bias toward retaining small particles was stronger for narrower palps than for wider palps. However, this effect was also mediated by flow speed, because it was only observed in the stronger flows. Thus, flow speed in the habitat can determine whether appendage sizes influence particle retention.

Selective retention can depend on particle characteristics other than size, e.g., shape, specific gravity, surface chemistry, and motility. A nonspherical particle (e.g., a pennate diatom encountered with its long axis parallel to that of the tentacle) can have a much larger contact area with the tentacle than does a sphere of equivalent volume. The surface texture of a particle can also influence how well it adheres to a tentacle (e.g., adhesion mechanisms discussed in Nachtigall, 1974; Kinloch, 1980). Indeed, deposit feeders (including spionids) that use mucus to adhere particles to their tentacles (as do many suspension feeders) show an apparent mechanical preference for rough particles over smooth ones (Self and Jumars, 1978). Although our retention model predicts that specific gravity is in most cases less important than particle size in determining selective retention (see Fig. 2), light particles might be less likely than heavy ones to be dropped by tentacles in very slow flow ($<1\text{ cm s}^{-1}$ local to the tentacle). Preference for particles of low specific gravity has been documented for tentaculate deposit feeders (Jumars et al., 1982; Self and Jumars, 1988). Natural particles also vary widely in surface chemistry, and hence in their stickiness (e.g., phytoplankton cells, Kiørboe and Hansen, 1993). Suspension-feeding ophiuroids have been found to preferentially capture beads with surface charges relative to uncharged beads (LaBarbera, 1978), while tentaculate deposit feeders have been shown to select mechanically for mineral grains with organic coatings relative to clean grains (Taghlon, 1982; Jumars, 1993). Motile particles (e.g., flagellated cells, zooplankton) differ by taxon and size in their ability to struggle against retention by suspension feeders. Struggling may enhance escape from some types of suspension feeders, whereas it may increase retention by others (e.g., prey struggling can induce nematocysts on cnidarian tentacles to fire).

Despite the variety of factors that can influence selective particle retention by tentaculate suspension feeders, the general effects due to ambient velocity and to particle and tentacle sizes should be similar to those we predicted and measured in this study.

Drag and lift forces increase with velocity, and the relative sizes of particle and tentacle can limit the contact area over which an adhesive bond can be formed (Fig. 3).

5.3. Particle handling

We found that spionids preferentially lost large particles, apparently by active rejection, after they were captured. The strength of handling selection was independent of both flow speed and palp width. We believe the rejection of large particles was due to behavioral preference rather than a passive mechanical obstruction to ingestion, because every worm had some large particles in its gut. Although post-capture rejection has been observed for spionids and other tentaculate suspension feeders (e.g., Pentreath, 1970; Winston, 1978; Dauer et al., 1981; Levin, 1981; Dauer, 1985; Holland et al., 1986), the rejection criteria have not been well documented. Passive, mechanical handling selection based on particle size has been observed (e.g., among sabellid polychaetes which use cilia to sort captured particles; Nicol, 1930; Bonar, 1972), but to our knowledge no tentaculate suspension feeder or tentaculate deposit feeder has previously been documented to reject particles actively by behavioral choice based only on particle size.

Because particle rejection during handling can depend on behavioral choice, simple physical models cannot predict selectivity during this step of feeding. Optimal foraging theory suggests that suspension feeders should preferentially ingest large particles because the caloric value of many suspended organic particles is directly related to their volume (Lehman, 1976; Shimeta, 1996). Our experimental particles had no food value, but the rejection of the large particles by suspension-feeding spionids is nonetheless surprising. The worms might have reacted to the plastic beads as though they were resuspended mineral grains, which generally have a nutritional value from surface films that scales to particle surface area rather than to volume. Optimal foraging theory for deposit feeders predicts preferential ingestion of small particles because of their relatively large ratio of surface area to volume (Taghlon et al., 1978).

5.4. Net influences of flow speed and palp size on selective ingestion

Size-selection among ingested particles was the net result of passive mechanical selection during encounter and retention, and behavioral selection during handling. Flow speed and palp width only influenced selection during the retention phase, however. Therefore, although selection occurred at each step of the feeding process, the influences of flow speed and palp size on overall feeding selectivity (i.e., ingestion) were due exclusively to the mechanics of particle retention.

The net result of encounter, retention, and handling produced the following patterns of selective ingestion. Worms with narrow palps ingested relatively fewer large particles (and more small particles) in fast flow than they did in slow flow. Furthermore, in fast flow worms with narrow palps ingested relatively fewer large particles than did worms with wider palps. In general, the spionids ingested a greater proportion of large particles than was available in suspension. However, ingestion was nonselective for worms with the smallest palps at the highest velocity (probably because under these conditions the encounter bias for large particles was offset by the retention and handling biases for

small particles). These effects of palp size and flow speed are similar to those measured during feeding experiments by Shimeta (1996).

The mechanics of particle retention may impose ontogenetic and environmental constraints on the feeding ecology of tentaculate suspension feeders like spionids. Because palp width and body size are directly correlated, juvenile spionids suspension feed on smaller particles when in strong flow compared to weak flow, and in strong flow juveniles suspension feed on smaller particles than do adults (Shimeta, 1996). When feeding on principally labile organic particles (e.g., algal cells, microzooplankters, detritus, and organic-rich aggregates), selectivity for smaller particles could result in a reduced caloric value of the diet on a per-particle basis. Variations in the flow environment could thereby have different effects for juveniles and adults as far as the caloric value of the food they can capture.

5.5. Comparisons with the mechanics of tentaculate deposit feeding

The mechanics of suspension feeding and deposit feeding with tentacles are similar in many ways, especially for animals like spionids that can feed in either mode. As in suspension feeding, contact between a deposit-feeding tentacle and particles on the substratum is biased toward large grains, while retention is biased toward small grains (Jumars et al., 1982). Taghon (1982) hypothesized that, in deposit feeding, drag forces in strong flow cause selective loss of large particles during post-capture transport to the mouth, which is a phenomenon analogous to the velocity effect on retention seen here in suspension feeding.

In contrast, the effect of tentacle width on selective encounter differs between suspension and deposit feeding. We measured no effect of palp width on the encounter bias toward large particles in suspension feeding, but the contact bias for large particles in deposit feeding is stronger on narrower tentacles than on wider tentacles (Hentschel, 1996). This difference can be understood by considering the encounter mechanics in each feeding mode. In suspension feeding by direct interception, encounter depends primarily on the size of a particle following a given streamline around the tentacle, while the tentacle width itself is relatively less important (Rubenstein and Koehl, 1977; Shimeta and Jumars, 1991; Shimeta, 1993). In contrast, tentacle width is more crucial in deposit feeding because contact depends directly on the surface area of the tentacle that is pressed onto the sediment. Models based on stereology predict a dependence of contact bias on tentacle width in deposit feeding (Whitlatch, 1989; Hentschel, 1996).

Retention mechanics in suspension feeding suggest by analogy the possible consequences of tentacle width for selective retention in deposit feeding. Narrower tentacles may preferentially retain smaller particles from deposits than do wider tentacles. This retention bias would counteract the contact bias toward large particles, which is stronger on narrow tentacles than on wide tentacles (Hentschel, 1996). The net result of these biases in contact and retention might explain why Hentschel (1996) found no net influence of palp width on selective ingestion by two spionid species deposit feeding in still water. However, Shimeta (1996) found that, when deposit feeding in strong flow, juvenile spionids ingested relatively fewer large particles than did adults. This influence

of palp size could have been due to an even greater retention bias on the small palps induced by the faster flow.

5.6. Generality of model

Our experimental results for spionid particle selectivity during the encounter and retention stages of feeding agree with the predictions of simple mechanical models of idealized particles and tentacles, in spite of the morphological complexities of spionid palps (e.g., non-circular cross-sectional shape, ciliation). This finding suggests that the variables included in these simple models, such as particle and tentacle size, and hydrodynamic forces on particles, are fundamental determinants of suspension-feeding performance. Therefore, the mechanics of particle selection we have modeled and tested in this study should apply to a wide range of tentaculate suspension feeders (e.g., various polychaetes, echinoderms, and cnidarians), and may include those with retention mechanisms other than mucous adhesion (e.g., nematocysts). Although we believe that the fundamental variables we have modeled set the baseline constraints on selectivity by tentaculate suspension feeders, we also stress that experiments should be done with other taxa and with various types of natural particles to assess the extent to which morphology, retention mechanism, and behavior might mediate the ultimate influence of these mechanical constraints on feeding ecology.

Acknowledgments

We thank D. Penry, R. Full, and D. Weston for use of laboratory space and equipment, and B. Hentschel for helpful discussions. The manuscript was improved with comments from P. Jumars and two anonymous reviewers. This work was supported by a Research Fellowship from the Miller Institute for Basic Research in Science (J.S.), a grant from the American Philosophical Society (J.S.), and ONR grant 00014-90-J-1357 (M.A.R.K.).

References

- Appelmanns, N., 1994. Sites of particle selection determined from observations of individual feeding larvae of the sand dollar *Dendraster excentricus*. *Limnol. Oceanogr.*, Vol. 39, pp. 404–411.
- Bonar, D.B., 1972. Feeding and tube construction in *Chone mollis* Bush (Polychaeta, Sabellidae). *J. Exp. Mar. Biol. Ecol.*, Vol. 9, pp. 1–18.
- Butman, C.A., 1986. Larval settlement of soft-sediment invertebrates: some predictions based on an analysis of near-bottom velocity profiles. In: *Marine interfaces ecophysiology*, edited by J.C.J. Nihoul, Elsevier Press, New York, pp. 487–513.
- Chapil, W.S., 1958. The use of evenly spaced hemispheres to evaluate aerodynamic forces on a soil surface. *IOS (Trans. Am. Geophys. Union)*, Vol. 39, pp. 397–404.
- Conklin, E.J. and R.N. Mariscal, 1976. Increase in nematocyst discharge in a sea anemone in response to mechanical stimulation. In: *Cnidellate ecology and behavior*, edited by G.O. Mackie, Plenum Press, New York, pp. 549–558.
- Conover, W.J., 1980. *Practical nonparametric statistics*. John Wiley, New York, second edition, 493 pp.

- Dauer, D.M., 1984. Functional morphology and feeding behavior of *Streblospio benedicti* (Polychaeta: Spionidae). In: *Proceedings of the first international polychaete conference*, Sydney, edited by P.A. Hutchings. The Linnean Society of New South Wales, pp. 418-429.
- Dauer, D.M., 1985. Functional morphology and feeding behavior of *Paraprionospio pinnata* (Polychaeta: Spionidae). *Mar. Biol.*, Vol. 85, pp. 143-151.
- Dauer, D.M., C.A. Maybury and R.M. Ewing, 1981. Feeding behavior and general ecology of several spionid polychaetes from the Chesapeake Bay. *J. Exp. Mar. Biol. Ecol.*, Vol. 54, pp. 21-38.
- Davies, C.N., 1973. *Air filtration*. Academic Press, London.
- Dennis, S.C.R. and G.-Z. Chang, 1970. Numerical solutions for steady flow past a circular cylinder at Reynolds numbers up to 100. *J. Fluid Mech.*, Vol. 42, pp. 471-489.
- Gibbs, R.J., 1985. Estuarine flows: their size, settling velocity, and density. *J. Geophys. Res.*, Vol. 90, pp. 3249-3251.
- Hentschel, B.T., 1996. Ontogenetic changes in particle-size selection by deposit-feeding spionid polychaetes: the influence of palp size on particle contact. *J. Exp. Mar. Biol. Ecol.*, in press.
- Holland, N.D., J.R. Strickler and A.B. Leonard, 1986. Particle interception, transport and rejection by the feather star *Oligometra serripinna* (Echinodermata: Crinoidea), studied by frame analysis of videotapes. *Mar. Biol.*, Vol. 93, pp. 111-126.
- Jackson, G.A., 1989. Simulation of bacterial attraction and adhesion to falling particles in an aquatic environment. *Limnol. Oceanogr.*, Vol. 34, pp. 514-530.
- Jørgensen, C.B., 1966. *Biology of suspension feeding*. Pergamon Press, Oxford, 357 pp.
- Jumars, P.A., 1993. Gourmands of mud: diet choice in deposit feeders. In: *Mechanisms of diet choice*, edited by R.N. Hughes. Blackwell Scientific, pp. 136-168.
- Jumars, P.A., R.F.L. Self and A.R.M. Nowell, 1982. Mechanics of particle selection by tentaculate deposit-feeders. *J. Exp. Mar. Biol. Ecol.*, Vol. 64, pp. 47-70.
- Keller, H.B. and H. Takami, 1966. Numerical studies of steady viscous flow about cylinders. In: *Numerical solutions of nonlinear differential equations*, edited by D. Greenspan, John Wiley and Sons, New York, pp. 115-140.
- Kiefer, D.A. and J. Berwald, 1992. A random encounter model for the microbial planktonic community. *Limnol. Oceanogr.*, Vol. 37, pp. 457-467.
- Kinloch, A., 1980. The science of adhesion. I. Surface and interfacial aspects. *J. Mat. Sci.*, Vol. 15, pp. 2141-2166.
- Kirby, T. and J.L.S. Hansen, 1993. Phytoplankton aggregate formation: observations of patterns and mechanisms of cell sticking and the significance of exopolymeric material. *J. Plankton Res.*, Vol. 15, pp. 993-1018.
- LaBarbera, M., 1978. Particle capture by a Pacific brittle star: experimental test of the aerosol suspension feeding model. *Science*, Vol. 201, pp. 1147-1149.
- Lahaye, M.C. and M. Jangoux, 1985. Functional morphology of the podia and ambulacral grooves of the comatulid crinoid *Aureolus bifida* (Echinodermata). *Mar. Biol.*, Vol. 86, pp. 307-318.
- Lehman, J.T., 1976. The filter-feeder as an optimal forager, and the predicted shapes of feeding curves. *Limnol. Oceanogr.*, Vol. 21, pp. 501-516.
- Leonard, A.B., J.R. Strickler and N.D. Holland, 1988. Effects of current speed on filtration during suspension feeding in *Oligometra serripinna* (Echinodermata: Crinoidea). *Mar. Biol.*, Vol. 97, pp. 111-125.
- Levin, L.A., 1981. Dispersion, feeding behavior and competition in two spionid polychaetes. *J. Mar. Res.*, Vol. 39, pp. 99-117.
- Lewis, J.B. and W.S. Price, 1975. Feeding mechanisms and feeding strategies of Atlantic reef corals. *J. Zool. London*, Vol. 176, pp. 527-544.
- Louden, C., 1990. Empirical test of filtration theory: particle capture by rectangular-mesh nets. *Limnol. Oceanogr.*, Vol. 35, pp. 143-148.
- Mariscal, R.N., 1974. *Nematocysts*. In: *Coelenterate biology*, edited by L. Muscatine and H.M. Lenhoff. Academic Press, New York, pp. 129-178.
- Mayer, S., 1994. Particle capture in the crown of the ciliary suspension feeding polychaete *Sabellia penicillus*: videotape recordings and interpretations. *Mar. Biol.*, Vol. 119, pp. 571-582.
- McFadden, C.S., 1986. Colony fission increases particle capture rates of a soft coral: advantages of being a small colony. *J. Exp. Mar. Biol. Ecol.*, Vol. 103, pp. 1-20.

- Nachtigall, W., 1974. *Biological mechanisms of attachment*. Springer-Verlag, Berlin.
- Nicol, E.A.T., 1930. The feeding mechanism, formation of the tube, and physiology of digestion in *Sabella pavonina*. *Trans. Roy. Soc. Edinburgh*, Vol. 56, pp. 537-598.
- Nowell, A.R.M. and P.A. Jumars, 1984. Flow environments of aquatic benthos. *Annu. Rev. Ecol. Syst.*, Vol. 15, pp. 303-328.
- Nowell, A.R.M. and P.A. Jumars, 1987. Flumes: theoretical and experimental considerations for simulation of benthic environments. *Oceanogr. Mar. Biol. Annu. Rev.*, Vol. 25, pp. 91-112.
- Okamura, B., 1984. The effects of ambient flow velocity, colony size, and upstream colonies on the feeding success of bryozoa. I. *Bugula stolonifera* Ryland, an arborescent species. *J. Exp. Mar. Biol. Ecol.*, Vol. 83, pp. 179-193.
- Okamura, B., 1985. The effects of ambient flow velocity, colony size, and upstream colonies on the feeding success of bryozoa. II. *Conopeum reticulatum* (Linnaeus), an encrusting species. *J. Exp. Mar. Biol. Ecol.*, Vol. 89, pp. 69-80.
- Patterson, M.R., 1984. Patterns of whole colony prey capture in the octocoral, *Alcyonium siderium*. *Biol. Bull.*, Vol. 167, pp. 613-629.
- Pentacoth, R.J., 1970. Feeding mechanisms and the functional morphology of podia and spines in some New Zealand ophiuroids (Echinodermata). *J. Zool. London*, Vol. 161, pp. 395-429.
- Rubenstein, D.I. and M.A.R. Koehl, 1977. The mechanisms of filter feeding: some theoretical considerations. *Am. Nat.*, Vol. 111, pp. 981-994.
- Sebens, K.P. and M.A.R. Koehl, 1984. Predation on zooplankton by the benthic anthozoans *Alcyonium siderium* (Alcyonacea) and *Metridium senile* (Actinaria) in the New England subtidal. *Mar. Biol.*, Vol. 81, pp. 255-271.
- Self, R.F.L. and P.A. Jumars, 1978. New resource axes for deposit feeders? *J. Mar. Res.*, Vol. 36, pp. 627-641.
- Self, R.F.L. and P.A. Jumars, 1988. Cross-phyletic patterns of particle selection by deposit feeders. *J. Mar. Res.*, Vol. 46, pp. 119-143.
- Shimeta, J., 1993. Diffusional encounter of submicrometer particles and small cells by suspension feeders. *Limnol. Oceanogr.*, Vol. 38, pp. 456-465.
- Shimeta, J., 1996. Particle-size selection by *Pseudopolydora paucibranchiata* (Polychaeta: Spionidae) in suspension feeding and in deposit feeding: influences of ontogeny and flow speed. *Mar. Biol.*, Vol. 126, pp. 479-488.
- Shimeta, J. and P.A. Jumars, 1991. Physical mechanisms and rates of particle capture by suspension-feeders. *Oceanogr. Mar. Biol. Annu. Rev.*, Vol. 29, pp. 191-257.
- Strathmann, R.R., 1987. Larval feeding. In: *Reproduction of marine invertebrates*, Vol. IX, edited by A.C. Giese. Boxwood Press, Pacific Grove, pp. 465-550.
- Taghon, G.L., 1982. Optimal foraging by deposit-feeding invertebrates: roles of particle size and organic coating. *Oecologia*, Vol. 52, pp. 295-304.
- Taghon, G.L., A.R.M. Nowell and P.A. Jumars, 1980. Induction of suspension feeding in spionid polychaetes by high particulate fluxes. *Science*, Vol. 210, pp. 562-564.
- Taghon, G.L., R.F.L. Self and P.A. Jumars, 1978. Predicting particle selection by deposit feeders: a model and its implications. *Limnol. Oceanogr.*, Vol. 23, pp. 752-759.
- Takami, H. and H.B. Keller, 1969. Steady two-dimensional viscous flow of an incompressible fluid past a circular cylinder. *Phys. Fluids*, Suppl. II, pp. II-51-II-56.
- Tate, M.W. and R.C. Clelland, 1957. *Nonparametric and shortcut statistics*. Interstate Printers and Publishers, Danville.
- Vogel, S., 1994. *Life in moving fluids: the physical biology of flow*. Princeton University Press, Princeton, second edition, 467 pp.
- Whitlatch, R.B., 1989. On some mechanistic approaches to the study of deposit feeding in polychaetes. In: *Ecology of marine deposit feeders*, edited by G. Lopez, G. Taghon and J. Levinton, Springer-Verlag, New York, pp. 291-308.
- Winston, J.E., 1978. Polypite morphology and feeding behavior in marine ectopros. *Bull. Mar. Sci.*, Vol. 28, pp. 1-31.

ONTOGENETIC SIZE AND SHAPE CHANGES
AFFECT THE MECHANICS OF JETTING IN THE
SCYPHOZOAN JELLYFISH *AURELIA AURITA*.

J.E. Jed, University of California, Berkeley.

jason2@garnet.berkeley.edu

Aquatic animals in a variety of phyla swim by jet propulsion. The ratio of inertial to viscous forces in the fluid environment (the Reynolds number (Re)) is an important factor for jetting animals. Animals with small body size will be hindered by viscous forces, but viscosity will not constrain jetting in animals with large body size. Cnidarian medusae are a good system for studying the effects of size on jetting since many species undergo substantial size and shape changes during ontogeny. For example, the scyphozoan jellyfish *Aurelia aurita* grows from a dorso-ventrally flattened, lobed ephyra less than a millimeter in bell diameter, into a bowl-shaped medusa with a bell diameter of many centimeters. Four size classes of free-swimming *A. aurita* were video-taped in the laboratory, and jetting kinematics examined by computer-based motion analysis. Ephyrae traveled up to 5 body lengths per second (bl/s) during the power stroke, with a Re of 1. Forward motion stopped abruptly at the end of each power stroke, and the ephyrae moved approximately 1 body length backward during the recovery stroke. Animals in larger size categories (mean bell diameters of 12, 24, and 76 mm) traveled 2, 1 and 0.4 bl/s, with Re 's of 200, 300 and 1200. In all larger size classes the animals continued to move forward during the recovery stroke due to inertial forces. Thrust production in medusae depends on the volume of the subumbrellar cavity, the area of the excurrent aperture, and the contraction rate of the bell.

(1996) Am. Zool. 35 : 7A

ONTOGENETIC CHANGES IN SIZE AND SHAPE AFFECT SWIMMING
PERFORMANCE IN THE SCYPHOZOAN MEDUSA *AURELIA AURITA*

Jason Eric Jed
University of California, Berkeley
Department of Integrative Biology
Berkeley, CA 94720-3140

Submitted to *Marine Biology*

Abstract

Ontogenetic Changes in Size and Shape Affect Swimming Performance in the Scyphozoan Medusa *Aurelia aurita*

by

Jason Eric Jed

Master of Arts in Integrative Biology

University of California, Berkeley

Professor Mimi A.R. Koehl, Chair

The free-swimming stage of the scyphozoan jellyfish *Aurelia aurita* increases 400-fold in bell diameter during ontogeny. Ephyrae (i.e. immature medusae) and three medusan size classes were studied using computer-based motion analysis. Morphological and kinematic measurements were used in a theoretical model of jet-propelled locomotion to predict hydrodynamic forces. In all cases, hydrodynamic forces (i.e. thrust, drag, acceleration reaction) and Froude propulsion efficiency (the ratio of thrust produced during bell contraction to resulting swimming velocity) increased with body size. Although pulsation rate decreased with increasing body size, swimming speed remained relatively constant for all size classes except ephyrae. All three medusan size classes were kinematically similar, but ephyrae had a higher swimming velocity in relation to their pulsation rate. Reynolds number (ratio of inertial to viscous forces) increased as a function of bell diameter. As *A. aurita* medusae grew larger, their bell shape became more oblate. Swimming performance, defined as the distance traveled per amount of mechanical energy expended, increased as a function of body size.

Introduction

Jet propulsion is a common mode of locomotion among aquatic animals. Cephalopod mollusks and cnidarian medusae are two groups well known for their ability to jet, but other mollusks (e.g. scallops; Dadswell and Weihs 1990), as well as some arthropods (e.g. dragonfly nymph; Mill and Pickard 1975) and urochordates (e.g. salps; Madin 1990), also use jet propulsion to locomote. It is interesting that while the jetting systems in each of these phyla have arisen independently, the mechanism for propulsion is very similar. Usually, part of the animal's body forms a chamber, the cavity of which is continuous with the external environment. Water within the chamber is forcefully ejected when muscles surrounding the chamber are contracted (contraction phase), propelling the animal in the opposite direction (Figure 1). Expansion and refilling of the chamber (expansion phase) often occurs passively due to the elastic recoil of the body wall, as in jellyfish (DeMont and Gosline 1988c), or by a combination of elastic recoil and active muscle contraction, as in squid (Gosline and Shadwick 1983). Although jetting is commonly associated with locomotion, it may serve additional functions in some groups. For example, jet pulses in jellyfish have been shown to improve feeding performance by moving water past the food capturing tentacles (Costello and Collin, 1994, 1995), and the increased flow of seawater through the mantle enhances respiration in cephalopods (Wells and Wells 1982).

Daniel (1983) developed a theoretical model of jet propulsion in jellyfish which can be used to estimate hydrodynamic forces acting on swimming medusae based on body

size and shape. This model predicts that net thrust will vary with bell diameter, suggesting that jet-propelled locomotion should be sensitive to body size. Increasing body size during ontogeny is a characteristic shared by most animals. When an animal grows larger and/or changes shape over the course of its life, the way that it physically interacts with its environment may change (e.g. Schmidt-Nielsen 1984; Vogel 1994). Growth, therefore, has the potential to alter swimming performance (distance traveled per amount of energy expended) and escape performance (distance traveled per time or per pulse) in an animal that locomotes by jet propulsion. If feeding is linked to jetting, as it is for some cnidarian medusae, an increase in body size may also affect feeding performance (amount of prey captured per time, per pulse, or per amount of energy expended). Ontogenetic changes in physiology and behavior, and changes in the mechanical properties of the jet system itself, might also affect swimming, feeding and escape performance. In this thesis, I focus on the effect that body size and shape have on swimming performance in one species of jellyfish, the medusoid phase of the scyphozoan *Aurelia aurita* (the common moon jellyfish).

Cnidarian Medusae

Cnidarian medusae are a useful system for studying the effects of growth on jet propulsion. Many jellyfish species undergo substantial size and shape changes during ontogeny, while their relatively simple morphologies and behaviors facilitate a quantitative analysis of their locomotory performance. Most studies of jellyfish locomotion (Daniel 1983, 1985; DeMont and Gosline 1988a,b,c; Gladfelter 1972, 1973) have dealt primarily with adult animals, and have not focused on ontogenetic changes in

size and shape. Although some studies of medusan feeding have taken body size into account (Costello and Colin 1994, 1995; Mills 1981), these studies have not looked at the trade-offs between feeding and swimming performance.

The body of a scyphozoan medusa is called the bell or umbrella because of its shape, with the volume enclosed by the bell referred to as the subumbrellar cavity (Figure 2a). The margin of the bell is usually lobed or scalloped. The bulk of the animal is composed of a thick, gelatinous mesoglea that contains elastic fibers (Chapman 1953). In the scyphomedusae, locomotion is brought about by a band of powerful ectodermal muscle fibers encircling the subumbrellar cavity. Their contractions produce rhythmic pulsations of the bell, with each pulse driving water out of the subumbrellar cavity. The elastic recoil of the compressed mesoglea provides the antagonistic force to restore the bell shape between contractions (Alexander 1964). While most scyphomedusae are active swimmers, their distribution is dictated by large-scale ocean currents. By swimming up or down, these animals may move into and out of currents which exist at different levels within the water column (Kopacz 1994). In addition, the ability to migrate vertically plays an important role in feeding, as their prey may also change position within the water column (Mills 1981).

Aurelia aurita has a complex life cycle consisting of a sessile asexual polyp stage, and a free-swimming sexual medusoid stage. As is the case for most scyphozoans, the young medusa, called an ephyra, is morphologically different from the adult (Figure 3). Unlike adult medusae which possess a bowl-shaped morphology, *A. aurita* ephyrae are dorso-ventrally flattened and have a deeply incised bell margin. When initially released

from the polypoid colony an *A. aurita* ephyra has a bell diameter of approximately 1 mm, whereas the bell diameter of a fully-grown medusa can reach 40 cm (Meinkoth 1995). The 400-fold increase in body size these animals undergo during their ontogeny will most likely affect the hydrodynamic forces they encounter.

Hydrodynamics of Jet Propulsion

Reynolds number (Re) is a dimensionless index that represents the relative importance of inertial forces to viscous forces in determining fluid motion (Vogel 1994),

$$Re = UL/\nu \quad (1)$$

where, in the case of a swimming jellyfish, U is the velocity of the medusa relative to the surrounding water, L is the bell diameter, and ν is the kinematic viscosity of seawater. A large or rapidly-moving jellyfish experiences an environment dominated by inertial forces (high Re), while a small or slowly-moving medusa may well experience a fluid environment dominated by viscous forces (low Re). The Reynolds number of the medusa should affect the way it moves. At the end of the contraction phase of the jet cycle a large medusa may continue to glide forward, while the motion of a small medusa (with less inertia) may be rapidly damped by the viscosity of the seawater surrounding it.

When a jellyfish moves through water it experiences a hydrodynamic force called drag that retards its motion. In a high Re environment, drag depends on the square of the velocity of the animal relative to the water and the projected area of the animal in the direction of motion (A_p). This type of drag is referred to as pressure drag (D_p) (Vogel 1994), and is given by

$$D_p = \frac{1}{2} C_d \rho A_p U^2 . \quad (2)$$

C_d is the drag coefficient, a dimensionless parameter which depends on the animal's shape, and ρ is the density of seawater. Although the exact value of the drag coefficient must be determined empirically, its value can be estimated for a hemisphere (approximating the shape of a medusa) as a function of Reynolds number (Daniel 1983):

$$C_d = 24/Re^{0.7} . \quad (3)$$

The force that propels a jellyfish forward is thrust (T). The magnitude of thrust produced by a medusa depends on the square of the rate of volume change of the subumbrellar cavity (dV/dt) squared, divided by and the area of the subumbrellar aperture (A_a) (Daniel 1983):

$$T = (\rho/A_a)(dV/dt)^2 . \quad (4)$$

Thrust acts in a direction opposite to the direction of the ejected fluid, so during the contraction phase of the jet cycle, when fluid is expelled from the oral surface, thrust acts in an aboral direction (towards the apex of the bell). During the expansion phase thrust has a smaller negative value, retarding the forward (i.e. aboral) motion of the animal, as water is drawn back into the subumbrellar cavity through the subumbrellar aperture.

When a medusa jets, its body continuously accelerates and decelerates. Acceleration reaction (G) and inertial resistance (I) are forces which resist changes in velocity of an object moving through a fluid (Denny 1993). These forces act rearward during the contraction phase of the jet cycle (retarding forward motion) and forward during the

expansion phase (tending to keep the animal moving forward). Acceleration reaction is given by

$$G = C_a \rho V (dU/dt) \quad (5)$$

and inertial resistance is given by

$$I = m (dU/dt) . \quad (6)$$

The magnitude of acceleration reaction depends on the volume of fluid displaced by the animal's body. Inertial resistance depends on the total mass of the medusa (m) which includes the mass of the animal's body and the mass of seawater contained within the subumbrellar cavity. Total mass fluctuates throughout the jet cycle as seawater is drawn in and expelled. The coefficient of added mass (C_a) is affected by the shape of the animal's body. Coefficient of added mass can be estimated for a hemisphere (approximating the shape of a medusa) based on its height (h) and radius (r) (Daniel 1983):

$$C_a = (h/r)^{1.4} . \quad (7)$$

During the contraction phase of the jet cycle the animal's body accelerates forward. Thrust acts in a forward direction, while drag, acceleration reaction and inertial resistance act backwards. During the expansion phase, water is drawn back into the bell. When operating at high Reynolds number, the medusa's body continues to move forward, but now thrust acts opposite to the direction of motion thereby slowing the animal. Drag continues to act backwards, since the animal is moving forward, but because its velocity

is decreasing both acceleration reaction and inertial resistance now act in a forward direction. These hydrodynamic forces continuously fluctuate throughout the jet cycle. The net hydrodynamic force (F_{total}) acting on a jetting medusa at any instant is the vector sum of the component hydrodynamic forces:

$$F_{total} = \frac{1}{2}C_d\rho A_p U^2 + (\rho/A_a)(dV/dt)^2 + C_a\rho V(dU/dt) + m(dU/dt) . \quad (8)$$

Size and Scaling of Jet Propulsion

Using Daniel's (1983) model, predictions can be made about how the component hydrodynamic forces should scale as a medusa grows larger (Figure 4). Thrust is proportional to bell diameter raised to the fourth power (subumbrellar volume squared divided by aperture area). Thrust should therefore increase at a greater rate as a medusa grows than either acceleration reaction or inertial resistance, both of which increase as a function of bell diameter cubed. Drag, which is proportional to the projected area of the bell, should increase at the lowest rate as bell diameter increases.

These predictions make a number of assumptions. They assume that the medusa remains geometrically similar as its size increases (isometric growth), and that velocity, acceleration, and the values of C_d and C_a all remain the same as the animal grows larger. They also assume that larger medusae are kinematically similar to smaller medusae. To be kinematically similar, the relationship between swimming velocity and pulsation rate must remain constant as a function of body size. Schmidt-Nelson (1984) uses this type of analysis to compare the swimming speeds of one species of fish. Large fish swim faster than small fish, but in that case the ratio of swimming velocity per body length versus tail

beat frequency remains constant. Medusae of different sizes can be compared in the same way. If the ratio of swimming velocity to the product of bell diameter times pulsation frequency (f) is the same for all sizes of medusae, then these animals remain kinematically similar as they grow:

$$(U/(Lf))_{\text{small}} = (U/(Lf))_{\text{large}} . \quad (9)$$

Body shape has a large influence on the hydrodynamic forces experienced by a medusa. The shape of a medusa's bell determines the value of S , C_d , and C_a , thereby directly affecting the magnitude of drag and acceleration reaction. The bell of an *A. aurita* medusa is radially symmetrical, and so a simple way to describe its shape is to calculate the ratio of bell height (h) to bell diameter (L), called the fineness ratio (Fi) (Vogel 1994):

$$Fi = h/L . \quad (10)$$

A high Fi means that the body of the medusa is prolate (cigar-shaped), while a low Fi means the body is oblate (bowl-shaped). Prolate objects with fineness ratios above 1 have low added mass coefficients, whereas oblate objects with fineness ratios below 1 have high coefficients.

Efficiency of Jet Propulsion

O'Dor and Webber (1986) found that the metabolic cost of jet-propelled locomotion in squid increases with body size. Vogel (1994) provides a set of formulae to calculate the efficiency of a jet-propelled system. Power output (P_{out}) of a jetting medusa can be

calculated by multiplying thrust by the difference between the jet velocity (U_2) and the velocity of the animal (U_1):

$$P_{out} = T(U_2 - U_1) . \quad (11)$$

Power input (P_{in}) is the kinetic energy of the medusa per unit time:

$$P_{in} = (m/2t)(U_2^2 - U_1^2) . \quad (12)$$

Dividing output by input yields the Froude propulsion efficiency (η_f):

$$\eta_f = 2U_1/(U_2 + U_1) . \quad (13)$$

In the case of a jet-propelled medusa, Froude propulsion efficiency represents the ratio of thrust produced during bell contraction to the resulting swimming velocity obtained. The ideal situation where the velocity of the animal is the same as the jet velocity yields the highest possible efficiency (infinitely high efficiency in the case of this model). In reality, forces such as drag and acceleration reaction reduce locomotor efficiency by decreasing body velocity relative to jet velocity.

How do the hydrodynamic forces experienced by an *Aurelia aurita* medusa change as it grows from an ephyra only 1 mm wide to an adult animal with a 40 cm bell diameter? To answer this question, I measure morphological and kinematic parameters for *A. aurita* in four size classes, and use these data in Daniel's theoretical model to calculate how swimming performance changes with growth. I also examine how body shape and swimming kinematics change as these animals grow larger. Finally, based on kinematic

data, I calculate the Froude propulsion efficiency for *A. aurita* medusae of different body size.

Materials and Methods

Animals

The *Aurelia aurita* medusae used in this study were raised in culture at the Monterey Bay Aquarium, in Pacific Grove, CA. Animals were grouped by size: ephyrae had a mean bell diameter (mbd) of 0.20 cm (standard deviation (SD) = 0.05, n = 3); "small" medusae had a mbd of 1.57 cm (SD = 0.20, n = 5); "medium" medusae had a mbd of 3.82 cm (SD = 0.22, n = 6); and "large" medusae had a mbd of 9.51 cm (SD = 1.79, n = 6). Bell diameters were determined by digitizing still video images of medusae at the point of maximum expansion (just prior to the onset of the contraction phase), with a measurement precision of 0.1 mm. Due to the availability of experimental animals, the largest medusa used in this study was approximately 25% the size of a full grown *A. aurita* medusa.

Video Recording

The swimming kinematics of animals in the three size classes of medusae were videotaped in plexiglas aquaria. Small and medium-sized animals were taped in a tank measuring 15×17×15 cm (h×w×d), while animals in the large size class were filmed in a tank measuring 61×65×28 cm. Both tanks were filled with filtered natural seawater at a temperature of 16° C. The video camera (Panasonic PV-S62D SVHS-C Camcorder) lens

was set parallel to the long side of each aquaria. Brine shrimp nauplii (*Artemia sp.*) were added to the water as flow marker particles. The swimming speeds of the brine shrimp were sufficiently slow (1.8 mm/s) relative to the swimming speeds of the medusae so as to be essentially motionless over the time-course of an individual trial. Prior to the start of a filming trial, a size scale was placed momentarily in the center of the tank. A single medusa was then placed carefully by hand in the center of the aquarium and allowed to swim normally. A videotaped trial ended when the animal moved out of the field of view of the camera. At the end of each trial the medusa was moved to a small holding tank while the aquarium was prepared for the next trial. Each medusa was filmed for 10 consecutive trials.

Ephyrae were placed individually in a 100 cc cell-culture well (1.5 cm diameter), and their swimming kinematics recorded using a video-equipped dissecting microscope (Wild dissecting microscope; Sony SSC-C374 video camera; Sanyo GVR-S955 SVHS VCR). The well was filled with filtered natural seawater at a temperature of 17° C. Brine shrimp nauplii were again used as flow marker particles. The swimming speed of the brine shrimp nauplii was less than 10% of the swimming speed of the ephyrae, and so remained essentially motionless over the time-course of an individual trial. Ephyrae were transferred into the cell-culture well using a pipette with a tip 3 mm wide. To reduce handling time, each ephyra was placed in the well once and allowed to swim freely for ten minutes. Separate "trials" were recorded as the animal moved into and out of the field of view of the video camera. After 10 minutes the animal was removed, the

seawater and brine shrimp nauplii replaced, and a new ephyra introduced into the filming chamber.

Motion Analysis

The SVHS-C recordings (60 fields/s) were transferred to standard SVHS cassettes before being analyzed. Motion analysis was performed using a Peak Performance Motus motion measurement system (Peak Performance Technologies, Inc.). This system was used to track changes in bell shape during the jet cycle, and to calculate swimming velocity and acceleration.

Within a given trial, individual jet cycles were chosen for analysis based on the following criteria: (1) at least one full jet cycle was completed within the field of view of the camera, (2) the animal was positioned relative to the camera so that a lateral view of its body was visible at all times during the jet cycle, and (3) the motion of the animal was not influenced by the ambient motion of the surrounding water (determined by the movement of flow marker particles). These same criteria were used for both ephyrae and medusae. Some trials contained a number of suitable jet cycle sequences which met these criteria, while other trials had few if any jet cycles that qualified for analysis.

For each jet cycle, ten fields were digitized during the contraction phase, and ten during the expansion phase, with an equal number of video fields skipped between successive digitized field. Six points were digitized on each captured video field: the outer and inner apex of the bell, the right and left edges of the bell margin at the opening of the subumbrellar aperture, and the right and left limits of the widest part of the bell

(Figure 2b). The bell of *Aurelia aurita* medusae is translucent, allowing the inner apex of the bell within the subumbrellar cavity to be clearly discerned. In most cases, when the bell was fully expanded the edges of the bell margin corresponded to the widest part of the bell. The motion analysis software automatically interpolated the positions of the six digitized points for all intervening video fields that were not digitized. Changes in the position of these six points relative to one another over the course of the jet cycle were used to quantify changes in bell morphology. Because *A. aurita* medusae are radially symmetric, it was possible to calculate the necessary parameters for Daniel's model based on the digitization of 2-dimensional images.

Calculations

Thrust, drag, acceleration reaction, and inertial resistance vary continuously throughout the jet cycle. The magnitudes of these forces were calculated for each time interval (i.e. 60 times per second). These calculations were performed for animals in the three medusoid size classes only. Ephyrae were omitted from these calculations for two reasons: (1) Because of their morphology, it was difficult to calculate such important morphological parameters as subumbrellar volume and projected area; (2) Daniel's model was developed for medusoid-shaped jellyfish, and it is not clear whether it can accurately describe the hydrodynamic forces experienced by ephyrae.

The motion analysis software generated horizontal and vertical velocity components for each of the six digitized points, as well as the resultant velocity vector. The algorithm used by the software relied on position data from seven video fields, the field in question

as well as three previous and three subsequent video fields. The resultant velocity vector of the bell apex was used as a measurement of swimming velocity.

Reynolds Number

Reynolds number was calculated using the distance between the right and left limits of the widest part of the bell as the length value, and the resultant velocity of the bell apex (Figure 2b). Both velocity and bell diameter change continuously throughout the jet cycle, and so an instantaneous Re was calculated for each time interval. In this calculation, and all subsequent calculations, the fluid density and kinematic viscosity values were estimated to be equal to that of seawater at 16° C ($\rho = 1.025 \times 10^3 \text{ kg/m}^3$; $\nu = 1.205 \times 10^{-6} \text{ m}^2/\text{s}$) (Kennish 1994).

Thrust

The two values necessary for calculating thrust are the area of the subumbrellar aperture and the rate of volume change of the subumbrellar cavity. Aperture area was calculated as the area of a circle with a diameter equal to the distance between the edges of the bell margin (Figure 2b). Once the subumbrellar cavity volume was calculated for each video field (as described below), the rate of volume change was determined by taking the volume difference between subsequent fields and dividing by the video field rate.

Pressure Drag

Pressure drag was calculated based on the swimming velocity and the projected area in the direction of motion. Swimming velocity was taken to be the resultant velocity of the bell apex. The projected area in the direction of motion was calculated to be the area of a circle with a diameter equal to the distance between the right and left limits of the widest part of the bell (Figure 2b). Drag coefficient was estimated as a function of Reynolds number (Equation 3) (Daniel 1983).

Acceleration Reaction

In addition to velocity vectors, the motion analysis software generated horizontal, vertical and resultant acceleration vectors for each digitized point. These values were derived using an algorithm which took into account position data from seven consecutive video fields.

The volume of the subumbrellar cavity was assumed to be the volume of a hemi-ellipsoid (V_{he}), its radius (r) being half the distance between the edges of the bell margin, and its height (h) being the distance from the plane of the aperture to the inner apex of the bell (Figure 2b):

$$V_{he} = 2/3 \pi h r^2 . \quad (14)$$

The volume of the animal's body was calculated in two steps. First, the volume of a hemi-ellipsoid was calculated based on a width measured from points half way between the edges of the bell margin and the widest parts of the bell, and a height measured from

the aperture plane to the outer apex of the bell (Figure 2b). The volume of the body alone was then assumed to be approximately equal to this volume minus the previously calculated volume for the subumbrellar cavity. Body volume was calculated once for each animal, based on an average of measurements taken while the bell was at its point of maximum expansion (just prior to the onset of the contraction phase).

The resultant acceleration vector of the bell apex, along with the bell volume, were used to calculate acceleration reaction. The coefficient of added mass was estimated based on the bell height and radius at each instant (Equation 7) (Daniel 1983).

Inertial Resistance

In order to calculate inertial resistance, the total mass of the animal must be known. Total mass is a combination of body mass and the mass of the water held within the subumbrellar cavity. The average density of medusa body tissue was determined by taking the ratio of body weight to body volume for one animal in each size class. The mean density of *Aurelia aurita* body tissue was found to be $1.06 \times 10^3 \text{ kg/m}^3$ (SD = 86.5). This value was used to estimate the body mass of each experimental animal based on its calculated bell volume. Body mass was added to the mass of seawater within the subumbrellar cavity to determine the total mass at each instant. Total mass fluctuates over the course of the jet cycle as water is drawn into and expelled from the subumbrellar cavity.

Net Hydrodynamic Force

The net force acting on a swimming medusa at any instant is the vector sum of the component hydrodynamic forces. Net force was calculated by summing the values of thrust, drag, acceleration reaction, and inertial resistance at each time interval (Equation 8). Gravitational and buoyant forces contributed less than 5% toward the total net force, and so for simplicity these forces were ignored in the calculation of net force.

Froude Propulsion Efficiency

In order to calculate Froude propulsion efficiency, jet velocity was measured at the time of maximum swimming velocity based on the motion of neutrally buoyant marker particles near the aperture of the subumbrellar cavity. Although a volume of fluid is ejected from the subumbrellar cavity, a two-dimensional analysis of the motion of marker particles was sufficient for determining jet velocity. Only particles within one body-length of the aperture of the subumbrellar cavity were analyzed, and of these particles only the velocity component opposite to the direction of motion was used to measure jet velocity. For each size class, one trial of one animal was chosen at random. Jet velocity was measured at the time of maximum swimming velocity for each contraction during that trial. These measurements were combined to yield the mean jet velocity at the time of maximum swimming velocity for that one animal, which was in turn used as an estimate of jet velocity at the time of maximum swimming velocity for all animals in that size class (Table 3).

Throughout this study, instantaneous morphological and kinematic measurements were used when calculating hydrodynamic forces. All measurements were either taken directly from video recordings or interpolated by the motion analysis software. Prior to analysis the raw data were filtered using a low-pass, fourth-order, zero-phase-shift Butterworth filter with a cut-off frequency of 10 Hz, in order to remove artifacts introduced through digitizing error. Each experimental trial contained numerous jet cycles, only some of which met the analysis criteria. Calculations were performed only on data from jet cycles which met the analysis criteria. The results of these calculations were pooled for each animal, yielding mean values for all parameters of interest (e.g. maximum thrust, mean Reynolds number) for that animal. The mean values for all animals within a size class were then used to calculate the overall mean value for that size class. The standard deviation of each overall mean was calculated based on the standard deviations of its component means (Ku 1966).

Statistical Analysis

A Kruskal-Wallis one-way analysis of variance by ranks was used to compare the means of each size class, and test for a significant difference at the $p=0.05$ level. When necessary, a Student-Newman-Keuls post hoc analysis was conducted to determine differences between two individual means. Statistics were computed using Jandel SigmaStat 2.01 software.

Results

Morphology

The "bell" of an ephyra consists of eight separate paddles joined by a central hub (Figure 3). When an ephyra bell is fully expanded, the paddles radiate outward with ends curved slightly in the aboral direction. Such a morphology is distinct from that of the bowl-shaped medusa. In most cases the resting fineness ratios of ephyrae are negative since the bell margin is positioned aboral to the bell apex. Ephyrae and medusae fineness ratios should therefore not be directly compared.

As medusae increased in size, the mean fineness ratio decreased (i.e. medusae became more oblate) (Figure 5). The mean fineness ratio of each medusoid size class was calculated (Equation 10) (Table 1) based on measurements of bell height and bell diameter taken when the bell was fully expanded, just prior to the onset of the contraction phase of the jet cycle. Fineness ratio does not remain constant, but rather changes continuously as the bell contracts and expands over the course of a jet cycle (Figure 9a). The decrease in fineness ratio with bell diameter was statistically significant.

Pulsation Frequency

Pulsation frequencies for ephyrae and all medusoid size classes were measured (Table 1). As *Aurelia aurita* increased in size, the mean frequency of bell contraction and re-expansion decreased significantly (Figure 6a).

Swimming Velocity

Whereas pulsation rate decreased significantly with an increase in body size, swimming velocity remained approximately constant for the small, medium and large size classes. Ephyrae swimming velocity was significantly higher than that of the medusoid size classes. Mean swimming velocity (calculated over the course of a complete jet cycle) and maximum swimming velocity were measured for all size classes (Table 1) (Figure 6b). Swimming velocity fluctuates throughout the jet cycle (Figure 9b).

Kinematic Similarity

The ratio of swimming velocity to the product of bell diameter times pulsation frequency was calculated for each size class (Equation 9) (Table 1) (Figure 6c). Both mean and maximum values remained roughly constant for the medusoid size classes (i.e. they were kinematically similar), but were significantly higher for ephyrae.

Reynolds Number

Mean Reynolds number (calculated over the course of a complete jet cycle) and maximum Reynolds number steadily increased as *Aurelia aurita* grew larger (Table 1) (Figure 6d). Except for ephyrae, this increase was due entirely to an increase in bell diameter since swimming velocity of the three medusoid size classes remained essentially constant. Reynolds number was calculated based on projected bell diameter and swimming velocity (Equation 1). Projected bell diameter and swimming velocity fluctuate continuously throughout the jet cycle, resulting in a continuously changing

Reynolds number value (Figure 9c). The increase in Reynolds number with body size was statistically significant.

Thrust

The magnitude of thrust produced during the jet cycle fluctuates with time. Thrust is positive during the contraction phase as water is ejected from the bell, and negative during the expansion phase when water is drawn back in (Figure 9d). Maximum forward and rearward thrust were calculated for the three medusoid size classes (Equation 4) (Table 2) (Figure 7a). In all cases, the increase in thrust magnitude with body size was statistically significant.

Pressure Drag

Pressure drag fluctuates throughout the jet cycle, as both swimming velocity and projected area change (Figure 9e). Both mean and maximum drag were calculated for each medusoid size class (Equation 2) (Table 2) (Figure 7b). Pressure drag increased significantly with body size.

Acceleration Reaction

Acceleration reaction acts rearward when the animal's body is speeding up, and forward when it is slowing down (Figure 9f). To compare these forces for medusae of different size classes, the maximum forward and maximum rearward acceleration reaction were calculated (Equation 5) (Table 2) (Figure 7c). Both maximum forward and maximum rearward acceleration reaction increased significantly with body size.

Inertial Resistance

The direction in which inertial resistance acts changes over the course of each jet cycle (Figure 9g). Maximum forward and maximum rearward inertial resistance were calculated for each medusoid size class (Equation 6) (Table 2) (Figure 7d). In all cases, inertial resistance increased significantly with body size.

Net Force

Both morphological and kinematic data were plotted as a function of time to show how these values fluctuate relative to one another (Figure 9). Net force was also calculated and plotted as a function of time (Equation 8) (Figure 9h). Net force reverses direction over the course of the jet cycle, acting forward during the contraction phase and rearward during the expansion phase. The maximum forward and maximum rearward net forces were calculated for each medusoid size class (Table 2) (Figure 7e), and were shown to increase significantly as a function of body size.

Net force at the time of peak thrust generation during both the expansion and the contraction phases of the jet cycle was also calculated for each of the three medusoid size classes (Table 2) (Figure 7f). As body size increased, forward and rearward net force at the time of peak thrust generation increased significantly. Taking the ratio of net force at the time of peak thrust generation during contraction to net force at the time of peak thrust generation during expansion for each medusoid size class reveals that as *Aurelia aurita* grow larger they produce higher forward force during contraction than rearward force during expansion (Table 2).

Froude Propulsion Efficiency

For each medusoid size class, Froude propulsion efficiency was calculated based on the mean power input and mean power output at the time of maximum swimming velocity (Equation 13) (Table 3). As body size increased, so did Froude propulsion efficiency (Figure 8). This increase was statistically significant.

Discussion

Important Aspects of Swimming Performance

Swimming performance can affect the survival of cnidarian medusae in a number of ways. *Aurelia aurita* are denser than seawater and sink slowly when not actively swimming upwards. The ability to change position within the water column may allow medusae to follow the vertical migrations of their prey (Mills 1981). Because the velocity and direction of prevailing ocean currents can change with depth, vertical position within the water column may also influence the large-scale horizontal movement of these animals (Kopacz 1994). Furthermore, feeding performance has been shown to be closely linked to swimming in some species of medusa. The currents that arise from bell pulsations increase prey capture rate by moving seawater past food capturing tentacles (Costello and Colin 1994, 1995). Swimming performance, defined as the distance traveled per amount of mechanical energy required, directly affects the metabolic cost of locomotion. As efficiency of locomotion increases the energetic cost of locomotion may drop, thereby improving *A. aurita* swimming performance.

Consequences of Bell Shape

Swimming performance is linked to the fundamental hydrodynamic forces that arise from the movement of seawater into and out of a medusa's bell. Body size and shape play a major role in determining the magnitude of these forces, and thus ultimately affect the way a medusa locomotes. Over the range of animal sizes observed in this study, bell shape became more oblate as bell diameter increased. This ontogenetic bell flattening was partially responsible for the increased pressure drag and acceleration reaction seen in larger animals. Bell shape is important in that it directly influences the magnitudes of pressure drag (by defining the projected area of the bell and affecting the drag coefficient) and acceleration reaction (by affecting the coefficient of added mass). Bell shape may also help influence the volume of the subumbrellar cavity and the area of the bell aperture, and thus indirectly determine the amount of thrust that a medusa can produce. A medusa with a streamlined bell experiences lower drag and acceleration reaction than a medusa with an bowl-shaped bell, and thus may accelerate more rapidly. A bowl-shaped bell has been shown to increase feeding performance in certain species of medusa (Costello and Colin 1994, 1995), and so in some cases such a shape may confer an advantage. Whether this decrease in fineness ratio has any affect on prey capture rate in *Aurelia aurita* is not yet known.

Consequences of Bell Size

As *Aurelia aurita* medusae grow larger they become more efficient at locomotion. When a large medusa pulses it achieves a greater power output relative to power input than does a small medusa. This result, based solely on kinematics, suggests that the

metabolic cost of transport may decrease as medusae grow larger. This finding for medusae contrasts with that of O'Dor and Webber (1986), who found that the metabolic cost of locomotion increases with increasing body size in three different species of squid. Squid also locomote by jet propulsion, but their jetting apparatus is different from that of medusae. Although further comparative study is necessary to reveal the reasons for this contrast, one possibility is that squid swimming velocity increases as these animals grow larger (O'Dor and Webber 1986), whereas *A. aurita* swimming velocity remains relatively constant during ontogeny.

While all medusae experience a net rearward force during the expansion phase of the jet cycle (due to water being drawn back into the subumbrellar cavity), large medusae produce a larger net forward force relative to net rearward force compared to small medusae. Furthermore, large medusae tend to continue to coast forward as they are reexpanding, whereas small medusae tend to move forward only during contraction. This finding is sensible in that smaller medusae experience a lower Reynolds number environment, and as body size increases so does the relative importance of inertia.

All three medusoid size classes of *Aurelia aurita* are kinematically similar. This means that, in relation to their body size, they all move in nearly an identical manner. A small medusa normally pulses at a higher frequency than a large medusa, but if that same small medusa were artificially enlarged and slowed down (for example, by magnifying a video image and playing it in slow motion) so that its bell diameter and contraction rate matched that of the large medusa, both animals would seem to swim at the same speed. Daniel's (1983) model suggests that the net hydrodynamic force acting on a medusa

increases with body size. While this seems to be the case for *A. aurita*, it is interesting to note that mean swimming speed remains relatively constant for all medusoid size classes. This is caused primarily by a decrease in bell pulsation rate. While both the net force per pulse and the distance traveled per pulse increase as a function of body size, a corresponding decrease in pulses per time causes overall swimming speed to remain roughly unchanged.

Ephyrae

Ephyrae exhibited significantly higher swimming speed than small medusae. While ephyrae pulse at a rate almost twice that of small medusae, this may only partially explain the difference in swimming speed. The morphology of an ephyra is radically different from that of a medusa. It is conceivable that the synchronized power-stroke of an ephyra's eight lappets produces greater thrust than the bell contraction of a small medusa. This idea is especially interesting in light of the low Reynolds number at which ephyrae operate. Jet propulsion is an inertial mode of locomotion, and would seem to be an inadequate (if not all together impossible) way to move about at viscosity-dominated low Reynolds numbers. An interesting comparison to make would be that of ephyrae to newly released hydrozoan medusae. Hydrozoans do not form ephyrae, but rather release small fully-formed medusae (on the order of 1 to 2 mm) from sessile polyps. These small hydromedusae most likely operate in a Reynolds number range similar to that of ephyrae. One major morphological difference between hydrozoan medusae and scyphozoan medusae is the presence of a shelf of tissue (called a velum) in hydromedusae which constricts the subumbrellar aperture. Since thrust is inversely proportional to the

diameter of the subumbrellar aperture, the presence of a velum should increase the thrust of these tiny medusae. While Daniel's model could be used to describe the hydrodynamics of newly released hydromedusae, it unfortunately does not adequately describe the hydrodynamic forces encountered by ephyrae flapping their eight lappets. A detailed analysis of ephyrae hydrodynamics merits further study.

Topics for Future Study

During the ontogeny of an individual medusa, changes in size and shape will have an effect on swimming performance. In order to survive, a medusa must function adequately at each stage of development. Of course, swimming performance is only one of many factors central to a medusa's survival. Furthermore, while body size and shape have a direct influence on swimming performance, other factors such as muscle physiology and neural control are also extremely important. Be that as it may, a drastic morphological change during ontogeny (such as the ephyra-to-medusa transition) raises a number of intriguing questions. Might this morphological shift be caused by some fundamental change in the way these animals interact with their fluid environment as they grow through the size range of 1 to 10 mm? This concept has been explored with respect to crustaceans who change from nauplii to other body forms as they grow (Williams 1994a,b). Hydrozoan cnidarians do not have an ephyra stage, but in spite of this they survive quite well. Does the increased thrust afforded by a velum allow hydrozoans to feed and locomote with a medusoid morphology at low Reynolds number, whereas scyphomedusae cannot? If it is possible for a medusoid-shaped morphology to function in a low Reynolds number environment, what advantage (if any) does being

shaped like an ephyra confer on tiny scyphozoans? Clearly many questions still remain to be addressed.

References

- Alexander, R.McN. (1964) Viscoelastic properties of the mesoglea of jellyfish. *J. Exp. Biol.* **41**: 363-369.
- Barnes, R.D. (1987) *Invertebrate Zoology, 5th Edition*. New York: Saunders College Publishing.
- Chapman, G. (1953) Studies of the mesoglea of coelenterates. II. Physical properties. *J. Exp. Biol.* **30**: 440-451.
- Costello, J.H. and S.P. Colin (1994) Morphology, fluid motion and predation by the scyphomedusa *Aurelia aurita*. *Mar. Biol.* **121**: 327-334.
- Costello, J.H. and S.P. Colin (1995) Flow and feeding by swimming scyphomedusae. *Mar. Biol.* **124**: 399-406.
- Dadswell, M.J. and D. Weihs (1990) Size-related hydrodynamic characteristics of the giant scallop, *Placopecten magellanicus* (Bivalvia: Pectinidae). *Can. J. Zool.* **68**: 778-785.
- Daniel, T.L. (1983) Mechanics and energetics of medusan jet propulsion. *Can. J. Zool.* **61**: 1406-1420.
- Daniel, T.L. (1985) Cost of locomotion: unsteady medusan swimming. *J. Exp. Biol.* **119**: 149-164.
- DeMont, M.E. and J.M. Gosline (1988a) Mechanics of jet propulsion in the hydromedusan jellyfish, *Polyorchis penicillatus*. I. Mechanical properties of the locomotor structure. *J. Exp. Biol.* **134**: 313-32.

- DeMont, M.E. and J.M. Gosline (1988b) Mechanics of jet propulsion in the hydromedusan jellyfish, *Polyorchis penicillatus*. II. Energetics of the jet cycle. *J. Exp. Biol.* **134**: 333-45.
- DeMont, M.E. and J.M. Gosline (1988c) Mechanics of jet propulsion in the hydromedusan jellyfish, *Polyorchis penicillatus*. III. A natural resonating bell; the presence and importance of a resonant phenomenon in the locomotor structure. *J. Exp. Biol.* **134**: 333-45.
- Denny, M.W. (1993) *Air and Water: The Biology and Physics of Life's Media*. Princeton, N.J.: Princeton University Press.
- Gladfelter, W.B. (1972) Structure and function of the locomotory system of *Polyorchis montereyensis* (Cnidaria, Hydrozoa). *Helgol. Wiss. Meeresunters* **23**: 38-79.
- Gladfelter, W.B. (1973) Comparative analysis of the locomotory system of medusoid Cnidaria. *Helgol. Wiss. Meeresunters* **25**: 228-72.
- Gosline, J.M. and R.E. Shadwick (1983) The role of elastic energy storage mechanisms in swimming: an analysis of mantle elasticity in escape jetting in the squid, *Loligo opalescens*. *Can. J. Zool.* **61**: 1421-1431.
- Kennish, M.J. (1994) *Practical Handbook of Marine Science, 2nd Edition*. Boca Raton: CRC Press.
- Kopacz, U. (1994) Evidence for tidally-induced vertical migration of some gelatinous zooplankton in the Wadden Sea area near Sylt. *Helgol. Wiss. Meeresunters* **48**: 333-342.
- Ku, H.H. (1966) Notes on the use of propagation of error formulas. *Journal of Research of the National Bureau of Standards – C. Engineering and Instrumentation*. **70C(4)**: 331-341.
- Madin, L.P. (1990) Aspects of jet propulsion in salps. *Can. J. Zool.* **68**: 765-777.

- Meinkoth, N.A. (1995) *National Audubon Society Field Guide to North American Seashore Creatures*. New York, N.Y.: Alfred A. Knopf, Inc.
- Mill, P.J. and R.S. Pickard (1975) Jet propulsion in isopteran dragonfly larvae. *J. Comp. Physiol.* **A97**: 329-338.
- Mills, C.E. (1981) Diversity of swimming behaviors in hydromedusae as related to feeding and utilization of space. *Mar. Biol.* **64**: 185-189.
- O'Dor and Webber (1986) The constraints on cephalopods: Why squid aren't fish. *Can. J. Zool.* **64**: 1591-1605.
- Schmidt-Nielsen, K. (1984) *Scaling: Why is Animal Size so Important?* Cambridge, U.K.: Cambridge University Press.
- Sullivan, B.K., C.L. Suchman and J.H. Costello (1997) Mechanics of prey selection by ephyrae of the scyphomedusa *Aurelia aurita*. *Mar. Biol.* **130**(2): 213-222.
- Vogel, S. (1994) *Life in Moving Fluids*. Princeton, N.J.: Princeton University Press.
- Wells, M.J. and J. Wells (1982) Ventilatory currents in the mantle of cephalopods. *J. Exp. Biol.* **99**: 315-330.
- Williams, T.A. (1994a) Locomotion in developing *Artemia* larvae: Mechanical analysis of antennal propulsors based on large-scale physical models. *Biol. Bull.* **187**: 156-163.
- Williams, T.A. (1994b) A model of rowing propulsion and the ontogeny of locomotion in *Artemia* larvae. *Biol. Bull.* **187**: 164-173.

Table 1 Morphology and kinematics. Values are means for the size class, with standard deviation given in parentheses. *p*-value calculated using a Kruskal-Wallis one-way ANOVA (d.f. = 19 for comparison of all size classes, d.f. = 16 for comparison of medusae only). Values marked with corresponding symbols (♣ ♦ ♥ ♠ •) were determined to be significantly different based on a Student-Newman-Keuls post hoc analysis.

	Ephyra	Small	Medium	Large	
Mean Fineness Ratio		0.41 [*] (0.04)	0.30 (0.02)	0.25 [*] (0.03)	$p < 0.005$
Pulsation Rate (pulses/s)	2.27 ^{***} (0.55)	1.49 ^{***} (0.20)	0.50 ^{**} (0.22)	0.42 ^{**} (0.31)	$p < 0.005$
Mean Swimming Velocity (cm/s)	1.96 (0.21)	1.21 (0.09)	1.40 (0.36)	1.48 (0.27)	$p = 0.082$
Maximum Swimming Velocity (cm/s)	3.21 (0.32)	2.43 (0.11)	2.61 (0.42)	2.90 (0.22)	$p = 0.075$
Mean U/Lf	4.32 ^{***} (0.88)	0.52 [*] (0.16)	0.73 [*] (0.33)	0.37 [*] (0.27)	$p < 0.005$
Maximum U/Lf	7.07 ^{***} (1.35)	1.04 [*] (0.78)	1.37 [*] (0.53)	0.73 [*] (0.39)	$p < 0.005$
Mean Re	21 [*] (5.4)	148 [*] (23.8)	681 [*] (102.9)	1490 [*] (127.2)	$p < 0.005$
Maximum Re	64 [*] (8.8)	274 [*] (31.5)	1439 [*] (131.9)	2509 [*] (187.4)	$p < 0.005$

Table 2 Forces during swimming. Values are means for the size class, with standard deviation given in parentheses. *p*-value calculated using a Kruskal-Wallis one-way ANOVA (d.f. = 16). Values marked with corresponding symbols (♣♦) were determined to be significantly different based on a Student-Newman-Keuls post hoc analysis.

	Small	Medium	Large	
Maximum Forward Thrust (mN)	0.30 [*] (0.03)	2.24 [*] (0.84)	36.30 [*] (5.61)	$p < 0.005$
Maximum Rearward Thrust (mN)	-0.09 [*] (0.03)	-0.71 [*] (0.46)	-13.90 [*] (4.11)	$p < 0.005$
Mean Pressure Drag (mN)	0.008 [*] (0.005)	0.013 [*] (0.008)	0.100 ^{**} (0.020)	$p < 0.005$
Maximum Pressure Drag (mN)	0.016 [*] (0.009)	0.029 [*] (0.008)	0.218 ^{**} (0.021)	$p < 0.005$
Maximum Forward Acceleration Reaction (mN)	0.39 [*] (0.02)	1.51 [*] (0.08)	11.00 [*] (1.92)	$p < 0.005$
Maximum Rearward Acceleration Reaction (mN)	-0.47 [*] (0.07)	-2.04 [*] (1.27)	-15.40 [*] (3.59)	$p < 0.005$
Maximum Forward Inertial Resistance (mN)	0.24 [*] (0.01)	0.90 [*] (0.19)	11.60 [*] (3.11)	$p < 0.005$
Maximum Rearward Inertial Resistance (mN)	-0.46 [*] (0.04)	-1.80 [*] (0.66)	-26.31 [*] (4.84)	$p < 0.005$
Maximum Forward Net Force (mN)	0.71 [*] (0.05)	3.57 [*] (1.99)	50.60 [*] (4.11)	$p < 0.005$
Maximum Rearward Net Force (mN)	-0.90 [*] (0.09)	-3.71 [*] (2.04)	-44.24 [*] (4.81)	$p < 0.005$
Net Force at time of Peak Forward Thrust (mN)	0.26 [*] (0.12)	1.67 [*] (0.85)	16.80 [*] (5.08)	$p < 0.005$
Net Force at time of Peak Rearward Thrust (mN)	-0.19 [*] (0.09)	-0.80 [*] (0.34)	-5.11 [*] (3.03)	$p < 0.005$
Net Force at time of Peak Forward Thrust / Net Force at time of Peak Rearward Thrust	1.36 [*] (0.21)	2.08 [*] (0.15)	3.29 [*] (0.26)	$p < 0.005$

Table 3 Froude propulsion efficiency. Values are means for the size class, with standard deviation given in parentheses. p -value calculated using a Kruskal-Wallis one-way ANOVA (d.f. = 16). Values marked with corresponding symbols (\clubsuit \diamond) were determined to be significantly different based on a Student-Newman-Keuls post hoc analysis.

	Small	Medium	Large	
Mean Jet Velocity at time of Maximum Swimming Velocity (cm/s)	3.0 (0.14)	3.1 (0.29)	3.4 (0.21)	$p = 0.071$
Mean Power Output at time of Maximum Swimming Velocity (J)	1.7×10^{-4} (6.0×10^{-5})	1.1×10^{-3} (7.5×10^{-4})	1.8×10^{-2} (7.1×10^{-4})	$p < 0.005$
Mean Power Input at time of Maximum Swimming Velocity (J)	1.5×10^{-4} (8.2×10^{-5})	7.0×10^{-4} (1.0×10^{-4})	1.2×10^{-3} (7.0×10^{-4})	$p < 0.005$
Froude Propulsion Efficiency	1.1^* (0.5)	1.6^* (1.2)	14.6^{**} (1.0)	$p < 0.005$

Figure 1. In *Aurelia aurita*, the jet cycle is comprised of two phases. During the contraction phase (t_2 , t_3) seawater is forcefully ejected from the subumbrellar cavity and the animal is driven forward. During the expansion phase (t_4) the recoil of the bell draws seawater back into the subumbrellar cavity. The animal may continue to move forward during the expansion phase, but negative thrust will cause it to decelerate.

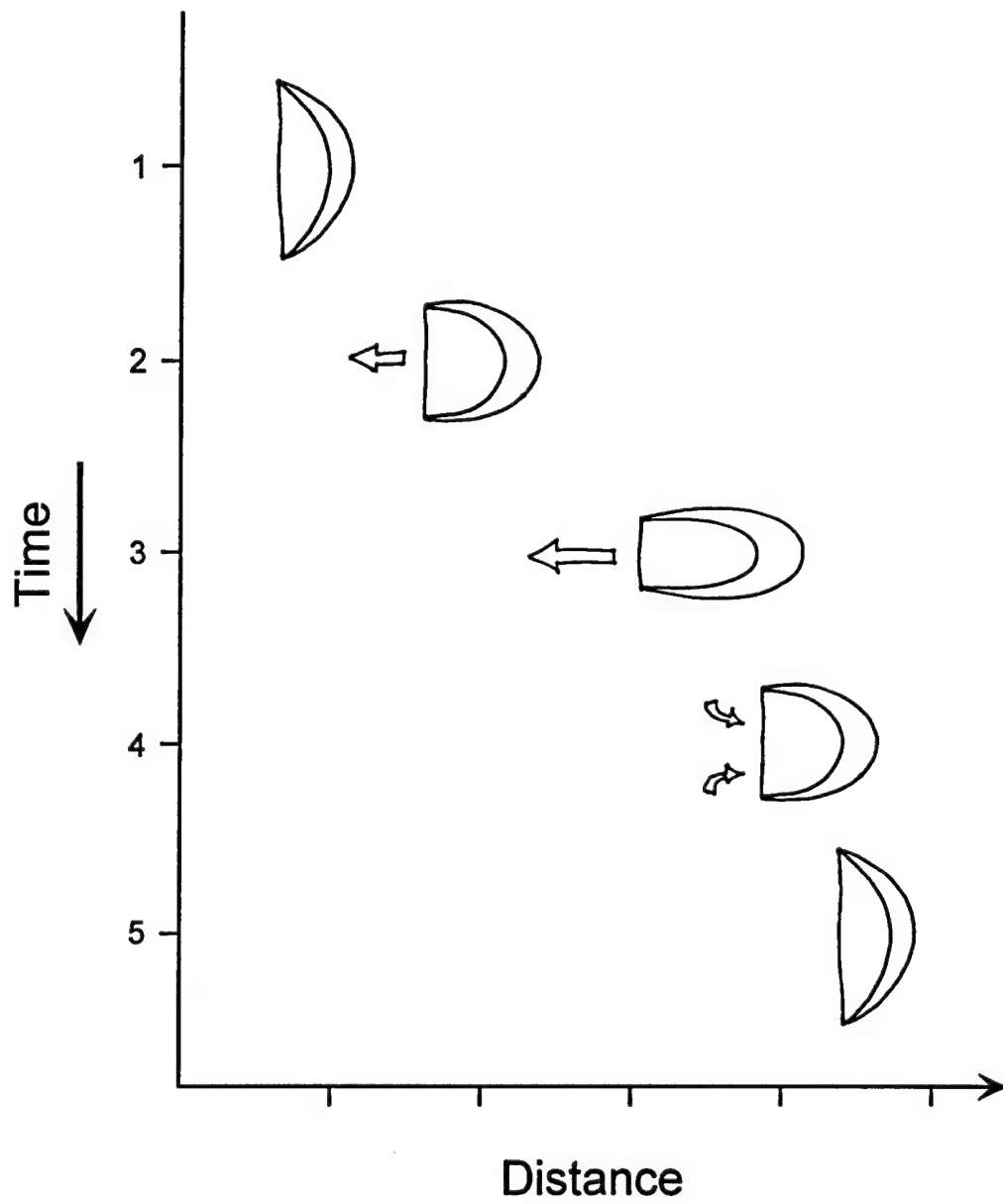


Figure 2. (A) *Aurelia aurita* morphology. (B) Six points on the bell were tracked over time. Bell diameter, bell height, aperture diameter and subumbrellar cavity height were calculated based on the relative location of these points.

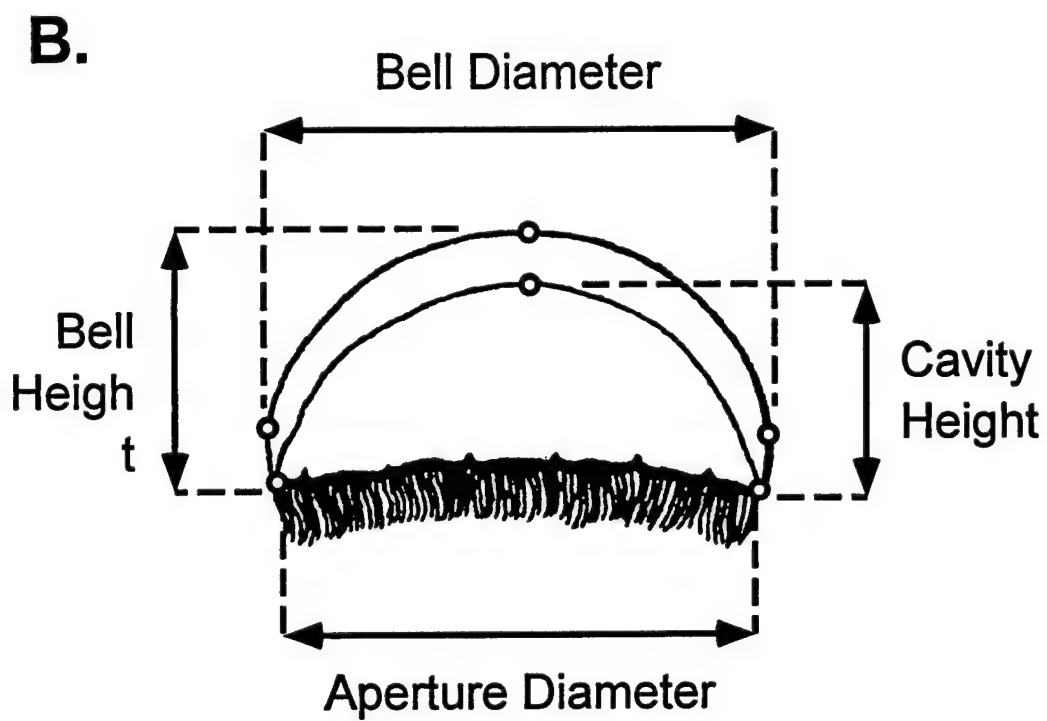
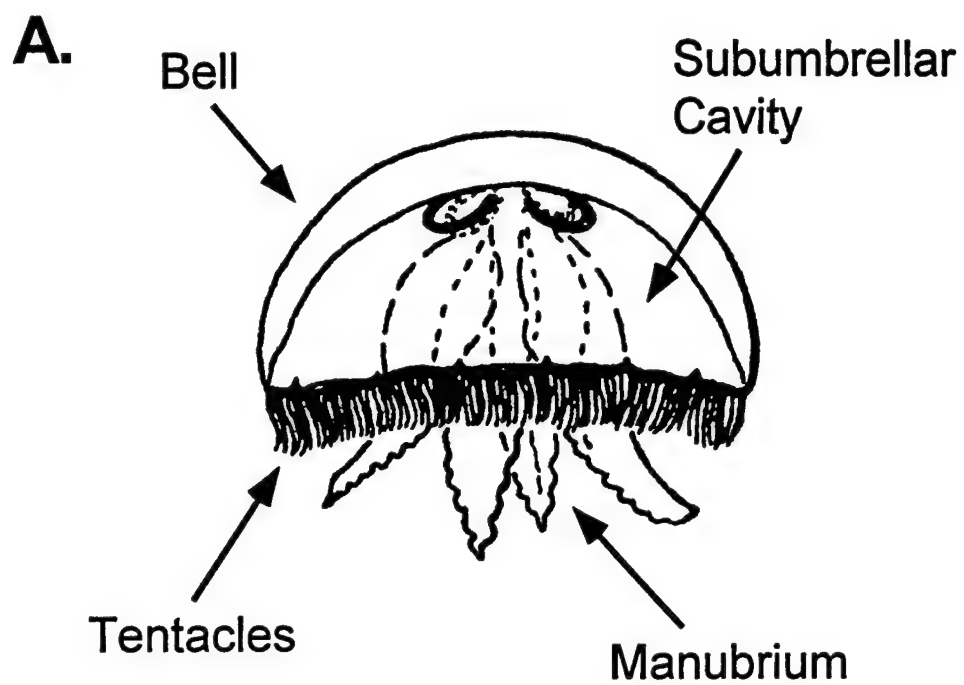


Figure 3. *Aurelia aurita* has a complex life cycle, alternating between a sessile asexual polyp stage and a free-swimming sexual medusoid stage. When initially released from the strobila, ephyrae (magnified insert) are approximately 1 mm in diameter and morphologically distinct from medusae. As ephyrae grow larger they take on the medusoid body shape. A full-grown medusa can achieve a bell diameter of over 40 cm, thus a 400-fold increase in body size occurs between the ephyra and the largest adult. Drawn using information presented in Barnes (1987).

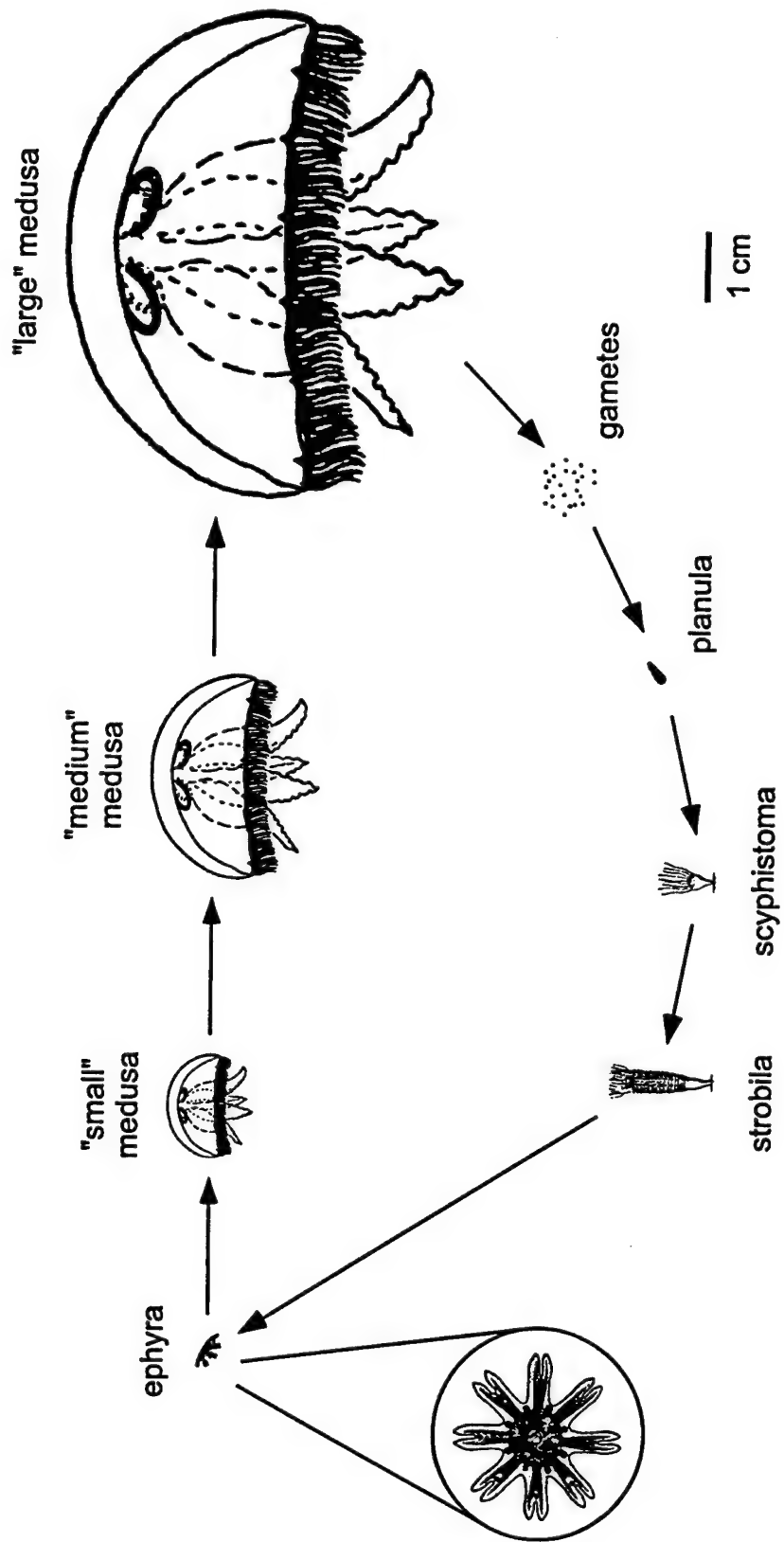


Figure 4. Hydrodynamic force as a function of bell diameter. Using Daniel's (1983) theoretical model of jet-propelled locomotion in medusae, the relative magnitudes of thrust, drag, acceleration reaction and inertial resistance can be calculated as functions of bell diameter. Thrust increases in proportion to length⁴, acceleration reaction and inertial resistance increase as length³, and drag increases as length².

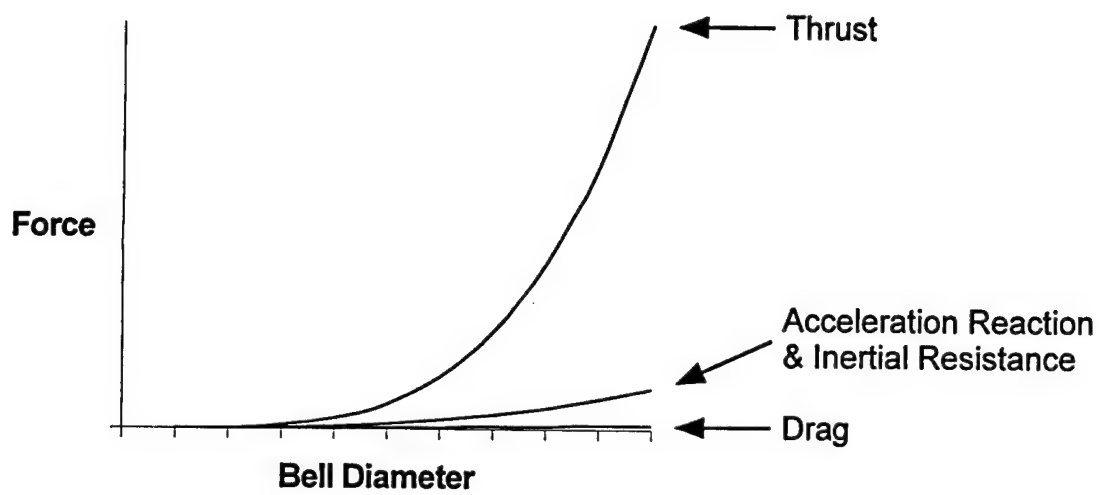


Figure 5. Fineness ratio as a function of size class. As an *Aurelia aurita* medusa grows larger, its bell becomes more oblate. Filled circle symbols (●) indicate the mean of each size class, error bars are one standard deviation. “Small” medusae had a mean bell diameter (mbd) of 1.57 cm (standard deviation (SD) = 0.20, n = 5); “medium” medusae had a mbd of 3.82 cm (SD = 0.22, n = 6); and “large” medusae had a mbd of 9.51 cm (SD = 1.79, n = 6).

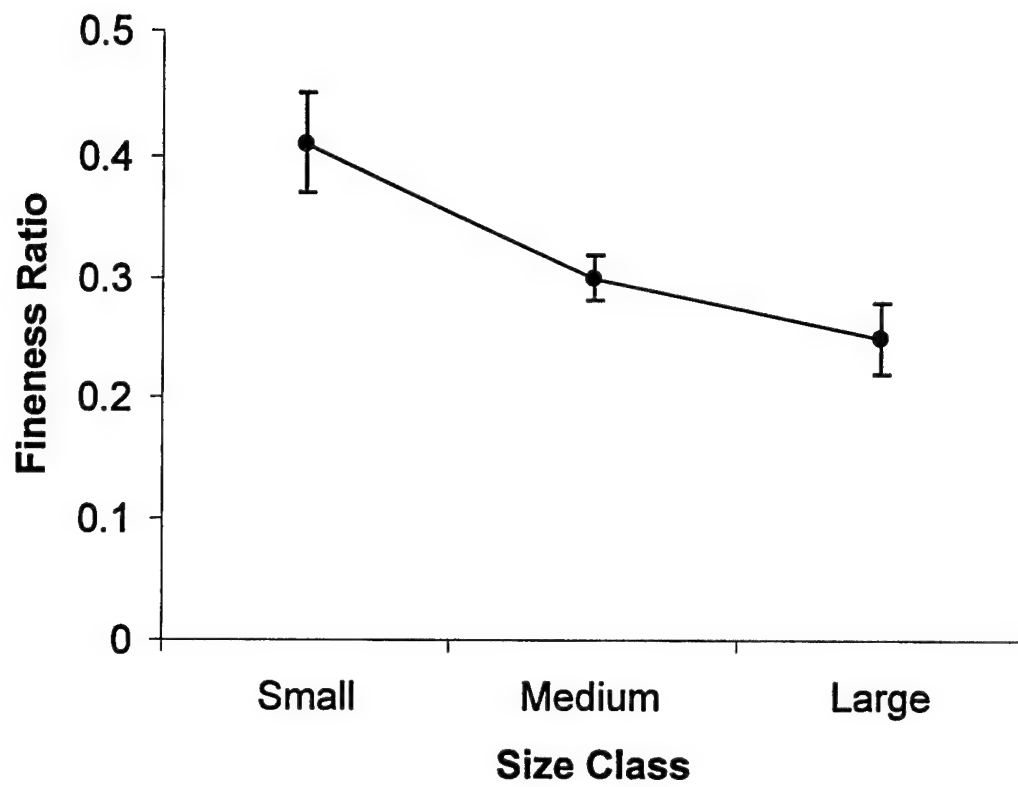


Figure 6. (A) Pulsation rate as a function of size class. Pulsation rate decreases significantly as body size increases. (B) Swimming velocity as a function of size class. Ephyrae swim significantly faster than medusae. Swimming velocity of medusae did not change significantly over the size range observed in this study. (C) The ratio of swimming velocity to the product of bell diameter times pulsation frequency as a function of size class. Small, medium and large medusae are kinematically similar to each other, but not to ephyrae. (D) Reynolds number as a function of size class. Reynolds number increases significantly as *Aurelia aurita* grow larger. Open square symbols (\square) indicate the mean of all maximum values in the size class, filled circle symbols (\bullet) indicate the mean of all mean values in the size class, error bars are one standard deviation. Ephyrae had a mean bell diameter of 0.20 cm (standard deviation = 0.05, $n = 3$).

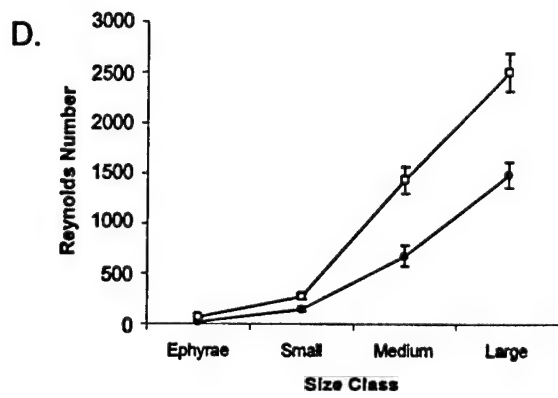
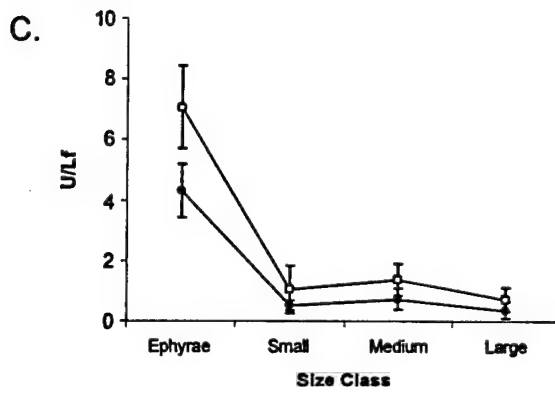
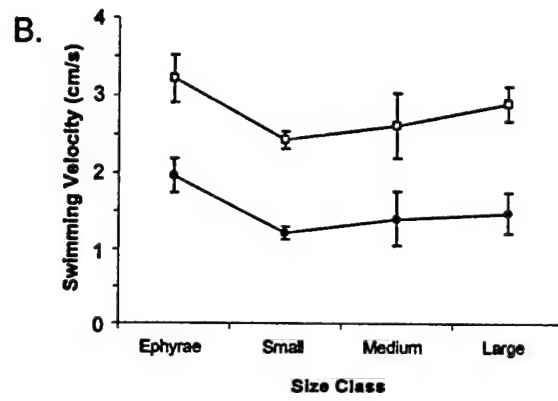
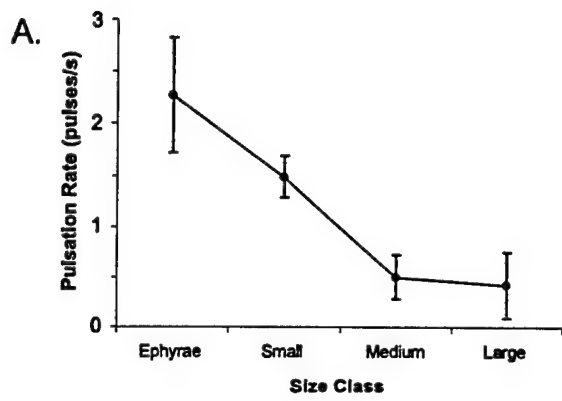


Figure 7. (A-E) Thrust, drag, acceleration reaction, inertial resistance, and net force as a function of size class. In all cases, hydrodynamic force increases significantly as a function of body size. (F) Net force at time of peak thrust as a function of size class (solid lines), and the ratio of net forward force at time of peak forward thrust to net rearward force at time of peak rearward thrust as a function of size class (dashed line). (A, C-F) Open square symbols (\square) indicate the mean of all maximum forward force values in the size class, filled circle symbols (\bullet) indicate the mean of all maximum rearward force values in the size class; (B) Open square symbols (\square) indicate the mean of all maximum values in the size class, filled circle symbols (\bullet) indicate the mean of all mean values in the size class. Error bars are one standard deviation. “Small” medusae had a mean Reynolds number (Re) of 148 (standard deviation (SD) = 23.8, n = 5); “medium” medusae had a mean Re of 681 (SD = 102.9, n = 6); and “large” medusae had a mean Re of 1490 (SD = 127.2, n = 6).

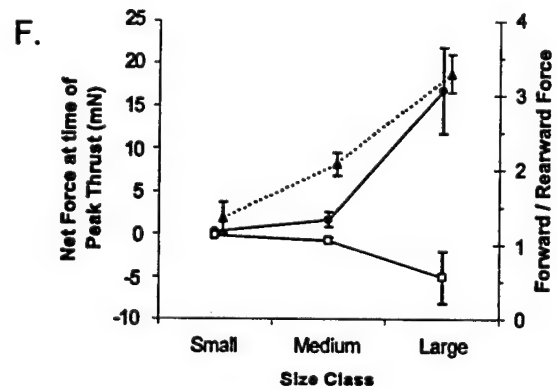
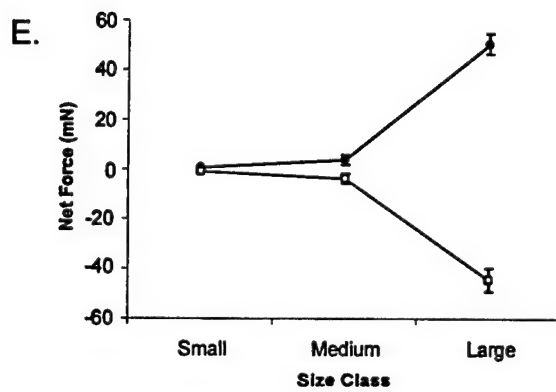
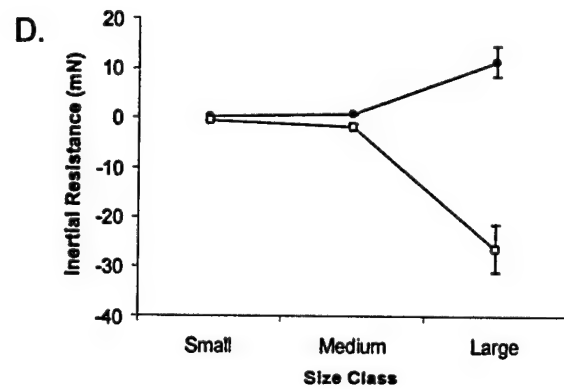
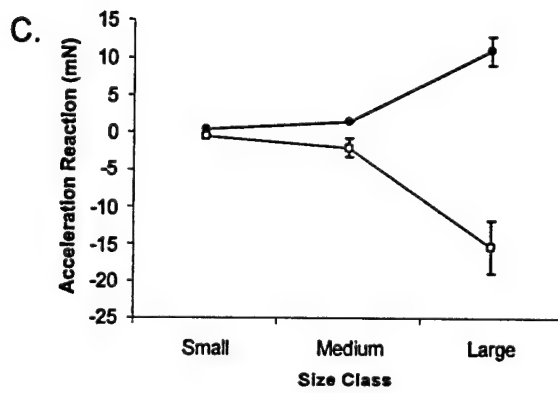
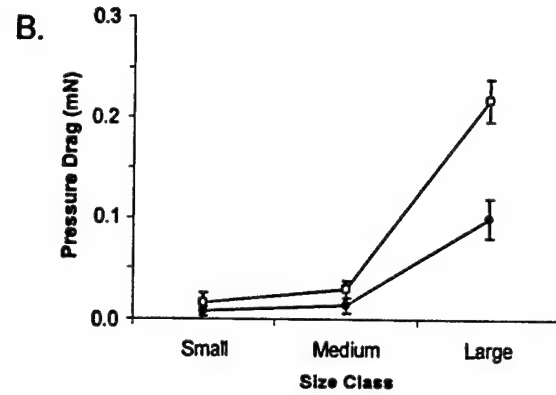
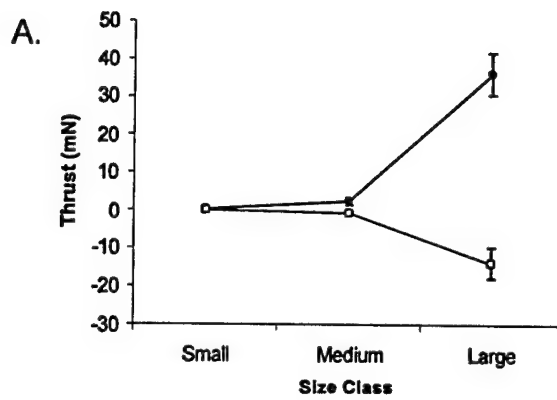


Figure 8. Froude propulsion efficiency as a function of size class. Efficiency increases as a function of body size. Filled circle symbols (●) indicate the mean of all mean values in the size class. Error bars are one standard deviation.

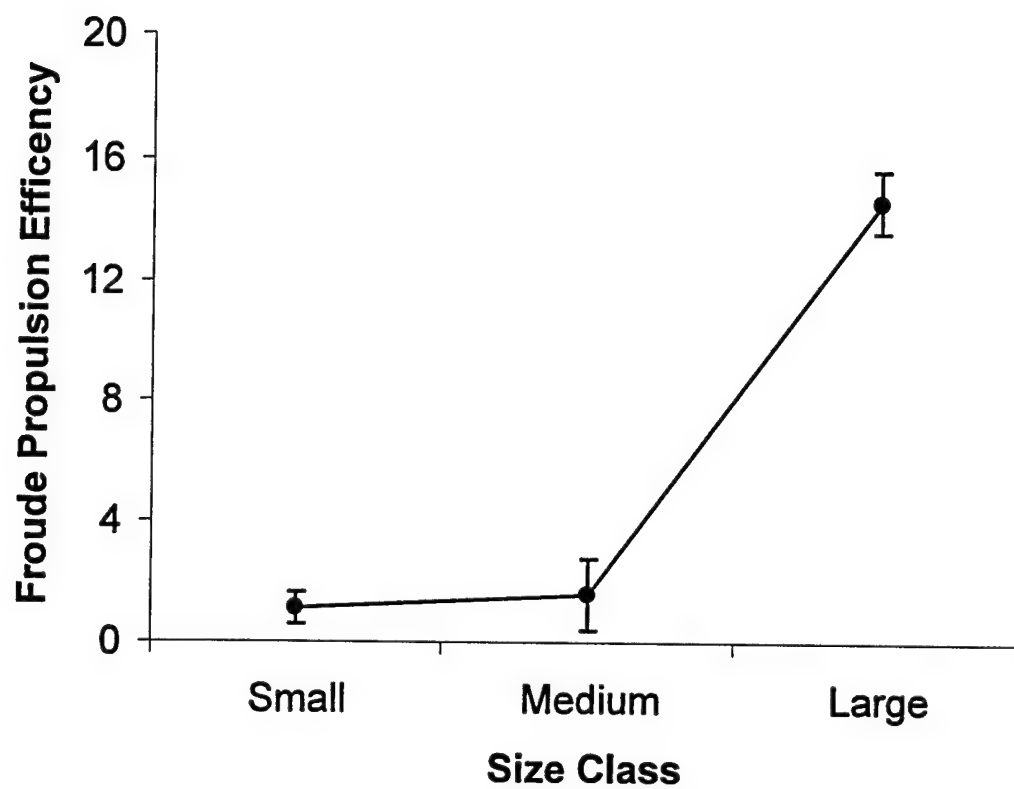
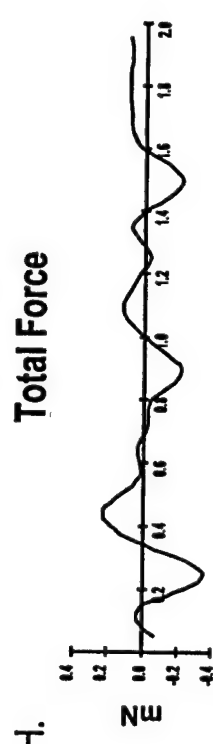
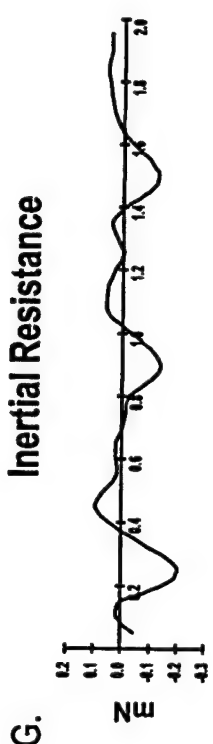
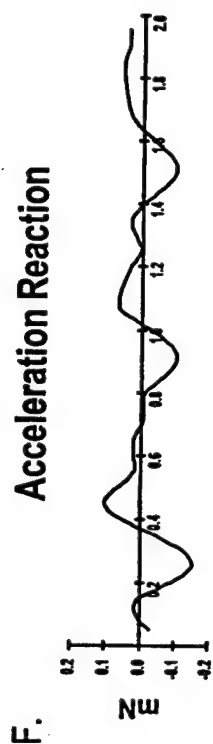
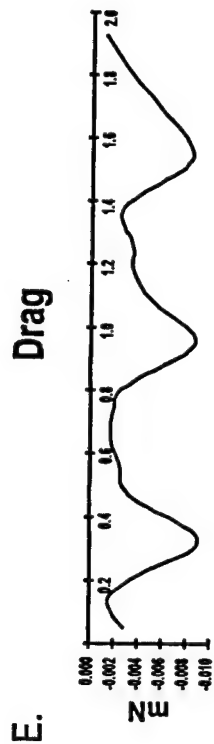
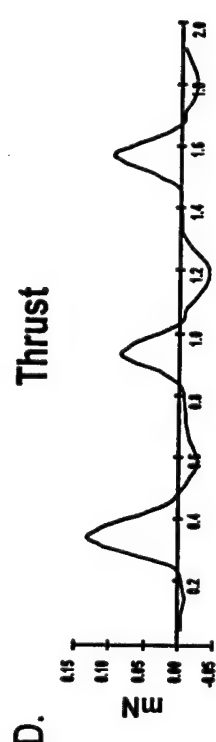
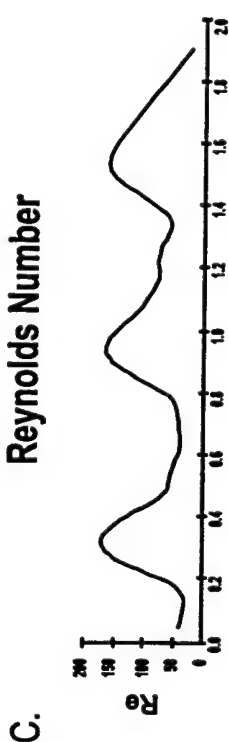
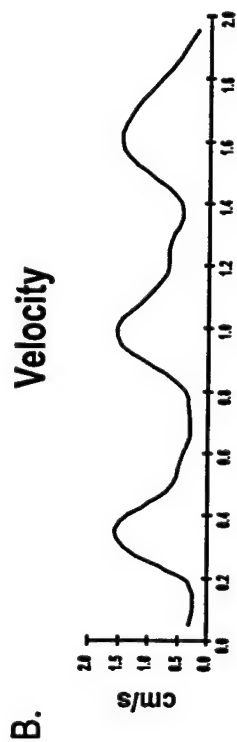
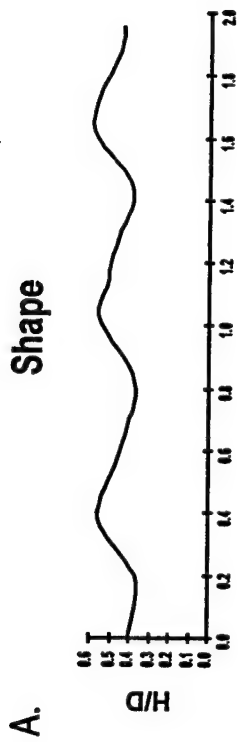


Figure 9. Morphology, kinematics and hydrodynamic forces as a function of time. Data from a single run of a small medusa, plotted to reveal how morphology, kinematics and hydrodynamic forces fluctuate relative to one another during the course of three jet cycles.



Time (seconds)

Time (seconds)

HYDRODYNAMICS OF THE CRAB *PACHYGRAPSUS*
CRASSIPES AT TWO DIFFERENT MICROHABITATS:
PROTECTED ESTUARY AND WAVE-SWEPT ROCKY
SHORE.....

W. Laur^a and M. Martinez, Univ. of California, Berkeley.
J23553@cctu.cc.tohoku.ac.jp,
marlenem@garnet.berkeley.edu.

Benthic locomoting animals, such as crabs, face the danger of being dislodged from the substratum by ambient water flow. Field measurements of water velocities in the microhabitats of *Pachygrapsus crassipes* showed that in the wave-swept site the flow is rapid, accelerational and oscillatory, while in the estuarine site it is slow and steady. Laboratory measurements of drag coefficients, lift coefficients and added mass coefficients of crabs from both sites were used to calculate the total hydrodynamic forces these animals may experience in the field. The tenacity (force with which a crab can hold on to the substratum) of *P. crassipes* standing still on different substrata was also measured in the lab and was found to be greater than the hydrodynamic forces that tend to wash them away.

(1996) Am. Zool. 35: 28A.

UNDERWATER PUNTING BY AN INTERTIDAL CRAB: A NOVEL GAIT REVEALED BY THE KINEMATICS OF PEDESTRIAN LOCOMOTION IN AIR *VERSUS* WATER

MARLENE M. MARTINEZ*, R. J. FULL AND M. A. R. KOEHL

Department of Integrative Biology, University of California at Berkeley, Berkeley, CA 94720, USA

*e-mail: marlenem@socrates.berkeley.edu

Accepted 22 June; published on WWW 25 August 1998

Summary

As an animal moves from air to water, its effective weight is substantially reduced by buoyancy while the fluid-dynamic forces (e.g. lift and drag) are increased 800-fold. The changes in the magnitude of these forces are likely to have substantial consequences for locomotion as well as for resistance to being overturned. We began our investigation of aquatic pedestrian locomotion by quantifying the kinematics of crabs at slow speeds where buoyant forces are more important relative to fluid-dynamic forces. At these slow speeds, we used reduced-gravity models of terrestrial locomotion to predict trends in the kinematics of aquatic pedestrian locomotion. Using these models, we expected animals in water to use running gaits even at slow speeds. We hypothesized that aquatic pedestrians would (1) use lower duty factors and longer periods with no ground contact, (2) demonstrate more variable kinematics and (3) adopt wider stances for increased horizontal stability against fluid-dynamic forces than animals moving at the same speed on land. We tested these predictions by

measuring the three-dimensional kinematics of intertidal rock crabs (*Grapsus tenuicrustatus*) locomoting through water and air at the same velocity (9 cm s^{-1}) over a flat substratum. As predicted from reduced-gravity models of running, crabs moving under water showed decreased leg contact times and duty factors relative to locomotion on land. In water, the legs cycled intermittently, fewer legs were in contact with the substratum and leg kinematics were much more variable than on land. The width of the crab's stance was 19 % greater in water than in air, thereby increasing stability against overturning by hydrodynamic forces. Rather than an alternating tetrapod or metachronal wave gait, crabs in water used a novel gait we termed 'underwater punting', characterized by alternating phases of generating thrust against the substratum and gliding through the water.

Key words: locomotion, biomechanics, crustacean, arthropod, gait, crab, *Grapsus tenuicrustatus*.

Introduction

Several lineages of benthic animals have made the evolutionary transition between an aquatic and a terrestrial habitat, notably the molluscs, annelids, arthropods and vertebrates. Whether a change of habitat takes place on an evolutionary time scale for a lineage or on a contemporary time scale for an amphibious individual (such as one that lives in the intertidal zone), the transition between two distinct physical environments may have significant mechanical consequences for walking and running. As an animal moves from air to water, its effective weight is substantially reduced by buoyancy, while the fluid-dynamic forces (e.g. lift and drag) are increased 800-fold. The changes in the magnitude of these forces are likely to have substantial consequences for locomotion as well as for resistance to overturning. Although pedestrian locomotion in air and swimming in water have been studied extensively (Alexander and Goldspink, 1977; Alexander, 1992; Full, 1997; Gans *et al.* 1997), only a few studies have explicitly considered the kinematics (Hui, 1992; Pridmore, 1994; Jamon and Clarac, 1995), kinetics (Clarac and Cruse, 1982; Grote, 1981; Klärner and Barnes, 1986), energetic cost (Houlihan and Innes, 1984;

Houlihan *et al.* 1984) or hydrodynamics (Pond, 1975; Maude and Williams, 1983; Blake, 1985; Bill and Hermkind, 1976) of aquatic pedestrian locomotion. No study to date provides a theoretical model of aquatic pedestrian mechanics comparable with those developed for legged terrestrial locomotion (Blickhan, 1989; Blickhan and Full, 1987, 1993; Cavagna *et al.* 1977; McMahon and Cheng, 1990). Most research on aquatic pedestrians has focused on inter-leg coordination and motor control (e.g. Chasserat and Clarac, 1983; Clarac, 1981, 1984; Clarac and Barnes, 1985; Clarac and Chasserat, 1983; Clarac *et al.* 1987; Cruse and Muller, 1986; Jamon and Clarac, 1995; Muller and Cruse, 1991). We contend that a synthesis of these fundamental studies of neural control with analyses of the mechanics of locomoting on underwater substrata is required before we can explain the differences between aquatic and terrestrial pedestrian locomotion and the transition to land.

Previous studies comparing pedestrian arthropods in water *versus* in air have revealed seemingly contrary patterns in locomotor posture and kinematics, including decreased duty factor or power stroke duration (Hui, 1992; Clarac *et al.* 1987),

increased stance width (Grote, 1981; Hui, 1992), no change in stance width (Hui, 1992), increased stride length (Grote, 1981; Pond, 1975), no change in stride length (Hui, 1992), increased stride frequency (Grote, 1981; Pond, 1975; Clarac *et al.* 1987) and no change in stride frequency (Hui, 1992) in water compared with air. The present study seeks a mechanistic explanation of these published observations on postural and kinematic differences. Furthermore, this study seeks to develop a unifying mechanical framework within which to consider pedestrian locomotion under varied conditions (including terrestrial, aquatic and lunar conditions). To accomplish these goals, we make direct kinematic comparisons between individual animals locomoting at the same speed in the same tank filled with either air or water. In doing so, we control for the effects of speed, substratum and the individual animal. We use the kinematic data to test several mechanically based hypotheses of aquatic pedestrian locomotion. This study also reveals basic information about mechanical aspects of the evolution of terrestriality and provides biological inspiration for the design of autonomous legged underwater vehicles (ALUVs; Greiner *et al.* 1996).

Experimental system

Crabs provide a useful system for investigation of the mechanics of locomoting in aquatic *versus* terrestrial environments because there are subtidal, intertidal (amphibious) and terrestrial crab species. This diversity permits both comparison across species and comparison of amphibious individuals with themselves as they locomote under water *versus* on land. Using amphibious animals offers the advantage of tighter control with paired comparisons for each individual, rather than comparisons of species averages.

Once we have determined the kinematic differences using amphibious animals, we can then make multiple-species comparisons that focus on quantifying the critical kinematic variables. Furthermore, there is already a rich background of information on the physiology and mechanics of terrestrial locomotion in crabs (e.g. Barnes, 1975; Blickhan and Full, 1987, 1993; Evoy and Fourtner, 1973; Full, 1987; Full and Herreid, 1983, 1984; Full and Weinstein, 1992; Hui, 1992). Using this breadth of knowledge from terrestrial locomotion in crabs may allow us more easily to predict how locomotion will change in an aquatic environment. The particular crab we chose was the Hawaiian intertidal rock crab *Grapsus tenuicrustatus*, a large, fleet-footed pedestrian both under water and on land (Johnson, 1965; Martinez, 1996).

Hypotheses of aquatic pedestrian locomotion

Using results from previous studies of locomotion in simulated reduced gravity (He *et al.* 1991; Kram *et al.* 1997; Margaria and Cavagna, 1964; Newman, 1992; Newman *et al.* 1994) as well as basic fluid-dynamic principles, we propose three hypotheses about the kinematics of animals locomoting under water *versus* on land.

Hypothesis 1: the kinematics of aquatic pedestrian locomotion can be predicted from reduced-gravity models of terrestrial locomotion

Since buoyancy reduces effective weight in water, we hypothesize that, during slow-speed locomotion, to which hydrodynamic forces make very little contribution, the kinematics can be predicted from reduced-gravity models of terrestrial locomotion (Fig. 1).

Like many animals, including humans, crabs locomoting on

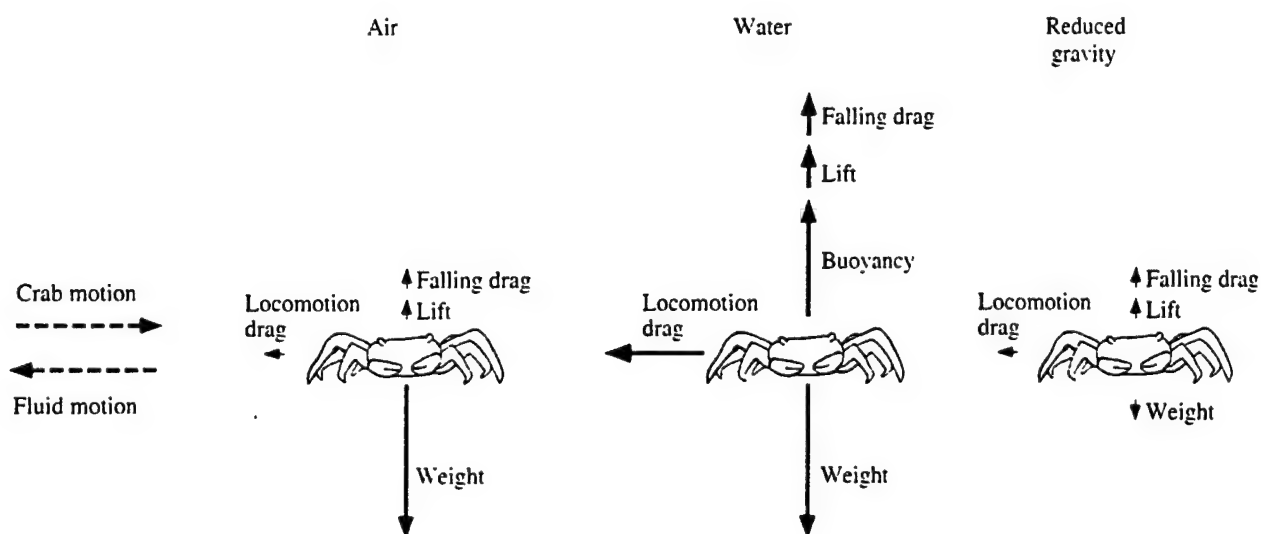


Fig. 1. Comparisons of forces on a crab locomoting in air, in water and under conditions of reduced gravity. In terrestrial pedestrian locomotion, an animal's weight is the predominant force it experiences as it locomotes. In water, buoyant forces can nearly balance gravitational forces, while hydrodynamic drag resists the motion of a body falling towards the substratum between steps. Horizontal locomotion may cause positive hydrodynamic lift on the body, acting at right angles to the direction of locomotion; such lift also supports the weight of the animal. The vertical forces on an animal can be similar in magnitude during aquatic and reduced-gravity pedestrian locomotion.

land at slow speeds use a walking gait, as defined by the inverted-pendulum mechanics of their center of mass (Blickhan and Full, 1987). Maximum exchange between potential and kinetic energy from the inverted-pendulum mechanism occurs when the magnitudes of the potential and kinetic energy fluctuations are equal and the fluctuations occur 180° out of phase with each other. The lower effective weight under water and reduced gravity affect the inverted-pendulum mechanics of pedestrian locomotion in much the same way. The lower effective weight (due to reduced gravity on land or increased buoyancy in water) uncouples the exchange of mechanical energy by reducing the magnitude of fluctuations in potential energy of the body, but not of fluctuations in kinetic energy (Margaria and Cavagna, 1964). This resulting mismatch produces an ineffective pendulum exchange of mechanical energy.

We can make predictions about inverted-pendulum walking using a simple model of dynamic similarity expressed as the Froude number (F) (Alexander, 1989):

$$F = u^2/(gl), \quad (1)$$

where u is the animal's forward speed, g is gravitational acceleration and l is the animal's effective leg length. The Froude number is the ratio of the centrifugal force (pulling the animal off the ground) to the gravitational force (pulling the animal back to the substratum). In theory, when centrifugal force balances or exceeds gravitational force (Froude number ≥ 1), an animal can no longer walk using inverted-pendulum mechanics and switches to a non-walking gait. According to this simple model, a lower effective gravity when in water (due to substantial buoyancy) would cause an animal to change from a walking- to a running-type (bouncing) gait at a lower speed than when in air (if we assume no change in the animal's effective leg length). Since the buoyant force in water decreases the effective gravity on a crab by approximately 10-fold, we expect that, even at the slowest speeds, a crab would use a running-type gait in water, where a running-type gait is defined by spring-mass motion, such as that seen in trotting, galloping and hopping.

Running on land has been successfully modeled as a simple, spring-mass system in a wide diversity of species (Blickhan, 1989; Blickhan and Full, 1993; Cavagna *et al.* 1977; Farley *et al.* 1993; McMahon and Cheng, 1990). The 'leg spring' represents the spring-like characteristics of the entire musculo-skeletal system. The mass is equivalent to body mass, upon which gravity acts. The stiffness of the leg spring is calculated as the ratio of the ground reaction force to the compression of the leg spring when the leg is maximally compressed (Blickhan, 1989). Buoyancy in water counteracts an animal's weight, producing an effect similar to reduced gravitational acceleration on the body mass, thereby decreasing ground reaction forces. Assuming that the stiffness of a crab's leg spring remains the same under water as on land, the spring-mass model predicts that aquatic pedestrians might contact the substratum only briefly and glide more relative to pedestrians on land.

Hypothesis 2: aquatic gaits are less constrained than terrestrial gaits

As gravity pulls an animal towards the substratum, the animal must readjust its legs to ensure support of its body before it falls to the ground. The time available for such an adjustment constrains the footfall patterns and gaits an animal can use while still keeping its body off the substratum. In water, where gravity is effectively less than on land, due to buoyancy, an animal's body is pulled towards the substratum more slowly, allowing more time for the legs to adjust before the animal hits the ground. Falling towards the substratum between steps also generates fluid-dynamic drag on the crab's body acting away from the substratum to support the weight of the animal (Fig. 1). A locomoting crab may even generate fluid-dynamic lift which acts perpendicular to the direction of locomotion. If such lift is positive (i.e. pulling the animal away from the substratum), it will further resist falling. Since drag and lift are proportional to the fluid density, these forces are 800 times greater in water than in air.

The higher buoyancy, drag and lift in water relative to those in air could allow a crab a longer time to fall and, consequently, a longer time to put down a stabilizing foot before its body strikes the substratum. This extra time may allow greater flexibility in the timing and placement of supporting feet during locomotion in water than in air. We therefore predict that a crab can exhibit more variable kinematics in water than in air.

Hypothesis 3: pedestrians adopt a more stable posture in water than in air

A running crab with a given posture incurs a greater risk of overturning in water than on land (Alexander, 1971). An animal will overturn, pivoting about its trailing (i.e. downstream) leg, when the overturning moments about its body exceed the stabilizing moments (Fig. 2). Assuming that all forces act at the center of mass, the overturning moment equals the drag times the vertical distance to the pivot, whereas

MOMENTS

Overturning = drag \times height

Stabilizing = (weight - buoyancy - lift) \times distance to trailing leg

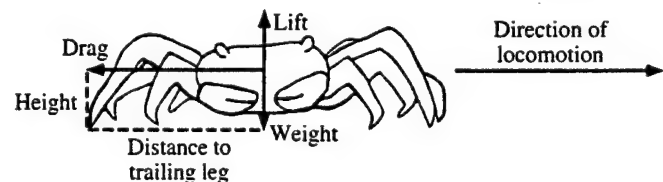


Fig. 2. Stability against overturning. An animal overturns, pivoting about its downstream leg, when the overturning moments about its body exceed the stabilizing moments. The overturning moment is the drag times the vertical distance to the pivot (the height of the carapace above the substratum). The stabilizing moment is the animal's effective weight (weight minus buoyancy minus lift) times the horizontal distance to the pivot (the distance from the center of mass to the trailing leg).

the stabilizing moment equals the animal's effective weight (weight minus buoyancy minus lift) times the horizontal distance to the pivot. Because the density of water is greater than that of air, the overturning moment on a crab locomoting in water is greater (due to higher drag) and the stabilizing moment is lower (due to higher lift and buoyancy) than on a crab in air. We predict that a crab will compensate for the greater likelihood of overturning in water by adopting a more stable posture under water than it uses on land. Crabs may increase the stabilizing moment by adopting a wider stance and may also minimize the overturning moment by adopting a body posture that reduces drag and lift forces on the body.

Materials and methods

Animals

Large male *Grapsus tenuicrustatus* Herbst (carapace width 53 ± 4 mm; mean \pm S.D., $N=6$; mass 74 ± 10 g, $N=6$) were collected along the rocky shore of Coconut Island, Hawaii. Crabs were maintained in seawater tables at ambient temperature ($25.5 \pm 0.5^\circ\text{C}$) and local photoperiod, fed freeze-dried brine shrimp daily and video-taped within 1 week of capture. Only intermolt crabs with a full complement of walking legs and chelipeds were video-taped.

Image capture

Crabs were video-taped as they moved freely along the length of a rectangular arena ($180\text{ cm} \times 40\text{ cm}$) through either air or still sea water. The arena was fitted with a felt substratum to provide adequate traction. The water was 20 cm deep, approximately 14 cm above the height of the crab. Before each trial, water motion in the tank was allowed to settle to the point where it could no longer be visually detected. At the beginning of a trial, crabs were occasionally prodded on the leg with a stiff rod to initiate movement. Trials were video-taped with two SVHS camcorders (Panasonic models PVS770 and PVS62) and one 8 mm camcorder (Sony CCD V9/V90) recording at 60 fields s^{-1} and synchronized with a light-emitting diode. Two camcorders were positioned 35° from horizontal, one at each end of the arena, and the third was positioned directly above the arena (Fig. 3). A calibration frame ($12\text{ cm} \times 6\text{ cm} \times 5\text{ cm}$) with eight non-coplanar control

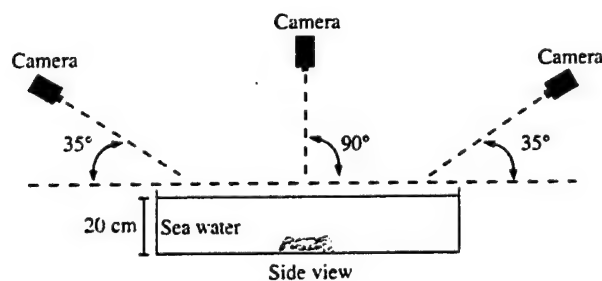


Fig. 3. Diagram of camera positions used to video-tape crabs. The arena ($180\text{ cm} \times 40\text{ cm}$) was filled to a depth of 20 cm with sea water for aquatic trials.

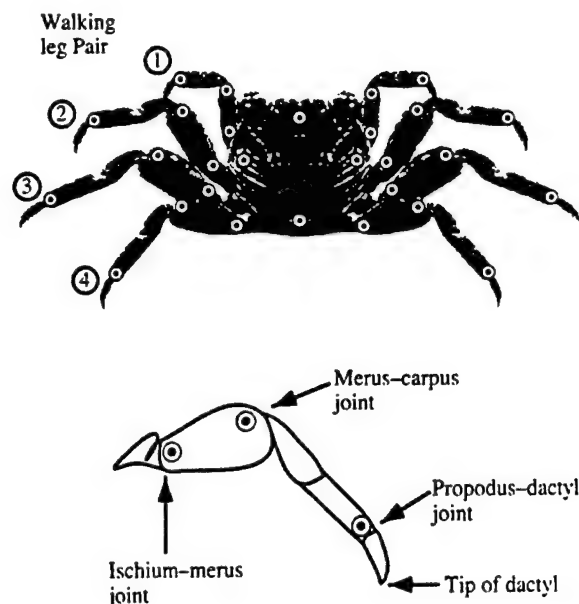


Fig. 4. Location of markers on a crab. Circles indicate points digitized on each crab in three camera views. The tip of the dactyl was also digitized for the first three pairs of walking legs.

points (see Biewener and Full, 1992) was video-taped by all three cameras.

To facilitate digitization of the video recordings, high-contrast white tabs were glued with cyanoacrylate adhesive to the crab's exoskeleton, adjacent to the ischium-merus, merus-carpus and propodus-dactyl joints on the walking legs (Fig. 4). Points on the carapace were marked with white paint (Liquid Paper).

Kinematic analysis

Video images were digitized using a motion analysis system (Peak Performance Technologies, Inc., version 5.0) to obtain three-dimensional coordinates for the marked points on the legs and carapace as well as the dactyl tips (Biewener and Full, 1992). As our coordinate system convention, we designated positive values of x as the direction of motion (lateral for a sideways-moving crab; Fig. 5). The resolution of the video images averaged 0.86 mm per pixel. Points in space could be located with mean squared errors of 0.083 mm, 0.098 mm and 0.114 mm for the x , y and z directions, respectively, yielding a 0.178 mm mean squared error for position. Data were filtered using a low-pass, fourth-order, zero-phase-shift Butterworth digital filter with a cut-off frequency of 10 Hz, a frequency that caused little signal distortion and allowed minimal noise to pass according to a residual analysis (see Biewener and Full, 1992). Filters below 8 Hz added signal distortion, whereas a 12 Hz filter included significant noise. Data from all camera views were filtered before direct linear transformation to three-dimensional coordinates.

Stride definition

A stride is conventionally defined as the complete motion

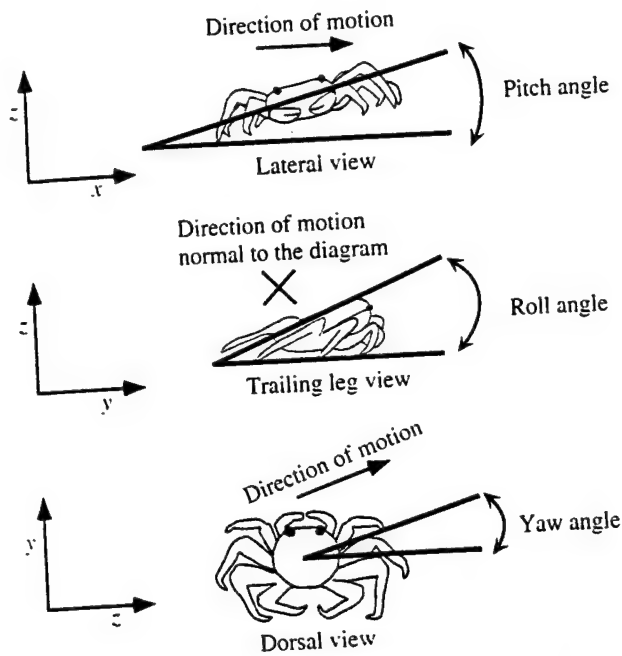


Fig. 5. Coordinate axes and carapace angles defined for a sideways-moving crab. In the trailing leg view, X indicates motion into the page.

cycle of a leg, within which all legs cycle with the same mean frequency. During aquatic locomotion, *G. tenuicrustatus* often cycled different pairs of legs at different rates, with some legs not cycling at all in the time examined. This variability during aquatic locomotion made the application of the conventional definition of a stride impossible. To compare cycles across different legs, we analyzed a complete cycle for legs that cycled throughout the period examined. The time period examined (approximately 2 s) was determined by the length of time that a crab stayed in the view of all three cameras. We defined the maximum stride period to be the longest time period taken by any individual leg to complete one cycle within the sampling period. If a leg did not cycle, it was not analyzed. Likewise, if a leg cycled more than once during that time, each cycle was analyzed and the data for that leg were averaged. A leg was said to cycle completely if it had a period of ground contact associated with protraction and retraction of the leg. The reference point used to determine the start of a cycle was either the beginning or the end of ground contact, whichever occurred first in that trial, for a particular leg. This operational definition of a stride did not bias our results for stride variables (e.g. stride length, duty factor and merus-carpus angle, defined below) because these variables were also analyzed for each individual leg cycle for all legs cycling within the maximum stride period. Defining the maximum stride period with respect to the longest observed leg cycle rather than with respect to the shortest leg cycle allowed inclusion of the greatest number of cycling legs in the time interval examined.

The animals moved at a mean velocity of $9.7 \pm 0.7 \text{ cm s}^{-1}$ (mean \pm S.D., $N=15$) in air and $11.4 \pm 2.0 \text{ cm s}^{-1}$ ($N=15$) under water, so we chose matched air and water trials at a velocity of $9 \pm 2 \text{ cm s}^{-1}$ for each of six individuals. One maximum stride

from each of these trials was analyzed, comparing each animal with itself in water versus in air. Of the two pairs of walking legs that cycled most consistently across trials, the first pair of walking legs showed the least variance in leg stride period (F -test of equal variance, $N=10$, $P=0.005$). To analyze a consistent number of fields across trials, we digitized 25 fields of the leg with the shortest leg stride period. Since the first pair of walking legs exhibited the shortest leg stride period of the four pairs of legs, expressing our sampling rate with respect to this leg pair yielded the largest consistent number of samples per maximum stride period. A comparison with 60 Hz sampling demonstrated that our sampling regime did not result in significantly different positions, angles or velocities. Chelipeds were not included in this analysis because *Grapsus tenuicrustatus*, unlike some other species (e.g. Sleinin and Silvey, 1980), were not observed to use them during locomotion.

Velocity and stride parameters

Instantaneous forward velocities were calculated by motion analysis software, using a fourth-order central difference algorithm (Biewener and Full, 1992), and were averaged over the trial. These mean velocities were consistent with independent calculations from times to traverse a known distance. For analysis, we chose only constant mean velocity trials in which the sum of increases and decreases in velocity was within 5% of the animal's mean velocity. For each cycling leg throughout the sampling period, stride length was determined from the distance traversed by the tip of a dactyl between successive periods of ground contact. A period of ground contact was defined as a time when a dactyl tip contacted the substratum (as determined from its z -axis coordinates) and did not move relative to the substratum (as determined from its x - and y -axis coordinates). There were no instances of dactyl slippage on the felt substratum. Leg stride period was taken as the time elapsed between successive beginnings or endings of ground contact, with stride frequency then calculated as the inverse of the stride period. Duty factors were calculated as the percentage of a cycle that a dactyl was in contact with the substratum, i.e. the contact time divided by that leg's stride period.

Because individuals almost always cycled more than one leg during a trial, we calculated the mean and variance of stride length, stride period and duty factor for each individual using all cycling legs. Using the mean and variance computed for each individual, we calculated group means and variances in air versus water. We compared means in air versus water using a Wilcoxon signed-rank test (the nonparametric equivalent of a paired t -test). Since we hypothesized that reduced gravity could remove the requirement for precise and regular leg movement, we also compared variances in air versus water using an F -test of equal variance. Statistical tests were performed using a statistical program (Statview 4.0 on a Power Macintosh).

Distance and angle measurements

For use in estimating overturning moments, we calculated

height at the center of the carapace (midway between the anterior and posterior digitized points on the carapace; Fig. 4) and the width of the stance between contralateral leg pairs using three-dimensional coordinates from the motion analysis software. We calculated maximum stance width as the greatest distance between the tips of the dactyls of any contralateral leg pair, regardless of ground contact, over the maximum stride period. We determined mean, maximum and minimum merus–carpus joint angles (Fig. 4) for every leg over a maximum stride period. We then calculated the means of each of these merus–carpus angles for each individual crab. In addition we determined pitch, roll and yaw angles of the carapace (Fig. 5). For a sideways-moving crab, pitch refers to rotation about the anterior–posterior axis of the carapace and roll refers to rotation about the lateral axis. Yaw is the angle between the lateral axis of the crab and the direction in which the animal moves.

Footfall pattern

Footfall patterns were determined from field-by-field analysis of video tapes by noting times of touch-down and lift-off of the dactyl for each walking leg throughout the stride analyzed. The total number of legs in contact with the substratum was determined for each video field. Over the course of the sampling period, the horizontal trajectories of each dactyl relative to the body determined the actual workspaces for each leg, in comparison with the potential workspaces (the area through which a leg could potentially swing, as determined by tracing the range of ground contact that the leg could achieve through maximum extension of all joints while the carapace is at the minimum height observed

during locomotion). Within these actual workspaces, the lateral and anterior–posterior excursion distances were quantified for each leg. In a sideways-moving crab, anterior–posterior excursion refers to the anterior–posterior axis of the animal, which (in the case of 0° yaw) is perpendicular to the direction of motion. Similarly, lateral refers to the lateral axis of the animal, parallel to the line of motion for a sideways-moving crab at 0° yaw. Workspace data for leading and trailing legs were analyzed separately, using Wilcoxon signed-rank tests. To determine the position of the crab's dactyls within the workspace, we compared the crab's lateral with its anterior–posterior stance width.

Whereas stride frequency, stride length, duty factor and contact time were analyzed only on legs that cycled completely, workspaces and stance width were measured without regard to cycling or ground contact, because a leg close to the ground can still provide timely support to a perturbed animal. Conversely, measures such as duty factor and contact time involve interactions with the substratum since they relate to propulsion.

Results

Buoyancy

The effective weight of *Grapsus tenuicrustatus* submerged in sea water (salinity 0.33 ‰) was only one-tenth of its weight in air. Subtracting each crab's submerged weight (0.073 ± 0.023 N, mean \pm S.D., $N=6$) from its weight in air (0.73 ± 0.097 N, $N=6$) yielded its buoyant force (0.65 ± 0.082 N, $N=6$) in sea water. *G. tenuicrustatus* had a specific gravity of 1.13 ± 0.035 ($N=6$).

Table 1. Kinematic variables in air versus water

	Air	Water	P
Speed (m s^{-1})	0.097 ± 0.007	0.114 ± 0.02	0.11 (0.50)
Stride length (m)			
Leg with maximum stride period	0.094 ± 0.02	0.088 ± 0.04	0.60 (0.09)
All legs	0.076 ± 0.0089	0.084 ± 0.0043	0.17 (0.80)
Stride frequency (Hz)			
Leg with maximum stride period	0.97 ± 0.14	1.19 ± 0.49	0.46 (0.008)
All legs	1.17 ± 0.150	1.13 ± 0.222	0.75 (0.40)
Stride period (s)			
Leg with maximum stride period	1.05 ± 0.163	0.94 ± 0.315	0.35 (0.09)
All legs	0.90 ± 0.097	0.98 ± 0.122	0.17 (0.63)
Contact time (s)			
Leg with maximum stride period	0.65 ± 0.196	0.39 ± 0.238	0.12 (0.34)
All legs	0.52 ± 0.047	0.37 ± 0.087	0.03 (0.20)
Duty factor			
Leg with maximum stride period	0.61 ± 0.102	0.40 ± 0.164	0.12 (0.16)
All legs	0.57 ± 0.021	0.38 ± 0.080	0.03 (0.01)

Values are means \pm one standard deviation; for P, values are for the means with P values for variances in parentheses.

$P < 0.05$ indicates a significant difference between water and air.

$N=6$ crabs except for speed, where $N=15$ crabs.

Table 2. Kinematic variables of leading versus trailing legs in air and in water

	Leading legs		Trailing legs	
	Air	Water	Air	Water
Stride length (m)	0.079±0.012	0.090±0.017	0.072±0.010	0.073±0.015†
Stride frequency (Hz)	1.11±0.206	1.08±0.154	1.23±0.192	1.28±0.331
Stride period (s)	0.94±0.144	1.00±0.109	0.87±0.112	0.87±0.184†
Contact time(s)	0.53±0.074	0.43±0.092	0.51±0.049	0.28±0.08†*
Duty factor	0.561±0.022	0.41±0.102	0.58±0.028	0.33±0.095*

Values are means ± one standard deviation; N=6 crabs.

† indicates a significant difference between leading and trailing legs for a given medium.

* indicates a significant difference between air and water for a given set of legs.

Kinematics

Rather than using an alternating tetrapod or metachronal gait, as seen on land, crabs in water usually pushed or pulled with only a few legs, occasionally cycling one leg several times before using a different leg. Thus, in water, the animals often cycled adjacent legs or even leading and trailing legs of the same pair at different rates, with some legs not cycling at all throughout the period examined. There were several instances (12 in water, one in air) where only one leg of a contralateral pair cycled completely during the maximum stride period, and several cases (eight in water, none in air) where neither leg of a contralateral pair cycled.

Stride period, frequency and length

During the maximum stride period, neither stride length nor stride period was significantly different between water and air trials (Table 1). Mean stride frequency was not significantly different between water and air trials during the maximum stride period (Table 1), although stride frequency was more variable in water than in air. Neither means nor variances of leg stride frequency, period or length were significantly different in water *versus* air for all cycling legs (Table 1). In water, leading legs had greater stride lengths and stride periods than trailing legs (Table 2). Leading legs did not show more variable kinematics than trailing legs (Table 2).

Contact time and duty factor

Mean leg contact times and duty factors in water were nearly half the values in air for all the legs that cycled completely. Contact time was also significantly lower in water, but was not more variable than in air (Table 1). Contact times for maximum stride periods did not differ in air *versus* water owing to large variations in both values. Duty factors were significantly lower and more variable in water than in air for all legs, but not for the legs with the longest stride periods (Table 1). In water, trailing legs had shorter contact times than leading legs (Table 2). Trailing legs in water also had shorter contact times and duty factors than trailing legs in air (Table 2).

Footfall pattern and leg cycling

Rather than an alternating tetrapod or metachronal gait,

crabs locomoting under water used a gait we shall call 'underwater punting,' characterized by alternating phases of gliding and thrust generation. Crabs moving under water had, on average, two fewer legs in contact with the substratum at any point in time than did animals moving on land (Table 3). On land, crabs almost never had fewer than three legs in contact with the ground at any time, whereas in water, they commonly had only one leg in contact with the substratum. We defined 'gliding' as the period when a crab did not have its center of mass surrounded by a tripod of supporting legs in contact with the substratum. Crabs moving on land virtually never glided (one crab for 0.03 s, which was 0.6 % of the mean maximum stride period), whereas four of the six crabs moving under water glided for a significant percentage of the maximum stride period ($57 \pm 27.6\%$, mean \pm s.d., $N=4$). One water trial included an 'aerial' period of 0.07 s, during which no legs contacted the substratum.

Water trials were characterized by a much more variable footfall pattern than air trials (Fig. 6). The number of legs cycling completely was significantly fewer and more variable in water than in air (Table 3), with four fewer legs cycling on average in water trials. In one of the water trials, only one leg cycled through the maximum stride period, whereas in air there was only one incident of a leg not cycling completely through the maximum stride period.

Leg stance and workspaces

Crabs adopted a wider stance in water than in air. The maximum lateral stance width in water was on average 1.2

Table 3. Leg participation in air versus water

	Air	Water	P
Number of dactyls in contact with ground	4.8±0.4	2.5±0.5	<0.001 (0.34)
Number of legs cycling through stride	7.8±0.4	4.2±1.6	0.028 (0.005)

Values are means ± one standard deviation; for *P*, values are for the means with *P* values for variances in parentheses.

$P < 0.05$ indicates a significant difference between water and air.

N=6 crabs.

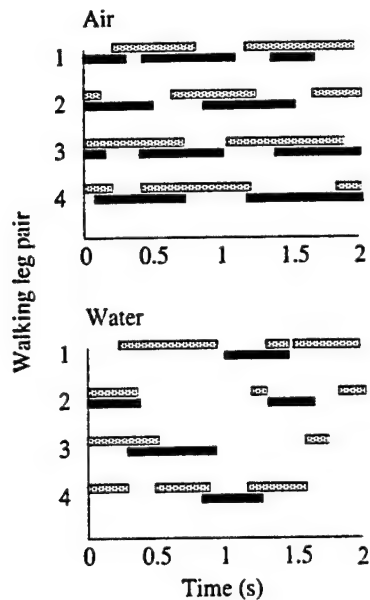


Fig. 6. Representative footfall patterns in air and water for each pair of walking legs plotted as a function of time. Bars represent times when the dactyls were in contact with the substratum. Leading legs (filled bars) and trailing legs (stippled bars) of each walking leg pair are plotted adjacent to one another. Footfall patterns illustrate that a crab locomoting under water showed greater gait variability and fewer legs in ground contact at any time than did a crab locomoting in air.

times that in air, with every individual adopting a greater stance width in water than in air (Table 4; Fig. 7). In fact, the narrowest lateral stance adopted by each crab in water did not differ from the widest stance adopted in air (paired *t*-test, $N=6$, $P=0.27$). In contrast, the maximum anterior-posterior stance width in water was not significantly different from that in air (Table 4). Carapace height was also not different between water and air trials (Table 4).

Dactyl movement within the workspaces differed between air and water trials. The actual workspaces used by the crabs (the two-dimensional horizontal trajectory followed by the dactyls) were very much smaller than the potential workspaces

Table 4. Stance width and carapace height in air versus water

Distance (m)	Air	Water	<i>P</i>
Stance width			
Anterior-posterior position	0.092±0.013	0.085±0.012	0.12 (0.78)
Lateral position	0.164±0.006	0.198±0.006	0.028 (0.90)
Carapace height	0.044±0.004	0.037±0.012	0.12 (0.02)

Values are means ± one standard deviation; for *P*, values are for the means with *P* values for variances in parentheses.

$P<0.05$ indicates a significant difference between water and air.

$N=6$ crabs.

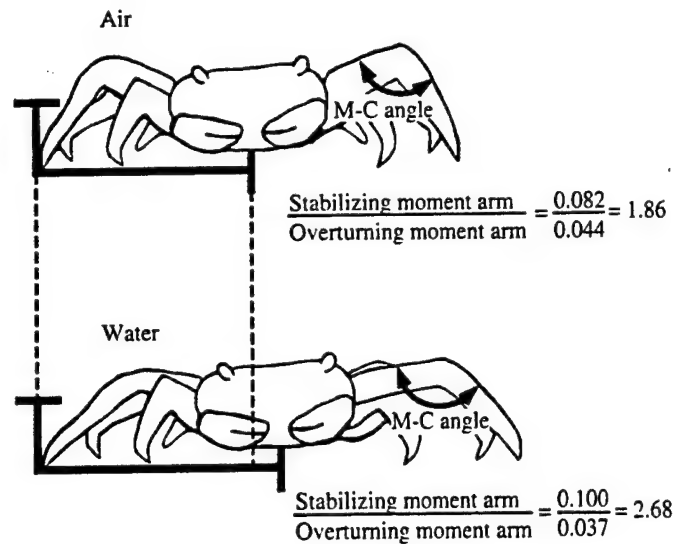


Fig. 7. Moment arms in air and water. Compared with crabs in air, those in water increased the distance between the center of mass and the trailing leg by increasing the merus-carpus (M-C) joint angle (Table 6). The ratio of mean stabilizing to mean overturning moment arms was greater for water postures than for air postures (data from Table 4).

(the range of motion through which dactyls could possibly move; Fig. 8). To compare the motion of a crab's dactyls relative to its body, we measured the excursions of the dactyls within their workspace along the anterior-posterior and lateral axes of the crab (Table 5; Fig. 8). The workspaces did not differ between the leading and trailing legs in either air or water trials. Water trials showed more variability than air trials in all directions except the lateral excursion of the leading leg (Table 5). The shape of the excursions differed noticeably between air and water trials. In air, the crabs used larger lateral excursions than anterior-posterior excursions for both leading and trailing legs (Table 5); in water, the lateral and anterior-posterior

Table 5. Leg excursions in air versus water

Excursions (m)	Air	Water	<i>P</i>
Anterior-posterior			
Leading	0.0156±0.0033	0.0219±0.0094	0.12 (0.02)
Trailing	0.0145±0.0031	0.0174±0.0093	0.6 (0.016)
Lateral			
Leading	0.0370±0.0050	0.0243±0.0075	0.03 (0.2)
Trailing	0.0356±0.0023	0.0181±0.0058	0.03 (0.03)

Values are means ± one standard deviation; for *P*, values are for the means with *P* values for variances in parentheses.

$P<0.05$ indicates a significant difference between water and air.

$N=6$ crabs.

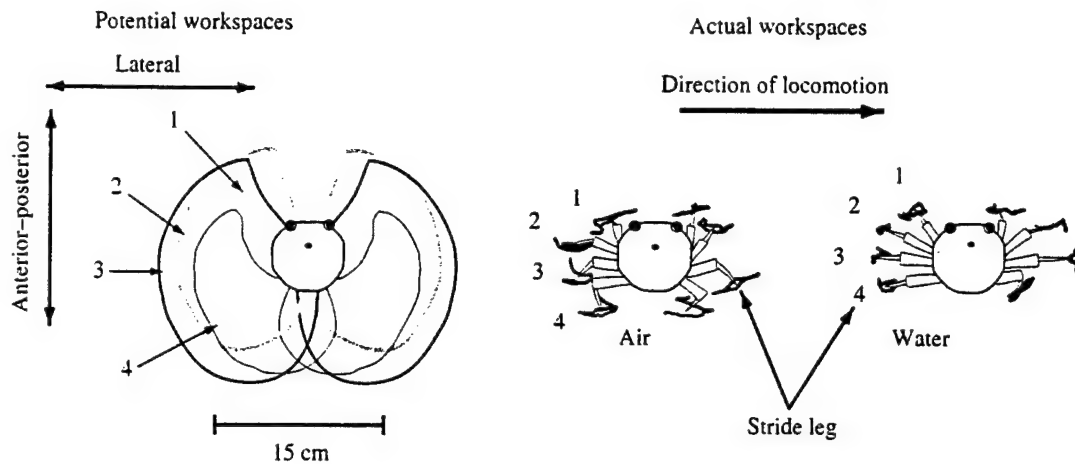


Fig. 8. Potential and actual workspaces. Potential workspaces show the range of motion possible for crab dactyls. Relative shading indicates the potential workspaces that each limb can achieve. Numbers denote the leg pairs corresponding to each of the workspaces. Actual workspaces are for the air and water trials of the same animal moving at 9 cm s^{-1} for one maximum stride period. Leg movements are shown relative to the stationary dot on the crab's carapace. These workspaces showed that most of the legs in water had smaller lateral excursions than on land. Crabs had a greater stance width when locomoting in water than in air.

excursions did not differ from each other. Crabs used smaller lateral excursions in water than they did in air (Table 5).

Joint angles and limb protraction

Mean, maximum and minimum merus–carpus angles were all greater and more variable in water trials than in air trials (Table 6; Fig. 7). Although crabs in water used greater absolute merus–carpus angles, they swept through a smaller range of angles than they did in air. The maximum and mean velocities achieved by a dactyl during its swing phase were significantly slower in water than on land for all four leg pairs (paired *t*-test, $N=4$, $P=0.00007$ for maximum velocity, $P=0.02$ for mean velocity).

Carapace angles

Mean pitch and roll angles did not differ between water and air trials (Table 7). Whereas variation about the mean angle from a given trial did not differ between air and water,

variation about the group mean angle for all trials was greater in water than in air (Table 7). The roll angles were much greater than the pitch angles. Crabs never achieved negative pitch or roll angles. Yaw angles did not differ between air and water trials and were evenly split between positive and negative values. Mean yaw angles were very small relative to pitch and roll angles.

Discussion

Hypothesis 1: the kinematics of aquatic pedestrian locomotion can be predicted from reduced-gravity models of terrestrial locomotion

Reduced-gravity models of locomotion on land provide a framework within which aquatic pedestrian locomotion can begin to be explained (Fig. 1). On the basis of simple inverted-pendulum and spring-mass models (Alexander, 1989; Blickhan, 1989; McMahon and Cheng, 1990), we predicted that *Grapsus tenuicrustatus* would use a running-type gait in water, even at its slowest speeds. While crabs in water did

Table 6. Merus–carpus angles in air versus water

Angle (degrees)	Air	Water	<i>P</i>
Mean	93±4	105±13	0.027 (0.007)
Maximum	119±4	127±11	0.046 (0.033)
Minimum	68±4	82±14	0.027 (0.007)
Range	51±4	45±5	0.027 (0.44)

Values are means ± one standard deviation; for *P*, values are for the means with *P* values for variances in parentheses.

$P<0.05$ indicates a significant difference between water and air.
 $N=6$ crabs.

Table 7. Pitch, yaw and roll angles in air versus water

Angle (degrees)	Air	Water	<i>P</i>
Pitch	3±2	10±10	0.12 (<0.001)
Yaw	1±5	2±7	0.75 (0.20)
Roll	30±5	37±9	0.07 (0.11)

Values are means ± one standard deviation; for *P*, values are for the means with *P* values for variances in parentheses.

$P<0.05$ indicates a significant difference between water and air.
 $N=6$ crabs.

exhibit the expected shorter contact times and duty factors (Table 1), the contact time was so brief and the kinematics so variable (Tables 2–5) that we argue that these crabs were not running, but were using a fundamentally different mode of locomotion, a gait we call ‘underwater punting’. The person operating a punt generates thrust by pushing on the river bottom with a pole, allowing the punt to glide before the next push.

At the slow speeds used by crabs during this study, *Grapsus tenuicrustatus* operated at Froude numbers that suggest that they can walk on land but are unlikely to walk under water. Crabs appeared to pivot primarily about their merus–carpus joints both on land and in water. Using the height of this merus–carpus joint as the effective leg length (air, 0.03 ± 0.003 m, mean \pm S.D., $N=6$; water, 0.02 ± 0.005 m, $N=6$) and incorporating a factor of 1/10 into the gravity term to account for buoyant force under water, we calculate a terrestrial Froude number of 0.027 and an aquatic Froude number of 0.41 for *G. tenuicrustatus* at 9 cm s^{-1} . In water, *G. tenuicrustatus* operate in the range of Froude numbers for which animals usually make a transition from a walking (i.e. inverted-pendulum) to a running (i.e. spring-mass) gait. Mammals and birds switch from a walk to a run at a Froude number of approximately 0.5 (e.g. Alexander, 1989; Gatesy and Biewener, 1991), a value only slightly higher than the aquatic Froude number we calculate for *G. tenuicrustatus*. Crabs in air change gait at the same stride frequency and speed as quadrupedal mammals (Blickhan and Full, 1987). Furthermore, Kram *et al.* (1997) have demonstrated that, even in reduced gravity, humans still prefer to change from a walk to a run at a mean Froude number of 0.45. Therefore, dynamic similarity suggests that crabs would probably not use inverted-pendulum mechanics in water at these speeds. The effective weight reduction in water appears to have forced the crabs at low speeds to adopt a gait more akin to running than to walking. Short contact times, low duty factors (Table 1), a reduction in the number of legs participating in propulsion (Table 3), longer gliding phases and the presence of an aerial phase in *G. tenuicrustatus* are all consistent with the use of a running gait under water at slow speeds. Ghost crabs show these same kinematic changes when running in air at very high speeds (Blickhan and Full, 1987; Burrows and Hoyle, 1973).

Changes in several significant kinematic variables associated with the air-to-water transition are predicted from running or spring-mass models subjected to reduced gravity. Let us assume that weight is reduced by 10-fold and leg spring stiffness does not change. In the mammals measured thus far, leg spring stiffness remains surprisingly constant over a range of speeds (McMahon and Cheng, 1990; Farley *et al.* 1993). Furthermore, leg spring stiffness in humans does not change as gravity is reduced in air (He *et al.* 1991). It has been predicted that, if the spring-mass system is to maintain its velocity and remain stable or re-entrant (i.e. similar initial conditions at landing and take-off) in reduced-gravity conditions, then the landing angle of the leg spring must increase (producing a more vertically orientated leg spring at

ground contact; Cavanga *et al.* 1972). Contact time and duty factor are reduced as the system is only briefly in contact the substratum. The reduced downward force decreases leg spring compression and the oscillation of the center of mass, thus giving the appearance of gliding. The reduction in weight decreases the vertical support forces required, which could then be produced by fewer or different legs than under higher loads.

Actual data on humans running in a reduced-gravity apparatus (He *et al.* 1991; Margaria and Cavagna, 1964) or under water (Newman, 1992; Newman *et al.* 1994) are consistent with some of these predictions. Gait transitions occur at lower speeds in reduced gravity compared with normal gravity (Kram *et al.* 1997). Duty factor always appears to decrease as effective weight is reduced. However, contact times, which are predicted to decrease as gravity is reduced, actually change very little (He *et al.* 1991).

While crabs locomoting in water made many of the same kinematic adjustments predicted from or measured in reduced-gravity studies, their aquatic kinematics were sufficiently different from those of running that we thought the aquatic pedestrian locomotion of this crab should be considered to be a new type of legged locomotion (‘underwater punting’). The exceptional variability allowed in this mode of locomotion prevents us from analyzing it in the same way that we would analyze regularly cycling gaits. In more typical rhythmic gaits, kinematic changes occur within each and every leg cycle. In contrast, leg cycling by this aquatic pedestrian crab can best be characterized as intermittent. We attempted to address this intermittency by determining both the kinematics of individual legs, while they were cycling, and of an overall stride represented by the leg with the maximum stride period (Table 1). Even this attempt failed to produce stride frequency and period data similar to those from studies on reduced-gravity running. When humans run in reduced gravity, they use lower stride frequencies and duty factors, but longer stride lengths, than they do in normal gravity (He *et al.* 1991; Newman, 1992). In contrast, punting crabs did not use significantly longer stride lengths or stride periods than they used on land (Table 1). We found no differences in stride length or frequency between water and air trials, in part because this novel mode of aquatic locomotion does not employ regular cycles of leg motion (Table 3). Rather than having longer leg stride periods, crabs in water used intermittent leg cycling, making use of longer ‘gliding’ times between cycles. A change from regimented leg cycling on land to intermittent leg cycling in water might produce the same dynamic effect as changes in leg stride length and period, but this possibility must be tested by measuring the forces acting on the center of mass. The irregularity of limb support and thrust generation might be understood in terms of controlling the motions of the body, but attempts to correlate ground contact with changes in pitch, roll and yaw of the body did not yield discernible patterns. A follow-up study of single-leg force production and dynamic stability is necessary to link leg function with whole-body dynamics.

Leg kinematics can also affect the hydrodynamic forces experienced by a leg. In the present study, crab legs moved more slowly in water (maximum dactyl velocity for leg pair 3 was 0.16 m s^{-1}) than in air (maximum dactyl velocity for leg pair 3 was 0.34 m s^{-1}) due to longer swing periods and gliding times. Since drag is proportional to the square of velocity, the 47% decrease in maximum velocity of a leg results in a 78% decrease in the drag on that leg in water relative to the drag that leg would experience if it moved at speeds characteristic of terrestrial kinematics.

Kinematic comparisons among aquatic pedestrian data in the literature are difficult because a common set of relevant mechanical variables is lacking. Crustacean pedestrians appear to adopt diverse strategies for locomoting under water, as shown by the varied findings of the few studies that contrast aquatic and terrestrial locomotion (Clarac *et al.* 1987; Grote, 1981; Hui, 1992; Pond, 1975). Whereas Grote (1981), Pond (1975) and Clarac *et al.* (1987) report differences in stride frequency between aquatic and terrestrial pedestrian locomotion, neither Hui (1992) nor the present study found significant differences. Grote (1981) and Pond (1975) found both increased stride length and increased stride frequency under water in forward-moving crayfish. Since both of these variables increased in concert, the animals necessarily moved at faster speeds in water than on land. In fact, Pond (1975) reported speeds in water twice as fast as speeds on land. Since both stride length and stride frequency can change as a function of speed (Blickhan and Full, 1987; Chasserat and Clarac, 1983), Pond's (1975) data do not allow us to determine which kinematic changes are due to a change in medium and which are due to a change in speed. Clarac *et al.* (1987) also found an increased stride frequency under water for sideways-moving crabs, but did not report stride lengths or locomotor speeds, so it is again impossible to know whether the increased stride frequency in water was due to a change in medium or in speed. Even though Hui (1992) found no differences in stride length or frequency in sideways-moving shore crabs in water *versus* in air, the data compare non-overlapping speed ranges or a large range of speeds. The Froude numbers for the shore crabs locomoting under water range from 0.02 to 0.76, calculated using a leg length of 0.015 m and an effective gravity of 20% normal gravity, based on buoyancy measurements from Hui (1992). These calculations show that aquatic data from Hui (1992) span the normal transition Froude number range, suggesting that this study may have included both walking and running gaits within one data set.

Despite the fact that the speed of locomotion has not always been controlled in the measurement of duty factor, all the studies of crayfish and crab locomotion under water *versus* on land, including the present study, report decreased duty factors or power stroke durations in water relative to those in air. Even electromyographic burst durations in shore crabs are shorter and the number of motor neurons activated is smaller during locomotion under water than on land (Clarac *et al.* 1987). While duty factor does change with speed, it is likely to be affected more strongly by a change in medium than by a

change in speed. Data on humans show that, while duty factor decreases with increasing speed, a reduction in gravity produces a larger decrease in duty factor than does an increase in speed (He *et al.* 1991; Donelan and Kram, 1997; Donelan *et al.* 1997). The effect of speed on duty factor is also not as great as the effect of speed on stride period in reduced-gravity studies (He *et al.* 1991). Thus, even though previous studies did not control for speed (Grote, 1981; Pond, 1975; Hui, 1992; Clarac *et al.* 1987), the lower duty factors reported for locomotion in water *versus* on land are likely to be, at least in part, a true effect of changing medium. The inability to detect a speed effect on duty factor in the shore crab *Pachygrapsus crassipes* (Hui, 1992) might be explained by a relatively weak relationship between duty factor and speed in the lower speed ranges as well as by the difficulty of assessing ground contact from only a top view of a crab that moves its dactyls underneath its body.

Sideways locomotion adds further to the challenge of kinematic comparisons because leading and trailing legs can adopt different roles with respect to sensing and propulsion. Primarily on the basis of their more variable kinematics, leading legs are often said to play a sensory role in arthropods (Full, 1997). Variable kinematics in the absence of ground reaction forces and electromyograms, however, leaves leg function less certain. Using electromyographic recordings, Clarac *et al.* (1987) found that the steps of the leading leg of the crab *Carcinus maenas* were more variable and longer in duration than those of the trailing legs both in water and on land. In water, *G. tenuicrustatus* showed a similar trend of longer stride periods and contact times in leading legs relative to trailing legs, but neither the contact time nor the stride period of the leading legs was more variable than in the trailing legs (Table 2). Whether the leading legs actually perform more or less of a sensory role in punting gaits is unknown. In air, *G. tenuicrustatus* showed no kinematic differences between leading and trailing legs (Table 2). Leading and trailing legs may also differ in their propulsive roles. At slow speeds in air, crabs can push with trailing legs or pull with leading legs (Blickhan and Full, 1987; Libersat *et al.* 1987). Burrows and Hoyle (1973) found that, at high speeds, ghost crabs in air use only two trailing legs alternately to generate force, while the leading legs act as skids. Clarac *et al.* (1987) concluded that electromyographic data provide more evidence for pushing propulsion with trailing legs. The present kinematic study showed that *G. tenuicrustatus* may use both the leading and trailing legs for propulsion in air and water. In water, however, crabs may be generating force over shorter periods with the trailing legs than with the leading legs, as suggested by the decreased stride length, stride period and contact time in trailing legs relative to leading legs (Table 2).

Furthermore, the leading and trailing legs could play different roles during locomotion in air *versus* water. Hui (1992) reported greater duty factors for trailing legs than leading legs in water, proposing that *Pachygrapsus crassipes* has to push harder to locomote in water over both rocky and smooth substrata. By contrast, *G. tenuicrustatus* had

significantly lower trailing leg duty factors in water than in air (Table 2). Perhaps as a manifestation of the kinematic variability permitted by lower effective gravity, the trailing legs require only brief periods to generate force effectively at slow speeds in water. Data from the crab *Carcinus maenas* show no effect of air *versus* water on leading *versus* trailing leg function (Clarac *et al.* 1987). Obviously, it is important to remember that kinematic data alone are insufficient to determine leg function. Direct measurements of individual leg ground reaction forces along with electromyograms are required to define a leg's role and will be our next focus.

In summary, data from previous studies clearly demonstrate that differences exist between aquatic and terrestrial pedestrian locomotion, but leave the nature of these differences unresolved. While the pioneering studies (Grote, 1981; Pond, 1975; Hui, 1992; Clarac *et al.* 1987) provided important first steps in exploring the differences between aquatic and terrestrial locomotion, the extreme variability in the variables measured thus far compel us to undertake a complete three-dimensional dynamic analysis of locomotion that includes kinematics, ground reaction forces and fluid-dynamic forces.

Hypothesis 2: aquatic gaits are less constrained than terrestrial gaits

Variability in the gaits of aquatic pedestrians has made the synthesis of general motor control principles challenging (Clarac, 1981; Full, 1997). Clarac (1981) reported that steps in crustaceans are incomplete or repeated 25% of the time. Data on crayfish reveal that inter-leg coupling varies depending on the conditions (i.e. treadmill *versus* free walking), the individual studied and the trial examined (Clarac and Barnes, 1985). A wide variety of gait patterns appear to be used even within a single locomotory bout of a given individual (Clarac and Barnes, 1985; Jamon and Clarac, 1995).

The slow-speed aquatic gaits of *G. tenuicrustatus* in the present study appeared so unconstrained that they do not conform to any traditionally recognized mode of locomotion. In water, compared with on land, the reduction in support force necessary and the increased recovery time from any instability, in addition to the large number of legs available for propulsion or correction, result in a redundant system in which no single kinematic solution should be expected. Even bipedal Apollo astronauts moving on the moon in one-sixth of the Earth's gravity freely chose new and different gaits (described by Jones, 1995). The inconsistent leg participation in thrust generation noted by Hui (1992) and demonstrated here (Table 3), together with extreme variability in leg kinematics, prompt us to consider underwater punting as a new mode of locomotion. Many kinematic variables of *G. tenuicrustatus*, including duty factor (Table 1), lateral and anterior-posterior excursion distance (Table 5), merus-carpus angle (Table 6) and pitch angle (Table 7) exhibited greater variability under water than on land. Greater variability in the number of legs cycling, the number of legs in the support phase (Table 3) and the overall footfall patterns (Fig. 6) can be tolerated during locomotion under water because animals unsupported by legs

fall to the substratum more slowly in water than they do in air. The relaxation of gravitational constraints on kinematics in water permits the use of gaits that are unavailable to animals locomoting in air at the slow speeds used by these crabs.

The combined effects of increased buoyancy in water and sideways locomotion may suspend the need even for the more tightly coupled ipsilateral leg coordination seen in aquatic walking by some crayfish and lobsters (e.g. Clarac, 1984; Jamon and Clarac, 1995; Muller and Cruse, 1991). While buoyancy decreases the requirement for more continuous vertical support, sideways motion allows the legs to move independently without physically interfering with other ipsilateral legs. Even though crayfish and lobsters have a specific gravity similar to that of crabs (e.g. the specific gravity of the crayfish *Procambarus clarkii* is 1.07; Grote, 1981) and hence similar buoyant forces, the lateral position of the legs on a forward-locomoting crayfish or lobster may prevent it from using a punting gait because asymmetric propulsion from contralateral legs would subject a forward-moving animal to large roll and yaw moments. Likewise, a forward-moving crab is unlikely to punt because the further a thrust-generating leg is from the axis of locomotion, the greater the moments it will generate about the center of mass.

Hypothesis 3: pedestrians adopt a more stable posture in water than in air

Although *G. tenuicrustatus* did not use a significantly lower body height under water, they did adopt a wider, more stable stance (Table 4). Crabs achieved this wider stance by using greater merus-carpus angles in water than they did on land (Table 6; Fig. 7). A wider stance stabilizes the crabs against overturning by hydrodynamic forces due to locomotion or to ambient water currents by increasing the moment arm over which the weight acts (Fig. 2). For example, an increase in stance width from 16 to 20 cm (increasing MA_s by 2 cm) translates directly into a 25% increase in the drag force (D) a crab could withstand before overturning, calculated from Alexander (1971):

$$D = F_v \frac{MA_s}{MA_o} \quad (2)$$

where F_v is the net vertical force on the crab (e.g. submerged weight 0.07 N). MA_s is the stabilizing moment arm (the distance from the center of mass to the trailing leg, 0.08 m) and MA_o is the overturning moment arm (the height of the center of mass above the substratum, 0.04 m; Fig. 2). Hui (1992) found that crabs locomoting sideways on rocky substrata used wider stances in water than they did on land, but he did not detect a difference on smooth substrata. Grote (1981) found that crayfish also used wider stances in water, but since the crayfish move forwards rather than sideways, this wider stance decreased the likelihood of being overturned by a cross current rather than by relative water motion due to locomotion. In contrast, *G. tenuicrustatus* did not show a significant difference in stance width perpendicular to the direction of motion (in the anterior-posterior direction; Table 4) in air *versus* in water.

We predicted that crabs would maintain lower pitch and roll angles of the carapace in water than in air, thereby reducing hydrodynamic forces resisting movement. Drag (resisting locomotion; Fig. 1) and lift (acting upwards) on the carapace due to locomotion are greater at greater positive pitch angles (Martinez, 1996). Greater positive roll angles cause a greater posteriorly directed component of lift on a sideways-moving crab. Contrary to our prediction, crabs used the same pitch and roll angles of the carapace under water as they did in air, but with more variable pitch angles in water (Table 7). The variation in mean pitch angle suggests that, at these slow speeds, crabs may not be subject to large hydrodynamic forces that might constrain gaits or that they are simply less able to control their body orientation under water. The hydrodynamic force due to locomotion in still water was too low to overturn the crabs even at high carapace angles, but the additional force from ambient currents might be sufficient to overturn them (Martinez, 1996).

Dynamics in aquatic versus terrestrial systems

The variability in the kinematic data of aquatic pedestrian locomotion in this and other studies suggests that we reassess our ideas concerning the neural control of locomotion. Perhaps instead of focusing on the control of leg positions and gait, we should consider the body and its dynamics. An assumption often implicit in the study of gait is that stepping pattern alone is sufficient to characterize the dynamics of the center of mass (e.g. Clarac *et al.* 1987; Cruse, 1990). However, Blickhan and Full (1987) found that whole-body ground reaction forces acting on the center of mass in ghost crabs locomoting in air were remarkably consistent, despite considerable variation in the pattern of leg movements. Determining the motion and forces acting on the body may be even more important in water because, as fluid-dynamic forces begin to dominate, the whole-body dynamics may become increasingly divorced from the pattern of leg movements. We believe new neural control hypotheses concerning the differences between aquatic and terrestrial pedestrian locomotion will emerge when kinematic and kinetic (i.e. fluid and ground reaction force) data are integrated.

Kinematic adjustments between water and land may be best understood in the context of the predominant destabilizing force: the vertical force resulting from the acceleration due to gravity is the principal factor determining locomotor dynamics for most animals on land (Alexander, 1989), whereas the horizontal hydrodynamic forces may equal or surpass the magnitude of the vertical forces under water. *G. tenuicrustatus* responded to this shift in destabilizing forces by adopting a wider stance in water, thereby increasing their resistance to overturning, and by reducing the number of legs in support phase, thereby decreasing their resistance to falling. While the decrease in vertical destabilizing forces may lessen the need for precise neural control of leg placement, the concomitant increase in horizontal destabilizing forces may substantially increase the need for control of the pitch, roll and yaw of the body.

On land, *G. tenuicrustatus* maintained its static stability (as defined by Gray, 1944) by keeping its center of mass within a triangle of supporting legs, whereas in water it relied on dynamic stability by making dynamic adjustments to ensure that, on average, the legs work to counteract gravity. As Pridmore (1994) noted for bottom-walking sharks, the change in overturning and stabilizing moments on an animal in aquatic versus terrestrial habitats allows the animal to achieve dynamic stability at much lower speeds under water than on land. Dynamic stability allows greater freedom of leg kinematics since animals do not require regular leg movements, or as many legs in contact with the ground, to ensure continuous support of body weight, so long as a supporting foot is put down in time to save the body from hitting the ground as it falls.

Hydrodynamic forces are likely to be low at slow speeds (Martinez, 1996); hence, reduced gravity makes a reasonable approximation of the forces on crustaceans locomoting under water. As the animals move more rapidly, however, hydrodynamic forces increase with the square of the speed and are likely to become an important component of the force balance on the animal. Using a drag coefficient of 0.1 (M. M. Martinez, in preparation), drag on *Grapsus tenuicrustatus* would equal its apparent weight in water at a speed of 42 cm s^{-1} . We are currently quantifying the hydrodynamic forces on *G. tenuicrustatus* at appropriate speeds and body postures to understand the mechanical implications for pedestrian locomotion in water.

Biological inspiration for robotics

The general principles learned from studying how legged locomotion differs on land versus under water have already provided biological inspiration for the design of autonomous legged underwater vehicles (ALUVs) which will be able to locomote in a variety of nearshore environments. Greiner *et al.* (1996) have developed an autonomous legged robot featuring the alternating tripod gait and distributed (as opposed to highly centralized) control shown in arthropod locomotion. Their most recent prototype, an amphibious surf-zone robot, emulates the sideways locomotion of a crab and employs a low-profile body to minimize the hydrodynamic forces while in the water. Like a crab, this surf-zone robot uses a wide stance and controls the pitch angle of its body to increase its stability under water. Since control of forces on a body is difficult in the surf-zone, they temporarily opted for a completely invertible design to minimize difficulties in the event of overturning. Most recently, H. Greiner is attempting to add punting behavior to reduce energy consumption and increase battery life. Our understanding of how amphibious animals change their kinematics and kinetics when locomoting in their two natural habitats will make possible even greater advances in the design of underwater pedestrian robots in the future.

This research was supported by an NSF Predoctoral Fellowship, a U. C. Berkeley Chancellor's Minority

Predoctoral Fellowship, a Pauley Grant-in-aid of Marine Research and a Sigma Xi Grant in Aid of research to M.M.M., ONR Grant N00014-92-J-1250 to R.F., Defense Advanced Research Projects Agency Grant N00014-93-C-0228 to R.F., M.A.R.K. and R. Caldwell, and ONR Grant N00014-90-J-1357 to M.A.R.K. Video recordings of crabs were made at the Hawaii Institute of Marine Biology (HIMB). We thank M. Atkinson, E. Reese, F. Thomas, D. Gulko and the staff at HIMB for their support and assistance. We thank J. Rhuman for help with data collection, W. Lau and K. Aarfa for help with data analysis and K. Quillin and R. Kram for helpful comments on the manuscript.

References

- ALEXANDER, R. MCN. (1971). *Size and Shape*. London: Edward Arnold Limited.
- ALEXANDER, R. MCN. (1989). Optimization and gaits in the locomotion of vertebrates. *Physiol. Rev.* **69**, 1199–1227.
- ALEXANDER, R. MCN. (1992). (ed.) *Mechanics of animal locomotion*. In *Advances in Comparative and Environmental Physiology*, vol. 11. Berlin: Springer-Verlag.
- ALEXANDER, R. MCN. AND GOLDSPIK, G. (1977). (eds) *Mechanics and Energetics of Animal Locomotion*. London: Chapman & Hall.
- BARNES, W. J. P. (1975). Leg co-ordination during walking in the crab, *Uca pugnax*. *J. comp. Physiol.* **96**, 237–256.
- BIEWENER, A. A. AND FULL, R. J. (1992). Force platform and kinematic analysis. In *Biomechanics: Structures and Systems, A Practical Approach* (ed. A. A. Biewener), pp. 45–73. Oxford: IRL Press at Oxford University Press.
- BILL, R. G. AND HERRNKIND, W. F. (1976). Drag reduction by formation movement in spiny lobsters. *Science* **193**, 1146–1148.
- BLAKE, R. W. (1985). Crab carapace hydrodynamics. *J. Zool., Lond.* **207**, 407–423.
- BLICKHAN, R. (1989). The spring-mass model for running and hopping. *J. Biomech.* **22**, 1217–1227.
- BLICKHAN, R. AND FULL, R. J. (1987). Locomotion energetics of the ghost crab. II. Mechanics of the centre of mass during walking and running. *J. exp. Biol.* **130**, 155–174.
- BLICKHAN, R. AND FULL, R. J. (1993). Similarity in multilegged locomotion: bouncing like a monopode. *J. comp. Physiol. A* **173**, 509–517.
- BURROWS, M. AND HOYLE, G. (1973). The mechanism of rapid running in the ghost crab, *Ocypode ceratophthalma*. *J. exp. Biol.* **58**, 327–349.
- CAVAGNA, G. A., HEGLUND, N. C. AND TAYLOR, C. R. (1977). Mechanical work in terrestrial locomotion: two basic mechanisms for minimizing energy expenditure. *Am. J. Physiol.* **233**, R243–R261.
- CAVAGNA, G. A., ZAMBONI, A., FARAGGIANA, T. AND MARGARIA, R. (1972). Jumping on the moon: power output at different gravity values. *Aerospace Med., April* 408–414.
- CHASSERAT, C. AND CLARAC, F. (1983). Quantitative analysis of walking in a decapod crustacean, the rock lobster *Jasus lalandii*. II. Spatial and temporal regulation of stepping in driven walking. *J. exp. Biol.* **107**, 219–243.
- CLARAC, F. (1981). Decapod crustacean leg coordination during walking. In *Locomotion and Energetics in Arthropods* (ed. C. F. Herreid and C. R. Fourtner), pp. 31–71. New York, London: Plenum Press.
- CLARAC, F. (1984). Spatial and temporal co-ordination during walking in Crustacea. *Trends Neurosci.* **7**, 293–298.
- CLARAC, F. AND BARNES, W. J. P. (1985). Peripheral influences on the coordination of the legs during walking in decapod crustaceans. *Sem. Ser. Soc. exp. Biol.* **24**, 249–269.
- CLARAC, F. AND CHASSERAT, C. (1983). Quantitative analysis of walking in a decapod crustacean, the rock lobster *Jasus lalandii*. I. Comparative study of free and driven walking. *J. exp. Biol.* **107**, 189–217.
- CLARAC, F. AND CRUSE, H. (1982). Comparison of forces developed by the leg of the rock lobster when walking free or on a treadmill. *Biol. Cybernetics* **43**, 109–114.
- CLARAC, F., LIBERSAT, F., PFLÜGER, H. J. AND RATHMAYER, W. (1987). Motor pattern analysis in the shore crab (*Carcinus maenas*) walking freely in water and on land. *J. exp. Biol.* **133**, 395–414.
- CRUSE, H. (1990). What mechanisms coordinate leg movement in walking arthropods? *Trends Neurosci.* **13**, 15–21.
- CRUSE, H. AND MÜLLER, U. (1986). Two coupling mechanisms which determine the coordination of ipsilateral legs in the walking crayfish. *J. exp. Biol.* **121**, 349–369.
- DONELAN, J. M. AND KRAM, R. (1997). The effect of reduced gravity on the kinematics of human walking: a test of the dynamic similarity hypothesis for locomotion. *J. exp. Biol.* **200**, 3193–3201.
- DONELAN, J. M., LETSON, B. G. AND KRAM, R. (1997). Effect of reduced gravity on running kinematics. *Med. Sci. Sports Exerc.* **29**, (suppl. 5), S81.
- EVOY, W. H. AND FOURTNER, C. R. (1973). Nervous control of walking in the crab *Cardisoma guanhumi*. III. Proprioceptive influences on intra- and intersegmental coordination. *J. comp. Physiol.* **83**, 303–318.
- FARLEY, C. T., GLASHEEN, J. AND MCMAHON, T. A. (1993). Running springs: speed and animal size. *J. exp. Biol.* **185**, 71–86.
- FULL, R. J. (1987). Locomotion energetics of the ghost crab. I. Metabolic cost and endurance. *J. exp. Biol.* **130**, 137–153.
- FULL, R. J. (1997). Invertebrate locomotor systems. In *The Handbook of Comparative Physiology* (ed. W. Dantzler), pp. 853–930. Oxford: Oxford University Press.
- FULL, R. J. AND HERREID II, C. F. (1983). Aerobic response to exercise of the fastest land crab. *Am. J. Physiol.* **244**, R530–R536.
- FULL, R. J. AND HERREID II, C. F. (1984). Fiddler crab exercise: the energetic cost of running sideways. *J. exp. Biol.* **109**, 141–161.
- FULL, R. J. AND WEINSTEIN, R. B. (1992). Integrating the physiology, mechanics and behavior of rapid running ghost crabs: slow and steady doesn't always win the race. *Am. Zool.* **32**, 382–395.
- GANS, C., GAUNT, A. AND WEBB, P. (1997). In *The Handbook of Comparative Physiology* (ed. W. Dantzler), pp. 55–214. Oxford: Oxford University Press.
- GATESY, S. M. AND BIEWENER, A. A. (1991). Bipedal locomotion-effects of speed, size and limb posture in birds and humans. *J. Zool., Lond.* **224**, 127–147.
- GRAY, J. (1944). Studies in the mechanics of the tetrapod skeleton. *J. exp. Biol.* **20**, 88–116.
- GREINER, H., SHECTMAN, A., WON, C., ELSLEY, R. AND BEITH, P. (1996). Autonomous legged underwater vehicles for near land warfare. In *Symposium on Autonomous Underwater Vehicle Technology*. Monterey, California.
- GROTE, J. R. (1981). The effect of load on locomotion in crayfish. *J. exp. Biol.* **92**, 277–288.

- HE, J., KRAM, R. AND MCMAHON, T. A. (1991). Mechanics of running under simulated low gravity. *J. appl. Physiol.* **71**, 863–870.
- HOULIHAN, D. F. AND INNES, A. J. (1984). The cost of walking in crabs: aerial and aquatic oxygen consumption during activity of two species of intertidal crab. *Comp. Biochem. Physiol.* **77A**, 325–334.
- HOULIHAN, D. F., MATHERS, E. AND EL HAJ, A. J. (1984). Walking performance and aerobic and anaerobic metabolism of *Carcinus maenas* (L.) in sea water at 15°C. *J. exp. mar. Biol. Ecol.* **74**, 211–230.
- HUI, C. A. (1992). Walking of the shore crab *Pachygrapsus crassipes* in its two natural environments. *J. exp. Biol.* **165**, 213–227.
- JAMON, M. AND CLARAC, F. (1995). Locomotion patterns on freely moving crayfish (*Procambarus clarkii*). *J. exp. Biol.* **198**, 683–700.
- JOHNSON, G. E. (1965). Behavioral observations of the rock crab, *Grapsus grapsus*, at Coconut Island, Kaneohe Bay, Oahu, Hawaii. Masters thesis, University of Hawaii.
- JONES, E. M. (1995). *Apollo Lunar Surface Journal*. <http://www.hq.nasa.gov/office/pao/History/alsj/>.
- KLÄRNER, D. AND BARNES, W. J. P. (1986). The cuticular stress detector (CSD2) of the crayfish. II. Activity during walking and influences on leg coordination. *J. exp. Biol.* **122**, 161–175.
- KRAM, R., DOMINGO, A. AND FERRIS, D. P. (1997). Effect of reduced gravity on the preferred walk–run transition speed. *J. exp. Biol.* **200**, 821–826.
- LIBERSAT, F., CLARAC, F. AND ZILL, S. (1987). Force-sensitive mechanoreceptors of the dactyl of the crab: single-unit responses during walking and evaluation of function. *J. Neurophysiol.* **57**, 1618–1637.
- MARGARIA, R. AND CAVAGNA, G. A. (1964). Human locomotion in subgravity. *Aerospace Med.* **35**, 1140–1146.
- MARTINEZ, M. M. (1996). Issues for aquatic pedestrian locomotion. *Am. Zool.* **36**, 619–627.
- MAUDE, S. AND WILLIAMS, D. (1983). Behavior of crayfish in water currents: hydrodynamics of eight species with reference to their distribution patterns in southern Ontario. *Can. J. Zool.* **40**, 68–77.
- MCMAHON, T. A. AND CHENG, G. C. (1990). The mechanics of running: how does stiffness couple with speed? *J. Biomech.* **23** (Suppl. 1), 65–78.
- MULLER, U. AND CRUSE, H. (1991). The contralateral coordination of walking legs in the crayfish *Astacus leptodactylus*. I. Experimental results. *Biol. Cybernetics* **64**, 429–436.
- NEWMAN, D. J. (1992). Human locomotion and energetics in simulated partial gravity. Doctoral thesis, Massachusetts Institute of Technology.
- NEWMAN, D. J., ALEXANDER, H. L. AND WEBBON, B. W. (1994). Energetics and mechanics for partial gravity locomotion. *Aviation Space env. Med.* **65**, 815–823.
- POND, C. M. (1975). The role of the 'walking legs' in aquatic and terrestrial locomotion of the crayfish *Austropotamobius pallipes* (Lereboullet). *J. exp. Biol.* **62**, 447–454.
- PRIDMORE, P. A. (1994). Submerged walking in the epaulette shark *Hemiscyllium ocellatum* (Hemiscyllidae) and its implications for locomotion in rhipidistian fishes and early tetrapods. *Zoology – Analysis of Complex Systems* **98**, 278–297.
- SLEINIS, G. AND SILVEY, G. E. (1980). Locomotion in a forward walking crab. *J. comp. Physiol. A* **136**, 301–312.

**RUNNING IN THE SURF:
HYDRODYNAMICS OF THE SHORE CRAB *GRAPSUS TENUICRUSTATUS***

By Marlene M. Martinez

*Department of Integrative Biology
University of California at Berkeley
Berkeley CA 94720 USA*

Running head: Underwater legged locomotion

Key words: hydrodynamics, locomotion, crustaceans, arthropods

Address correspondence to:

Marlene Martinez

Department of Integrative Biology

University of California at Berkeley

Berkeley, CA 94720 USA

Phone 510-643-9048

FAX 510-643-6264

e-mail marlenem@socrates.berkeley.edu

Summary

When locomoting in water, animals experience hydrodynamic forces due to ambient water motion and their own motion through the water. Because an aquatic pedestrian must maintain contact with the substratum to locomote, hydrodynamic forces which can dislodge an animal have the capacity to constrain the postures, gaits and speeds an animal can use. This study measured hydrodynamic forces on the amphibious shore crabs *Grapsus tenuicrustatus* in aquatic and terrestrial postures. The crabs' locomotory speeds and ambient water velocities in their habitat were considered in predicting the conditions under which a crab is likely to overturn or wash away. A crab using the terrestrial posture while locomoting in water experiences greater drag and acceleration reaction forces than it does in the aquatic posture. Thus a crab using the aquatic posture could locomote more quickly or through a faster water flow environment than it could in the terrestrial posture. In faster flow environments like wave-swept rocky shores, a crab in either posture would have to actively grasp the substratum to keep from being dislodged. Thus in slower flow environments, animals can locomote faster and take advantage of different gaits that are not available to them in faster flow environments.

Introduction

Studies of legged locomotion have historically concentrated on terrestrial locomotion or on swimming (reviewed in Full, 1997; Gans *et al.*, 1997), but have more recently begun to explore aspects of pedestrian locomotion in water (e.g. Pond, 1975; Bill and Herrnkind, 1976; Grote, 1981; Houlihan and Innes, 1984; Houlihan *et al.*, 1984; Clarac *et al.*, 1987; Hui, 1992; Jamon and Clarac, 1995; Martinez, 1996; Martinez *et al.*, 1998). While weight is the largest external force imposed on an animal during terrestrial locomotion, buoyancy and hydrodynamic forces may be as important as an animal's weight in aquatic locomotion (Martinez, 1996; Martinez *et al.*, 1998). While the increased buoyant force in water explains many of the kinematic differences exhibited by pedestrians when in still water versus in air (Martinez *et al.*, 1998), the role of hydrodynamic forces in determining the dynamics of aquatic pedestrian locomotion remains uncertain.

Locomotion in air versus in water

Several studies report that amphibious animals using pedestrian locomotion use different kinematics when in air versus in water (Pond, 1975; Clarac *et al.*, 1987; Grote, 1981; Hui, 1992; Martinez *et al.*, 1998). The amphibious shore crab, *Grapsus tenuicrustatus* changes body postures as well as kinematics, using a different locomotory gait in air than in water (Martinez *et al.*, 1998). The crabs walk on land at slow speeds, but in water at these same speeds, the crabs use a more variable gait (submerged punting), characterized by alternating thrust generation and gliding. Unlike other gaits crabs might use underwater, the submerged punting gait does not allow crabs to actively grasp the substratum while locomoting.

Animals' kinematic changes between air and water can be understood in terms of the mechanical loads characteristic of these different fluid environments. The increased buoyancy and hydrodynamic forces in water compared to on land can cause a shift in the predominant destabilizing forces an animal experiences. Whereas on land the destabilizing forces are predominantly vertical (due to

gravity), in water the horizontal destabilizing forces (due to hydrodynamic forces) may equal or exceed the vertical forces (Martinez, 1996). Martinez *et al.* (1998) show that many of the kinematic adjustments made by *Grapsus tenuicrustatus* in water at slow speeds can be predicted from reduced gravity models of locomotion. As animals move more rapidly, however, hydrodynamic forces increase and are likely to become an important component of the force balance on the animal.

Hydrodynamic forces on an animal walking or running underwater are due not only to its motion through the water, but also to the ambient water flow in the animal's habitat. The net hydrodynamic force on an animal affects the force the animal has to exert to locomote and determines whether the animal washes off the substratum or overturns. Of the few studies that consider hydrodynamic forces on legged animals, most focus on swimming rather than on pedestrian locomotion (e.g. Alexander, 1990; Blake, 1985; Fisher, 1975; Plotnik, 1985; Jacklyn and Ritz, 1986). While the importance of hydrodynamic forces has been demonstrated for many sessile organisms (e.g. Koehl, 1977, 1982, 1984; Carrington, 1990; Gaylord *et al.*, 1994) and for animals using adhesive locomotion (Denny *et al.*, 1985, 1988; Dudley, 1985; Denny, 1994; Denny and Gaylord, 1996), little is known about the effects of hydrodynamic forces on aquatic legged locomotion.

The hydrodynamic forces on an animal are not prescribed simply by the water flow environment, but are also modified by the animal's reaction to the flow conditions. Not only do pedestrian animals use different postures in still water than they use in air (Grote, 1981; Hui, 1992; Martinez *et al.*, 1998), but they also change their postures and orientations in response to water flow (Maude and Williams, 1983; Nishimoto and Herrnkind, 1978). Changes in posture and orientation can have large effects on the hydrodynamic forces an animal experiences (Pond, 1975; Bill and Herrnkind, 1976; Koehl, 1977, 1982; Jacklyn and Ritz, 1986; Weissenberger *et al.*, 1991). Few studies on aquatic pedestrians have explicitly considered the significance of ambient water flow or an animal's posture on the hydrodynamic forces that animal experiences, although Bill and

Herrnkind (1976) measured the effect of antennal orientation and inter-lobster spacing on the drag experienced by lobsters walking in a queue.

Consequences of hydrodynamic forces

The hydrodynamic forces on the body of an animal (Fig. 1, A) impact the dynamics of aquatic pedestrian locomotion in many ways, including resisting forward motion, keeping the animal in contact with the substratum, or dislodging the animal from the substratum. Dislodgment from the substratum is a serious problem for pedestrian animals since they must maintain contact with the substratum in order to generate thrust. Hydrodynamic forces can dislodge an animal by causing it to overturn or wash away. Assuming that an animal does not actively grip the substratum, it will overturn, pivoting about its downstream leg, when the overturning moment about the animal's center of mass exceeds the stabilizing moment (Fig. 1, B) (Alexander, 1971). The conditions under which an animal will overturn can be expressed in terms of the forces on the animal's body:

$$\frac{(D + A)h}{(W - B - L)d} > 1 \quad (1)$$

where D is the drag force, A is the acceleration reaction force, h is the height of the center of mass, W is the weight of the animal, B is the buoyant force, L is the lift force, and d is the distance from the center of mass to the downstream or trailing leg. Positive lift (away from the substratum) contributes to the likelihood that an animal will become dislodged, but if an animal generates negative lift, this will assist the animal in maintaining ground contact.

Another mechanism by which hydrodynamic forces can dislodge an animal is to shear it off the substratum, washing it away. An animal will wash away when the net horizontal force on the body (drag plus acceleration reaction) exceeds the force resisting that motion (Fig. 1, C). Unless an animal actively grasps the substratum, only friction between the animal and the substratum keeps the animal from washing away. The frictional force resisting dislodgment

is proportional to the net vertical force on the animal (weight minus buoyancy and lift).

Hydrodynamic forces can constrain aquatic locomotion in several ways. The need to actively hold onto the substratum when exposed to ambient water flow can limit the conditions under which an animal can locomote or the gaits and postures the animal can use while locomoting. Even if an animal does not become dislodged from the substratum, hydrodynamic forces may limit the speed and accelerations of the animal by greatly increasing the horizontal forces and power output the animal must exert to locomote.

Objectives

The present study addresses three hypotheses concerning the role of hydrodynamic forces in aquatic pedestrian locomotion: 1) Drag, lift and acceleration reaction contribute significantly to the force balance on an animal locomoting through an aquatic environment. 2) Adopting different locomotory postures alters the hydrodynamic forces an animal experiences. 3) Hydrodynamic forces (due to locomotion or ambient water flow) constrain an animal's postures, speeds, accelerations, and kinematics as well as the environmental conditions under which the animal can locomote. These hypotheses are tested using the Hawaiian intertidal rock crab, *Grapsus tenuicrustatus*, which inhabits a wide range of water flow environments, from slow-flow lagoons to wave-swept rocky shores. This study employs a quasi-steady state hydrodynamic analysis, considering steady state drag and lift as well as acceleration reaction forces on the body of a crab. These forces are assessed at speeds and accelerations characteristic of locomotion and ambient water velocity measured in three different habitats: a lagoon, a protected bay, and a wave-swept site. Based on the total force on the body of a crab, predictions were made about when a crab will overturn or wash away while locomoting in its natural environment. *G. tenuicrustatus* are convenient animals for this hydrodynamic study not only because of the diversity of water flow environments they inhabit, but also because they use distinct postures in air and water (Martinez *et al.*, 1998).

Materials and methods

Animals

Many *Grapsus tenuicrustatus* (not captured) were videotaped in the field to determine their fate in waves. Large adult *G. tenuicrustatus* (0.070 ± 0.02 kg) were collected near Coconut Island, HI. Weight in air and in water were measured to the nearest 0.001 kg with a Mettler balance. Live crabs were videotaped to determine preferred locomotory speeds in air and in water. Different live crabs were used in tenacity measurements. Exoskeletons from these crabs were made into models for lift, drag and added mass measurements.

Speeds of locomotion

To estimate a crab's preferred locomotory speed, five crabs were videotaped locomoting freely through air and through still seawater over a flat substratum. Crabs were occasionally prodded to initiate movement. Handling of crabs was minimized and crabs were allowed to rest for several hours between trials. Videotapes were digitized using motion analysis software (Peak Performance Inc., Version 5.0) to obtain average velocity over a one meter path. Trials were discarded when crabs tripped, turned, did not move steadily, or ran alongside walls. Crabs used two distinct gears that corresponded to slow and fast speeds underwater (Fig. 2), but this pattern did not show a trial effect; i.e. crabs did not locomote more slowly or more quickly after several trials. Mean slow and fast speeds were calculated for each crab. Group means for slow and fast speeds were then calculated to be used in overturning calculations.

Tenacity

Tenacity measurements in air were made on five live crabs on rugose volcanic rock similar to that commonly found in the crabs' habitat. Each crab was allowed to settle on the rock for several seconds and then was pulled in the horizontal or vertical directions with an AMETEK (LKG-5) force transducer via a wire loop attached to the center of the crab's carapace. Each crab was pulled until it detached from the rock. Maximum force was determined to the nearest 0.01 kg from ten replicates.

The coefficient of friction was determined for each epoxy-filled crab model used in the hydrodynamic experiments. Weight of the specimens was determined to the nearest 0.001 kg using a Mettler balance. Frictional force (± 0.001 kg) was measured with a Pesola force transducer as the models were pulled along the wet surface of both the volcanic rock used in tenacity measurements and a flatter, less rugose shale rock.

Ambient water velocity

For an estimate of the ambient water velocities and accelerations that a crab might encounter, water velocities were measured in *G. tenuicrustatus* habitats on several days in January 1995 along rocky shores on Oahu, Hawaii. These data represent non-stormy conditions over a range of weather conditions, as indexed by wind speed. Three sites were chosen to represent the different water flow environments that the crabs inhabit: a wave-swept site at Makapuu State Beach Park, a protected lagoon at Coconut Island and a semi-protected site in Kaneohe Bay. Ambient water velocity was measured during flooding tide, using an electromagnetic flow probe (Marsh-McBirney, Model 511), the electrodes of which were placed above the substratum at the approximate height of a crab (0.06 m). At all three sites the probe was placed above the substratum at a location where an adult *G. tenuicrustatus* had been observed. The electromagnetic flow probe measures flow in two perpendicular axes. The probe was oriented to measure the horizontal components of velocity, with one axis parallel to the direction of the highest velocity at each site.

Flow velocities were recorded using a DAQBook data acquisition system (OMB-DAQBOOK-100) on a Texas Instruments 486Dx2/50 Travelmate notebook computer, sampled at 2 Hz. Accelerations were calculated over each 0.5 s sampling interval. While the sensing volume of the flow probe yields accelerations on a spatial scale relevant to *G. tenuicrustatus*, this method of measurement underestimates instantaneous acceleration. Therefore a range of water accelerations were considered for calculations of overturning and washing away. Koehl and Cooper (unpublished data) have measured water velocities at a sampling rate of 25 Hz with a sensing volume of 1cm³. Their data yields

maximum water accelerations of 0.9 m/s^2 and 1.3 m/s^2 for sites with similar water velocities and flow characteristics as the lagoon and bay sites used in the present study. Water accelerations in the surf zone on rocky shores may commonly reach 400 m/s^2 (Denny, 1988). While these values provide a broad sense of the water accelerations in the intertidal zone, their applicability is ambiguous for determining the forces on a large organism such as *Grapsus tenuicrustatus*. Water accelerations cannot generate a force of substantial magnitude on an organism if the bulk of accelerating water encompasses only part of the organism at a given time (Gaylord, 1997).

Hydrodynamic forces

Models and postures

Crab exoskeletons were filled with epoxy and positioned in different postures by adjusting the ischium-merus (Fig. 3) and merus-carpus joints and securing the joint positions with remeltable plastic (Friendly Plastic), which was smoothed and sanded to the contour of the legs. Hex nuts were embedded in the ventral and posterior side of the crabs' bodies and made flush with the surface of the body with epoxy.

Hydrodynamic forces were measured on each crab model in two postures, a sprawled aquatic posture and a more upright terrestrial posture, as determined from a three-dimensional kinematic analysis of these crabs locomoting in air and water (Martinez *et al.*, 1998). For the aquatic posture, crabs were positioned with a relatively wide lateral stance (0.20 m, 364% of the mean carapace width). For the terrestrial posture, crabs were positioned with a narrower lateral stance (0.16 m, 291% of the mean carapace width), with smaller merus-carpus joint angles (Fig. 3). Crabs in both aquatic and terrestrial postures were positioned with their centers of mass approximately 0.04 m above the substratum as determined from the kinematic analysis (Martinez *et al.*, 1998). The crab models were attached to force transducers via the ventral hex nut (for drag and acceleration reaction measurements) and then via the posterior hex nut (for lift measurements).

Kinematic analysis (Martinez *et al.*, 1998) showed that *G. tenuicrustatus* used angles of attack (angle at which the animal meets the oncoming flow, rotation about the anterior-posterior axis for a sideways-moving crab) between 0° and +4° more than 65% of the time when locomoting through air or still water. Although *G. tenuicrustatus* did not use negative angles of attack at slow speeds (Martinez *et al.*, 1998), negative angles of attack provide a potential stabilizing mechanism against overturning and were consequently considered in this study.

Justification of a quasi-steady state approach

To verify the validity of a quasi-steady state approach in analyzing the hydrodynamic forces on *G. tenuicrustatus*, the period parameter was calculated for the epoxy-filled crab models, assuming conditions of a wave-swept environment. The period parameter is used as an index of whether time-dependent effects will have a significant influence on hydrodynamic coefficients. Period parameter (K) is given by

$$K = (T U_{max}) / l \quad (2)$$

where T = wave period, U_{max} = maximum water velocity, l = characteristic length of organism in the direction of flow. Using the crabs' maximum length in flow (width of lateral stance in aquatic posture: 0.2 m), the average wave period (average of ten consecutive waves at the wave-swept site: 12.5 s), and the mean maximum water velocity (mean of the maximal water velocity from each wave: 0.5 m/s), yields a period parameter value of 31.3. A period parameter greater than 30 allows one to reasonably assume quasi-steady state conditions (Keulegan and Carpenter, 1958).

Importance of a substratum

It is important to consider proximity to a substratum when measuring hydrodynamic forces on a benthic animal because the substratum can affect the local flow and thus affect the fluid dynamic forces experienced by the animal.

The proximity of a surface can interfere with fluid flow around an animal, decreasing drag and increasing lift experienced by the animal (Martinez, 1996). When fluid flows over a substratum, a velocity gradient (boundary layer) develops above the substratum (Vogel, 1981). Reduced flow and high shear in the steep gradient of a boundary layer can significantly alter the forces an animal experiences.

When an animal locomotes through still water, the substratum and the water move with respect to the animal but not with respect to each other; therefore no boundary layer develops over the substratum. However, for an animal either standing or locomoting in ambient water flow, the water also moves with respect to the substratum, creating a velocity gradient. Yet *Grapsus tenuicrustatus* are unlikely to feel the effects of a boundary layer in their environment because these large crabs do not dwell within the steep gradient of a boundary layer that would develop over rough substrata in shallow water (Denny, 1988). In addition, crabs do not experience boundary layer effects on wave-swept shores because thick boundary layers do not have sufficient time to develop under these conditions (Denny, 1988).

Using a unidirectional flow tank, I modeled three situations: a crab locomoting through still water, a crab standing still in moving water, and a crab locomoting through moving water. In a typical unidirectional flow tank (Vogel, 1981), water moves past a specimen which is fixed relative to the substratum. In order to simulate a crab locomoting in still water, I positioned the crab model over an underwater treadmill with the belt speed matched to the speed of the water. To simulate water moving past a crab standing still, I circumvented the effects of a boundary layer by placing the crab model at the leading edge of a flat plate. This method is effective because boundary layers do not appear instantaneously, but take time and distance to develop. Preliminary measures of drag force on a crab model positioned over the underwater treadmill did not differ from drag measured on the model positioned at the leading edge of a flat plate (within one cm of the edge) (Paired T-test, two-tailed, $P = 0.82$, $N = 6$ speeds). Therefore, all subsequent hydrodynamic measurements were made over a flat plate rather than over a treadmill.

Drag and lift

Drag and lift were measured on five crab models in a unidirectional water flow tank with a working section of 0.35 m x 0.50 m x 2.00 m. Forces were measured at seven different water velocities ranging between 0.15 to 1.00 m/s, approximating my measurements of both the crabs' locomotory speeds in water and water velocities in the habitat. Water velocity in the flow tank was measured with an acoustic doppler anemometer (SonTek, Inc.) to the nearest 0.001 m/s. The crabs did not significantly affect flow through the flow tank since they obstructed less than 3% of the flume's cross-section (largest crab cross-sectional area: 0.003 m², cross-section of tank: 0.13 m²) (Vogel, 1981).

Since crabs locomote with their left or right sides leading, the models of *G. tenuicrustatus* were placed with their left side facing upstream in the flow tank. Drag and lift on the models were measured with force transducers (e.g. Vogel, 1981; Koehl, 1977). The force signal was passed through a bridge amplifier (Measurements Group, Model 2100) to a desktop computer (Gateway 2000) via LabView software (Version 3.0.1, National Instruments). Force signals were sampled at 10 Hz and averaged over two minute intervals. Three replicate measures of forces were made on each crab in each posture and angle of attack at each speed. Mean forces and coefficients were calculated for each crab and group means were calculated for each posture.

Crabs' projected areas and planform areas were measured on video images (to the nearest 0.01 cm²), using NIH Image software (version 1.52) on a MacIntosh PowerPC 7200/120 desktop computer. Since some studies report drag coefficients (C_D) calculated using frontal area and others using planform area, this study included C_D 's calculated both ways for comparison. The choice of which area to use for this calculation can profoundly affect the interpretation of the data (Alexander, 1990). The ratios of planform to frontal areas are likely not the same for two animals being compared. Therefore, determining which animal has a lower drag coefficient may depend on which reference area is used in the calculation.

Drag coefficient (C_D) was calculated from the following equation:

$$C_D = D / (0.5 \rho u^2 S) \quad (3)$$

where D is the measured drag force, ρ is the fluid density, u is the water velocity relative to the crab, and S is the projected or planform area of the crab. Lift coefficient (C_L) was calculated from the following equation:

$$C_L = L / (0.5 \rho u^2 S_p) \quad (4)$$

where L is the measured lift force, and S_p is the planform area (top view). Preliminary hydrodynamic measurements indicated that lift, but not drag, was sensitive to these small changes in angle of attack (Kruskal-Wallis test, $df = 2$, $P = 0.006$ for lift, $P = 0.97$ for drag). Thus lift measurements were made at $+4^\circ$, 0° and -4° . Drag measurements were made only at 0° angle of attack.

Acceleration reaction

Using the apparatus and methods described in Denny and Gaylord (1996), acceleration reaction forces were measured on crabs accelerating in a tow tank. During the force measurements, crab models were oriented as for drag and lift measurements and positioned next to a substratum that accelerated with the crabs. Ten force measurements were made for each of seven individual crab models (mean body mass of live crabs = 0.070 ± 0.013 kg) in each posture. Inertia coefficients (C_M) (for modeling fluid accelerating past a crab) were calculated from the following equation:

$$C_M = A / (\rho V a) \quad (5)$$

where A = acceleration reaction force, ρ = water density, V = volume of the crab, and a = acceleration of water relative to the crab. Accelerations were measured by a force transducer acting as an accelerometer as it was towed along the with

crab model. Crab volumes (V) were calculated from the models' weights in air and submerged weights using the following equation:

$$V = (m - m_{app}) / \rho \quad (6)$$

where m = mass of the crab, m_{app} = apparent mass of the crab in water (submerged weight divided by gravity), and ρ = water density. Added mass coefficients (C_A) (appropriate for modeling a crab accelerating through still fluid) were calculated from the following equation:

$$C_A = C_M - 1 \quad (7)$$

(Denny, 1988). Mean coefficients were calculated for each crab and group means were calculated for each posture.

Critical velocity calculations

Overturning

Critical velocities required to overturn a crab under various conditions were calculated using equation (1). The crabs' mean slow and mean fast punting speeds (measured from videotape) were used to determine whether or not a crab would overturn while punting through still water. Even during locomotion at a constant average speed, an animal accelerates and decelerates its body during each stride (e.g. Full, 1989). The only data available for body accelerations of *G. tenuicrustatus* were determined from kinematics (Martinez *et al.*, 1998), a process that returns questionable values for accelerations. Therefore a sensitivity analysis was used to explore the effects of body accelerations on the likelihood of overturning for a crab using different postures and angles of attack. Since in punting there are times when a crab has no legs in contact with the substratum, crabs cannot actively grasp the substratum while using the submerged punting gait (Martinez *et al.*, 1998). Accordingly calculations of overturning during punting locomotion excluded active tenacity.

For a crab in ambient water flow, the maximum water velocities and accelerations measured at each of three sites were used in the calculations. All calculations involving ambient water flow were made with the assumption that crabs were fully submerged in shallow water, either in oscillatory flow characteristic of flow along the substratum under waves passing overhead or in the shoreward surge and seaward backwash after a wave has broken. Under these assumptions this study did not address the effects of pressure distribution or air bubbles under breaking waves or the impact forces associated with a wall of water hitting an emersed animal (Denny, 1988). A crab locomoting in ambient flow was considered during the worst-case scenario of punting upstream. Accelerations used in these calculations were the maximum accelerations measured for comparable water velocities in the crab's habitat; e.g. for velocities less than 0.30 m/s, the maximum acceleration measured in the lagoon environment was used; for velocities greater than 0.50 m/s, the maximum acceleration measured at the wave-swept site was used.

Washing away

Critical velocities for washing away were calculated for a crab in each posture at an angle of attack of 0°. For these calculations, the crab was assumed to wash away if drag (in steady currents) or drag plus acceleration reaction (in waves) exceeded the frictional force resisting a crab's lateral movement across the substratum. The frictional force (F_f) is given by

$$F_f = (W_{app} - L) \Phi \quad (8)$$

where W_{app} is the crab's apparent weight in water (weight minus buoyancy), L is the hydrodynamic lift on the body of the crab (where positive lift acts away from the substratum), and Φ is the coefficient of friction for a crab on rock. For a crab actively grasping the substratum, the maximum horizontal tenacity of a crab was added to the frictional force. Critical water velocities for washing away were calculated over a range of water accelerations for crabs in the aquatic and terrestrial postures.

Fate of crabs in waves

Using a zoom lens so as not to disturb natural behavior of these skittish crabs, *Grapsus tenuicrustatus* were videotaped (Panasonic model PVS62, 60 fields/second) in the field along the coast of Hawaii at several locations representing a range of water flow conditions: 1) a protected lagoon (Coconut Island), 2) semiprotected sites (Kaneohe Bay, Aloha Tower), and 3) rocky shores exposed to heavy wave action (Makapuu, Kona Coast of Hawaii, Kapapa Island). The videotapes were analyzed to determine the fates of crabs in waves. Each crab and each wave was only counted once, yielding statistically independent samples. In video sequences where several crabs were subjected to many waves, events were sampled systematically in a counter-clockwise direction from the top right corner of the camera view. Approximate wave heights were determined from the videotapes, using crabs as a size scale. Crabs were assumed to have a carapace width of 0.05 m. With this method, wave heights were approximated with a precision of 0.2 m. Waves were categorized as small (0 - 0.5 m), medium (0.5 - 1 m) or large (1.0 - 2.0 m).

Statistics

Drag, lift and acceleration reaction forces were compared using Paired T-tests. Hydrodynamic coefficients were compared using Wilcoxon Signed Rank tests. All statistical tests were performed on a MacIntosh PowerPC (6100/60), using Statview (Version 4.5).

Results

Speeds of locomotion

When locomoting under water, crabs used a slow punting speed of 0.11 ± 0.02 m/s and a fast punting speed of 0.40 ± 0.08 m/s (Fig. 2). The fastest speed recorded for underwater punting was 0.67 m/s, whereas for terrestrial running the fastest speed recorded was 1.4 m/s.

Tenacity

Crabs' mean maximum tenacity on rugose rock exceeded their weight in air by more than an order of magnitude (horizontal tenacity 13.0 ± 7.7 N, vertical tenacity 11.3 ± 3.3 N). On the slate rock, the crab models had a mean friction coefficient of 0.32 ± 0.06 . On the volcanic rock, the dactyls of the models caught in holes, greatly increasing the force needed to drag the models across the rock. The force to pull crab models across the volcanic rock were in excess of 5.6 ± 0.7 N, the force to break a leg off the model. The pliant legs of live crabs grasped the substratum with 130% more force than it took to break a model crab's leg.

Measurements of water flow in the field

Water flow in the lagoon and bay environments was characterized by turbulent velocity fluctuations superimposed upon relatively slow unidirectional currents. The wave-swept environment was characterized by oscillatory water movement, with much greater water velocities and accelerations than the other sites (Fig. 4). The peak water velocity in the wave-swept site was almost three times the peak velocity at the bay site and 13 times the peak velocity at the lagoon site (Fig. 4). The peak accelerations measured at each sites were 0.17 m/s^2 at the lagoon site, 1.05 m/s^2 at the bay site, and 1.71 m/s^2 at the wave-swept site.

Hydrodynamic forces

Drag

As expected for this Reynolds number range ($10^4 - 10^5$), drag increased with the square of the velocity for crabs in both postures ($r^2 > 0.997$). Crabs experienced greater drag in the terrestrial posture than they did in the aquatic posture (Paired T-tests, two tailed, $P < 0.05$, $N = 5$) at all speeds except the slowest speed (Fig. 5). Drag coefficients (C_D 's) did not show a significant association with Reynolds number for either posture (Kendall Rank Correlation, $P > 0.05$, $N = 7$). Mean drag coefficients were greater at each speed for crabs in the terrestrial posture than for crabs in the aquatic posture (Wilcoxon Signed Rank test, $P = 0.018$, $N = 7$ speeds) (Table 2). While models in the terrestrial posture had a smaller planform area than they did in the aquatic posture, this change accounted for only 14% of the difference in drag coefficient (based on planform

area) between these two postures. Drag measures were at 0° angle of attack because angle of attack did not affect drag coefficients on either posture (see Methods).

Lift

The lift force was sensitive to angle of attack for both the aquatic and the terrestrial postures (Fig. 6). Over the span of just a few degrees, the effect of the lift force switched from pulling a crab off the substratum to pushing it down onto the substratum. At 0° angle of attack, crabs in the aquatic posture experienced, on average, positive lift (away from the substratum), while crabs in the terrestrial posture experienced, on average, negative lift (toward the substratum) (Fig. 5, Table 2). A +4° angle of attack always produced positive lift and a -4° angle of attack always produced negative lift. At all angles of attack, the aquatic posture generated lift of greater magnitude than did the terrestrial posture (Paired T-test, 2 tailed, $P < 0.05$, $N = 7$), although due to the difference in planform areas, the lift coefficients for -4° angle of attack are similar for the two postures (Wilcoxon Signed Rank Test, $P > 0.05$, $N = 7$) (Table 2).

Lift coefficient showed a significant negative association with Reynolds number for the terrestrial posture, but not for the aquatic posture, at all three angles of attack measured (Kendall Rank Correlation, $P < 0.005$, $N = 7$). At 0° and +4° angle of attack, lift coefficients on crabs were greater in the aquatic posture than in the terrestrial posture (Wilcoxon Signed Rank Test, $P < 0.05$, $N = 7$) (Table 2).

Acceleration Reaction

Added mass coefficients were greater for crabs in the terrestrial posture than in the aquatic posture (Table 2). Since added mass coefficients did not show a significant correlation with crab size in either posture (Kendall Rank Correlation tests, $P > 0.05$, $N = 7$), group mean coefficients for each posture were used in overturning calculations.

Comparison of forces

At locomotory speeds in air, weight was by far the greatest force on a crab, whereas at locomotory speeds in water, the hydrodynamic forces were sometimes much larger than a crab's submerged weight. In still air at a crab's maximum recorded terrestrial speed (1.4 m/s), weight was 384 times greater than the drag force (on a crab using the terrestrial posture) (Fig. 7, A). Even at an angle of attack of $+4^\circ$, drag was 10 times greater than the lift force, but only 0.3% of the weight (Fig. 7, A). In contrast, in still water at their maximum recorded locomotory speed in water (0.67 m/s), drag on *Grapsus tenuicrustatus* was 2.3 times greater than the crab's submerged weight and 17 times greater than lift at 0° angle of attack for a crab using the aquatic posture. At an angle of attack of $+4^\circ$ at this speed, *G. tenuicrustatus* generated positive lift greater than its apparent weight in water. Lift at this angle of attack was still less than half the drag on a crab (Fig. 7, A).

For a crab standing still in a wave-swept environment, drag was still the predominant force, but acceleration reaction also imposed a significant force. On a wave swept shore with water velocities and accelerations of 1.6 m/s and 1.7 m/s^2 , the magnitude of the acceleration reaction force was 20% of the drag force on a crab using the aquatic posture and 11% of the drag force on a crab using the terrestrial posture (Fig. 7, B).

Aquatic vs. terrestrial posture

Posture greatly influenced the hydrodynamic forces on the body of a crab. Compared to a crab using the aquatic posture, a crab using the terrestrial posture in wave swept conditions (water velocity = 1.6 m/s, water acceleration = 1.7 m/s^2) experiences 111% greater drag, 53% less lift (and negative rather than positive lift), and 12% more acceleration reaction force (Fig. 7, B). The different forces cause a crab in the terrestrial posture to wash away in slower water flow than a crab in the aquatic posture. In fact, a crab in the aquatic posture could withstand 44% faster flow in a steady current and 200% faster flow in waves (slow flow regime, water acceleration = 0.17 m/s^2) than it could withstand in the terrestrial posture (Table 1) before washing away. Furthermore, the difference

in forces imposed on the two postures affects the maximum speed at which a crab could locomote underwater. A crab could locomote 50% faster in the aquatic posture than in the terrestrial posture before overturning in still water (at 0° angle of attack, without tenacity), assuming that the crab is not accelerating its body during the maximum acceleration of the water around it (Table 1).

Calculations

Overturning

Even if crabs do not accelerate their bodies at the same time that waves maximally accelerate over them, crabs punting upstream while using the terrestrial posture overturn in any of the three flow environments considered (Table 3) even without consideration of acceleration reaction forces. In contrast, crabs punting upstream in the aquatic posture (at 0° angle of attack) are stable against overturning in the lagoon environment at both slow and fast punting speeds if water accelerations are low (Table 3). In the wave-swept environment, crabs punting at the slow speed are unstable in either posture even without water acceleration. The critical speed for overturning in still water (at 0° angle of attack, no body accelerations) is 0.66 m/s for a crab in the aquatic posture and 0.44 m/s for a crab in the terrestrial posture (Table 1). For comparison, a crab locomoting on land (using the terrestrial posture at 0° angle of attack, no body accelerations) would overturn at 41.3 m/s.

Critical speeds for overturning are highly dependent on the body acceleration assumed (Fig. 8). Crabs in the terrestrial posture must punt with accelerations lower than 1.3 m/s^2 . In contrast, crabs in the aquatic posture can punt with accelerations up to 2 m/s^2 . A crab using a -4° angle of attack in the aquatic posture does not overturn at any speed for body accelerations less than 2 m/s^2 . For 0° and $+4^\circ$ angle of attack as well as for the terrestrial posture, using higher accelerations drastically reduces the speeds at which a crab can punt without overturning.

Washing away

Critical speeds for washing away are lower than critical speeds for overturning. Furthermore, the critical speed at which a crab washes away depends on whether the crab relies on friction or actively grasps the substratum. If a crab in steady currents relies on friction, it washes away at 0.24 m/s in the aquatic posture and at only 0.17 m/s in the terrestrial posture. However, if a crab grasps the substratum with its maximum horizontal tenacity, it can resist washing away at velocities up to 5.72 m/s in the aquatic posture and 3.98 m/s in the terrestrial posture, greater than the peak water velocities measured at all sites. Increasing water acceleration decrease the water velocity a crab can withstand before washing away (Fig. 9)

Behavior in waves

While most crabs maintained their positions, a few crabs washed away in waves in all three size categories (Table 4). Surprisingly, five percent of the total number of crabs were observed to continue walking through waves of medium and large sizes. No crabs were observed walking through waves of the smallest size, although this may be due to small sample size. Sometimes as a large wave broke over a crab, the crab flattened itself against the rock. This flattening behavior appeared to prevent crabs from washing away.

Crabs were observed to use non-punting gaits in the field, especially while climbing a vertical wall or while locomoting upside down under a ledge. These non-punting gaits were characterized by constant contact with the substratum. Usually a crab had at least two legs in contact with the ground, one on either side of the body, allowing the crab to grip the substratum with a pinching behavior. Occasionally a crab dangled from one leg while climbing.

Discussion

An animal using pedestrian locomotion under water must contend with hydrodynamic forces that can prevent it from locomoting quickly or that can cause it to overturn or wash away. Thus, hydrodynamic forces can limit how and when an animal can locomote. In addition to an animal's morphology, factors such as posture, behavior and water flow environment dramatically influence the hydrodynamic forces the animal experiences.

Comparisons with other animals

Comparison of hydrodynamic coefficients with those of other animals gives a relative measure of how an animal's morphology influences the hydrodynamic forces it experiences. Comparing benthic crustaceans using data from the literature is difficult primarily because these data are collected under different circumstances. To determine the hydrodynamic forces an aquatic pedestrian experiences, measurements should be made on intact animals, in appropriate postures, in biologically relevant flow conditions, and next to a substratum. Blake (1985) and Plotnik (1985) determined the components of force generated by crabs' carapaces, but did not measure forces on entire animals. Both Pond's data (1975) and the present study (Figs. 6-7) show that leg positions influence the forces experienced by an animal, suggesting that legs can contribute significantly to the hydrodynamics of the whole body. While several studies have measured hydrodynamic forces on benthic crustaceans, most of these studies (Pond, 1975; Blake, 1985; Plotnik, 1985; Jacklyn and Ritz, 1986; Alexander, 1990) have focused on swimming rather than on pedestrian locomotion and have thus measured forces on bodies far from a substratum. Animals very near a surface experience decreased drag and increased lift relative to animals far from a surface (Withers and Timko, 1977; Martinez, 1996).

Given these caveats, hydrodynamic comparisons can still be made among benthic crustacean data in the literature. The drag coefficients measured for *Grapsus tenuicrustatus* are smaller than those reported for benthic and swimming crabs (Blake, 1985), lobsters (Bill and Herrnkind, 1976), crayfish

(Maude and Williams, 1983; Pond, 1975, calculated in Maude and Williams, 1983), and isopods (Alexander, 1990) (Fig. 10, A-B), indicating that *G. tenuicrustatus* has a relatively streamlined shape. The only other crab that has a drag coefficient as low as that of *G. tenuicrustatus* is *Callinectes sapidus* (Blake, 1985, Plotnik, 1985), a crab known for rapid swimming (Spirito, 1972) (Fig. 10, B).

Few data are available for lift on benthic crustaceans. *G. tenuicrustatus* has a large planform area, yielding a very low lift coefficient compared to crabs measured without legs (Blake, 1985) and for lobsters executing tail flips (Jacklyn and Ritz, 1986) (Fig. 10, C).

The present study is the first to report added mass coefficients for a benthic animal using legged locomotion, enabling evaluation of the hydrodynamic forces imposed by accelerating water in the intertidal habitat. *G. tenuicrustatus* have added mass coefficients in the range reported for various sessile or slowly-moving intertidal invertebrates (Denny et al., 1985), but lower than reported for sea urchins (Denny and Gaylord, 1996).

Mechanisms for resisting dislodgment

One mechanism by which a crab can avoid dislodgment from the substratum is by altering its posture. Of the two postures examined in this study, (described for *Grapsus tenuicrustatus* in Martinez et al., 1998), the aquatic posture confers greater stability against overturning and washing away than does the terrestrial posture. This greater stability allows a crab to locomote up to 50% faster through water in the aquatic posture than in the terrestrial posture (Table 1). Using the aquatic posture also allows a crab to be active in faster flow environments than it could be if it used the terrestrial posture (Table 3).

Two mechanisms contribute to the greater stability of the aquatic posture relative to the terrestrial posture: 1) the aquatic posture's wider stance increases the moment-arm over which the stabilizing forces act (Fig. 1B; Martinez et al., 1998); and 2) the lower drag coefficient and added mass coefficient associated with the aquatic posture result in smaller forces acting about the overturning moment-arm (Fig. 1B, Table 2). Martinez et al. (1998) predicted that a crab in the aquatic posture could withstand 25% more drag than in the terrestrial posture

before overturning in a steady current. However the present study reveals that the stability of the aquatic posture is somewhat reduced by positive lift, resulting in a smaller increase in drag force (6%) that a crab could withstand before overturning.

Another aspect of posture that affects hydrodynamic forces is the angle of attack. Since the lift on *G. tenuicrustatus* is very sensitive to angle of attack, a crab could substantially alter its stabilizing moment simply by changing its angle of attack by a few degrees (Fig. 6). The aquatic posture affords more opportunity for control of lift than does the terrestrial posture because the aquatic posture shows greater sensitivity of lift to changes in angle of attack (Fig. 6). Yet in faster flow environments, a small increase in angle of attack could result in a much larger lift force, causing the crab to overturn or wash away as it climbed over rugose terrain. Crabs punting slowly in still water do use variable angles of attack, but this variation is limited to shallow positive angles (Martinez, et al., 1998). A crab's risk of overturning increases at faster relative water velocities and accelerations. Since negative angles of attack greatly increase a crab's stability (Tables 1, 3), crabs may use negative angles of attack at higher locomotory speeds and in ambient water flow to help them maintain contact with the substratum and to keep from overturning.

A crab's tenacity provides a very effective mechanism to resist overturning or washing away. A crab's tenacity augments its weight, increasing the hydrodynamic force necessary to dislodge it from the substratum. On a substratum with sufficient availability of footholds, tenacity could increase by more than an order of magnitude the relative water flow an animal could withstand (Table 1). Actively grasping the substratum (hence using a different gait than submerged punting) allows *Grapsus tenuicrustatus* to locomote in its wave-swept habitat, even through breaking waves (Table 4; See Results, Behavior in Waves).

Hiding in a crevice allows a crab to withstand greater ambient water velocities. Koehl (1977) showed that flow microhabitats can be protected even in high flow sites. Furthermore, wedging against the sides of the crevice increases

the water velocity necessary to wash away a crab, although the crab's behavior is still limited by the flow.

Hydrodynamic forces constrain locomotion

Hydrodynamic forces have the potential to constrain the speeds and accelerations an animal can attain while locomoting because at high velocities or accelerations, these forces contribute a large portion to the force balance on the animal (Fig. 7). The power output to locomote at a constant speed is given by the product of the speed at which an animal locomotes and the drag force on the animal at that speed. Assuming a power output of 1.2 W/kg (value for *Ocypode quadrata* running on land, Blickhan and Full, 1987), a 0.07 kg *G. tenuicrustatus* could locomote at a constant speed of 4.45 m/s on land, 0.59 m/s in water using the aquatic posture, or 0.46 m/s using the terrestrial posture. Aside from the power to overcome drag at a given speed, an animal must generate power to accelerate, which can be calculated as the product of acceleration reaction force and the change in speed. The power output required to accelerate a crab using the aquatic posture is 53% greater in water than on land.

Ambient water flow in a habitat can constrain the gait choice and kinematics of aquatic pedestrians. While *Grapsus tenuicrustatus* uses a punting gait in slow water (Martinez *et al.*, 1998), the present study reveals that it could not use this gait in faster water flow because it would overturn (Table 3) unless it used negative angles of attack (which it does not use in slow punting). Maude and Williams (1983) have shown that while standing still, crayfish adopt a lower, more streamlined posture and a negative angle of attack in response to increasingly faster water flow. Because flow habitat can greatly affect pedestrian kinematics (Martinez *et al.*, 1998; Hui, 1992; Maude and Williams, 1983; Grote, 1981; Clarac *et al.*, 1987), the next step in kinematic studies will be to incorporate field flow conditions as well as an animal's behavior in those flow conditions.

In addition to influencing an animal's gait, ambient water motion can constrain or completely inhibit an animal's locomotion. In the very slow flow of the lagoon environment, *Grapsus tenuicrustatus* (using the aquatic posture) incur very little risk of dislodgment; however, in the faster flows of the bay and wave-

swept environments, crabs are constrained to actively grasp the substratum while locomoting or to locomote downstream (Table 3). The lobster *Homarus gammarus* stops locomoting in moderately slow flow and washes away in flow approaching 50 cm/s on a gravel substratum (Howard and Nunny, 1983). Similarly, crayfish may be limited in their distribution by hydrodynamic interaction and their ability to hold onto the substratum to keep from washing away (Maude and Williams, 1983). Likewise, Le Roux et al. (1990) have suggested that green crabs (*Carcinus maenas*) do not invade wave-swept shoreline because they are inhibited by the ambient flow. Restrictions on mobility affect not only an animal's behavior, but consequently its interactions with other organisms. Sea urchins reduce their locomotion and feeding rates in faster flow (Kawamata, 1998). In the intertidal zone, limpets forage less when waves are high (Wright, 1978) and carnivorous gastropods impose low predation intensity at high flow sites (Leonard *et al.*, 1998).

Not only are the dynamics of pedestrian locomotion drastically different in air versus in water, but also in still water compared to in currents or waves. The hydrodynamic forces imposed by ambient water flow constrain how, when, and where a pedestrian may locomote because the animal must generate enough force to overcome hydrodynamic resistance to movement as well as keep from being dislodged from the substratum. In order to assess the role of hydrodynamic forces in pedestrian locomotion, it is critical to consider water flow conditions in the environment as well as the postures and behaviors an animal uses in those water flow conditions.

Acknowledgments

This research was supported by a NSF Predoctoral Fellowship, a U. C. Berkeley Chancellor's Minority Predoctoral Fellowship, a Pauley Grant-in-Aid of Marine Research, and a Sigma Xi Grant in Aid of research to M. Martinez, ONR Grant N00014-92-J-1250 to R. Full, Defense Advanced Research Projects Agency Grant N00014-93-C-0228 to R. Full, M. Koehl, and R. Caldwell, ONR Grant N00014-96-1-0594 and NSF Grant OCE92-17338 to M. Koehl. I thank M. Denny and B. Gaylord for the use of their facilities and the computer software to analyze added mass coefficient data. M. Koehl and T. Cooper generously shared unpublished water flow data. I thank M. Koehl for the use of her videotapes of *G. tenuicrustatus* behavior in waves, and M. Atkinson, E. Reese, and F. Thomas, D. Gulko and the staff at HIMB for their support and assistance. I gratefully acknowledge M. Koehl, W. Lau, R. J. Full and the biomechanics group at UC Berkeley for helping to shape my ideas about this project. W. Lau, B. Waggoner, S. Park and J. Rhuman assisted with data collection and D. Gulko, J. Harriman, and F. Te helped to collect crabs. K. Quillin, M. Koehl, and R. Full provided helpful comments on the manuscript.

Table 1. *Critical speeds (m/s) in aquatic vs. terrestrial postures at 0° angle of attack.*

	Aquatic Posture	Terrestrial Posture
<hr/>		
Washing Away*		
Without active tenacity	0.09	0.03
With maximum tenacity	5.72	3.98
Overturning[^]		
Without active tenacity (e.g. punting)	0.66	0.44
With maximum tenacity	8.20	5.50

*Critical water velocity (with appropriate accelerations measured in the field) to wash away a crab standing still.

[^]Critical speed to overturn a crab locomoting through still water, assuming no body accelerations.

Table 2. *Hydrodynamic coefficients*

	Aquatic Posture*	Terrestrial Posture*	<i>P</i> [†]
Drag coefficient			
Planform area = S_p	0.10 ± 0.02	0.24 ± 0.01	0.018
Projected area = S	0.47 ± 0.08	0.68 ± 0.02	0.018
Lift coefficient			
+4° angle of attack	0.038 ± 0.003	0.026 ± 0.006	0.028
0° angle of attack	0.005 ± 0.001	-0.003 ± 0.004	0.018
-4° angle of attack	-0.033 ± 0.002	-0.036 ± 0.003	0.091
Added mass coefficient	0.48 ± 0.08	0.67 ± 0.18	0.018

*Means of all crabs at all speeds (\pm one standard deviation). $N = 7$ speeds, except for added mass coefficient for which $N = 7$ crabs.

[†] $P < 0.05$ indicates significant difference between aquatic and terrestrial posture.

Table 3. *Washing away and overturning at three field sites.*

	Lagoon ($u = 0.12 \text{ m/s}$)*	Bay ($u = 0.55 \text{ m/s}$)*	Wave-swept ($u = 1.57 \text{ m/s}$)*
Wash away standing still?†			
Aquatic Posture	No (0.15 m/s^2)^	Yes	Yes
Terrestrial Posture	No (0.12 m/s^2)^	Yes	Yes
Overturn punting upstream?‡			
Aquatic posture slow punt	No (1.47 m/s^2)^	No (0.04 m/s^2)^	Yes
Aquatic posture fast punt	No (0.50 m/s^2)^	Yes	Yes
Terrestrial posture slow punt	Yes	Yes	Yes
Terrestrial posture fast punt	Yes	Yes	Yes

Calculations assume 0° angle of attack and no active tenacity.

*Peak water velocity measured at site.

†Due to drag and lift forces only.

^Critical acceleration to wash away or overturn crab under these conditions, assuming that crab does not accelerate into accelerating flow.

‡Slow punting speed = 0.11 m/s . Fast punting speed = 0.40 m/s .

Table 4. *Fate of crabs in waves.*

	Washed away	Did not move	Kept walking
Small wave			
(0 - 0.5 m)* (N = 17)	24%	76%	0%
Medium wave			
(0.5 - 1.0 m)* (N = 32)	6%	88%	6%
Large wave			
(1.0 - 2.0 m)* (N = 17)	6%	88%	6%

5.5 hours of videotape yielded 66 independent crab-waves from six different sites.

*Wave height (before breaking) estimated from video images, using crabs as a size scale.

References

- Alexander, D. E. (1990). Drag coefficients of swimming animals: effects of using different reference areas. *Biol. Bull.* **179**,86-190.
- Alexander, R. McN. (1971). *Size and shape*. London: Edward Arnold Limited.
- Bill, R.G., and W.F. Herrnkind. (1976). Drag reduction by formation movement in spiny lobsters. *Science* . **193**,1146-1148.
- Blake, R.W. (1985). Crab carapace hydrodynamics. *J. Zool. Lond.* **207**,407-423.
- Blickhan, R., and R.J. Full. (1987). Locomotion energetics of the ghost crab II. Mechanics of the centre of mass during walking and running. *J. exp. Biol.* **130**,155-174.
- Carrington, E. (1990). Drag and dislodgement of an intertidal macroalga: consequences of morphological variation in *Mastocarpus papillatus* Kutzing. *J. exp. biol. ecol.* **139**,185-200.
- Clarac, F., Libersat, F., Pflugger, H. J. and Rathmayer, W. (1987). Motor pattern analysis in the shore crab (*Carcinus maenas*) walking freely in water and on land. *J. exp. Biol.* **133**,395-414.
- Denny, M. and B. Gaylord. (1996). Why the urchin lost its spines: hydrodynamic forces and survivorship in three echinoids. *J. exp. Bio.* **199**,717-729.
- Denny, M. W. (1988). *Biology and the mechanics of the wave-swept environment*. Princeton: Princeton University Press.
- Denny, M. W. (1994). Roles of hydrodynamics in the study of life on wave-swept shores. *Ecological morphology*. Eds. P. C. Wainwright and S. M. Reilly. 169-204. Chicago: The University of Chicago Press.
- Denny, M. W., T. L. Daniel, and M. A. R. Koehl. (1985). Mechanical limits to size in wave-swept organisms. *Ecological monographs*. **55**(1):69-102.
- Dudley, R. (1985). Fluid-dynamic drag of limpet shells. *The Veliger*. **28**(1):6-13.
- Fisher, D. C. (1975). Swimming and burrowing in *Limulus* and *Mesolimulus*. *Fossils and Strata*. **4**,281-290.
- Full, R. J. (1989). Mechanics and energetics of terrestrial locomotion: bipeds to

- polypeds. In W. Wieser and E. Gnaiger (eds.), *Energy transformations in cells and organisms*. 175-182. New York:Georg Thieme Verlag Stuttgart.
- Full, R. J. (1997). Invertebrate locomotor systems. *The handbook of comparative physiology*. Ed. W. H. Dantzler. (vol. 2) 853-930. Oxford: Oxford University Press.
- Full, R. J, and M. A. R. Koehl. (1993). Drag and lift in running insects. *J. exp Biol.* **176**,89-103.
- Gans, C., A. Gaunt, and P. Webb. (1997). Vertebrate locomotion. *The handbook of comparative physiology*. Ed. W. H. Dantzler. (vol. 1) 55-214. Oxford: Oxford University Press.
- Gaylord, B. (1997). Implications of hydrodynamic length scales for the ability of fluid acceleration to limit the sizes of wave-swept organisms. Western Society of Naturalists annual meeting. Dec 26-30. Monterey, California.
- Gaylord, B., C. A. Blanchette, and M. W. Denny. (1994). Mechanical consequences of size in wave-swept algae. *Ecological monographs*. **64**(3):287-313.
- Grote, J. R. (1981). The effect of load on locomotion in crayfish. *J. exp. Biol.* **92**,277-288.
- Hayami, I. (1991). Living and fossil scallop shells as airfoils: an experimental study. *Paleobiology*. **17**(1):1-18.
- Houlihan, D.F., and A.J. Innes. (1984). The cost of walking in crabs: aerial and aquatic oxygen consumption during activity of two species of intertidal crab. *Comp. Biochem. Physiol. A*. **77**(2):325-334.
- Houlihan, D.F., E. Mathers, and A.J. El Haj. (1984). Walking performance and aerobic and anaerobic metabolism of *Carcinus maenas* (L.) in sea water at 15° C. *J. Exp. Mar. Biol. Ecol.* **74**,211-230.
- Howard, A. E., and R. S. Nunny. (1983). Effects of near-bed current speeds on the distribution and behaviour of the lobster, *Homarus gammarus* (L.). *J. exp. mar. biol. ecol.* **71**,27-42.
- Hui, C. A. (1992). Walking of the shore crab *Pachygrapsus crassipes* in its two natural environments. *J. exp. Biol.* **165**,213-227.
- Jacklyn, P. M., and D. A. Ritz. (1986). Hydrodynamics of swimming in scyllarid

- lobsters. *J. exp. mar. biol. ecol.* **101**,85-99.
- Jamon, M., and F. Clarac. (1995). Locomotion patterns on freely moving crayfish (*Procambarus clarkii*). *J. exp Biol.* **198**,683-700.
- Kawamata, S. (1998). Effect of wave-induced oscillatory flow on grazing by a subtidal sea urchin *Strongylocentrotus nudus* (A. Agassiz). *J. exp. mar. biol. ecol.* **224**, (1):31-48.
- Keulegan, G. H., and L. H. Carpenter. (1958). Forces on cylinders and plates in an oscillating fluid. *J. Res. N. B. Stand.* **60**(5):423-440.
- Koehl, M. A. R. (1977). Effects of sea anemones on the flow forces they encounter. *J. exp. Biol.* **69**,87-105.
- Koehl, M. A. R. (1982). The interaction of moving water and sessile organisms. *Sci. Am.* **Dec.**,124-133.
- Koehl, M. A. R. (1984). How do benthic organisms withstand moving water? *Am. Zool.* **24**,57-70.
- Le Roux, P. J. , G. M. Branch, and M. A. P. Joska. (1990). On the distribution, diet and possible impact of the invasive European shore crab *Carcinus maenas* (L.) along the South African Coast. *S. Afr. J. mar. sci.* **9**,85-93.
- Leonard, G. H., J. M. Levine et al. (1998). Flow-driven variation in intertidal community structure in a Maine estuary. *Ecology.* **79**, (4):1395-1411.
- Martinez, M. M. (1996). Issues for aquatic pedestrian locomotion. *Am. Zool.* **36**,619-627.
- Martinez, M. M., R. J. Full, and M. A. R. Koehl. (1998). Underwater punting by an intertidal crab: a novel gait revealed by the kinematics of pedestrian locomotion in air vs. water. *J. exp. Biol.* **201**,2609-2623.
- Maude, S. H., and D. D. Williams. (1983). Behavior of crayfish in water currents: hydrodynamics of eight species with reference to their distribution patterns in southern Ontario. *Can. J. Fish. Aq. Sci.* **40**,68-77.
- Nakamura, R. (1994). Lift and drag on inclined sand dollars. *J. exp. mar. biol. ecol.* **178**,275-285.
- Nishimoto, R. T., and W. F. Herrnkind. (1978). Directional orientation in blue crabs, *Callinectes sapidus* Rathbun: escape responses and influence of wave direction. *J. exp. mar. biol. ecol.* **33**,93-112.

- Plotnik, R.E. (1985). Lift based mechanisms for swimming in eurypterids and portunid crabs. *Trans. Roy. Soc. Edin.* 76,325-337.
- Pond, C.M. (1975). The role of the 'walking legs' in aquatic and terrestrial locomotion of the crayfish *Austropotamobius pallipes* (Lereboullet). *J. exp. Biol.* 62,447-454.
- Spirito, C. P. (1972). An analysis of swimming behavior in the portunid crab *Callinectes sapidus*. *Mar. behav. phys.* 1,261-276.
- Torres, J. J. (1984). Relationship of oxygen consumption to swimming speed in *Euphausia pacifica* II. Drag, efficiency and a comparison with other swimming organisms. *Mar. Biol.* 78,231-237.
- Vogel, S. (1981). *Life in moving fluids* Princeton: Princeton University Press.
- Weissenberger, J., H.-C. Spatz, et al. (1991). Measurement of lift and drag forces in the mN range experienced by benthic arthropods at flow velocities below 1.2 ms^{-1} . *Freshwater Biol.* 25,21-31.
- Withers, P. C., and P. L. Timko. (1977). The significance of ground effect to the aerodynamic cost of flight and energetics of the black skimmer (*Rhyncops nigra*). *J. exp. Biol.* 70,13-26.
- Wright, W. G. (1978). Aspects of the ecology and behavior of the owl limpet, *Lottia gigantea* Sowerby 1834. *West. Soc. Malac. Ann. Rep.* 11:7.

Figure Legends

Figure 1.A. Forces acting on the body of a crab locomoting through a fluid environment. The crab in the diagram is locomoting with its left side leading and is moving upstream against an ambient water current. The fluid motion relative to the crab is the vector sum of the flow due to the ambient current and the flow due to the motion of the crab. Buoyancy counteracts the crab's weight. Lift, which acts perpendicular to the relative fluid motion, counteracts the weight (positive lift, acting away from the substratum) or augments the weight (negative lift, acting toward the substratum). Drag acts in the direction of relative fluid motion, resisting locomotion and tending to push the crab downstream. Acceleration reaction resists changes in velocity, augmenting drag as a crab accelerates relative to the fluid and counteracting drag as the crab decelerates. B. A crab overturns, pivoting about its downstream leg, when the overturning moment about its center of mass exceeds the stabilizing moment. The overturning moment is the net horizontal force times the height of the center of mass. The stabilizing moment is the net vertical force times the distance from the center of mass to the trailing leg. C. A crab that does not actively grasp the substratum washes away when the net horizontal force on its body exceeds the frictional force resisting dislodgment.

Figure 2. Speeds of five different crabs locomoting through still water over a flat substratum. Each data point represents one trial for an individual crab. Circles indicate slow punting and triangles indicate fast punting. A mean speed for each of these gaits was calculated for each crab; the overall mean for each gait (shown at the right of the graph) was calculated as the mean of the mean speeds of the five crabs.

Figure 3. The two postures of *Grapsus tenuicrustatus* (from Martinez et al., 1998) effected by changes in the ischium-merus joint and the merus-carpus joint.

Figure 4. Water flow records from the lagoon, bay and wave-swept sites, measured at the approximate height of a crab (0.06 m above the substratum). Mean and maximum velocities measured for the trials shown were 0.02 m/s, 0.04 m/s (lagoon), 0.21 m/s, 0.40 m/s (bay), and 0.30 m/s, 0.91 m/s (wave-swept site).

Figure 5. Hydrodynamic forces on the body of a crab using the terrestrial and aquatic postures at 0° angle of attack. Each data point represents the mean of five trials for an individual crab. Error bars indicate \pm one standard deviation. Reynolds numbers (based on maximum lateral width of a crab) range from 2.5×10^4 to 2.0×10^5 . Drag force was significantly different for the two postures at all velocities except 0.15 m/s. Lift force was not significantly different for the two postures. Arrows indicate the mean slow and mean fast punting speeds.

Figure 6. Lift force on the body of a crab as a function of angle of attack. Data points represent the means of the means of five crabs at a velocity of 0.98 m/s for one individual crab in the aquatic and the terrestrial posture. Error bars indicate \pm one standard deviation. These data illustrate the results shown for each of the crabs tested, although the actual values varied: the absolute value of the magnitude of the lift at angles of attack of $+4^\circ$ or -4° were greater for the aquatic posture than for the terrestrial posture, and lift acted upwards at angle of attack = $+4^\circ$ but downwards at angle of attack = -4° .

Figure 7. The mean of the mean values for all crabs were used to calculate an estimate of forces acting on the body of a crab using different postures in various flow conditions. Fluid motion relative to the crab is right-to-left. Longer arrows represent larger forces. In air crabs are shown only in the terrestrial posture. W_{app} = apparent weight (weight-buoyancy); A = acceleration reaction; D = drag; L = lift. A. Crab is locomoting through still fluid (water or air). Fastest punting speed in water = 0.67 m/s. Fastest

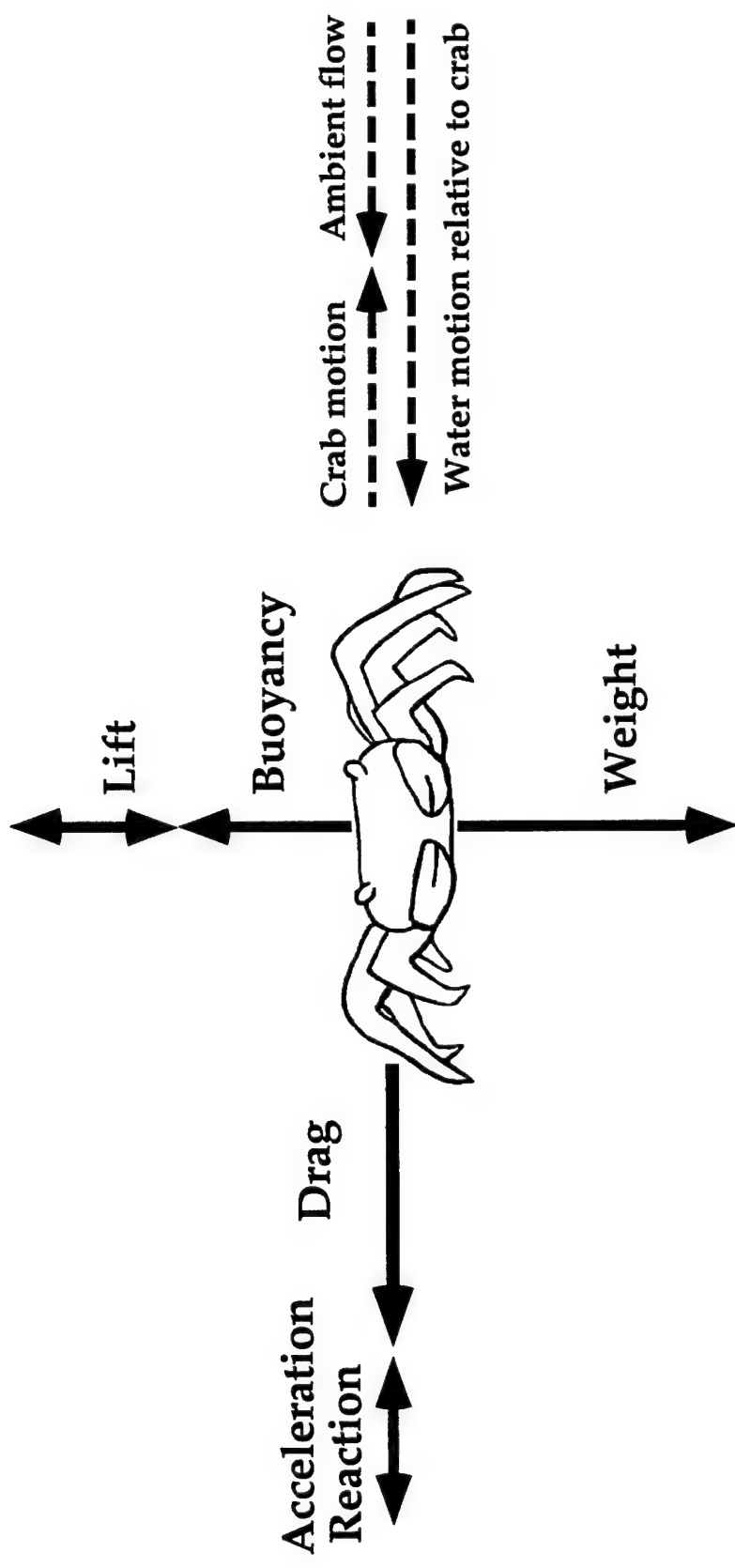
recorded run on land = 1.4 m/s. Crab is locomoting at +4° angle of attack. Body acceleration = 1.13 m/s². B. Crab is standing in moving fluid (water or air). Fastest water flow measured in the field at wave-swept site = 1.6 m/s, 1.71 m/s². Air speed in hurricane ≈ 45 m/s. Crab is standing with 0° angle of attack relative to oncoming flow. Acceleration reaction force was not calculated in the terrestrial hurricane condition because acceleration data appropriate to the size scale of a crab were not available. Note that a crab locomoting in water at its fastest punting speed generates positive lift greater than its effective weight if that crab were to use a +4° angle of attack.

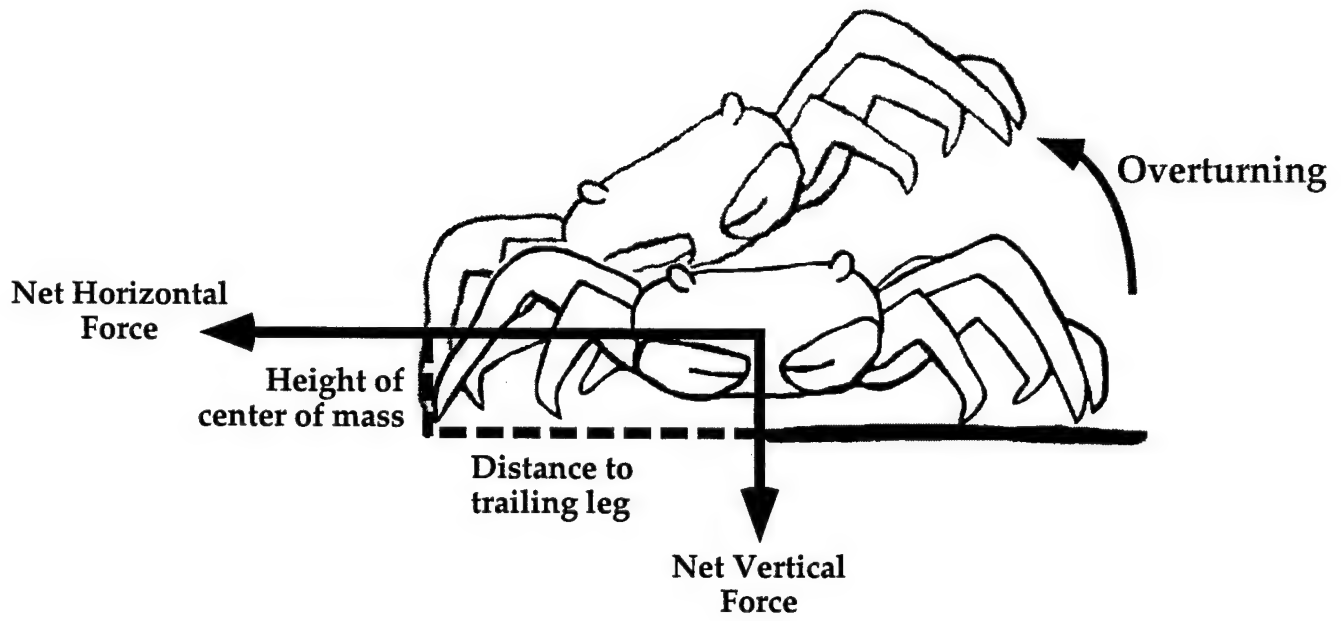
Figure 8. Effect of body acceleration on the critical punting speed to overturn a crab in still water. Mean of mean measurements for five crabs were used to calculate critical punting speed. Filled symbols and solid lines represent a crab in the aquatic posture. Open symbols and dashed lines represent a crab in the terrestrial posture. Circles, squares and triangles indicate -4°, 0°, and +4° angles of attack, respectively. At slow speeds, the submerged weight of the animal contributes substantially to its stabilizing moment, allowing the animal to locomote slowly even if the ratio of its drag to lift is somewhat greater than the ratio of the lift moment-arm to the drag moment-arm. Drag and lift forces increase at the same rate with an increase in velocity, whereas submerged weight and acceleration reaction forces are independent of velocity. Thus it is possible for an animal to be stable at any speed (below a critical acceleration value) if it generates negative lift such that the lift times its moment-arm is greater than the drag times its moment-arm. *Grapsus tenuicrustatus* uses body accelerations of 1.1 m/s² during slow punting in water (Martinez et. al, 1998). Ghost crabs, *Ocypode quadrata*, use body accelerations of 0.27 m/s² during a fast walk on land and 3.12 m/s² during a fast run on land (Blickhan and Full, 1987).

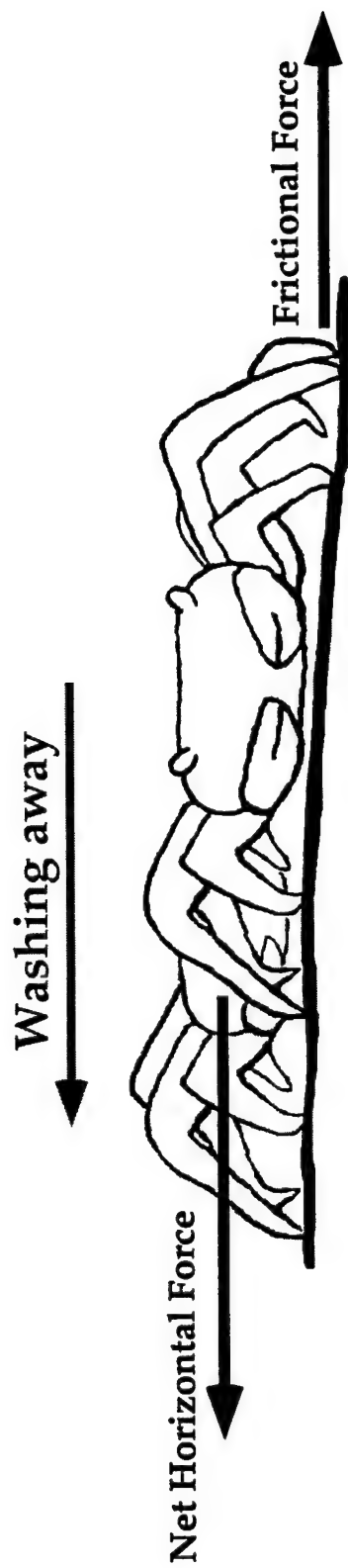
Figure 9. Effect of water acceleration on the critical ambient water velocity necessary to wash away a crab standing with an angle of attack of 0°. Calculations assumed crabs grasped the substratum with maximum

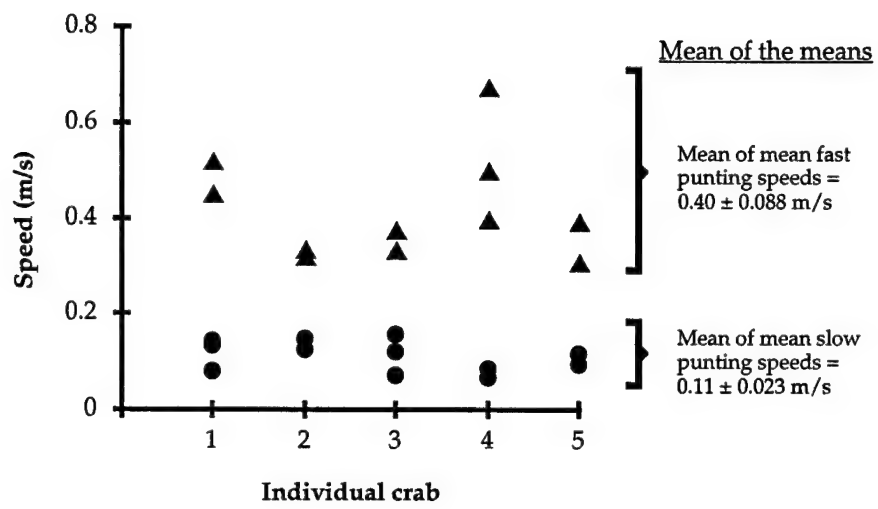
horizontal tenacity (13 N). Mean of mean measurements for five crabs were used to calculate critical water velocities. Grey symbols indicate a crab using the aquatic posture. Open symbols represent a crab using the terrestrial posture in water.

Figure 10. Drag and lift coefficients as a function of Reynolds number for various animals. Black and grey diamonds indicate data for *Grapsus tenuicrustatus* in the aquatic and terrestrial postures, respectively. Diamonds represent data measured on animals near a substratum. Circles represent data measured on animals far from a substratum. (A, B, C) crabs (Blake, 1985); (D) crab (Plotnik, 1985); (E, F) crayfish (Maude and Williams, 1983); (G) lobster (Bill and Herrnkind, 1976); (H) lobster in tail-flip posture (Jacklyn and Ritz, 1986); (I, J) isopods (Alexander, 1990); (K) euphausid (Torres, 1984); (L) eurypterid (Plotnik, 1985); (M, N) cockroaches (Full and Koehl, 1993); (O) barnacle, (P) snail, (Q, R) limpets (Denny et al., 1985); (S) scallop (Hayami, 1991); (T) sea urchin (Denny and Gaylord, 1996); (U) inclined sand dollar (Nakamura, 1994); (V) sea anemone (Koehl, 1977). Lift coefficients measured at positive angles of attack: *G. tenuicrustatus* +4°; (A, B, C) +5°; (S) +25°.

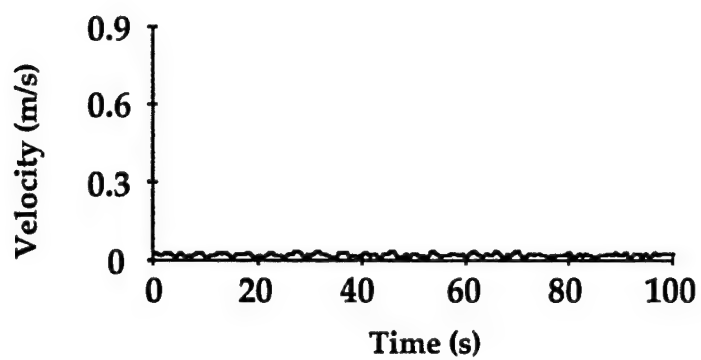




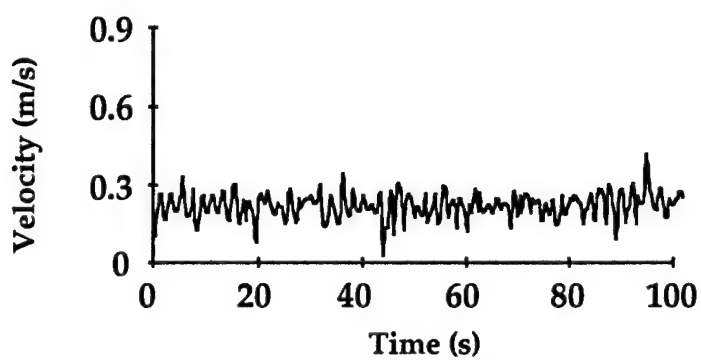




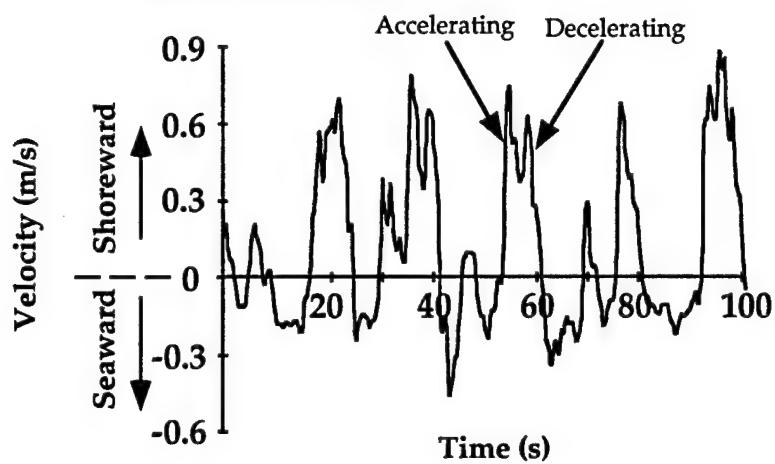
Lagoon site

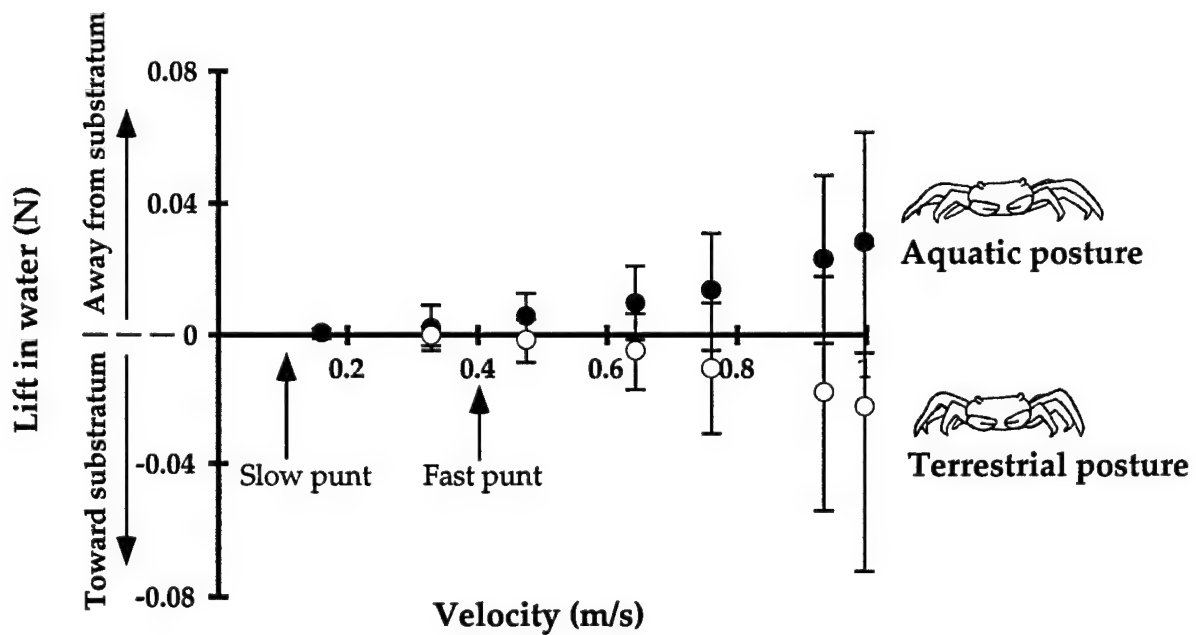
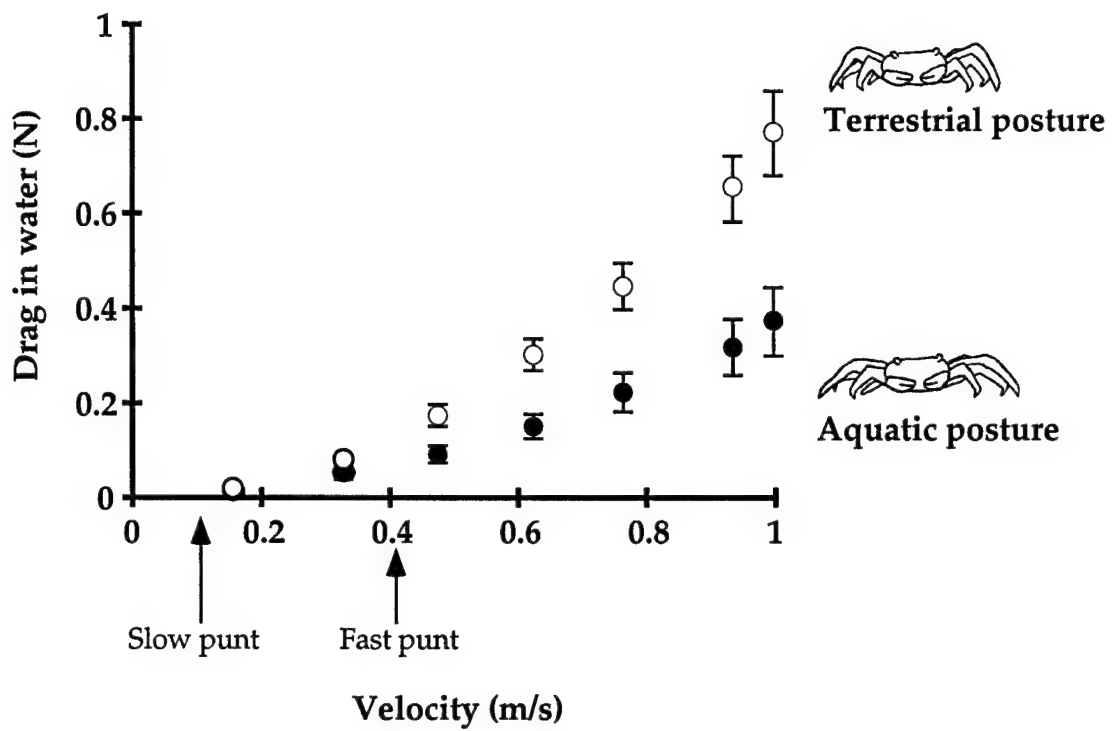


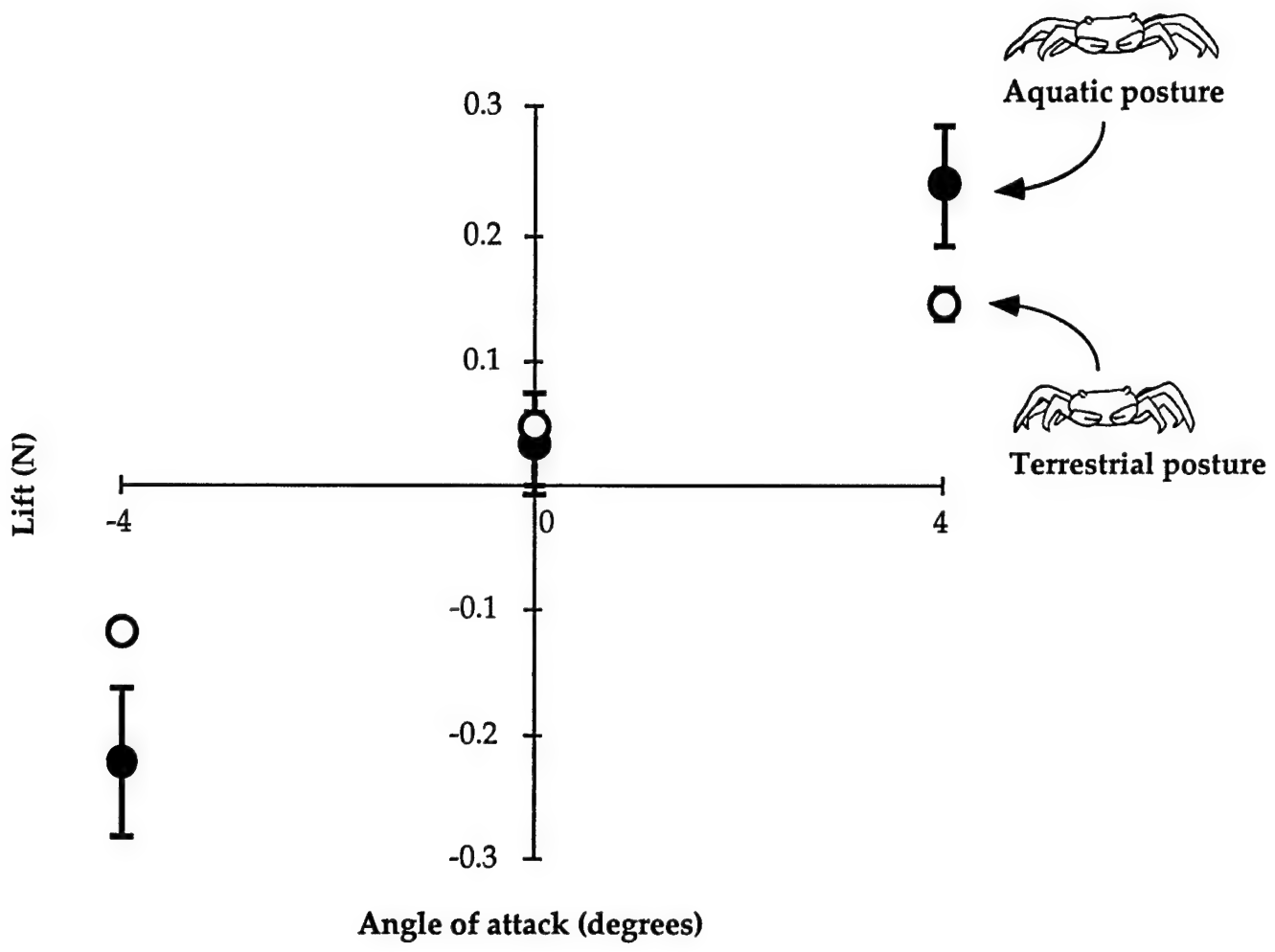
Bay site



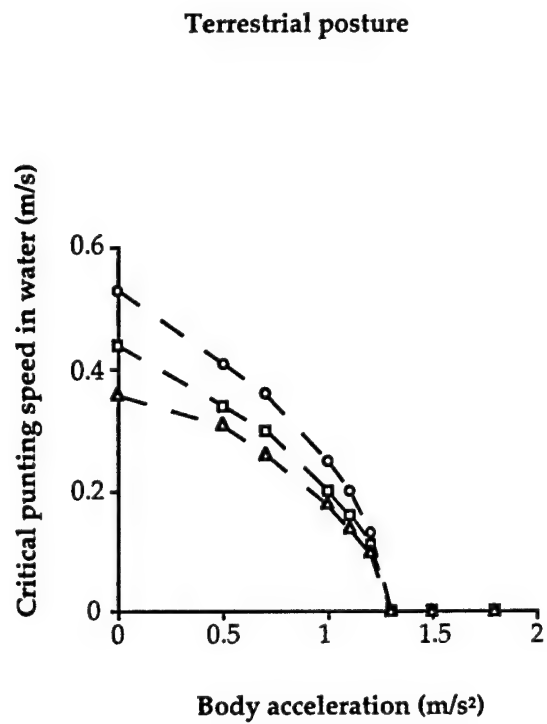
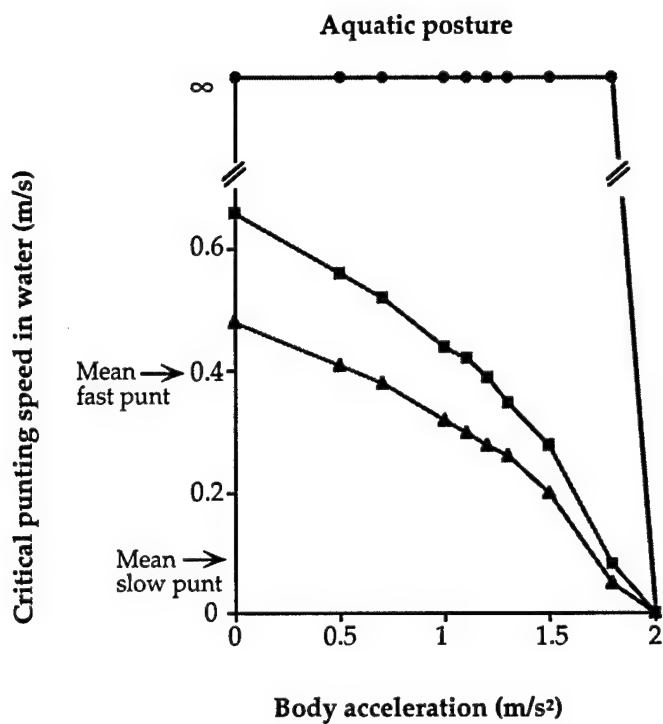
Wave-swept site

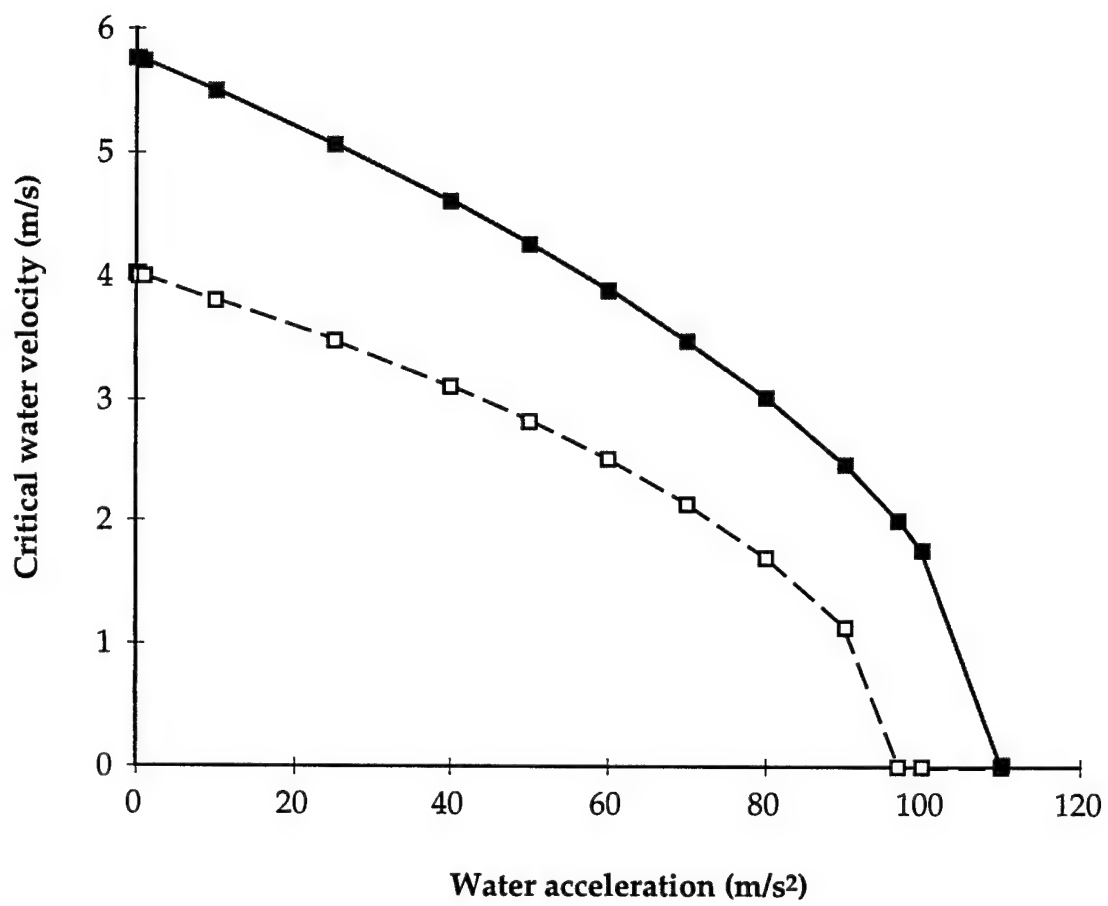


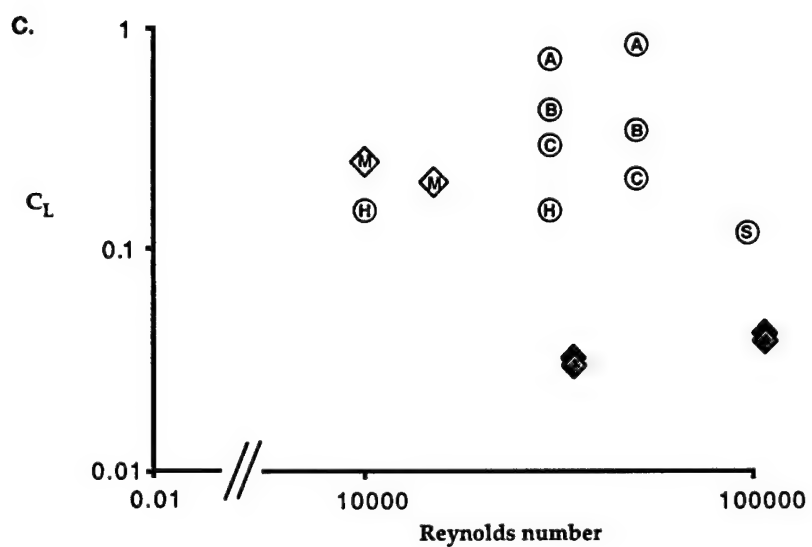
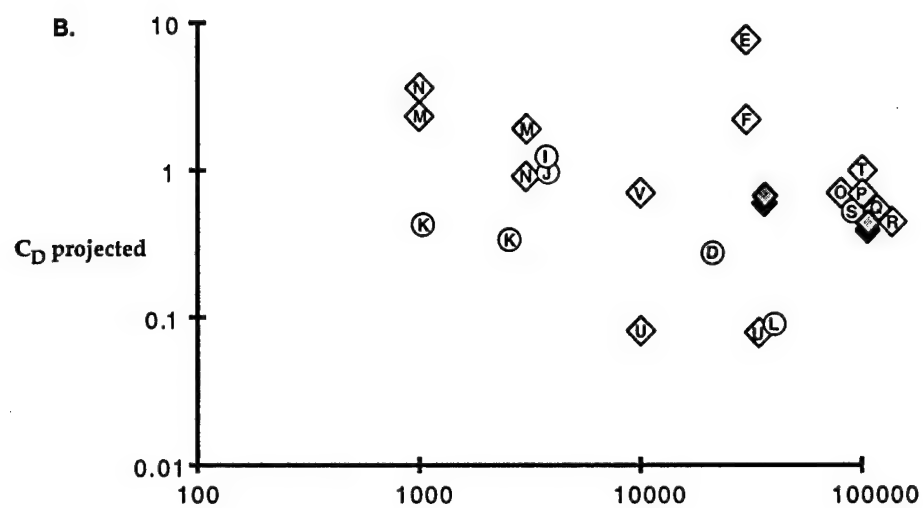
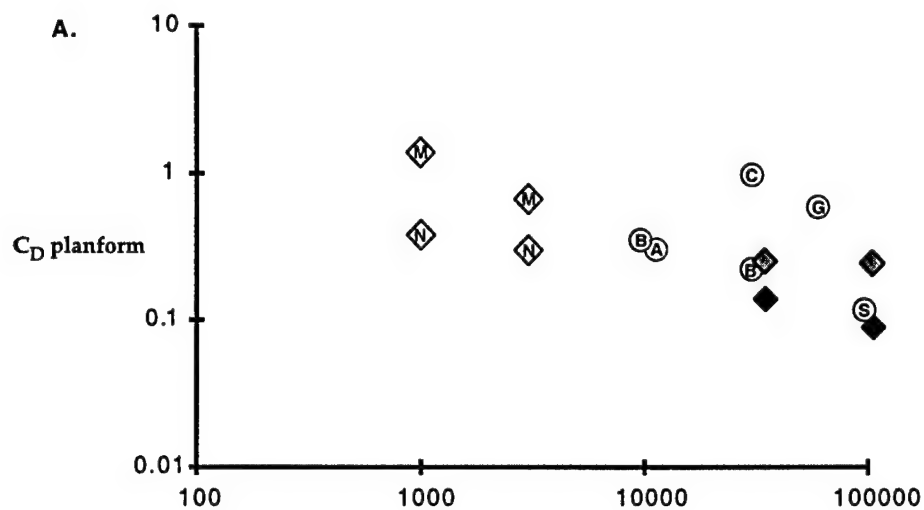




	IN WATER	IN AIR
A.	<p><u>Still water</u> <u>Fastest recorded punting speed</u></p> <p>Aquatic posture</p> <p>Terrestrial posture</p>	<p><u>Still air</u> <u>Fastest recorded run</u></p>
B.	<p><u>Fast ambient flow</u> <u>Standing still</u></p> <p>Aquatic posture</p> <p>Terrestrial posture</p>	<p><u>Fast ambient flow</u> <u>Standing still</u></p>







LOCOMOTOR PERFORMANCE OF SUBTIDAL,
INTERTIDAL AND SEMI-TERRESTRIAL CRABS IN
AIR VS. WATER. Marlene M. Martinez, University of
California, Berkeley. marlenem@garnet.berkeley.edu

Studying how the mechanics of pedestrian locomotion changes in water versus on land will contribute to our understanding of the evolutionary transition between aquatic and terrestrial environments as well as of the behavior and ecology of amphibious legged animals. Seven benthic crab species were chosen as subtidal, intertidal, and semi-terrestrial representatives of a lineage, allowing comparison within an individual as well as across the lineage. Performance differences were predicted for locomotion on land versus in water since in water, effective weight is substantially reduced by buoyancy while the fluid dynamic forces are increased 800-fold compared to on land. Maximum average sprinting speed as a function of air versus water and over two types of substratum (sand and textured rock) was obtained for several individuals of each species. Performance correlated with natural habitat: semi-terrestrial crabs *Grapsus tenuicrustatus* and *Ocypode quadrata* showed greatest speeds on land, subtidal *Cancer magister* showed greatest speed in water, whereas the intertidal crab *Carcinus maenas* showed no difference as a function of either water versus air or as a function of substratum type. Important features that affect performance include the ability to support the body above the substratum and dactyl penetration of the substratum. Neither *Cancer* nor *Carcinus* could support their body weight on land, necessitating dragging the body along the substratum with each step. Furthermore, *Cancer* could manage only very slow speeds in sand on land as its legs sliced through the wet sand.

(1996) Am. Zool. 35: 8A.

AERODYNAMIC STABILITY AND
MANEUVERABILITY OF GLIDING FROGS.
M.G. McGay. University of California at Berkeley.
mccav@gamet.berkeley.edu

Although many studies of the origin of animal flight have focused on aspects of gliding or parachuting performance such as distance traveled or time aloft, the aerodynamics of maneuverability has received less attention. Maneuverability, the ability to change the direction of the glide path, is highly dependent on the aerodynamic stability of the animal. A more stable animal better resists perturbations to its motion. While high stability means that the animal needs to perform less postural adjustments in response to disturbances from gusts, high stability also means the animal will resist intentional disturbances such as the initiation of maneuvers by the animal. Thus, a trade-off exists in that stable flyers require less active control to stay on course, but are less maneuverable than gliders with reduced stability. The motion of Rhacophoridae tree frogs (*Rhacophorus leucomystax*) gliding in a tilted wind tunnel were analyzed to assess stability versus maneuverability. The frog was filmed in two views by 8mm video cameras, and 3-D kinematic analysis was performed to quantify the frog's posture during gliding as well as postural responses to disturbances. Motion analysis reveals several stereotyped postures used for steady gliding, maneuvering, and attitude stabilization. The frog's reactions to disturbances indicate strong overall longitudinal stability, but weak lateral-directional stability. Relatively few postural changes were observed in response to disturbances about the pitch axis, while active control using postural changes was required to recover from disturbances about the roll and yaw axes. These observed behaviors indicate high maneuverability in the roll and yaw axes, thus enhancing turning performance.

(1996) Am. Zool. 35: 8A.

AERODYNAMIC STABILITY AND MANOEUVRABILITY
OF GLIDING FROGS. *McCay, M. G. University of
California, Berkeley, USA*

Although many studies of the origin of animal flight have focused on aspects of gliding or parachuting performance such as distance traveled or time aloft, the aerodynamics of manoeuvrability has received less attention. Manoeuvrability, the ability to change the direction of the glide path, is highly dependent on the aerodynamic stability of the animal. A more stable animal better resists perturbations to its motion. While high stability means that the animal needs to perform less postural adjustments in response to gusts, high stability also means that the animal will resist intentional disturbances such as the initiation of manoeuvres by the animal. Thus, a trade-off exists in that stable gliders require less active control to stay on course, but are less manoeuvrable than gliders with reduced stability. The motion of macophond tree frogs (*Rhacophorus leucomystax*) gliding in a tilted wind tunnel was analysed to assess stability versus manoeuvrability. The frog was filmed in two views by 8 mm video cameras, and three-dimensional kinematic analysis was performed to quantify the frog's posture during gliding. Motion analysis reveals stereotyped postures used during gliding and manoeuvring. Relatively low variability in pitch angle, and high variability in roll and yaw angles indicate strong overall longitudinal stability, and weak lateral-directional stability. The observed behaviours indicate high manoeuvrability in the roll and yaw axes, thus enhancing turning performance.

(1997) J. Morph. 282: 294.

51
A COMPARISON OF THE AERODYNAMIC
STABILITY OF THREE SPECIES OF
NEOTROPICAL TREE FROG: HOW DOES
STABILITY CHANGE WITH GLIDING ABILITY?
M.G. McCay, Univ. of California, Berkeley.
mccay@socrates.berkeley.edu

A critical step in the evolution of flight is developing the ability to control direction of flight. Aerodynamic stability affects both maintaining direction of flight, and maneuvering. Aerodynamic stability permits a gliding animal to maintain its direction of flight without actively steering. Aerodynamic stability also resists intentional disturbances to direction of flight such as the initiation of turning maneuvers. Gliding has originated independently in 2 families of frogs: Rhacophoridae and Hylidae. Gliding tree frogs possess a suite of morphologies and behaviors associated with gliding such as enlarged, extensively webbed hands and feet. Among Phyllomedusinae, a subfamily of Hylidae, gliding has evolved in the genus *Agalychnis*. To assess how stability changes with gliding ability, I compared the aerodynamic stability of 3 *Agalychnis* species. The species chosen represent 3 stages in the development of gliding within this genus: 1) *Agalychnis callidryas*, a frog with minimal webbing on its hands and feet, 2) *A. calcarifer*, a frog with an intermediate amount of webbing on its hands and feet, and 3) *A. spurrelli*, a frog with extensively webbed hands and feet. Aerodynamic stability and maneuverability were assessed using aerodynamic forces and torques measured from physical models of the frog species in a wind tunnel.

(1998) Amer. Zool 38: 150A

TWITCHING, TWISTING, AND TWIRLING IN
TUNICATE TADPOLE TODDLERS: THE
KINEMATICS OF SWIMMING IN ASCIDIANS.
M.J. McHenry, Univ. of California, Berkeley, CA.
mchenry@socrates.berkeley.edu

The tadpole larvae of ascidians function solely for dispersal by undulatory swimming. How does the undulatory motion of the morphologically simple larval tail facilitate both thrust generation and orientation behavior? This question was addressed by studying the undulatory movement and swimming trajectory in the colonial *Borystoides* in three dimensions with high-speed video. As in larval fishes and amphibians, lateral amplitude increased as waves traveled posteriorly. Unlike vertebrates, the body rolled continuously around the axis of progression, the tail-beat amplitude and frequency were relatively large (e.g. 1.6 mm at 19.5 Hz in a 2.8 mm individual), and the tail fin twisted and beat wider from right to left than the opposite direction. The trajectory of this unusual swimming was in the shape of a narrow left-handed helix, which is characteristic orientation behavior of many ciliated and flagellated microorganisms, but was unexpected because tadpole larvae swam at an intermediate Reynolds number ($Re = 50$). Changes in the radius the helix were correlated with lateral displacement of the tail and its pitch was positively correlated with swimming speed ($p < 0.05$). These results suggest that tadpole larvae generate thrust like larval vertebrates, but their peculiar form of undulatory motion also functions to orient movement like microorganisms.

(1997) Amer. Zool. 38: 194A

LIKE FISH AND FLAGELLATES: THE 3D
KINEMATICS OF SWIMMING MANEUVERS BY
ASCIDIAN LARVAE (*DISTAPLIA OCCIDENTALIS*)
M.J. McHenry and E. Azizi. Univ. of California,
Berkeley. mchenry@socrates.berkeley.edu.

The 'tadpole' larvae of ascidians swim by lateral undulations of the tail. Although this motion resembles fish swimming, ascidian larvae move along a helical trajectory like flagellated microorganisms. How does the body of an ascidian larva move to be able to follow a helix and how are these movements altered to change the direction of swimming? We addressed these questions by analyzing the three-dimensional kinematics of individuals of *Distaplia occidentalis* filmed with high-speed video (500 fps). Individuals swam with bilaterally asymmetric undulations having greater head yaw to the left and faster wavespeed (up to 20%) in bends directed concave-right. The degree of asymmetry remained constant when individuals swam along a straight helix. The radius of such a helix was wider in individuals swimming with a greater degree of asymmetry. When asymmetry did change, the axis of the helix curved and larvae changed their direction of swimming. Therefore, bilateral asymmetry appears to be important for swimming along a helix and asymmetry may be modulated to change swimming direction.

(1998) Amer. Zool 37: 451A

SIZE, SPEED, AND STINK: HOW THE BOUNDARY^{2/1}
LAYER SURROUNDING STOMATOPOD
CHEMOSENSORY SETAE DURING OLFACTORY
FLICKING CHANGES AS THE ANIMALS GROW.
K.S. Mead. Department of Integrative Biology,
University of California, Berkeley.
kmead@socrates.berkeley.edu

Stomatopods, like many crustaceans, sample their chemical environment by flicking their antennules. This abrupt movement facilitates odorant access to the chemosensory setae (aesthetascs) on the lateral flagellum of the antennule. Previous studies have shown that the Reynolds numbers describing flow around stomatopod aesthetascs during flicking change dramatically as the animals grow from juveniles to adults. This study examines changes in the structure of the boundary layer that occur between the outward and return strokes of the flick and between large and small specimens of *Gonodactylus mutatus*. Large scaled physical models of aesthetasc-bearing antennule segments from large and small stomatopods were dragged through Karo syrup in a large tow tank. Flow was visualized by seeding the Karo syrup with neutrally buoyant reflective particles and illuminating them with lasers arranged to provide discrete light sheets. Boundary layer structure and sample volume per flick were determined from measurements of particle velocities relative to the models.

(1998) *Amer. Zool* 38: 82A

ONTOGENETIC SCALING OF HYDROSTATIC SKELETONS: GEOMETRIC, STATIC STRESS AND DYNAMIC STRESS SCALING OF THE EARTHWORM *LUMBRICUS TERRESTRIS*

KIM J. QUILLIN

Department of Integrative Biology, University of California, Berkeley, CA 94720-3140, USA

e-mail: quillin@socrates.berkeley.edu

Accepted 23 March; published on WWW 21 May 1998

Summary

Soft-bodied organisms with hydrostatic skeletons range enormously in body size, both during the growth of individuals and in the comparison of species. Therefore, body size is an important consideration in an examination of the mechanical function of hydrostatic skeletons. The scaling of hydrostatic skeletons cannot be inferred from existing studies of the lever-like skeletons of vertebrates and arthropods because the two skeleton types function by different mechanisms. Hydrostats are constructed of an extensible body wall in tension surrounding a fluid or deformable tissue under compression. It is the pressurized internal fluid (rather than the rigid levers of vertebrates and arthropods) that enables the maintenance of posture, antagonism of muscles and transfer of muscle forces to the environment. The objectives of the present study were (1) to define the geometric, static stress and dynamic stress similarity scaling hypotheses for hydrostatic skeletons on the basis of their generalized form and function, and (2) to apply these similarity hypotheses in a study of the ontogenetic scaling of earthworms, *Lumbricus terrestris*, to

determine which parameters of skeletal function are conserved or changed as a function of body mass during growth (from 0.01 to 8 g). Morphometric measurements on anesthetized earthworms revealed that the earthworms grew isometrically; the external proportions and number of segments were constant as a function of body size. Calculations of static stresses (forces per cross-sectional area in the body wall) during rest and dynamic stresses during peristaltic crawling (calculated from measurements of internal pressure and body wall geometry) revealed that the earthworms also maintained static and dynamic stress similarity, despite a slight increase in body wall thickness in segment 50 (but not in segment 15). In summary, the hydrostatic skeletons of earthworms differ fundamentally from the rigid, lever-like skeletons of their terrestrial counterparts in their ability to grow isometrically while maintaining similarity in both static and dynamic stresses.

Key words: biomechanics, scaling, hydrostatic skeleton, earthworm, *Lumbricus terrestris*, ontogeny, size.

Introduction

Body size influences almost every aspect of the biology of an organism, from its physiology and ecology to the mechanical functioning of its skeleton (reviewed in Gould, 1966; Currey, 1970; Alexander, 1971; Pedley, 1977; McMahon, 1973, 1975; McMahon and Bonner, 1983; Peters, 1983; Calder, 1984; Schmidt-Nielsen, 1984). Studies on the scaling of skeletons have concentrated on vertebrates, arthropods and trees whose rigid bones, exoskeletons and trunks, respectively, are loaded as beams and columns by their own body weight. Other studies have examined the scaling of structures loaded in pure tension (e.g. fruit stems and kelp stipes; Peterson *et al.* 1982; Johnson and Koehl, 1994). While these studies have established a foundation of useful scaling principles, they are not directly applicable to the problem of how hydrostatic skeletons scale.

Soft-bodied organisms with hydrostatic skeletons are abundant and diverse. Body mass differs by at least 13 orders of magnitude from giant squid (*Architeuthis* sp., 20 m long

including tentacles) to minute nematode worms (less than 1 mm length) (Ruppert and Barnes, 1995). Body size also increases by orders of magnitude during the growth of many soft-bodied organisms, for example by four orders of magnitude in body mass in the earthworm *Lumbricus terrestris*. Clearly, size is an important variable for soft-bodied organisms, but what effect does body size have on the biomechanical functions of hydrostatic skeletons?

The hydrostatic skeletons of most soft-bodied organisms are constructed from an extensible body wall in tension surrounding a fluid or deformable tissue under compression (Chapman, 1958; Wainwright, 1988). The fluid under compression becomes pressurized, and it is this pressure (rather than the rigid levers of vertebrates and arthropods) that enables stiffening of the organism, antagonism of muscles and transfer of muscle forces to the environment (e.g. Chapman, 1958; Currey, 1970; Trueman, 1975). Hydrostatic skeletons may encompass whole organisms, either for an entire lifetime

(e.g. earthworms) or for one life-history stage (e.g. caterpillars), or alternatively may occur in just parts or appendages of an organism (e.g. tongues in vertebrates and tube feet in echinoderms). Hydrostatic appendages whose requisite incompressible fluid is contained within deformable muscle cells are called muscular hydrostats (e.g. elephant trunks and squid tentacles; Kier and Smith, 1985). In contrast, hydrostatic skeletons describe a body cavity filled with sea water, blood, coelomic fluid and/or deformable organ tissues (e.g. sea anemones, roundworms and earthworms; see Kier, 1992).

Objectives

How does a soft-bodied organism grow by orders of magnitude in body size yet maintain the biomechanical functions of its hydrostatic skeleton? The objectives of the present study were (1) to generate the geometric, static stress and dynamic stress similarity scaling hypotheses for hydrostatic skeletons on the basis of their form and function, and (2) to apply these similarity hypotheses to the ontogeny of the earthworm *Lumbricus terrestris* to determine which aspects of skeletal function are conserved or altered as a function of size during growth.

Scaling hypotheses

Whether a particular functional aspect of a skeleton is conserved or altered in relation to body mass is typically expressed in terms of a scaling hypothesis. Some hypotheses are based on form ('geometric similarity') whereas others are based on function (e.g. 'stress similarity'). The functional similarity hypotheses have been defined previously in terms of the mechanism of mechanical function of lever-like skeletons. Since hydrostatic skeletons function by a qualitatively different mechanism from lever-like skeletons, both the predictions of the similarity hypotheses and their relationships to one another must be derived anew.

Geometric similarity

If two organisms are geometrically similar, or isometric, then linear dimensions are proportional to volume raised to the one-third power. Linear dimensions scale as (body mass)^{1/3} because mass is proportional to volume which is proportional to the cube of length, when body density is constant (e.g. Thompson, 1917; Alexander, 1971; Schmidt-Nielsen, 1984; Fig. 1). The exponential relationship between linear dimensions and body mass can be expressed by the function $y = am_b^b$ (Huxley, 1932), where m_b is body mass, y is a linear dimension, a is a constant and b is the exponent (1/3 in the case of geometric similarity). If the exponent is significantly different from 1/3, scaling is said to be allometric.

Most hydrostatic skeletons are cylindrical in shape, having an approximately round or elliptical cross section and an easily identifiable longitudinal axis (Wainwright, 1988). Therefore, the most important linear dimensions are length (L), diameter (d) and body wall thickness (t), all of which scale as $m_b^{1/3}$ in geometrically similar organisms in comparable postures, such

as resting posture. If the cylindrical body of a hydrostat is divided into segments (as in annelids), then the number and linear dimensions of segments scale as m_b^0 and $m_b^{1/3}$, respectively, in geometrically similar organisms.

Static stress similarity

Static stress is the force (F) per cross-sectional area (A) of a skeletal element bearing the force when an organism is standing still (Thompson, 1917; Hill, 1950; McMahon, 1975). Static stress similarity occurs when static stress is constant as a function of body mass (i.e. $\text{stress} \propto m_b^0$). The loading of beam-like skeletons by body weight precludes the possibility that they are both geometrically and statically stress similar. Weight is proportional to the cube of the linear dimension, while the cross-sectional area of a skeletal element is proportional only to the square of the linear dimension. Therefore, static stress in a self-loaded beam can only remain constant as a function of body size if diameter increases at a greater rate than length (e.g. McMahon, 1975; Fig. 1). Bending beams must scale allometrically, not geometrically, to maintain static stress similarity.

The major source of static load on the body wall of a hydrostatic skeleton is internal pressure (P). Pressure can be generated by the contraction of muscles in the body wall surrounding the incompressible fluid and/or by mechanisms such as ciliary pumps (e.g. in sea anemones; Batham and Pantin, 1950), osmotic pressure (e.g. notochords; Adams *et al.* 1990) and gravitational pressure (the gradient of pressure produced in a static fluid by its own weight; e.g. Ellers and Telford, 1992). The magnitude of tensile stress in the body wall of a cylindrical hydrostatic skeleton is given by:

$$\sigma_c = \frac{Pr}{t} \quad \text{and} \quad \sigma_l = \frac{Pr}{2t}, \quad (1)$$

(Fig. 2A; Chapman, 1950), where σ_c is the circumferential tensile stress, σ_l is the longitudinal tensile stress, P is the internal pressure, r is the radius and t is the body wall thickness. The stress is distributed uniformly over the thickness of the wall provided that the wall is very thin (generally indicated by a ratio r/t that is greater than 10; Gere and Timoshenko, 1984). The thicker the wall relative to the radius, the more important shear stress becomes because of the differential in tensile stress between the outside and the inside of the wall. The maximum shear stress (τ_{\max}) in the body wall is given by:

$$\tau_{\max} = \frac{Pr}{2t} + \frac{P}{2}, \quad (2)$$

where the last term is generally disregarded when the ratio r/t is high (Gere and Timoshenko, 1984). Since shear stress is directly proportional to tensile stress for a given cylinder, and since maximum tensile stress is generally of greater magnitude than maximum shear stress, tensile stress will be the focus of the remainder of this study.

Unlike the case for rigid skeletons, static stress similarity is

Fig.
con
org:
ver:
skel
det:
wal
due
are:
load
inte
reac

not
and
the
stro
pre
sin
on
pre
pol
res
(Cl
ma
fall
mu
geo
as
Th
by:

	LEVER-LIKE SKELETONS	HYDROSTATIC SKELETONS
Geometric Similarity	$d \propto m_b^{1/3}$ $L \propto m_b^{1/3}$ $d \propto L$	$d \propto m_b^{1/3}$ $L \propto m_b^{1/3}$ $t \propto m_b^{1/3}$ $d \propto L \propto t$
Static Stress Similarity	$\frac{F_w}{A} \propto m_b^0$ $d \propto L^2$	$\frac{P_R r}{t} \propto m_b^0$ $d \propto L \propto t$
Dynamic Stress Similarity	$\frac{F_w + F_{acc}}{A} \propto m_b^0$ <p>(depends on behavior)</p>	$\frac{P r}{t} \propto m_b^0$ <p>(depends on behavior)</p>

Fig. 1. Schematic comparison and contrast of the similarity hypotheses for organisms with lever-like skeletons versus organisms with hydrostatic skeletons. See Introduction for further details. d , diameter; L , length; t , body wall thickness; m_b , body mass; F_w , force due to body weight; A , cross-sectional area of a skeletal element bearing the load; P_R , internal pressure during rest; P , internal pressure; r , radius; F_{acc} , ground reaction force.

not excluded by geometric similarity in hydrostatic skeletons. and *vice versa*; hydrostats that are geometrically similar (and therefore possess the same r/t ratio) may or may not show static stress similarity depending on the magnitude of internal pressure. Likewise, hydrostats that are *not* geometrically similar may or may not show static stress similarity depending on the magnitude of internal pressure.

The scaling of static stress depends on the source of internal pressure in animals at rest. Many animals, such as the marine polychaete *Arenicola marina*, maintain muscle tension during rest to stiffen the body and maintain a resting posture (Chapman and Newell, 1947; Trueman, 1966), much as we maintain tension in our leg muscles to keep ourselves from falling down when we are standing still. In such cases, where muscle tension is the only source of internal pressure (P_m), geometrically similar hydrostats will be stress similar as long as muscle stress (σ_m) does not vary with body size ($\sigma_m \propto m_b^0$). The internal pressure resulting from muscle tension is given by:

$$P_m = (\sigma_m A_m) A_i^{-1}, \quad (3)$$

where both the cross-sectional area of the muscle (A_m) and the projected inside area of the hydrostat (A_i ; Fig. 2B) scale as $m_b^{2/3}$ such that:

$$P_m \propto m_b^{0+2/3-2/3}, \quad (4)$$

hence

$$P_m \propto m_b^0. \quad (5)$$

Thus, geometrically similar organisms with internal pressure derived from muscle tension should show static stress similarity unless the muscle properties or the behavior of the organisms change with body size. Note that body wall stress will necessarily equal muscle stress only when the body wall thickness is composed entirely of one muscle layer.

If the total internal pressure (P) in a hydrostat is derived from sources other than or in addition to P_m , then the scaling of these sources must also be considered. Gravitational pressure (P_g) is insignificant in most aquatic soft-bodied organisms because the pressure gradient outside the body wall due to the weight of the water column is the same as the pressure gradient within (Ellers and Telford, 1992). Gravitational pressure may, however, be an important variable

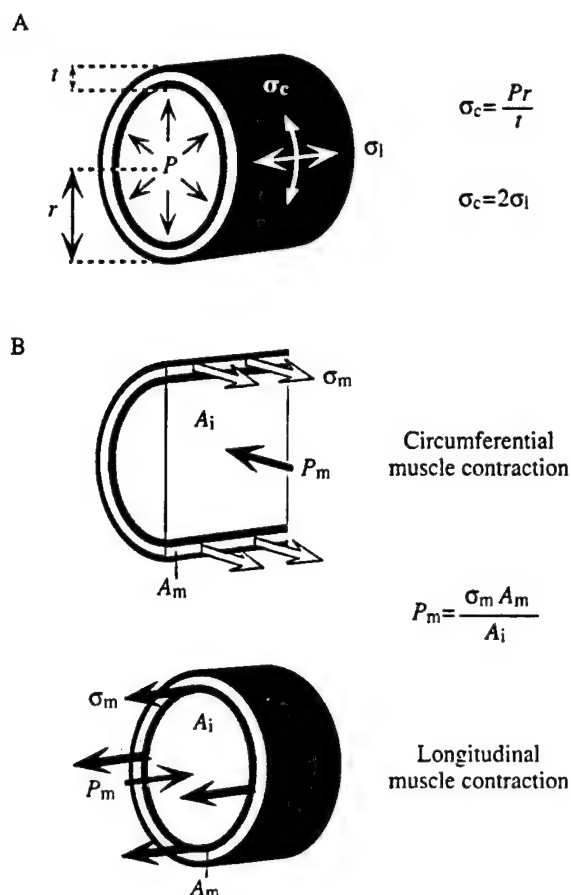


Fig. 2. Simplified diagram of an earthworm-like hydrostatic skeleton composed of a body wall in tension surrounding a fluid in compression. The body wall is composed of a layer of longitudinal muscle (dark gray), a layer of circumferential muscle (light gray) and a layer of epidermis and cuticle (black). (A) The circumferential stress (σ_c) in a cylindrical hydrostatic skeleton of uniform radius (r) and thickness (t) is the product of internal pressure (P) and the ratio of radius to thickness. The magnitude of longitudinal stress (σ_l) is half the magnitude of circumferential stress. (B) The magnitude of internal pressure resulting from muscle tension (P_m) for both circumferential and longitudinal muscle contractions is determined by the muscle stress (σ_m), the cross-sectional area of muscle (A_m) and the projected inside area of the hydrostat (A_i).

in some terrestrial hydrostats. Gravitational pressure at a given point in an organism is given by:

$$P_g = \rho g z, \quad (6)$$

where ρ is the density of the fluid and tissue, g is the acceleration due to gravity, and z is the vertical distance from the upper surface of the organism to that point (Ellers and Telford, 1992). A larger organism will have a greater maximum P_g than a geometrically similar smaller organism because of its greater vertical linear dimension (z), such that $P_g \propto m_b^{1/3}$ when body density is constant (unless the larger organism is sufficiently flexible to flatten slightly under its own weight). Thus, geometrically similar organisms for which P_g is an important source of pressure may not maintain static stress similarity.

Dynamic stress similarity

Animals experience dynamic stresses in their skeletons when they move. The dynamic strain similarity hypothesis of Rubin and Lanyon (1984; so-named because they calculated stresses from their measurements of bone strains) states that the maximum stress experienced by a skeletal element during vigorous locomotion is independent of body size and thus scales as m_b^0 (Fig. 1). Maximum stress during locomotion in legged animals is greater than resting stress owing to the addition of the ground reaction forces (F_{acc}) required to accelerate and decelerate the animal. The magnitude of ground reaction forces is dependent not only on the weight of the organism but also on the gait it uses. Therefore, the dynamic strain similarity hypothesis as applied to rigid skeletons is neither excluded nor predicted by geometric similarity alone: it must be measured while the organisms are in motion.

The maximum stress experienced by the body wall of a hydrostatic skeleton likewise depends on the organism's behavior. The internal pressures in most hydrostats fluctuate (Zuckerlandl, 1950), but tend to peak when muscle contractions peak (e.g. Chapman and Newell, 1947; Newell, 1950). However, hydrostats tend to be highly deformable, and the maximum r/t may not coincide with the pressure maximum. The maximum tensile stress occurs when and where the product of P and r/t is greatest (see equation 1). If the main source of internal pressure is muscle tension (P_m , which is likely to be the case) and if muscle properties do not vary with body size, then geometrically similar hydrostats should show dynamic stress similarity as long as behavior does not change during growth. Thus, internal pressure and body wall geometry must be measured in living hydrostats in order to test hypotheses of dynamic stress similarity.

Application of scaling hypotheses to *Lumbricus terrestris*

The first objective of the present study was to generate predictions for the geometric, static stress and dynamic stress scaling hypotheses for hydrostatic skeletons on the basis of their form and function. Given the formulated predictions, the next objective was to apply the similarity hypotheses to the ontogeny of the earthworm *Lumbricus terrestris* to determine which aspects of skeletal function are conserved or altered as a function of size during growth. *L. terrestris* was chosen as the experimental system because of its abundance, ease of study in the laboratory, and the availability of a large ontogenetic size range. Its segmented skeleton is composed of a body wall (cuticle, epithelium, two layers of muscle and connective tissue) surrounding coelomic fluid and deformable organ tissues. The volume of coelomic fluid within each segment is constant (Newell, 1950). Thus, when the circumferential muscles of a segment contract, the segment becomes long and slim as the passive longitudinal muscles are stretched. When the longitudinal muscles contract, the segment becomes short and wide and the circumferential muscles are stretched (Seymour, 1969). Alternating waves of circumferential and longitudinal muscle contractions travel posteriorly along the body, enabling

for
193
7
me:
as a
eat
stre
pres
scal
pres
obs:
peri
eat
surf
nam
drav
peri
Artl
as a
wal

E
0.3
Raf
Ran
(Ma
sup
coll
whi
Berl
for
A
of t
relat
body
effe
scal
wide
segr

Fig.
(10)
meas
stres
(10²
of th
scale
ontog

forward progression by peristalsis (e.g. Gray and Lissmann, 1938).

The experimental objectives of the present study were (1) to measure the resting geometry of the skeletons of earthworms as a function of size, (2) to measure internal pressures in resting earthworms in order to calculate the scaling of static tensile stresses in the body wall, and (3) to measure dynamic internal pressures in locomoting earthworms in order to calculate the scaling of dynamic tensile stresses in the body wall. The present study focuses on the earthworms during their most observed and understood activity – surface crawling – although peristalsis is also used by this species to burrow. Whereas most earthworm species are either geophagous (earth-eaters) or surface feeders, *Lumbricus terrestris* is both: as its common name 'night crawler' suggests, it feeds on the surface at night, drawing leaves and other organic materials into its semi-permanent burrows and digesting them within (Darwin, 1881; Arthur, 1965; Satchell, 1967). Thus, surface crawling is used as a pragmatic first assessment of dynamic stresses in the body wall.

Materials and methods

Experimental animals

Earthworms (*Lumbricus terrestris* L.) ranging in size from 0.3 to 8.0 g were obtained from Idaho (Loch Lomond Bait, San Rafael, CA, USA) and maintained at 6°C in Magic Worm Ranches using Magic Worm Bedding and Magic Worm Food (Magic Products Inc., Amherst Junction, WI, USA). I supplemented this size range with juveniles (0.01–0.3 g) collected from an outdoor enclosure in Berkeley, CA, USA, in which I maintained *L. terrestris* from Canada (Berkeley Bait, Berkeley, CA, USA). Fig. 3 summarizes the size ranges used for each of the scaling variables examined.

Although earthworm segments are similar along the length of the body, some regionalization does occur. I chose two relatively dissimilar segments for comparison of diameter, body wall thickness, internal pressure and stress to assess the effects, if any, of this regionalization on the function and scaling of the hydrostatic skeleton. Segment 15 lies in the widest region of the worm near the anterior end, where segments are relatively long and wide and contain specialized

digestive and reproductive organs. Segment 50, by contrast, lies in the relatively homogeneous midregion of the worm, where segments are narrower and shorter and are occupied primarily by the intestine (Fig. 4).

Pressure measurement

I made continuous measurements of internal pressure using a low-volume gauge pressure transducer (PX170, Omega Engineering, Stamford, CT, USA) designed to read pressures up to 7 kPa. I connected the transducer to a piece of water-filled flexible polyethylene tubing attached to a terminal cannula constructed from a 27 gauge hypodermic needle. The transducer was calibrated before each series of measurements by inserting the needle through the wall of a 2 cm vertical Nalgene tube that was open at the top. The tube height was raised so that the meniscus of the water level increased in height at 1 cm intervals with respect to the center of the transducer. The data were collected at 50 scans s⁻¹ by LabVIEW software (version 3.0.1: National Instruments, Austin, TX, USA) on a Gateway 2000 computer.

Prior to insertion of the cannula, the earthworms were calmed by placement in dilute ethanol (1–5% in spring water) for 20–40 min (response time to the anesthetic varied). After this procedure, worms did not thrash when handled but did exhibit typical locomotory peristalsis as observed in earthworms without a cannula inserted. I then placed the earthworms into a tray of fresh water 1 cm deep (meniscus level adjusted to the height of the center of the pressure transducer) rather than in air to keep the needle-tip submerged between measurements and to keep the tubing still while the worm crawled 'in place' in the water, avoiding pressure artifacts due to movement of the apparatus. I inserted the needle laterally into the coelom of each worm, just under the body wall in segments 15 and 50 or the adjacent segments (pressure among adjacent segments did not differ measurably).

The following variables were measured from the pressure records (to the nearest 10 Pa; Fig. 5): (1) maximum pressures during circumferential muscle contractions ($P_{C.M.}$), (2) maximum pressures during longitudinal muscle contractions ($P_{L.M.}$) and (3) resting pressures (P_R). The dynamic pressure measurements were averaged over 10 cycles of peristalsis. Resting pressures were recorded as often as possible but only

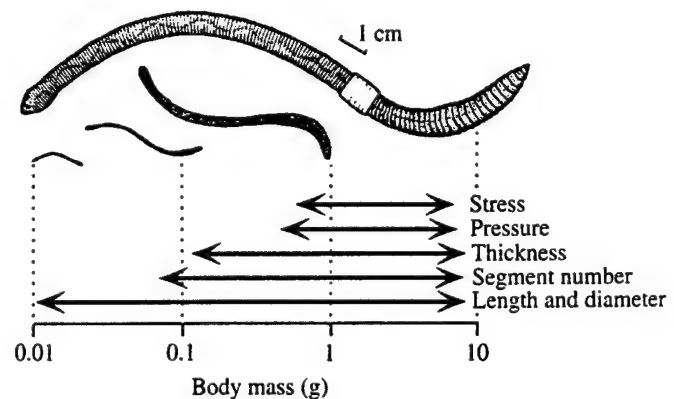


Fig. 3. Diagram illustrating the order-of-magnitude of size ranges (10^0) in body mass of *Lumbricus terrestris* used for each measurement: dynamic stress ($10^{1.1}$), internal pressure and static stress ($10^{1.2}$) and morphometrics ($10^{2.9}$), with segment number ($10^{2.1}$) and body wall thickness ($10^{1.7}$) measured in the upper end of the morphometric range. Earthworms are drawn to the same scale at order-of-magnitude intervals in body mass to illustrate the ontogenetic size range used.

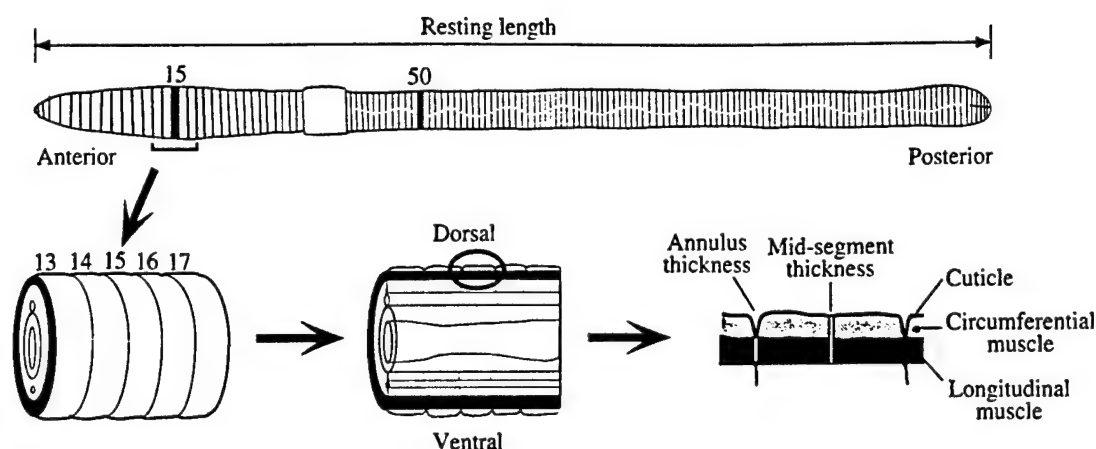


Fig. 4. Diagram illustrating the morphometric measurements made on *Lumbricus terrestris*. Resting length and the number of segments of the entire body, and resting lengths, lateral diameters and body wall thicknesses of segments 15 and 50 were measured on anesthetized earthworms as described in Materials and methods.

as they occurred between bouts of peristalsis (rather than in anesthetized or otherwise quiescent earthworms) to ensure that the cannula was not clogged. The number of pressure records available for each individual varied from zero to five; the mean resting pressure was calculated when more than one record was available.

Morphometrics

I anesthetized the earthworms to compare the dimensions of their highly extensible skeletons in comparable postures. First, I submerged the earthworms in spring water and slowly added drops of 50% ethanol for 30–60 min. When the earthworms no longer responded to stimulation, I blotted them dry and measured the mass of the large and medium worms on a three-beam balance and the smallest worms on a Mettler balance (model AE 163) to two significant figures (i.e. to the nearest 0.1 g for the largest worms and to the nearest 0.0001 g for the smallest worms). I then counted the number of segments and measured body length with a ruler or digital calipers to the nearest 1 mm (or 0.1 mm in the case of very small worms) and

the widths of segments 15 and 50 with calipers to the nearest 0.1 mm.

Body wall thickness was measured using frozen sections rather than standard histological sections to minimize shrinkage due to fixation. I rapidly froze anesthetized earthworms by sliding them off a straight edge into 95% ethanol chilled to -78°C using cubes of dry ice. Small worms froze immediately while large worms required 2–3 s; body dimensions did not change measurably during this period. I removed each frozen worm and cut it first transversely with a razor blade to remove two sections composed of segments 13–17 and 48–52, and then sagittally to produce two lateral halves of each section (Fig. 4). Images of these halves were captured using a high-resolution color video camera (Sony CCD-Iris SSC-C374) affixed to a Wild Heerbrugg dissecting microscope (model M5A). I used a RasterOps frame-grabber board to select individual video frames, and NIH Image software (Version 1.59) on a Power Macintosh 7100/80 to measure body wall thickness in the middle of segments 15 and 50 and at the annuli adjacent to these segments (Fig. 4).

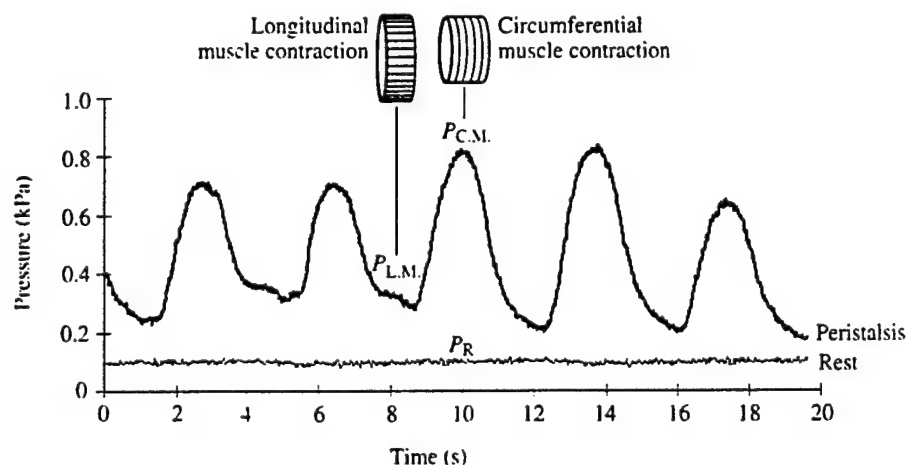


Fig. 5. Typical records of internal pressure during earthworm peristalsis (upper record) and during rest (lower record) showing the variables measured: maximum pressure during circumferential muscle contraction ($P_{C.M.}$), when the segment is long and narrow; maximum pressure during longitudinal muscle contraction ($P_{L.M.}$), when the segment is short and wide; and resting pressure (P_R), when the segment is relaxed.

Thickness was measured to the nearest 0.01 mm, and dorsal and ventral thicknesses were averaged. Segment length was measured to the nearest 0.01 mm. Circumferential muscle cross-sectional area was measured to the nearest 0.01 mm². The lower size limit of worms sectioned (Fig. 3) was determined by the lack of pigmentation in small worms, which rendered tissue layers difficult to distinguish.

Stress calculations

Static body wall tensile stresses were calculated from equation 1 using resting pressure and the resting radius and thickness values obtained from morphometric measurements of the same individuals. Since the body walls of earthworms do not have uniform thickness (Fig. 4), the annulus body wall thickness was used to calculate maximum resting longitudinal stress (because only the longitudinal muscles bear longitudinal loads). The mid-segment thickness was used to calculate resting circumferential stress (because both longitudinal and circumferential muscles bear circumferential loads and because circumferential stress is resisted by the muscular septae at each annulus).

Dynamic body wall tensile stresses were calculated using pressures obtained during maximum contractions of circumferential and longitudinal muscles and using radius and thickness values calculated from the resting dimensions of the segments and the maximum shape changes observed in the segments during peristalsis. I video-taped the shape changes of segments 15 and 50 of crawling earthworms through a Wild Heerbrugg dissecting microscope using a SONY CCD-Iris (SSC-C374) high-resolution color video camera and a time/date generator (Panasonic WJ-810). I used RasterOps Video Capture software on a Power Macintosh 7100/80 to grab video frames, and NIH Image software (Version 1.59) to measure the minimum and maximum length and lateral diameter of the segments to the nearest 0.1 mm. During longitudinal muscle contraction, the shapes of segments 15 and 50 did not differ from those of resting earthworms; therefore, the resting radius and thickness values were used for calculation of circumferential stress during longitudinal muscle contraction. During circumferential muscle contraction, the length of segments 15 and 50 of earthworms of all sizes increased by a factor of 1.6 ± 0.2 ($N=20$), while the diameter decreased by a factor of 0.75 ± 0.06 (means \pm S.D., $N=15$) (K. J. Quillin, unpublished data). Using these values, I solved for the annulus thickness of the extended segments assuming that the volume of the body wall is constant.

Statistical analysis

The allometric relationships between each of the measured variables and body mass (g) were analyzed using linear regressions of log-transformed data, where the equation of the log-transformed allometric relationship is given by:

$$\log y = \log a + b \log m_b \quad (7)$$

Ordinary regression analysis tends to underestimate the slope (b) owing to the incorrect assumption that there is no

measurement error in the x variate. In this case body mass (Harvey and Pagel, 1991). The degree of underestimation of the slope may, however, be corrected using the reliability ratio (κ_{xx}) as described by Fuller (1987):

$$\beta = b(\kappa_{xx})^{-1} \quad (8)$$

where b is the attenuated slope as calculated by ordinary regression analysis and β is the corrected slope. For continuous variables such as body mass, the reliability ratio (κ_{xx}) is the correlation coefficient between two determinations of the same characteristic. I measured the body mass of 10 individuals on separate days (the first day they were unanesthetized, a week later they were anesthetized). I then plotted the body mass from the first day against the body mass from the second day and calculated the correlation coefficient r ($r = \kappa_{xx}$) and from this calculated each corrected slope β . The reliability ratio κ_{xx} calculated for body mass was 0.995; therefore, all regression slopes plotted as a function of body mass were increased by a factor of 1.005.

Student's t distribution was used to test slopes where the null hypothesis was $\beta=0$ or $\beta=1/3$. Analysis of covariance (ANCOVA) tests of homogeneity of slopes were performed to test whether observed slopes were significantly different from each other (Sokal and Rohlf, 1969). Independent-sample and paired-sample t -tests were performed to compare internal pressures in segment 15 versus segment 50. All statistical analyses were performed using Systat for Windows, version 5. Values are given as means \pm standard deviations (S.D.).

Results

Geometric similarity

The external dimensions of the earthworms increased isometrically. Segment number (n) varied among individuals (147 ± 13 , $N=111$), but did not increase with body mass m_b over the two orders of magnitude size range investigated ($n \propto m_b^{0.01}$; the slope was not significantly different from zero, $P>0.10$; Fig. 6), indicating that the earthworms grew by enlarging each

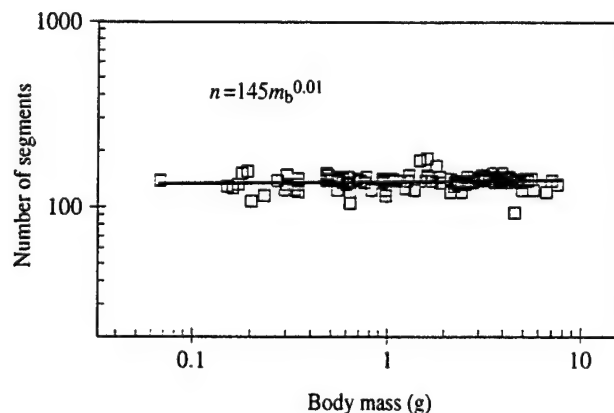


Fig. 6. Segment number n as a function of body mass m_b on logarithmic coordinates. The slope of the linear regression is not significantly different from zero ($P>0.10$; $N=111$; $r^2=0.01$).

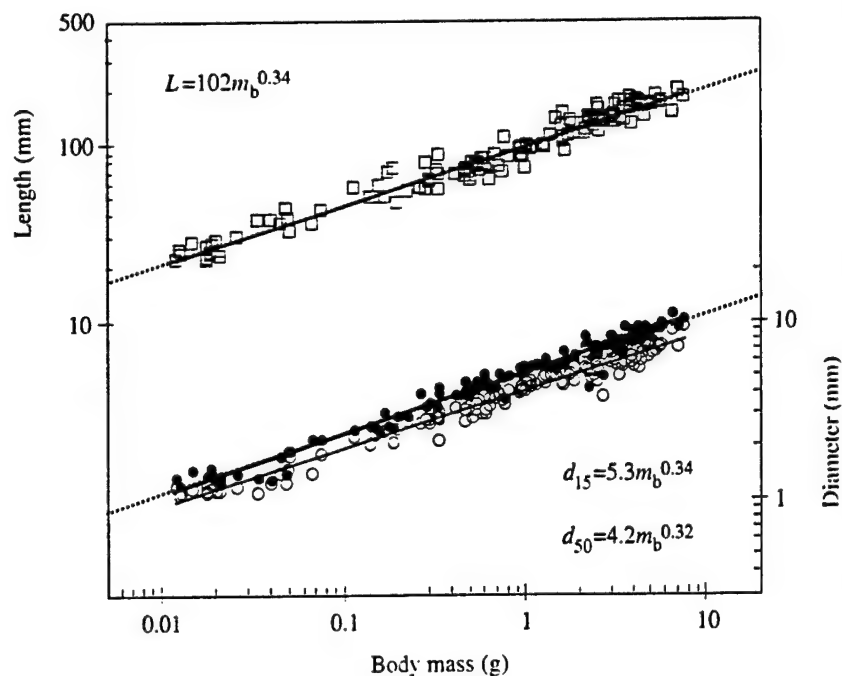


Fig. 7. Resting body length L (\square ; $N=164$; $r^2=0.99$; $P<0.001$ compared with a slope of zero) and lateral diameter of segments 15, d_{15} (\bullet ; $N=160$; $r^2=0.98$; $P<0.001$), and 50, d_{50} (\circ ; $N=162$; $r^2=0.98$; $P<0.001$), as a function of body mass m_b on logarithmic coordinates. None of the slopes of the linear regressions is significantly different from 0.33 (broken lines), the slope predicted by isometry ($P>0.10$ for length: $P=0.061$ for both diameters).

segment rather than by adding segments. Furthermore, the resting lengths L_s of segment 15 ($L_s=0.011m_b^{0.32}$; $r^2=0.82$, $N=19$) and segment 50 ($L_s=0.007m_b^{0.34}$; $r^2=0.79$, $N=19$) increased at the rate predicted by geometric similarity (the slopes were significantly different from zero, $P<0.001$, but not significantly different from 0.33, $P>0.10$). The resting diameters (d_{15} , d_{50}) of both segments also increased as predicted by geometric similarity ($d_{15}\propto m_b^{0.34}$, $d_{50}\propto m_b^{0.32}$; $P=0.061$ for both compared with a slope of 0.33, $P<0.001$ for both compared with a slope of zero; Fig. 7), indicating that earthworms increased their segment dimensions isometrically. The resting length of the entire body increased with body mass at the same rate as predicted by geometric similarity ($L\propto m_b^{0.34}$; $P>0.10$ compared with a slope of 0.33, $P<0.001$ compared with a slope of zero, $N=164$; Fig. 7). The mean length/diameter ratio over the entire size range was 21.8 ± 4.0 ($N=135$).

Body wall thickness increased isometrically in segment 15, but allometrically in segment 50 (Fig. 8). The mid-segment and annulus thicknesses of segment 15 increased isometrically as $m_b^{0.37}$ and $m_b^{0.38}$ respectively ($P>0.10$ compared with a slope of 0.33, $P<0.001$ compared with a slope of zero). However, the mid-segment and annulus thicknesses of segment 50 grew allometrically as $m_b^{0.42}$ ($P=0.004$ compared with a slope of 0.33) and $m_b^{0.45}$ ($P<0.001$), respectively. The allometric increase in body wall thickness reflects an allometric increase in the cross-sectional area of the muscles; the mid-sagittal cross-sectional areas of circumferential muscle in the body wall of segments 15 and 50 increased as $m_b^{0.90}$ ($r^2=0.90$, $N=20$) and $m_b^{0.91}$ ($r^2=0.81$, $N=20$), respectively, which were both greater than the slope 0.67 predicted by isometry ($P=0.006$ for segment 15, $P=0.037$ for segment 50).

Despite allometry in body wall thickness, the longitudinal and circumferential muscles maintained their relative

proportions during growth (Fig. 8). The slopes of the mid-segment body wall thicknesses (a measure of circumferential muscle plus longitudinal muscle plus epidermis and cuticle thickness) were not significantly different ($P>0.10$) from the slopes of the annulus body wall thicknesses (a measure of longitudinal muscle plus epidermis and cuticle thickness; see Fig. 4).

Static stress similarity

Resting pressures P_R differed greatly from individual (115 ± 45 Pa; $N=19$), but scaled independently of body mass over the one-order-of-magnitude range in body mass observed ($P_R\propto m_b^{-0.003}$; $P>0.10$ compared with a slope of zero; Fig. 9). Resting pressures in segments 15 and 50 were not significantly different (independent t -test, $P>0.10$), so these data were pooled for the calculation of stress.

Static tensile stress in the body wall of the earthworms was constant as a function of body mass. The static circumferential stress σ_c in the mid-segment body wall scaled as $m_b^{-0.07}$ and $m_b^{-0.09}$ in segments 15 and 50, respectively, neither of which was different from a slope of zero ($P>0.10$; Fig. 10). The static longitudinal stress σ_l in the longitudinal muscle layer scaled as $m_b^{0.10}$ and $m_b^{0.07}$ in segments 15 and 50, respectively, neither of which was significantly different from a slope of zero ($P>0.10$; Fig. 9). The mean static circumferential stresses were 830 ± 330 Pa and 710 ± 300 Pa ($N=19$) for segments 15 and 50, respectively. The mean static longitudinal stresses were 64 ± 15 Pa and 55 ± 13 Pa ($N=19$) for segments 15 and 50, respectively.

Dynamic stress similarity

Since the mean internal pressures during maximum circumferential muscle contraction $P_{C.M.}$ in segments 15

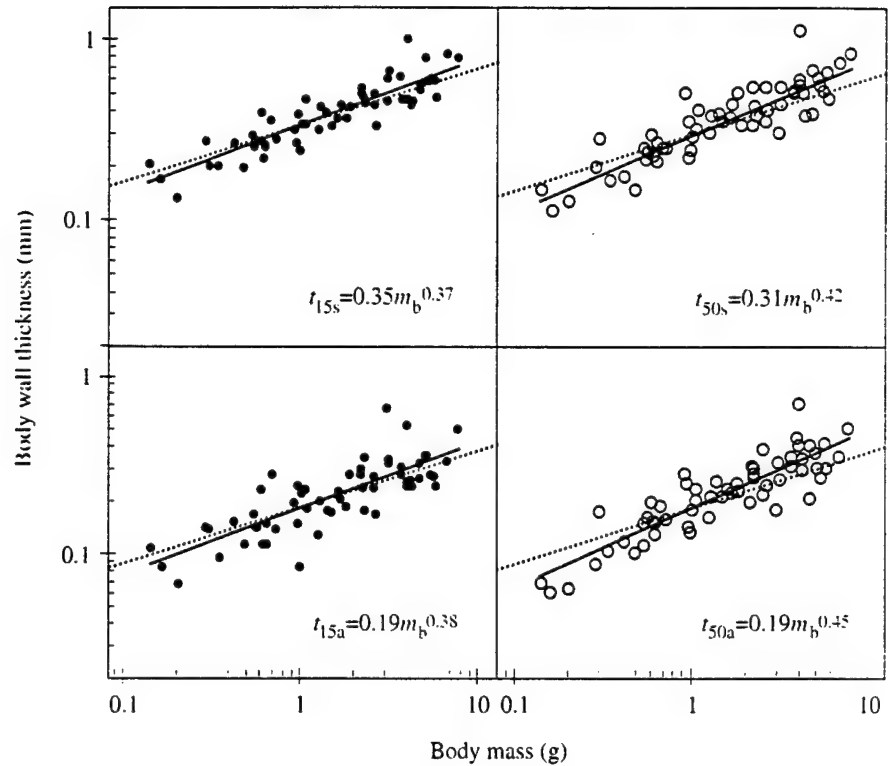


Fig. 8. Body wall thickness as a function of body mass m_b on logarithmic coordinates ($N=59$). The slopes of the linear regressions for mid-segment thickness (t_{15s} ; $r^2=0.80$) and annulus thickness (t_{15a} ; $r^2=0.65$) for segment 15 (\bullet) are significantly different from a slope of zero ($P<0.001$), but not significantly different from 0.33, the slope predicted by isometry (broken lines: $P>0.10$). The slopes of the linear regressions for mid-segment thickness (t_{50s} ; $r^2=0.78$) and annulus thickness (t_{50a} ; $r^2=0.79$) for segment 50 (\circ) are significantly greater than 0.33 (broken lines: $P=0.004$ and $P<0.001$, respectively).

(580 ± 220 Pa) and 50 (670 ± 300 Pa) were not significantly different ($P>0.10$), these data were pooled for the calculation of stress. However, the internal pressures during maximum longitudinal muscle contraction $P_{L.M.}$ in segments 15 (300 ± 220 Pa) and 50 (550 ± 260 Pa) were significantly different ($P=0.018$), and so were not pooled for the calculation of stress.

Maximum dynamic stresses in the body wall during peristalsis were independent of body mass (Fig. 10). The mean maximum pressure during circumferential muscle contraction $P_{C.M.}$ scaled as $m_b^{0.04}$ (Fig. 9), and the resulting maximum longitudinal stress σ_l in the body wall scaled as $m_b^{0.01}$ and $m_b^{-0.19}$ in segments 15 and 50, respectively (Fig. 10). The mean maximum pressure during longitudinal muscle contraction $P_{L.M.}$ scaled as $m_b^{-0.05}$ (Fig. 9), and the resulting maximum circumferential stress σ_c in the body wall scaled as $m_b^{-0.07}$ and $m_b^{-0.09}$ in segments 15 and 50, respectively. None of the regression slopes was significantly different from zero ($P>0.10$), indicating that earthworms show dynamic stress similarity in peristaltic crawling as they grow. The amplitude

of stress fluctuation during peristalsis was higher in segment 15 than in segment 50 ($P<0.001$; Fig. 10), but the amplitude did not change significantly as a function of body mass ($P>0.10$).

In the resting earthworm, circumferential tensile stress was greater than longitudinal tensile stress (Fig. 10). In the crawling earthworm, however, longitudinal tensile stress

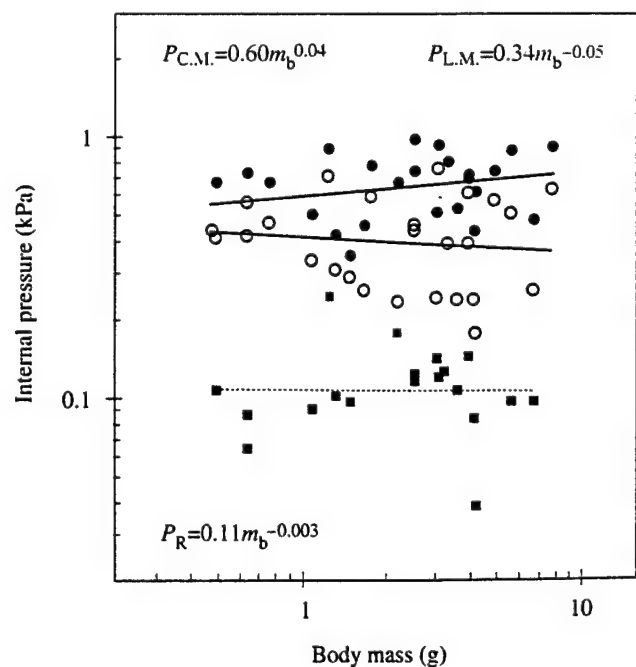
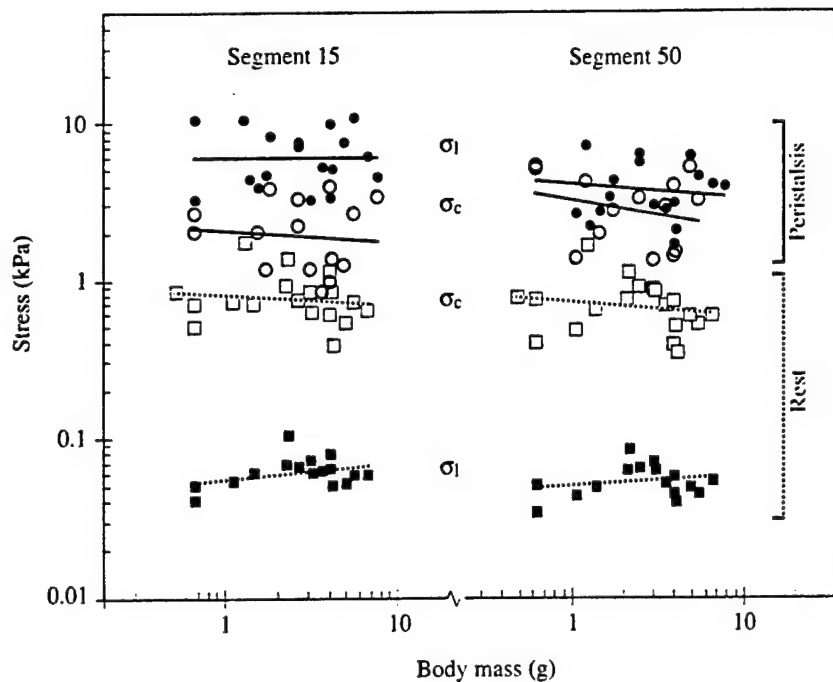


Fig. 9. Internal pressure as a function of body mass m_b on logarithmic coordinates. The slopes of the linear regressions for maximum internal pressure during circumferential muscle contraction ($P_{C.M.}$; \bullet ; $N=26$; $r^2=0.01$), maximum internal pressure during longitudinal muscle contraction ($P_{L.M.}$; \circ ; $N=22$; $r^2=0.01$), and rest (P_R ; \blacksquare ; $N=19$; $r^2=0.00003$) are not significantly different from zero ($P>0.10$). $P_{C.M.}$ and P_R of segments 15 and 50 were not significantly different ($P>0.10$) and so were pooled. Values of $P_{L.M.}$ in segment 15 ($P_{L.M.15}=0.34m_b^{-0.05}$; $r^2=0.01$) were significantly lower ($P<0.001$) than those in segment 50 ($P_{L.M.50}=0.44m_b^{-0.002}$; $r^2=0.00001$) but are shown pooled here for clarity.

Fig. 10. Body wall stress as a function of body mass m_b on logarithmic coordinates. In segment 15, longitudinal stress σ_l in the body wall during maximum circumferential muscle contraction (\bullet ; $\sigma_l = 6.1m_b^{0.01}$, $N=19$; $r^2=0.001$) was greater than circumferential stress σ_c during maximum longitudinal muscle contraction (\circ ; $\sigma_c = 2.1m_b^{-0.07}$, $N=17$; $r^2=0.01$) during surface peristalsis. Static circumferential stress (\square ; $\sigma_c = 0.8m_b^{-0.07}$, $N=19$; $r^2=0.02$) was greater than static longitudinal stress (\blacksquare ; $\sigma_l = 0.03m_b^{0.10}$, $N=16$; $r^2=0.12$). Likewise in segment 50, longitudinal stress in the body wall during maximum circumferential muscle contraction (\bullet ; $\sigma_l = 4.1m_b^{-0.09}$, $N=19$; $r^2=0.03$) was greater than circumferential stress during maximum longitudinal muscle contraction (\circ ; $\sigma_c = 3.2m_b^{-0.19}$, $N=14$; $r^2=0.07$) during surface peristalsis. Static circumferential stress (\square ; $\sigma_c = 0.7m_b^{-0.09}$, $N=19$; $r^2=0.04$) was greater than static longitudinal stress (\blacksquare ; $\sigma_l = 0.03m_b^{0.07}$, $N=16$; $r^2=0.05$). None of the slopes of the linear regressions was significantly different from zero ($P>0.10$).



during circumferential muscle contraction was greater than circumferential tensile stress during longitudinal muscle contraction as a result of the higher pressures generated during circumferential muscle contraction (Fig. 9) and smaller cross-sectional area of the body wall experiencing longitudinal forces (Fig. 4).

The highest pressures recorded in the present study occurred during violent, whole-body contractions rather than during normal peristaltic crawling. Pressures reached 6.2 kPa in a 5.5 g earthworm and 4.3 kPa in a 1.8 g earthworm. The resulting circumferential stresses were calculated as 44 and 33 kPa, respectively.

Discussion

The earthworm *Lumbricus terrestris* grows isometrically while maintaining static and dynamic stress similarity. Unlike rigid skeletons, for which geometric similarity and static stress similarity are mutually exclusive hypotheses, hydrostatic skeletons can simultaneously maintain similarity in both form and this aspect of mechanical function as they grow.

Gravity and the scaling of hydrostatic skeleton function

The main source of loading on the skeleton of most terrestrial organisms with rigid skeletons is body weight. In earthworms, the main source of loading on the skeleton is internal pressure (generated by body wall muscles contracting against a constant volume of internal fluid). The pressure measurement apparatus used in the present study necessitated submerging the earthworms in a shallow bath of water to prevent air from entering the system and to prevent pressure artifacts due to the movement of the apparatus. Thus,

gravitational pressure (P_g) was essentially eliminated as a source of total internal pressure. A horizontally oriented earthworm that is 1 mm in dorsoventral diameter should have a dorsoventral gradient in pressure that ranges from zero at the dorsal perimeter to a maximum P_g of 10 Pa at the ventral perimeter. An earthworm that is 10 mm in dorsoventral diameter should have a pressure gradient that ranges from zero to a maximum P_g of 100 Pa. These pressures lie within the variation in resting pressure measured in the present study (Fig. 9), and thus would not affect the resting pressure regression appreciably. Furthermore, the estimated gravitational pressures are considerably smaller than the pressures that occurred during peristalsis and therefore appear to be relatively unimportant. Vertically oriented earthworms (e.g. in vertical burrows) would not necessarily have higher gravitational pressures than horizontally oriented earthworms since muscular septae divide the coelom into constant-volume segments which prevent the transfer of pressure along the length of the body. Overall, the decoupling of body weight and skeletal function probably accounts to a great extent for the ability of a terrestrial hydrostatic skeleton to grow isometrically while maintaining stress similarity.

Lumbricus terrestris is generally considered to be a large earthworm compared with other temperate species (e.g. Arthur, 1965; Pearce, 1983), but several 'giant' species, measuring meters in length, can be found in the tropics (Stephenson, 1930). The upper limit to the size of hydrostatic skeletons is unclear, but some of the possible limitations to giant earthworms include (1) a decreased respiratory surface area due to the low surface-to-volume ratio compared with that of smaller earthworms, (2) an increased importance of gravitational pressure as a source of load on the body wall, (3) an increased frictional resistance to burrowing, and (4) the

exponential increase in the cost of tunnel construction with increasing body diameter (Gans, 1973). Present evidence suggests that larger earthworm species generally possess a higher length/diameter ratio and more segments than smaller earthworm species (Arthur, 1965; Pearce, 1983); this allometry may enable earthworms to reach the upper limit of body mass for terrestrial hydrostatic skeletons.

Scaling of segment shape

Segments are the constant-volume functional units of the skeletons of earthworms. Some species add segments during post-emergent growth (Evans, 1946; Pearce, 1983), but *Lumbricus terrestris* possesses the same number of segments throughout its lifetime (unless segments are lost as a result of predation; Evans, 1946). The number of segments and their dimensions are important for several reasons. In general, the greater the degree of segmentation of the skeleton, the greater the potential for localization of forces, pressures and shape changes in the skeleton and, hence, the greater the potential for complex motions (Clark, 1964). Furthermore, since the muscular septae between segments radially reinforce the cylindrical structure, the number of segments for a given body length may affect the resistance of the body to circumferential bulging and sagging (e.g. Seymour, 1970). A large number of septae per body length may also diminish the pressure gradient established along the length of an earthworm oriented vertically in its burrow.

The number and dimensions of the segments are also important in determining the velocity advantage of a hydrostatic skeleton. The velocity advantage is expressed by the ratio U_2/U_1 , where U_1 is the rate of contraction of a muscle and U_2 is the maximum resulting velocity of an attached skeletal element (e.g. Alexander, 1983). In vertebrates and arthropods, the amplification of velocities is accomplished by rigid levers rotating about pivots. The velocity advantage of hydrostatic skeletons is determined by the simple geometric relationship between length and diameter in a constant-volume deformable cylinder (Fig. 11; Chapman, 1950; Kier and Smith, 1985). Both segments 15 and 50 have resting length/diameter ratios less than 1. This means, for example, that only a slight shortening of the longitudinal muscles is necessary for a large and rapid increase in diameter, enabling the earthworm to anchor quickly. Since the length and diameter of segments 15 and 50 did not differ significantly as a function of body mass, the segments of large and small worms appear to possess the same velocity advantage. Velocity advantage and mechanical advantage tend to be inversely related, but mechanical advantage has yet to be measured in hydrostatic skeletons.

The length/diameter ratio of an earthworm is not only important to the mechanical function of the skeleton, but also to the physiology of the organism. Gaseous exchange in earthworms occurs by diffusion across the skin (for a review, see Edwards and Bohlen, 1996), and the rate of water loss is also likely to be proportional to body surface area (Pearce,

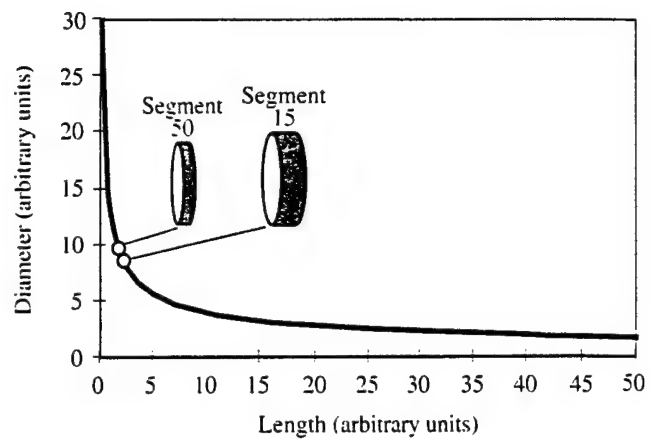


Fig. 11. Relationship between the diameter and length of a constant-volume cylinder in arbitrary units. Although segments 15 and 50 of the earthworm *Lumbricus terrestris* have different volumes, their resting dimensions are plotted on the same curve for comparison. Both segments have a resting diameter/length ratio greater than 1. Thus, only a small length change is required to cause a large change in diameter.

1983). Since the surface area of *L. terrestris* decreases relative to its body mass during ontogeny (growth is isometric; thus, surface area $\propto m_b^{2/3}$), either larger earthworms have a lower respiratory rate and activity level than smaller earthworms or the decrease in relative surface area is compensated by other physiological variables such as the degree of vascularization of the body wall or the oxygen-carrying capacity of hemoglobin.

Whereas I observed isometric growth in *L. terrestris* ($L \propto d^{1.05}$), Pearce (1983) observed an increase in the length/diameter ratio as a function of body mass ($L \propto d^{1.28}$) in preserved specimens of the same species, such that larger worms were skinnier relative to their length than were smaller worms. All of the individuals observed by Pearce (1983) possessed a lower length/diameter ratio ($L/d=18$) than I observed in the present study ($L/d=22$). Preservation artifacts or interpopulational differences in diet and habitat are possible sources of this discrepancy.

Scaling of internal pressure

Neither resting pressure nor peak pressures during peristalsis changed as a function of body mass, and values were comparable to, but on average lower than, those reported for adult worms of the same species by Seymour (1969; mass range 4–6 g) and Newell (1950; mass range not provided). Since both body geometry and internal pressures were essentially independent of body mass in *L. terrestris*, I predict that the maximum force exerted on the environment by an earthworm per area of force application will be constant as a function of body mass ($F/A \propto m_b^0$), providing that muscle stress is constant. However, given the allometric increase in body wall thickness of segment 50, maximum internal pressures and thus the maximum force exerted by the mid-

region of large earthworms may be greater than that in small earthworms during burrowing. I am currently testing these alternative hypotheses.

One might expect internal pressure to peak during both circumferential and longitudinal muscle contractions, since these muscles are said to antagonize one another *via* internal pressure (e.g. Chapman, 1950). In the present study, internal pressure peaked during circumferential muscle contraction but decreased (sometimes nearly to resting pressure) during longitudinal muscle contraction (Fig. 5). Seymour (1969) hypothesized that the body wall, which is stiffened by the collagen-fiber-reinforced cuticle and subepidermal connective tissue, may act as a spring, storing potential energy upon circular muscle contraction which can be released to aid the longitudinal muscles in shortening upon the relaxation of the circumferential muscles. This spring-like behavior of segments may also be a simple byproduct of the dynamic shape changes of the constant-volume segments. Clark and Cowey (1958) established that a unit length of an open-ended cylinder bounded by crossed-helical collagen fibers contains the greatest volume when the angle between the fibers and the longitudinal axis of the cylinder is $54^{\circ}44'$ (see Fig. 1 in Clark and Cowey, 1958). The fiber angle of an adult earthworm cuticle is approximately 45° when the animals are at rest (Richards, 1974; Lepescheux, 1988). Since the volume of a segment is constant, the volume cannot decrease when the circumferential muscles contract (causing the segment to become longer and slimmer and the fiber angle to decrease), resulting in an increase in internal pressure. Likewise, the volume of a segment cannot increase when the longitudinal muscles contract (causing the segment to become short and wide and the fiber angle to increase), so the pressure decreases. It is not known how the fiber angle of the cuticle scales, nor how the material properties of the intact body wall scale (including the passive and active material properties of the muscle). Such information would help to determine the importance of elastic energy storage in explaining the observed patterns of segment shape change and internal pressure fluctuation.

In conclusion, soft-bodied organisms with hydrostatic skeletons are abundant and diverse and range in body mass over many orders of magnitude both within and among taxa. The present study used earthworms (*Lumbricus terrestris*) as an experimental system to begin an examination of how hydrostatic skeletons scale during ontogeny. Earthworms show geometric similarity and maintain static and dynamic stress similarity as they grow over several orders of magnitude in body mass. The hydrostatic skeletons of earthworms, therefore, differ fundamentally from the rigid lever-like skeletons of their terrestrial counterparts in their ability to grow isometrically while maintaining static stress similarity. Overall, the qualitatively distinct manner of mechanical function of hydrostatic skeletons and the relative unimportance of gravitational loads probably account to a great extent for the difference between the scaling of hydrostatic skeletons and terrestrial lever-like skeletons.

List of symbols

a	y-intercept of log-transformed allometric power-law function
A	cross-sectional area of a skeletal element bearing a force (m^2)
A_f	external area of application of force (m^2)
A_i	projected inside area of a hydrostat (m^2)
A_m	cross-sectional area of muscle (m^2)
b	exponent of allometric power-law function
d	diameter (m)
d_{15}	lateral diameter of segment 15 (m)
d_{50}	lateral diameter of segment 50 (m)
F	force (N)
F_{acc}	ground reaction force (N)
F_w	force due to the weight of the organism (N)
g	gravitational acceleration (m s^{-2})
L	resting body length (m)
L_s	resting segment length (m)
m_b	body mass (g)
n	number of segments
P	internal pressure (N m^{-2})
$P_{\text{C.M.}}$	internal pressure during circumferential muscle contraction (N m^{-2})
P_g	gravitational pressure (N m^{-2})
$P_{\text{L.M.}}$	internal pressure during longitudinal muscle contraction (N m^{-2})
P_m	internal pressure due to muscle tension (N m^{-2})
P_R	internal pressure at rest (N m^{-2})
r	radius (m)
t	body wall thickness (m)
t_{15a}	annulus body wall thickness of segment 15 (m)
t_{15s}	mid-segment body wall thickness of segment 15 (m)
t_{50a}	annulus body wall thickness of segment 50 (m)
t_{50s}	mid-segment body wall thickness of segment 50 (m)
U_1	rate of contraction of a muscle (m s^{-1})
U_2	maximum velocity of a skeletal element (m s^{-1})
z	distance from upper surface of organism (m)
β	regression slope corrected for attenuation
κ_{xx}	reliability ratio
ρ	fluid density (kg m^{-3})
σ_c	circumferential stress (N m^{-2})
σ_l	longitudinal stress (N m^{-2})
σ_m	muscle stress (N m^{-2})
τ_{max}	maximum shear stress in the wall of a cylinder (N m^{-2})

This research was supported by an NSF Graduate Research Fellowship, a University of California at Berkeley Frankhauser Fellowship and a Sigma Xi Grants-in-Aid of Research to K.Q., by NSF Grant 92-20525 to M. Koehl and R. Keller, and ONR Grant 444095-23068 to M. Koehl. I am especially grateful to M. Koehl for helpful discussion and advice, and to the members of the biomechanics group at the University of California at Berkeley for their insights and suggestions. I am grateful to M. Koehl, O. Ellers, M. Martinez and two anonymous referees for critical reading of this manuscript.

References

- ADAMS, D. S., KELLER, R. AND KOEHL, M. A. R. (1990). The mechanics of notochord elongation, straightening and stiffening in the embryo of *Xenopus laevis*. *Development* **110**, 115–130.
- ALEXANDER, R. MCN. (1971). *Size and Shape*. London: Edward Arnold.
- ALEXANDER, R. MCN. (1983). *Animal Mechanics*. Second edition. Oxford: Blackwell Scientific Publications.
- ARTHUR, D. R. (1965). Form and function in the interpretation of feeding in lumbricid worms. *Viewpoints Biol.* **4**, 204–251.
- BATHAM, E. J. AND PANTIN, C. F. A. (1950). Muscular and hydrostatic action in the sea-anemone *Metridium senile*. *J. exp. Biol.* **27**, 264–289.
- CALDER, W. A. (1984). *Size, Function and Life History*. Cambridge, MA: Harvard University Press.
- CHAPMAN, G. (1950). On the movement of worms. *J. exp. Biol.* **27**, 29–39.
- CHAPMAN, G. (1958). The hydrostatic skeleton in the invertebrates. *Biol. Rev.* **33**, 338–371.
- CHAPMAN, M. A. AND NEWELL, G. E. (1947). The role of the body fluid in relation to movement in soft-bodied invertebrates. I. The burrowing of *Arenicola*. *Proc. R. Soc. Lond. B* **134**, 431–455.
- CLARK, R. B. (1964). *Dynamics of Metazoan Evolution*. Oxford: Clarendon Press.
- CLARK, R. B. AND COWEY, J. B. (1958). Factors controlling the change of shape of certain nemertean and turbellarian worms. *J. exp. Biol.* **35**, 731–748.
- CURREY, J. D. (1970). *Animal Skeletons*. New York: St Martin Press.
- DARWIN, C. (1881). *The Formation of Vegetable Mould through the Action of Worms, with Observations of their Habitats*. London: Murray.
- EDWARDS, C. A. AND BOHLEN, P. J. (1996). *Biology and Ecology of Earthworms*. New York: Chapman & Hall.
- ELLERS, O. AND TELFORD, M. (1992). Causes and consequences of fluctuating coelomic pressure in sea urchins. *Biol. Bull. Mar. Biol. Lab., Woods Hole* **182**, 424–434.
- EVANS, A. C. (1946). Distribution of number and segments in earthworms and its significance. *Nature* **158**, 98–99.
- FULLER, W. A. (1987). *Measurement of Error Models*. New York: John Wiley & Sons.
- GANS, C. (1973). *Biomechanics: An Approach to Vertebrate Biology*. Ann Arbor: The University of Michigan Press.
- GERE, J. M. AND TIMOSHENKO, S. P. (1984). *Mechanics of Materials*. Second edition. Boston: PWS Engineering.
- GOULD, S. J. (1966). Allometry and size in ontogeny and phylogeny. *Biol. Rev.* **41**, 587–640.
- GRAY, J. AND LISSMANN, H. W. (1938). Studies in locomotion. VII. Locomotory reflexes in the earthworm. *J. exp. Biol.* **15**, 506–517.
- HARVEY, P. H. AND PAGEL, M. D. (1991). *The Comparative Method in Comparative Biology*. Oxford: Oxford University Press.
- HILL, A. V. (1950). The dimensions of animals and their muscular dynamics. *Sci. Prog.* **38**, 209–230.
- HUXLEY, J. S. (1932). *Problems of Relative Growth*. London: Methuen.
- JOHNSON, A. S. AND KOEHL, M. A. R. (1994). Maintenance of dynamic strain similarity and environmental stress factor in different flow habitats: thallus allometry and material properties of a giant kelp. *J. exp. Biol.* **195**, 381–410.
- KIER, W. M. (1992). Hydrostatic skeletons and muscular hydrostats. In *Biomechanics (Structures and Systems): A Practical Approach* (ed. A. A. Biewener), pp. 205–231. Oxford: IRL Press.
- KIER, W. M. AND SMITH, K. K. (1985). Tongues, tentacles and trunks: The biomechanics of movement in muscular hydrostats. *J. Linn. Soc.* **83**, 307–324.
- LEPESCHEUX, L. (1988). Spatial organization of collagen in annelid cuticle: order and defects. *Biol. Cell* **62**, 17–31.
- MCMAHON, T. (1973). Size and shape in biology. *Science* **179**, 1201–1204.
- MCMAHON, T. A. (1975). Using body size to understand the structural design of animals: Quadrupedal locomotion. *J. appl. Physiol.* **39**, 619–627.
- MCMAHON, T. A. AND BONNER, J. T. (1983). *On Size and Life*. New York: W. H. Freeman & Company.
- NEWELL, G. E. (1950). The role of the coelomic fluid in the movements of earthworms. *J. exp. Biol.* **27**, 110–121.
- PEDLEY, T. J. (1977). *Scale Effects in Animal Locomotion*. New York: Academic Press.
- PETERS, R. H. (1983). *The Ecological Implications to Body Size*. Cambridge: Cambridge University Press.
- PETERSON, J. A., BENSON, J. A., NGAI, M., MORIN, J. AND OW, C. (1982). Scaling in tensile 'skeletons': structures with scale-independent length dimensions. *Science* **217**, 1267–1270.
- PIEARCE, T. G. (1983). Functional morphology of lumbricid earthworms, with special reference to locomotion. *J. nat. Hist.* **17**, 95–111.
- RICHARDS, S. (1974). The ultrastructure of the cuticle of some British lumbricids (Annelida). *J. Zool., Lond.* **172**, 303–316.
- RUBIN, C. T. AND LANYON, L. E. (1984). Dynamic strain similarity in vertebrates: an alternative to allometric limb bone scaling. *J. theor. Biol.* **107**, 321–327.
- RUPPERT, E. E. AND BARNES, R. D. (1995). *Invertebrate Zoology*. Sixth edition. New York: Saunders College Publishing.
- SATCHELL, J. E. (1967). Lumbricidae. In *Soil Biology* (ed. A. Burgess and F. Raw), pp. 259–322. London: Academic Press.
- SCHMIDT-NIELSEN, K. (1984). *Scaling: Why is Animal Size so Important?* Cambridge: Cambridge University Press.
- SEYMOUR, M. K. (1969). Locomotion and coelomic pressure in *Lumbricus terrestris* L. *J. exp. Biol.* **51**, 47–58.
- SEYMOUR, M. K. (1970). Skeletons of *Lumbricus terrestris* L. and *Arenicola marina* (L.). *Nature* **228**, 383–385.
- SOKAL, R. R. AND ROHLF, F. J. (1969). *Biometry*. San Francisco, CA: W. H. Freeman & Company.
- STEPHENSON, J. (1930). *The Oligochaeta*. Oxford: Oxford University Press.
- THOMPSON, D. W. (1917). *On Growth and Form*. Cambridge: Cambridge University Press.
- TRUEMAN, E. R. (1966). Observations on the burrowing of *Arenicola marina* (L.). *J. exp. Biol.* **44**, 93–118.
- TRUEMAN, E. R. (1975). *Locomotion in Soft-bodied Animals*. London: Edward Arnold.
- WAINWRIGHT, S. A. (1988). *Axis and Circumference*. Cambridge, MA: Harvard University Press.
- ZUCKERKANDL, E. (1988). Coelomic pressure in *Sipunculus nudus*. *Biol. Bull. mar. Biol. Lab., Woods Hole* **98**, 161–173.

KINEMATIC SCALING OF HYDROSTATIC
SKELETONS: PERISTALTIC CRAWLING IN
EARTHWORMS

K.J. Quillin. U.C. Berkeley.
quillin@violet.berkeley.edu

The mechanical consequences of size changes are relatively well-studied for rigid skeletal systems, but not for hydrostatic skeletons, which are composed of a flexible body wall in tension surrounding a compression-resisting fluid under pressure. An ontogenetic size range of earthworms (*Lumbricus terrestris*) was used to examine how the kinematics of peristaltic crawling scale with body size. Preferred crawling speed, stride length, stride frequency, and duty factor all scale as would be predicted by isometry: crawling speed and stride length scale as body mass^{1/3} while stride frequency and duty factor are independent of body mass. Preferred crawling speed, however, varied widely among individuals, with fast worms generally crawling more rapidly than slow worms by taking bigger steps rather than by taking more steps per unit time. Larger steps are accomplished by engaging more segments in anterior protrusion rather than extending each segment to a greater degree. Hydrostatic skeletons are commonly composed of viscoelastic materials; extent of deformation is dependent not only on the magnitude of load but also on the rate of loading. Both the longitudinal and circumferential extension ratios (final length/original length) and extension rates of the body wall of segments 15 and 50 were found to be independent of body mass in *Lumbricus terrestris* during peristaltic crawling.

(1996) Am. Zool. 35: 9A.

ONTOGENETIC SCALING OF FORCE PRODUCTION IN
HYDROSTATIC SKELETONS

K.J. Quillin. Univ. of California, Berkeley, CA.,
quillin@socrates.berkeley.edu

The mechanical consequences of size changes are relatively well-studied for rigid skeletal systems, but not for hydrostatic skeletons. The present study uses the earthworm *Lumbricus terrestris* as the experimental system to examine how force production scales with body size during ontogeny. Worms ranging in size from hatchlings (0.01 g) to adults (8 g) exerted maximum forces during active radial expansion of their burrows by their anteriormost segments. These radial forces were typically seven times greater in magnitude than the normal radial anchoring forces of worms crawling within burrows. When the earthworms pushed against the closed end of a soil burrow, the maximum axial and radial forces were comparable in magnitude. All radial and axial forces scaled as body mass raised to the 2.5 power; the hatchlings could push 500 times their own body weight, while the large adults could push only 10 times their own body weight. Both the stride length (normalized to body length) and stride frequency of burrowing earthworms were constant as a function of body mass.

(1997) Amer. Zool 37: 176A